Evolution of a microcontinent during continental break-up: re-evaluating the Falklands Plateau

Roxana-Mihaela Stanca

Submitted in accordance with the requirements for the degree of

Doctor of Philosophy

The University of Leeds

School of Earth and Environment

August 2021

Declaration

The candidate confirms that the work submitted is their own, except where work which has formed part of jointly authored publications has been included. The contribution of the candidate and the other authors to this work has been explicitly indicated below. The candidate confirms that appropriate credit has been given within the thesis where reference has been made to the work of others.

The work in two of the chapters has been accepted for publication and subsequently edited and included in the thesis. Changes from the submitted version include the addition of more figures, associated text edits, and text clarifications where required. The status of the manuscripts is as follows:

Chapter 4: Stanca, R. M., Paton, D. A., Hodgson, D. M., McCarthy, D. J., and Mortimer, E. J. 2019. A revised position for the rotated Falkland Islands microplate. Journal of the Geological Society, 176, pp. 417–429, https://doi.org/10.1144/jgs2018-163

As lead author, I was responsible for data analysis, interpretation, and figure and manuscript preparation. The contribution of the other authors was limited to discussion of the results and manuscript review and editing.

Chapter 5: Stanca, R. M., McCarthy, D. J., Paton, D. A., Hodgson, D. M., and Mortimer, E. J. 2021. The tectono-stratigraphic architecture of the Falkland Plateau Basin; implications for the evolution of the Falkland Islands Microplate. Gondwana Research, https://doi.org/10.1016/j.gr.2021.09.014

As lead author, I was responsible for data analysis, interpretation, and figure and manuscript preparation. The contribution of the other authors was limited to discussion of the results and manuscript review and editing.

Acknowledgements

I extend my most honest thanks

to my supervisors, Dave Hodgson and Estelle Mortimer, for all the support, encouragements, and trust shown over the past years. You made this whole experience so enjoyable, and I am forever grateful for this. Thank you to both for the useful advice and help during job hunting, for your general enthusiasm and kind discussions, which kept me motivated.

to my industry supervisor, Dave McCarthy, for all the help offered during the project, for all the talks and encouragements, for having the best dog that made our Zoom meetings even better, and, of course, for taking the time to co-found Whiskey Wednesdays. I thank him and his colleagues from the British Geological Survey for the support offered during my placements at their office. I am grateful to Erica Greenhalgh for the help offered with the gravity modelling stage of the project and to Phil Stone and Graham Leslie for the insightful comments on the two manuscripts submitted during these years.

to Douglas Paton for support and constructive discussions in the early stages of my project. I would not have been here if it were not for your enthusiasm for structural geology that has been an inspiration since my master's degree.

to Graeme Eagles for providing me with early access to the magnetic data acquired by the Alfred Wegner Institute over my area of study.

to journal reviewers for the positive and constructive comments and for making the whole publication process easy and enjoyable.

to Moh Gouiza and Ezekiel Yusuf Yenne for not getting tired of my questions and for always being keen to help. Moh, thank you for the many roles you have undertaken during my PhD, as a friend, honorary supervisor, and gravity modelling connoisseur.

to people from the department for the helpful chats and encouragements. I would like to particularly thank Charlotte Botter, Sergio Gamez Galicia, Ulises Rodriguez, Rebecca Schlegel, Mike Shotton, Sissy Vasileiou, and Rachel Whitty for the laughs (and cries), runs, all the top-notch cake decorating, and cat therapy.

to Georgian Manuc for all the moral support offered throughout the entirety of this project. I could not have asked for a better roommate and friend. Thanks for the cakes and late-night drinks and chats and for dealing with all my anxieties like a champ!

to friends from home and not only for keeping me motivated, distracted when needed, and just being there when I needed a pep talk or a virtual hug. I thank Cristina Accotto, Sarah Iliuta, Theo Istrate, Delia Lazar, Lucian Luta, Mihnea Micu, Simon Oldfield, Iasmina Stefan, Alex Tamas, and others for just making my life better by being in it!

to Matt for being my rock for these past years. There's nothing more special than the bond between a geoscientist and their rock! Thank you for believing in me even when I did not. Thank you for the support, for accepting my quirks, for the games and strolls and delicious puddings.

and to my family, Alina, Violeta, and Vasile, for all the love and support. There is nothing that helps me recharge more than a phone or video call with either of you or a visit home. Thank you for being there when I needed you, for always accepting and supporting my choices, and for just being by my side even when not knowing how to help. Vă mulțumesc!

This project was funded through the Leeds/York NERC Doctoral Training Programme and BUFI (BGS University Funding Initiative).

Abstract

Continental break-up is associated with the formation of complex margins, of which transform margins remain less understood due to their varied crustal architectures. This limits our understanding of the processes that accompany the fragmentation of supercontinents, which impacts the reliability of plate tectonic models. The Falkland Plateau (FP) is an example of a transform margin that developed along one of the most long-lived and long-offset transform faults on Earth. The evolution of the plateau is linked to south-western Gondwana break-up and its present-day morphology has been associated with vertical-axis rotation of an extensive microplate (the Falkland Islands Microplate – FIM). Therefore, the FP represents an ideal example to improve our understanding of transform margin development, block rotation mechanisms, and early stages of Gondwana break-up.

Here, the FP architecture and evolution is constrained by integrating seismic reflection and potential field data, and building rigid and deforming plate models. The results support an ~80° Middle-Late Jurassic FIM clockwise rotation. Rapid stress variations affected south-western Gondwana before and during the FIM rotation. The rotation was initiated by the East Antarctica southward drift, and resulted in continental crust extension, intrusion, underplating, and oceanic crust generation in the Falkland Plateau Basin. The resulting architecture displays similarities with other transform margins. Furthermore, the FIM structural network supports intra-block deformation during rotation, and shows that current deformation models are applicable to larger scales. This thesis emphasises a need for re-evaluating the deformation interpreted along South America during Gondwana break-up, and disproves recent interpretations of West Antarctic evolution.

This study highlights the importance of integrating diverse datasets and methodologies in understanding tectonically complex areas. The updated interpretation of the FP provides more information about transform margin evolution and constraints on the pre-break-up Gondwana configuration, which will inform future research on resource distribution and climate evolution.

Contents

List of tables

List of figures

Chapter 1 Introduction

1.1 Motivation

Understanding how continents amalgamate, break-up and disperse is important from an economic point of view (i.e. resource distribution) but also for understanding the formation of oceanic basins (Macdonald et al., 2003; Donnadieu et al., 2016; Mueller and Jokat, 2017). Dispersal of supercontinents and changes in the configuration of the resulting continents have profound implications on oceanic connectivity and the development of oceanic current circulation, which in turn directly impact present-day climate (Barker and Thomas, 2004). Therefore, a better understanding of the processes related to the fragmentation of continents and supercontinents can provide more insights into how these influence the evolution of Earth's geomorphology, biota, and climate.

One of the consequences of continental break-up consists of the formation of continental margins. Numerous studies have been carried out on passive margins, due to their industrial importance; these have contributed to the development of continental break-up models (Biari et al., 2021 and references therein). Transform margins represent 16% of continental margins (Figure 1.1) and have been the topic of numerous studies since the 1970s. However, they remain less understood due to their complexity and variability (Rabinowitz and Labrecque, 1979; Scrutton, 1979; Mascle and Blarez, 1987; Mutter and Larson, 1989; Lorenzo et al., 1991; Basile et al., 1993, 2013; Lorenzo, 1997; Sage et al., 2000; Berndt et al., 2001; Mercier de Lépinay et al., 2016; Nemčok et al., 2016; Loncke et al., 2020), which has limited the development of models for their formation and evolution. This impacts their integration in plate reconstructions and the understanding of their pre-break-up morphology and configuration. In addition, this also results in uncertainties in current plate models that do not account for the pre-break-up extent and shape of transform margins. Nonetheless, recent efforts have been made to compile the available information for these margin types and their highly complex sub-types (transform marginal plateaus) (Basile, 2015; Mercier de Lépinay et al., 2016; Nemčok et al., 2016; Loncke et al., 2020). This compilation approach has allowed the structural and crustal architectures commonly identified along transform margins to be summarized.

Furthermore, continental break-up and the formation of continental margins (commonly transform margins) can be accompanied by large-scale wrenching which can result in fragmentation of the crust and lithosphere and the rotation of the resulting blocks around a vertical axis (Mascle and Blarez, 1987; Lorenzo et al., 1991). Although several models for the mechanism and deformation seen along these rotating blocks exist (Beck, 1976; Ron et al., 1984; England et al., 1985; Garfunkel and Ron, 1985; McKenzie and Jackson, 1986; Nelson and Jones, 1987; Sonder et al., 1994; Peacock et al., 1998), there are still a lot of uncertainties remaining about the applicability of these models at regional scale.

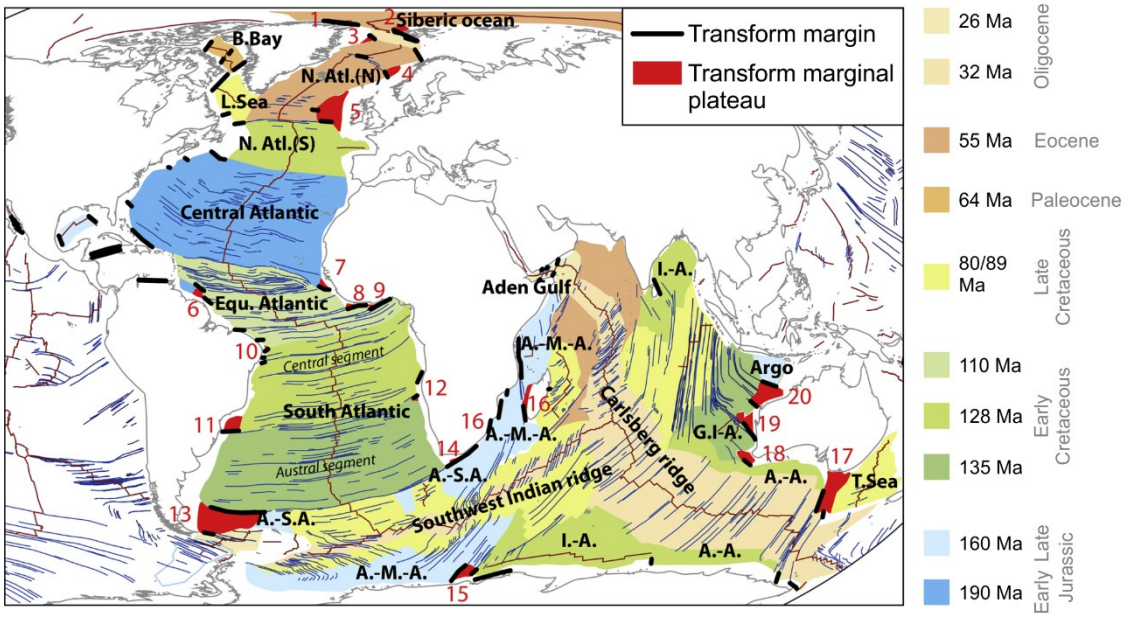

Figure 1.1 Global distribution of transform margins and marginal plateaus (modified after Mercier de Lépinay et al., 2016 and Loncke et al., 2020); 1. Morris Jesup Rise; 2: Yermarck Plateau; 3: NE Greenland Plateau;4: Vøring Plateau; 5: Faroe-Rockall Plateau; 6: Demerara Plateau; 7: Guinea Plateau; 8: Liberia; 9: Côte d'Ivoire - Ghana; 10: Potiguar Plateau; 11: Sao Paulo Plateau; 12: Walvis Plateau; 13: Falklands Plateau; 14: Agulhas Plateau; 15: Gunnerus Ridge; 16: Morondava Plateau, 17: Tasman Plateau; 18: Naturaliste Plateau; 19: Wallaby-Cuvier Plateau; 20: Exmouth Plateau; A.-A.- Australia-Antarctic; A.-M.-A. - Africa-Madagascar-Antarctic; A.-S-A - Africa-South America; B.Bay - Baffin Bay; Equ Atlantic - Equatorial Atlantic; G.I.-A. - Greater India-Australia; I.A. - India-Antarctic; L.Sea - Labrador Sea; N.Atl (N) - Northern North Atlantic; N.Atl(S) - Southern North Atlantic; T.Sea -Tasman Sea.

This thesis is a contribution to the current knowledge base of transform margins by focusing on one such margin, the Falkland Plateau, offshore Argentina, and the way it relates to its conjugate, the Agulhas margin, offshore South Africa

(Figure 1.2). These two areas have developed along the Agulhas-Falkland Fracture Zone (AFFZ), which is a trans-Atlantic transform with one of the longest offsets on Earth (1200 km; Ben-Avraham et al., 1997). Both margins were active for ~50 Myrs (Lorenzo and Wessel, 1997) which classifies them as two of the most long-lived transform margins (Mercier de Lépinay et al., 2016). The Falkland side, which represents the topic of this thesis, is believed to have undergone far more deformation than its northern counterpart with some authors invoking vertical-axis rotation of the Falkland Islands (Adie, 1952a; Mitchell et al., 1986; Marshall, 1994; Thomson, 1998; Trewin et al., 2002; Macdonald et al., 2003). Furthermore, it has remained well preserved, except for the southern boundary, which is now further complicated by compression along the North Scotia Ridge. It therefore represents a pertinent example to improve understanding of these types of margins and the processes associated with their formation (e.g. block rotation). This in turn will add to the current understanding of the break-up of south-western Gondwana and of continental fragmentation and dispersal in general.

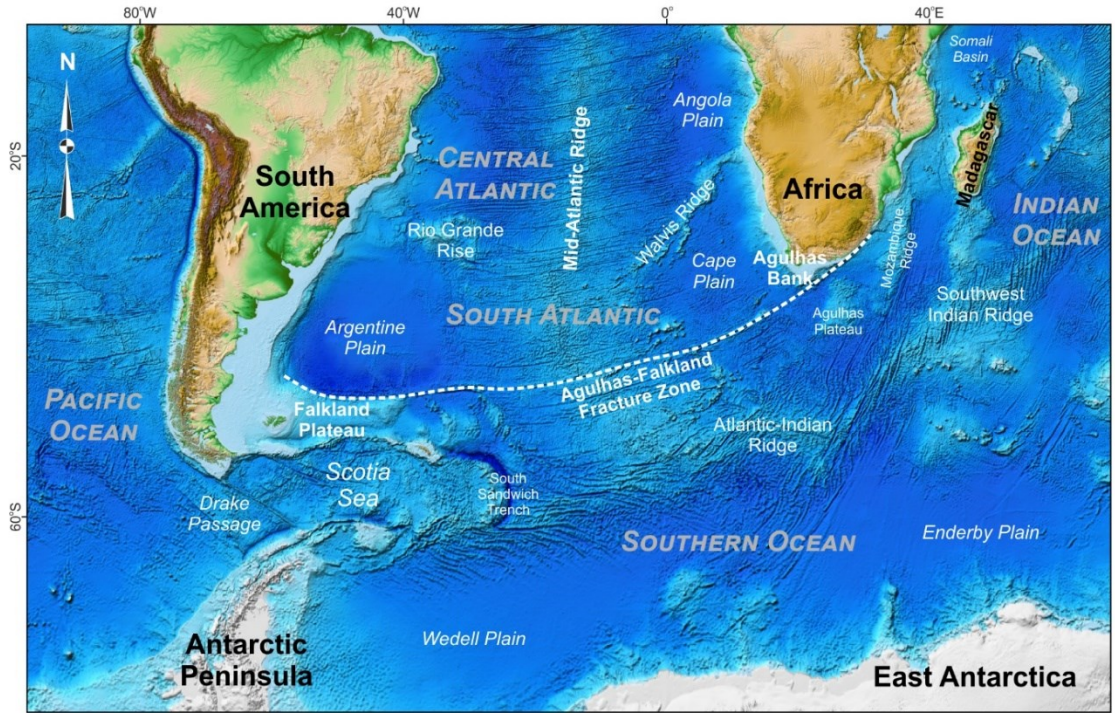

Figure 1.2 Present-day configuration of the South Atlantic region showing the location of the Falkland Plateau and the extent of the Agulhas-Falkland Fracture zone; ETOPO1 global relief model (NOAA National Geophysical Data Centre, 2009; Amante and Eakins, 2009)

1.2 Aim and objectives

The Falkland Plateau has been the focus of several studies (Lorenzo and Mutter, 1988; Richards et al., 1996a; Lorenzo and Wessel, 1997; Richards and Fannin, 1997; Kimbell and Richards, 2008; Schreider et al., 2011; Baristeas et al., 2013; Lohr and Underhill, 2015; Schimschal and Jokat, 2017). However, its structural and crustal architecture remain the subject of numerous debates, which has resulted in different reconstructions and interpretations for the evolution of south-western Gondwana (Macdonald et al., 2003; König and Jokat, 2006; Muller et al., 2019; Eagles and Eisermann, 2020). This thesis aims to address the uncertainties related to the structure and evolution of the Falkland Plateau by carrying out a thorough analysis of the plateau with the following specific objectives:

(a) to determine if a vertical-axis rotation of the Falkland Islands Microplate has occurred and, if so, to assess the amount and timing of rotation through correlative analysis between the structural frameworks on- and offshore (northern and eastern sedimentary basins) the islands and on- and offshore South Africa, South America, West and East Antarctica;
(b) to document the crustal, structural, and stratigraphic architecture of the Falkland Plateau Basin and the Falkland Plateau in general, and to use the results to further constrain the position of the Falkland Islands relative to the Maurice Ewing Bank and South Africa prior to the break-up of Gondwana;
(c) to assess the impact of these results on processes and mechanisms that facilitate vertical-axis rotations, on our understanding of transform faults, and on the palaeogeographic reconstruction of south-western Gondwana.

The study will contribute to our understanding of the evolution of the Falkland Plateau, which will add to current knowledge of processes occurring during the fragmentation of supercontinents by offering insights into the evolution of transform margins, and by constraining the pre-break-up plate configuration of south-western Gondwana. An integration of seismic reflection, gravity, and magnetic data, gravity modelling and inversion, and rigid and deforming plate models will be used to achieve this and answer the following research questions:

1. *What are the implications of the reconstruction of the Falkland Islands Microplate on the fragmentation of south-western Gondwana and how do microplates control regional reconstructions?*

Rationale: Understanding the evolution of the Falkland Plateau is crucial for a better understanding of the break-up of Gondwana. The position and original extent of the plateau control how close together South America, Antarctica, and Africa were prior to the fragmentation of Gondwana. Uncertainties in the tectonic evolution of the plateau (i.e. rotation vs. no rotation of the Falkland Islands) translate into difficulties in reliably estimating the displacement that occurred during the intra-continental transform stage of the AFFZ, which affects the fit between South America and Africa. This in turn impacts the amount of deformation included in plate models for South America and results in vastly different fragmentations and configurations of the South American plate within Gondwana reconstructions (Figure 1.3; Macdonald et al., 2003; König and Jokat, 2006; Torsvik et al., 2009; Muller et al., 2019). Furthermore, the southern part of the Falkland Plateau was the conjugate of the Weddell Sea/West Antarctic region (Filchner-Ronne Shelf; Figure 1.3), but it was deformed during the Late Cretaceous - Cenozoic development of the North Scotia Ridge and opening of the Scotia Sea (Barker and Griffiths, 1972; Dalziel et al., 2013). Nonetheless, understanding the pre-break-up architecture of the Falkland Plateau and its tectonic evolution can provide insights into the configuration of the sub-blocks of the West Antarctic region where several pre-break-up models currently exist (e .g. Storey et al., 1992; Dalziel and Lawver, 2001; König and Jokat, 2006; Eagles and Eisermann, 2020).

As the Falkland Plateau has developed at the junction between South America, Africa, East and West Antarctica (Figure 1.3), the deformation of the infill of its sedimentary basins and overall crustal architecture can provide information on the stress variations that preceded the break-up of Gondwana. Furthermore, developing a model for the structural and crustal evolution of the plateau and comparing and correlating it with the structural networks documented along Africa, South America, and Antarctica can help understand how the wrenching between these three major plates has affected the area between them. This will further constrain the plate models that currently exist for south-western Gondwana and the processes that accompanied the early stages of break-up.

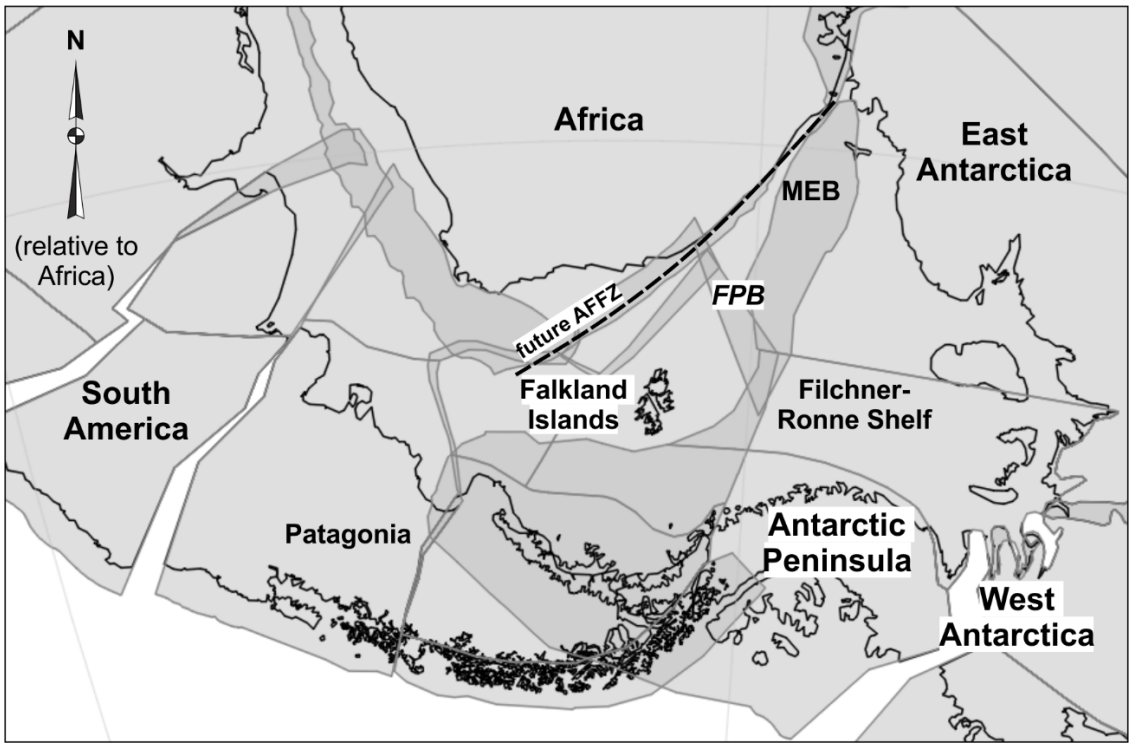

Figure 1.3 Reconstruction of Gondwana at ~180 Ma (Müller et al., 2019) showing an example of fragmentation and configuration of the South American plate, West Antarctic region, and Falkland Plateau; AFFZ – Agulhas Falkland Fracture Zone; FPB – Falkland Plateau Basin; MEB – Maurice Ewing Bank

2. *How do blocks/microplates form, rotate, and deform in wrenching settings?*

Rationale: Currently there are several studies on the delimitation and release of microplates and multiple models for their rotation and intra-plate deformation (Beck, 1976; Ron et al., 1984; England et al., 1985; Garfunkel and Ron, 1985; McKenzie and Jackson, 1986; Nelson and Jones, 1987; Sonder et al., 1994; Peacock et al., 1998; Nemcok et al., 2016). However, it is unclear if areas the size of the Falkland Islands Microplate, which are interpreted to have undergone up to ~120° rotation (Adie, 1952a) abide by the rules invoked by these models.

The fragmentation of previously documented rotated blocks (Martinez and Taylor, 1996; Peacock et al., 1998; Platt and Becker, 2013; Ingersoll and Coffey, 2017) is predominantly controlled by Riedel geometries (Ron et al., 1984; Garfunkel and Ron, 1985; McKenzie and Jackson, 1986; Peacock et al., 1998). More irregular fragments are invoked by Horst et al. (2018), whereas Szatmari and Milani (1999), Salamon et al. (2003), Nemcok et al. (2016), and Glerum et al. (2020) argue for a control of structural inheritance on the

geometry of the final blocks. However, more information is needed to understand the impact of pre-existing structures on the delimitation and release of blocks, particularly for areas like the Falkland Islands Microplate where the areal extent of the block reaches hundreds of thousands of km^2 (e.g. as defined by Storey et al., 1999).

In areas like California and Northern Iceland (Luyendyk et al., 1985; Horst et al., 2018), rotations comparable to, or larger than the one invoked for the Falkland Islands Microplate were documented and explained through previously published models (Ron et al. , 1984; Garfunkel and Ron, 1985; McKenzie and Jackson, 1986; Nelson and Jones, 1987; Sonder et al., 1994). The driving forces for documented rotations are represented either by drag along the edge of the blocks and/or basal drag either from a ductile lower crust, for crustal blocks (confined to the upper crust), or from the upper mantle, for microplates (Beck, 1976; Nelson and Jones, 1987; Schouten et al., 1993; Searle et al., 1993; Neves et al., 2003). The contribution of each of these forces can vary, and understanding the mechanism for the large potential rotation of the Falkland Islands Microplate can offer more insights into the importance of each of these forces on initiating and maintaining rotations of microplates.

Furthermore, the behaviour of the blocks during rotation can vary (Beck, 1976; Ron et al., 1984; England et al., 1985; Garfunkel and Ron, 1985; Nelson and Jones, 1987; Peacock et al., 1998) and, where documented, the deformation can result in complex fault networks (Neves et al., 2003; Salamon et al., 2003; Horst et al., 2018) or more typical geometries predicted by published models (Martinez and Taylor, 1996; Peacock et al., 1998; Ingersoll and Coffey, 2017). However, it is unclear if larger blocks (microplates), such as the Falkland Islands Microplate behave rigidly during rotation or deform according to predicted geometries.

Understanding the processes that led to the separation of the Falkland Islands Microplate and the timing and mechanisms that initiated vertical-axis rotation can help understand similar areas where large blocks have undergone significant rotations, such as the Ellsworth Whitmore Terrane (Watts and Bramall, 1981). Furthermore, better understanding the mechanics of these rotations can shed more light onto the complex processes that accompany continental break-up.

3. *What crustal, structural, and stratigraphic architectures can be seen along transform margins?*

Rationale: Transform margins and marginal plateaus display significant variability in crustal, structural, and stratigraphic architectures due to the fact that the latter have commonly undergone several stages of deformation before the transform motion (Mercier de Lépinay et al., 2016; Loncke et al., 2020). This makes developing models to account for their evolution difficult. An understanding of the processes associated with the formation of these margin types can be gained from compilations summarizing common structural styles, crustal distribution, and stratigraphic geometries (Basile, 2015; Mercier de Lépinay et al., 2016; Loncke et al., 2020).

The structural architecture documented along transform margins and transform marginal plateaus is complex, with normal and reverse faults superimposed by wrenching-related deformation and geometries (Basile et al., 1993; Benkhelil et al., 1995; Pryer et al., 2002; Attoh et al., 2004; Antobreh et al., 2009; McHarg et al., 2018; l'Anson et al., 2019). Furthermore, the distribution of crustal types along these margins can vary as well (Loncke et al., 2020). Although included in the category of continental margins, Loncke et al. (2020) showed that the crust underlying transform marginal plateaus can vary (Figure 1.4) from continental crust, which can be highly intruded and underplated and/or capped by volcanics, to igneous or thick oceanic crust (Lorenzo et al., 1991; Berndt et al., 2001; Klingelhöfer et al., 2005; Fromm et al., 2017; Planert et al., 2017; Schimschal and Jokat, 2019b). The volcanism and magmatism identified along these margins can be associated either with the transform margin development or with any of the deformational stages that preceded it (Loncke et al., 2020). During the transform margin development, vertical movements occur in the vicinity of the transform fault (Basile, 2015; Mercier de Lépinay et al., 2016). The processes associated with these uplifts can vary as well and each of their contribution and control remain uncertain (Le Pichon and Fox, 1971; Scrutton, 1979; Mascle and Blarez, 1987; Lorenzo et al., 1991; Basile and Allemand, 2002; Attoh et al., 2004). In order to easily separate which processes are commonly found along transform margins, more examples need to be documented and discussed against these published compilations.

The Falkland Plateau is one such transform marginal plateau (Mercier de Lépinay et al., 2016; Loncke et al., 2020). Its evolution has been impacted by deformational stages preceding the break-up of Gondwana and has culminated with its separation from Africa along the AFFZ. Furthermore, the Falkland

Plateau is one of the most extensive and long-lived marginal plateaus (Mercier de Lépinay et al., 2016). Therefore it represents an ideal example to further our understading of the processes related to transform margin formation.

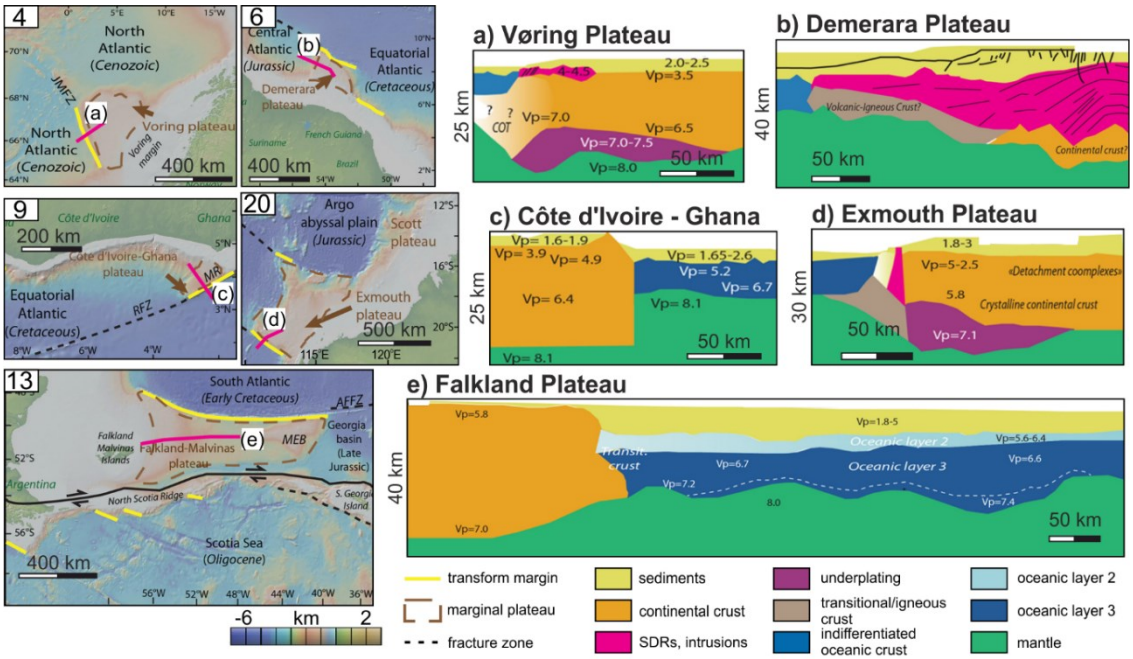

Figure 1.4 Example of crustal architecture along transform marginal plateaus (modified from Loncke et al., 2020); numbers on location maps correspond to plateaus number identifiers in Figure 1.1

1.3 Thesis structure

This thesis is structured in seven chapters. Three of these comprise of results that answer the research questions mentioned in the previous section. Chapter 2 consists of an overview of the concepts discussed and the geological background of the area of study. Chapter 3 presents the data available for this thesis and the methodology used. Chapter 4 is the first results chapter and presents a revised estimation of the Falkland Islands Microplate rotation based on a correlative analysis between the Southern North Falkland Basin and published data from the Outeniqua Basin. Chapter 5 discusses the interpreted structural framework from the western part of the Falkland Plateau Basin and structural styles from the western part of the Falkland Islands Microplate in the context of south-western Gondwana evolution. Chapter 6 discusses the crustal architecture of the Falkland Plateau as constrained by seismic reflection, gravity, and magnetic data, gravity modelling and inversion, and deforming plate modelling. Chapter 7 is the thesis discussion and summarises the findings from the three results chapters, presents updated reconstructions of south-

western Gondwana that incorporate the Falkland Plateau revised architecture, and addresses the research questions posed in Section 1.2.

As stated in the declaration, Chapter 4 has been published in the Journal of the Geological Society and subsequently incorporated in the thesis with several minor changes, and Chapter 5 has been accepted for publication in Gondwana Research and subsequently edited to be included in the thesis.

Chapter 2 Geological background

Each results chapter (Chapters 4-6) will have a separate section on the geological background relevant to the topic analysed and discussed. This chapter will focus on the geological concepts used, regional geology, and details of the local geology not presented within the chapters themselves.

2.1 Transform settings

2.1.1 Transform margins

Transform margins are defined as the transition between continental and oceanic crust across a transform fault (Mercier de Lépinay et al., 2016). Laterally, they are delimited by divergent margins and their meeting points are known as inner and outer corners (Figure 2.1). The initiation of the controlling transform fault can vary from margin to margin and can pre-date the formation of oceanic crust (Basile, 2015) or form simultaneously (Taylor et al., 2009). It was previously considered that these faults exploit areas of crustal weakness, developing along older structures as shown by examples in the Gulf of Aden, the Gulf of Suez, the East African Rifts (Bellahsen et al., 2013), and Nigeria (Wright, 1976), but there are numerous cases where the transform faults cut across previous structures (the Agulhas-Falkland Fracture Zone as shown by Ben-Avraham et al., 1993; fracture zones in the Equatorial Atlantic as described by Basile et al., 2005).

The evolution of transform margins can be summarized in three stages: 1) intra-continental shearing, when anastomosing strike-slip faults develop (Scrutton, 1979; Benkhelil et al., 1995; Antobreh et al., 2009), which can be associated with rotation of continental blocks (Mascle and Blarez, 1987; Lorenzo et al., 1991; Figure 2.1a); 2) continent – ocean active transform faulting, or the active transform margin stage (Basile, 2015), when the spreading centre and further hot oceanic lithosphere is juxtaposed against cold continental lithosphere, resulting in thermal isostasy. This stage can also be accompanied by volcanism (magmatic intrusions and/or lava flows) (Lorenzo et al., 1991; Benkhelil et al., 1995; Berndt et al., 2001; Bird, 2001; Figure 2.1b); 3) continent – ocean contact across an inactive transform fault, or the passive transform margin stage (Basile, 2015), when both the continental and oceanic crust cool down, but at different rates, leading to differential subsidence

(Lorenzo and Wessel, 1997; Figure 2.1c). The amount of mechanical coupling between the adjacent continental and oceanic plates acts as a constraint for the thermal uplift and subsequent differential subsidence (Lorenzo and Wessel, 1997; Lorenzo, 1997; Basile et al., 1998).

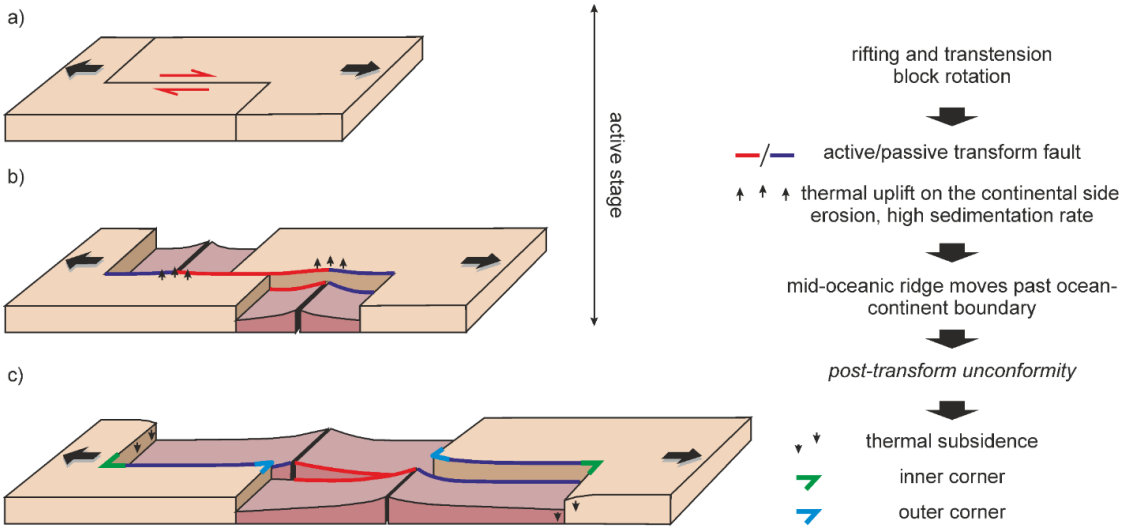

Figure 2.1 Three stage model for transform margin formation (after Mascle and Blarez, 1987; Lorenzo, 1997); a) intra-continental shearing; b) continent-ocean active transform fault stage; c) passive transform margin stage

During the evolution of transform margins, vertical movements on both sides of the transform fault can lead to a complex tectono-stratigraphy and the generation of marginal ridges (Basile, 2015; Mercier de Lépinay et al., 2016). A consensus on the formation of the latter is yet to be reached, but three potential mechanisms have been proposed:

1. thermal uplift induced in the continental lithosphere by juxtaposition against the spreading ridge (Scrutton, 1979; Mascle and Blarez, 1987). However, there is little known on the stability of a ridge generated in this manner. Furthermore, Nemčok et al. (2013) argues that modelled thermal uplift is significantly less than what has been observed. This, in combination with the expected subsequent cooling stage of the lithosphere, raises questions around this process as the main mechanism of marginal ridge formation (Basile, 2015);
2. flexural processes caused by erosion during the intra-continental and continent-ocean stages (Basile and Allemand, 2002), similar to uplift of rift shoulders due to unloading. The lack of response observed at the Moho level represents one of the drawbacks of this model (Basile,

2015). Furthermore, other studies argue against a significant flexural response to unloading along transform faults (Nemčok et al., 2016);

3. crustal thickening due to transpression along the transform fault (Attoh et al., 2004) and/or underplating (Lorenzo et al., 1991), or the transport and juxtaposition of thicker continental blocks against the transform fault (Le Pichon and Fox, 1971). Most observations, however, do not support the presence of a thickened crust beneath the marginal ridges (Basile, 2015).

The volcanic activity associated with transform margins varies with location, and its timing in the transform evolution remains debated (Berndt et al., 2001; Loncke et al., 2020). Lava flows, magmatic intrusions, and underplating have been documented along some transform margins (i.e. Exmouth Plateau in Mutter and Larson, 1989; Lorenzo et al., 1991, Vøring Plateau in Berndt et al., 2001; see Figure 1.1 for location). The uncertainties come from the interpretation of the effect of the cooler continental crust on the melt production. The dynamic model of Mutter et al. (1988) argues for the formation of secondary convection cells in the upper mantle due to the juxtaposition of hot oceanic crust against colder continental crust. This could lead to more melt production and emplacement on the continental side even in the later stages of transform margin evolution (Lorenzo et al., 1991), rather than only during rifting when melt is generated through decompression (Mutter and Larson, 1989). In a second interpretation, the thermal gradient occurring across the transform fault would result in a temperature decrease in the upper mantle and, thus, in lower melt production (Berndt et al., 2001).

2.1.2 Transform marginal plateaus

In some instances, transform margins are associated with deep and extensive submarine plateaus bounded to one side by the transform fault (e.g. Falklands, Agulhas, Vøring, South Tasman Plateau/Rise, Walvis, Rockall, Demerara, Guinea, Exmouth; see Figure 1.1 for location; Mercier de Lépinay et al., 2016). These have been termed transform marginal plateaus (*sensu* Loncke et al., 2020) and are normally associated with several deformational stages prior to transform margin formation (Mercier de Lépinay et al., 2016). The polyphase evolution of transform marginal plateaus results in even more complex structural and crustal architectures when compared to typical transform margins. Depending on their pre-transform deformation history, the plateaus can consist of extended continental crust with (Lorenzo et al., 1991; Berndt et al., 2001; Evain et al., 2015; Fromm et al., 2017) or without (Sage et al., 2000;

Parsiegla et al., 2007, 2009) significant magmatic additions, or a mosaic of continental and oceanic crust (Ewing et al., 1971; Evain et al., 2015; Fromm et al., 2017; Schimschal and Jokat, 2017). The volcanism associated with them can be varied, and can pre-date (be coeval with pre-transform rifting stages), be synchronous with, or post-date transform margin development (Lorenzo et al., 1991; Benkhelil et al., 1995; Berndt et al., 2001; Schimschal and Jokat, 2017; Loncke et al., 2020). The fault networks documented along transform marginal plateaus show a marked variability due to their multi-stage evolution, but a common factor is represented by the wrenching component which can result in transpressional (e.g. folds, reverse faults), transtensional (e.g. normal faults, pull-apart basins), and en-échelon geometries (Basile et al., 1993, 2013; Benkhelil et al., 1995; Pryer et al., 2002; Antobreh et al., 2009; McHarg et al., 2018; I'Anson et al., 2019).

2.1.3 Intra-continental shearing

The incipient stages of transform margin formation, represented by intra-continental shearing, is of particular interest, as it is accompanied by significant deformation. Aside from leading to the development of transform margins, this style of deformation can occur in a variety of settings, along any lithospheric plates moving horizontally past each other (Basile and Allemand, 2002). Analogue settings can be found in areas like the San Andreas Fault and the Dead Sea Transform (Mascle and Blarez, 1987; Weber et al., 2009). The regions affected by shearing can be tens to hundreds of kilometres wide and, depending on the underlying structural grain of the affected regions, can comprise areas of releasing and restraining bands, and anastomosing faults, which give rise to separations of blocks that can undergo vertical-axis rotations during the lateral movement along the faults (Mascle and Blarez, 1987; Jackson and Molnar, 1990; Platt and Becker, 2013; Ingersoll and Coffey, 2017). The deformation can be trans-crustal, as seen in the case of the Dead Sea Transform and the San Andreas Fault (Weber et al., 2004, 2009). The isolated blocks can vary in areal extent from tens to hundreds of thousands of km^2 and be restricted to the upper, brittle crust (*crustal blocks*; Scrutton, 1979; Jackson and Molnar, 1990; Ingersoll and Coffey, 2017), or be bound by lithospheric structures and consist of completely separated *microplates* (Nemcok et al., 2016). The amount of vertical-axis rotation varies and, depending on the mechanistic explanation invoked for the rotation, can account for complex structural architectures as detailed in the next section.

2.2 Deformational models for blocks undergoing vertical-axis rotations

Besides transform or strike-slip settings, tectonic vertical-axis rotations can occur in divergent and convergent environments as well (Lamb, 1987; Giorgis et al., 2004) but this section will mostly focus on wrenching-related motion. Several models have been proposed to explain the mechanism of the rotation in shear zones and the deformation expected within the rotated blocks and surrounding areas (Beck, 1976; Garfunkel and Ron, 1985; McKenzie and Jackson, 1986; Nelson and Jones, 1987; Peacock et al., 1998). These can be loosely grouped into three main categories:

1. *Discrete (rigid) models* use the concept of bookshelf tectonics to explain block rotations in shear zones. The blocks are bounded by strike-slip faults of opposing kinematics to the main shear zone and behave rigidly during the rotation (Ron et al., 1984; Garfunkel and Ron, 1985; McKenzie and Jackson, 1986; Figure 2.2b).
2. *Continuous models* consider that the lithosphere behaves like a viscous layer and no discrete faulting is accommodating the rotation (England et al., 1985; Nelson and Jones, 1987; Kimura et al., 2004; Kimura et al., 2011; Figure 2.2c)
3. *Quasi-continuous models* incorporate the rest of the models in which deformation within the upper and lower crust is accommodated differently during rotation or intra-block deformation is represented by discrete faulting (Figure 2.2d-f). These include: i) the small blocks model of Nelson and Jones (1987) and Sonder et al. (1994) where upper crust fragmentation and rotation due to ductile deformation of the substratum increases towards the shear zone, ii) the ball bearing model of Beck (1976) where rigid, rounded to sub-rounded blocks rotate freely between strike-slip faults above a ductile substratum, and iii) the model of Peacock et al. (1998) which shows similarities to the bookshelf tectonics but argues for a high degree of discrete small-scale intra-plate deformation accommodating large block rotations (Figure 2.2d-f).

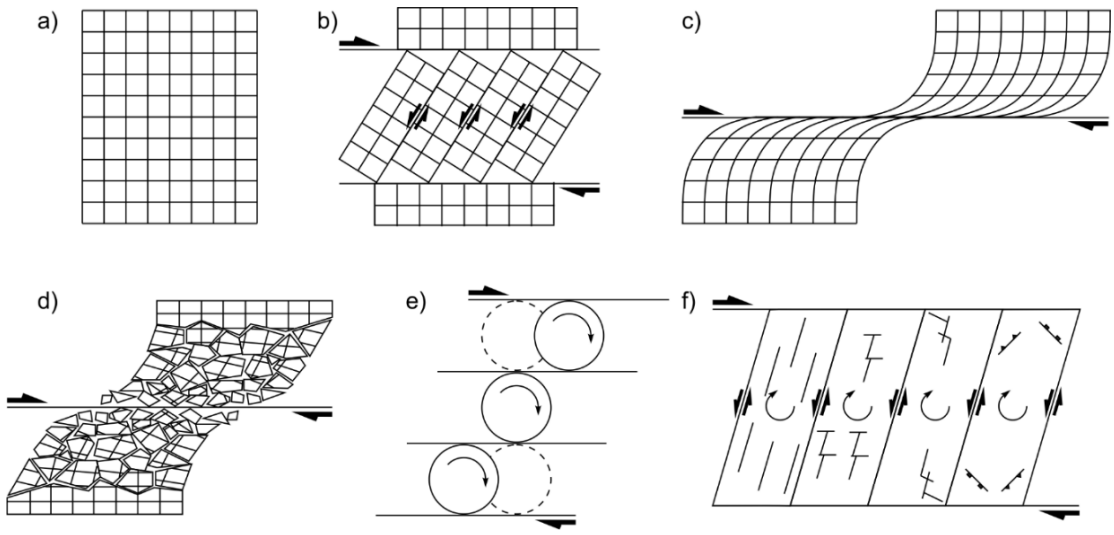

Figure 2.2 Kinematic models for block rotation in strike-slip systems; a) undeformed state; b) discrete (rigid) model (after Ron et al., 1984; Garfunkel and Ron, 1985; McKenzie and Jackson, 1986); c) continuous model (after England et al., 1985; Nelson and Jones, 1987); d) quasi-continuous model with deformation increasing towards the fault plane (after Nelson and Jones, 1987; Sonder et al., 1994); e) quasi-continuous ball-bearing model (after Beck, 1976); f) quasi-continuous model showing four styles of discrete intra-block deformation (after Peacock et al., 1998)

Although numerous studies demonstrate the applicability of each of these models (Figure 2.3; Peacock et al., 1998; Platt and Becker, 2013; Ingersoll and Coffey, 2017; Horst et al., 2018), it is unclear if they can be used to explain the rotation and deformation of microplates where the driving mechanisms may vary. Studies on rotating oceanic microplates, either in strike-slip or rift systems, show a predominance of the edge-driven mechanism, where coupling with the surrounding plates acts as the driving force for rotation (Schouten et al., 1993 and references therein; Searle et al., 1993). However, there are instances where basal drag from the upper mantle can affect this rotation, as in the case of the Easter microplate (Neves et al., 2003). Intra-plate deformation adhering to the mechanistic model of Ron et al. (1984) and Garfunkel and Ron (1985) has been documented in the Bismarck Sea (Figure 2.3a, b; Martinez and Taylor, 1996), but it is not certain if larger and/or continental microplates behave in the same way. The added force exerted by upper mantle drag, along with the crustal anisotropy expected along most continental microplates due to inheritance, can influence the way the deformation is accommodated during rotation (Glerum et al., 2020).

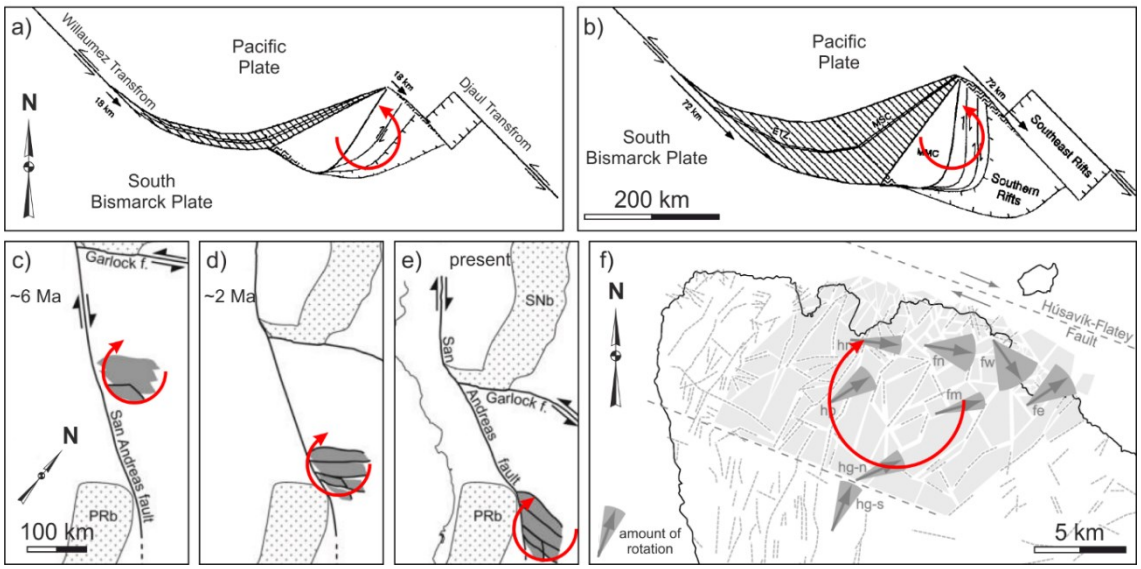

Figure 2.3 Example of block rotations; a) and b) show different stages of counter-clockwise rotation of the Manus Microplate (modified after Martinez and Taylor, 1996); c), d) and e) show different stages of clockwise rotation of the Eastern Transverse Ranges (modified after Ingersoll and Coffey, 2017); f) block fragmentation and clockwise rotations in Northern Iceland (modified after Horst et al., 2018)

The sizes of the blocks and microplates mentioned in this section vary between several tens of km^2 to 1.6 x 10^5 km^2, and underwent rotations of up to 90° (Santa Catalina in Luyendyk et al., 1985; Martinez and Taylor, 1996; Neves et al., 2003; Ingersoll and Coffey, 2017) or even more for blocks under 10 km^2 (Horst et al., 2018). The rotations occurred (or still occur in some cases) in strike-slip, rift (but predominantly bounded by transform and strike-slip faults), or back-arc settings (between transforms accommodating back-arc rifting), and the driving mechanism along with the intra-plate/block deformation due to rotation for these examples can provide insights into the general processes that lead to microplate rotation and structures that accommodate intra-plate deformation.

Understanding transform margins in general and the behaviour of smaller blocks or sub-plates is crucial in understanding the processes occurring during continental break-up. Vertical-axis rotations of blocks and microplates during transform margin development has been invoked for the fragmentation and dispersal of Gondwana, and the following section focuses on the area between South America, Africa, and Antarctica which, as will be evidenced, was the locus of extensive wrenching-related deformation.

2.3 The evolution of the south-western Gondwana

Following the intermittent orogeneses along the southern margin of Gondwana, a pervasive structural fabric was generated, following the trends of Sierra de la Ventana (South America), Cape Fold Belt (Africa), D1 fold belt in the Falkland Islands, and Ellsworth and Pensacola Mountains (Antarctica) (Figures 2.4 and 2.5; Du Toit, 1927; Hälbich, 1993; Trouw and De Wit, 1999; Curtis, 2001). These mountainous belts were part of the Permo-Triassic Gondwanide orogeny, controlled at depth by an intra-crustal mega-décollement (Paton et al., 2006; Lindeque et al., 2011; Pángaro and Ramos, 2012; Stanca et al., 2019). On the South American side, the orogenesis was preceded by the accretion of several terranes throughout the Paleozoic: Pampia, Cuyania, Chilenia, Paracas, and Patagonia (Pankhurst and Rapela, 1998; Pankhurst et al., 2006; Ramos, 2008; Ramos et al., 2010). In Africa, several episodes of contraction and extension preceded the formation of the Cape Fold Belt, which included the Namaqua-Natal and Pan-African orogeneses (Shone et al., 1990; Hälbich, 1993; Thomas et al., 1993; Veevers et al., 1994). The accretion of several terranes (Wilson, Bowers, Robertson Bay) prior to the Gondwanide Fold and Thrust Belt formation occurred in Antarctica as well during the Ross Orogeny (Trouw and De Wit, 1999; Collinson et al., 2006). The resulting structural fabric played an important role in the subsequent break-up and dispersal of Gondwana (Macdonald et al., 2003).

The driving mechanism for the initiation of fragmentation of Gondwana, and supercontinents in general, is still disputed. The presence of mantle plumes impinging on continental lithosphere and far-field drag along subduction zones have been postulated by most studies (Sengör and Burke, 1978; Storey, 1995; Lovecchio et al., 2020). Extensive volcanism occurring in south-western Gondwana prior to and during its fragmentation (e.g. Karoo-Ferrar, Central Atlantic Magmatic Province, Chon Aike magmatic province, Paraná-Etendeka flood-basalt province; Figure 2.5; Encarnación et al., 1996; Pankhurst et al., 1998; Marzoli et al., 1999; Trumbull et al., 2007; Hastie et al., 2014; Foulger, 2018) has been related to rifting initiation. However, a control of far-field stresses (e.g. drag at the Panthalassa Ocean – SW Gondwana subduction zone) is considered by other authors to play an important part in the break-up of Gondwana (Storey, 1995; Peace et al., 2020). Here, the areas of interest are represented by the separation of East and West Gondwana and the opening of the southern South Atlantic.

2.3.1 The southern South Atlantic region

The opening of the South Atlantic was a result of the Mesozoic fragmentation of south-western Gondwana. Continental break-up and generation of the first oceanic crust is believed to have occurred between the Barremian and Berriasian (126.5 – 138 Ma; Rabinowitz and Labrecque, 1979; Nürnberg and Müller, 1991; Channell et al., 1995; Jokat et al., 2003; Heine et al., 2013; Collier et al., 2017). The rifting that preceded passive margin formation propagated northwards (Rabinowitz and Labrecque, 1979), and the intra-plate deformation that accommodated the extension shows significant lateral variability and a strong pre-Jurassic tectonic inheritance (Heine et al., 2013; Paton et al., 2016).

Early extension in the southern South Atlantic region was accompanied in the Jurassic by the emplacement of the Chon Aike magmatic province in Patagonia (Figure 2.5; Pankhurst et al., 1998) and followed an oblique to sub-perpendicular trend to the subsequent mid-Atlantic ridge, believed to be related to the pre-existent structural fabric. A reactivation in an extensional regime of the Paleozoic to Triassic thrusts resulted in Triassic (?) to Early Cretaceous sedimentary basins, bounded by faults trending NW-SE to WNW-ESE, developing across South America (Uliana et al., 1989; Lovecchio et al., 2020) and southern Africa (Muntingh, 1993; Paton and Underhill, 2004). The control of the Gondwanide orogeny on the way extension was accommodated across the two major plates is readily visible in the changes in strike between the Colorado, Orange, and Outeniqua basins (Muntingh, 1993; Paton and Underhill, 2004; Pángaro and Ramos, 2012; Paton et al., 2016) occurring at the Colorado, Garies, Cape, and Port Elizabeth oroclinal bends of the Permo-Triassic fold and thrust belt (Figure 2.4; De Beer, 1992; De Beer, 1995; Johnston, 2000; Pángaro and Ramos, 2012; Paton et al., 2016). Sedimentary basins following a more NNW-SSE trend formed along the western margin of South America (parallel to the south-western margin of Gondwana; Figure 2.4) and were related to retroarc extension (Lovecchio et al., 2020). A more N-S oriented trend developed along the western margin of southern Africa, which was controlled by the Pan-African fabric, and resulted in the Early Cretaceous opening of the South Atlantic (Uchupi, 1989; Maslanyj et al., 1992; Mohammed et al., 2017). The early stages of break-up in the southern South Atlantic are believed by several authors to have included clockwise rotation of the Falkland Islands of up to 180° (Adie, 1952a; Mitchell et al., 1986; Taylor and Shaw, 1989; Marshall, 1994; Thomson, 1998; Storey et al., 1999; Trewin et al., 2002;

Macdonald et al., 2003), and of the Deseado and North Patagonia massifs by ~20°-50° and ~25°-30°, respectively (Geuna et al., 2000; Somoza et al., 2008).

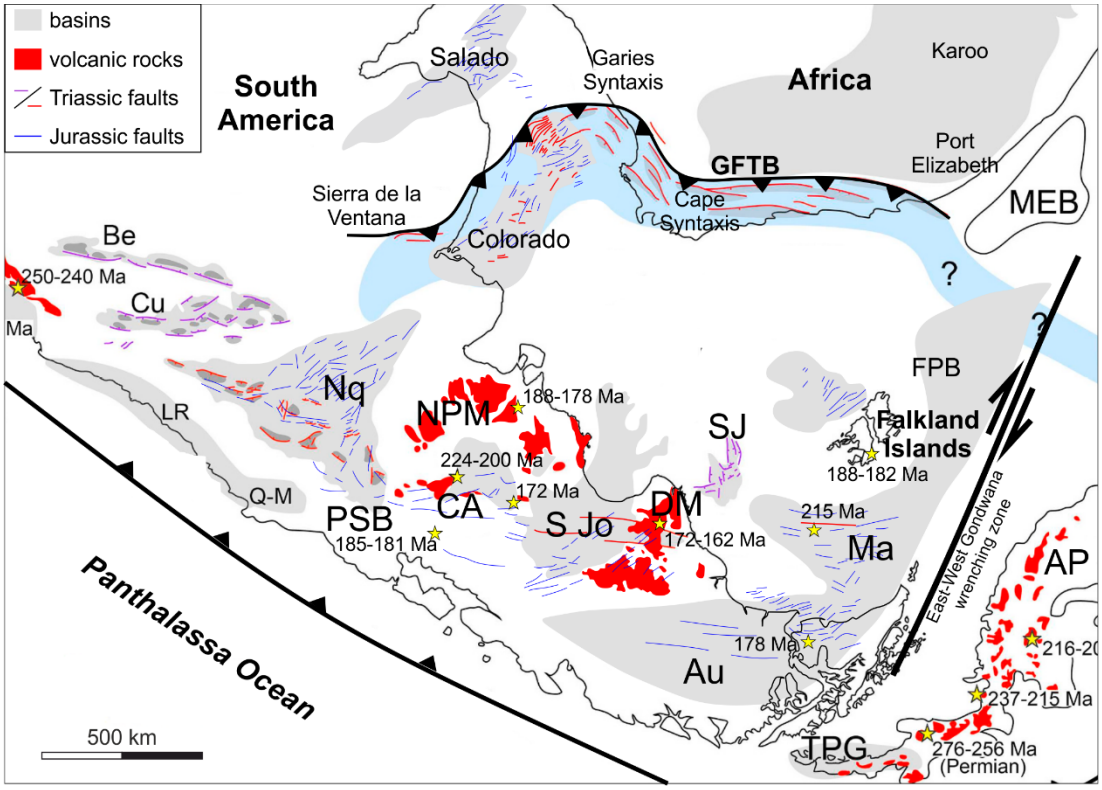

Figure 2.4 Early-Mid Jurassic South Atlantic reconstruction showing main fault trends along the South American plate and the Gondwanide orogeny trend (modified after Lovecchio et al., 2020); AP – Antarctic Peninsula; AU – Austral Basin; Be – Bermejo; CA – Cañadón Asfalto Basin; Cu – Cuyo; DM – Deseado Massif; FPB – Falkland Plateau Basin; GFTB – Gondwana Fold and Thrust Belt; LR - La Ramada; Ma – Malvinas Basin; MEB – Maurice Ewing Bank; NPM – North Patagonian Massif; Nq – Neuquén basins; PSB - Patagonian Subcordilleran Batholith; Q-M - El Quereo-Los Molles basin; SJ – San Julian Basin; S Jo – San Jorge Basin; stars indicate locations with absolute ages for volcanic rocks; TPG – Trinity Peninsula Group

The significant amounts of intra-plate deformation that affected the South American and African plates prior to and during the break-up of Gondwana have been integrated variously in numerous South Atlantic plate models, particularly when it comes to South America (Figures 2.5 and 2.6). Since the rigid reconstruction of Bullard et al. (1965), several ways of fragmenting and deforming the South American plate have been postulated (Lawver et al., 1999; Macdonald et al., 2003; König and Jokat, 2006; Torsvik et al., 2009; Heine et al., 2013; Müller et al., 2019). A few of these reconstructions require the existence of a number of trans-continental strike-slip zones to account for a close fit between the southern part of South America and southern Africa

(Lawver et al., 1999; Macdonald et al., 2003; König and Jokat, 2006; Torsvik et al., 2009). The most controversial of these is the dextral Gastre Fault System, which was considered the onshore continuation of the Agulhas-Falkland Fracture Zone (Rapela and Pankhurst, 1992) along which South America drifted away from Africa. However, no evidence of Mesozoic dextral activity was found in subsequent studies (von Gosen and Loske, 2004).

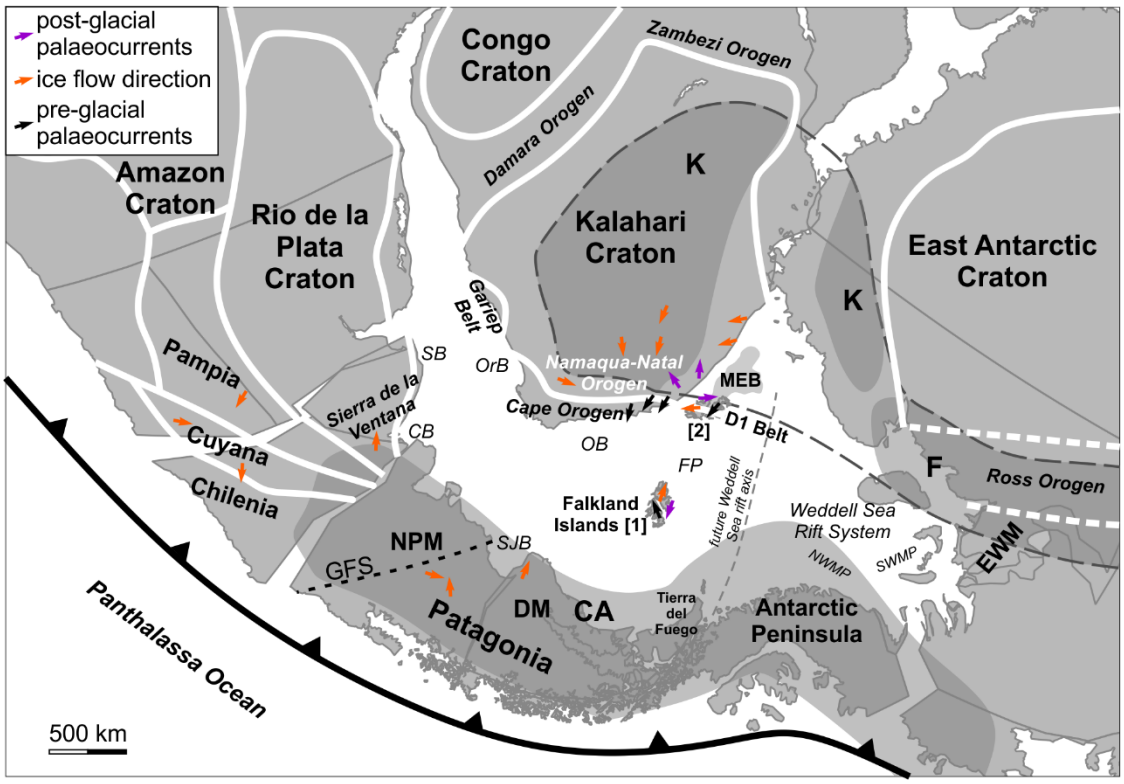

Figure 2.5 Early Jurassic Gondwana configuration; terranes in South America after Ramos et al. (2010) and Santos et al. (2019); cratons and orogens in Africa after Van Hinsbergen et al. (2011); cratons and orogens in Antarctica after Harley and Kelly (2007); Chon Aike after Pankhurst et al. (2000); Karoo-Ferrar large igneous province extent after Stone (2016); Gastre Fault and future Weddell Sea ridge positions after König and Jokat (2006); CA – Chon Aike; CB – Colorado Basin; DM – Deseado Massif; EWM – Ellsworth Whitmore Mountains; F – Ferrar; FP – Falkland Plateau; GFS – Gastre Fault System; K – Karoo; MEB – Maurice Ewing Bank; NPM – North Patagonian Massif; OB – Outeniqua Basin; OrB – Orange Basin; SB – Salado Basin; SJB – San Jorge Basin; Falkland Islands position [1] after Müller et al. (2019) and [2] after Trewin, et al. (2002); plate model after Müller et al. (2019); pre- and post-glacial palaeocurrent directions from Johnson (1991) and Trewin et al. (2002); ice flow directions from Frakes and Crowell (1967), Frakes and Crowel (1969) and Crowell and Frakes (1972)

Besides extensional episodes related to the fragmentation of Gondwana across the South American plate (e.g. Colorado, Salado, San Jorge, San Julian

basins; Uliana et al., 1989; Fitzgerald et al., 1990; Homovc and Constantini, 2001; Lovecchio et al., 2018, 2020), several compressional episodes were also documented throughout Jurassic and during the Cenozoic across Patagonia (Fitzgerald et al., 1990; Naipauer et al., 2012; Navarrete et al., 2016, 2019). This makes a plate model representation of the behaviour of South America more challenging.

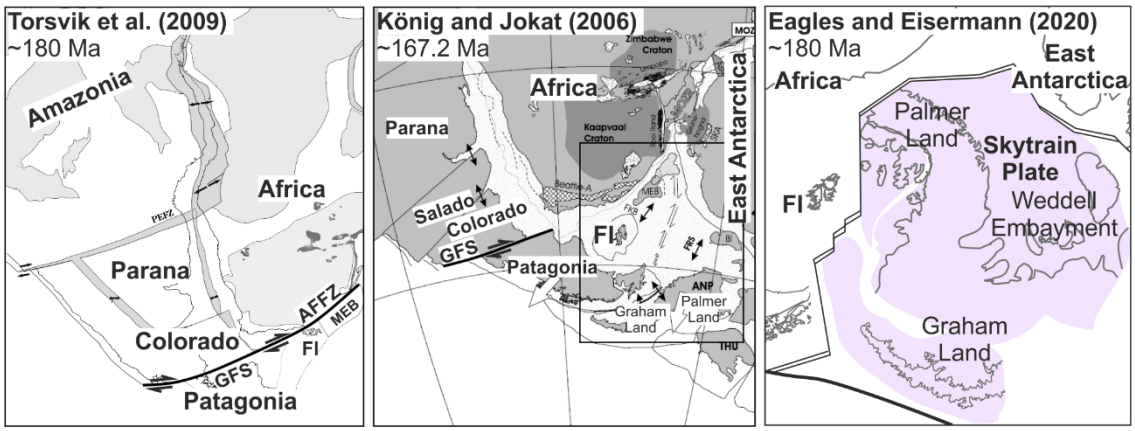

Figure 2.6 Examples of models for the fragmentation and configuration of South America and Weddell Sea; modified and/or drawn after König and Jokat (2006), Torsvik et al. (2009), and Eagles and Eisermann (2020); rectangle in middle inset – approximate extent of plate configuration after Eagles and Eisermann (2020); AFFZ – Agulhas Falkland Fracture Zone; ANP – Antarctic Peninsula; FI – Falkland Islands; FRS - Filchner-Ronne Shelf; GFS – Gastre Fault System; MEB – Maurice Ewing Bank; THU - Thurston Island

2.3.2 The evolution of the Antarctic blocks

The separation of eastern and western Gondwana, along with the events that led to it remain uncertain. There is a wide range of dates (between 165 Ma and 183 Ma) for the drift initiation of Antarctica provided by several studies based on correlations of magnetic reversal isochrons, regional fracture zones, and magmatic and volcanic flow and intrusions analysis (Coffin and Rabinowitz, 1987; Reeves and De Wit, 2000; Marks and Tikku, 2001; König and Jokat, 2006; Jourdan et al., 2007; Eagles and König, 2008). However, early signs of this fragmentation occurred during the Early Permian formation of the Karoo rifts (Macgregor et al., 2018). Extensive volcanism occurred during the Early Jurassic (174-190 Ma; Riley et al., 2005; Jourdan et al., 2007; Klausen, 2009) resulting in the formation of the Karoo-Ferrar large igneous province (Figure 2.5; Macdonald et al., 2003; Jourdan et al., 2007; Peace et al., 2020). This episode of magmatism led to the intrusion of several dyke swarms and lava flow emplacement onshore Africa and East Antarctica (Encarnación et al.,

1996; Riley et al., 2005; Jourdan et al., 2007; Klausen, 2009; Hastie et al., 2014).

The subsequent Jurassic rifting did show some reactivation of the Permian structures (Papini and Benvenuti, 2008), although this was not the predominant case along the entire eastern margin of Africa (Macgregor et al., 2018). The drift of East Antarctica was preceded by intense deformation occurring between East and West Antarctica, in the Weddell region. The Ellsworth Whitmore (Mountains) Terrane (Figure 2.5) was interpreted to have undergone ~90° of counter-clockwise rotation before 180-175 Ma (Watts and Bramall, 1981; Grunow et al., 1987; Curtis and Storey, 1996; Martin, 2007). Extension between the Antarctic Peninsula and East Antarctica between ~178 and ~155 Ma resulted in the formation of the Weddell Sea rift system and its two North and South Weddell Magnetic Provinces (SWMP, NWMP; Grunow, 1993; Jordan et al., 2017; Riley et al., 2020). Roughly N-S wrenching between East and West Gondwana (Figure 2.4; König and Jokat, 2006) is believed to have generated an area of weakness (dashed line along future Weddell Sea rift axis in Figure 2.5), potentially affecting the subducting Panthalassan plate from the south-west, that controlled the location of the subsequent rifting occurring between East Antarctica and SW Gondwana (Lovecchio et al., 2019). Continued extension in the Weddell region led to break-up and oceanic crust formation in the Weddell Sea at ~147 Ma (König and Jokat, 2006). A more recent study argues for a more complex tectonic evolution of the Weddell region where the southern part of the Antarctic Peninsula and the Weddell Embayment are part of a separate Skytrain plate (Figure 2.6) that started rifting away from the Falkland Plateau at the end of the Early Jurassic (Eagles and Eisermann, 2020). This model postulates a development of the South Georgia block along the boundary between the Skytrain plate and west Gondwana, which contrasts with previous interpretations of the island originating off the south-east coast of Tierra del Fuego (Dalziel et al., 1975, 2013, 2021; Macdonald et al., 1987).

The configuration and timing of break-up and dispersal of south-western Gondwana remain uncertain despite numerous studies (Grunow et al., 1987; Curtis and Storey, 1996; Marks and Tikku, 2001; Jokat et al., 2003; König and Jokat, 2006; Eagles and König, 2008; Torsvik et al., 2009; Heine et al., 2013; Collier et al., 2017; Riley et al., 2020). Questions about the pre-break-up configuration of the South Atlantic (i.e. intra-plate deformation along South America, South America – Africa fit, movement along the AFFZ) and East-West

Antarctica remain, as evidenced by various current interpretations of their evolution (Macdonald et al., 2003; König and Jokat, 2006; Torsvik et al., 2009; Heine et al., 2013; Müller et al., 2019; Eagles and Eisermann, 2020). The region sitting between Africa, South America, and Antarctica is represented by the Falkland Plateau and understanding its tectonic evolution is key to addressing these questions.

2.4 Geological setting of the Falkland Plateau

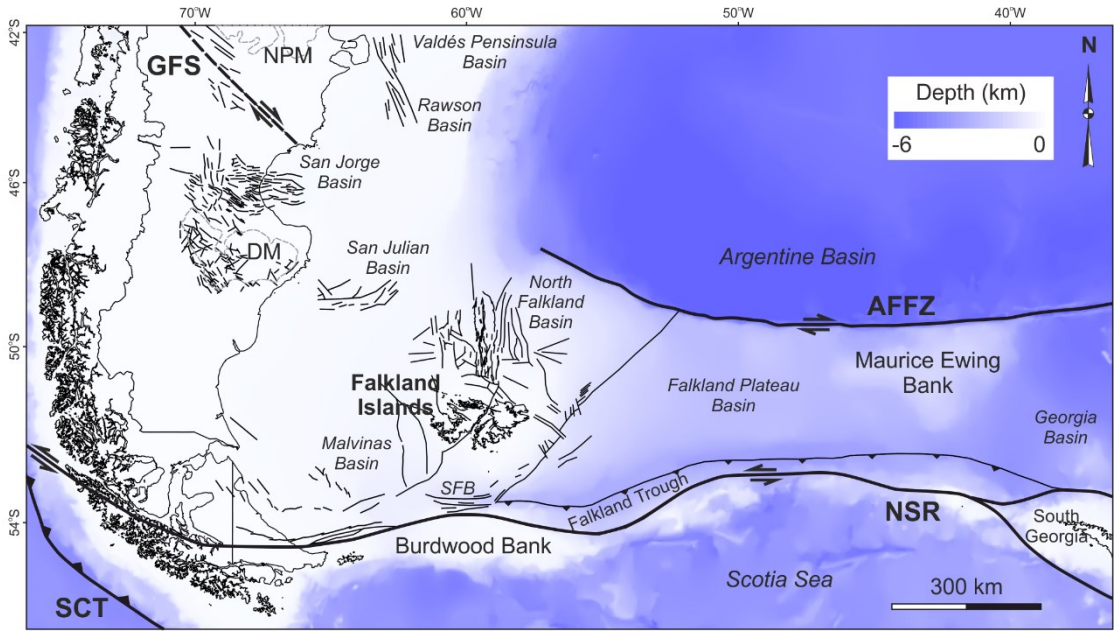

Figure 2.7 Mesozoic structural framework of the South American margin; offshore fault network for the Falkland Plateau compiled after Richards et al. (1996a), Richards and Fannin (1997), Cunningham et al. (1998), Galeazzi (1998), Tassone et al. (2008), and Ramos et al. (2017); the structure of the San Jorge and El Tranquilo basins and the Deseado Massif redrawn after Fitzgerald et al. (1990), Figari et al. (2015), and Moreira and Fernández (2015); Deseado Massif and North Patagonian Massif extents drawn after Ramos et al. (2017); main fracture and subduction zones in South America drawn after Rapela and Pankhurst (1992); AFFZ – Agulhas-Falkland Fracture Zone; DM – Deseado Massif; GFS – Gastre Fault System; NPM – North Patagonian Massif; NSR – North Scotia Ridge; SCT – Southern Chile Trench; SFB – South Falkland Basin

The fragmentation and dispersal of south-western Gondwana resulted in the formation of numerous sedimentary basins and structurally complex regions. The Falkland Plateau (FP) is one of the most prominent areas in the South Atlantic that developed during the break-up of the super-continent.

Understanding its evolution can offer key insights into processes related to break-up of supercontinents but also the development of transform margins.

The plateau is located east of Argentina and comprises, from west to east, the following provinces: the Malvinas Basin, the Falkland Islands (FI) with the North Falkland Basin to the north and the South Falkland Basin to the south, the Falkland Plateau Basin (FPB), and the Maurice Ewing Bank (MEB; Figure 2.7).

The plateau stretches ~2000 km between the South America coast and the Georgia Basin (Figure 2.7). An escarpment represented by the dextral Agulhas - Falkland Fracture Zone (AFFZ) delimitates the plateau to the north whereas to the south it terminates against the Falkland Trough and the North Scotia Ridge (NSR; Ludwig, 1983).

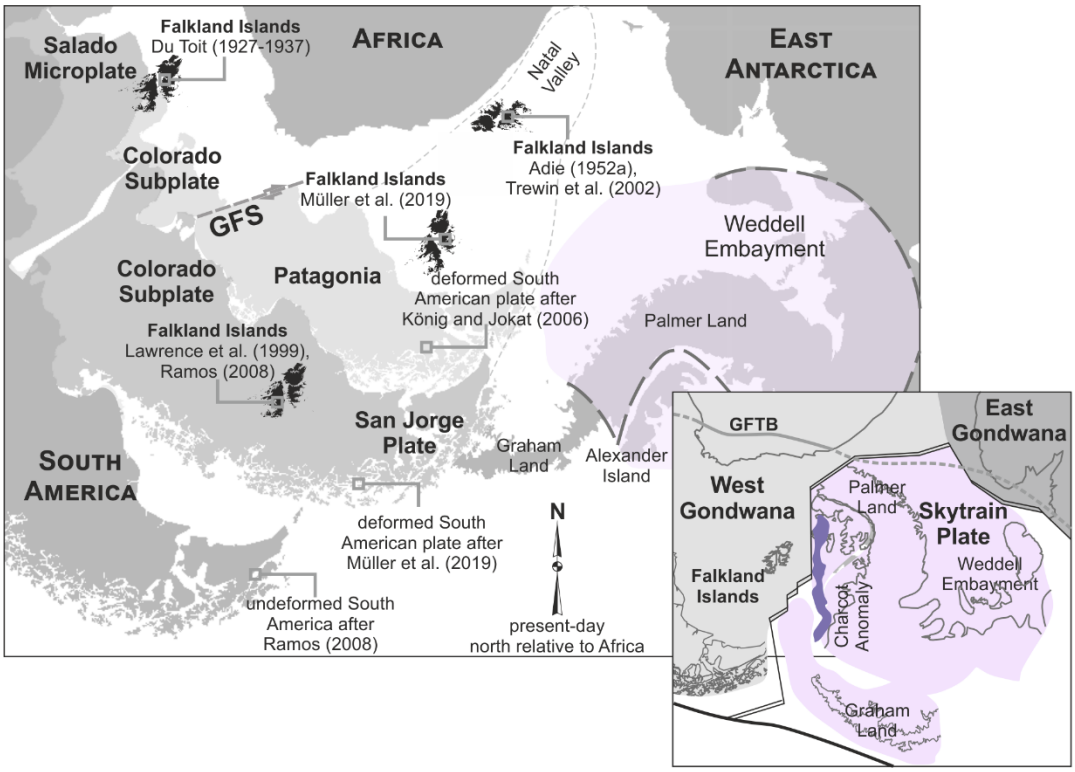

Figure 2.8 Early Jurassic palaegeographic reconstructions of the Falkland Islands along with the corresponding reconstruction of the South American Plate; plate model for East and West Antarctica in the main map after Müller et al. (2019); plate model for the West Antarctic region in inset after Eagles and Eisermann (2020); GFS – Gastre Fault System; GFTB – Gondwana Fold and Thrust Belt

The current morphology of the FP has been significantly influenced by the break-up of Gondwana and the opening of the Atlantic Ocean in the Mesozoic (Late Triassic – Late Cretaceous). Its pre-break-up position remains controversial. Early reconstruction models placed the Falkland Islands between

South America and South Africa (Du Toit, 1927-37), whereas recent studies advocate for a position of the FP immediately adjacent to the south-eastern African margin, in the Natal Valley (Figure 2.8; Adie, 1952a; Mitchell et al., 1986; Marshall, 1994; Curtis and Hyam, 1998; Lawver et al., 1999; Macdonald et al., 2003). The behaviour of the FP during the fragmentation of Gondwana remains controversial as well, some arguing that it was accompanied by the rotation of the Falkland Islands, whilst others support an E-W or NE-SW directed extension of the plateau (Figure 2.8; König and Jokat, 2006; Schimschal and Jokat, 2019b; Eagles and Eisermann, 2020).

2.4.1 Geology of the Maurice Ewing Bank

The Maurice Ewing Bank marks the eastward termination of the FP. It consists of ~29 km thick continental crust (Schimschal and Jokat, 2019a). The lithologies of the bank were constrained by five DSDP sites (327, 329, 330, 511, 512) and consist of an igneous-metamorphic complex unconformably overlain by Middle (?) Jurassic to Cenozoic sediments (Barker, 1977; Beckinsale et al., 1977; Lorenzo and Mutter, 1988). The basement lithologies have been dated (Rb-Sr) at 399±10 Ma - 535±66 Ma and are similar in composition to the Cape Meredith Complex in southern West Falkland, their difference in age being interpreted as a result of re-crystallisation (Beckinsale et al., 1977; Tarney, 1977). More recent U-Pb and Lu-Hf zircon isotopic analysis confirmed the correlation with the Cape Meredith Complex and yielded ages of 1006±13 Ma – 1233±8 Ma (Chemale et al., 2018). Recent petrological and geochemical studies support affinities of the Maurice Ewing Bank to the Kalahari Craton in Africa and its origin in the Namaqua-Natal-Maud belt (Vargas et al., 2021).

2.4.2 Geology of the Falkland Islands

The FI represent the only area of FP situated above sea level, and their stratigraphy and structural features have been thoroughly studied by Curtis and Hyam (1998), Aldiss and Edwards (1999), and references therein. The sedimentary deposits cropping out onshore the islands are all Paleozoic. However, they are interpreted to underlie the sedimentary basins offshore the islands, and a short review of their distribution will aid with the analysis of the basins. Furthermore, the Paleozoic succession has been affected by Paleozoic and post-Paleozoic deformation, which has controlled to some degree the style of deformation seen offshore the islands (Richards and Fannin, 1997), and intruded by Jurassic and Early Cretaceous dykes (Taylor and Shaw, 1989; Mussett and Taylor, 1994; Stone et al., 2008) of importance in understanding

stress configuration during this period. A complete review of the Falkland Islands onshore geology has been done by Stone (2016).

2.4.2.1 Stratigraphy

The main stratigraphic units of the FI are represented by the Cape Meredith Complex, the West Falkland Group, and the Lafonian Supergroup (Curtis and Hyam, 1998; Aldiss and Edwards, 1999). The Cape Meredith Complex is represented by Proterozoic gneisses that only crop out at Cape Meredith in the southernmost West Falkland (Curtis and Hyam, 1998; Stone, 2015). The complex was dated at 980 – 1100 Ma using K-Ar and Rb-Sr methods (Cingolani and Varela, 1976; Rex and Tanner, 1982 in Curtis and Hyam, 1998). These gneisses are unconformably overlain by the West Falkland Group, which covers the rest of the West Falkland, the northern part of the East Falkland, and Beauchêne Island (Aldiss and Edwards, 1999; Stone, 2015). This Siluro-Devonian group consists of the arkosic sandstones and quartz conglomerates of the Port Stephens Formation (Curtis and Hyam, 1998). These are overlain by sandstones intercalated with shales and siltstones comprising the Fox Bay Formation and covered by the sandstones and mudstones of the Port Stanley Formation (Curtis and Hyam, 1998).

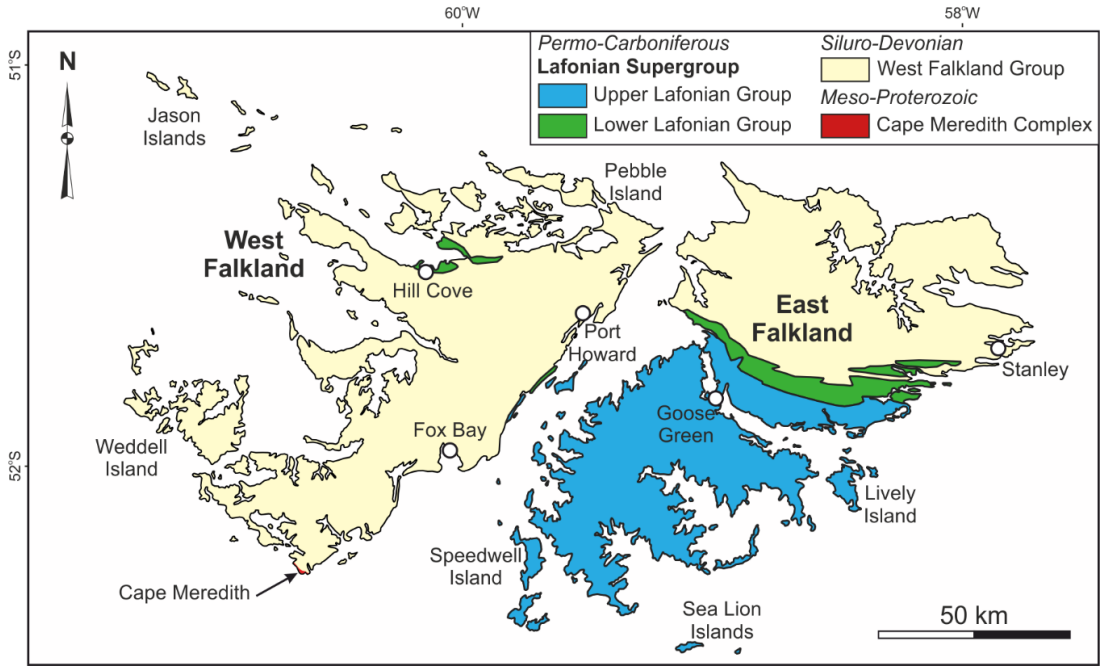

Figure 2.9 Simplified stratigraphy of the Falkland Islands (after Aldiss and Edwards, 1999)

The Permo-Carboniferous Lafonian Supergroup covers southern East Falkland, crops out locally on the eastern coast of the West Falkland (Figure 2.9), and consists of two groups: the Lower and Upper Lafonian Groups (Curtis and

Hyam, 1998). The former is represented by the Bluff Cove Beds glaciomarine deposits, the Lafonian Diamictite Formation or the Fitzroy Tillite Formation, and the Port Sussex Formation consisting of the organic-rich mudstones of the Black Rock Member and the mudstone-sandstone sequence of the Shepherds Brook Member (Curtis and Hyam, 1998; Aldiss and Edwards, 1999). The Permian Upper Lafonian Group is represented by an alternation of sandstones and shales of the Brenton Loch and Bay of Harbours formations (Curtis and Hyam, 1998). The differences in the units along the West and East Falkland have been associated with the presence of a major, long-lived NE-SW trending fault (the Falkland Sound Fault; Figure 2.10). This structure may have controlled the thicker deposition of the Lafonian Supergroup on East Falkland (Marshall, 1994; Curtis and Hyam, 1998; Aldiss and Edwards, 1999).

2.4.2.2 Deformation phases

Five deformation phases (D1 to D5) were identified across the FI and described in detail by Aldiss and Edwards (1999). The first phase (D1) is characterised by structures trending E-W (Figure 2.10) and affecting strata of up to Early Permian age (Aldiss and Edwards, 1999; Stone, 2016). D2 structures (Figure 2.11), such as the Hornby Anticline and the Coast Ridge (West Falkland), along with D3 (Figure 2.12), trend roughly NE-SW and were associated with dextral NE-SW transpression (Aldiss and Edwards, 1999; Curtis and Hyam, 1998). Movement on the Falkland Sound Fault (Figure 2.10) is interpreted to control this dextral movement between East and West Falkland (Marshall, 1994; Curtis and Hyam, 1998; Aldiss and Edwards, 1999). However, there are few constraints on the amount and age of lateral movement that has occurred along this speculated fault. The inferred displacements along it vary between 3.3 km and 300 km (Thomas et al., 1997; Curtis and Hyam, 1998; Aldiss and Edwards, 1999). The time of activity has been considered coeval with the D2 and D3 deformation stages (Thomas et al., 1997; Curtis and Hyam, 1998; Aldiss and Edwards, 1999) although there have been authors arguing for a Mesozoic activity or Cenozoic reactivation (Thomas et al., 1997; Lawrence et al., 1999). Richards et al. (1996a) have postulated a continuation of the Falkland Sound Fault to the south based on gravity data but no evidence for it was found on seismic. The same authors related some of the faulting in the North Falkland Basin with movement along the Falkland Sound Fault. However, no evidence of this has been reported in the northern sedimentary basins along the strike of the Falkland Sound Fault by more recent studies (Lohr and Underhill, 2015; Stanca et al., 2019). The fourth phase of deformation (D4) consists of WNW-

ESE striking thrusts and folds (Figure 2.13) (e.g. the Pebble Island Thrust, Sand Grass Thrust) affecting strata of the Port Stephens Formation and cross-cut by the last extensional deformation stage (D5; Figure 2.14) (Aldiss and Edwards, 1999).

Regarding the timing of deformation, deposits as young as Permian are affected by the D1 deformation (Curtis and Hyam, 1998; Stone, 2016) whereas Ar-Ar dating on fault zone micas carried by Hodgkinson (2002) yielded Permian ages. Early Jurassic dykes seem to cross-cut D4 structures (Figure 2.13) suggesting an older age for the latter (Aldiss and Edwards, 1999; Stone, 2016). D5 faults are considered the youngest as they were documented to displace D4 thrusts and Early Jurassic dykes (Aldiss and Edwards, 1999). Based on these observations, the D1-D4 deformation stages were considered coeval with the Permo-Triassic Gondwanide orogeny, whilst the D5 was interpreted as being generated during the Mesozoic fragmentation of Gondwana (Stone, 2016).

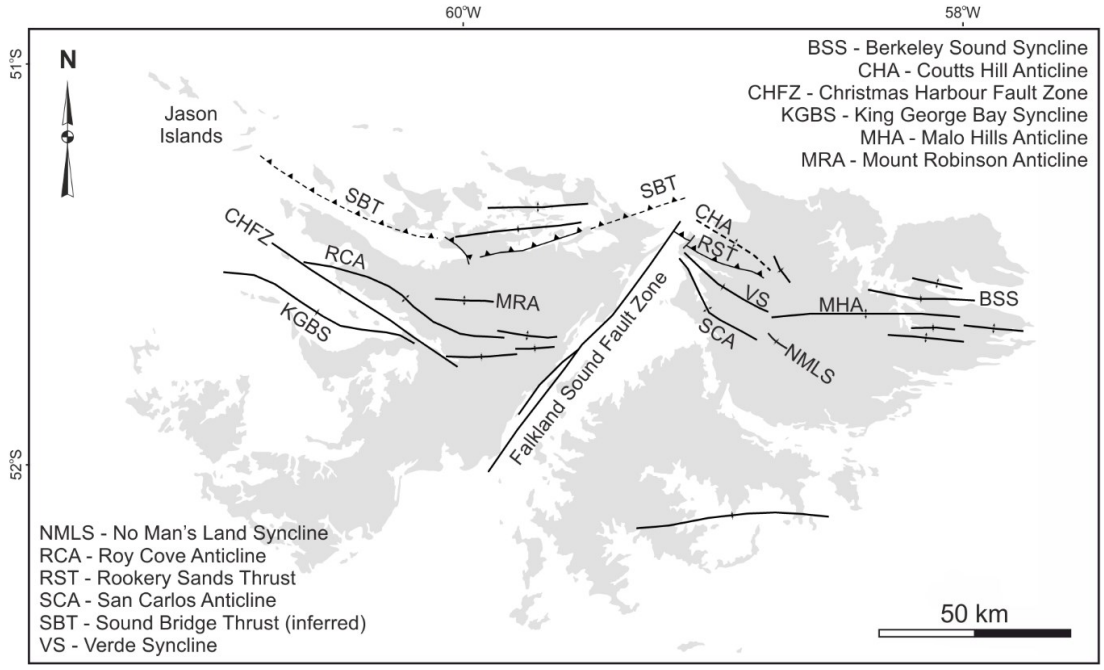

Figure 2.10 D1 structures (after Aldiss and Edwards, 1999)

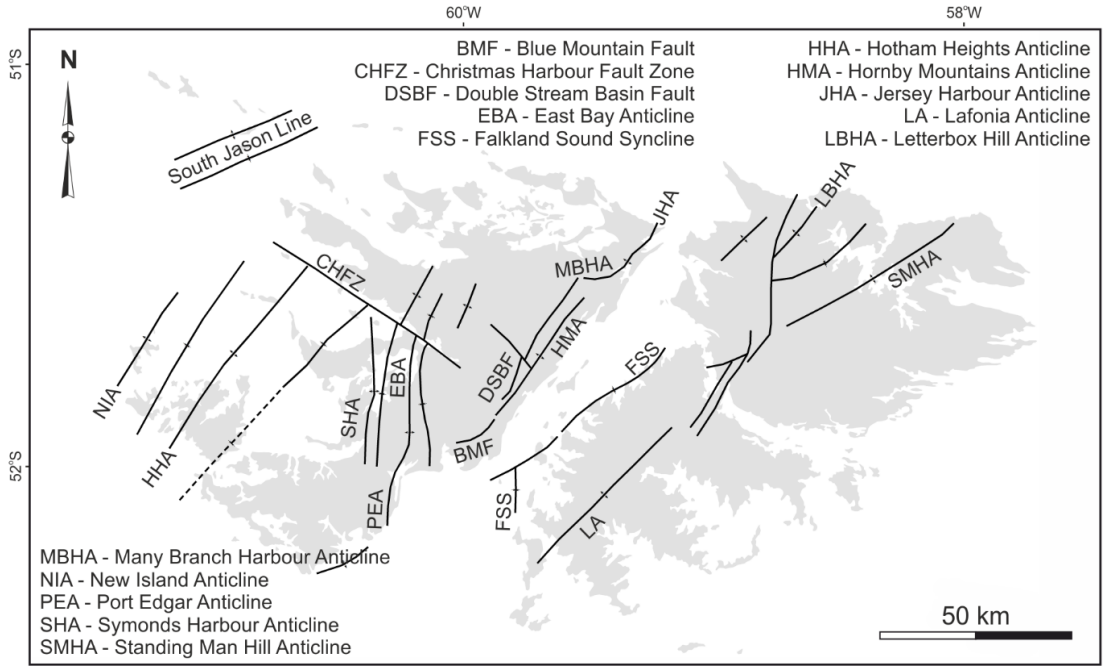

Figure 2.11 D2 structures (after Aldiss and Edwards, 1999)

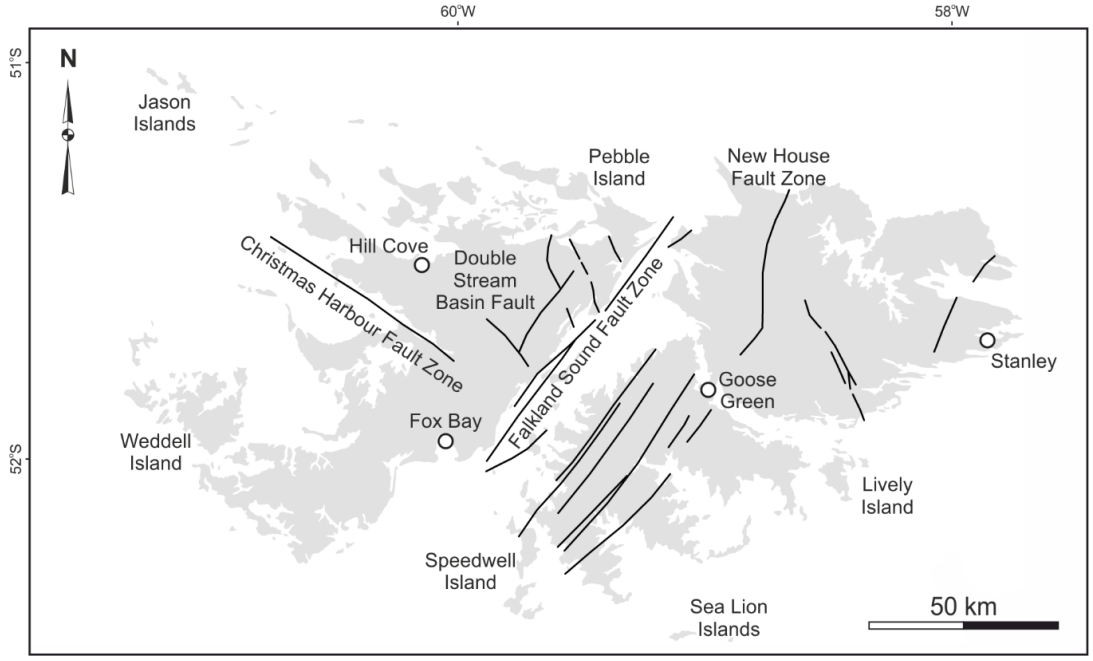

Figure 2.12 D3 structures (after Aldiss and Edwards, 1999)

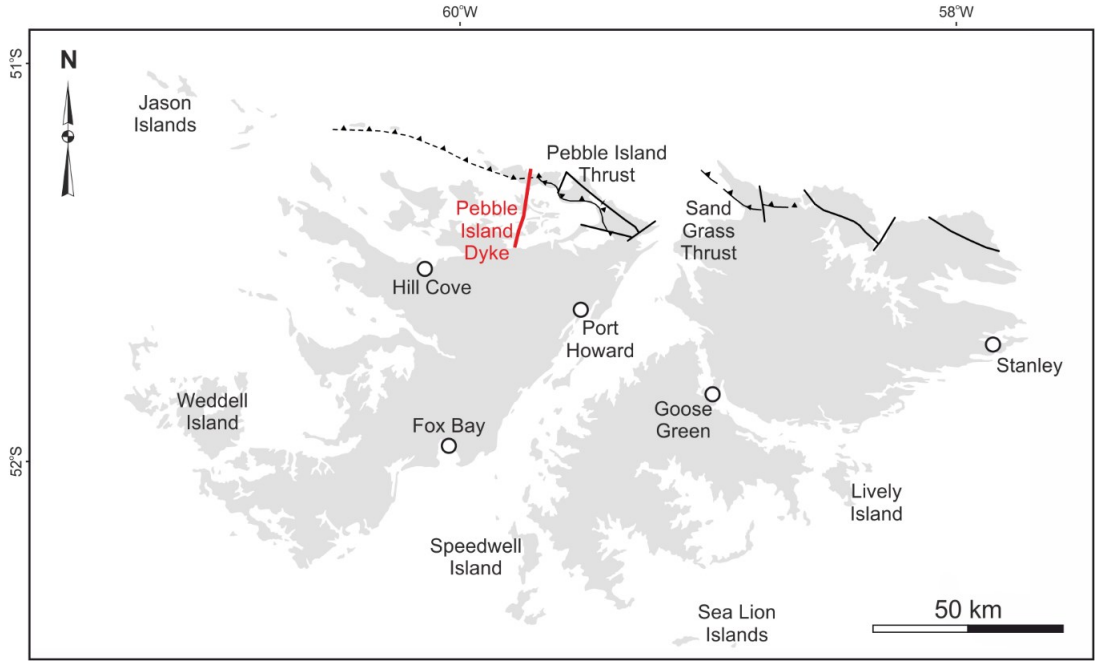

Figure 2.13 D4 structures (after Aldiss and Edwards, 1999)

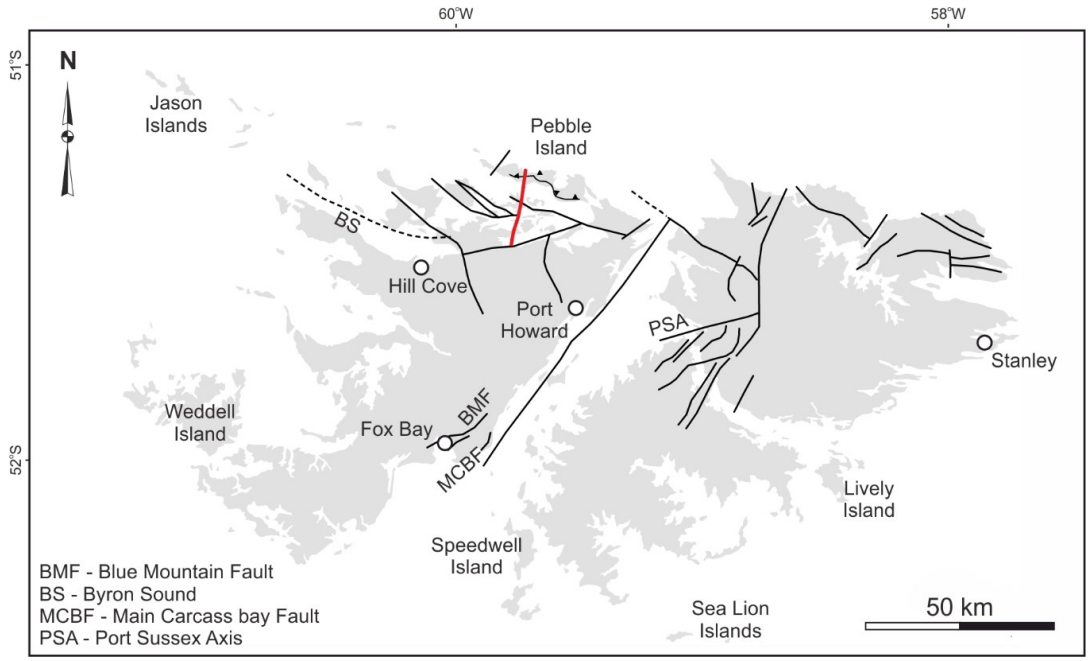

Figure 2.14 D5 structures (after Aldiss and Edwards, 1999)

2.4.3 Geology of the Falkland Plateau basins

The area offshore the Falkland Islands consists of four sedimentary basins: North Falkland Basin, Malvinas Basin, South Falkland Basin, and Falkland Plateau Basin. Their Mesozoic to Cenozoic sedimentary infill records deformation and isostatic changes related to the break-up of Gondwana which makes their analysis key to understanding the evolution of the Falkland Plateau during the dispersal of Gondwana.

2.4.3.1 Falkland Plateau Basin

The Falkland Plateau Basin has undergone less exploration compared to the northern and western sedimentary basins surrounding the Falkland Islands. The crust type distribution under this basin is still subject to debate. Continental crust is interpreted nearshore and along the Maurice Ewing Bank (Beckinsale et al., 1977; Schimschal and Jokat, 2017, 2019a) but the architecture within the basin itself is yet to be confirmed. Several studies on seismic reflection, refraction and gravity data pointed towards either thinned and underplated continental crust or thick oceanic crust (Ewing et al.,1971; Lorenzo and Mutter, 1988; Kimbell and Richards, 2008). More recent seismic refraction and aeromagnetic data have been used to argue for an oceanic nature of the FPB (Schimschal and Jokat, 2019b; Eagles and Eisermann, 2020).

The contentious crustal architecture of the FPB is covered by up to 12 km of Jurassic (or older) to Recent deposits as characterised by seismic reflection and refraction data, gravity modelling, available DSDP sites and exploration wells (Barker, 1977; Richards et al., 1996a; Del Ben and Mallardi, 2004; Schimschal and Jokat, 2017). The sediment infill is bounded to the west by NE-SW trending normal faults (Figures 2.15 and 2.16a) and is affected by Permo(?)-Jurassic normal faults in the more distal parts of the FPB (Lorenzo and Mutter, 1988; Richards et al., 1996a). However, the ages of the deformation postulated in these studies remain speculative due to a lack of well constraints.

2.4.3.2 North Falkland Basin

The present-day structure of the North Falkland Basin (NFB) is the result of two rifting events: a Jurassic one that resulted in the opening of the Southern North Falkland Basin (SNFB) and an Early Cretaceous extensional episode during which the North Falkland Graben formed (Lohr and Underhill, 2015). The North Falkland Graben and its secondary half-grabens are superimposed on the Jurassic rift system and are bounded by N-S striking normal faults (Richards and Fannin, 1997; Lohr and Underhill, 2015). These transition southward to the NW-SE normal faults of the SNFB (Richards and Fannin, 1997) (Figure 2.15). As suggested by their geometries and shallow dips, the Jurassic normal faults are considered to have exploited older Palaeozoic thrust planes, their strike being associated with the Gondwanide orogeny (Richards et al., 1996a; Richards and Fanning, 1997; Bransden et al., 1999; Hodgkinson, 2002). The infill of the basins is considered to start with Jurassic to Valanginian fluvio-lacustrine deposits. These transition to lacustrine and deltaic deposits, which

are unconformably overlain by fluvial to marine mudstones (Figure 2.16b; Richards and Hillier, 2000; Lohr and Underhill, 2015).

2.4.3.3 South Falkland Basin

The FPB connects to the SW to the South Falkland Basin (SFB), which separates the former from the Malvinas Basin (Figure 2.15; Richards et al., 1996a). The SFB is an asymmetrical basin, plunging to the south where it terminates against the NSR (Figure 2.16c; Richards and Fannin, 1997). The SFB is affected by E-W trending normal faults that downthrow northward. These are interpreted as predominantly Jurassic to Early Cretaceous in age (Richards et al., 1996a). This normal fault trend is further complicated by widespread thrusting occurring in the southern part of the basin as a consequence of oblique compression along the North Scotia Ridge (Bry et al., 2004).

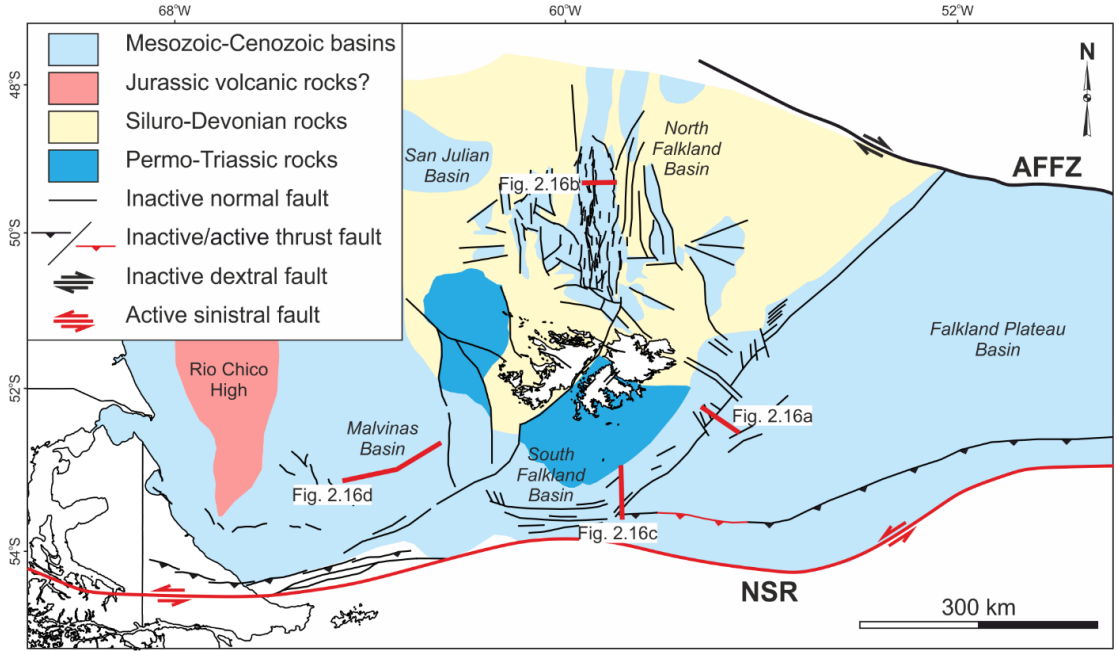

Figure 2.15 Falkland Plateau and the fault network in its basins (based on Richards et al., 1996a, Richards, 2002, Cunningham et al., 1998, Galeazzi, 1998, and Stone, 2016); extent and infill age of the sedimentary basins after Richards et al., 1996a

2.4.3.4 Malvinas Basin

The Malvinas Basin lies between the Falkland Islands to the east and the Rio Chico High to the west (Figure 2.15; Richards et al., 1996a). It has a complex structure represented by the superimposition of two fault trends along NW-SE and NE-SW directions (Galeazzi, 1998; Ghiglione et al., 2010; Baristeas et al., 2013). The generation of these faults was correlated with back-arc extension

and the opening of the Weddell Sea, respectively (Baristeas et al., 2013). These faults were overprinted by Cenozoic E-W trending normal, thrust, and strike-slip faults (Galeazzi, 1998) affecting a thick sedimentary infill represented by Triassic to Cenozoic volcanics and fluvial to marine deposits (Figure 2.16d; Richards et al., 1996a; Lovecchio et al., 2019).

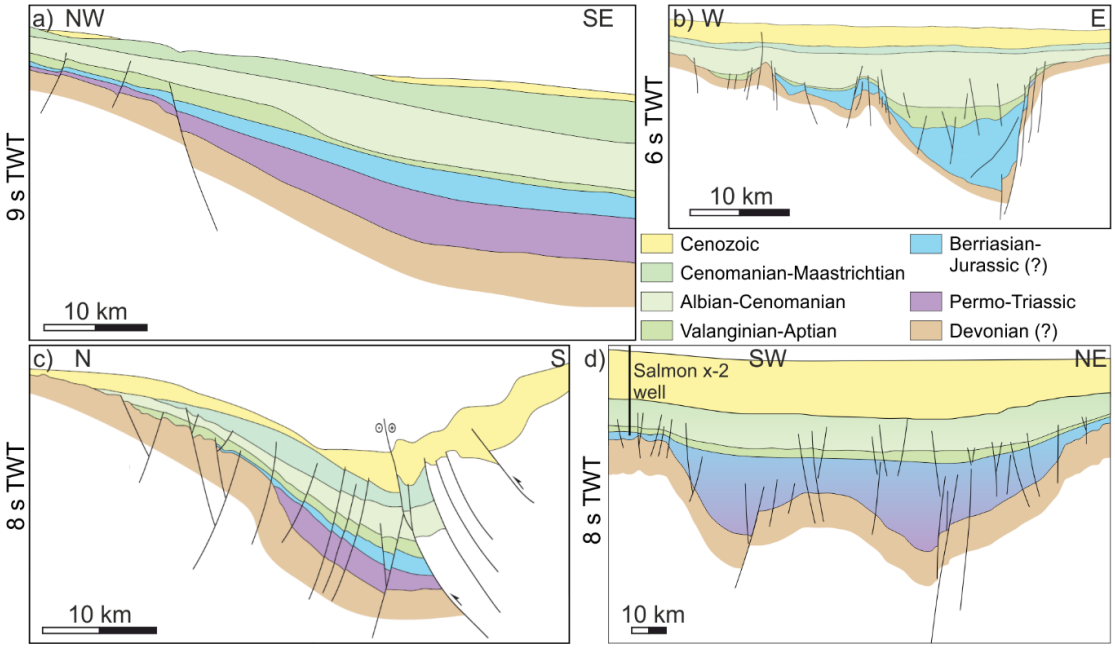

Figure 2.16 Representative sections through the four sedimentary basins; a) Falkland Plateau Basin (modified after Richards et al., 1996a); b) North Falkland Basin (modified after Richard and Hillier, 2000 and Stone, 2016); c) South Falkland Basin (modified after Stone, 2016); d) Malvinas Basin (drawn from Lovecchio et al., 2019); approximate line locations shown in Figure 2.15

2.4.4 Volcanism

Evidence of volcanism has been documented both on- and offshore the Falkland Islands and related to different stages in the fragmentation of Gondwana. An understanding of the distribution of volcanic and magmatic elements can give indications on stress configuration and other processes related to the dispersal of Gondwana.

Several dyke swarms were identified onshore the Falkland Islands (Figure 2.17) based on field observations and aeromagnetic data (Taylor and Shaw, 1989; Mussett and Taylor, 1994; Aldiss and Edwards, 1999; Stone et al., 2009). These follow three main trends as observed on aeromagnetic data (Stone et al., 2009), although bigger variations in directions were observed locally in Cape Orford, south-west West Falkland (Aldiss and Edwards, 1999). K-Ar and Ar-Ar dating has yielded Early Jurassic ages for E-W trending dykes and one

dyke from Cape Orford. Ages spanning the Jurassic were obtained for NE-SW trending dykes, and Early Cretaceous ages for N-S trending dykes (Mussett and Taylor, 1994; Stone et al., 2008). The Jurassic dykes were related to the emplacement of the Karoo-Ferrar magmatic province based on their petrology and geochemistry (Mitchell et al., 1999; Hole et al., 2016), whilst the Cretaceous swarm was interpreted as being coeval with the opening of the South Atlantic (Stone et al., 2008; Hole et al., 2016). Offshore, volcanic edifices, lava flows and/or plutonic bodies, and sills were interpreted based on seismic reflection, gravity, and magnetic data (Lorenzo and Mutter, 1988; Richards et al., 1996a, 2013; Barker, 1999; Schimschal and Jokat, 2017).

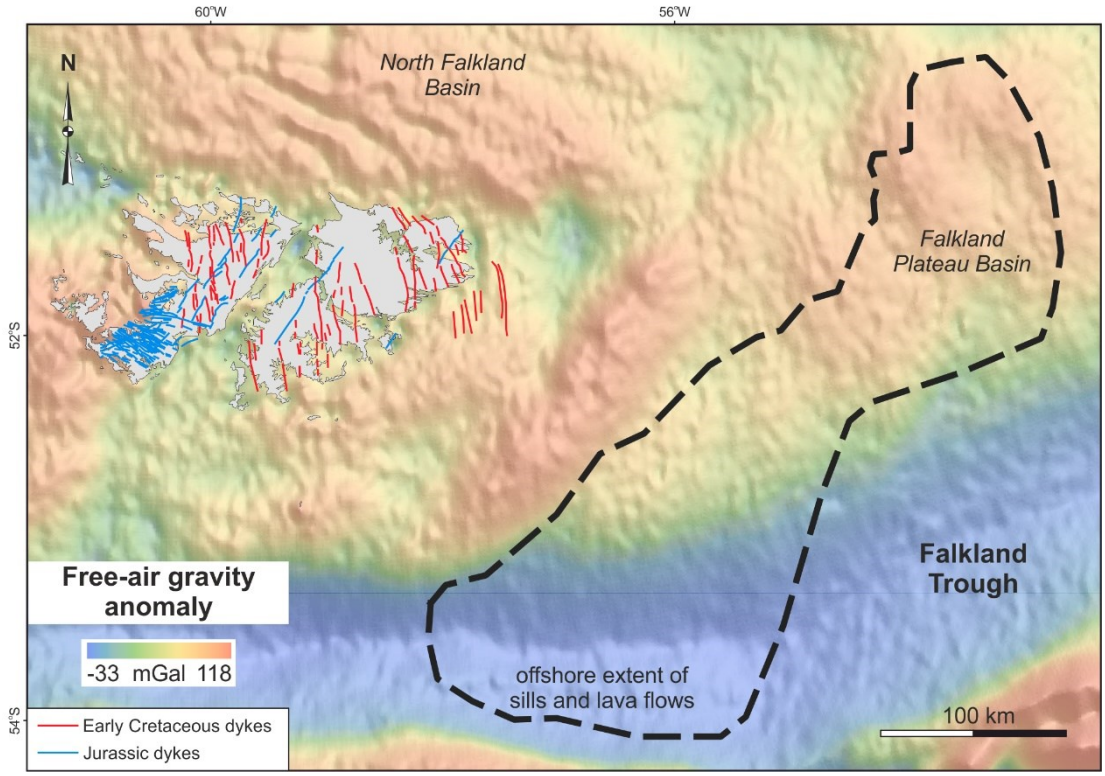

Figure 2.17 Distribution of volcanism on- and offshore the Falkland Islands; on- and nearshore dykes drawn after Richards et al. (2013); free air gravity anomaly map from Sandwell et al. (2014)

2.5 Palaeogeographic reconstructions of the Falkland Islands

The present-day architecture of the Falkland Plateau and its subsequent evolution are a direct consequence of the original configuration of the Falkland Islands. The break-up of Gondwana and the separation of South America and the Falkland Plateau from Africa are interpreted by some authors to have been accompanied by the rotation of the Falkland Islands (Adie, 1952a; Mitchell et al., 1986; Thomson, 1998; Trewin et al., 2002). However, this tectonic evolution

model of the plateau is not unanimously accepted (Lawrence et al., 1999; Ramos et al., 2017; Eagles and Eisermann, 2020; Lovecchio et al., 2020). Two end-model reconstructions of the Falkland Islands are currently incorporated in the South Atlantic plate models (Macdonald et al., 2003; König and Jokat, 2006; Müller et al., 2019), which significantly affect the interpretation of the tectonic history of the plateau (Figure 2.8).

2.5.1.1 Rotational model

Similarities between the D1 fold belt onshore the Falkland Islands and the Cape Fold Belt in South Africa and Sierra Australes in South America were first documented by Du Toit (1927). In his model, the islands were reconstructed off the coast of Cape of Good Hope (south-west South Africa; Figure 2.8) so that the Sierra Australes, the D1 fold and thrust belt, and the Cape Fold Belt formed a continuous feature (Du Toit, 1927). Further stratigraphic and structural analysis confirmed a correlation between the Cape Fold Belt and the Falkland Islands (Adie, 1952a). However, similarities between the Lafonian Supergroup onshore the Falkland Islands and the Karoo Basin in South Africa and correlation between ice flow directions between the two landmasses led Adie (1952a) to put forward a novel reconstruction of the islands off the coast of south-east South Africa and rotated by ~180° (Figures 2.8 and 2.18). Palaeomagnetic analyses carried out on Jurassic dykes (Mitchell et al., 1986; Mussett and Taylor, 1994) and on sedimentary successions of the Lafonian Supergroup (Thistlewood and Randall, 1998 in Stone, 2016), one aeromagnetic study (Stone et al., 2009), palaeontological, stratigraphic, structural, and palaeocurrent data (Marshall, 1994; Curtis and Hyam, 1998; Trewin et al, 2002) were used in support of this hypothesis where the islands were located ~200 km away from Ecca Pass in South Africa, at a palaeolatitude between 42±6°S and 47±5°S (Figure 2.18; Mitchell et al., 1986; Trewin et al., 2002).

The basement lithologies and metamorphic fabrics of the Cape Meredith Complex onshore West Falkland were correlated with the Namaqua-Natal-Maud belt extending across South Africa and East Antarctica after the rotation of the FI (Thomas et al., 1997; Thomas et al., 2000; Jacobs et al., 1999; Jacobs et al., 2003; Jacobs and Thomas, 2004; Vorster et al., 2016). Detrital zircons of the same age as the Cape Meredith Complex were documented in south-eastern South Africa (KwaZulu Natal) and interpreted to have been sourced from the Falkland Islands when in a rotated reconstruction (Vorster et al., 2016). Based on fossil assemblages and palaeocurrent data, Adie (1952b; in Marshall, 1994), Curtis and Hyam (1998), and Trewin et al. (2002) correlated

the Devonian deposits of the West Falkland Group to the Bokkeveld Group in South Africa. Palaeocurrent directions towards the SSW documented in the pre-glacial deposits in South Africa matched the rotated towards NNE flow recorded in the West Falkland Group (Figures 2.5 and 2.18; Scasso and Mendia, 1985; Johnson, 1991; Curtis and Hyam, 1998; Trewin et al., 2002). The Fitzroy Tillite Formation deposits from the Falkland Islands were correlated with the Dwyka Group from South Africa (Frakes and Crowell, 1968; Curtis and Hyam, 1998), both consisting of Permo-Carboniferous glacial deposits with archaeocyathan fauna (Stone and Thomson, 2005). Ice flow directions from W-SW to E-NE in the Fitzroy Tillite Formation (Frakes and Crowell, 1967) are consistent with the striae in South Africa (Crowell and Frakes, 1972) after a 180° rotation of the islands and suggest a clast provenance from the Shackleton Limestone in East Antarctica (Figures 2.5 and 2.18; Stone and Thomson, 2005). The overlying Permian deposits of the Upper Lafonian Group have been correlated with the Ecca and Beaufort Groups in South Africa based on stratigraphy, trace fossils, and sediment provenance (Figure 2.18; Trewin et al., 2002). Palaeocurrent directions for the post-glacial deposits show some variability compared to the ones recorded in South Africa oriented towards the NW, whilst in the Falkland Islands the documented flow was towards the WSW (Figure 2.5; Johnson, 1991; Trewin et al., 2002). The local variation of the sediment flow in the Falkland area was related to the presence of a depocentre related to an easterly downthrow of the Falkland Sound Fault (Trewin et al., 2002). The structural style of the Falkland Islands and the vergence and ages of deformation are also in accordance with the ones in the Eastern Cape Fold Belt in South Africa prior to rotation (Adie, 1952a; Curtis and Hyam, 1998).

The rotation of the Falkland Islands is interpreted to have occurred in stages: 120º prior to the South Atlantic opening and 60º during the opening of the ocean (Mitchell et al., 1986). Taylor and Shaw (1989), Ben-Avraham et al. (1993), and Storey et al. (1999) suggested that the islands rotated only 105º before the Atlantic opening. The rotational model requires that the FI are part of a microplate that underwent isolated movements during the break-up of Gondwana (the Falkland Islands Microplate – FIM; the Falkland Platform of Marshall, 1994; the Falkland Islands Block of Storey et al., 1999; the Lafonia Microplate of Ben Avraham et al., 1993 and Dalziel et al., 2013). As mentioned in section 2.1.3, a microplate is bounded by trans-lithospheric structures (plate boundaries). The FIM is believed to be delimited to the north by the AFFZ (Marshall, 1994; Richards et al., 1996b), to the south by the North Scotia Ridge, and to the east by the NE-SW striking fault bounding the FPB to the

west (Richards et al., 1996b). The western extent of the micro-plate remains uncertain, although Marshall (1994) placed the limit between the FI microplate and Argentina along a high-velocity ridge described by Ludwig et al. (1968). Storey et al. (1999) and Macdonald et al. (2003) believe that the microplate is confined to the area of high free air gravity anomalies and does not reach the AFFZ in the north. Although there are uncertainties regarding the scale of the eastern and western boundaries, the area comprising the Falkland Islands will be referred to as *microplate* or *microcontinent* (a microplate consisting of continental crust) throughout the thesis. The term *block* will be used as a general term when the nature of boundaries is unknown (i.e. restricted to the upper crust or lithospheric).

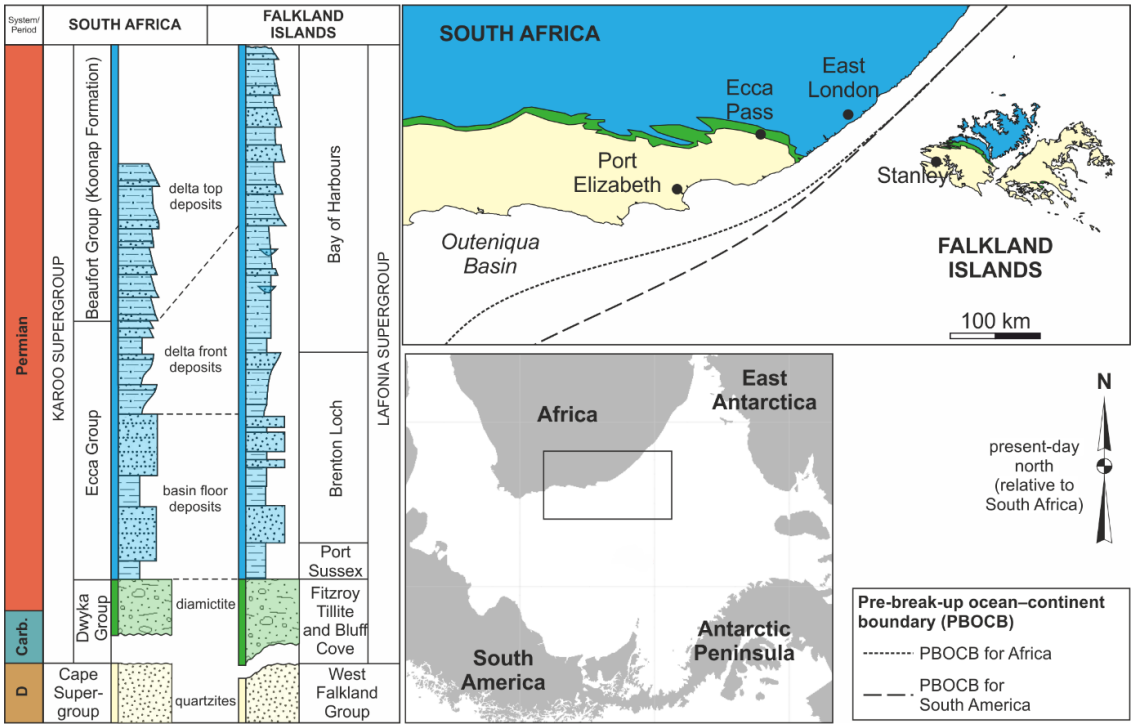

Figure 2.18 Rotated Early Jurassic reconstruction of the Falkland Islands showing stratigraphical correlations with onshore South Africa after Trewin et al. (2002); the PBOCB is based on gravity data and drawn after Lawver et al. (1999) and Macdonald et al. (2003); south-western Gondwana configuration after Müller et al. (2019)

Another requirement of the rotational model which positions the FI offshore East London (South Africa) pre-rotation is the existence of a (south) Patagonian plate that was, prior to the break-up of Gondwana, closer to South Africa than the rest of the South America (Figure 2.8). The boundary between this Patagonian plate and South America could be represented by a right-lateral shear zone located north of the North Patagonian Massif, along the Huincul Fault (Ben-Avraham et al., 1993; Pankhurst et al., 2006; Mosquera and

Ramos, 2006). Rapela and Pankhurst (1992) argue for a southern Patagonian plate separated by the North Patagonian Massif by a dextral strike-slip fault - the Gastre Fault System (GFS; Figure 2.8) - the onshore equivalent of the AFFZ. The latter has been a recurring element of more recent reconstructions of South America (König and Jokat, 2006; Torsvik et al., 2009). However, field observation carried out along the Gastre Fault System do not support its dextral nature (von Gosen and Loske, 2004).

Few authors have inferred a separation between the East and West Falklands reconstruction in a rotational model along the Falkland Sound Fault believed to run between the two main islands (Figure 2.10; Thomas et al., 1997). However, the displacement and timing of activity along this major structure has been difficult to constrain (Marshall, 1994; Richards et al., 1996a; Thomas et al., 1997; Curtis and Hyam, 1998; Aldiss and Edwards, 1999).

2.5.1.1.1 Timing of rotation

The timing of potential FIM rotation has been highly debated over the decades. Based on the preliminary analysis of palaeomagnetic measurements on Jurassic dykes, Mitchell et al. (1986) argues for a rotation of the FIM of 120º occurring during the early stages of Gondwana break-up with further 60º occurring during the opening of the Atlantic. The paleomagnetic analysis carried by Taylor and Shaw (1989) suggests a 500 km southward translation of the FIM and a clockwise rotation of ~100º interpreted as being related to the rifting between Africa and Antarctica between 200-125 Ma. Marshall (1994) supports the theory of rotation prior to 130 Ma but places it after the onset of extension in the Falkland Plateau Basin as the geometry inferred for the FIM would not have allowed for rotation happening while the Falkland Plateau was still adjacent to the Agulhas Plateau (AP). However, Scrutton (1973) pointed towards an oceanic nature of the AP, giving it an age of formation after the westwards drift of South America. This theory is confirmed by recent seismic refraction and reflection studies (Gohl and Uenzelmann-Neben, 2001). Thomson (1998) argued for a Valanginian rotation of the islands based on correlations between the North Falkland and Outeniqua basins. However, no evidence of rotation was documented in the adjacent basins (Richards et al., 1996a), which has led emerging studies to favour a rotation preceding the opening of the sedimentary basins offshore the Falkland Islands, but after (or during) the emplacement of the Early Jurassic dykes onshore the Islands (Storey et al., 1999). Barker (1999) suggested that the rotation and formation of the Falkland Plateau Basin occurred simultaneously between 190 Ma and 165 -

160 Ma. Recent reconstruction models of Gondwana support the completion of the FIM rotation by 165 Ma (Macdonald et al., 2003). Recent Ar-Ar dating of the NE-SW and N-S trending FI dyke swarms carried by Stone et al. (2008) gave a time frame for rotation constrained to the Middle Jurassic (post-178 Ma).

2.5.1.1.2 Mechanisms for rotation

Taylor and Shaw (1989) associated the rotation of the FIM with dextral strike-slip movement occurring between Africa and Antarctica in their early stages of rifting. N-S trending folds onshore the Falkland Islands along with the Hornby Mountains Anticline were interpreted as proof for this dextral motion between West and East Gondwana (Storey et al., 1999). A more recent study invokes dextral-transtension occurring between Antarctica and the Falkland Plateau prior to the opening of the Weddell Sea, due to the velocity of the southward drift of Antarctica overcoming the velocity of south-westward drift of Patagonia (König and Jokat, 2006). Differential movement occurring along the Gastre Fault System and the AFFZ is proposed as an alternative driving force for rotation by Marshall (1994). A synchroneity and correlation between the causative events for the opposite senses of rotation for the FIM and the Ellsworth Whitmore Mountains was suggested (Macdonald et al., 2003) and explained through a ‘double-saloon-door’ model (Martin, 2007).

Several studies invoke mantle flow as driving the rotation of the FIM (Ben-Avraham et al., 1993; Storey, 1995; Storey et al., 1999). Ben-Avraham et al. (1993) discuss the possibility that the large rotations affecting the microplates between East and West Gondwana, including the FIM, might be driven by mantle suction forces generated along the subduction front of West Gondwana (Figures 2.4 and 2.5) due to slab rollback. Late Triassic to Late Jurassic differential rollback along the south-western margin of Gondwana is supported by recent studies on coeval trenchward migration of magmatism along Patagonia and rotation in the extension direction along south-western Gondwana (Echaurren et al., 2017; Lovecchio et al., 2019, 2020). Doming above the Karoo plume followed by movement on a viscous substratum is invoked by Storey (1995) as a facilitator for the rotation, much like the interpretation suggested by Molnar and Gipson (1994; in Storey et al., 1999) in southern California.

2.5.1.2 Rigid model

The rotation model, however, is not unanimously accepted. Field studies on the Gastre Fault System point towards a late Permian sinistral strike-slip rather

than a dextral movement synchronous with the break-up of Gondwana (Franzese and Martino, 1998 in Ramos et al., 2017, Von Gosen and Loske, 2004). In the absence of a structure along which Patagonia is reconstructed in a tight position to Africa, a rotation of the FIM would result in space being generated between the microplate and South America (Ramos et al., 2017). Inconsistencies in the palaeomagnetic measurements (Richards et al., 1996a, Hodgkinson, 2002), the wide range of rotations estimated from the modelling of aeromagnetic anomalies (Stone et al., 2009), the lack of a mechanism for the large rotation of a microplate the size of the FIM, and the lack of documented evidence offshore the islands resulted in several studies favouring a non-rotational evolution of the Falkland Islands in which the Falkland Plateau is fixed to the South America plate and it underwent a rotation of only 60^{o} during the opening of the South Atlantic (Figure 2.8; Lawrence et al., 1999, Ramos et al., 2017; Lovecchio et al., 2019; Eagles and Eisermann, 2020).

Evidence supporting this model consists of zircon analysis results, which correlates the West Falkland Group with the Sierra Grande quartzites, their common source being considered the Deseado Massif (Ramos et al., 2017). Furthermore, archaeocyaths were discovered in the Sauce Grande Formation diamictite of the Ventania System, Argentina (Gonzáles et al., 2013) which was suggested as being coeval to the Fitzroy Tillite Formation by Ramos et al. (2017). However, no equivalent of the Permian Upper Lafonian Group was documented on the Patagonian side. The opposite vergence of the thrusts and folds onshore the Falkland Islands compared to the Cape Fold Belt is explained through the existence of similar south-verging structures in the north-eastern North Patagonian Massif (von Gosen, 2003), which led Ramos et al. (2017) to disagree with the requirement for a rotation of the Falkland Islands. The almost orthogonal trends identified along the North Falkland Basin (Lohr and Underhill, 2015) were related to the opening of the NW-SE trending sedimentary basins on- and offshore South America (e.g. El Tranquilo, San Jorge, Río Mayo basins) and the N-S trending Península Valdes and Rawson basins (Ramos et al., 2017).

The debate about the contentious rotation of the Falkland Islands is ongoing and hugely impacts the overall evolution of the Falkland Plateau and, in turn, the reconstruction of the south-western Gondwanan plates. Chapters 4-6 will be looking into evidence for the tectonism along the plateau as seen in the sedimentary basins north and south of the Falkland Islands.

Chapter 3 Data and methodology

3.1 Data

This project was based on the analysis of open-source gravity data, magnetic data courtesy of the Alfred Wegener Institute, well and seismic reflection data courtesy of the Falkland Islands Government, and open-source well and seismic reflection data.

3.1.1 Gravity data

The gravity data consist of the V24.1 1-minute satellite altimetry free-air gravity anomaly grid of Sandwell et al. (2014). The dataset combines the altimeter information from Geosat, ERS-1, CryoSat-2, and Jason-1 to generate a gravity field with an accuracy of ~2mGal and a spatial resolution of down to ~6 km (Garcia et al., 2014; Sandwell et al., 2014). An ASCII XYZ file extending from 69°W to 30°W and from 47°S to 57°S was extracted from the Satellite Geodesy research group at Scripps Institution of Oceanography, University of California San Diego website. This was further gridded in Geosoft's Oasis Montaj using a 2 km grid increment and the Minimum Curvature algorithm chosen in order to minimize the roughness of the interpolation (Figure 3.1). The free-air gravity anomaly for the southern part of South Africa was extracted in a similar manner (18°W to 29°E and 31°S to 38°S; Figure A.1 in Appendix). The following geotiff files were also downloaded from the same website: N0E0 and S40W60 for the two regions.

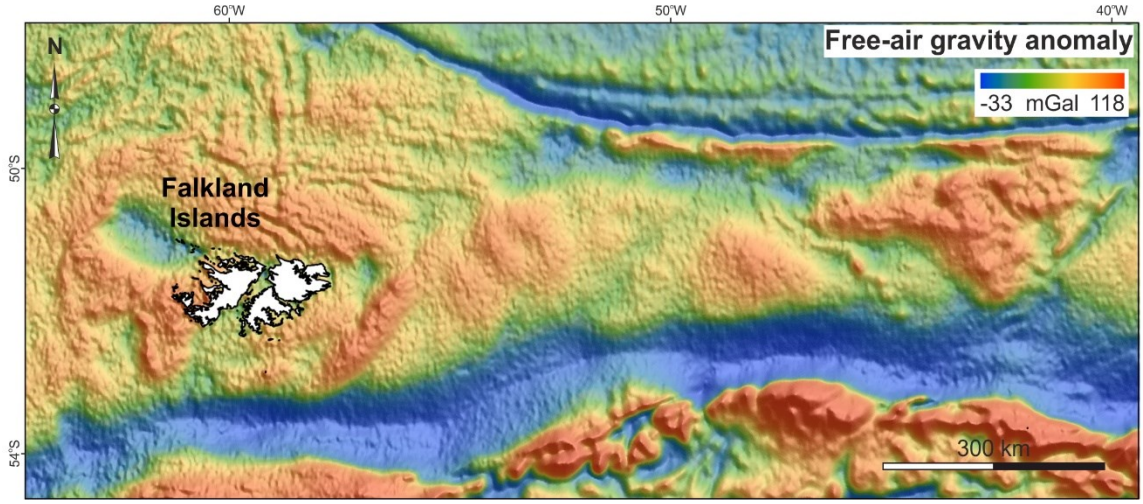

Figure 3.1 Map of the free-air gravity anomaly of Sandwell et al. (2014) along the Falkland Plateau

3.1.2 Magnetic data

The magnetic data consist of the AIRLAFONIA aeromagnetic survey acquired by the Alfred Wegener Institute over the Falkland Plateau Basin in 2017-2018 (Figure 3.2). The survey comprises 25185 km of magnetic lines acquired at 2000 ft (with some portions acquired at 1000-3000 ft) above sea-level, oriented E-W and NE-SW, and spaced at ~12 km. The grid, provided by the Alfred Wegner Institute, was further extended eastward and northward by using marine and helicopter legacy data levelled to the AIRLAFONIA survey in Geosoft's Oasis Montaj. The data have been made available via PANGAEA.

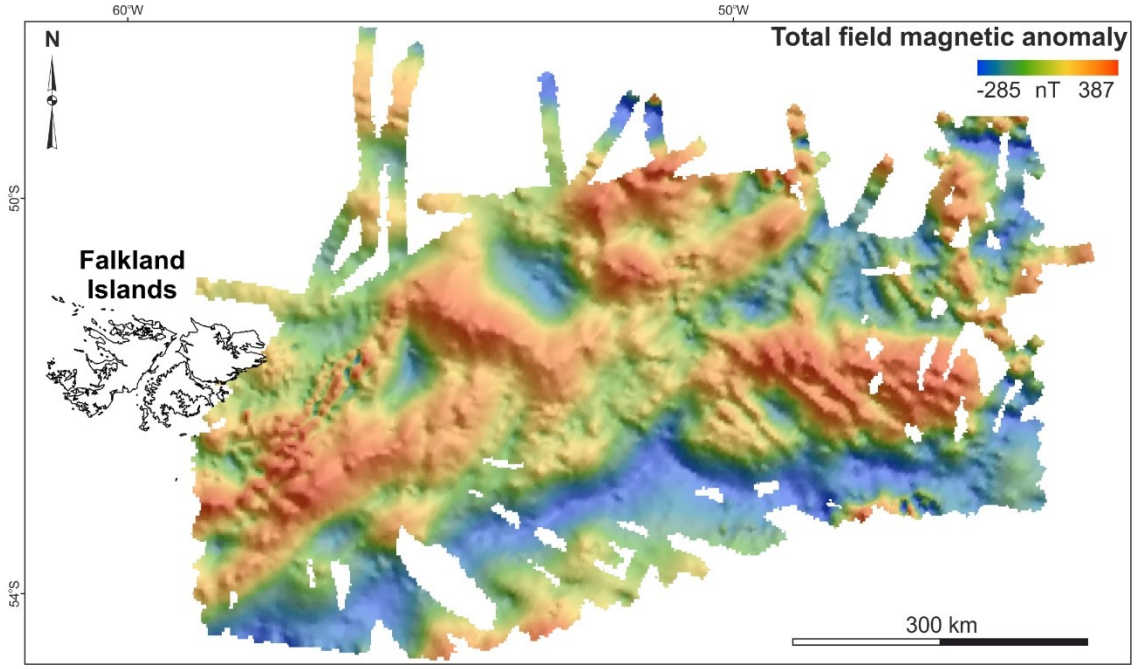

Figure 3.2 Total field magnetic anomaly along the Falkland Plateau Basin (Eagles, 2019)

3.1.3 Seismic and well data

The seismic reflection data used for this study comprise 2D and 3D survey data from 18 different vintages acquired between 1977 and 2014 (Figure 3.3). Survey details along with acquisition parameters (where available) can be found in Table 3.1. Seismic reflection data (with the exception of the Lamont-Doherty Geological Observatory survey from 1978) have been made available through the Falkland Island Government. Data acquired by the Falkland Islands Government under Exploration Licences or Production Licences can be made available for exploration or academic purposes, under certain conditions (interested parties can contact the Department of Mineral Resources by email info@mineralresources.gov.fk). The Lamont-Doherty Geological Observatory

survey is available freely from the Marine Geoscience Data System (https://www.marine-geo.org/index.php).

Table 3.1 Details for the used seismic reflection data

Survey	Year	Survey type	Line length (km)	Area (km^2)	Shot point interval (m)	Fold of cover	Record length (s)
Amerada Hess	1997	2D	1738.56	N/A			6
BIRPS	1980s	2D	1021.67	N/A	50	30	18
Desire	1998	2D	2540.97	N/A			6.7
Falkland Oil and Gas	2007	2D	10349.87	N/A	25	120	8
Geophysical Service Incorporated	1977	2D	3281.15	N/A			6
IPC Falklands	1996	2D	1600.33	N/A			8
Lamont-Doherty Geological Observatory	1978	2D	8160.84	N/A	50		4-12
Noble Energy FISA	2013	3D	N/A	5500			9
Noble Energy FIST	2013	3D	N/A	1120			9.2
Noble Energy FINA	2013	3D	N/A	5750			9.1
Rockhopper Exploration	2006	2D	871.85	N/A	25	120	8
Rockhopper Exploration	2008	2D	1965.61	N/A	25	120	8
Spectrum	1993	2D	7427.37	N/A		90	8

Spectrum	1995	2D	3736.14	N/A		90	7
Spectrum	1997	2D	3108.64	N/A		90	8
Veritas DGC	2000	2D	1832.91	N/A	25	90	8
WesternGeco	1993	2D	9999.83	N/A	40		9
WesternGeco	1977	2D	6068.27	N/A			6

For the entire plateau, 24 wells, located in the basins north, east, and south of the islands, were made available by the Falkland Islands Government (Figure 3.3; see paragraph above for availability). To this, information from five deep sea drilling projects were added from the Deep Sea Drilling Project reports and publications website. Out of these, eight wells were located in the basins that underwent detailed analysis (25\05-1, 26/06-1, and 14/24-1 north of the islands, and 31/12-1, 42/07-1, 61/05-1, 61/17-1, and 61/25-1 east of the islands) and were directly tied to the seismic. Three of the DSDPs (327, 330, and 511) penetrated the Mesozoic section and were located near regional seismic lines and were tied to these to provide age constraints on the eastern margin of the Falkland Plateau Basin.

Table 3.2 Summary of available wells; shaded wells have not been used in the seismic reflection data interpretation stage of this thesis

Well name	Location	Operator	Year	TD (m)	Formation at TD
14/05-1A	NFB	Shell	1998	4525	Lower Cretaceous
14/09-1	NFB	Amerada Hess	1998	2615	Middle Jurassic - Devonian
14/09-2	NFB	Amerada Hess	1998	2371	Lower Cretaceous
14/10-1	NFB	Shell	1998	3005	Lower Cretaceous
14/10-2	NFB	Rockhopper	2010	2744	Lower Cretaceous
14/10-3	NFB	Rockhopper	2011	2830	Lower Cretaceous
14/10-4	NFB	Rockhopper	2011	2800.7	Lower Cretaceous
14/10-5	NFB	Rockhopper	2011	2726.4	Lower Cretaceous
14/10-6	NFB	Rockhopper	2011	2706	Lower Cretaceous
14/10-7	NFB	Rockhopper	2011	2696	Lower Cretaceous

14/10-8	NFB	Rockhopper	2011	2635	Lower Cretaceous
14/13-1	NFB	Lasmo	1998	1550.5	Lower Cretaceous and Devonian (?)
14/15-1	NFB	Desire	2010	2877	Lower Cretaceous
14/15-1Z	NFB	Desire	2010	3418	Lower Cretaceous
14/15-2	NFB	Desire	2010	3052	Lower Cretaceous
14/19-1	NFB	Desire	2010	3667	Lower Cretaceous
14/24-1	NFB	IPC Falklands	1998	2938.9	Upper Jurassic (?)
25/05-1	NFB	Desire	2010	1697	Lower Cretaceous
26/06-1	NFB	Rockhopper	2010	2240	Jurassic (?)
31/12-1	FPB	FOGL	2012	5555	Lower Cretaceous
42/07-1	FPB	FOGL	2012	4043	Upper Cretaceous
61/05-1	FPB	BHP Billiton	2010	2476	Middle (?) Jurassic – Upper Triassic (?)
61/17-1	SFB	Borders and Southern	2012	4876	Lower Cretaceous
61/25-1	SFB	Borders and Southern	2012	3060	Eocene
DSDP327	FPB	DSDP	1974	2880.5	Lower Cretaceous
DSDP330	FPB	DSDP	1974	3211.5	Middle (?) to Upper Jurassic and Precambrian basement
DSDP511	FPB	DSDP	1980	3234	Upper Jurassic

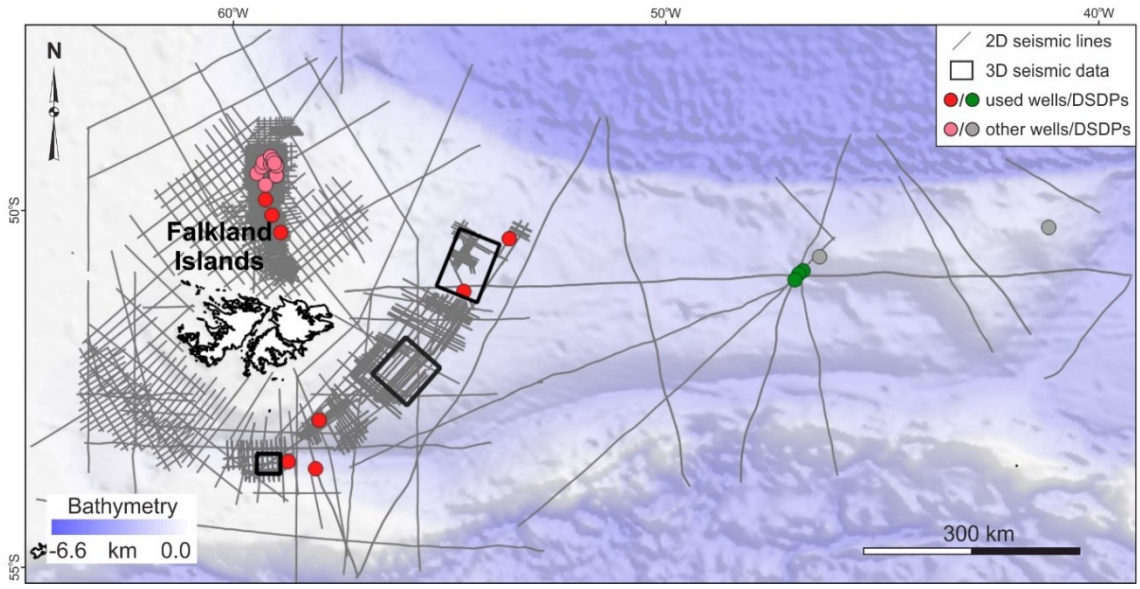

Figure 3.3 Seismic reflection data and wells used in this project

3.2 Methodology

Each chapter provides an account of the used methodologies. The following sections cover a description of the holistic approach in the methodology undertaken throughout the project, general concepts, technical details, and particularities in the way the interpretation was carried out.

3.2.1 Data integration

The Falkland Plateau has been the subject of multiple studies largely due to continued interest in hydrocarbon exploration. However, despite the extensive seismic reflection and well data acquired along the plateau, there are still numerous uncertainties in its crustal architecture and structural network in areas with little seismic coverage. For this particular reason, the seismic reflection data interpretation carried out in this project was integrated with gravity and magnetic data interpretation and analysis. Crustal boundaries and structural trends were constrained with the aid of potential field data and compared against the seismic interpretation. Where uncertainties remained regarding the nature of the crust, 2D gravity modelling was undertaken along regional seismic reflection profiles. To evaluate the reliability of the modelling results in the context of a laterally varied plateau in terms of crustal and structural architectures, 3D gravity inversion was carried out for the Falkland Plateau Basin area. The inversion was constrained by: (a) a plateau-wide depth-to-Moho isostatically compensated model of the area available from literature (Kimbell and Richards, 2008); (b) a 2D seismic refraction profile

available from literature (Schimschal and Jokat, 2019b); and (c) open-source bathymetric data from soundings and gravity-derived (Smith and Sandwell, 1997) and depth-to-basement from seismic reflection data interpretation. The distribution of crustal types along with the interpreted tectonic evolution were used as an input for plate reconstruction. Although the plate model was considered one of the main outcomes of the project, the deformable networks module of the reconstruction carried in GPlates was used iteratively as a validation tool for the crustal model generated from seismic, gravity, and magnetic data. Five scenarios for the evolution of the Falkland Plateau were considered and the results compared to the present-day configuration of the plateau as seen on seismic reflection and potential field data and as estimated from gravity inversion.

3.2.2 Potential field data

3.2.2.1 Data enhancement and interpretation

Data enhancement and filtering of the gravity and magnetic data was undertaken to facilitate the interpretation stage. The magnetic data were reduced to the magnetic pole before any filters were applied (Baranov and Naudy, 1964). The total horizontal (Cordell and Grauch, 1985; Figure A.3 in Appendix; Chapter 5) and tilt derivatives (Miller and Singh, 1994; Verduzco et al., 2004; Oruç and Keskinsezer, 2008; Chapters 5 and 6) of the free-air gravity anomaly and the reduced to pole total field magnetic anomaly, the first vertical derivative (Evjen, 1936; Figure A.2) of the free-air gravity anomaly, and the analytic signal of the total magnetic anomaly (Roest et al., 1992; Figure A.4) were computed to enhance linear structures and block boundaries. The free-air gravity anomaly underwent Butterworth bandpass filtering in order to eliminate the effect of low and high extremes of source depths. The range of wavelengths and the filter order were chosen by trial, making sure known regional feature were enhanced whilst minimizing ringing artefacts produced by high filter orders. The cut-off wavelengths that yielded most favourable results were 5-70 km for a filter order of 8. The free-air gravity anomaly along the southern part of South Africa underwent only a Butterworth bandpass filtering with cut-off wavelengths of 10 and 85 km, chosen by trial to highlight the same structures as along the Falkland Plateau, present in South Africa at different depths. All the derivatives and filtered maps were computed in Geosoft's Oasis Montaj. A short description of each of the derivatives and filters can be found below.

The *Total Horizontal Derivative* enhances the edges of the magnetic source or gravity contrasts (e.g. block boundaries, faults), and its calculation is carried out using the following formula:

$$THD = \sqrt{\left(\frac{\partial f}{\partial x}\right)^2 + \left(\frac{\partial f}{\partial y}\right)^2}$$

where f is the potential field used and $\frac{\partial f}{\partial x}$ and $\frac{\partial f}{\partial y}$ are the two horizontal derivatives of the field in the x and y directions (Cordell and Grauch, 1985).

The *First Vertical Derivative* is used to sharpen anomalies and enhance the effect of local or shallow features (Evjen, 1936).

$$VD = \frac{\partial f}{\partial z}$$

Similarly, the *Tilt Derivative* is used to sharpen anomalies. Its benefit comes from the equalization of strong and weak amplitudes (Verduzco et al., 2004).

$$TDR = tan^{-1}\left(\frac{VD}{THD}\right) = tan^{-1}\left(\frac{\partial f/\partial z}{\sqrt{(\partial f/\partial x)^2 + (\partial f/\partial y)^2}}\right)$$

The *Analytic Signal* is a function of the derivatives along all the x, y, and z directions. It is independent of the magnetic field orientation and therefore its maxima normally correspond to the edges of the magnetic source (Roest et al., 1992).

$$AS = \sqrt{\left(\frac{\partial f}{\partial x}\right)^2 + \left(\frac{\partial f}{\partial y}\right)^2 + \left(\frac{\partial f}{\partial z}\right)^2}$$

The *Butterworth Bandpass Filter* allows the pass of a predetermined wavenumber range (i.e. attenuates the effect of sources falling outside this range).

$$BP = \begin{cases} \dfrac{1}{[1 + (k/k_0)^n]} & if\ k_0 < k \\ \dfrac{k_1 - k}{k_1 - k_0} \cdot \dfrac{(k/k_0)^n}{[1 + (k/k_0)^n]} + \dfrac{k - k_0}{k_1 - k_0} \cdot \dfrac{1}{[1 + (k/k_1)^n]} & if\ k_0 \le k \le k_1 \\ \dfrac{(k/k_1)^n}{[1 + (k/k_1)^n]} & if\ k > k_1 \end{cases}$$

where k_0 and k_1 are the low and high wavenumber cut-offs in cycles/ground unit, and *n* is a positive integer which determines the degree of cut-off sharpness (Geosoft Inc., 2020).

The Bouguer anomaly was computed in Geosoft's Oasis Montaj along with its tilt derivative (Figure 3.4) in order to check the completeness of mapped features. However, the free-air gravity anomaly will be used throughout the thesis. This is because the filtering used to reduce the track noise introduced by the bathymetric data in the computation of the Bouguer anomaly minimised the gravimetric response of some of the features associated with faults on seismic data.

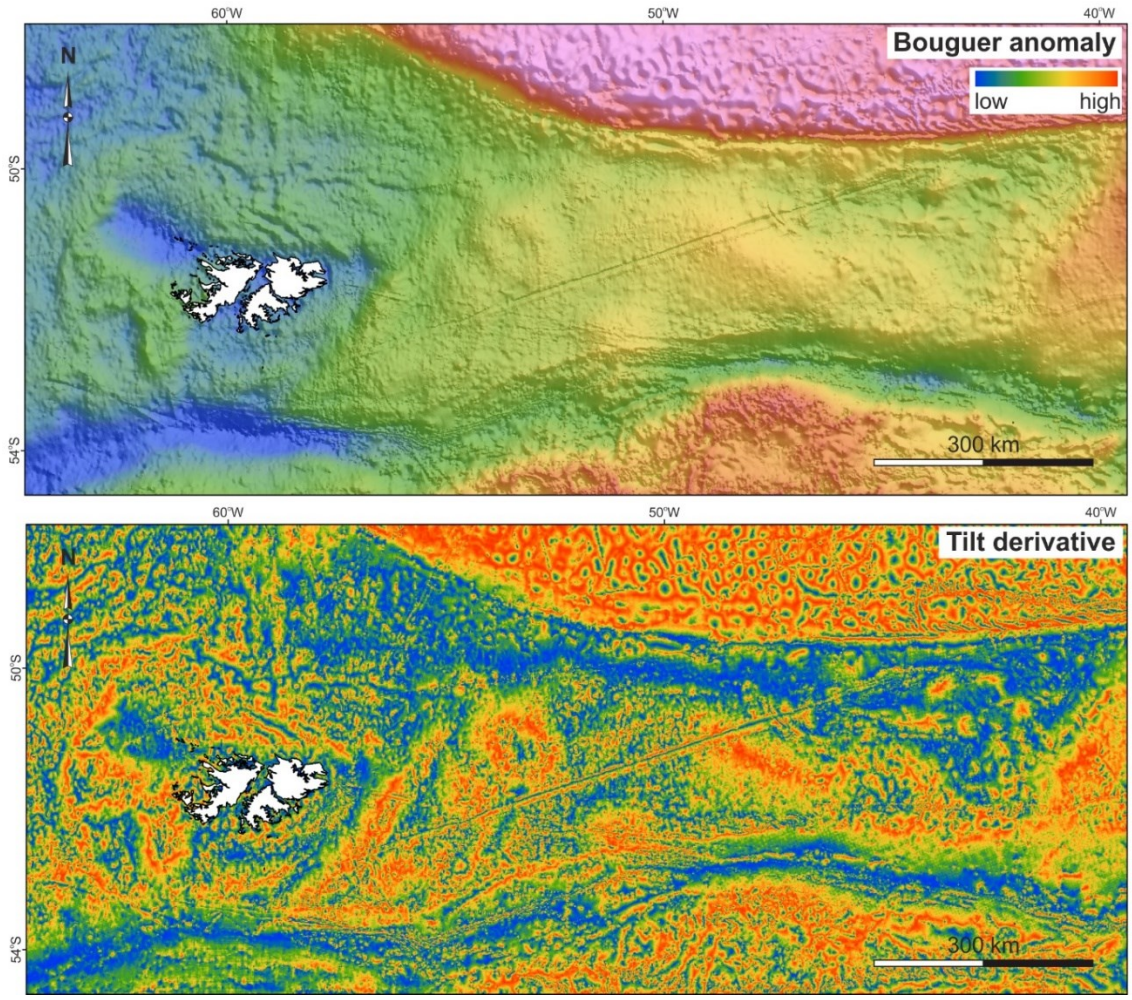

Figure 3.4 Bouguer anomaly computed using formulas given by Heiskanen and Moritz (1967) and a 2.67 g/cc reduction density (top); the tilt derivative of the Bouguer anomaly (bottom); the linear track noise can be seen along both maps, particularly in the central part

The interpretation of lineaments on the potential field data was carried out in ArcGIS and QGIS by mapping the zero-value contour on the first vertical and tilt derivatives and the maxima on the total horizontal derivative and analytical signal. Breaks or truncations of trends and changes in the magnetic and gravimetric signature were interpreted as tectonic or compositional crustal boundaries (Figure 3.5). The azimuth of the mapped lineaments was calculated

in ArcGIS and QGIS and further used to generate Rose Diagrams in Rick Allmendinger's Stereonet software.

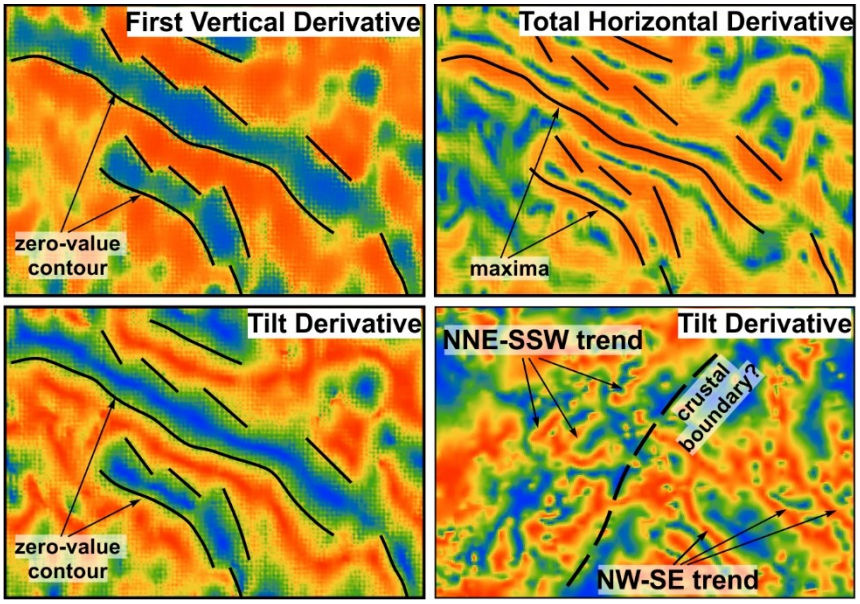

Figure 3.5 Example of lineaments mapping along the zero-value contour for the first vertical and tilt derivatives and along the maxima for the total horizontal derivative, and crustal boundary definition where potential field signature changes

3.2.2.2 Gravity modelling and inversion

For the 2D forward modelling and 3D inversion in GM-SYS and VPmg, respectively, inputs from seismic data interpretation and literature were used. Depth-converted horizon interpretations were converted to points in Petrel and exported as ASCII files (x, y, depth).

During the preparation of the 2D models, interpretations were imported in databases in Geosoft's Oasis Montaj and gridded using the minimum curvature algorithm and a grid increment of 15 km to obtain a good fit along the used profiles. The point distribution along the profiles was quasi-continuous, but sparser on either side of it. Therefore, a larger grid increment will be used during inversion when the entire horizon interpretation will be used. The grid file of the depth to Moho from Kimbell and Richards (2008) and bathymetry from Sandwell et al. (2014) were imported and gridded as well, using grid increments of 20 km. A mid-crust surface was generated at the mid-point between the top basement and the Moho using the Grid Math tool. The depth values for each of the used interfaces were extracted to separate databases along the modelled profiles using the Grid Profile tool in Oasis Montaj. The 2D models were built from map profiles, using the free-air gravity anomaly of Sandwell et al. (2014) as input. The horizons were added to the GM-SYS

model as depth surfaces. The depth converted seismic profiles were loaded as a backdrop to check the fit of the gridded horizons and add more interfaces, where needed, in the sedimentary succession. For the scenario using the Moho from Schimschal and Jokat (2019b) along the main modelled profile (Chapter 6), the interface corresponding to the seismic refraction-derived Moho was digitised from the published sections loaded as backdrops in GM-SYS. The starting densities and optimisation of the models are described in the methodology of Chapter 6.

For the 3D inversion, the ASCII files exported from Petrel or Oasis Montaj (digitised Moho from 2D model after Schimschal and Jokat, 2019b) were used as inputs for the layers and pierce points needed during the inversion process. A detailed overview of the methodology can be found in Chapter 6. Mira Geoscience's Geoscience Analyst was used for visualisation purposes. The Moho resulted from geometrical inversion was exported as an .xyz file, loaded back into Oasis Montaj and gridded using a grid increment of 20 km. Crustal thickness maps were computed for the modelled scenarios using the Grid Math tool. Thinning factors were calculated using the following formula:

$$\gamma = 1 - \frac{t_f}{t_i}$$

where t_f is the modelled crust thickness and t_i is the original crust thickness (Hellinger and Sclater, 1983), here considered 35 km.

3.2.3 Seismic and well data

3.2.3.1 Well ties

A time-depth relationship (Figure A.5) for key formation tops was available for most wells and used to tie them to the seismic reflection data. These were the result of a conventional well tie workflow consisting of a calibration of the sonic logs using vertical seismic profiling (VSP) data and synthetic generation from the calibrated sonic and density logs. The reliability of the time-depth relationships was validated by repeating the well tying process in Petrel using the Seismic well tie module. Similar to the workflow of the provided data, a sonic calibration was carried out using the available VSP data. Prior to this, a conditioning of the sonic and density logs was done, consisting of de-spiking and interpolation (Figure A.6) along areas with missing measurements. The calibrated sonic and conditioned density logs were used as an input in the synthetic generation stage. An iterative analysis was applied to evaluate the type of wavelet to be used for the synthetic, with the deterministic method and

extended white algorithm yielding the best results (Figure 3.6). This method uses the seismic data around the well and the provided well logs to determine the characteristics of the wavelet (Oldenburg et al., 1981).

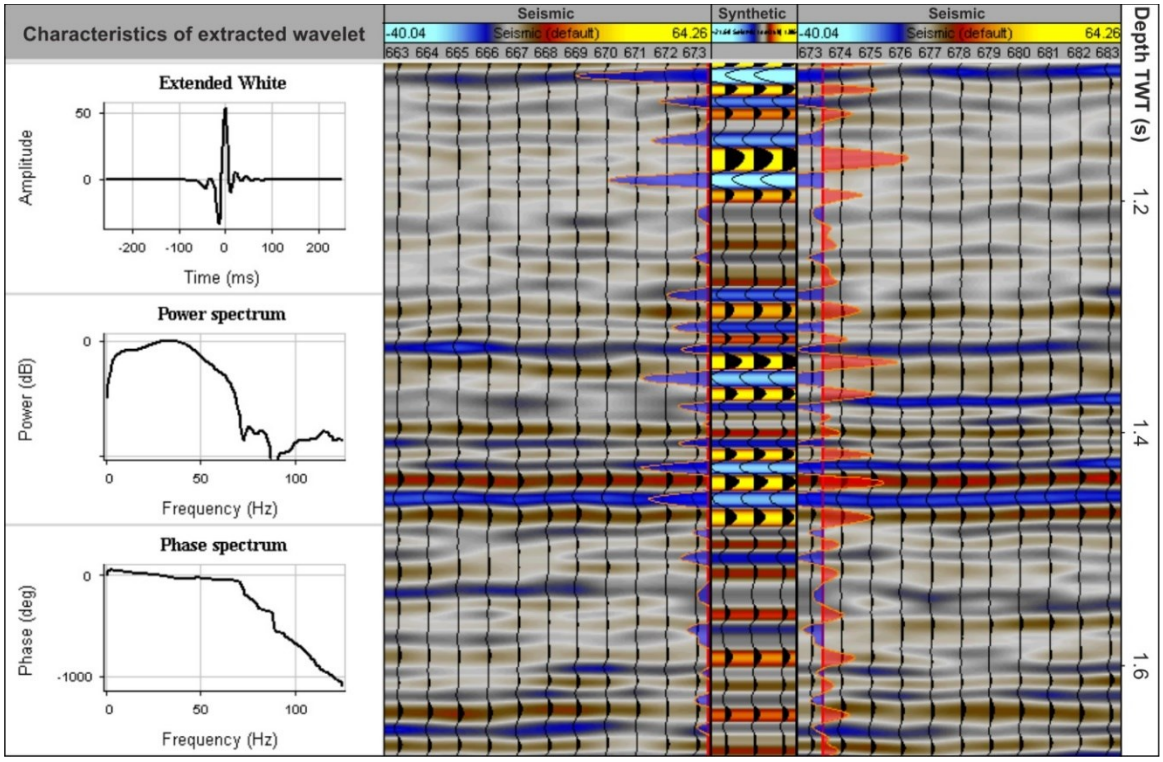

Figure 3.6 Example of synthetic generated for well 26/6-1

The DSDPs were tied to the seismic using the time-depth relationships provided by Barker (1977) and Ludwig et al. (1983) for key formation tops.

3.2.3.2 Seismic quality control, enhancement, and interpretation

The seismic reflection data were interpreted using Schlumberger's Petrel Software. Prior to interpretation, the 18 survey vintages were analysed in Petrel's Mis-tie manager. Vertical mis-ties were computed for a fixed interval (-0.25 to -2.5 s) between intersecting surveys. The datum for the corrections was set to the datum of the 3D cubes. Constant corrections were applied to the 2D vintages to avoid the distortion of the seismic lines. Corrections were applied in turns, starting with the ones directly intersecting the cubes and then fixing the corrected ones and recomputing and correcting the mis-ties for the next intersecting survey. For the older datasets (1970-1980 vintages) with poorer resolution and lower quality, a structural smoothing filter (filter size: 1.5 traces x 1.5 samples) was applied in order to increase the reflector continuity (Figure 3.7). Major bounding surfaces were mapped based on stratal terminations of reflectors and internal geometries of seismic facies (Figure 3.8; Mitchum et al. 1977; Hubbard et al. 1985a, b). Depending on the amplitude strength, each of

the mapped horizons were associated with either a peak or a trough. Both the 2D and 3D datasets were interpreted using the loop tying principle. For the seismic cubes, seed-grids were generated during the interpretation and further used for 3D autotracking for the shallower and more continuous horizons. In areas of uncertainty, seismic facies analysis was used to separate between different stratigraphic sequences following the methodology of Mitchum et al. (1977).

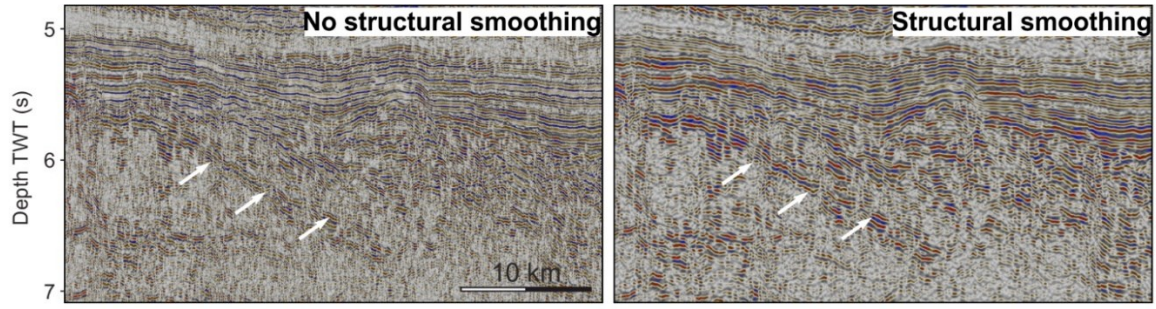

Figure 3.7 Example of seismic section before and after the application of a structural smoothing filter

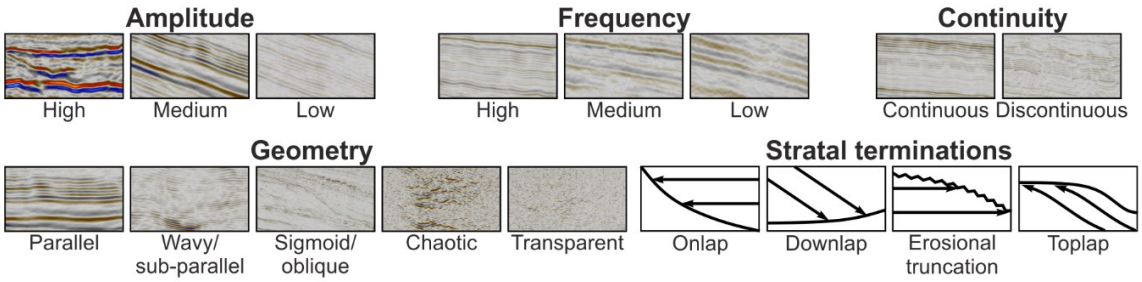

Figure 3.8 Reflector geometry and seismic facies terminology used (after Mitchum et al., 1977)

Surfaces were generated for the picked horizons. The gridding was carried out in Petrel using the Minimum Curvature interpolation algorithm chosen by trial and error. This algorithm generated smoother surfaces with no unrealistic geometries (e. g. angular geometries) and in conformity with the input data. The parameters of the algorithm were set as half-cell influence radius and inverse distance squared point weighting. The dimensions of the grid varied depending on the density of the seismic coverage. The surfaces computed along the 3D cubes or locally, above half-grabens, where different 2D seismic surveys generated a dense network of seismic lines, had grid increments of 1 km x 1 km. More regional surfaces along which the coverage of 2D lines varied had grid increments of 5 km x 5 km.

The interpretation of faults was carried by identifying breaks and/or offsets in reflections or a decrease in amplitudes (Figure 3.9a, c). The sense of slip was

determining by using the seismic polygon ghost in Petrel which allowed for correlations of reflection packages across the fault plane – section intersection. The lateral fault plane extent was interpreted differently on the 2D compared to 3D data. For the 2D seismic profiles, correlation of faults between different sections was done in two ways: (a) for areas where multiple faults were present and closely spaced together or a large spacing existed between adjacent seismic lines, faults were correlated based on fault plane geometry and/or fault throw, making sure their variation was geologically plausible; and (b) where available, using intersecting seismic lines and the loop-tying principle. For the 3D seismic data, the lateral interpretation of fault planes was done either by looking at changes and offsets in amplitude along timeslices or, most predominantly, by making use of timeslices through a previously generated variance cube (Figure 3.9a, b). This is a volume edge-detection attribute emphasizing horizontal discontinuities in amplitudes. The variance was generated in Petrel as well, using iteratively chosen inline and crossline ranges of 3 traces, a vertical smoothing of 15 samples, and no dip correction.

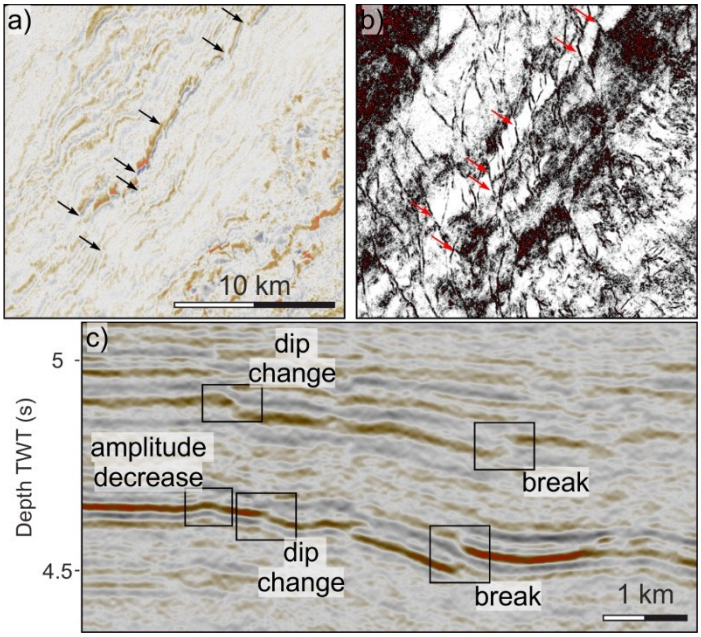

Figure 3.9 Example of faults on seismic on a) a timeslice; b) a timeslice with the variance attribute applied; c) on a seismic section

3.2.3.3 Depth conversion

Depth conversion was applied to specific sections for the purpose of comparison with the literature or as an intermediate step for gravity modelling and inversion using the Advanced Velocity Model module in Petrel. Several horizon-generated surfaces were used to separate units of different velocities (see individual chapter methodologies for details). For the sedimentary section

not penetrated by wells and for the acoustic basement, P-wave velocity values from literature were used. These were derived from seismic refraction studies (Ludwig et al., 1978; Schimschal and Jokat, 2017, 2019a, b) carried along the Falkland Plateau. For the shallower units, where well constraints were available, either average interval velocities or linear velocity functions were used (see individual chapter methodologies for details). These were obtained from the interval velocities derived from the calibrated sonic logs in Excel either by averaging them along the section between two horizons (Table 3.3) or by plotting the interval velocities against depth and fitting a linear trend through their distribution (Figure 3.10). The intercept and slope of the fitted line give the velocity at the datum (v_0) and the velocity gradient (k) to be used as inputs in Petrel's advanced velocity model (n.b. the velocity function used in Petrel comprised the velocity v_0 at the top of the interval and the calculated velocity gradient). If multiple wells were used, an average between them was used.

Table 3.3 Average interval velocities derived from the calibrated sonic logs for the Southern North Falkland Basin

	Cenozoic	Cretaceous	Jurassic	Well
Average Interval Velocity (m/s)	1741.23	2660.81	3889.23	**14/24-1**
	1813.14	2426.86		**25/5-1**
	2126.7	2769.96		**26/6-1**
	1893.69	*2619.21*	*3889.23*	

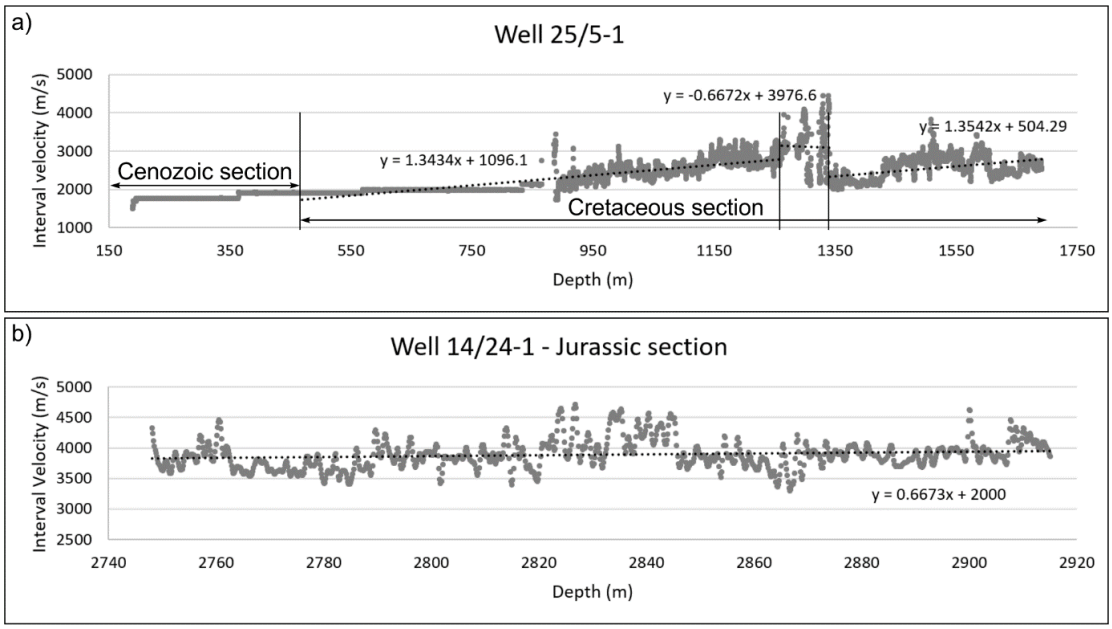

Figure 3.10 Example of the velocity analysis carried prior to depth conversion for a) well 25/5-1 (for the model, constant interval velocities were used for these sections); b) well 14/24-1 showing the calculation of the velocity gradient for the Jurassic section

3.2.4 Plate reconstruction

The plate reconstruction was built on a modified version of the plate model of Müller et al. (2019) (see Chapter 6 for details). The Falkland Plateau was split into two subplates, and the plate IDs (an identification number unique for each plate) were modified accordingly in the rotation file. The finite rotations of the subplate corresponding to the Falkland Islands Microplate (FIM) were calculated relative to the San Jorge Plate (see Table 6.2 in Chapter 6 for the finite rotations; Figure 3.11) for the rotation scenario. When no rotation was invoked, the FIM was kept fixed to the San Jorge Plate. The finite rotations for the FIM during rotation were calculated using the Pole Manipulation section in GPlates to alter the position of the FIM so that in the pre-break-up position of the block the structural features north of the islands align with the ones offshore South Africa (after Stanca et al., 2019; Chapter 4) and gaps between plates are minimised. Finite rotations for intermediate positions were calculated in a similar way, aligning structural features along the FIM with their equivalent in south-western Gondwana (~150-155 Ma; see Chapter 5) or bringing the FIM in a post-rotation position relative to the San Jorge Plate (~145 Ma; see Chapter 6 for rationale behind the timing of rotation). The visual fitting technique was preferred for this study due to the complexity of the tectonic evolution of the plateau.

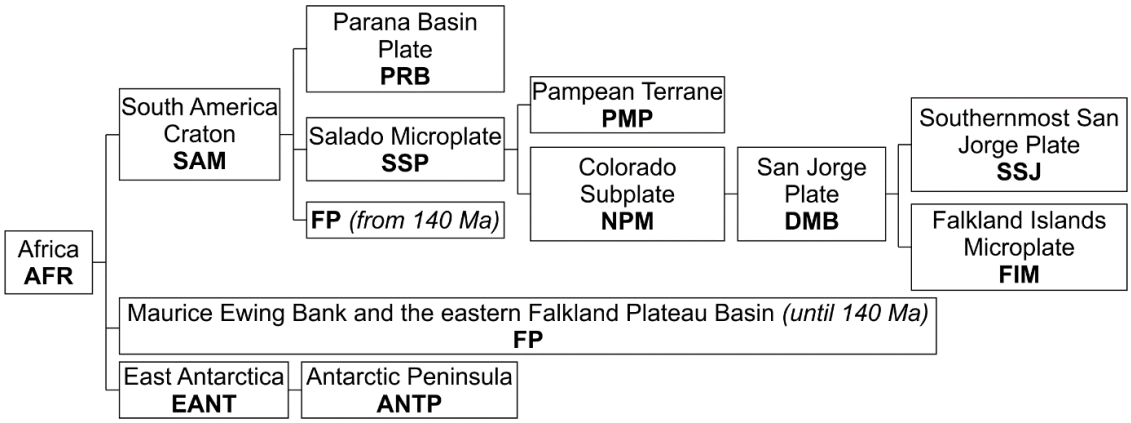

Figure 3.11 Plate hierarchy of the plate models presented in Chapter 6 (finite rotations shown in Chapter 6 for each plate are relative to the plate on their left in this figure)

The extent of the topological networks used during the deforming plate model construction was chosen by trial and error (see Chapter 6 for details). The boundaries were fixed to the surrounding plates by giving them the corresponding plate IDs. Points and rigid blocks were added to the interior of the topological network to constrain the deformation using the Topology section

in GPlates and the tools within to build and edit the topologies. The resulting reconstructed scalar coverages (crustal thickness distribution in this case) were exported as .xyz files, imported in databases in Oasis Montaj, and gridded using grid increments of 20 km. Residuals between the thicknesses resulted from the deforming plate models and the crustal thickness from the gravity models were computed using Grid Math. For the generation of images at different time instants, raster files consisting of maps and/or shapefiles with structural features were imported into GPlates at 0 Ma. The Assign Plate IDs tool was used to partition the raster files using the plate boundary polygons and assign the ID of the plate into which the structural features or partitioned raster fragments were located at 0 Ma. This would allow for the features within a specific plate boundary to stay fixed to that plate during the reconstruction.

A secondary plate model which incorporated a more northern position of the FIM in line with previous studies was also generated (See Chapter 6). As this required a modification of the position of the southernmost part of South America (outside the area of study) to eliminate gaps between this plate and the FIM, its effect on the estimated crustal thickness represented the topic of discussion in Chapter 7. The comparison between a rotational and non-rotational model from Chapter 6 was based on the reconstruction incorporating the South America fragmentation and reconstruction of Müller et al. (2019) for consistency.

More details about when and how each of the methods were implemented can be found in the upcoming results chapters (Chapters 4-6). The integrated approach of the methodology used throughout this thesis was chosen to overcome the uneven coverage of the available data and to constrain tectonically complex areas more reliably.

Chapter 4 A revised position for the rotated Falkland Islands Microplate

Summary

The early stages of transform margin formation are associated with crustal fragmentation and block rotation. The restricted size of the resultant microcontinental blocks precludes palaeogeographical reconstructions and reliable estimations of the amount of rotation they can undergo. An example considered here is the Falkland Plateau. This is located adjacent to the Agulhas–Falkland Fracture Zone and its westernmost province is the Falkland Islands microcontinent. The position of the plateau and the islands prior to Gondwana break-up remains contentious. This chapter integrates seismic reflection and gravity data to propose a revised position of the Falkland Islands microcontinent constrained by (1) the presence of a mega-décollement, controlling the Gondwanide Orogen, described north of the Falkland Islands and underneath South Africa and the Outeniqua Basin, and (2) the similar architecture of fault networks mapped north of the islands and in the northernmost Outeniqua Basin. This revised position requires a re-evaluation of the timing and rate of rotation of the Falkland Islands microcontinent and affects the expected crustal architecture adjacent to the islands. The model yields rotation rates between 5.5° and 8° Ma−1 and two potential times for rotation and predicts more unstretched crust beneath the basin east of the Falkland Islands than previous models.

4.1 Introduction

Transform margins are associated with a complicated tectono-stratigraphy (Scrutton, 1979; Basile and Allemand, 2002; Mercier de Lépinay et al., 2016) and a unified model for their evolution is yet to be established. Commonly, their incipient development stages can be associated with crustal fragmentation and block rotation (Mascle and Blarez, 1987). Typically, the resultant microcontinental blocks have a limited outcrop extent. This paucity of information hinders palaeogeographic reconstructions of these blocks, which are crucial for understanding the pre-break-up configuration of transform margins. A more reliably constrained palaeoposition of the transform-related microcontinental blocks can also bring insights into the amount of rotation that can affect these blocks and also on the architecture of the continental crust adjacent to them.

A pertinent example considered here is the Falkland Plateau transform margin (Figure 4.1). Its position prior to Gondwana break-up is highly dependent on the position of the Falkland Islands microcontinent.

Reaching a consensus on reconstructions of the southern Gondwanan margin prior to the opening of the South Atlantic Ocean has been hampered by conflicting models that try to account for the position and orientation of the Falkland Plateau. Palaeogeographic reconstructions of Gondwana during the Permo-Triassic recognize a Gondwanide fold and thrust belt that extended from South America through South Africa to Antarctica (Du Toit, 1937; Trouw and De Wit, 1999; Dalziel et al., 2000). The first to recognize a link between this fold and thrust belt and the Falkland Islands was Du Toit (1927) while Adie (1952a) further argued for a positioning of the islands east of South Africa in a rotated position as an extension of the Cape Fold Belt. Subsequent studies (Mitchell et al., 1986; Marshall, 1994; Mussett and Taylor, 1994; Curtis and Hyam, 1998; Thistlewood and Randall, 1998 in Stone, 2016; Thomson, 1998; Trewin et al., 2002) favoured this reconstruction but the associated uncertainties in interpretation and drawbacks of the model led also to the emergence of a rigid (non-rotational) model (Richards et al., 1996a; Lawrence et al., 1999; Ramos et al., 2017) with the islands and the Falkland Plateau fixed to the South American plate.

Extensive work has been carried across the Falkland Islands (Curtis and Hyam, 1998; Aldiss and Edwards, 1999) and their adjacent sedimentary basins (Ludwig et al., 1979; Lorenzo and Mutter, 1988; Platt and Philip, 1995; Richards et al., 1996a; Richards and Fannin, 1997; Thomson, 1998; Del Ben and Mallardi, 2004; Baristeas et al., 2013; Lohr and Underhill, 2015). However, deep crustal studies in the offshore region have not been equally widespread, being mainly focused on the Falkland Plateau Basin (Ewing et al., 1971; Lorenzo and Mutter, 1988; Lorenzo and Wessel, 1997; Schreider et al., 2011; Kimbell and Richards, 2008; Schimschal and Jokat, 2017). There is, nonetheless, a well constrained crustal model for the southern South African margin and its offshore basins (Dürrheim, 1987; Hälbich, 1993; Paton and Underhill, 2004; Paton et al., 2006). The offshore North Falkland Basin is well known only at the scale of its sedimentary infill. Therefore, a direct comparison between the Falkland Islands Microplate and the southern South African margin, at a crustal scale, is hard to accomplish. This scarcity of information regarding the deep structure also precludes a more accurate positioning of the islands prior to the break-up of Gondwana.

In this chapter, offshore seismic reflection and gravity data from the Southern North Falkland Basin (SNFB) are integrated to bring new insights into the crustal architecture of the Falkland Islands Microplate and better constrain its palaeoposition. The specific objectives are as follows: (1) to map the major tectonic features across the North Falkland Basin, (2) to compare the structural architecture of the SNFB and the Outeniqua Basin offshore South Africa, (3) to constrain the pre-break-up position of the Falkland Islands, and (4) to discuss the implications of the results.

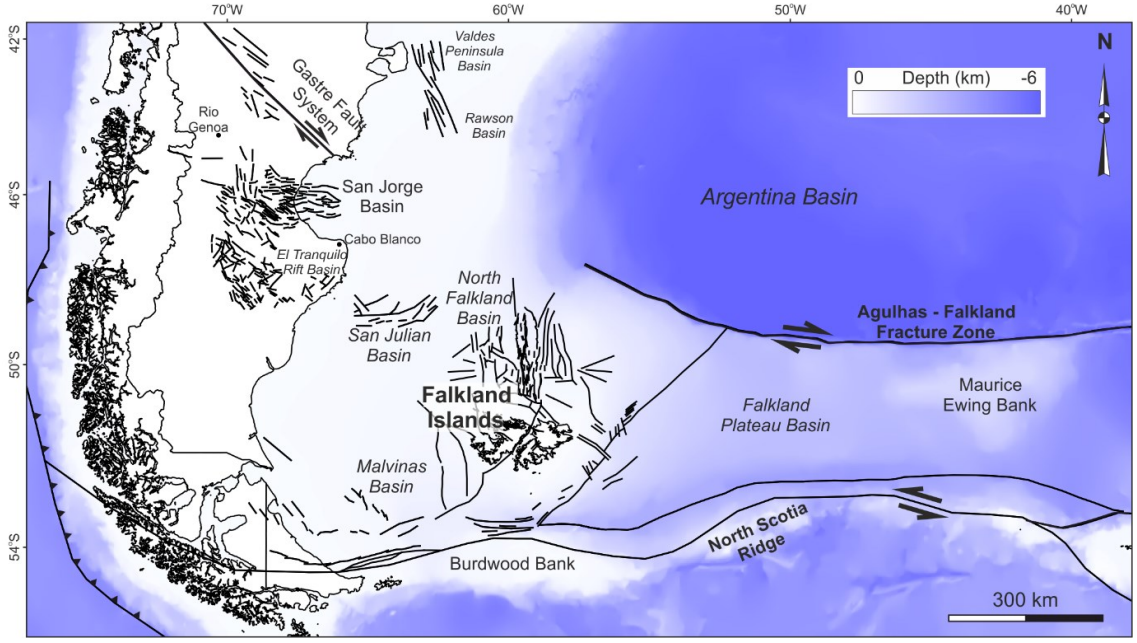

Figure 4.1 Present-day configuration and structural framework of the Falkland Plateau; offshore fault network for the Falkland Plateau compiled after Richards et al. (1996a), Richards and Fannin (1997), Cunningham et al. (1998), Galeazzi (1998), Tassone et al. (2008), and Ramos et al. (2017); the structure of the San Jorge and El Tranquilo basins and the Deseado Massif redrawn after Fitzgerald et al. (1990), Figari et al. (2015), and Moreira and Fernández (2015); Deseado Massif and North Patagonian Massif extents drawn after Ramos et al. (2017); main fracture and subduction zones in South America drawn after Rapela and Pankhurst (1992)

4.2 Geological background

4.2.1 General tectonic setting of south-western Gondwana

The crustal evolution of the southern margin of Gondwana was characterised by repeated reactivation of older structural features in an extensional or compressional regime (Paton and Underhill, 2004). After passive margin conditions (1600–1200 Ma), compression ensued between 1200 and 900 Ma

(Hälbich, 1993; Thomas et al., 1993). This was accompanied by subduction either on a north-dipping (Tankard et al., 2009) or south-dipping (Lindeque et al., 2011) plane, leading to the obduction of oceanic crust and the generation of the Gondwana suture during the Namaqua-Natal Orogeny (Hälbich, 1993; Thomas et al., 1993). Reworking of this suture zone material resulted in the deposition of the Pre-Cape Group in basins that opened parallel to this suture from 900 to 600 Ma (Tankard et al., 1982; Hälbich, 1993; Paton and Underhill, 2004). Between 600 and 450 Ma, the Pan African Orogeny led to basin inversion, north-verging thrusts, and a south dipping mega-décollement (Tankard et al., 1982; Shone et al., 1990; Hälbich, 1993). During the Ordovician to Carboniferous (450–300 Ma) the Cape Supergroup was deposited, followed by the Cape Orogeny (280–235 Ma; Tankard et al., 1982; Hälbich, 1993; Paton and Underhill, 2004); the latter was accompanied by the deposition of the Karoo foreland sequence (Hälbich, 1993; Veevers et al., 1994). This later collisional episode led to the formation of the Gondwanide orogen, which extended through the Sierra de la Ventana (South Argentina), Cape Mountains (South Africa), Falkland Islands, Ellsworth Mountains, and Pensacola Mountains (Antarctica) (Du Toit, 1937; Thomas et al., 1993; Trouw and De Wit, 1999; Dalziel et al., 2000).

Evidence of an updip continuation of the mega-décollement interpreted by Hälbich (1993) is presented by Lindeque et al. (2011). Their study documents a south-dipping interface beneath the Karoo Basin, lying between ~5 and 11 km depth and separating the deformed Karoo and Cape supergroup sequences from the Mesoproterozoic basement (Lindeque et al., 2011). This interface has been interpreted as an angular unconformity by Lindeque et al. (2011) but the fact that thrusts coalesce onto it suggests that it acted as a decoupling plane and its depth correlates with the depth of the mega-décollement interpreted by Hälbich (1993); this décollement is believed to have had been partially reactivated during the Cape Orogeny (Hälbich, 1993).

During the Middle Jurassic to Early Cretaceous break-up of Gondwana many Cape Fold Belt structures were reactivated in an extensional regime (Paton and Underhill 2004; Paton, 2006). During this time, there were high rates of exhumation across southern South Africa (Richardson et al., 2017), with sediment supplied to offshore extensional basins such as the Outeniqua and Southern Outeniqua basins (Figure 4.2; Tinker et al., 2008). At the same time, offshore the Falkland Islands, the North Falkland Basin, the Falkland Plateau Basin, the South Falkland Basin, and the Malvinas Basin developed (Figures

4.1 and 4.3; Richards et al., 1996a; Macdonald et al., 2003). The extension was the result of the westward drift of South America along the dextral Agulhas-Falkland Fracture Zone (AFFZ), away from Africa, and the opening of the South Atlantic (Ben-Avraham et al., 1997; Macdonald et al., 2003).

4.2.2 Outeniqua Basin

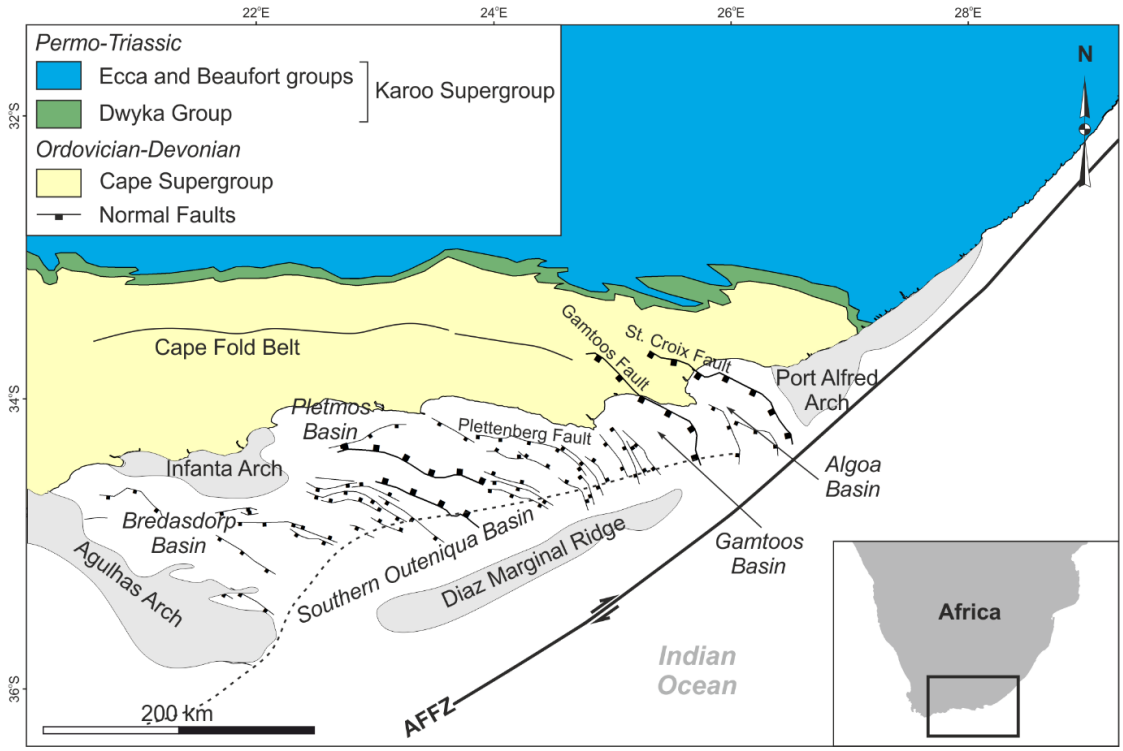

Figure 4.2 Map of South Africa and its offshore basins (after Paton et al., 2006; Parsiegla et al., 2009); AFFZ – Agulhas-Falkland Fracture Zone

Rifting in the broader Outeniqua Basin is thought to have occurred between Middle Jurassic and Valanginian with sedimentation into four depocentres: Bredasdorp, Pletmos, Gamtoos, and Algoa (McMillan et al., 1997). These are bounded by west-dipping normal faults (from west to east respectively: Plettenberg Fault, Gamtoos Fault, Port Elizabeth Fault, and St. Croix Fault) with displacements in excess of 10 km or by basement highs (Agulhas and Infanta Arches; McMillan et al., 1997; Figure 4.2). The dip angles of the controlling faults consistently increase towards the SW from 24° across the St. Croix Fault to 60° across the Plettenburg Fault (Paton et al., 2006) and coalesce onto a south-dipping mega-décollement (Hälbich, 1993; Paton et al., 2006). This configuration results in a southward change in structural style from thin-skinned to thick-skinned (Paton et al., 2006). These depocentres are bounded to the south by the Southern Outeniqua Basin, which is in turn

separated from the AFFZ by the Diaz Marginal Ridge (Parsiegla et al., 2009; Figure 4.2).

The basin-fill of each of these depocentres consists of Middle Jurassic to Early Cretaceous terrestrial and shallow marine sediments that unconformably overlie the Ordovician-Devonian Cape Supergroup onshore and offshore in the early rift stages, and show a transition to deep-water deposits offshore in the late rift stages (McMillan et al., 1997; Paton and Underhill, 2004; Paton, 2006). The post-rift sequence is represented by shallow marine deposits (McMillan et al., 1997).

4.2.3 North Falkland Basin

The structure of the North Falkland Basin (NFB) is controlled by the superimposition of two rift systems: the Late Jurassic Southern North Falkland Basin (SNFB) and the overlying Early Cretaceous North Falkland Graben (Lohr and Underhill, 2015; Figures 4.1 and 4.3). The SNFB is bounded by NW-SE striking normal faults, which are overprinted to the north by the N-S striking normal faults of the younger North Falkland Graben and its secondary half-grabens (Richards and Fannin, 1997; Thomson and Underhill, 1999; Lohr and Underhill, 2015). The Jurassic normal faults have low dip angles, thought to suggest that they originated as thrust faults (Richards et al., 1996a; Richards and Fannin, 1997; Thomson and Underhill, 1999). Their strike is similar to the onshore structures associated with the Gondwanide orogeny (Richards and Fannin, 1997; Brandsen et al., 1999).

The onset of post-rift sedimentation in the SNFB is interpreted as coeval with the deposition of syn-rift sediments in the North Falkland Graben and its subsidiary basins (Lohr and Underhill, 2015). The infill of the basins is considered to comprise Jurassic to Valanginian fluvio-lacustrine deposits passing to lacustrine and deltaic deposits during the post-rift phase of the North Falkland Graben and overlain by fluvial to marine mudstones of Late Cretaceous to Cenozoic age (Richards and Hillier, 2000; Richards et al., 2006; Lohr and Underhill, 2015).

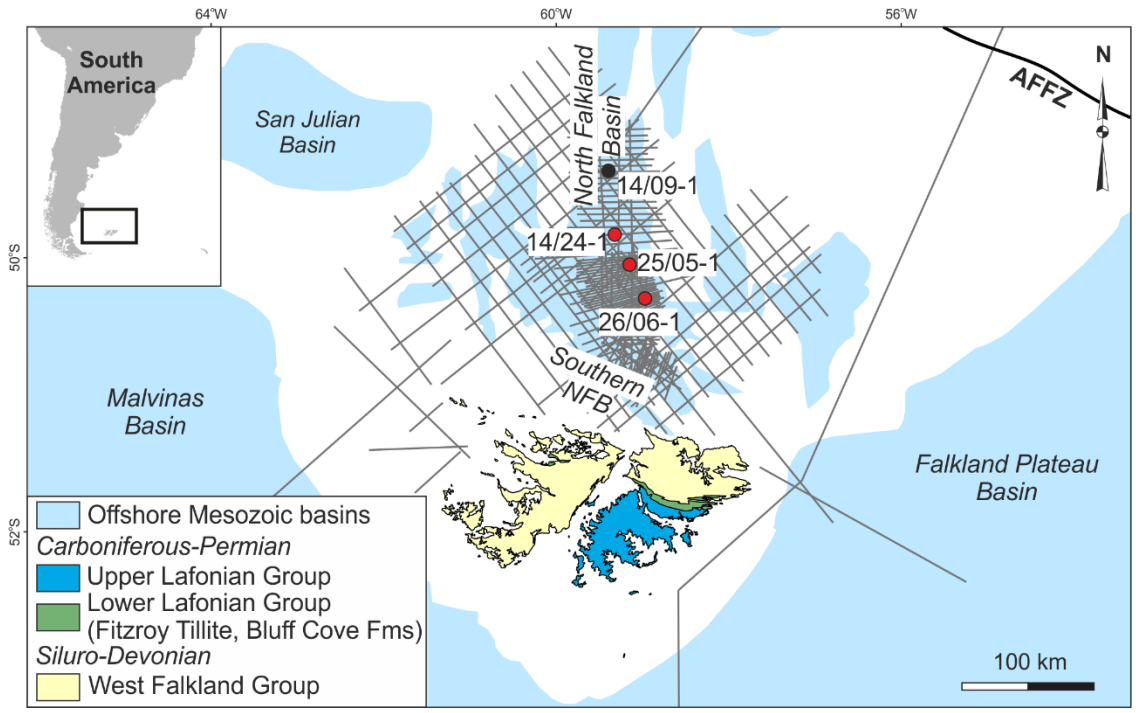

Figure 4.3 Map of the Falkland Islands (after Aldiss and Edwards, 1999) and their offshore basins (based on Richards et al., 1996a); grey lines - the position of the 2D seismic reflection lines used in this chapter; red circles – wells used in this chapter; black circle – unused well

4.2.4 Falkland Islands within Gondwana

Du Toit (1927) first suggested that the Falkland Islands might represent a displaced segment of the Cape Fold Belt (CFB) and placed the islands between South America and South Africa. Adie (1952a) built upon that hypothesis and suggested that the islands rotated ~180° having originated from offshore east South Africa (Figure 4.4a). This assertion was based on stratigraphic correlations, fossil assemblages, ice flow directions, and structural similarities between the Falkland Islands and the South African margin. This hypothesis is further supported by more recent palaeomagnetic, aeromagnetic, stratigraphic, palaeontological, and structural data analysis (Mitchell et al., 1986; Mussett and Taylor, 1994; Marshall, 1994; Curtis and Hyam, 1998; Trewin et al., 2002; Stone et al., 2009). The palaeomagnetic measurements were carried out on dykes identified onshore the Falkland Islands (Mitchell et al., 1986; Taylor and Shaw 1989; Stone et al., 2008) and on Permian sediments (Thistlewood and Randall, 1998 in Stone, 2016). The dykes trend E-W to NE-SW and N-S and are of Early Jurassic to Early Cretaceous age, respectively (Mussett and Taylor, 1994; Thistlewood et al., 1997; Stone et al., 2008; Richards et al., 2013). Their emplacement is related to the Karoo-Ferrar

magmatism in South Africa and Antarctica for the Jurassic dykes (Mitchell et al., 1999) and the opening of the South Atlantic for the Cretaceous swarm (Richards et al., 2013). Five deformation phases (D1 to D5) were identified by Aldiss and Edwards (1999) onshore the Falkland Islands; the first four were interpreted as being synchronous to the Permo-Triassic CFB in South Africa (Curtis and Hyam, 1998; Stone, 2016). The West Falkland Group, which crops out on West Falkland, the northern part of East Falkland, and Beauchêne Island (Aldiss and Edwards, 1999; Stone, 2015), has been correlated with the Table Mountain, Bokkeveld, and Witteberg groups in South Africa (Adie, 1952b in Marshall, 1994), whereas the Fitzroy Tillite Formation from the Falkland Islands is considered coeval with the Dwyka Group (Figure 4.5) of South Africa (Curtis and Hyam, 1998) based on ice flow directions (Frakes and Crowell, 1967; Crowell and Frakes, 1972) and fossil assemblages from erratic clasts from the glacial diamictites (Stone and Thompson, 2005; Stone et al., 2012). The overlying Permian deposits of the Upper Lafonian Group have been correlated with the Ecca and Beaufort groups in South Africa based on stratigraphy, trace fossils, and sediment provenance (Trewin et al., 2002; Figure 4.5).

These correlations led to the positioning of the Falkland Islands east of the south-eastern coast of South Africa (Curtis and Hyam, 1998; Trewin et al., 2002; Figure 4.4a) with the Maurice Ewing Bank, now located at the eastern end of the Falkland Plateau (Figure 4.1), adjacent to the Durban Basin (Marshall, 1994). In this model, the Falkland Islands underwent a clockwise rotation of up to 180° during the break-up of Gondwana (120° prior to the opening of the South Atlantic and 60° during the drifting of the South American plate; Mitchell et al., 1986).

As part of the rotational model, the Falkland Islands are considered to be part of a microplate that underwent vertical-axis rotation during the break-up of Gondwana. However, the northern and western boundaries of this microplate remain uncertain, whereas the southern and eastern boundaries are considered to coincide with the present-day North Scotia Ridge and the NE-SW striking fault bounding the Falkland Plateau Basin, respectively (Marshall, 1994; Richards et al., 1996b; Storey et al., 1999; Figure 4.1).

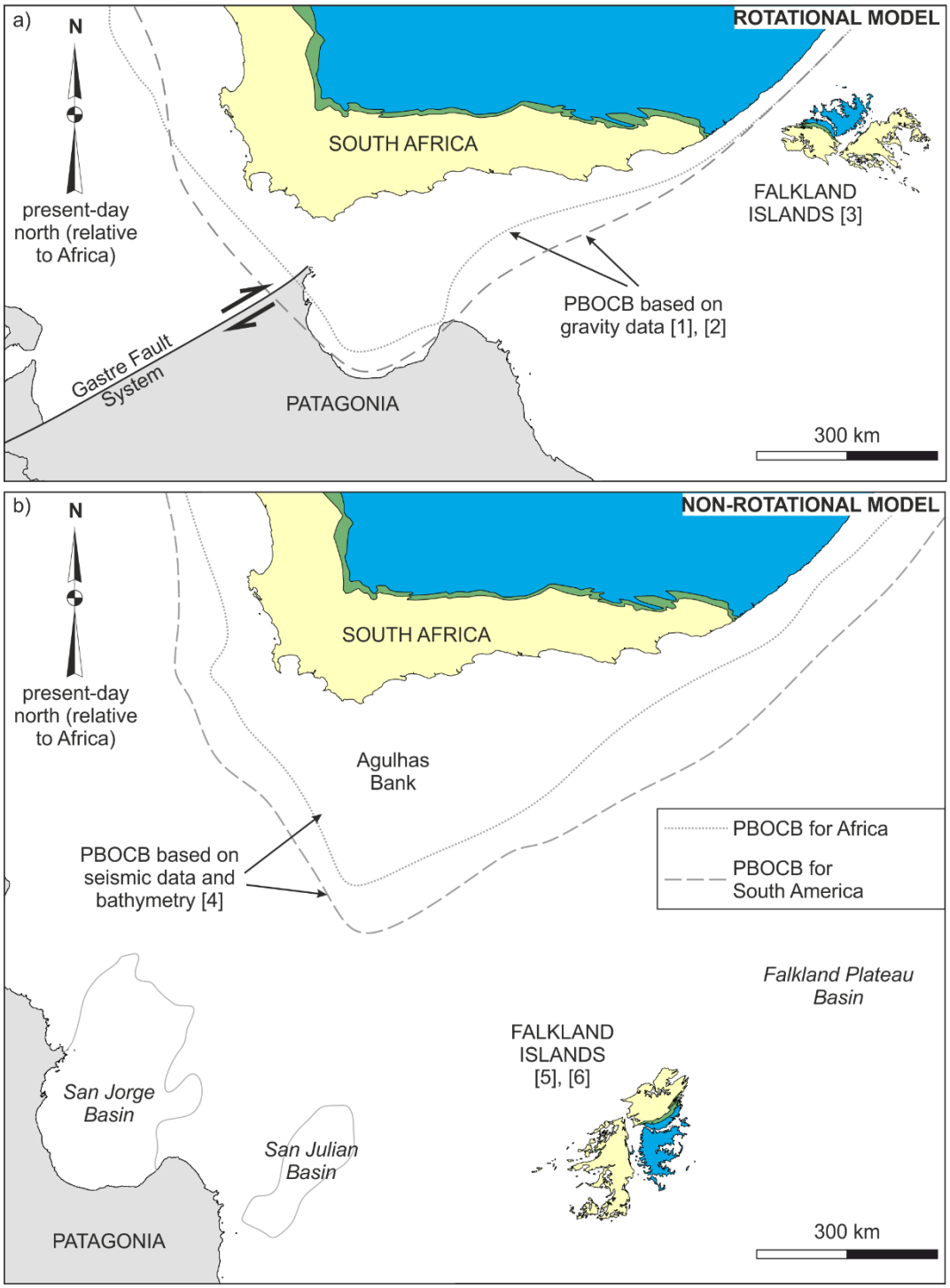

Figure 4.4 Two models for the palaeogeographic reconstruction of the Falkland Islands: (a) rotational and (b) non-rotational; [1] – Lawver et al. (1999), [2] – Macdonald et al. (2003), [3] – Trewin et al. (2002), [4] – Martin et al. (1981), [5] – Lawrence et al. (1999), [6] – Ramos (2008), PBOCB – pre-break-up ocean – continent boundary; the stratigraphic correlation and colour code are shown in Figure 4.5

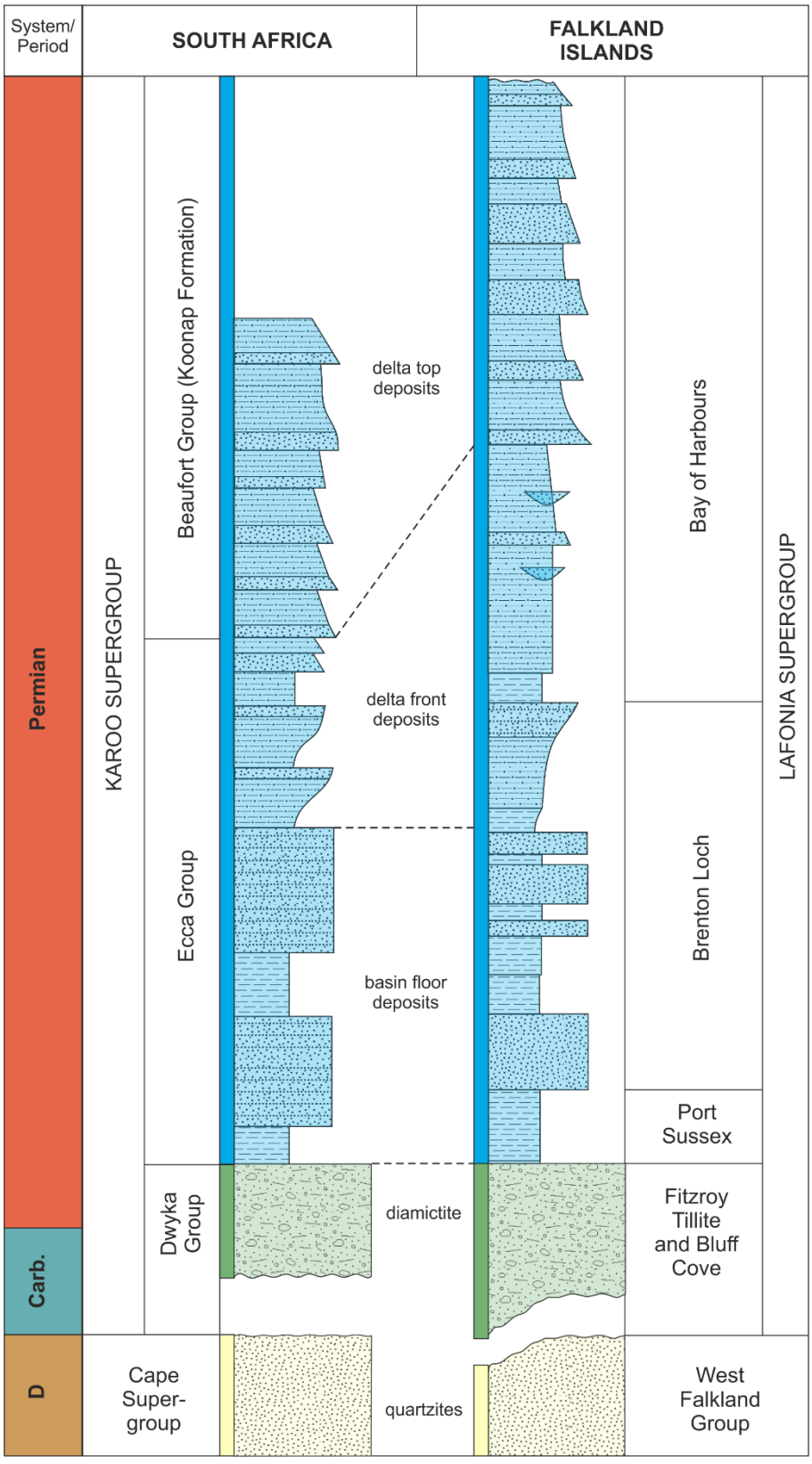

Figure 4.5 Lithostratigraphy of the Devonian to Permian deposits of the Falkland Islands and South Africa along with the correlations (dashed lines) presented by Trewin et al. (2002); ages after Curtis and Hyam (1998) and Paton et al. (2006)

A further implication of this reconstruction of the islands consists of space issues, which require the presence of a right-lateral fault north of the North Patagonian Massif (Ben-Avraham et al., 1993) or south of it, along the Gastre Fault System (Rapela and Pankhurst, 1992; Figures 4.1 and 4.4a) to account for a more eastern position of Patagonia prior to the break-up of Gondwana. However, field observations along the Gastre Fault contradict its predicted dextral nature (Franzese and Martino, 1998 in Ramos et al., 2017; Von Gosen and Loske, 2004) and provide an additional argument against the rotational model.

Furthermore, no deformation affecting the sedimentary basins offshore the Falkland Islands has been identified in previous studies (Richards et al., 1996a), which led to the conclusion that the rotation occurred prior to the opening of these basins in the mid-Jurassic (Stone et al., 2008). However, there is little movement recorded along the AFFZ at this time (Broad et al., 2006 in Tankard et al., 2009) in support of this hypothesis. In addition, the uncertainty around palaeomagnetic measurements (Richards et al., 1996a; Hodgkinson, 2002) and the absence of a pertinent mechanism to account for the rapid and substantial rotation of the islands resulted in numerous studies advocating a contrasting rigid (non-rotational) evolution of the Falkland Islands, in which the islands are part of a Falkland Plateau fixed to the South American plate (Figure 4.4b). In this scenario the Falkland Islands undergo a rotation of only 60° during the opening of the South Atlantic (Lawrence et al., 1999; Ramos et al., 2017).

In the rigid model the opposite vergence of the thrusts and folds onshore the Falkland Islands compared to the Cape Fold Belt is explained through the existence of similar south-verging structures in the north-eastern North Patagonian Massif (Von Gosen, 2003; Ramos et al., 2017). The West Falkland Group is interpreted as being coeval with same age deposits from northern Patagonia, their common source being the Deseado Massif, whereas the equivalent of the diamictite in the Falkland Islands is interpreted as being the Sauce Grande Tillite of the Ventania System, Argentina (Ramos et al., 2017). Furthermore, the trend of the Jurassic Southern North Falkland Basin is correlated to basins along the South American margin (Figure 4.1), having the same trend and age (Ramos et al., 2017), their opening being associated either with back-arc extension along the southern margin of Gondwana or the southward movement of Antarctica and early extension in the Weddell Sea

(Uliana et al., 1989; Baristeas et al., 2013; Reeves et al., 2016; Ramos et al., 2017).

4.3 Data and methods

This chapter was based on the analysis of open-source gravity data (Figure 4.6) and seismic reflection and well data (Figure 4.3) courtesy of the Falkland Islands Government.

The gravity data consist of the V24.1 1-minute satellite altimetry free-air gravity anomaly grid of Sandwell et al. (2014). The seismic reflection data used for this study comprise 2D lines from seven different vintages acquired between 1980s and 2008 by BIRPS, WesternGeco, Spectrum, Rockhopper Exploration, and Desire Petroleum. The shot point interval ranges from 25 m for the more recent datasets to 50 m for the regional traverse east of the islands, whereas the geophone coverage varies between 120-fold and 30-fold, respectively. The line spacing ranges from 2 to 30 km and the maximum record lengths between 6.7 and 18 seconds TWT. All seismic sections have a vertical axis in two-way-time (TWT), a depth conversion being undertaken on type-sections post-interpretation. Three wells, 26/06-1 (Rockhopper Exploration), 25/05-1 (Desire), and 14/24-1 (IPC Falklands), were used for this chapter with formation top markers and were tied to the seismic reflection data. Vertical seismic profile surveys were available for each well and provided velocity information that facilitated the subsequent depth conversion.

The total horizontal derivative of the free-air gravity anomaly (Cordell and Grauch, 1985), first vertical derivative (Evjen 1936), and tilt derivative (Miller and Singh, 1994; Verduzco et al., 2004; Oruç and Keskinsezer, 2008) were computed (Figure 4.6) for edge detection and to enhance linear structures. The main gravity lineaments were mapped along the entire NFB (Figure 4.6) and show a close correlation with fault trends mapped on the seismic reflection data (Figure 4.8).

Five key surfaces were mapped across the SNFB (Figure 4.7) based on stratal terminations of reflectors and internal geometries of seismic facies (Mitchum et al., 1977; Hubbard et al., 1985a, b), and used to define three mega-sequences: pre-rift, syn-rift, and post-rift. The latter sequence is separated into four packages by an intra-Lower Cretaceous reflector, the top Lower Cretaceous, and the base Cenozoic regional unconformity. Within the syn-rift sequence two unconformities, described in detail by Lohr and Underhill (2015), were mapped

along the extent of the basin-fills of the half-grabens (Figures 4.9, 4.10, and 4.11). The SNFB pre-rift sequence is associated with a semi-transparent seismic facies capped by a high amplitude reflector that is onlapped by wedge-shaped syn-rift deposits. These display a chaotic seismic character in the lower section and sub-parallel to parallel reflectors in the upper part. The Cretaceous post-rift sequence comprises wavy to hummocky and sub-parallel to divergent deposits overlain by the sub-horizontal Cenozoic post-rift sequence (Figures 4.9, 4.10, and 4.11).

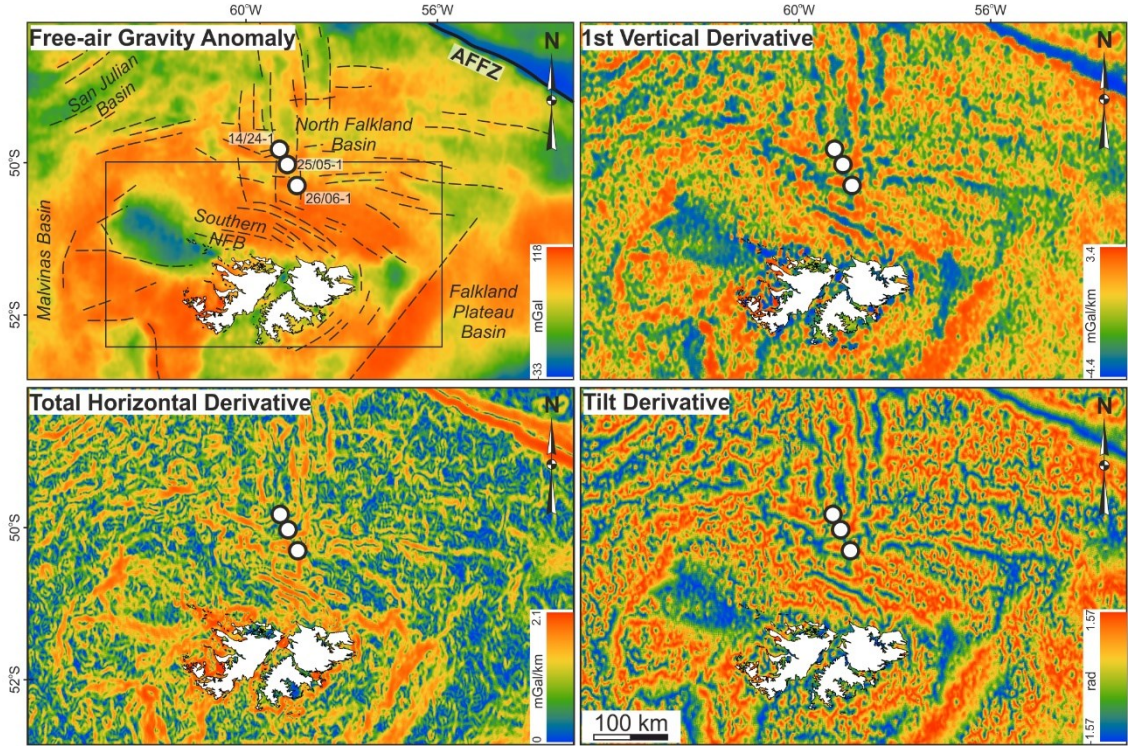

Figure 4.6 Open-source gravity data (Sandwell et al., 2014) and the first vertical, total horizontal, and tilt derivatives for offshore Falkland Islands; gravity lineaments (dashed lines) interpreted based on the computed derivatives are superimposed on the free-air gravity anomaly; rectangle shows the extent of the map in Figure 4.8

The oldest sediments penetrated by two of the used wells are represented by Upper (?) Jurassic volcaniclastic deposits. Deposits of potentially Middle Jurassic age have been penetrated by well 14/09-1 further north, in the NFB (Figure 4.3), and correlated by Lohr and Underhill (2015) with deposits associated with the SNFB syn-rift sequence. Across the faults, the Upper Jurassic reflector is correlated with the top syn-rift of the SNFB. This horizon is not continuous southward across the shoulders of the half-grabens. The age of the infill of the southernmost half-graben is inferred based on stratal geometries alone assuming coeval deposition across the SNFB.

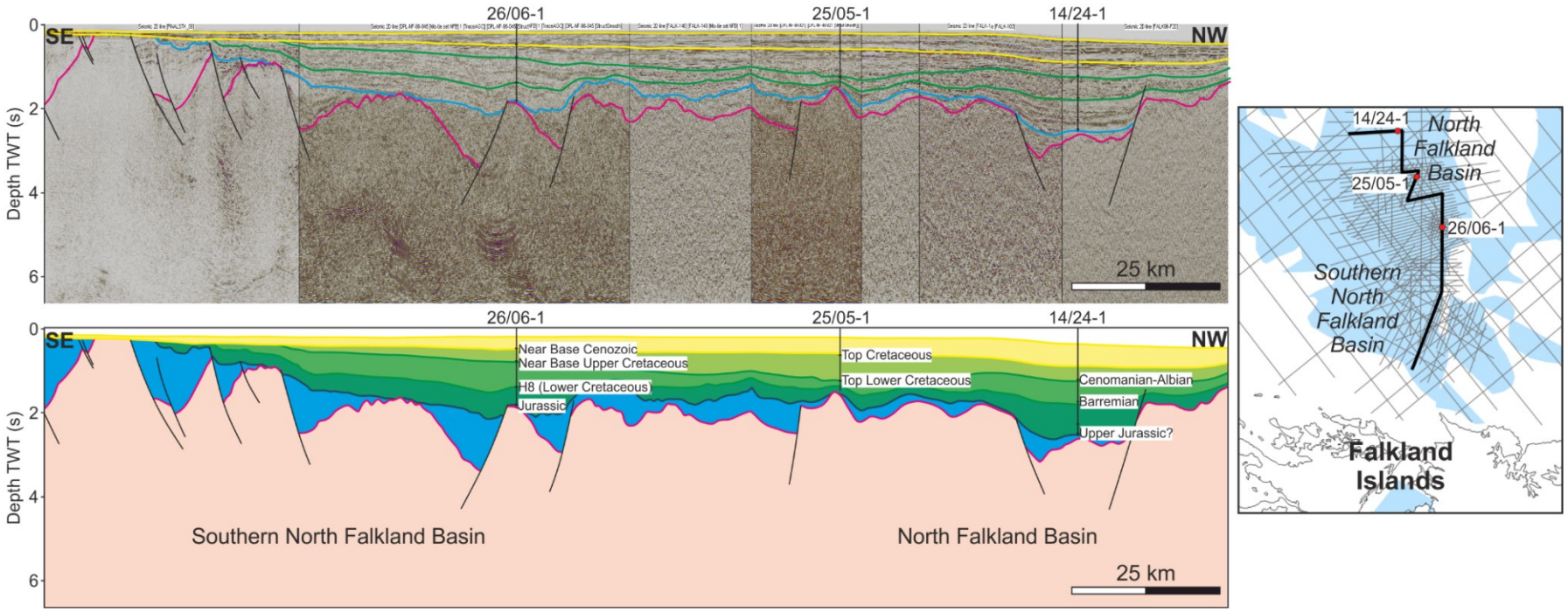

Figure 4.7 Composite seismic section through the used wells showing the pre-rift (Paleozoic to Proterozoic; light pink), syn-rift (Jurassic; blue), and post-rift (Cretaceous-Cenozoic; green and yellow), and their variation in geometry from the Southern North Falkland Basin to the North Falkland Basin

Faults at the SNFB pre-rift level were mapped (Figures 4.8–4.12) and superimposed onto the interpreted gravity features shown in Figure 4.6 for comparison and correlation. Two deep high-amplitude intervals were identified, the shallower (-3.5 s to -8.2 s TWT) being mapped across the entire SNFB (Figures 4.8, 4.13a, b, c, 4.14) on two of the vintages, whereas the deeper feature (-11 s to -12 s TWT) was interpreted only on the regional traverse east of the islands (Figure 4.13c, d).

A regional cross-section was constructed perpendicular to the main structural grain of the basin to allow a direct comparison with published sections from onshore Falkland Islands and South Africa. To assess the geometry of the faults more reliably, the section was depth converted using velocity information from the borehole seismic surveys available for all wells. The Cenozoic and Cretaceous post-rift sequences were depth converted using interval velocities of 1900 and 2600 m/s, respectively. A v_0-k function was used for the syn-rift deposits (v_0 = 3000 m/s at the top of the formation and k = 0.6; derived from the available well data), whereas the pre-rift down to a depth of 8s TWT was depth converted using a constant velocity of 5200 m/s (averaged from Ludwig et al., 1978 and Schimschal and Jokat, 2017). The same velocity model was used to depth convert type-section across the major WNW-ESE faults to estimate the thickness of the half-graben infills and the dips of the faults more accurately.

4.4 Results

The deformation in the SNFB was accommodated by three main NW-SE to WNW-ESE striking reactivated thrust faults (A to C in Figure 4.8), up to ~150 km long, and with depocentres ~3000 ms TWT (~5 km) deep. The WNW-ESE trend of these faults can be tracked on the gravity data derivatives, where they are associated with linear anomalies (Figure 4.6). Further north, this WNW-ESE trend of the gravity lineaments is overprinted by roughly E-W striking features, swinging through NE-SW to N-S on the west of the islands, and the N-S trend of the Early Cretaceous main graben (Figure 4.6). Sections through both the WNW-ESE trending faults of the SNFB and the main N-S trending faults in the NFB show a clear separation of the syn-rift deposits (Figure 4.9), although locally some indication of Jurassic activity along N-S trending faults was identified (Figure 4.9b).

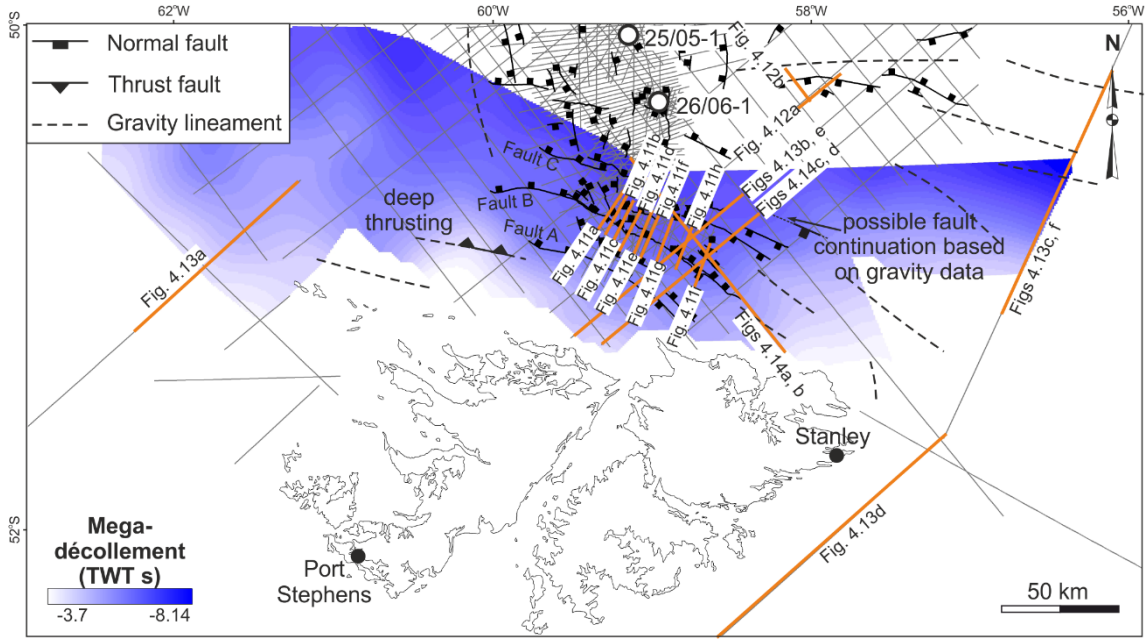

Figure 4.8 Normal faults interpreted based on seismic reflection data in the SNFB superimposed on the TWT map of the mega-décollement; the faults are following the same orientation as the WNW-ESE gravity lineaments mapped across the SNFB; grey line network represents the seismic reflection profiles used for interpretation

The WNW-ESE trending normal faults have low depth converted dips of 20-40° (with the exception of Fault A, which steepens up to 60° closer to the surface), dominantly with a downthrow to the NE, and are associated with splay faults and smaller-scale synthetic and antithetic faults within their hanging-walls (Figures 4.8 and 4.11).

The syn-rift deposits associated with these faults reach a thickness of ~2000 ms TWT but a greater thickness was likely to have existed as the southernmost half-graben infills have since been uplifted and eroded (Figure 4.10h). The syn-rift sequence was deposited in three stages, separated by unconformities interpreted within the package (Figures 4.10 and 4.11). Lateral variations in the sediment thickness within these syn-rift packages have been identified (Figure 4.10e-h). For the longest fault in the basin, Fault B, three main depocentres can be readily noticed on the pre-rift TWT map (Figure 4.10a). The isochron maps of the three syn-rift sequences show that these depocentres developed at different times (Figure 4.10e-g). The syn-rift most probably overlies the same formations that crop out onshore (Thomson and Underhill, 1999; Lohr and Underhill, 2015). Locally, high upper crust reflectivity was identified in the pre-rift (Figure 4.10h), potentially related to the top of the crystalline basement known to crop out onshore the islands. The syn-rift sequence was further inverted and deformed into harpoon structures and gentle folds along with the

overlying Cretaceous post-rift units (Figure 4.11). The whole sequence is capped unconformably by Cenozoic deposits.

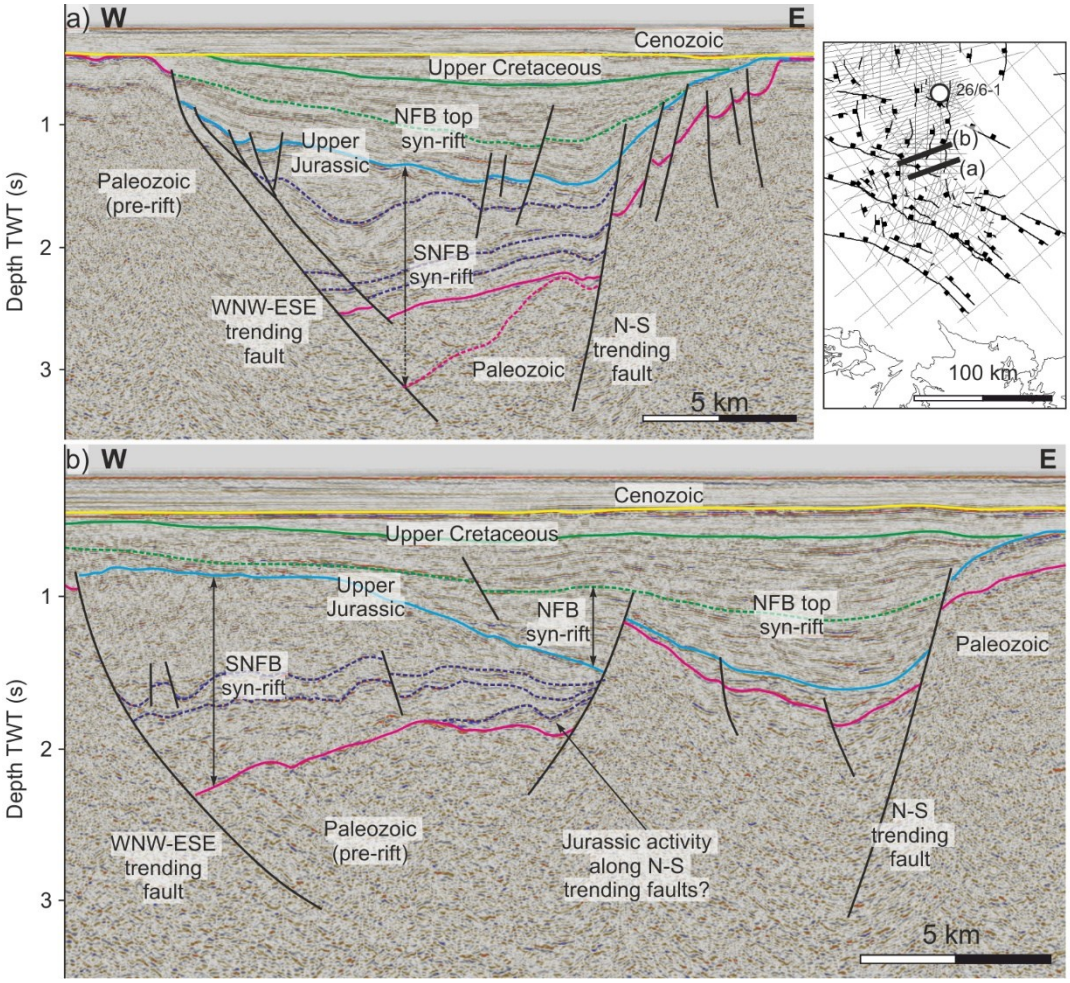

Figure 4.9 Sections intersecting both the WNW-ESE trending faults of the SNFB and the N-S trending faults of the NFB showing the separation of their syn-rift deposits

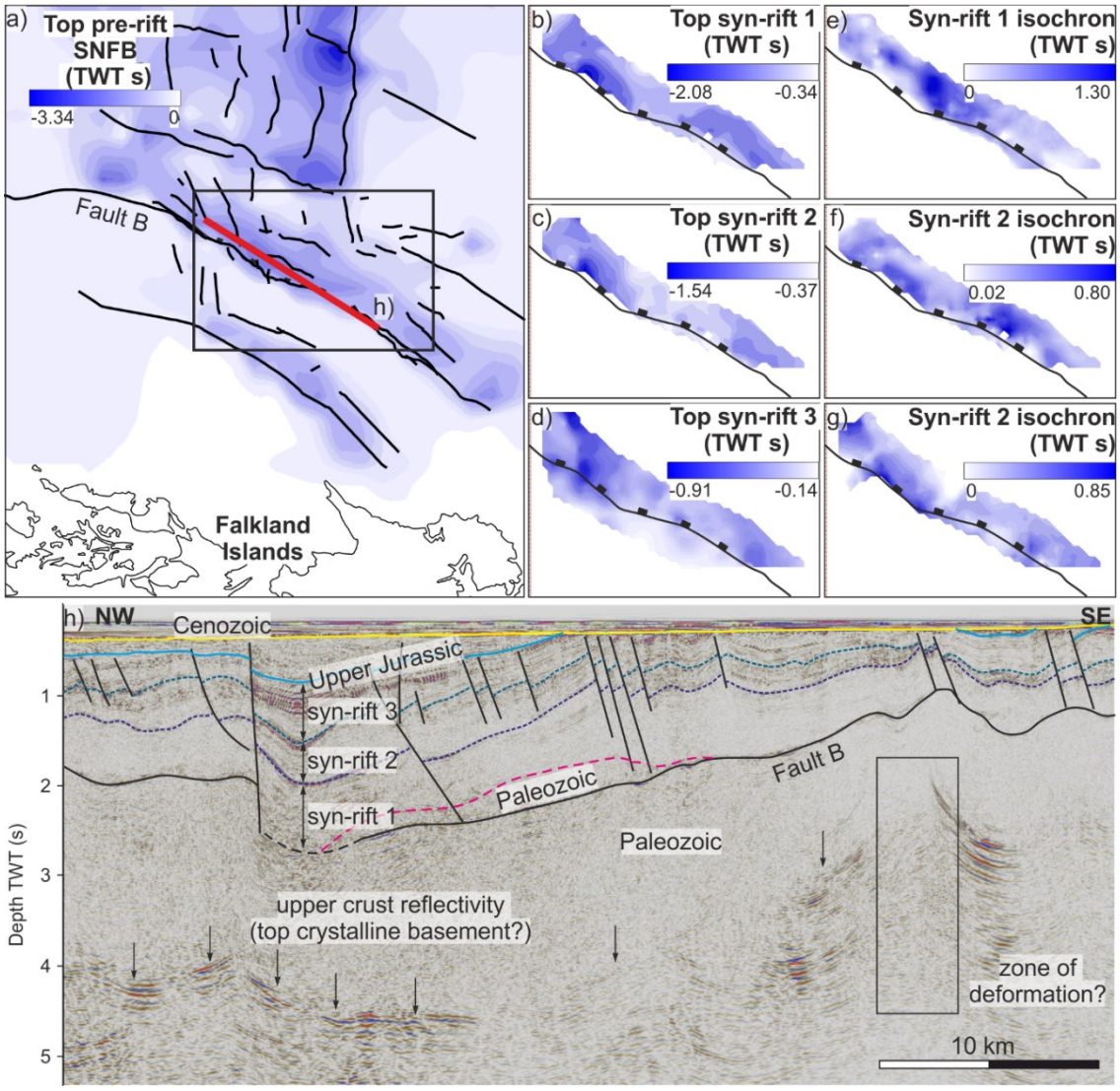

Figure 4.10 a) TWT map of the SNFB pre-rift; rectangle – extent of maps in (b) – (g); b) TWT map of the top syn-rift 1 showing main depocentres along the WNW-ESE segments of Fault B; c) TWT map of the top syn-rift 2 showing main depocentres along the WNW-ESE segments of Fault B; d) TWT map of top syn-rift 3 (top Upper Jurassic) showing main depocentre towards the centre of Fault B; e) syn-rift 1 isochron showing maximum thickness along an E-W trending segment of Fault B; f) syn-rift 2 isochron showing maximum thickness along WNW-ESE trending segments of Fault B; g) syn-rift 3 isochron showing maximum thickness in the central part of Fault B; h) section along the strike of Fault B showing the lateral variation in the syn-rift thicknesses

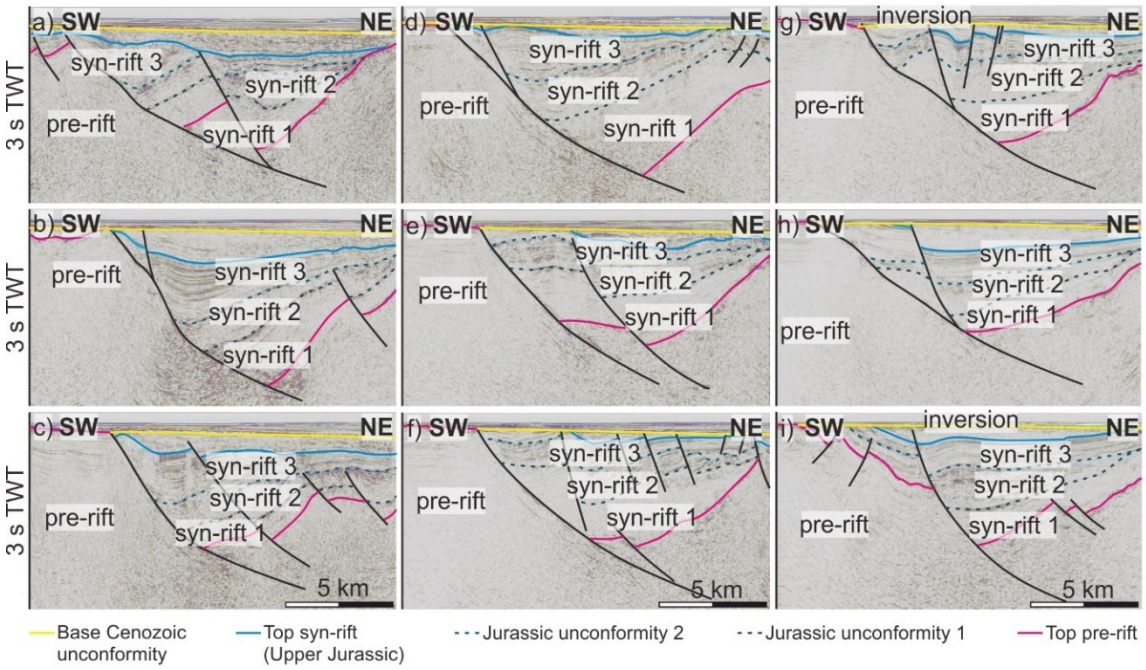

Figure 4.11 Compilation of seismic sections across Fault B from west (a) to east (i) showing how the geometry of the syn-rift package varies along the fault; position of the lines is shown in Figure 4.8

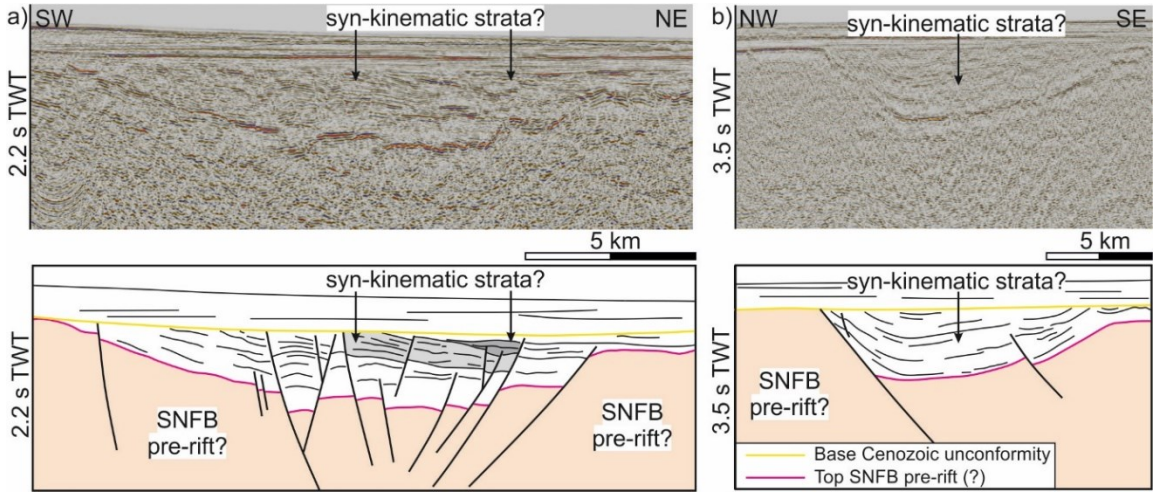

Figure 4.12 Sections across E-W trending features associated with (a) fracture zones generating structural lows and (b) half-grabens; sedimentary packages showing slight thickening into faults are shaded in grey; position of the lines is shown in Figure 4.8

The roughly E-W trending features mapped on the gravity data (Figure 4.6) correlate with depressions and fractured zones within the seismic reflection data (Figure 4.12). A high amplitude reflector correlated with the top SNFB pre-rift (Figure 4.12) can be mapped across these structures; the geometry of the strata overlying it shows a slight thickening south-westwards whereas further up the succession strata thicken north-eastwards (grey-shaded packages in

Figure 4.12a). The infill of these structural lows is unconformably overlain by Cenozoic deposits (Figure 4.12).

Across the SNFB a high-amplitude north-dipping set of reflectors was interpreted between -3.5 s and -8.2 s TWT (-8 to -20 km; Figure 4.13a, b, c). The ‘surface’ can be mapped out to ~100 km from the coastline where the imaging becomes poorer and/or its depth exceeds the maximum recorded length of the data. Towards the south, the interface is visible nearshore Stanley where it shallows both southwards and south-eastwards, disappearing around 51°42’S (Figure 4.8). This feature has been characterised as an interval of high amplitudes as it appears as a discrete interface only updip (Figure 4.13a). Further downdip, the area widens and becomes more convoluted, being characterised by an irregular top and the presence of lenticular features most likely generated through thrusting (Figures 4.13b, 4.14). East and NE of the islands another set of reflectors was picked between -11 s and -12 s TWT (Figure 4.13c, d); the two sets of reflectors seem to converge northeast of the Falkland Islands (Figure 4.13d, f).

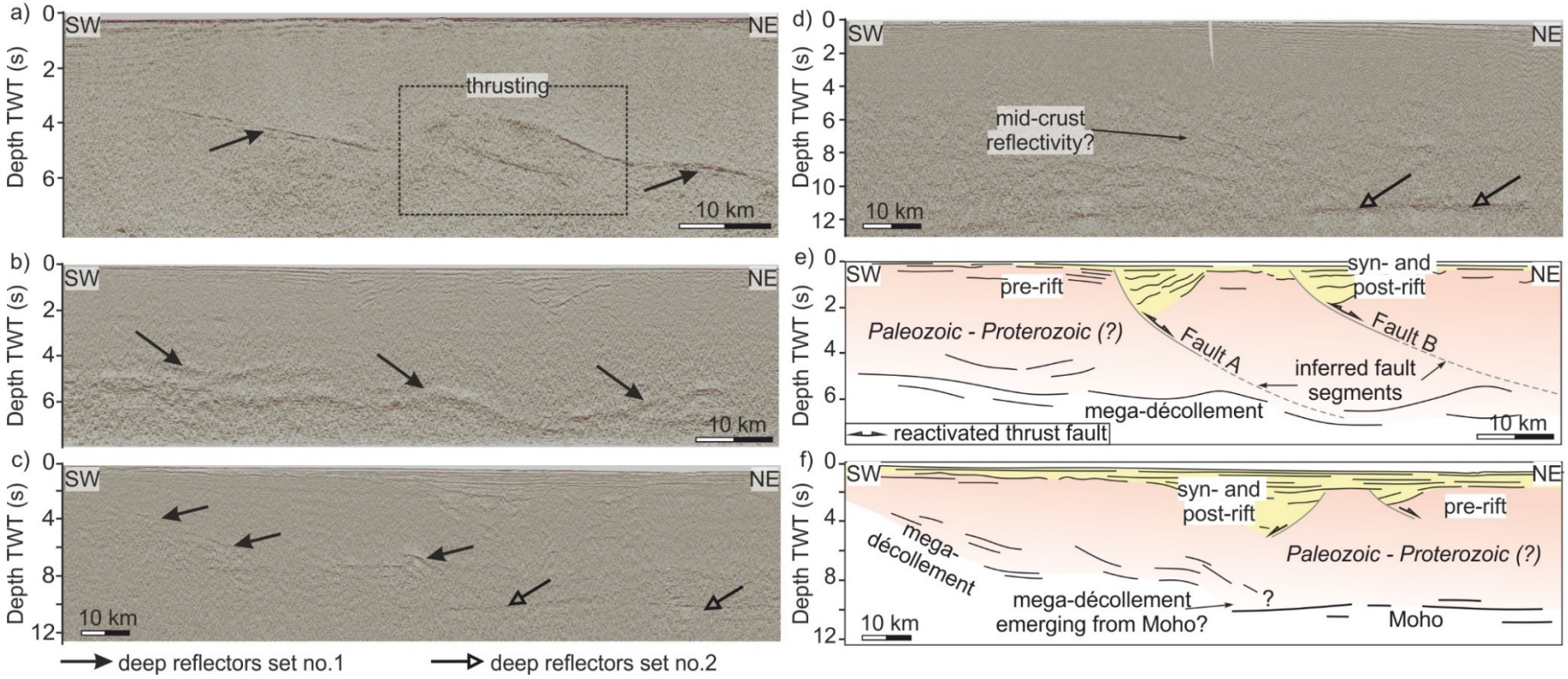

Figure 4.13 Seismic sections showing: (a), (b) the morphology of the shallower set of deep reflectors interpreted as a mega-décollement; (c), (d) the extent of the second set of deep reflectors correlated with Moho; (e) line drawing and interpretation of section in (b) showing the interaction between the reactivated thrust faults mapped across the SNFB and the mega-décollement along with their common sense of vergence; (f) line drawing and interpretation of section in (c) showing a potential merging between the mega-décollement and the Moho discontinuity; location of the profiles is shown in Figure 4.8

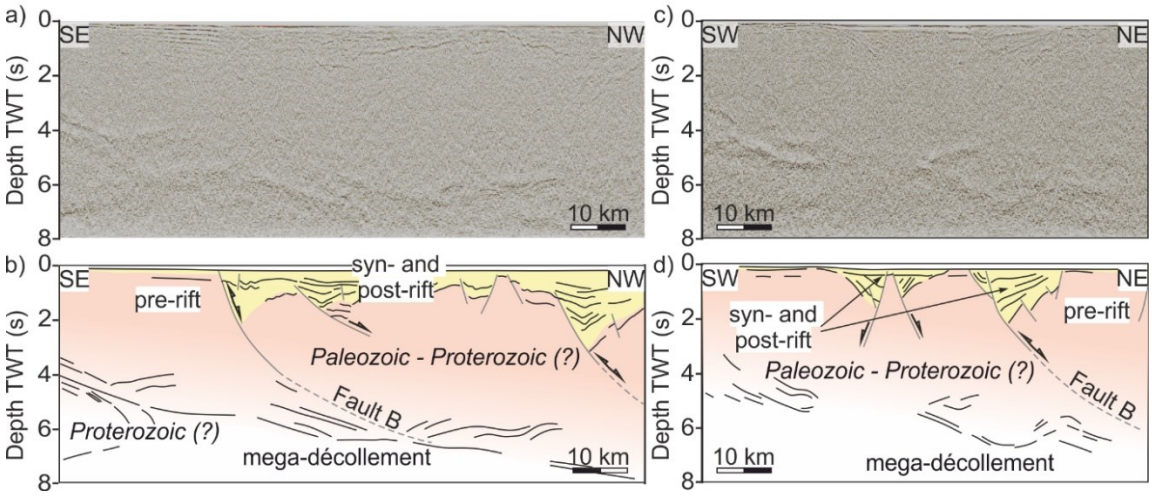

Figure 4.14 Seismic sections showing the morphology of the shallower set of deep reflectors interpreted as a mega-décollement (a, c) and their interpretation (b, d) emphasising the complex morphology of the mega-décollement; location of the profiles is shown in Figure 4.8

4.5 Discussion

4.5.1 SNFB fault geometry and formation

The NW-SE to WNW-ESE normal faults mapped in the SNFB have low dip angles, are downthrown predominantly to the NE, and have a similar orientation to the D4 thrust faults described onshore the Falkland Islands by Aldiss and Edwards (1999). This suggests that they exploited pre-existing thrust planes (Richards et al., 1996a) developed during the Gondwanide orogeny much like the faults on the southern margin of South Africa (Paton et al., 2006; Paton, 2006). However, unlike its conjugate (Paton et al., 2006), the faults in the SNFB do not show a consistent steepening away from the deformation front, their mean depth converted dips being in the 20°–40° range (Figure 4.15a). The south-westward steepening of the faults in the Outeniqua Basin has been recorded across a wide area of over 200 km, which is in direct contrast to the narrow extent of the analysed SNFB (~60 km). It is possible that this limited extent does not cover the deep rooted, higher angle faults and that these may underlie the northernmost part of the NFB.

The present-day preserved SNFB is therefore characteristic only of a narrow deformational domain. Its equivalent on the conjugate South African margin based on the range of dips could correspond to the transitional area between the thin-skinned and thick-skinned domains described by Paton et al. (2006), namely the area between the St. Croix Fault and the Gamtoos Fault (Figure 4.15).

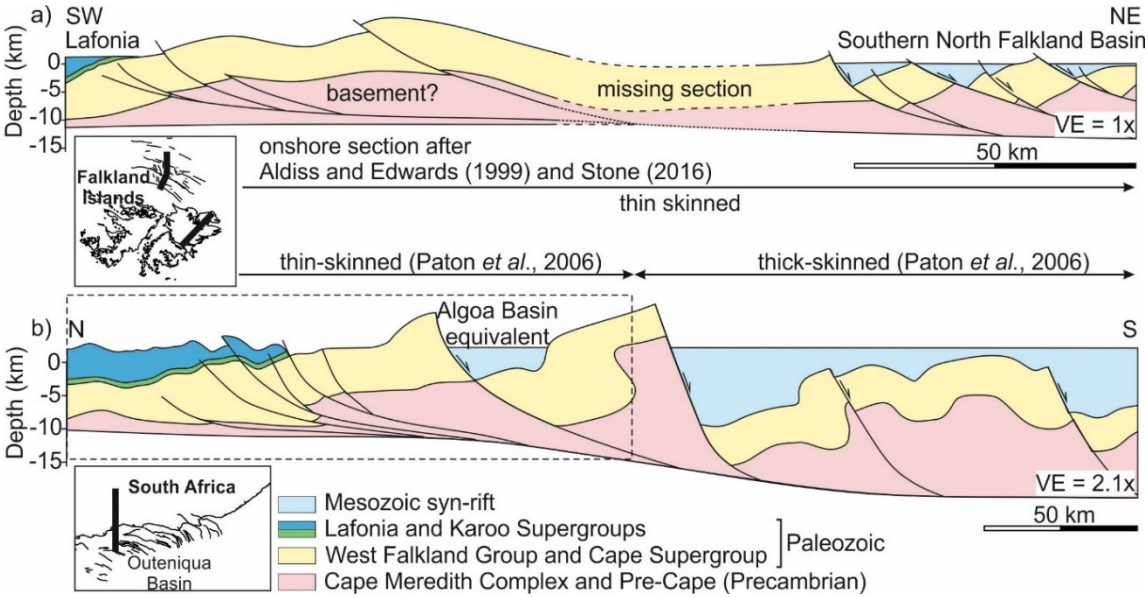

Figure 4.15 (a) Depth converted section across the SNFB extrapolated onshore based on published data from Aldiss and Edwards (1999) and Stone (2016); (b) section across the South African margin and its offshore basins showing the steepening of the faults south-westwards (after Paton et al., 2006); dashed rectangle shows the extent of the South African equivalent of the section in (a); both sections are restored to the top syn-rift

There are, however, basins along the South American margin (e.g. Cañadón Asfalto, San Jorge, El Tranquilo, San Julián, Río Mayo basins) that underwent rifting along the same NW-SE trend as the SNFB or have similar infills, suggesting a synchronous opening within the same stress field (Uliana et al., 1989; Brandsen et al., 1999; Ramos et al., 2017). The normal faults bounding the grabens and half grabens in these basins situated along strike from the SNFB are nonetheless steeply dipping (Fitzgerald et al., 1990; Soares et al., 2000; Echavarría et al., 2005) and point towards a different evolution prior to the Jurassic rifting.

The similarities in trend between the SNFB and the South American basins have been previously invoked as an argument for the rigid (non-rotational) model (Ramos et al., 2017), but this does not explain the origin of the crustal anisotropy beneath the Falkland Islands and its northern basin. The south-verging deformation documented by Von Gosen (2003) in the North Patagonian Massif was correlated with the accretion of Patagonia during Late Paleozoic (Ramos, 2008) and used to explain the present-day vergence of the Falkland Islands deformation front (Ramos et al., 2017). Evidence of south-verging thrusts can be seen up to 150 km away from the western coast of the Falkland Islands (Figure 4.13a; McCarthy et al., 2017), but there is however no

documentation of a south-verging fold and thrust belt further west to support a correlation with Patagonia. The opening of the SNFB due to the same stress regime as the one in the South American NW-SE trending basins is still a pertinent interpretation but does not preclude a rotation of the islands prior to this rifting event.

The ~E-W gravity lineaments mapped across the NFB (Figure 4.6) are associated with fractured zones interpreted as extensional or transtensional features (Figure 4.12). The timing of activity on these faults is difficult to constrain because some of these features are not covered by the available seismic data, their infill was partly eroded, and well data cannot be extrapolated across the fault shoulders. The changes in the location of the depocentre along Fault B (Figure 4.10), which suggests that different oriented segments of the fault were active at different times, could give an indication of the timing of formation of these E-W trending faults. The isochron maps of the three syn-rift packages along Fault B point towards a fault activity switching between E-W and more WNW-ESE oriented segments of the fault (Figure 4.10e-g). The concentration of deformation on an E-W trending segment during the deposition of syn-rift 1 (Figure 4.10e) could indicate that the local stress configuration was favourable for the formation of the E-W trending structures identified across the NFB at this time. Along these E-W trending structures, the geometry of the strata overlying the interpreted top SNFB pre-rift shows a slight thickness variation (grey-shaded packages in Figure 4.12) suggesting a diachronous activity of the faults bounding the structures. However, because of the lack of well data on the platform and scarcity of seismic reflection data the timing of activity on these faults along with the sense of movement (dip-slip, strike-slip) remains speculative.

The E-W trend of these lineaments changes to a more ENE – WSW orientation westwards (Figure 4.6). As this area is not constrained by seismic reflection data, the nature of these gravity lineaments remains unknown. Their formation can be simultaneous either with the event that generated the E-W trending features or with the Triassic – Late Jurassic opening of the San Julian Basin (Soares et al., 2000) where a NE – SW gravity trend is noticeable parallel to the eastern margin of the basin (Figure 4.6).

4.5.2 Mega-décollement

The north dipping high-amplitude interval mapped between -3.5 s and -8.2 s TWT (-8 to -20 km after depth conversion) is interpreted as a mega-décollement onto which the major faults bounding the three half-grabens of the

SNFB coalesce (Figures 4.13e–4.15a). Further south the interface can be mapped until 51°42'S.

Based on previous crustal studies carried out by Kimbell and Richards (2008) and Schimschal and Jokat (2017) on the Falkland Plateau, the Moho discontinuity is located at 34-36 km depth on the continental shelf east of the islands and shallows northwards to 30 km based on gravity modelling. Using the P-wave velocities published by Schimschal and Jokat (2017) for the continental shelf crust, the reflectors interpreted between 11 and 12 s TWT off the east coast of the Falkland Islands would be situated at a converted depth of 33-36 km; this led to a correlation of the reflectors with the Moho discontinuity (Figure 4.13f). Taking into account the present-day depth distribution of the Moho north of the Falkland Islands as shown by Kimbell and Richards (2008) and the dip of the mega-décollement, it can be deduced that the latter emerges from the Moho between 48°S and 50°S (present-day coordinates; double line in Figure 4.16).

The presence of a similar regional décollement dipping south has been inferred by Hälbich (1993) to be controlling the deformation in South Africa. Based on a deep seismic reflection profile along the Agulhas Bank (Dürrheim, 1987, [1] in Figure 4.16), the depth of this décollement would be -6.5 s or -18 km underneath the Outeniqua Basin (Hälbich, 1993), which is in the depth range estimated for the décollement under the SNFB. The interpretation of a more recent seismic reflection transect ([2] in Figure 4.16) acquired between Prince Albert and Slingersfontein (South Africa) shows the presence of a crustal interface that dips 3° southwards and separates the shallower thrusted sequence of the CFB and Karoo Basin from the Mesoproterozoic basement (Lindeque et al., 2011). Extrapolating this plane southwards, its estimated depth underneath the Agulhas Bank is ~20 km, which correlates it with the mega-décollement of Hälbich (1993). This depth variation of the mega-décollement was also proposed by Paton et al., (2006). The detachment is located underneath the Cape Supergroup in the southern part of the Karoo Basin (Lindeque et al., 2011) and is thought to displace Proterozoic deposits further south (Paton et al., 2006; Figure 4.15b).

The Moho for the South African margin shallows southwards from 50 km underneath the Karoo Basin to ~30 km near the coast and 25-26 km beneath the Agulhas Bank (Nguuri et al., 2001; Stankiewicz et al., 2008; Stankiewicz and de Wit, 2013). Taking into account the dip of the décollement (~3° based on Lindeque et al., 2011) and the present-day depth of the Moho offshore

South Africa, a merging of the decoupling plane with the Moho can be estimated to occur at ~35°S (dashed grey double line in Figure 4.16) which is in accordance with the interpretation of Hälbich (1993).

4.5.3 South African connections

Cross-sections across both the southern South African onshore to offshore margin and the Falkland Islands and their northern basin exhibit similar deformation styles (Figure 4.15). Given the uncertainty in the relative positions during the initial phases of rifting during the break-up of Gondwana, the terms foreland and hinterland will be used to refer to different parts of the cross-sections.

The foreland portion in both areas comprises Carboniferous to Permian deposits of the Karoo and Lafonia supergroups exposed onshore South Africa and Eastern Falkland, respectively (Figure 4.15). These are affected by open to isoclinal folds with symmetric to highly asymmetric limbs controlled at depth by thrusting (Aldiss and Edwards, 1999; Stone, 2016; Paton et al., 2006).

Towards the hinterland, thrusts active during the Cape orogeny underwent negative structural inversion during the Mesozoic rifting event. Closer to the CFB deformation front, the extension resulted in low angle (20°–40°) listric normal faults that bound half grabens filled with Upper Jurassic terrestrial to shallow marine deposits across the SNFB and the South African Algoa and Gamtoos Basins (Figure 4.15). Away from the deformation front, the normal faults accommodating the extension steepen (Figure 4.15b) and it has been proposed that these originated as normal faults during the Cape Supergroup deposition and were further exploited during the subsequent compressional and extensional regimes (Paton et al., 2006; Paton, 2006). These steeply dipping faults were not identified offshore the Falkland Islands. The E-W trending features mapped north of the SNFB and the subsequent opening of the North Falkland Graben are most likely overprinting their effect. On both margins, at depth, the deformation is controlled by the presence of a mega-décollement onto which the thrusts and normal faults coalesce (Figure 4.15).

4.5.4 Palaeogeographic implications

Existing palaeogeographic reconstructions of the Falkland Islands have associated drawbacks from the absence of a mechanism that explains the substantial rotation of the islands in the rotational model to the lack of continuation of a south verging fold and thrust belt east and west of the islands in the rigid (non-rotational) model.

Given the new observations in this study, the geometry of the normal faults bounding the SNFB half grabens could correspond to the deformation domain between the St. Croix and Gamtoos Faults, suggesting that the reactivated Paleozoic thrusts north of the Falkland Islands were an along strike continuation of the present-day Algoa Basin region. This translates in a change in trend of the Cape Fold Belt from WNW-ESE to NNW-SSE eastwards. This abrupt change in orientation is supported by the strike change of the St. Croix, Port Elizabeth, and Gamtoos faults (Figure 4.16), which has been referred to as the Port Elizabeth Antitaxis (Johnston, 2000). This strike variation has been related to the pre-existing crustal fabric developed during the Cape Orogeny rather than later movements along the AFFZ (Paton and Underhill, 2004). Similar oroclinal bends of the Ventana–CFB are seen in western South Africa and Argentina at the Cape and Colorado syntaxes, respectively (De Beer, 1992; Pángaro and Ramos, 2012; Paton et al., 2016). The rotation expected to affect the Falkland Islands Microplate would be ~140° in this scenario (~80° if the rotation occurring during the opening of the South Atlantic is subtracted (Mitchell et al., 1986)).

This repositioning of the Falkland Islands Microplate would mean that the points at which the mega-décollement branches off from the Moho are distributed along a trend similar to the trend of the CFB across the restored AFFZ (Figure 4.16) and has implications for the extension expected in the Falkland Plateau Basin.

The available data do not allow for latitudinal constraints in repositioning the microplate, the extent of the Falkland Plateau Basin fitted between the Eastern Falkland and the AFFZ remaining uncertain. However, the revised position predicts more unstretched crust between the microplate and the Maurice Ewing Bank block, which is thought to have originated south of the Tugela Cone (Marshall, 1994). Therefore, less extension is required in order to achieve the present-day relative position of the two continental blocks.

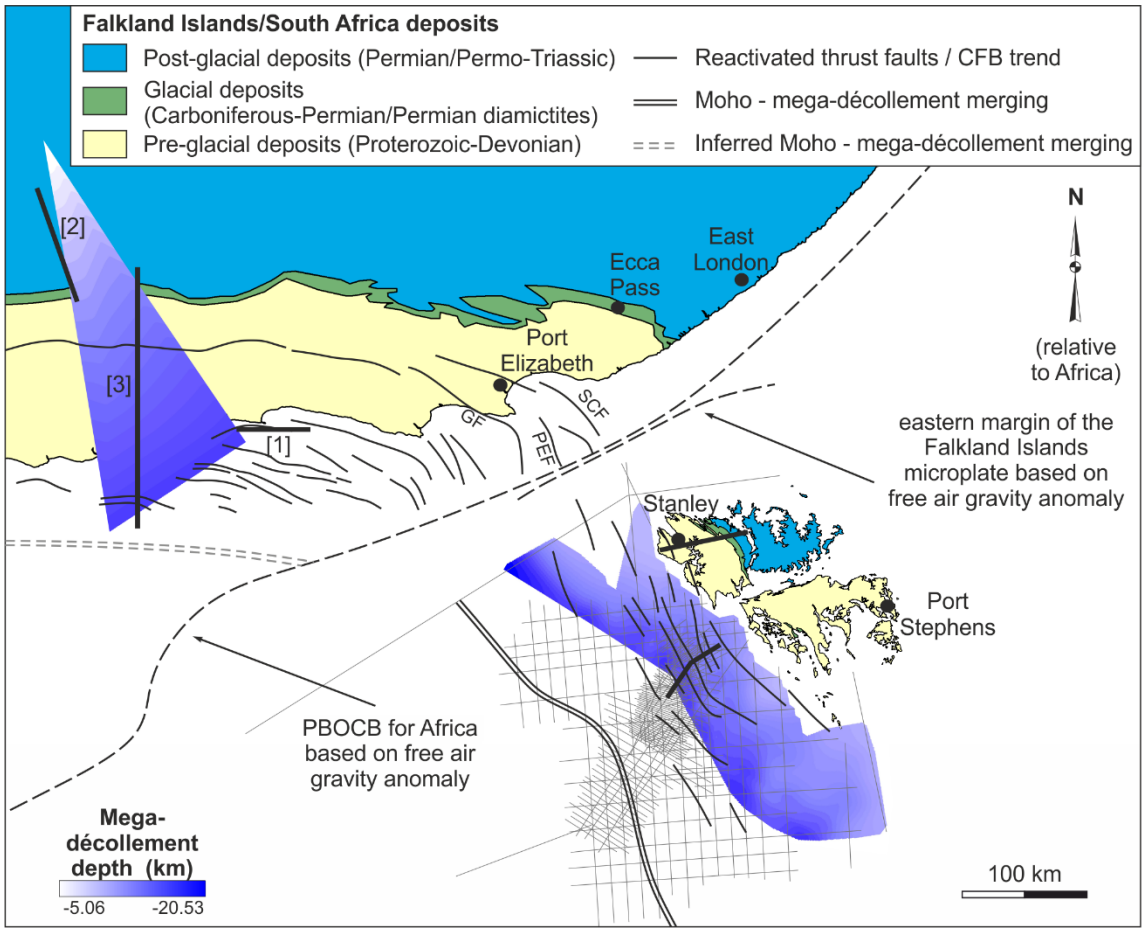

Figure 4.16 Revised position of the Falkland Islands Microplate at ~180 Ma; the depth of the mega-décollement in South Africa is constrained by two seismic lines: [1] (Dürrheim, 1987) and [2] (Lindeque et al., 2011) and extrapolated until it intersected Moho as modelled by Nguuri et al. (2001) and Stankiewicz and de Wit (2013); mega-décollement inferred on profile [3] (Paton et al., 2006) is used for comparison and validation; the mega-décollement underneath the SNFB was truncated at depths of 30-35 km (based on this study, Kimbell and Richards (2008), and Schimschal and Jokat (2017)); faults in the Outeniqua Basin are drawn based on Paton et al. (2006) and Parsiegla et al. (2009); GF – Gamtoos Fault, PEF – Port Elizabeth Fault, SCF – St. Croix Fault; faults in the SNFB are drawn based on the seismic reflection (grey lines) and gravity data available for this study; faults onshore Eastern Falkland are based on Aldiss and Edwards (1999); the position of the section in Figure 4.15a is shown onshore and offshore the Falkland Islands

Regarding the timing of rotation of the Falkland Islands Microplate, two scenarios are available based on the stress regime that led to the opening of the SNFB.

Considering a WSW-ENE extension direction during the opening of the SNFB similar to the Late Jurassic extensional episode inferred for the Gamtoos Basin

(Paton and Underhill, 2004), the SNFB/Falkland Islands Microplate should have been in a pre-rotation position in the Late Jurassic. Between the two rifting events that led to the formation of the SNFB and the North Falkland Graben, the microplate underwent a rapid clockwise rotation possibly exploiting the E-W to ENE-WSW lineaments described previously. Based on the detailed study carried out by Lohr and Underhill (2015) in the North Falkland Basin, the time interval between the two extensional episodes is ~10 Myr, although a longer time-frame is possible owing to the extensive Tithonian hiatus marking the end of the SNFB formation. A rotation rate of maximum 12° Myr^{-1} is estimated for this scenario for a rotation of 120° consistent with the existing rotational model. For the same time interval, the revised model yields a rotation rate of 8° Myr^{-1}. The latter is closer to the range of rates documented for strike-slip-related vertical-axis block rotations (Little and Roberts, 1997; Ingersoll and Coffey, 2017).

However, if the SNFB opened simultaneously with the NW-SE oriented basins along the South American margin (Uliana et al., 1989; Baristeas et al., 2013; Ramos et al., 2017), the Falkland Islands Microplate should have already been in the rotated position in Late Jurassic when the SNFB was undergoing rifting. Based on the Ar-Ar dating carried out on one of the NE-SW dykes onshore the Falkland Islands, the microplate is thought to have rotated after 178 Ma (Stone et al., 2008). This would limit the time interval for the rotation to Middle Jurassic which, is in accordance with the time frame suggested by Stone et al. (2008), giving rotation rates of ~8.2° Myr^{-1} and 5.5° Myr^{-1} for the 120° and 80° scenarios, respectively.

4.6 Conclusions

The North Falkland Basin was affected by two rifting episodes during the break-up of Gondwana, the older of which led to the formation of the Southern North Falkland Basin. This study reveals that the Paleozoic thrusts exploited during the opening of this basin emerge from a north-dipping mega-décollement, much like the faults in the Outeniqua Basin, offshore South Africa, which coalesce on a south-dipping mega-décollement. Based on the range of fault dips in the SNFB and the inferred latitude at which the mega-décollement merges with the Moho, a repositioning of the Falkland Islands Microplate is proposed so that the SNFB sat along-strike from the Algoa Basin prior to the break-up of Gondwana. The implications of the revised position of the islands are threefold: (1) the position is in agreement with the presence of an antitaxis

of the Cape Fold Belt at Port Elizabeth; (2) the amount of extension expected to have affected the Falkland Plateau Basin is reduced compared to previous rotational models; (3) the amount of rotation and the estimated rotation rate of the Falkland Islands Microplate are reduced, the latter being now comparable to block rotation rates in strike-slip systems.

The orientation of the extensional regime that led to the opening of the SNFB can be either WSW-ENE and related to the separation between South America and Africa or NW-SE rifting related to the southward movement of Antarctica or back-arc extension. Based on these two scenarios, the timing of rotation is restricted to Tithonian–Berriasian or Middle Jurassic, respectively.

Chapter 5 The tectono-stratigraphic architecture of the Falkland Plateau Basin; implications for the evolution of the Falkland Islands Microplate

Summary

Commonly, intra-continental wrenching is associated with a high degree of crustal faulting and fragmentation. The resulting continental blocks can undergo vertical-axis rotations, which in turn can lead to the generation of intricate fault networks within and along their boundary regions. Investigations into these structural complexities can support understanding of when and how these continental blocks rotate, and what their position was prior to transform margin formation. In the case of the Falkland Islands Microplate (part of the Falkland Plateau transform margin), its position between South Africa, South America, and East Antarctica prior to the break-up of Gondwana is still debatable. This uncertainty affects the reliability of plate models for this region. In this chapter, an integration of gravity and 2D and 3D seismic reflection data from the eastern (west side of the Falkland Plateau Basin) and western margins of the microplate is used to provide insights into the tectono-stratigraphic architecture of this area from Jurassic onwards, and into the evolution of the Falkland Islands Microplate. The results provide evidence of a potential western boundary of the microplate. Furthermore, the findings show that the western part of the Falkland Plateau Basin is an integral part of the microplate, and it underwent deformation in a relatively fast-changing stress regime. Stress field configuration estimates across the Falkland Islands Microplate support an alternation between a NE-SW and NW-SE/WNW-ESE orientation of σ_3 during the Jurassic and an ENE-WSW oriented σ_3 during the Early Cretaceous. Correlations of this local stress configuration with the regional stress support a Middle to Late Jurassic rotation of the microplate in a predominantly extensional setting facilitated by the early fragmentation of south-western Gondwana.

5.1 Introduction

Typically, intra-continental wrenching is associated with high degrees of crustal fragmentation and rotations of the resulting crustal and lithospheric blocks (Scrutton, 1979; Mascle et al., 1987; Nemcok et al., 2016; Ingersoll and Coffey, 2017). This leads to structurally complex isolated blocks where smaller, secondary fault systems within and along their boundaries accommodate relatively large rotations (Ron et al., 1984; McKenzie and Jackson, 1986; Peacock et al., 1998; Platt and Becker, 2013). The analysis of these fault networks can offer more insights into the temporal variation in the stress regime that affected the blocks, which can be used to aid reconstruction models. The Falkland Islands Microplate (FIM) is an example of an isolated block formed in an intra-continental wrenching setting. The FIM is part of the larger Falkland Plateau transform margin that underwent intense deformation during the fragmentation of Gondwana and the opening of the South Atlantic in the Mesozoic due to wrenching between East and West Gondwana, and South America and Africa (Rabinowitz and Labrecque, 1979; Lorenzo and Mutter, 1988; Platt and Philip, 1995; Richards et al., 1996a, b; Richards and Fannin, 1997; Bry et al., 2004; Del Ben and Mallardi, 2004; König and Jokat, 2006; Kimbell and Richards, 2008; Baristeas et al., 2013; Lohr and Underhill, 2015; Schimschal and Jokat, 2017, 2019a, b).

Extensive work has been undertaken looking at the deformation affecting the FIM, which resulted in onshore to offshore fault network compilations and crustal architecture models (Ludwig et al., 1978; Lorenzo and Mutter, 1988; Platt and Philip, 1995; Richards et al., 1996a; Richards and Fannin, 1997; Thomson, 1998; Curtis and Hyam, 1998; Aldiss and Edwards, 1999; Bry et al., 2004; Del Ben and Mallardi, 2004; Kimbell and Richards, 2008; Schreider et al., 2011; Baristeas et al., 2013; Lohr and Underhill, 2015; Schimschal and Jokat, 2019b). However, no detailed structural analysis has been published for the eastern boundary of the FIM (the western margin of the Falkland Plateau Basin). Furthermore, the location of the western boundary of the microplate remains uncertain (Marshall, 1994; Storey et al., 1999). This scarcity of information hinders attempts to generate a reliable reconstruction model for the microplate and the entire plateau.

This chapter aims to document the western part of the Falkland Plateau Basin, and its constituent depocentres: the Volunteer and Fitzroy sub-basins. Their present-day tectono-stratigraphy reflects the complexities of transform margins and was in addition influenced by the development of the plateau between

South America, Africa, and East Antarctica. The chapter focuses on the area that would have sat between the Falkland Islands and South Africa in a rotational reconstruction model (Adie, 1952a; Mitchell et al., 1986; Marshall, 1994; Curtis and Hyam, 1998; Thomson, 1998; Trewin et al., 2002; Stanca et al., 2019) by assessing the fault network and stratigraphic architecture of this region. The findings are integrated with data from the western boundary of the FIM which facilitates the delimitation of the FIM and the analysis of the nature of the deformation that occurs within and around the margins of a rotated microplate. Furthermore, the results are discussed in the context of south-western Gondwana by comparing the local and regional stress regimes.

5.2 Geological background

5.2.1 Overview of the Falkland Plateau

The Falkland Plateau (FP) is located east of Argentina, extending eastward ~2000 km away from the Argentinian coast. It is bounded to the north by the dextral Agulhas - Falkland Fracture Zone (AFFZ) and to the south by the North Scotia Ridge (NSR) (Ludwig, 1983; Richards et al., 1996b) (Figure 5.1). The formation of the FP was associated with the break-up of Gondwana (Lorenzo and Mutter, 1988; Macdonald et al., 2003) and the opening of the Atlantic Ocean in the Mesozoic (Late Triassic – Late Cretaceous; Uliana et al., 1989; Heine et al., 2013) and was subsequently affected by oblique compression and transpression related to sinistral strike-slip movement during the development of the NSR (Cunningham et al., 1998; Eagles, 2000; Bry et al., 2004). The behaviour of the FP during the break-up remains controversial. Correlations between geological and geophysical data from the Falkland Islands and South Africa led to the development of the rotational theory which argues that the formation of the FP was accompanied by up to 120° rotation of the Falkland Islands (Adie, 1952a; Mitchell et al., 1986; Marshall, 1994; Mussett and Taylor, 1994; Thomson, 1998; Curtis and Hyam, 1998; Storey et al., 1999; Trewin et al., 2002; Macdonald et al., 2003; Stone et al., 2009; Stanca et al., 2019). The lack of documented evidence for this rotation in the sedimentary infill of the basins surrounding the islands (Richards et al., 1996a), and the absence of a mechanism to accommodate this rotation led several authors to favour a non-rotational model. In this model, the Falkland Islands were in a similar position relative to South America prior to the break-up of Gondwana as today (Lawrence et al., 1999; Ramos et al., 2017; Lovecchio et al., 2019; Eagles and

Eisermann, 2020), and the fragmentation of the supercontinent was recorded by extension in the sedimentary basins around the islands.

Regardless of the movement of the Falkland Islands, the fragmentation of Gondwana and the initial rifting in the South Atlantic resulted in a series of structural and crustal provinces along the FP. These are, from west to east: the Malvinas Basin, the Falkland Islands (FI) with the North Falkland Basin to the north and the South Falkland Basin to the south, the Falkland Plateau Basin (FPB), and the Maurice Ewing Bank (Figure 5.1). The North Falkland Basin is further subdivided in the Jurassic Southern North Falkland Basin (SNFB) and the Late Jurassic - Early Cretaceous North Falkland Graben (Lohr and Underhill, 2015; Stanca et al., 2019). The FPB consists of the Volunteer sub-basin to the north-west and the Fitzroy sub-basin in the west and south-west, the two being separated by the Berkeley Arch basement high (Rockhopper Exploration Plc., 2012; Dodd and McCarthy, 2016; Figure 5.1).

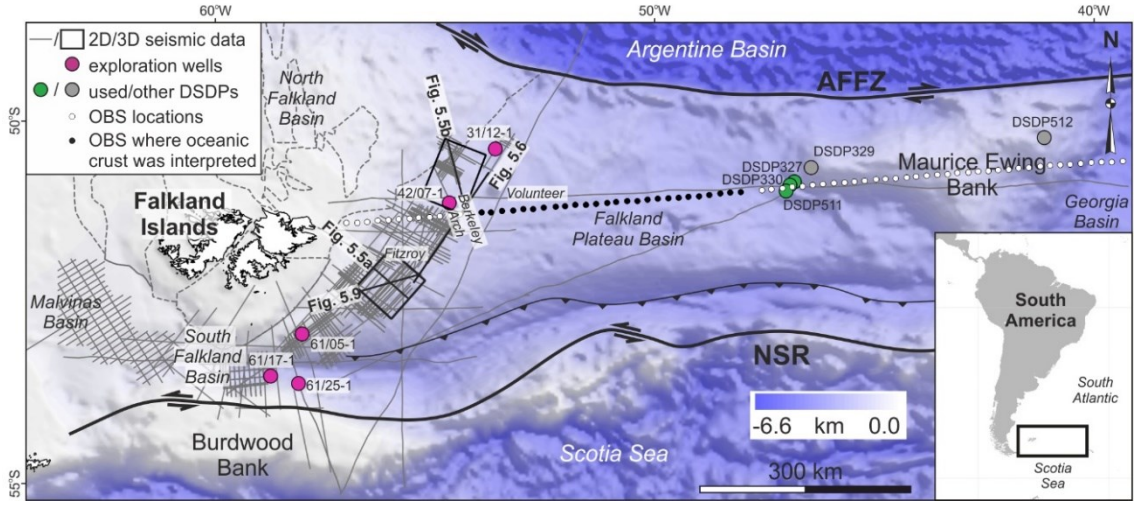

Figure 5.1 Bathymetric map (GEBCO Compilation Group, 2020) of the Falkland Plateau (FP), overlain by the seismic reflection, exploration well, and Deep Sea Drilling Project (DSDP) data utilised in this chapter; the map shows the FP constituent basins (grey, dashed lines) and the regional structures bounding it (dextral and sinistral Agulhas – Falkland Fracture Zone and North Scotia Ridge, respectively, and the thrust front of the North Scotia Ridge); ocean bottom seismometer (OBS) position from Schimschal and Jokat (2019b); AFFZ – Agulhas-Falkland Fracture Zone; NSR – North Scotia Ridge

5.2.2 Architecture of the Falkland Plateau Basin

5.2.2.1 Structure

The distribution of crustal types under the FPB is still uncertain. The Falkland Islands and the Maurice Ewing Bank were part of a continuous block, as

suggested by geochemical and isotopic analyses of their basement lithologies (Thomas et al., 2000; Chemale et al., 2018), which underwent extension and/or potential break-up during the fragmentation of Gondwana (Chemale et al., 2018). Gravity modelling studies (Richards et al., 1996a; Kimbell and Richards, 2008) and the interpretation of seismic reflection and refraction data (Ludwig, 1983; Lorenzo and Mutter, 1988) show that the resulting basin is underlain by either thick oceanic crust or thinned and underplated continental crust. Recent studies have revealed more evidence on the presence of oceanic crust in the FPB (Schimschal and Jokat, 2017, 2019b; Eagles and Eisermann, 2020) but the extent of the oceanic domain remains uncertain. The results of the refraction study of Schimschal and Jokat (2017, 2019b) show the presence of high P-wave velocities indicative of oceanic crust along an E-W trending profile across the FPB (Figure 5.1), but with no constraints on the N-S extent of this potential oceanic domain. Similarly, Eagles and Eisermann (2020) present a crustal model of the FPB based on newly-acquired magnetic data where the entire FPB, with the exception of the AFFZ-adjacent area, is interpreted as oceanic or igneous crust. However, magnetic reversal isochrons indicative of typical oceanic crust are present only in the south-eastern part of the basin (Eagles and Eisermann, 2020).

The FPB is bounded to the west by NE-SW trending normal faults that down-throw to the south-east (Richards et al., 1996a, b), and to the east by the Maurice Ewing Bank. Most of the normal faults interpreted from seismic reflection data along the basin terminate at the top Jurassic (Lorenzo and Mutter, 1988). Rifting within the FPB was interpreted to have occurred either between Middle Jurassic and Early Cretaceous (Lorenzo and Mutter, 1988), during the Early Jurassic (Marshall, 1994; Richards et al., 1996a), or during the late Middle Jurassic (Ben-Avraham et al., 1993), although some authors argue for an earlier onset of rifting during the Permo-Triassic (Richards et al., 1996a). No wells penetrated the oldest syn-rift deposits, rendering the timing of rifting initiation speculative.

5.2.2.2 Stratigraphy

Gravity modelling and seismic reflection and refraction data interpretation revealed the presence of an up to 12 km thick sediment infill in the FPB (Richards et al., 1996a; Schimschal and Jokat, 2017). This sedimentary succession is constrained by well data on the western part of Maurice Ewing Bank (DSDP sites 327, 330, 511, 329, and 512) and east of the Falkland Islands (61/05-1, 31/12-1) (Figures 5.1 and 5.2). The remaining part of the

basin fill is interpreted on the basis of seismic facies analysis (Ludwig et al., 1983; Del Ben and Mallardi, 2004).

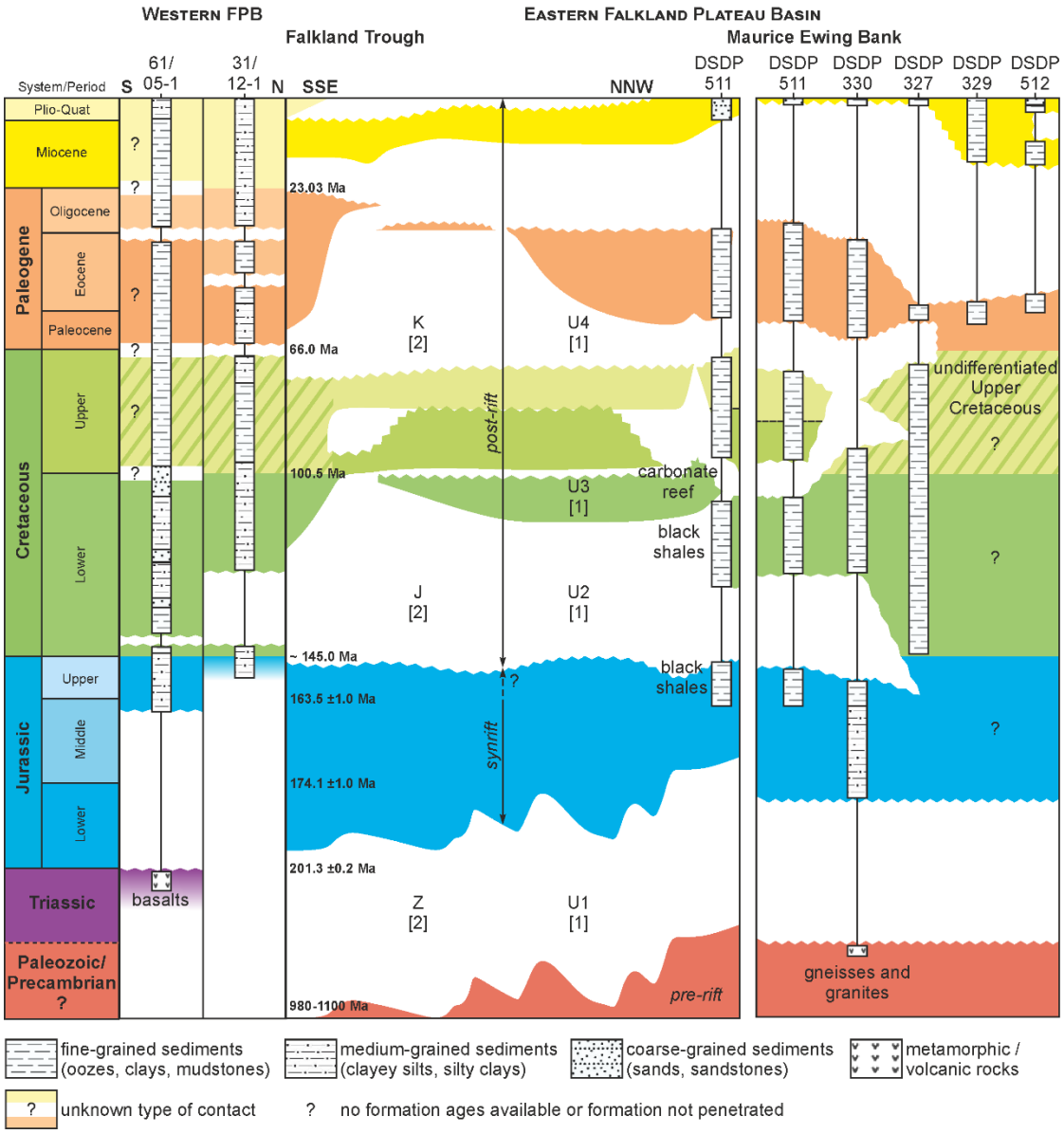

Figure 5.2 Chronostratigraphic diagram for the Falkland Plateau Basin based on well data (Western FPB), the interpretation of the seismic reflection profile I95167 from Del Ben and Mallardi (2004) (Eastern FPB), and DSDP information (Eastern FPB and Maurice Ewing Bank; Barker, 1977; Ludwig et al., 1980, 1983; Lorenzo and Mutter, 1988); main unconformities and nomenclature from [1] Lorenzo and Mutter (1988) and [2] Del Ben and Mallardi (2004); unconformities and formation ages along the Western FPB from BHP Billiton Petroleum (2010) and Falkland Oil and Gas Limited (2013); geometries of unconformities along the Eastern FPB redrawn after Del Ben and Mallardi (2004); correlation of unconformities along the Maurice Ewing Bank redrawn after Lorenzo and Mutter (1988); units are colour-coded to reflect their ages; FPB – Falkland Plateau Basin

The Middle to Upper Jurassic recorded a relative sea-level rise (Thompson, 1977) that accounted for the deposition of open shelf deposits rich in terrigenous material. Middle Jurassic to Oxfordian sandstones, siltstones, and claystones interbedded with limestones (Barker, 1977) are overlain by Middle Jurassic non-marine sandstones and siltstones with lignitic intervals (Thompson, 1977). From the end of the Jurassic and throughout the Early Cretaceous up to late Aptian time, claystones and mudstones rich in organic matter and interbedded with micritic limestone were deposited in a restricted basin environment (Barker, 1977; Thompson, 1977; Ludwig, 1983). The Albian, Late Cretaceous, and the Cenozoic were associated with open marine conditions (Thompson, 1977) and the deposition of pelagic carbonates, zeolitic oozes and clays, and chalk. Throughout the Cretaceous, the western margin of the basin recorded the deposition of deltaic sandstones and sand-rich deep marine fans intercalated with claystones (Richards et al., 1996b; BHP Billiton Petroleum, 2010; Falkland Oil and Gas Limited, 2013). Paleocene to Early Oligocene sediment drift deposits are interpreted in the Cenozoic succession (Lorenzo and Mutter, 1988; Del Ben and Mallardi, 2004) overlain by Pliocene to Recent gravels, siliceous sands, and foraminiferal oozes (Barker, 1977; Ludwig, 1983) (Figure 5.2).

Major uncertainty remains on the age of the oldest sediments in the FPB. DSDP 330 cored Middle Jurassic deposits resting on a Precambrian basement (Barker et al., 1977), but older sedimentary rocks are inferred from seismic velocities and gravity modelling with syn-rift deposition potentially starting in the Permo-Triassic (Richards et al., 1996a).

Several regional unconformities have been identified on seismic reflection data: a Tithonian to Early Cretaceous unconformity spanning 30 Myr (‘U2’ in Lorenzo and Mutter (1988) and ‘J’ in Del Ben and Mallardi (2004)), a Middle Cretaceous unconformity marked ‘U3’ in Lorenzo and Mutter (1988), and an unconformity at the Cretaceous/Cenozoic boundary (‘U4’ in Lorenzo and Mutter (1988) and ‘K’ in Del Ben and Mallardi (2004)) (Figure 5.2).

5.2.2.3 Volcanism

The break-up of SW Gondwana was associated with extensive volcanism and magmatism resulting in the formation of the widespread Karroo – Ferrar large igneous province (Encarnación et al., 1996; Macdonald et al., 2003). This event has been related to the emplacement of several dyke swarms identified onshore the Falkland Islands trending predominantly E-W and NE-SW although a higher variability in orientations has been observed across West Falkland

(Aldiss and Edwards, 1999; Mitchell et al., 1999; Stone et al., 2009; Hole et al., 2016; Stone, 2016). E-W and NE-SW trending dykes yielded K-Ar and Ar-Ar ages of 188 ± 2 to 190 ± 4 Ma and 162 ± 6 to 178.6 ± 4.9 Ma, respectively (Mussett and Taylor, 1994; Thistlewood et al., 1997; Stone et al., 2008; Stone et al., 2009), although a maximum age of 193 ± 4 Ma was also obtained for a NE-SW trending dyke (Mussett and Taylor, 1994). A N-S trending dyke swarm varying in age from 121 ± 1.2 Ma to 138 ± 4 Ma (Stone et al., 2008; Richards et al., 2013) has been related to the early opening of the South Atlantic (Stone et al., 2009; Stone, 2016). N-S trending dykes have also been interpreted nearshore the Falkland Islands on magnetic data (Barker, 1999).

Proof of volcanic activity has been invoked in the interpretation of seismic reflection data from the FPB in the form of volcanic edifices and dipping reflectors within the basement (Lorenzo and Mutter, 1988). The presence of the latter was supported by Barker (1999) and Schimschal and Jokat (2017) who correlated potential seaward-dipping reflector packages with velocities of over 4 km/s. Positive magnetic and gravity anomalies along the western margin of the FPB were also interpreted as being generated by basaltic flows and/or the presence of plutonic bodies (Richards et al., 1996a; Barker, 1999) whereas seismic reflection data revealed the presence of sills intruded in the FPB sediment pile and interpreted as Early Cretaceous in age (Richards et al., 2013).

5.2.3 Falkland Islands Microplate – current reconstruction models

The evolution and overall structure of the FPB is strongly correlated with the behaviour of the Falkland Islands during the fragmentation of Gondwana. Similarly, the pre-break-up structural grain of the Falkland Islands Microplate was inherited from the Permo-Triassic Gondwanide orogeny, which resulted in WNW-ESE trending folds and thrusts and NE-SW trending folds related to NNE-SSW compression and NE-SW dextral transpression, respectively (Curtis and Hyam, 1998; Aldiss and Edwards, 1999; Hodgkinson, 2002).

Stratigraphic and structural correlations between the Falkland Islands and South Africa along with fossil assemblages, Late Paleozoic ice flow directions, and palaeomagnetic data analysis have been used to reconstruct a rotated position of the islands in a Gondwana pre-break-up configuration. The angle of rotation between the pre-Jurassic and current day position has been estimated between ~80° and 120°, with an additional ~60° occurring during the opening of the South Atlantic (Adie, 1952a; Mitchell et al., 1986; Marshall, 1994; Mussett and Taylor, 1994; Curtis and Hyam, 1998; Trewin et al., 2002; Stone et al.,

2009; Stanca et al., 2019; Figure 5.3). This scenario positions the Falkland Islands off the south-east coast of South Africa, with the basement cropping out onshore the islands representing a fragment of the Namaqua-Natal-Maud belt extending across South Africa and East Antarctica (Thomas et al., 1997; Jacobs et al., 1999; Jacobs et al., 2003; Jacobs and Thomas, 2004; Vorster et al., 2016). A separation between the East and West Falkland reconstruction has been interpreted along the Falkland Sound Fault which has been inferred to run between the two main islands (Figure 5.4a; Thomas et al., 1997). However, the sense of movement, displacement, and timing of activity along this major structure has been difficult to constrain (Marshall, 1994; Richards et al., 1996; Thomas et al., 1997; Curtis and Hyam, 1998; Aldiss and Edwards, 1999).

The rotated reconstruction requires a fragmentation of the FP so that the islands are part of a separate microplate (the FIM) that underwent isolated clockwise vertical-axis rotation. Definition of FIM boundaries is still subject to debate. The microplate is considered to continue north all the way up to the Agulhas-Falkland Fracture Zone by some authors (Marshall, 1994) whereas others put the boundary further south, along the gravity positive anomaly corresponding to the Southern North Falkland Basin (Storey et al., 1999; Figure 5.4b, c). Its western extent is interpreted to be marked by the arcuate positive gravity anomaly along the edge of the Malvinas Basin (Figure 5.4a-c) which corresponds in the northern part with a high-velocity ridge (Ludwig et al., 1968). This ridge was associated with a potential tectonic boundary between the Falkland Plateau and Patagonia (Marshall, 1994). The eastern boundary is thought to coincide with the NE-SW trending positive gravity anomaly (Storey et al., 1999; Figure 5.4a-c). The minimum southern extent corresponds to the NSR (Figures 5.1 and 5.4b, c).

Studies favouring the rotation of the Falkland Islands argue for a more northern position of the islands relative to South Africa (Figure 5.3). This would require significant displacement along a right-lateral fault between Patagonia and the remainder of the South American plate (Rapela and Pankhurst, 1992; Ben-Avraham et al., 1993) which has been challenged by subsequent studies (von Gosen and Loske, 2004; Franzese and Martino, 1998 in Ramos et al., 2017). More recent global and South Atlantic reconstructions achieve a closer fit between Patagonia (and the islands) and South Africa by taking into account intra-plate deformation of South America during the fragmentation of Gondwana (Heine et al., 2013; Müller et al., 2019).

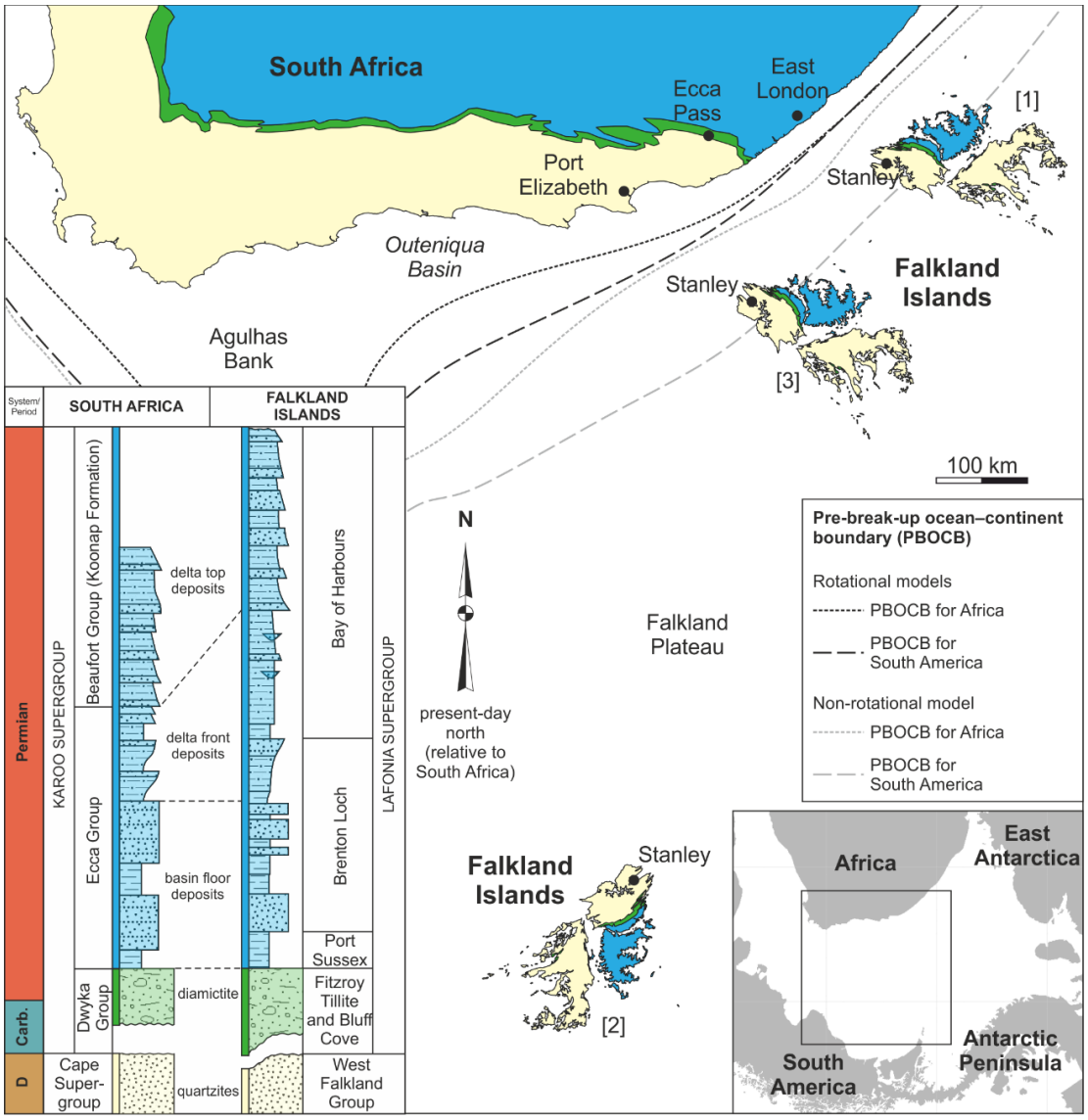

Figure 5.3 Jurassic rotational ([1] and [3]) and non-rotational ([2]) reconstruction models of the Falkland Islands after [1] Trewin et al. (2002), [2] Ramos (2008), and [3] Chapter 4 and Stanca et al. (2019); the stratigraphy and correlation between the Falkland Islands and South African onshore sedimentary deposits is based on Trewin et al. (2002); the PBOCB for the rotational models is based on gravity data and drawn after Lawver et al. (1999) and Macdonald et al. (2003); the PBOCB for the non-rotational model is based on seismic and bathymetric data and drawn after Martin et al. (1981); inset in bottom, right corner shows the south-western configuration of Gondwana after Müller et al. (2019) with Africa fixed in its present-day position

The lack of documented deformation in the sedimentary basin-fills offshore the islands (Richards et al., 1996a) that would support the rotation, along with the absence of a mechanism for it occurring at the FIM scale, led to several authors favouring a non-rotational evolution model. In this model, the Falkland

Islands remain fixed to the South American plate (Figure 5.3) throughout the Mesozoic, and the present-day morphology of the FP is either the result of extension coeval with the opening of the South Atlantic (Lawrence et al., 1999; Ramos et al., 2017; Lovecchio et al., 2019; Schimschal and Jokat, 2019b) or the plateau represents the conjugate to the Weddell Sea and undergoes extension related to the break-up and drift of the Antarctic plates (Eagles and Vaughan, 2009; Eagles and Eisermann, 2020). Arguments supporting these models are based on stratigraphic and structural correlations carried between the Falkland Islands and Patagonia (Lawrence et al., 1999; Ramos et al., 2017; Chemale et al., 2018; Lovecchio et al., 2019) and magnetic reversal isochrons and magnetic anomaly correlations between the FP on one side, and the Central Scotia Sea and the Weddell Sea on the other side (Eagles and Eisermann, 2020).

5.3 Data and methodology

5.3.1 Gravity data – availability and interpretation

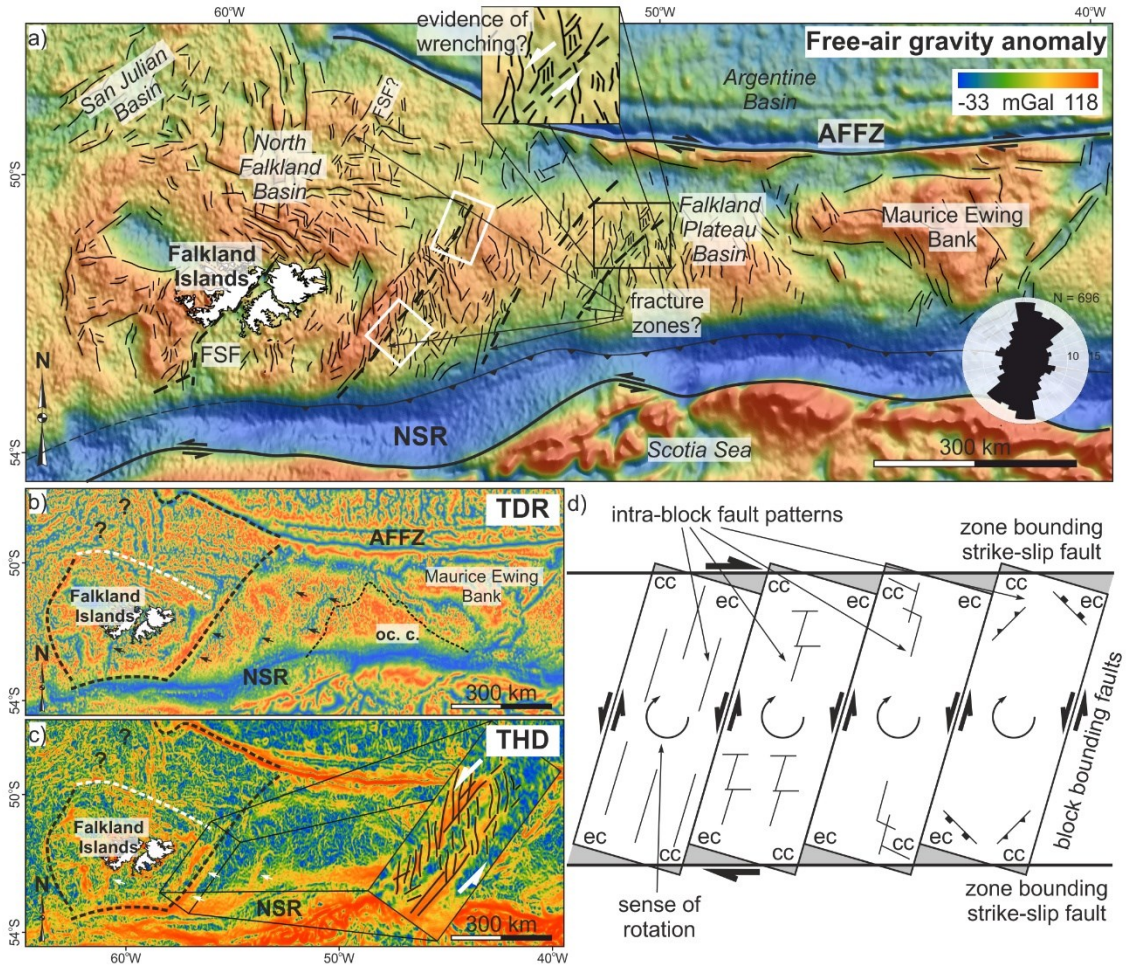

Figure 5.4 See next page for caption

Figure 5.4 a) Free air gravity anomaly (Sandwell et al., 2014) across the Falkland Plateau along with gravity lineaments showing the variation in structural grain; stippled black lines - potential intra-plate fracture zones accommodating the rotation of the FIM; an area-weighted rose diagram of the mapped features is also shown; white rectangles – seismic cubes; b) tilt derivative (TDR); black arrows - potential regional fracture zones; c) total horizontal derivative (THD); white arrows - potential regional fracture zones; inset showing the structural grain along the western margin of the Falkland Plateau Basin; black, thick stippled lines in (b) and (c) mark the potential boundaries of the FIM, white stippled line marks an alternative northern boundary of the FIM after Storey et al. (1999) and black question marks show uncertainties in the location of the western FIM boundary; thin stippled lines in (b) mark the extent of magnetic reversal isochrons from Eagles and Eisermann (2020) (oc. c. – oceanic crust); d) map-view of potential intra-block fault networks accommodating block rotation after Peacock et al. (1998); grey areas mark the regions gained and lost during block rotation assuming an original rectangular shape of the blocks; the change in shape is accommodated through intra-block faulting; potential fault patterns that may occur are drawn after Peacock et al. (1998) and are, from left to right: one fault network consisting of faults parallel to the block bounding faults, two fault networks parallel to the block and zone bounding faults, conjugate strike-slip faults in the corners where compression is expected, thrusts and normal faults occurring in the contractional (cc) and extensional (ec) corners, respectively; deformation exhibits a fractal behaviour and block widths vary between 10 mm and 100 km in the model of Peacock et al. (1998); AFFZ - Agulhas-Falkland Fracture Zone; NSR – North Scotia Ridge; FSF – Falkland Sound Fault

The gravity data consist of the V24.1 1-minute satellite altimetry free-air gravity anomaly grid of Sandwell et al. (2014) for the entire FP. Total horizontal (Cordell and Grauch, 1985) and tilt derivatives (Miller and Singh, 1994; Verduzco et al., 2004; Oruç and Keskinsezer, 2008) were computed using Geosoft's Oasis Montaj software and used to map gravity lineaments across the entire FP (Figure 5.4). The nature of the interpreted structures was constrained using seismic reflection data.

5.3.2 Seismic reflection data – availability and interpretation

The seismic reflection data comprise 2D and 3D survey data (courtesy of the Falkland Islands Government) from seven vintages acquired between 1977 and 2014 by Falklands Oil and Gas Limited, WesternGeco, Noble Energy, Lamont-Doherty Earth Observatory, and Geophysical Service Incorporated (GSI) (Figure 5.1). The Falkland Oil and Gas Limited 2D survey from 2007 was the main 2D dataset used for the interpretation due to its resolution and coverage

of the western margin of the FPB. It consists of 154 lines with variable spacing on a grid predominantly orientated parallel (NE-SW to ENE-WSW) and sub-perpendicular (WNW-ESE to NNW-SSE) to the shelf (Figure 5.1). The record length of this survey is 8 s TWT, with shot and receiver spacing of 25 m and 12.5 m, respectively. The coverage of this dataset was complemented by 22 lines from the 1993 WesternGeco survey (reprocessed in 2003). These have a record length of 9 s TWT and a shot and receiver spacing of 40 m and 10 m, respectively. Two 3D seismic cubes (FINA along the Berkeley Arch and Volunteer sub-basin and FISA in the Fitzroy sub-basin) aided with the interpretation of smaller scale faults and with the assessments of the 3D distribution of these fault networks and of the magmatic plumbing. The FINA and FISA cubes cover areas of ~5750 km^2 and ~5500 km^2, respectively, and have record lengths of ~9 s TWT. Older regional surveys (two lines from the RC2106 1978 Lamont-Doherty Earth Observatory survey, one line from the 1978 GSI survey, and four lines from the 1977 Western survey) were used for correlations between the western margin of the FPB and the DSDPs on the eastern side. These have record lengths between 4 and 12 s TWT and a poorer data quality compared to the more recent surveys but provided regional information about the basement geometries and the main stratigraphic packages. Five wells (31/12-1, 42/07-1, 61/05-1, 61/17-1, and 61/25-1) and three DSDPs (327, 330, and 511) were tied to the seismic reflection data for the horizon interpretation stage.

Four horizons were mapped across the Fitzroy and Volunteer sub-basins (western part of the FPB) and associated with mega-sequences based on stratal terminations and internal geometries of seismic facies (Mitchum et al., 1977; Hubbard et al., 1985a, b). These horizons are: (1) the Upper Cretaceous Claystone and (2) Valanginian unconformity within the transitional to post-rift section, (3) near top Jurassic as the top syn-rift, and (4) near top Paleozoic as the top of the pre-rift sequence (Figure 5.5). Jurassic deposits were only penetrated by well 61/05-1 and DSDPs 330 and 511, reducing the reliability of correlation of Jurassic strata across the Berkeley Arch and into the Volunteer sub-basin. Volcanic rocks of Triassic (?) age were penetrated by well 61/05-1 (Figure 5.2) but their extent remains uncertain.

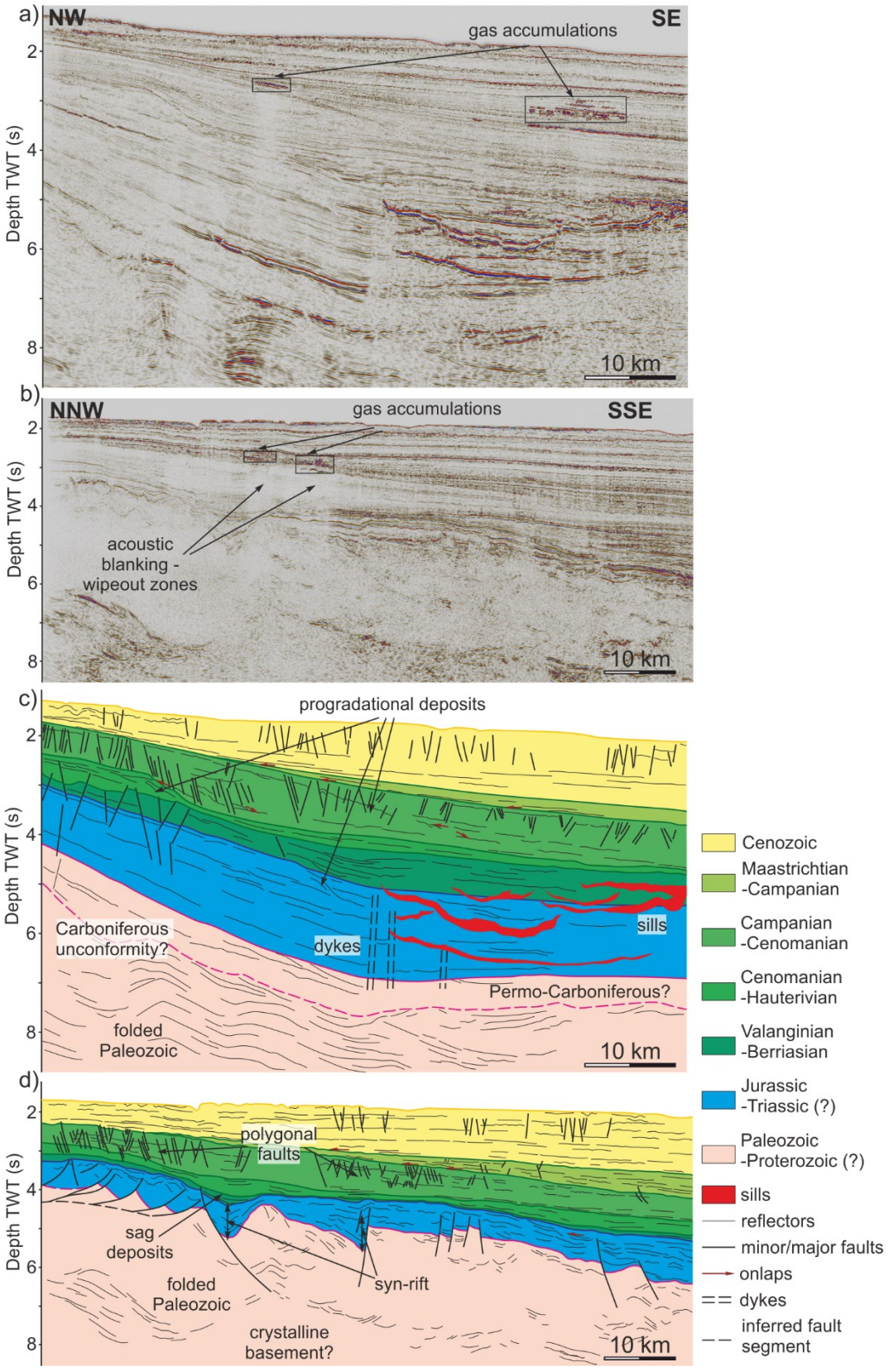

Figure 5.5 a) and b) Uninterpreted seismic sections along the Fitzroy sub-basin and the Berkeley Arch, respectively; c) and d) interpreted sections showing the sedimentary sequences, fault network, and evidence of magmatism; lines position shown in Figure 5.1

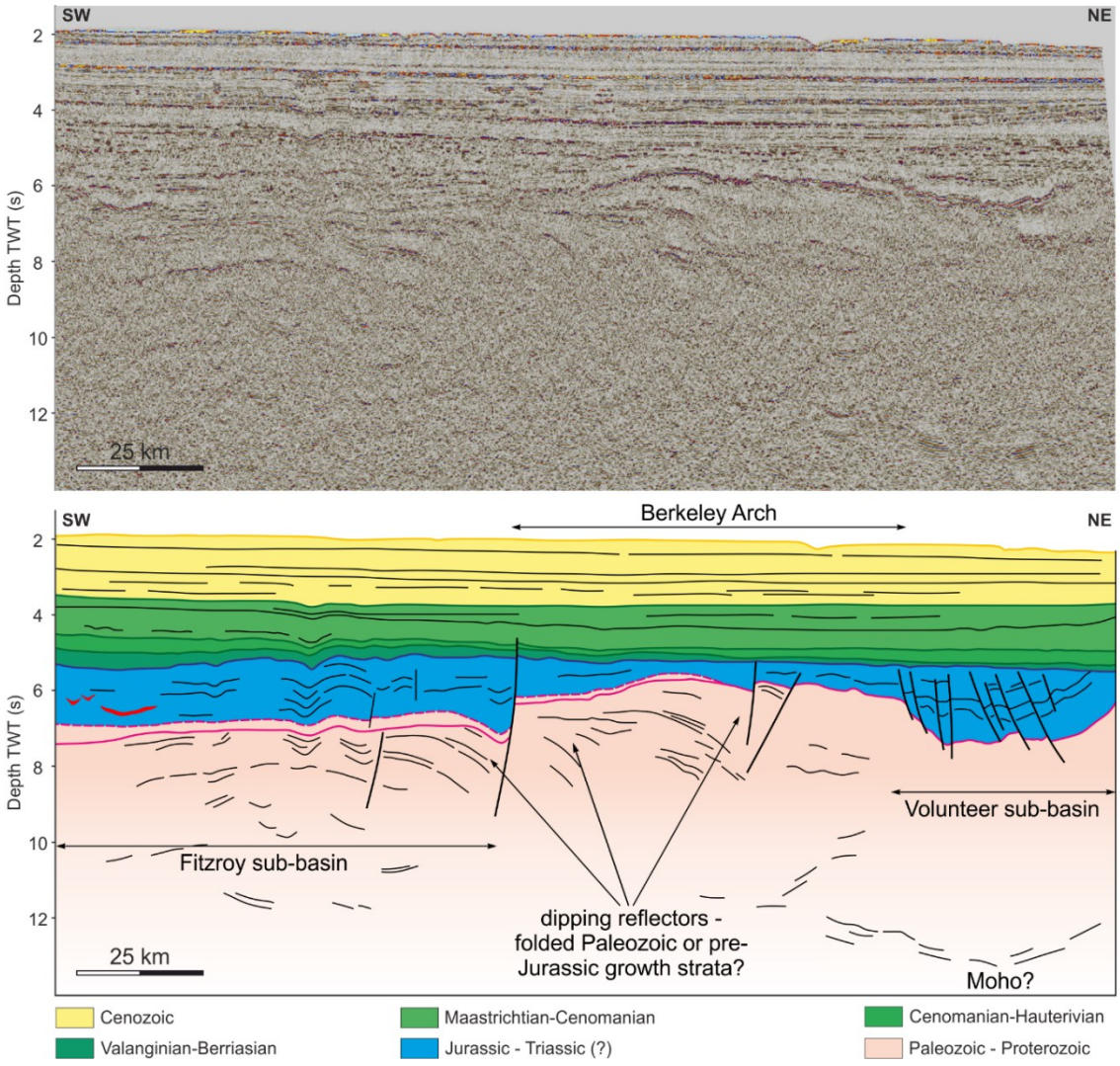

Figure 5.6 Uninterpreted and interpreted section parallel to the Falkland Islands eastern shelf and across the Berkeley Arch showing pre-rift reflectivity associated with pre-Mesozoic deformational stages and the distribution of the Cenozoic to Mesozoic sediment infill; deep reflectivity was associated with the Moho discontinuity; the shallow part of the Paleozoic-Proterozoic section (between the dashed and continuous magenta lines) correlates with the Permo-Carboniferous deposits in Figure 5.5c; line location shown in Figure 5.1

Wavy low to high amplitude reflectors are readily observed within the pre-rift in the Fitzroy sub-basin and are truncated by a section of relatively constant thickness marked by subparallel to oblique reflectors and areas of transparency (Figure 5.5a, c). These deposits are associated with wavy to oblique discontinuous reflectors further north, across the Berkeley Arch and in the Volunteer sub-basin, where the upper part of the pre-rift is characterised by higher amplitudes and semi-continuous reflectors (Figure 5.5b, d), which make the differentiation from the Mesozoic sediments challenging. Regions of high

reflectivity have been identified in this area in the lower part of the pre-rift (Figure 5.5b, d).

The main syn-rift phase was correlated with Jurassic and older deposits. The continuous reflectors within this mega-sequence have very low to high amplitudes and are disrupted in the Fitzroy sub-basin by sub-vertically stacked pockmarks. The deposits up to the Upper Valanginian unconformity record the transitional/sag phase. The latter two sections are crosscut by high amplitude saucer-shaped bodies. The younger Cretaceous section up to Campanian shows sigmoidal to oblique geometries with the Maastrichtian and younger deposits onlapping on the former (Figure 5.5).

Isochron maps were computed in order to analyse the migration of the depocentres in the FPB as a response to the tectonic activity and sediment source/input (Figure 5.7). Faults were mapped across the Volunteer and Fitzroy sub-basins and the Berkeley Arch. The variance was the primary edge detection attribute used to identify small-scale discontinuities in the seismic reflection data related to normal or oblique-slip faults.

The available wells did not allow for an extrapolation of the mapped horizons west of the Falkland Islands. Age constraints for near top Jurassic were added from Lovecchio et al. (2019) derived from well Salmon x-2 from the Malvinas Basin (Chapter 2, Figure 2.16d). Aside from this horizon, faults and changes in the seismic facies were also interpreted west of the Falkland Islands in order to assess the presence of the western FIM boundary and the deformation occurring along it.

5.4 Structural and stratigraphic characteristics of the Falkland Plateau Basin from seismic and gravity data

5.4.1 Basin depocentre migration during Mesozoic

The pre-rift section of the western FPB has been interpreted as folded and faulted strata and correlated with the Siluro-Devonian deposits cropping out onshore the Falkland Islands and unconformably overlain by Permo-Carboniferous deposits. Upper crust reflectivity (Figure 5.5b, d, 5.12a, e, and A.8a) has been correlated with the presence of crystalline basement. The stratigraphic architecture of the infill overlying the Paleozoic deposits was controlled by the tectonic activity affecting the plateau from Mesozoic and throughout the Cenozoic. The top pre-rift TWT map shows the two depocentres corresponding to the Volunteer sub-basin in the north and the Fitzroy sub-basin

in the central area separated by a basement high, the Berkeley Arch (Figure 5.7a, b). The top pre-rift to Valanginian isochron shows a similar stratigraphic architecture, with sedimentation confined to the two sub-basins and little to no deposits above the Berkeley Arch. A southward migration of the Fitzroy sub-basin depocentre is visible on the Valanginian-Campanian isochron. The Late Cretaceous recorded a progradation of the deposits from the south-west (Figure A.7) with the Cenozoic marking the merging of the two sub-basins in the larger FPB. Little sedimentation occurred at this point along the south-western and northern margins of the basin (Figure 5.7c, d and e).

Locally, the Berkeley Arch and Volunteer sub-basin show a higher variability in their stratigraphic architecture throughout the Jurassic and Cretaceous, which is related to tectonic structures present in the area (Figure 5.7f-i). The TWT map of the pre-rift shows fault-bounded WNW-ESE trending depocentres in the northern part of the Berkeley Arch and within the Volunteer sub-basin (Figure 5.7f), and minor NNW-SSE striking depocentres in the central and southern part of the Berkeley Arch, deepening towards the east (Figure 5.7f). A similar distribution is observed for the Jurassic deposits with the Volunteer sub-basin as the main depocentre and little sedimentation occurring above the Berkeley Arch (Figure 5.7g). Thermal sag deposits that follow the trend of the underlying fault-controlled depocentres were eroded at the end of the Valanginian particularly in the north-eastern part of the area covered by the seismic cube (Figure 5.7h). The Lower Cretaceous sees the erosion of Valanginian deposits along a WNW-ESE direction potentially controlled by further sag along the WNW-ESE faults and/or uplift from the north, which focuses these deposits along the Jurassic depocentres (Figure 5.7i). During the Late Cretaceous, the accommodation space increases northwards with little sedimentation occurring along the Berkeley Arch (Figure 5.7d). From Maastrichtian onwards, the FPB is established as the main depocentre (Figure 5.7c).

The structural control of the Fitzroy sub-basin is less apparent, the depocentre variation being similar to the one described for the entire western margin of the FPB. Local features characteristic of this sub-basin are represented by post-Valanginian Early Cretaceous channel systems and shelf-incised canyon-fills (Figure 5.8).

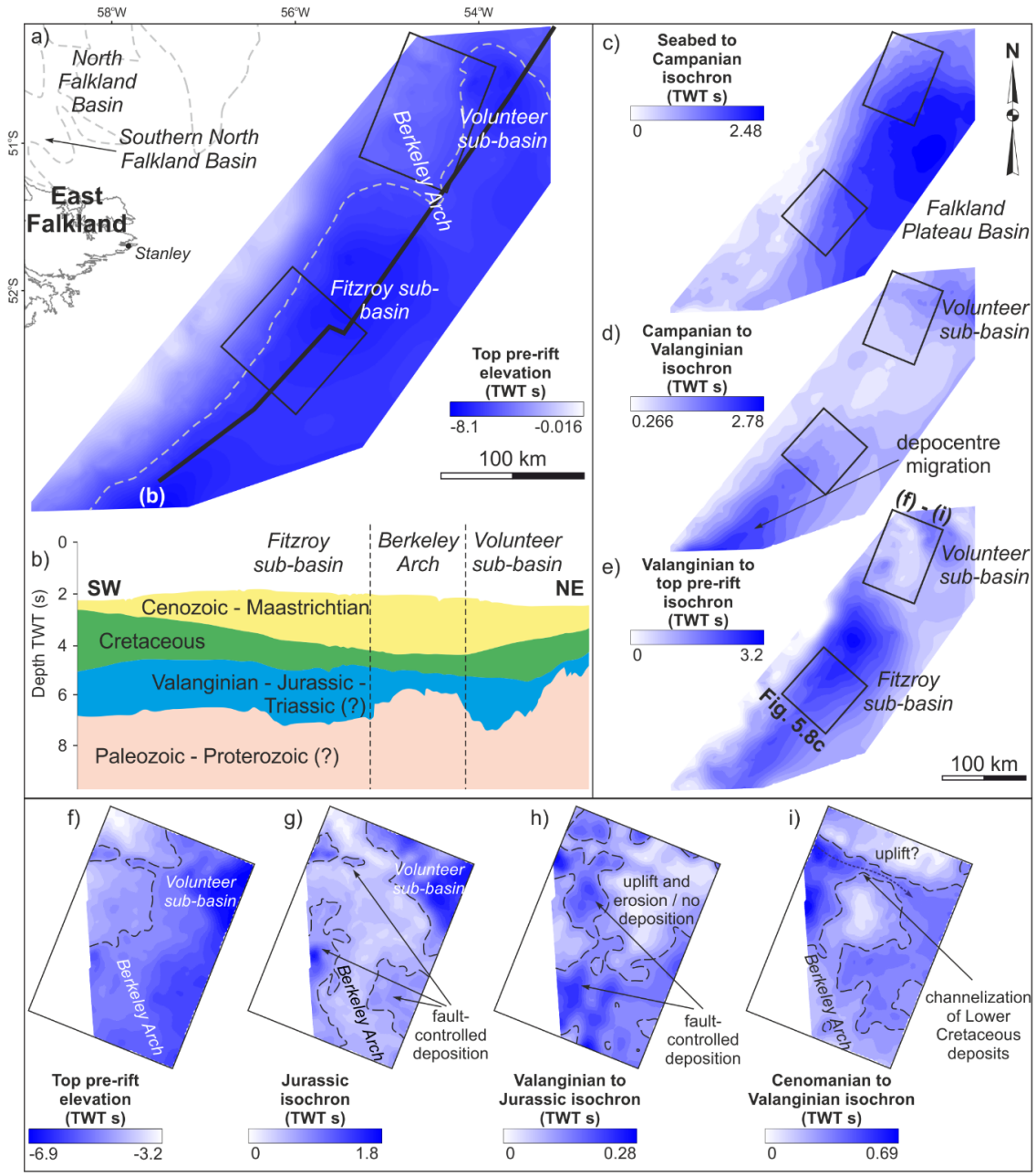

Figure 5.7 a) Morphology of the pre-rift topography; b) strike section along the shelf showing the main mega-sequences and basins; c), d), e) thickness maps of the overlying deposits showing depocentre migration as a result of sediment input and tectonism; black rectangles – position of the two 3D seismic cubes; f) top pre-rift TWT map showing the Volunteer sub-basin, WNW-ESE fault-controlled depocentres, and the Berkeley Arch; g) thickness of Jurassic section showing fault controlled deposition; h) thickness of Valanginian-Berriasian deposits showing extensive erosion and fault-controlled depocentres; i) thickness of the Lower Cretaceous section showing the uplift from the north controlling the sediment pathway into the basin; location of (f) - (i) shown in (e); black stippled lines – outlines of main depocentres

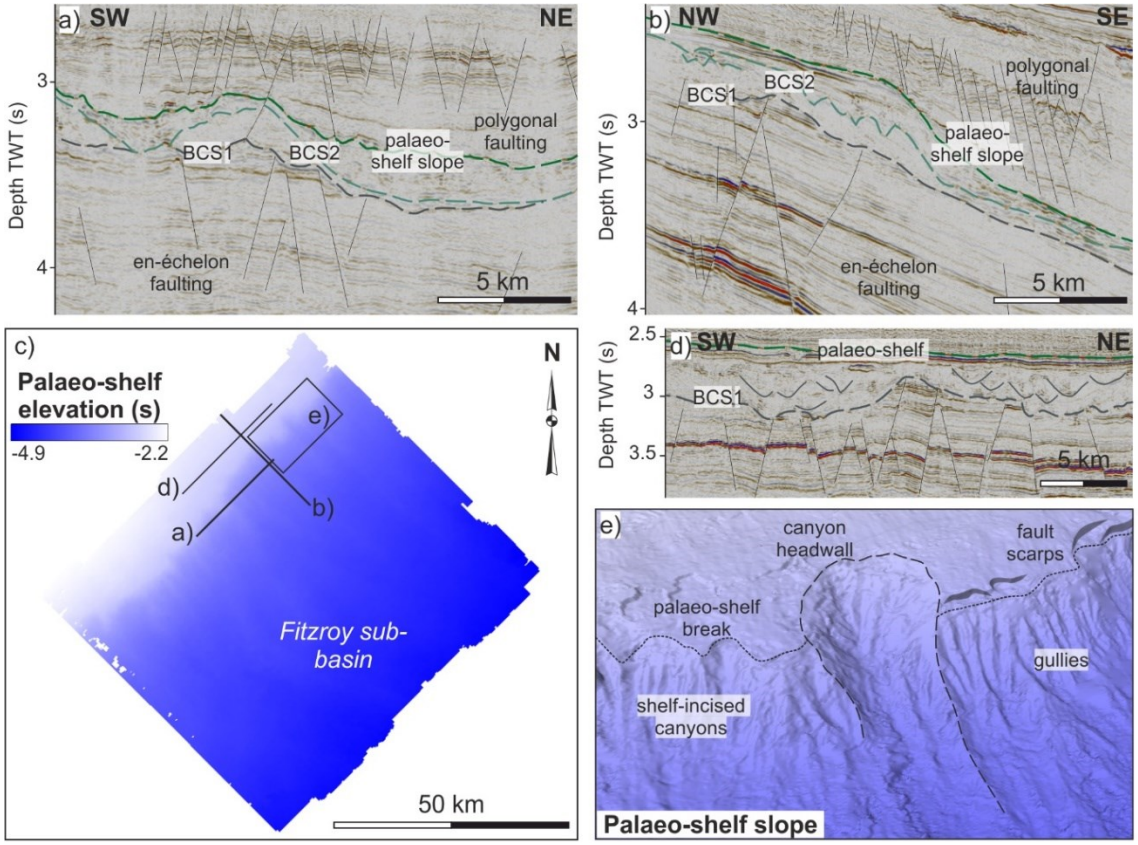

Figure 5.8 Evidence for shelf-incised canyons (a, b, d, e) and stacked channels (a, b, d) during the Early Cretaceous in the Fitzroy sub-basin (southern rectangle in Figure 5.7); BCS – base channel system; palaeo-shelf surface in (c) and (e) corresponds to the palaeo-shelf (green dashed line) in (a), (b) and (d)

5.4.2 Volcanism and magmatism

Evidence for volcanic activity was identified in both the Volunteer and Fitzroy sub-basins. In the Fitzroy sub-basin, the correlation of vertically or sub-vertically stacked pockmarks (Figure 5.9) resulted in a network of N-S trending features (Figure 5.14) showing no evidence of vertical or horizontal displacement. These features are consistent with an interpretation of igneous dykes following the rationale of Magee and Jackson (2019).

Stacked saucer-shaped bodies with high amplitudes and step-like geometries were mapped across the extent of both sub-basins (Figures 5.12c, A.7, A.8a) but were particularly extensive in the Fitzroy sub-basin (Figures 5.10, 5.11). They are restricted to the Triassic (?) – Valanginian stratigraphic level and associated with deformation of the surrounding sedimentary deposits. Their 3D geometry and distribution as shown by the 3D seismic data in the Fitzroy sub-basin can be seen in Figure 5.10. Their western extent, as constrained by the 2D and 3D seismic reflection data, can be seen in Figure 5.14. These features

are interpreted as sills and their emplacement was associated with the force-folding of the intruded sediments. The relative age for this volcanic event is constrained by onlapping geometries (Figure 5.11b, d). Folding of the Valanginian and Aptian-Albian markers and onlap geometries identified in the pre- and post-Valanginian successions indicate an emplacement spanning the Early Cretaceous (Figures 5.11, A.7b). These sills can also be identified above some of the dykes, and the emplacement of the two is interpreted here as coeval.

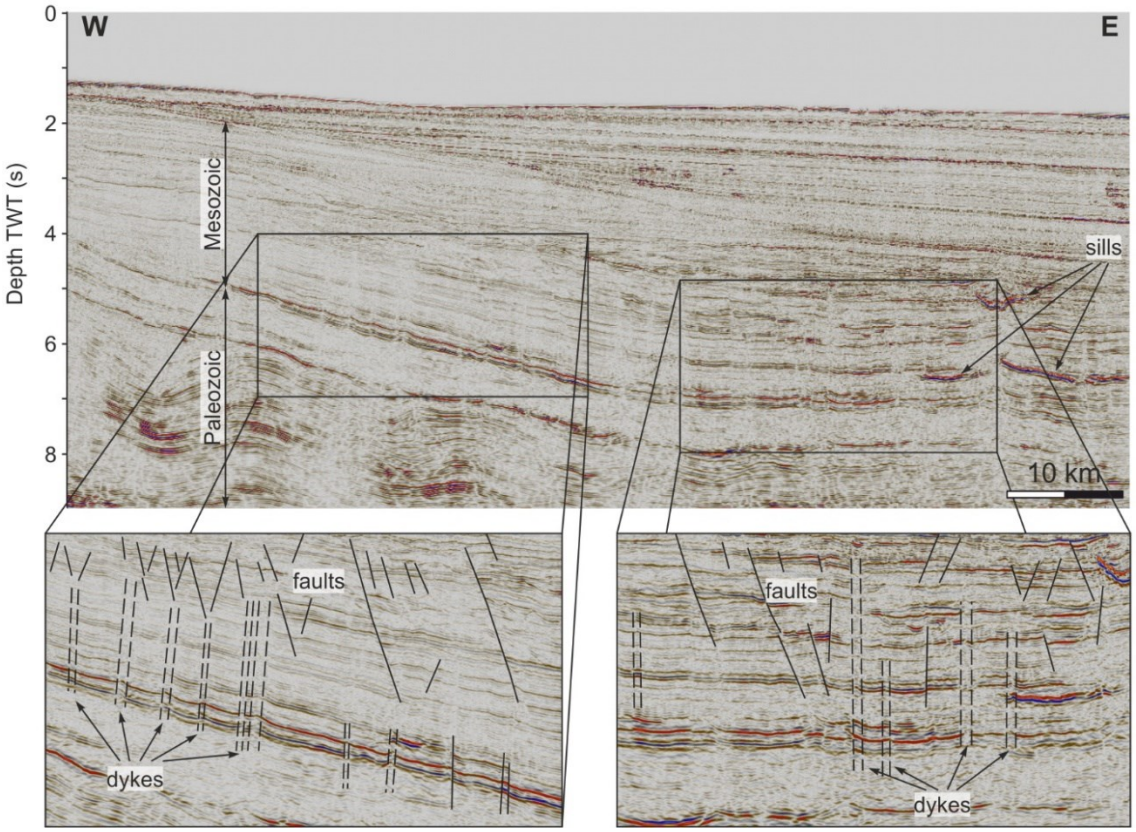

Figure 5.9 Pockmarks interpreted as dykes (stippled lines) in the Fitzroy sub-basin; line position shown in Figure 5.1

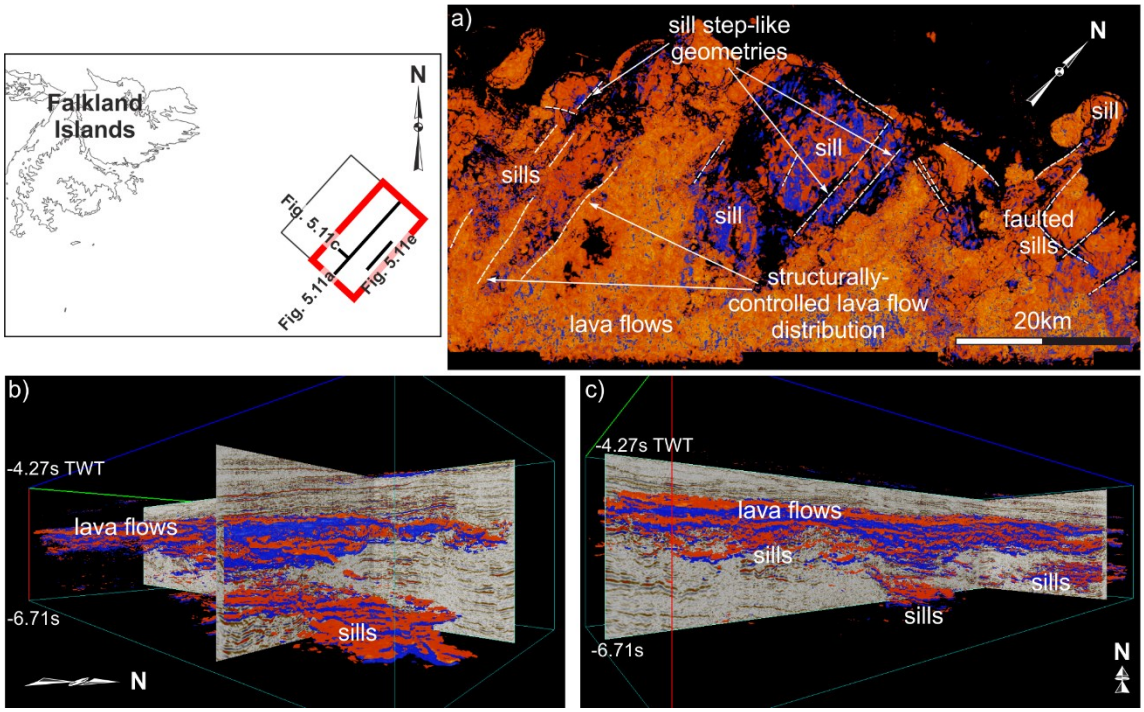

Figure 5.10 3D opacity rendering of the south-eastern part of the FISA cube showing a) top view of the sills and lava flows and the control of the N-S trending structures on their distribution; b) view from the east and c) view from the south of the sills and lava flows

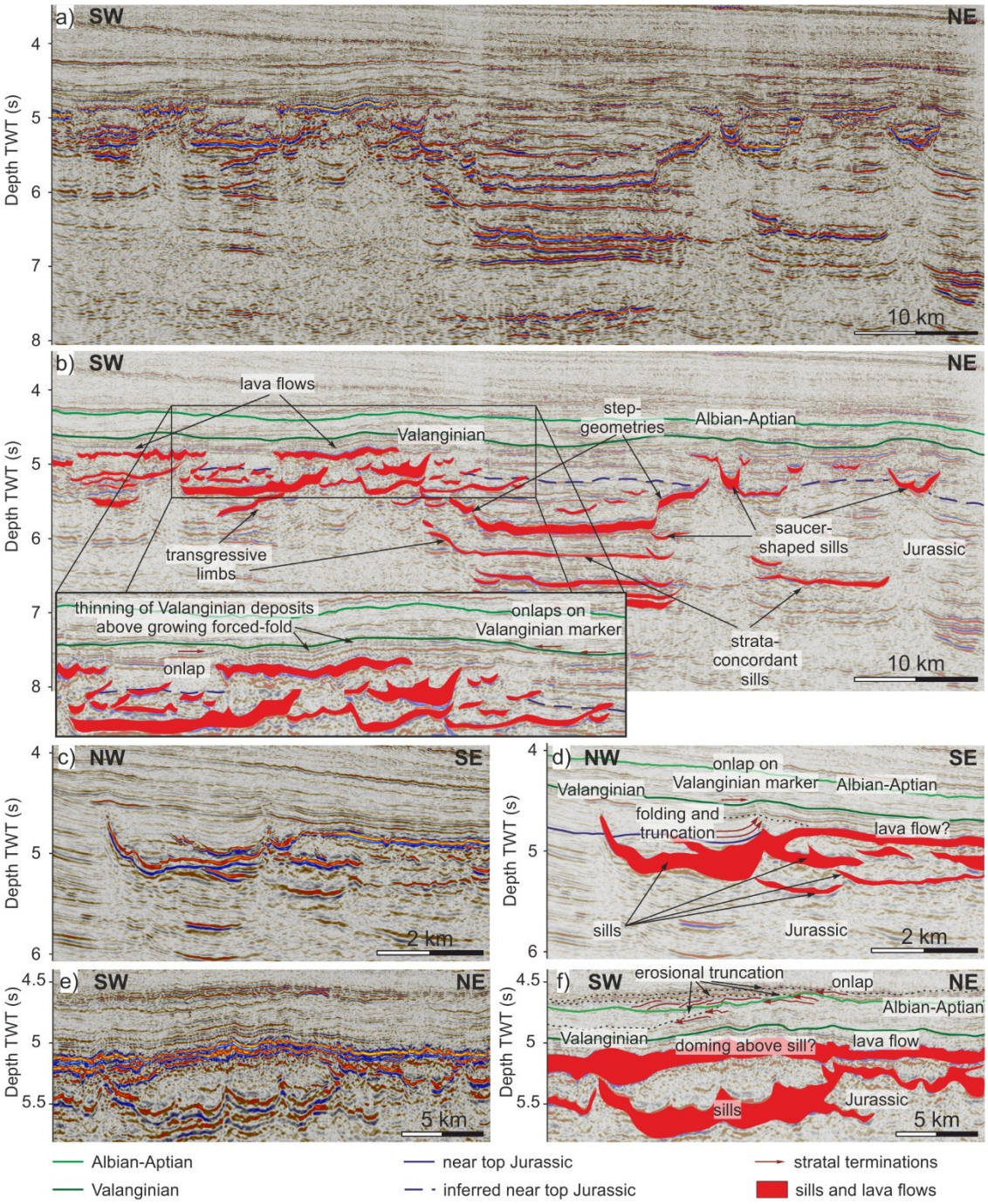

Figure 5.11 Sills and lava flow distribution and associated forced-folds in the Fitzroy sub-basin; a) uninterpreted strike line; b) interpretation of section in (a) showing lava flows and sill geometries and extent, and pre- and post-Valanginian evidence of forced-folding coeval with the sills emplacement; c) uninterpreted dip line; d) interpretation of section in (c) showing folding and truncation above the Jurassic marker and in the post-Valanginian section; e) uninterpreted strike line; f) interpretation of section in (e) showing erosional truncation and onlapping below and above the Aptian-Albian marker; lines position shown in Figure 5.10

Locally, the magma feeding the sills and dykes reached the surface resulting in lava flows (Figure 5.11b, d, f). These are more extensive in the south-eastern part of the seismic cube in the Fitzroy sub-basin (Figure 5.10) and their extrusion and distribution shows a N-S trending structural control (Figure 5.10a), parallel to the trend of the interpreted dykes. Further evidence of volcanism along this margin of the FPB can be seen in the lower section of the Volunteer sub-basin as high amplitude reflectors (Figure 5.17a) interpreted as (pre-)Jurassic volcanic deposits.

5.4.3 Structural architecture

Three predominant structural trends were identified and mapped across the entire FP with the aid of free-air gravity anomaly data and its computed derivatives and seismic reflection data:

- NW-SE to WNW-ESE: corresponding to the Jurassic SNFB faults, the western margin of the Maurice Ewing Bank and the northern part of the Berkeley Arch (Figure 5.4a);
- NE-SW: reflecting the structural grain along the western margin of the FPB, the eastern Maurice Ewing Bank, and the area west of West Falkland; larger scale structures (stippled black lines in Figure 5.4a) following the same NE-SW trend were interpreted across the FPB, parallel to the Falkland Sound Fault inferred between the East and West Falkland; a potential continuation of the NE-SW trend of the Falkland Sound Fault can be seen on the gravity data east of the North Falkland Basin (Figure 5.4a);
- N-S to NNW-SSE: comprising the Late Jurassic – Early Cretaceous North Falkland Graben, the coeval features in the main FPB and the area west and south-west of the Falkland Islands (Figure 5.4a).

5.4.3.1 Western margin of the Falkland Plateau Basin

This tridirectional structural distribution is evident along the eastern shelf of the FIM. WNW-ESE striking normal faults displace deformed Paleozoic deposits and, along the western margin of the FPB, were identified and mapped exclusively in the northern part of the Berkeley Arch (Figure 5.13).

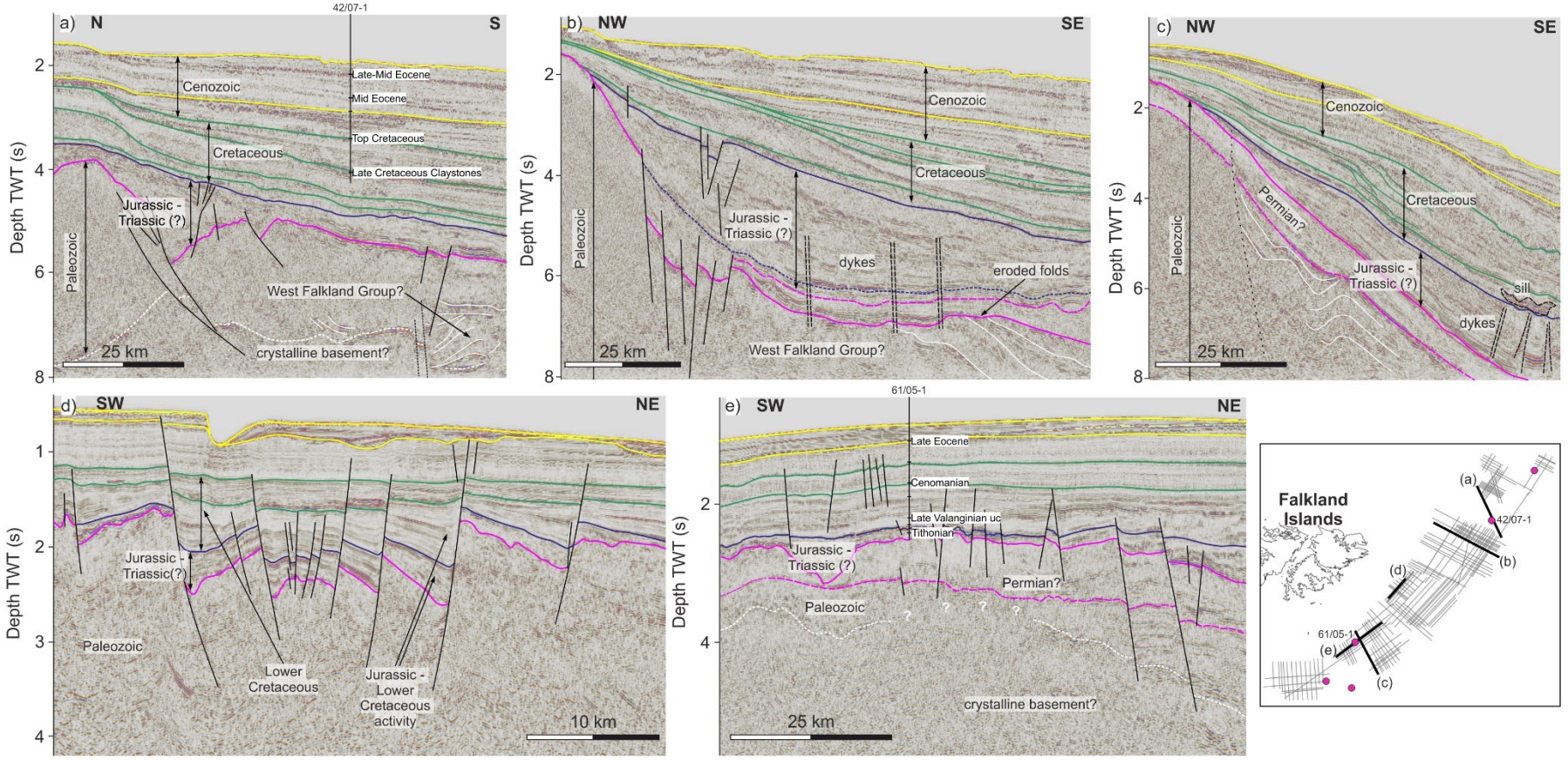

Figure 5.12 a), b), and c) Dip sections across and d) and e) strike sections along the western margin of the Falkland Plateau Basin showing changes in faulting style from north to south and evidence of normal faulting affecting the whole margin; two of the used wells tied to the seismic are shown in (a) and (e)

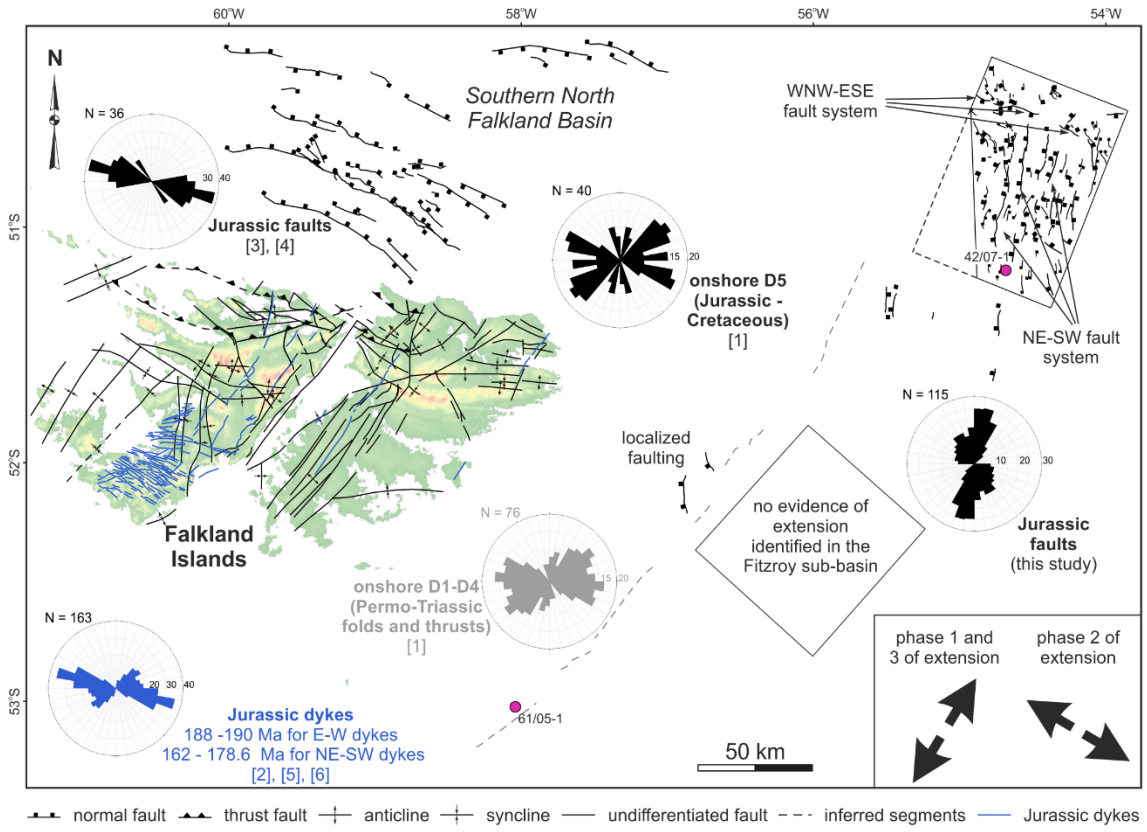

Figure 5.13 Compiled Jurassic structural map of the Falkland Islands on- and offshore areas ([1] Aldiss and Edwards, 1999; [2] Stone et al., 2009; [3] Lohr and Underhill, 2015; [4] Stanca et al., 2019 and Chapter 4, and this chapter) along with area-weighted rose diagrams for every deformational stage and fault network, showing extension directions throughout Jurassic assumed to be perpendicular on the onshore dyke swarms and offshore normal faults; ages of onshore dykes after [5] Mussett and Taylor (1994) and [6] Stone at al. (2008); arrows show extension direction and their orientation is equivalent to the orientation of σ_3

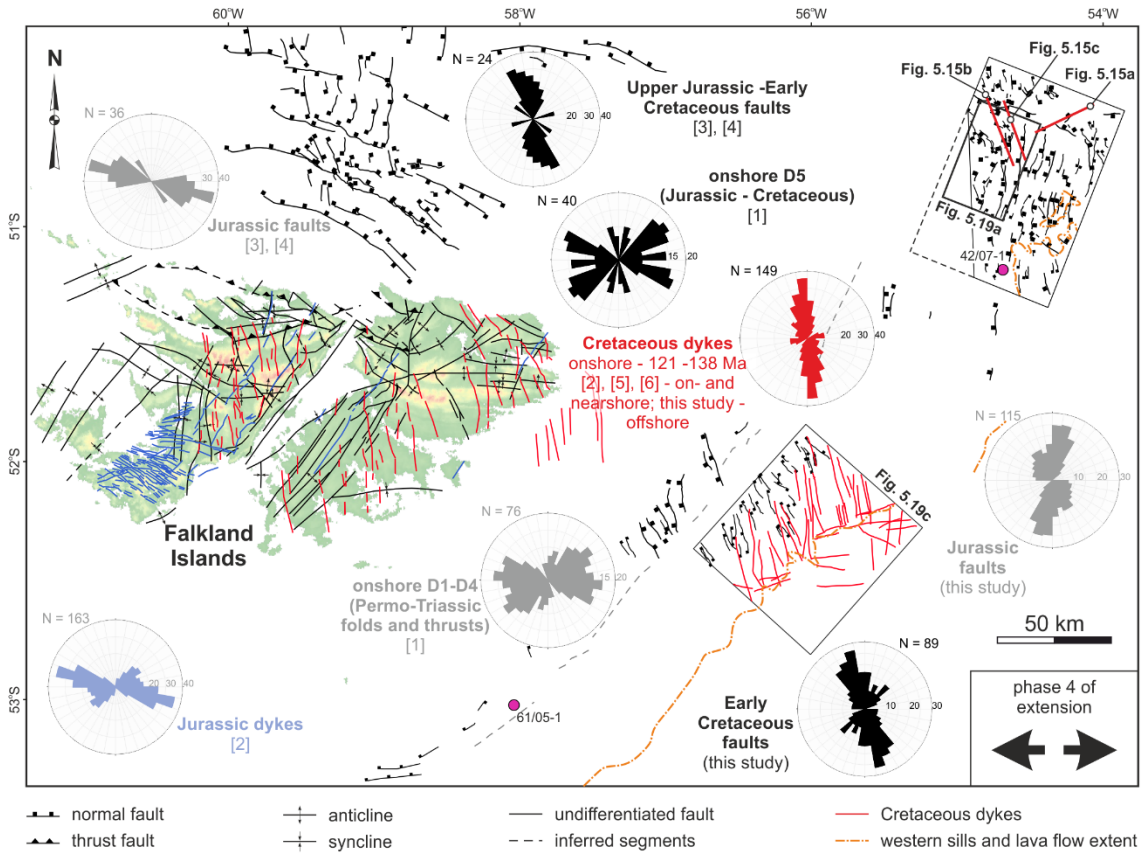

Figure 5.14 Compiled Cretaceous structural map of the Falkland Islands on- and offshore areas ([1] Aldiss and Edwards, 1999;[2] Stone et al., 2009; [3] Lohr and Underhill, 2015; [4] Stanca et al., 2019 and Chapter 4, and this chapter) along with area-weighted rose diagrams for every deformational stage and fault network, showing extension direction during Cretaceous assumed to be perpendicular on the onshore dyke swarms and offshore normal faults and dykes; ages of onshore dykes after [5] Stone et al. (2008) and [6] Richards et al. (2013); arrows show extension direction and their orientation is equivalent to the orientation of σ_3

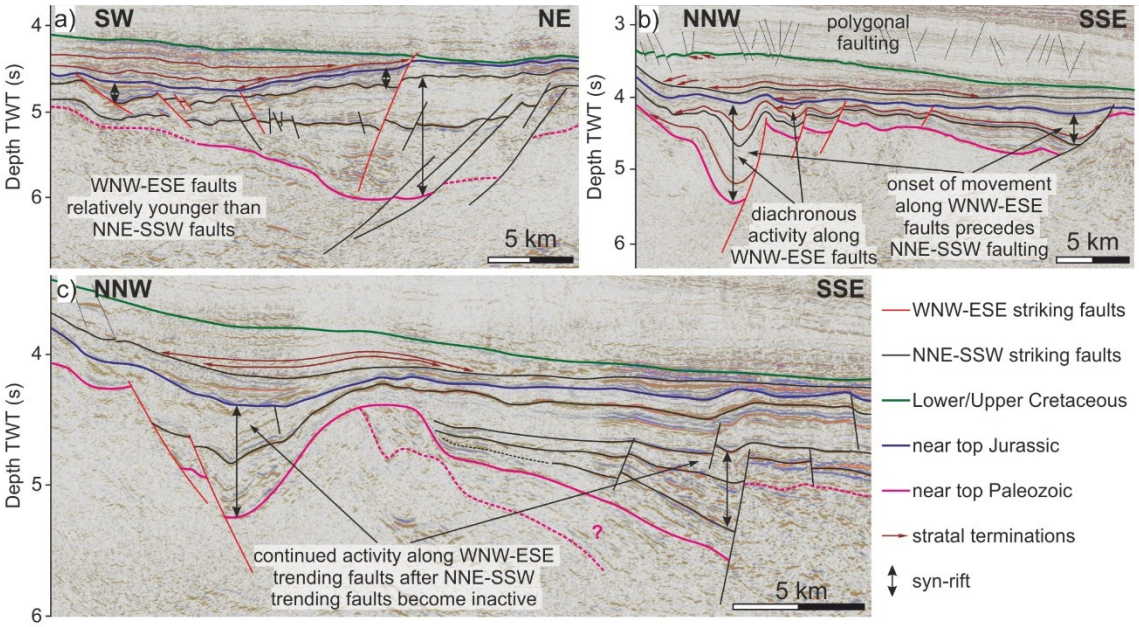

Figure 5.15 Relative ages of the WNW-ESE and NNE-SSW trending normal faults in the Volunteer sub-basin and along the Berkeley Arch showing a secondary separation of the same-strike faults based on their ages; motion on NNE-SSW trending faults occurs both before and after the formation on the WNW-ESE trending faults, but both sets are restricted to the Jurassic interval; line positions shown in Figure 5.14

NNE-SSW striking normal faults affect the rest of the basement high, the Volunteer sub-basin, and are inferred to control the entire western margin of the Fitzroy sub-basin (Figures 5.12, 5.13). The syn-kinematic deposits associated with both fault sets are predominantly Jurassic (Figures 5.12a, b, 5.15, 5.16c, A.8) and are consistent with an alternation between almost orthogonal extension directions resulting in the formation and reactivation of NNE-SSW and WNW-ESE striking faults (Figures 5.13 and 5.15).

N-S to NNW-SSE trending normal faults are interpreted along the entire western margin of the FPB and are distributed in either a left- or right-stepping en-échelon geometry (Figures 5.12d, 5.13, 5.14, and 5.19a- e). The faults in this set have small displacements, with a few exceptions along the western margin of the Fitzroy sub-basin (Figure 5.12d). Their syn-rift deposits are restricted to either the Jurassic section along the Berkeley Arch (Figure 5.19f) or offset the Valanginian unconformity in the Fitzroy sub-basin and the northern part of the Berkeley Arch (Figures 5.12d, 5.16, and 5.19f, g). Although these normal faults are predominantly interpreted on the 3D seismic reflection data, a similar trend can be observed on the gravity data, at a larger scale, along the

western margin of the FPB (Figure 5.4c) and locally, albeit with more uncertainty, along the more eastern interpreted fracture zones (Figure 5.4a).

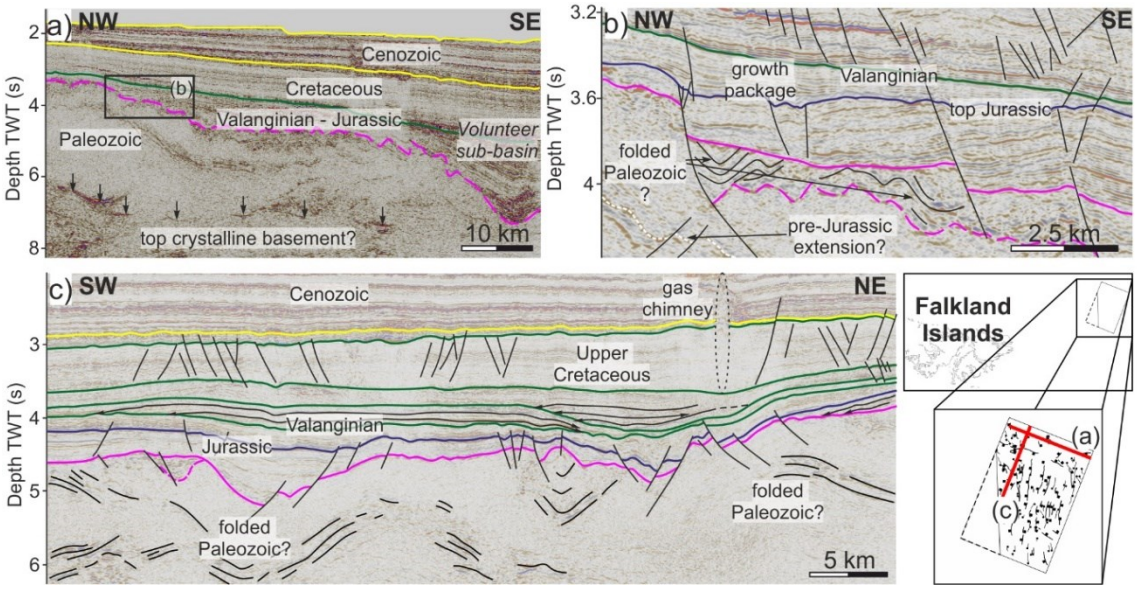

Figure 5.16 Sections through the FINA cube showing evidence of Early Cretaceous faulting in the north of the cube (b, c) and Jurassic faulting in the NW of the cube (c); upper crust reflectivity and deformation can also be seen in sections (a)-(c)

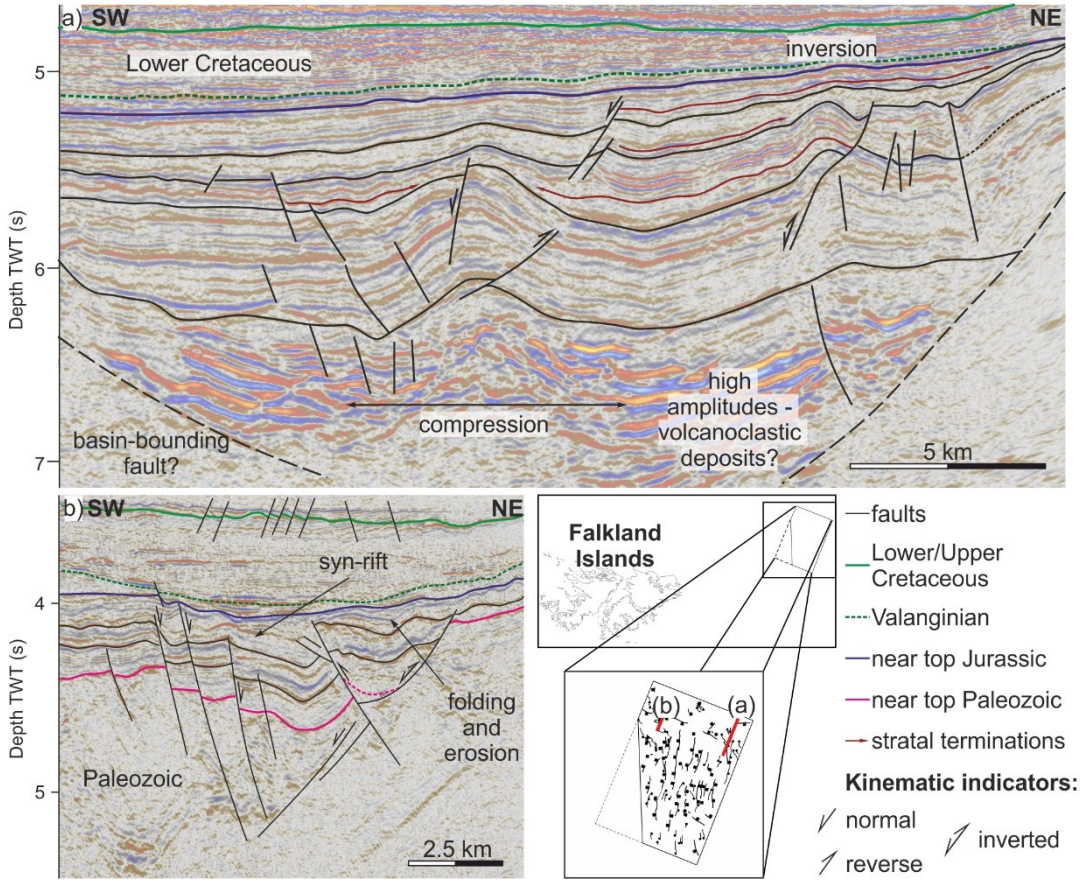

Figure 5.17 See next page for caption

Figure 5.17 Evidence for a) compression and b) positive inversion and cross-cutting relationships in the Volunteer sub-basin in the form of folds and reverse faults; sense of movement for the hanging-wall of the faults indicated; onlaps on folds shown as syn-kinematic indicators

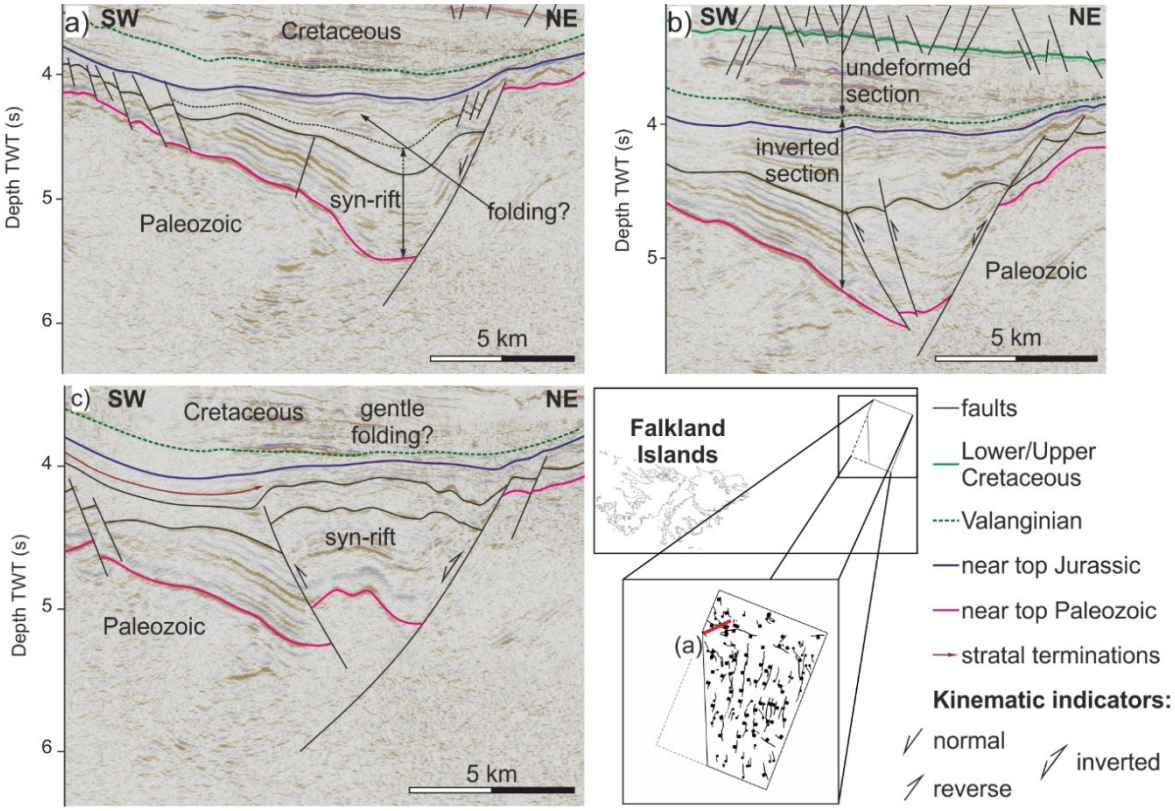

Figure 5.18 Evidence for positive inversion along a segment of a WNW-ESE trending normal faults in the Volunteer sub-basin; sense of movement for the hanging-wall of the faults indicated; onlaps on folds shown as syn-kinematic indicators; compression increases westwards (from a to c); sections (b) and (c) are parallel to section (a) shown in the location map and west of it (distance between sections too small to reproduce on the map of the cube)

Evidence of localized compression in the form of periclinal folds and WNW-ESE trending reverse faults with lengths of up to 4 km can be seen in the Volunteer sub-basin and along the Berkeley Arch, respectively (Figures 5.17, 5.18). These are restricted to the Jurassic level (Figures 5.17, 5.18b), albeit a small degree of deformation of the Valanginian marker is noticeable along some of the inverted fault segments (Figure 5.18c). Locally, reverse faults reactivate or displace Jurassic WNW-ESE trending normal faults, suggesting a younger relative age for the compression event (Figures 5.17b, 5.18).

The post-Valanginian up to present-day section is relatively undeformed with the exception of polygonal faulting (Figures 5.5c, d, 5.15b, 5.16c).

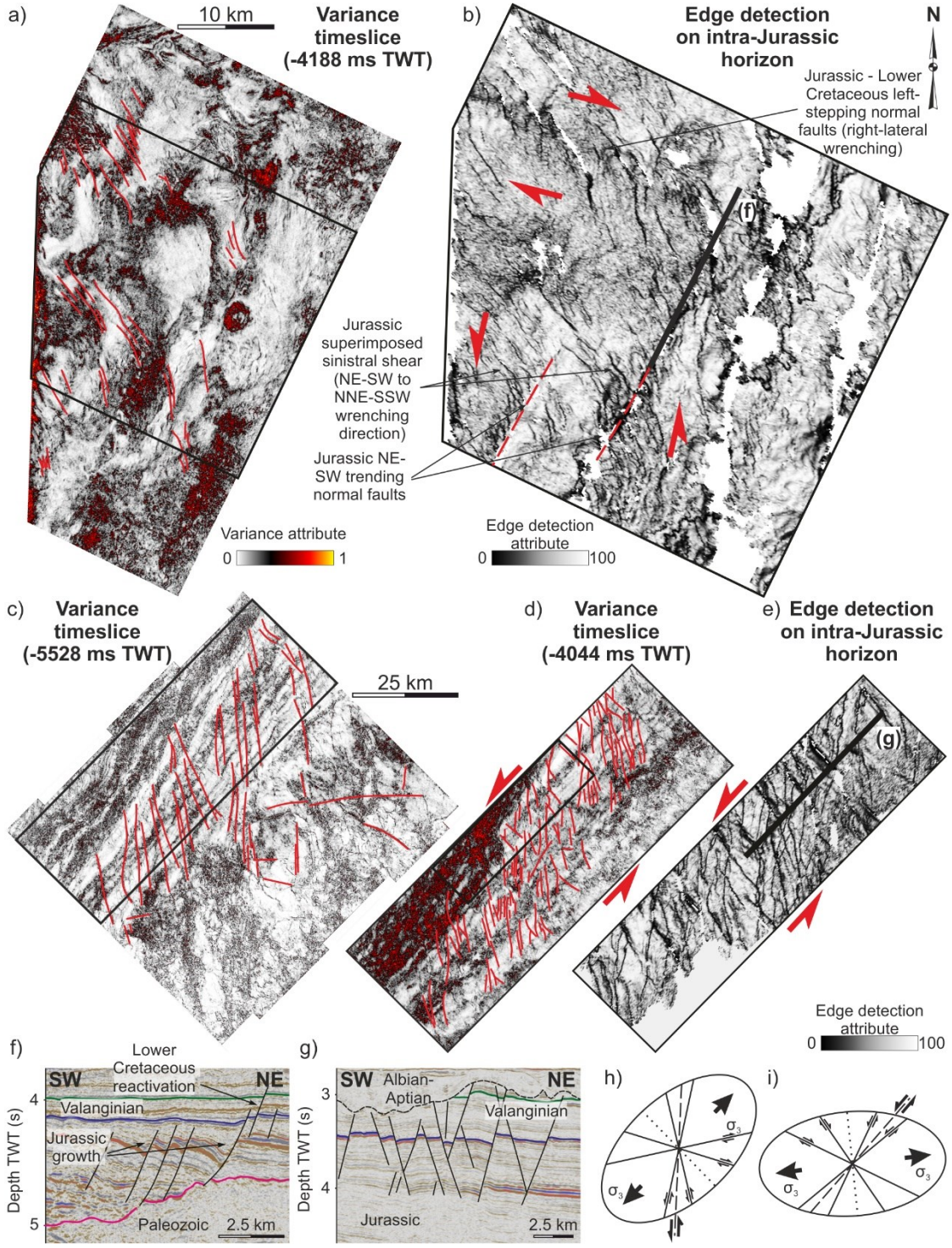

Figure 5.19 See next page for caption

Figure 5.19 a) Variance timeslice across the Berkeley Arch showing the distribution of en-échelon faults; black polygon – inset in (b); b) edge detection attribute along an intra-Jurassic horizon showing right and left-stepping en-échelon fault networks; c) faults and dykes distribution on the 3D seismic in the Fitzroy sub-basin; black rectangle - inset in (d); d) en-échelon faults and the sense of shear estimated from their orientation; black rectangle – inset in (e); e) edge detection attribute along an intra-Jurassic horizon showing the complex fault and fracture network generated by sinistral wrenching; f) section through the en-échelon faults in (b); g) section through the en-échelon faults in (e); h) strain ellipse with the orientation of the minimum horizontal stress for (a) and (b); i) strain ellipse with the orientation of the minimum horizontal stress for (c), (d) and (e); direction of arrows mark extension direction and their orientation is equivalent to the orientation of σ_3; position of timeslices in (a) and (c) shown in Figure 5.14

5.4.3.2 Western margin of the Falkland Islands Microplate

West and south-west of the Falkland Islands the tilt derivative of the free-air gravity anomaly shows a complex structure with an arched, roughly N-S trending linear anomaly on the westernmost part, ENE-WSW trending features between this and the islands, and N-S lineaments SW of West Falkland (Figure 5.20 – map inset). The available seismic data do not cross the central and northern part of the arched anomaly. However, east of this structure the data image the mega-décollement controlling the deformation across the Falkland Islands Microplate described in Chapter 4 just west of the islands with folded Palaeozoic deposits in the upper section (Figure 4.13a in Chapter 4). Gentle folding can be seen just SW of the islands (Figure 5.20a) where a N-S pattern is distinguishable on the tilt derivative (Figure 5.20 – map inset). The semi-continuous reflectors associated with the Palaeozoic succession cannot be followed west of this area where the gravity has a more chaotic character (Figure 5.20 – map inset). This region has semi-transparent seismic facies with discontinuous reflectors in the superior part and continues west into the Central Graben of the Malvinas Basin (Figure 5.20a). The infill of this graben is poorly imaged by the seismic data, showing evidence of deformation and progradational geometries from the shoulders of the graben (Figure 5.20a, b).

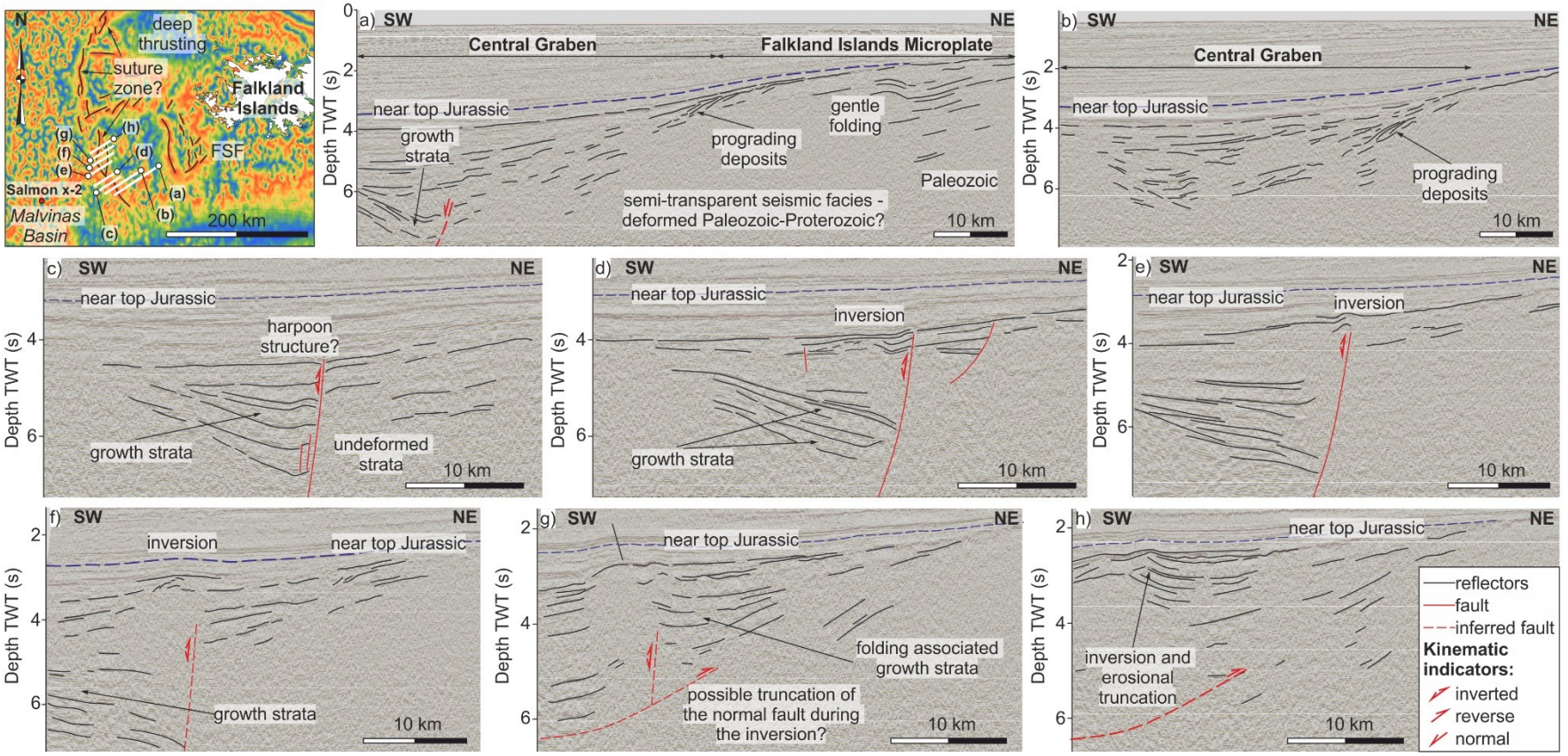

Figure 5.20 Map - tilt derivative across western FIM showing the arcuate gravity anomaly and the position of the seismic sections in (a) to (h); a) seismic section showing a change from Paleozoic(?) deposits to the Central Graben infill; b) sediment geometry in the Central Graben; (c), (d), (e) the main normal fault associated with the arcuate gravity anomaly and inversion along it generating a harpoon structure; (f) transparent seismic facies of the inverted section; inverted normal fault is inferred; (g) growth strata associated with folding, with deeper reflectors pointing towards a potential truncation of the original normal fault; (h) erosional truncation of the inverted section suggesting a Jurassic (?) relative age for the inversion; deep thrusting domain from Chapter 4 (Figure 4.13a); FSF – Falkland Sound Fault

A wedge-shaped package was identified on most of the NE-SW striking seismic lines from this area and associated with the presence of an NNW-SSE normal fault down-thrown to the west (Figure 5.20c, d, e). The uppermost section of the syn-rift shows evidence of inversion which becomes more prominent northwards where the feature resembles more a classical harpoon structure (Figure 5.20c-f). The folding is interpreted to decouple from the underlying fault further north (Figure 5.20g). Truncation of the folded deposits by a pre-top Jurassic surface (Figure 5.20h) and gentle folding of the near top Jurassic marker visible on the northernmost sections (Figure 5.20f-h) provide a relative age for the inversion. The inverted fault and the folded deposits coincide with the southern segment of the arched gravity anomaly (Figure 5.20 – map inset).

5.5 Discussion

5.5.1 The evolution of the western Falkland Plateau Basin

The present-day morphologies of the Volunteer and Fitzroy sub-basins are the result of extension along the Falkland Plateau associated with the fragmentation of Gondwana and the opening of the South Atlantic. They are further influenced by the movement along the AFFZ and the formation of the NSR. The contrasting structural frameworks and stratigraphic architectures of the two constituent sub-basins point towards different tectono-stratigraphic histories.

The Volunteer sub-basin and the Berkeley Arch show extensive deformation of Paleozoic deposits with two sets of normal faults subdivided based on their orientation: one trending NE-SW and one WNW-ESE (Figure 5.13). The syn-rift deposits show that NW-SE directed extension both preceded and followed the formation of the WNW-ESE trending fault set (Figure 5.15), although an alternation between WNW-ESE and roughly NE-SW extension is more likely (Figures 5.21, 5.22). On the free-air gravity anomaly map (Figure 5.4a), the WNW-ESE trend correlates with the reactivated faults from the SNFB, suggesting a coeval rifting stage during the Jurassic (Lohr and Underhill, 2015; Stanca et al., 2019; Chapter 4). As the oldest SNFB syn-rift deposits have not been penetrated by wells, one can argue for an onset of extension synchronous to the emplacement of the Early Jurassic onshore E-W trending dykes (188 ± 2 to 190 ± 4 Ma; Mussett and Taylor, 1994; Ramos et al., 2017; Figure 5.22a). Extension perpendicular to the western NE-SW trending margin of the FPB potentially started during the Early to Middle Jurassic when dykes following the same trend were emplaced onshore the Falkland Islands (162 ± 6

to 178.6 ± 4.9 Ma; Thistlewood et al., 1997; Stone et al., 2008; Figures 5.21a, 5.22b). Variations in the configuration of stress components are seen throughout the Jurassic, resulting in N-S trending en-échelon normal faults superimposed on the first generations of faults (Figure 5.19b), and suggestive of secondary sinistral and dextral shearing along NE-SW and WNW-ESE directions, respectively. Locally, evidence of (Late?) Jurassic compression and positive inversion are seen in the Volunteer sub-basin (Figure 5.17). Although the deposition of the Cretaceous and younger section shows some control of the underlying structures (Figure 5.7h, i), the only active faults at this level are polygonal (Figures 5b, d and 5.15b) with evidence of restricted WNW-ESE dextral shearing occurring in the northern part of the seismic cube from this area (Figure 5.19b, f) during the Early Cretaceous.

In contrast, the Fitzroy sub-basin shows little faulting of the Paleozoic deposits, the depth of its depocentre pointing towards subsidence due to loading as a result of a high input of sediments rather than crustal thinning. Discrete faulting could occur basinward, underneath the sills where the seismic imaging is poor (Figure 5a, c). Localized evidence of Jurassic faulting is interpreted along the shelf (Figures 5.12d, 5.13). However, the faulting within the sub-basin is restricted to the Lower Cretaceous interval when N-S to NNW-SSE normal faults were generated with intrusion of dykes and extrusion of lavas that follow the same trend (Figures 5.10a, 5.19c-e and g). The en-échelon distribution of these faults suggests a sinistral strike-slip component. The extensive formation and filling of submarine canyons and channels in the Fitzroy sub-basin (Figure 5.8) suggest an increase in sediment supply during the Hauterivian-Albian, and/or a relative sea-level fall (Covault, 2011) which might be related to a larger scale isostatic adjustment.

Although small-scale faults control the stratigraphic architecture in the study area, the overall morphology of the FPB was strongly impacted by large-scale tectonism, such as movement along the AFFZ and the formation of the NSR. The wrenching and active transform motion period of the AFFZ, as documented on the South African side, occurred between 134 and 92 Ma (Valanginian - Turonian) and resulted in a gradual westward migrating uplift in the Outeniqua Basin (Baby et al., 2018). In the Volunteer sub-basin, the deposition of the Valanginian-Cenomanian sequence is focused along a WNW-ESE direction (sub-parallel to the AFFZ) and onlaps onto the Valanginian deposits, which could suggest uplift from the north, along the AFFZ (Figure 5.7i). A large-scale unconformity is interpreted along the South African margin during the Aptian-

Albian (McMillan, 2003; Baby et al., 2018) and related to large scale tectonic events that could explain the canyon incision seen at this time along the western margin of the FPB (Figure 5.8).

Compression and uplift along the NSR are thought to have started in the Late Cretaceous (Bry et al., 2004), which resulted in the southward tilt of the Falkland Plateau (Ewing et al., 1971). This is expressed as a south-eastward increase in accommodation space during this time in the FPB (Figure 5.7c).

5.5.2 The structural evolution of the western margin of the Falkland Islands Microplate

The region west and south-west of the Falkland Islands shows the highest degree of Mesozoic deformation occurring in the south-westernmost part, along the Central Graben of the Malvinas Basin (Figure 5.20a-h). The rifting in this part of the basin is believed to have started in Middle (?) Jurassic (Baristeas et al., 2013) or as early as Late Triassic (Lovecchio et al., 2019). The main fault bounding the Central Graben to the east undergoes increasing inversion northwards during the (Late?) Jurassic with the folding associated with this inversion following the trend of the linear gravity anomaly west of the Falkland Islands (Figure 5.20 – map inset, Figure 5.20c-h). The northern segment of this anomaly corresponds to the high-velocity ridge of Ludwig et al. (1968) and was associated with a potential suture zone between the Falkland Plateau and Patagonia (Storey et al., 1999; Marshall, 1994; Richards et al., 1996a, b). The age of this contentious suture is debatable, being either a result of the Mesozoic fragmentation of Gondwana or older, following the Carboniferous collision of Patagonia with south-western Gondwana as discussed by Pankhurst et al. (2006). The presence of a crustal scale structure would act as a weak zone during subsequent deformational events and would explain the localization of deformation in the Malvinas Basin along this boundary, in the Central Graben. The depth of the Central Graben (Figure 5.20) along with the inversion occurring along it (Figure 5.20c-h) points towards more complex tectonism than sole extension resulting in the opening of the Malvinas Basin. This style of deformation could be associated with wrenching between FIM and Patagonia.

5.5.3 Mesozoic structural evolution of the Falkland Islands Microplate

The seismic reflection data interpreted along the western boundary of the FPB does not show a crustal scale feature that could be associated with the eastern

boundary of the FIM (Figure 5.5). Furthermore, the deformation related to wrenching is relatively localised and suggests little sinistral displacement along what was interpreted to be the margin of the microplate (Figure 5.19). Therefore, the region comprising the Fitzroy and Volunteer sub-basins is considered here as part of the FIM, and the NE-SW trending gravity anomalies interpreted as fracture zones (Figure 5.4a, b and c) are interpreted to accommodate the intra-plate deformation during rotation of the FIM, with the easternmost fracture zone potentially acting as the eastern FIM boundary.

Subsequent to the Gondwanide orogeny, which resulted in WNW-ESE trending folds and thrusts and NE-SW trending folds across the FIM (Curtis and Hyam, 1998; Aldiss and Edwards, 1999), the incipient stages of continental fragmentation resulted in a complicated fault network affecting the microplate. Situated between three major plates, the microplate underwent faulting and dyke emplacement related to the undocking and drifting of East Antarctica and South America away from Africa (Figure 5.21).

During the Early Jurassic, the early stage of Karoo-Ferrar magmatism was marked by WNW-ESE to W-E oriented dyke intrusion in the southern part of West Falkland (188-190 Ma). This was followed by NW-SE directed extension resulting in the emplacement of another dyke swarm (162-179 Ma) onshore the islands, assuming dyke intrusion occurred perpendicular to σ_3. This stage was potentially synchronous with normal faulting in the Volunteer sub-basin and along the Berkeley Arch (Figure 5.22a, b) and extension in the main depocentre of the Malvinas Basin. The Middle (?) - Late Jurassic sees a rotation in the extension direction to NNE-SSW allowing for the reactivation of the Permo-Triassic thrusts in an extensional regime seen both in the Southern North Falkland Basin and the Volunteer sub-basin (Figure 5.22c, d). The structural inheritance given by the presence of older WNW-ESE trending thrusts does not require the extension direction to be perpendicular to these thrusts in order for them to reactivate. Experimental studies on oblique rifting show that pre-existing structures can reactivate with a predominantly normal dip-slip component for angles between 45° and 135° between their trend and the extension direction (Withjack and Jamison, 1986; Henza et al., 2010). For angles outside this range, oblique-slip or strike-slip faults tend to develop (Withjack and Jamison, 1986; Henza et al., 2010). The reactivated thrusts in the SNFB show predominantly normal displacements to oblique-slip suggesting an extension direction between NNW-SSE and NE-SW which would allow

multiple stages of movement along these faults throughout the Jurassic (Figure 5.22a, c, and d).

Jurassic en-échelon faulting along the margin of the FPB (Figure 5.19a, b) is consistent with sinistral and dextral wrenching generated by a NE-SW oriented σ_3 (Figures 5.19h and 5.22c, d). However, the predominantly small displacements associated with these faults along with the lack of age constraints for the Jurassic section make their relative dating in the context of SNFB rifting difficult. From the end of the Jurassic and into the Early Cretaceous σ_3 oscillates around a roughly E-W orientation, leading to the opening of the North Falkland Basin, normal faulting in the Fitzroy sub-basin, and the onshore and offshore emplacement of an Early Cretaceous generation of dykes between 121 ± 1.2 Ma to 138 ± 4 Ma (Figure 5.22e, f). Sinistral and dextral shearing occurs at this time locally, along the western margin of the FPB (Figure 5.19c, d, e) and in the northern part of the Berkeley Arch (Figure 5.19b), respectively, potentially related to the onset of wrenching along the AFFZ (at 134 Ma; Baby et al., 2018). However, these right and left-stepping en-échelon faults could be reactivated Jurassic structures that accommodated the FIM intra-plate deformation during its rotation, in a similar way to the NE-SW trending regional fracture zones (Figure 5.4a) but on a much smaller scale (Peacock et al., 1998; Figure 5.4d).

5.5.4 Stress orientation variation across the FIM in the context of Gondwana

5.5.4.1 Plate model considerations

In the context of a pre-break-up configuration of south-western Gondwana, the stress variation interpreted across the FIM could help constrain the timing of microplate rotation. This can be done by comparing structures of similar age identified across south-western Gondwana with the aforementioned structural framework. To do this, a modified version of the South Atlantic reconstruction after Müller et al. (2019) with Africa fixed to its present-day position is used. The Falkland Plateau is considered to consist of two sub-plates: the FIM and the Maurice Ewing Bank region. The FIM is defined as the area bounded to the north, west, and south by the black stippled lines in Figure 5.4b, c, and extends eastward up until the magnetic stripes from Eagles and Eisermann (2020) (oc. c. region in Figure 5.4b, c). These were interpreted as magnetic reversal isochrons associated here with the presence of oceanic crust, although a more extensive oceanic domain has been interpreted by Schimschal and Jokat (2019b) based on P-wave velocities (black dots in Figure 5.1) and by Eagles

and Eisermann (2020) based on magnetic data. The Maurice Ewing Bank sub-plate represents the remainder of the plateau. The amount of rotation for the Falkland Islands Microplate during the Early Jurassic is based on Chapter 4 (after Stanca et al., 2019) but its exact location remains debatable. Here the islands are positioned further south than Stanca et al. (2019) and the reconstruction shown in Chapter 4 in order to eliminate the space between the FIM and South America in the Jurassic reconstruction while not invoking dextral movement along the Gastre Fault. A more northern position could be accomplished by further deformation of the South American plate. These scenarios are not addressed here; rather, the sole aim of the reconstruction is to carry out a qualitative comparison between the stress fields and structures across the FIM and south-western Gondwana. Similarly, Schimschal and Jokat (2017, 2019b) and Eagles and Eisermann (2020) interpreted oceanic crust underlying the whole Falkland Plateau Basin. Although the seismic data presented here show folded Paleozoic deposits indicative of a more extensive continental crust in the east of the FIM than suggested by these studies, this chapter does not refute the presence of oceanic crust in the eastern part of the Falkand Plateau Basin. This would change the extent of the two sub-plates of the Falkland Plateau, but it would not affect the fact that the structural features of the Falkland Islands, North Falkland Basin, and the Volunteer and Fitzroy sub-basins are part of the same microplate and underwent the same amount of rotation. Therefore, the extent of the sub-plates and the overall crustal architecture of the plateau should not have implications for the purpose of this comparison between the local (FIM) and regional (south-western Gondwana) stresses. In the following section, the orientation of the regional σ_3 is mentioned relative to the fixed Africa (Figure 5.21), whereas the local orientation is relative to the present-day position of the Falkland Islands (Figure 5.22).

5.5.4.2 Local vs. regional stress orientation

The Early Jurassic E-W trending dyke swarm onshore the Falkland Islands is thought to have compositional affinities with the now N-S trending Rooi Rand basalts in Lebombo, SE Africa (Armstrong et al. (1984) in Mitchell et al. (1999)), which were in turn correlated with the early E-W rifting between Africa and Antarctica (Reeves, 2000; Figure 5.21a). However, more recent dating of the Rooi Rand dyke swarm yielded ages between 164.7 and 177.8 Ma (Jourdan et al., 2007; Hastie et al., 2014) and therefore younger than the Early Jurassic dykes onshore the Falkland Islands (188 ± 2 to 190 ± 4 Ma). Older dyke swarms that mark the beginning of the Karoo-Ferrar magmatism and early

stages of Gondwana fragmentation are the N-S striking dykes in the northern part of the Lebombo monocline in south-east Africa, although E-W regional extension might have started as early as 190 Ma with the emplacement of the ENE-WSW trending dykes from Ahlmannryggen region, Dronning Maud Land (Antarctica) (Riley et al., 2005; Jourdan et al., 2007; Klausen, 2009). The pre-break-up position of the Falkland Islands, incorporating the rotation from Stanca et al. (2019), would result in a NW-SE to N-S orientation of the oldest Jurassic dyke swarm relative to Africa. This is sub-parallel to the North Lebombo and the reconstructed Dronning Maud Land dykes, suggesting that their emplacement could have occurred in a similar stress regime (Figure 5.21a). The Early Jurassic dykes onshore the Falkland Islands show a more radial distribution (ENE-WSW swinging to WNW-ESE) which could suggest a continuation of their intrusion coeval with the Okavango and Save-Limpopo dyke swarms in Africa, discussed below, and a conjugate relationship with the NE-SW dykes onshore the Falkland Islands as suggested by Musset and Taylor (1994).

The Jurassic NE-SW (present-day orientation) oriented dyke swarm (162 ± 6 to 178.6 ± 4.9 Ma) has the same orientation as the Jurassic normal faults mapped along the Berkeley Arch and suggest a NW-SE to WNW-ESE orientation of σ_3 (Figure 5.22b). The regional stress orientation during Early Jurassic relative to a fixed Africa was controlled by NNW-SSE to N-S-oriented extension between East Antarctica and West Gondwana as inferred from field analysis of the Okavango and Save-Limpopo dyke swarms in Africa (Le Gall et al., 2002, 2005; Jourdan et al., 2007; Klausen, 2009; Hastie et al., 2014). At this time, NNW-SSE, NNE-SSW, and NE-SW striking dykes were emplaced in the Straumsvola, Ahlmannryggen, and Vestfjella regions, respectively, on the East Antarctic side (Riley et al., 2005; Curtis et al., 2008). The variation in the orientation of the Dronning Maud Land dyke swarms is considered to be suggestive of radial intrusions around a plume head (Curtis et al., 2008) rather than controlled by the regional stress field but are shown here in the interest of completeness. Rifting in the Weddell Sea Rift System (~175-180 Ma) and across Patagonia and the Malvinas Basin (Figure 5.21a) is considered to have occurred during the Early to Middle Jurassic (Jordan et al., 2017; Lovecchio et al., 2019; Riley et al., 2020), which is consistent with a roughly NNW-SSE regional extension relative to Africa. A counterclockwise rotation of the FIM to its original position would align the Early to Late Jurassic dykes perpendicular to the regional extension direction (Figure 5.21a). However, the age range of these dykes is relatively wide and the age of the NE-SW trending normal faults

along the Berkeley Arch is poorly constrained. These are speculated to be synchronous to the dyke emplacement based on their orientation alone. Faults and dykes with a similar trend would be generated during stage 2 of the Middle Jurassic extension (Figures 5.21a) when the σ_3 rotates to an NNW-SSE orientation as East Antarctica drifts southwards (at ~167.2 Ma; König and Jokat, 2006). This would align the now WNW-ESE to NW-SE trending dykes of Middle Jurassic age (~170 Ma) from northern Patagonia (Rapalini and Lopez De Luchi, 2000; López De Luchi and Rapalini, 2002) with the Early to Late Jurassic dyke swarm from onshore the Falkland Islands and relate them to the same extensional episode (stage 2 of the Middle Jurassic deformation in Figure 5.21a). This switch in the extension direction could also have led to the undocking of the FIM from Africa.

During the Late Jurassic, the thrust faults in the SNFB undergo negative structural inversion and NW-SE to WNW-ESE trending normal faults are generated along the Berkeley Arch. These suggest a NNW-SSE to NE-SW orientation of σ_3 (Figure 5.22d). WSW-ENE directed extension is registered in the Outeniqua Basin (Paton and Underhill, 2004) related to the drifting of South America (Figure 5.21a). This would require the FIM to be in an intermediary rotated position during the Late Jurassic. The reactivated thrusts in the SNFB are in an orientation relative to the regional horizontal minimum stress that favours reactivation during the Early and Middle Jurassic as well when E-W extension occurs between Africa and Antarctica (Figure 5.21a) accompanied in the later stages by the emplacement of the Rooi Rand dykes (between 164.7 and 177.8 Ma; Jourdan et al., 2007) and the formation of the Northern Weddell Magnetic Province (~155-175 Ma; Grunow, 1993; Riley et al., 2020; Figure 5.21a). This would point towards multiple phases of thrust reactivation in an extensional regime as suggested by the multiple syn-rift packages associated with them (Lohr and Underhill, 2015; Stanca et al., 2019; Chapter 4). E-W striking faults (present-day orientation) documented in Chapter 4 and by Stanca et al. (2019) north of the Falkland Islands would be generated synchronously to extension in the SNFB.

Little evidence for compression can be seen during this period in the north-eastern (Volunteer sub-basin and Berkeley Arch; Figure 5.17) and south-western (Malvinas Basin; Figure 5.20) corners of the FIM. This could be due either to clockwise rotation against the Maurice Ewing Bank and the South American plate, respectively, or related to the wrenching between eastern and western Gondwana. The compression identified in the FPB can also be related

to early wrenching between Africa and the Falkland Plateau. However, the small and localised scale of this compression suggests that the space into which the FIM rotated was in an overall extensional regime (i.e. the overall movement between Africa, South America, and Antarctica resulted in space being created at the same rate or faster than the FIM rotated, favouring the formation of predominantly extensional features over compressional or transpressional).

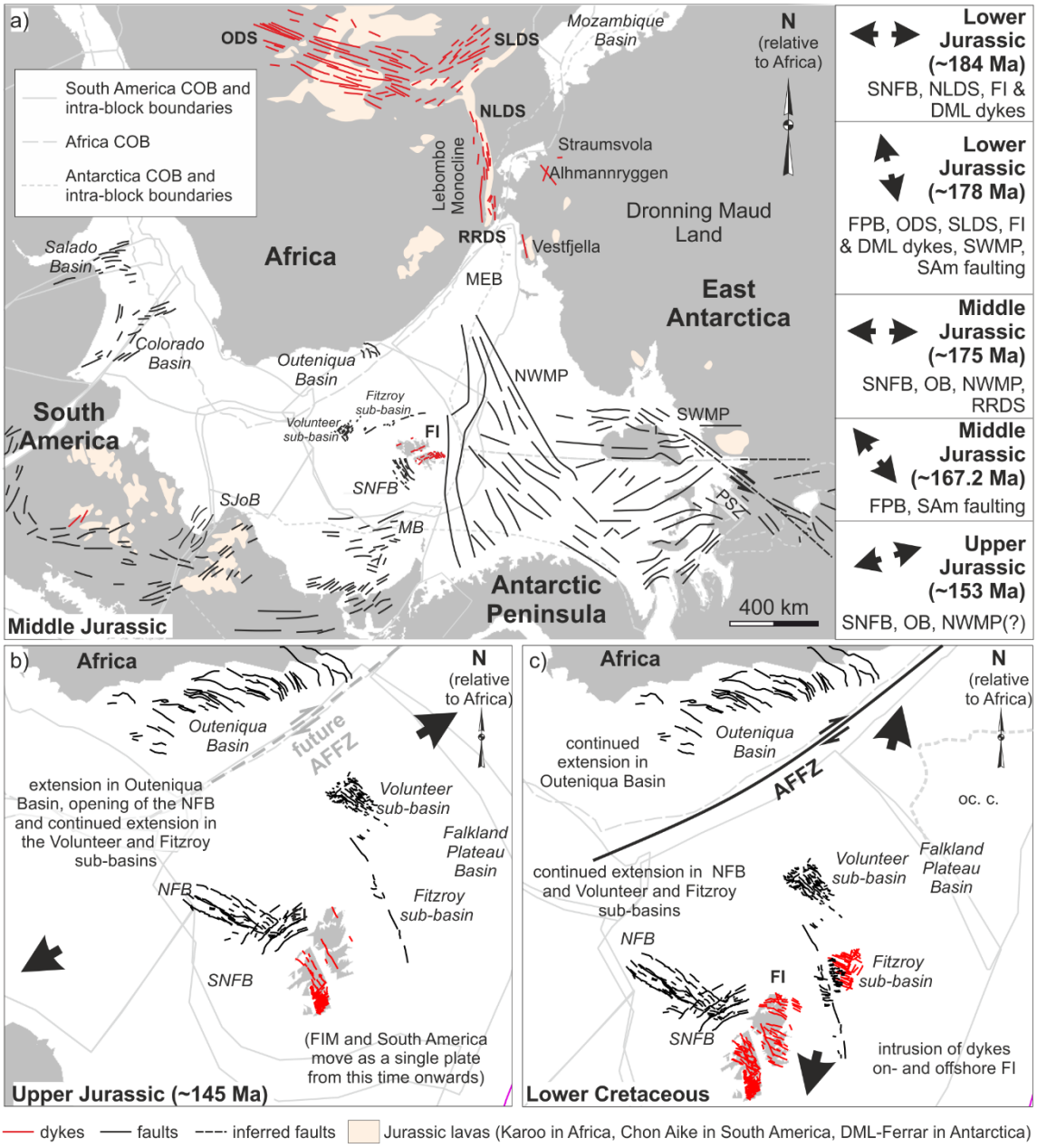

Figure 5.21 See next page for caption

Figure 5.21 Correlation between the position of the Falkland Islands and south-western Gondwana based on the orientation of σ3 for a rotated reconstruction of the FIM; a) Middle Jurassic plate configuration showing the change in the regional orientation of σ_3 from Early to Late Jurassic (right panel) and the structural features used for its estimation; b) NE-SW extension direction (Paton and Underhill, 2004) and plate configuration during Late Jurassic; c) NNE-SSW directed extension (Paton and Underhill, 2004) marked by the emplacement of now N-S trending Early Cretaceous dykes on- and offshore the Falkland Islands; rotation of the FIM from Chapter 4 (after Stanca el al., 2019); Falkland Islands Microplate and the South American plate rotate clockwise with the remaining ~60° during the opening of the South Atlantic (Mitchell et al. 1986) to reach their present-day position; onset of wrenching along the Agulhas – Falkland Fracture Zone after Baby et al. (2018); FI – Falkland Islands; MB – Malvinas Basin; NFB – North Falkland Basin; NLDS – Northern Lebombo dyke swarm; NWMP – Northern Weddell Magnetic Province; OB – Outeniqua Basin; oc. c. – oceanic crust (based on magnetic reversal isochrons from Eagles and Eisermann, 2020); ODS – Okavango dyke swarm; PSZ – Pagano Shear Zone; RRDS – Rooi Rand dyke swarm; SJoB – San Jorge Basin; SLDS – Save Limpopo dyke swarm; SWMP – Southern Weddell Magnetic Province; SWMP and NWMP framework from Jordan et al. (2017); South Africa simplified dyke network drawn after Gomez (2001); East Antarctica dykes drawn after Curtis et al. (2008); Falkland Islands onshore and nearshore dykes drawn after Stone et al. (2009); Outeniqua Basin fault network after Paton et al. (2006) and Parsiegla et al. (2009); SNFB and NFB fault networks after Lohr and Underhill (2015) and Chapter 4 (Stanca et al., 2019); South America fault network after Lovecchio et al. (2019); Karoo lavas extent after Jourdan et al. (2007); Chon Aike lavas extent after Bouhier et al. (2017); DML-Ferrar lavas extent after Elliot (1992) and Elliot et al. (1999); arrows show extension direction and their orientation is equivalent to the orientation of σ_3

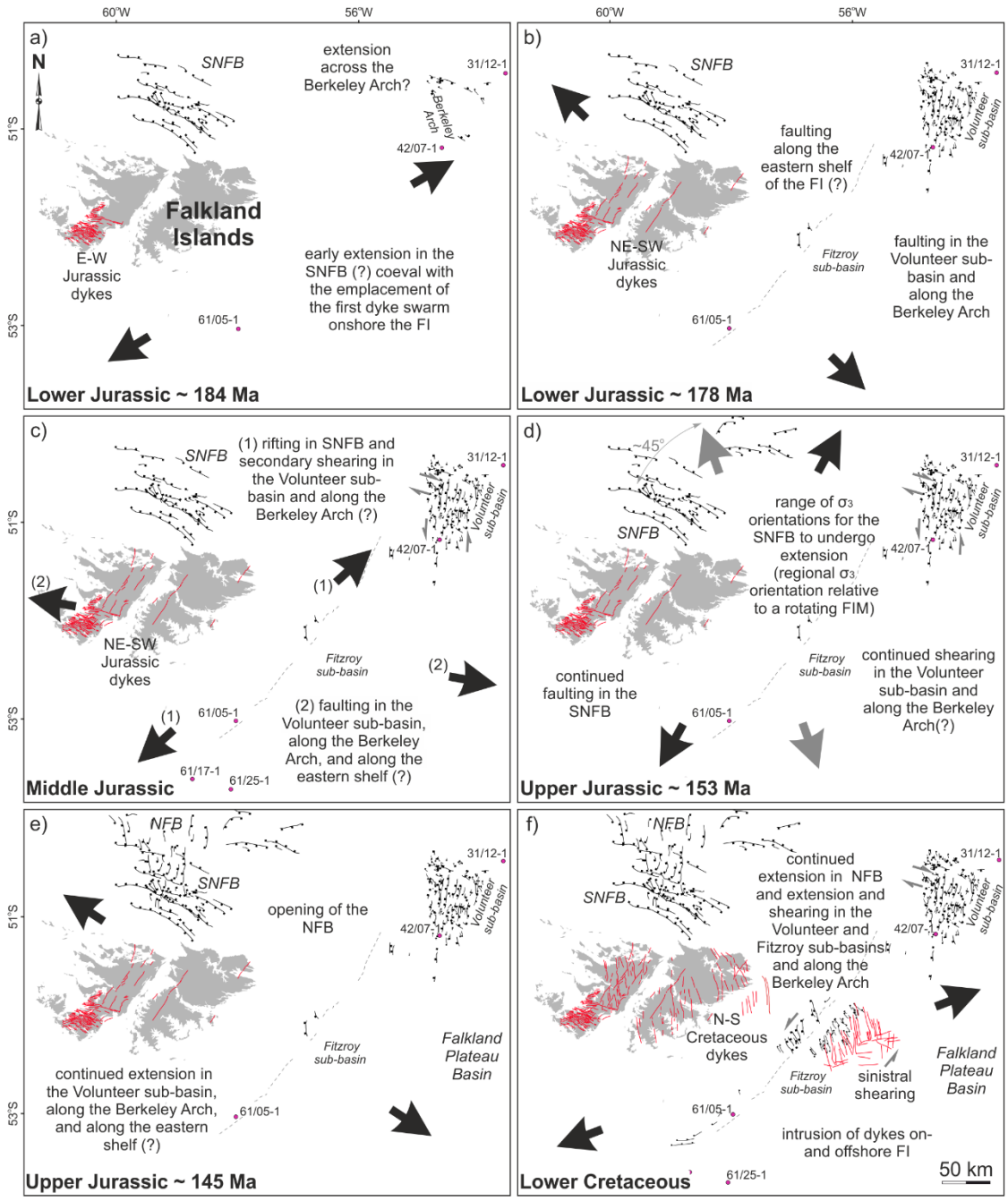

Figure 5.22 See next page for caption

Figure 5.22 Stress field evolution across the Falkland Islands Microplate (based on the structures from this chapter and literature, and the regional stress compilation in Figure 5.21) throughout the Jurassic and Early Cretaceous showing: a) Early Jurassic emplacement of dykes onshore the islands and potential extension occurring in the Southern North Falkland Basin and across the Berkeley Arch; b) extension along the eastern shelf of the Falkland Islands and the emplacement of a NE-SW trending dyke swarm onshore; c) reactivation of the Southern North Falkland Basin faults and secondary shearing occurring in the Volunteer sub-basin area, followed by continued WNW-ESE directed extension in the Fitzroy and Volunteer sub-basins; d) reactivation of the faults in the Southern North Falkland Basin and continued shearing in the Volunteer sub-basin region; e) opening of the North Falkland Basin and extension along the eastern shelf of the Falkland Islands; f) Early Cretaceous emplacement of dykes on-and offshore the Falkland Islands and continued extension and wrenching in the offshore basins; NFB – North Falkland Basin; SNFB – Southern North Falkland Basin; onshore and nearshore dykes drawn after Stone et al. (2009); SNFB and NFB fault networks after Lohr and Underhill (2015) and Stanca et al. (2019); no onshore structural features besides dykes are shown for simplicity (see Figures 5.13 and 5.14 for the detailed map); arrows show extension direction and their orientation is equivalent to the orientation of σ_3

The Late Jurassic to Early Cretaceous normal faults in the NFB and Fitzroy sub-basin and the Early Cretaceous (121 ± 1.2 Ma to 138 ± 4 Ma) on- and offshore dykes are consistent with a NE-SW regional extension direction (Paton and Underhill, 2004) related to the opening of the South Atlantic (Figure 5.21b, c). This indicates that, at this stage, the FIM was roughly in its present-day position relative to South America (Figure 5.21b, c).

Jurassic to Early Cretaceous en-échelon normal faults in the Fitzroy sub-basin and along the Berkeley Arch suggest that some degree of sinistral wrenching occurred along the western NE-SW trending margin of the FPB during this time and WNW-ESE dextral shearing along the Berkeley Arch (Figures 5.4, 5.19). This is consistent with intra-plate deformation related to a clockwise rotation of the FIM throughout the Jurassic. Further plate reorganization and/or wrenching related to movement on the AFFZ occur as late as Early Cretaceous when evidence of WNW-ESE dextral shearing is identified along the Berkeley Arch and NE-SW sinistral wrenching is interpreted in the Fitzroy sub-basin (Figures 5.4, 5.19). Large-scale NE-SW features (Figure 5.4a, b and c) were identified further east on the plateau which were interpreted as regional intra-plate sinistral shear zones that accommodated the rotation of the FIM with the small-scale en-échelon faults allowing further deformation along and between these

features. Although geometries indicative of sinistral wrenching were identified on the gravity data (Figure 5.4a, c), the amount of horizontal displacement along these potential fracture zones remains difficult to constrain.

Besides the NE-SW fault zones interpreted within the FPB, the Falkland Sound Fault, running between the West and East Falkland (Figure 5.4a), follows the same trend and one could argue for a common origin. Studies carried along the Falkland Sound Fault suggest that these shear zones might be long-lived basement structures with activity recorded as early as late Paleozoic (Aldiss and Edwards, 1999; Stone, 2016) and re-established as left-lateral faults during the Mesozoic. However, based on the current data, the amount of displacement along these potential fracture zones cannot be quantified. Dextral movement in the range of 3.3 – 300 km was interpreted along the Falkland Sound Fault during the Permo-Triassic or coeval with the break-up of Gondwana (Thomas et al., 1997; Curtis and Hyam, 1998; Aldiss and Edwards, 1999). However, no evidence of Jurassic or sinistral reactivation has been documented by more recent studies in the offshore sedimentary basins along-strike the Falkland Sound Fault (Richards et al., 1996a; Lohr and Underhill, 2015; Stanca et al., 2019) which contributes to the uncertainty regarding the nature and age of this potential fracture zone. This precludes a correlation with the eastern fracture zones following the same trend and hinders a more detailed reconstruction of the microplate and an understanding of its overall geometry prior to the break-up.

5.5.4.3 Implications for the FIM rotation mechanism

Invoking the kinematic models of Ron et al. (1984), McKenzie and Jackson (1986), and Peacock et al. (1998) for the rotation of the FIM is a novel explanation. The extent of the blocks/microplates that have undergone this style of deformation related to large amounts of rotations in transform margin settings is sparsely documented. Examples of large recorded rotations, comparable to the FIM case, include the Santa Catalina Island (~90°) in South California (Luyendyk et al., 1985), albeit affecting a much smaller block (thousands versus hundreds of thousands of km^2), and the Ellsworth-Whitmore Terrane (~90°) in Western Antarctica (comparable in areal extent to the FIM; Curtis and Storey, 1996). Instances where the deformation related to rotation was accommodated by strike-slip faults anthithetic to the main shear zone (Ron et al., 1984; McKenzie and Jackson, 1986) are reported in the eastern and western Transverse Ranges in Southern California (Platt and Becker, 2013; Ingersoll and Coffey, 2017), and the oceanic Manus microplate (Bismarck Sea)

in a back-arc spreading system (Martinez and Taylor, 1996). However, in none of these examples this style of deformation was both documented and led to >80° rotation of a microplate the size of the FIM.

In this chapter, evidence of sinistral wrenching across the FIM is reported, potentially on several NE-SW striking shear zones (Figure 5.4a, b and c). This observation is consistent with the kinematic models of Ron et al. (1984) and McKenzie and Jackson (1986), considering that the rotation of the FIM occured in an overall dextral shear zone developed between Africa and Antarctica, and Africa and South America. Furthermore, fault networks that are several orders of magnitude smaller, and suggestive of conjugate dextral and sinistral shearing have been interpreted along the eastern shelf of the Falkland Islands (Figure 5.19). This is consistent with the model proposed by Peacock et al. (1998) where high degrees of block rotation can be accomodated through small-scale faulting and increased deformation within the block itself (Figures 5.4a, d and 5.19). Although these models can be used to interpret the current structural architecture of the FIM, more data are required to constrain whether the microplate rotated as a whole, or whether the NE-SW shear zones are responsible for a further fragmentation of the FIM. Furthermore, the answer to why this particular transform margin has seen such high degrees of rotation affecting a microplate several hundred of kilometers wide remains elusive. Possibly this is a consequence of the origin of the microplate at a junction of multiple tectonic plates, where rapid variations in the stress configuration are expected, followed by its evolution along one of the most long-lived and long-offset transform faults on Earth. Alternatively, it is the result of deeper processes that preconditioned this scale of rotation, and ultimately led to the break-up of Gondwana (Ben-Avraham et al., 1993; Storey, 1995; Dalziel et al., 2000). Nonetheless, this study advocates testing the kinematic models of Ron et al. (1984), McKenzie and Jackson (1986), and Peacock et al. (1998) in other settings where comparable scales of microplates and amount of rotation require a mechanistic explanation (e.g. the Ellsworth Whitmore Terrane).

5.6 Conclusions

The western margin of the Falkland Plateau Basin recorded a series of rapid changes in the orientation of σ_3 during the Jurassic and Early Cretaceous related to a vertical-axis rotation of the Falkland Islands Microplate. This rotation took place under a complex stress regime corresponding to the region

located between South America, Africa, and East Antarctica and the early stages of transform margin formation.

The clockwise rotation resulted in the generation of NE-SW and WNW-ESE trending faults in the northern part of the margin (along the Berkeley Arch and in the Volunteer sub-basin) superimposed by N-S striking en-échelon normal faults extending into the Fitzroy sub-basin. When collated with information from the North Falkland Basin and onshore the Falkland Islands, the larger structural framework supports a complex tectonic history of the FIM. The orientation of the minimum horizontal stress across the FIM alternated between roughly NE-SW and NW-SE/WNW-ESE during the Jurassic and switched to a NE-SW orientation during the Early Cretaceous.

Interpretation of seismic reflection data along the eastern shelf of the FIM points towards a larger eastern extent of the microplate than previously constrained. The revised microplate comprises the region of the Volunteer and Fitzroy sub-basins. The western extent of the FIM is interpreted as following the high arcuate gravity anomaly bounding the Malvinas Basin to the east and along which evidence of Jurassic extension and inversion was identified. A comparison of the newly defined FIM local stress configuration with the regional stress in the reconstructed south-western Gondwana suggests that the rotation of the microplate started during or after the intrusion of the Jurassic NE-SW trending dykes onshore the Falkland Islands (during the drift initiation of East Antarctica in Middle Jurassic) and continued throughout the Late Jurassic. During the incipient stages of rotation, a small degree of compression occurred in the north-eastern and south-western corners of the microplate, but the predominant extensional structures suggest that the early fragmentation of Gondwana generated enough space during the clockwise rotation of the islands to limit the widespread occurrence of compression.

Chapter 6 Implications of the crustal architecture of the Falkland Plateau Basin for plate reconstructions in the South Atlantic: insights from gravity and deformable plate modelling

Summary

Continental break-up is commonly associated with intra-continental wrenching that can lead to the generation of transform margins. The wrenching phase is typically associated with complex processes (e.g. vertical-axis rotations of crustal blocks and microplates), which result in heterogeneous structural and crustal architectures. This high degree of complexity makes understanding the evolution of such tectonic settings difficult. The Falkland Plateau is such an area where regional wrenching accompanying continental break-up has resulted in a mosaic of crustal types underlying its largest basin: the Falkland Plateau Basin. The uncertainties in crustal boundaries have resulted in several models for the evolution of the plateau which hinder the development of a reliable plate model for this area. This chapter integrates seismic reflection, gravity, and magnetic data, gravity modelling and inversion, and deforming plate modelling to propose an updated crustal architecture of the Falkland Plateau Basin. The results show that the basin is underlain by extended continental crust in the west and north. The eastern and central part consists of a complex juxtaposition of intruded and underplated continental crust and thick oceanic crust, crosscut by shear zones. Furthermore, the deforming plate models show that a rotation of the Falkland Islands Microplate is more compatible with the present-day architecture of the plateau.

6.1 Introduction

Intra-continental shear zones formed during the incipient stages of transform margin formation or generally during continental break-up are associated with a complex tectono-stratigraphy and crustal architecture that reflects early-stage fragmentation of the crust and vertical-axis block rotation of the newly formed continental blocks (Scrutton, 1979; Basile and Allemand, 2002; Mercier de Lépinay et al., 2016; Nemčok et al., 2016). The resulting crustal provinces exhibit high degrees of faulting, volcanism, localized tectonic, thermal and/or flexural uplift (Scrutton, 1979; Mascle, Blarez, 1987; Basile and Allemand, 2002; Attoh et al., 2004; Basile, 2015), and a high lateral crustal variability. Therefore, assessment of their evolution is challenging, and an integrated

approach to analysis is crucial to understand the structure of these environments.

The Falkland Plateau is an example of a transform margin that formed at the junction between Africa, South America and Antarctica during the break-up and dispersal of Gondwana. Numerous studies, based on seismic reflection and refraction, gravity, and magnetic data, have documented offshore fault networks and developed stratigraphic and crustal models for the plateau (Ludwig et al., 1978; Lorenzo and Mutter, 1988; Bry et al., 2004; Del Ben and Mallardi, 2004; Kimbell and Richards, 2008; Schreider et al., 2011; Baristeas et al., 2013; Lohr and Underhill, 2015; Schimschal and Jokat, 2017, 2019a, b; Eagles and Eisermann, 2020). However, there are still uncertainties in the crustal architecture of the plateau, which impact the amount of deformation and extension interpreted along it. This limits the elucidation of the evolution and reconstruction of the Falkland Plateau Basin which in turn impacts the pre-break-up plate configuration in south-western Gondwana.

In this chapter, integration of regional 2D and 3D seismic reflection data, global open-source gravity data (Sandwell et al., 2014), and magnetic data (Eagles, 2019) enables the assessment of the crustal architecture of the Falkland Plateau Basin. This is further constrained using 2D forward gravity modelling, 3D inversion, and iterative stages of deforming plate modelling. The implications of the results on the overall crustal architecture of the Falkland Plateau and its evolution are discussed.

6.2 Geological background

6.2.1 Tectonic context of the Falkland Plateau

The Falkland Plateau (FP) is a transform margin representing the eastward continuation of the continental shelf of South America (Kimbell and Richards, 2008). The northern boundary of the plateau corresponds to the Agulhas - Falkland Fracture Zone (AFFZ) which accommodated ~1200 km of dextral offset during the opening of the South Atlantic (Ben-Avraham et al., 1997). To the south, the plateau is bounded by the sinistral North Scotia Ridge (NSR) (Ludwig, 1983), and to the east it merges with the Georgia Basin (Lorenzo and Mutter, 1988; Figure 6.1).

The FP was generated during the break-up of Gondwana and was subsequently affected by the opening of the Atlantic Ocean in the Mesozoic and Late Cretaceous - Cenozoic oblique compression and transpression from

the south related to the development of the NSR (Lorenzo and Mutter, 1988; Cunningham et al., 1998; Eagles, 2000; Bry et al., 2004). The former predominantly extensional episodes resulted in a series of crustal and structural provinces along the plateau. The Falkland Islands Microplate is the most controversial domain and is surrounded by the Malvinas Basin to the west, the North Falkland Basin to the north, the South Falkland Basin (SFB) to the south, and the Falkland Plateau Basin (FPB) to the east. The easternmost province of the plateau is the Maurice Ewing Bank (MEB). The North Falkland Basin (NFB) is further subdivided in the Middle to Late Jurassic Southern North Falkland Basin (SNFB) and the Late Jurassic - Early Cretaceous North Falkland Graben (Lohr and Underhill, 2015; Stanca et al., 2019; Chapter 4). The FPB consists of the Volunteer sub-basin to the northwest and the Fitzroy sub-basin in the west and southwest; the two sub-basins are separated by the Berkeley Arch basement high (Rockhopper Exploration Plc., 2012; Dodd and McCarthy, 2016).

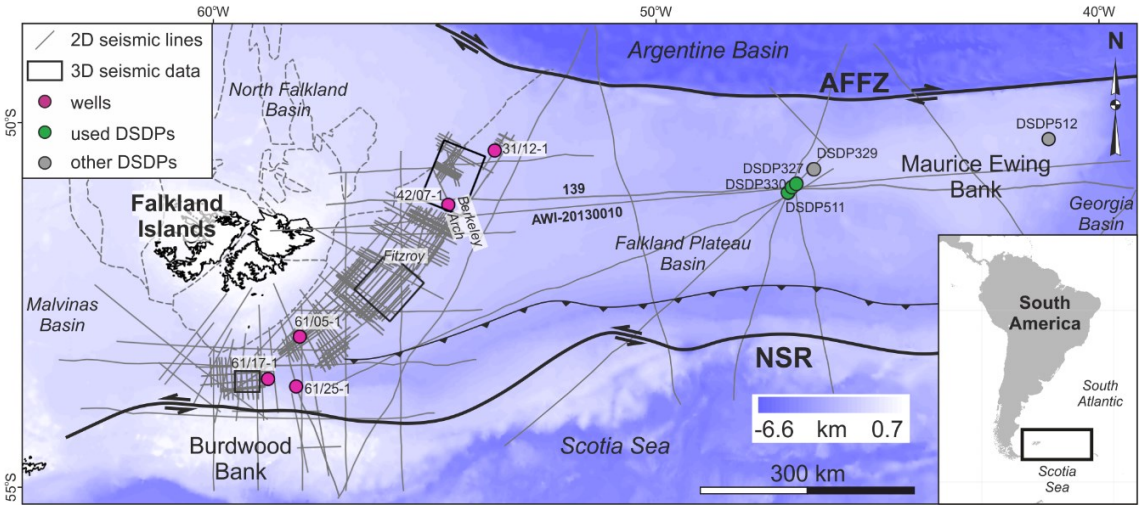

Figure 6.1 Present-day extent of the Falkland Plateau showing the bounding fracture zones (dextral AFZ and sinistral NSR along with the NSR thrusting front) overlain by the available seismic reflection data and wells used in this chapter; AAFZ – Agulhas – Falkland Fracture Zone; NSR – North Scotia Ridge

The nature of the crust underlying the Falkland Plateau remains subject to debate and is directly controlled by the evolution of the Falkland Islands Microplate during the fragmentation of Gondwana. Correlations between geological and geophysical data from the Falkland Islands and South Africa led to the development of the rotational theory which argues for rotation of the Falkland Islands Microplate of up to 120° (Adie, 1952a; Frakes and Crowell, 1967; Crowell and Frakes, 1972; Mitchell et al., 1986; Marshall, 1994; Mussett

and Taylor, 1994; Thomas et al., 1997; Thomson, 1998; Curtis and Hyam, 1998; Storey et al., 1999; Trewin et al., 2002; Macdonald et al., 2003; Stone et al., 2009; Dalziel et al., 2013; Stanca et al., 2019; Chapter 4). The lack of documented evidence for this rotation in the sedimentary infill of the basins surrounding the islands (Richards et al., 1996a), and the absence of a mechanism to accommodate this rotation led several authors to favour a non-rotational model. In this model, the Falkland Islands were in a similar position relative to South America prior to the break-up of Gondwana as today (Lawrence et al., 1999; Ramos et al., 2017; Lovecchio et al., 2019), and the fragmentation of the supercontinent was recorded by extension in the sedimentary basins around the islands.

6.2.2 Architecture of the Falkland Plateau

6.2.2.1 Tectono-stratigraphy of the Falkland Plateau

The tectono-stratigraphic architecture of the Falkland Plateau is the result of multiple tectonic events that started as early as the Permian and ended with the formation of the Scotia Sea (Cunningham et al., 1998; Hodgkinson, 2002; Stone, 2016). Evidence of the Permo-Triassic collisional episode, which resulted in the formation of the trans-Gondwanian orogen, seen today in the Sierra de la Ventana (South Argentina), Cape Mountains (South Africa), Ellsworth Whitmore Terrane / Ellsworth Mountains Block, and Pensacola Mountains (Antarctica), was recorded by the onshore geology of the Falkland Islands (Du Toit, 1937; Thomas et al., 1993; Trouw and De Wit, 1999; Dalziel et al., 2000), and influenced the architecture of the offshore Mesozoic sedimentary basins that formed during the break-up of Gondwana (Richards and Fannin, 1997).

Currently, the only area of the Falkland Plateau above sea level are the Falkland Islands outcrops, which range in age from Neoproterozoic gneisses (Cape Meredith Complex) through Siluro-Devonian quartz-rich sandstones and conglomerates with intercalated siltstones and mudstones (West Falkland Group) to Permo-Carboniferous glacial deposits and mudstone-dominated successions (Lafonian Supergroup; Curtis and Hyam, 1998; Aldiss and Edwards, 1999). The architecture of the islands was strongly influenced by Permo-Triassic E-W/WNW-ESE and NE-SW trending folds and thrusts associated with N-S compression and NE-SW dextral transpression, respectively (Curtis and Hyam, 1998; Aldiss and Edwards, 1999; Stone, 2016). The inheritance of this structural grain played a major role in the formation of the northern and eastern sedimentary basins (Richards and Fannin, 1997; Lohr

and Underhill, 2015; Stanca et al., 2019; Chapters 4 and 5). During and following the fragmentation of Gondwana, the FP underwent extension which resulted in the formation of four sedimentary basins: the Malvinas Basin, the North Falkland Basin, the South Falkland Basin, and the Falkland Plateau Basin.

The Malvinas Basin lies west of the Falkland Islands (Richards et al., 1996a). It has a complex structure which was the result of two extensional episodes that generated normal faults trending NW-SE and NE-SW, which were correlated with back-arc extension and the opening of the Weddell Sea, respectively (Galeazzi, 1998; Ghiglione et al., 2010; Baristeas et al., 2013). The North Falkland Basin (NFB) to the north of the islands is the result of two rifting events: a Jurassic one that resulted in the opening of the WNW-ESE trending Southern North Falkland Basin (SNFB), which reactivated Permo-Triassic thrusts, and a Late Jurassic - Early Cretaceous extensional episode during which the N-S trending North Falkland Graben formed (Richards and Fannin, 1997; Richards and Hillier, 2000; Lohr and Underhill, 2015). South of the Falkland Islands lies the asymmetrical South Falkland Basin. This basin plunges southward where it terminates against the NSR (Richards and Fannin, 1997). The deformation within it was accommodated by E-W striking normal faulting (Richards et al., 1996a) superimposed by thrusting related to movement along the North Scotia Ridge (Richards et al., 1996a).

The Falkland Plateau Basin (east of the islands) is bounded to the west by a series of NE-SW trending normal faults (Richards et al., 1996a, b), and to the E by the Maurice Ewing Bank. Seismic reflection data interpretation showed that normal faults within the basin predominantly terminate at the top Jurassic (Lorenzo and Mutter, 1988). Based on this, FPB rifting between Early Jurassic and Early Cretaceous was interpreted (Lorenzo and Mutter, 1988; Marshall, 1994; Richards et al., 1996a). There are studies supporting an earlier onset of extension during the Permo-Triassic (Richards et al., 1996a). However, no age constraints from well data exist for the oldest syn-rift deposits to verify this. New seismic reflection data, presented and interpreted in Chapter 5, show the presence of Jurassic NE-SW and WNW-ESE trending faults in the northern part of the margin (along the Berkeley Arch and in the Volunteer sub-basin). These faults are superimposed by Jurassic to Early Cretaceous N-S striking en-échelon normal faults extending into the Fitzroy sub-basin, suggesting a wrenching element associated with the Mesozoic break-up and extension.

The fragmentation of Gondwana was also associated with extensive volcanism, both onshore and offshore the islands. The Paleozoic succession cropping-out onshore was intruded by E-W and NE-SW trending Jurassic dykes, coeval to the Karoo-Ferrar large igneous province formation, and N-S striking Early Cretaceous dykes related to the opening of the South Atlantic (Mussett and Taylor, 1994; Mitchell et al., 1999; Stone et al., 2008; Richards et al., 2013; Hole et al., 2016; Stone, 2016). N-S trending Early Cretaceous dykes and sills have been interpreted nearshore and offshore the Falkland Islands, in the Fitzroy and Volunteer sub-basins (Barker, 1999; Richards et al., 2013; Chapter 5).

6.2.2.2 Crustal distribution along the Falkland Plateau

The fragmentation of Gondwana associated with the rotation of the Falkland Islands Microplate (Adie, 1952a; Mitchell et al., 1986; Marshall, 1994; Mussett and Taylor, 1994; Thomson, 1998; Curtis and Hyam, 1998; Storey et al., 1999; Trewin et al., 2002; Macdonald et al., 2003; Stone et al., 2009; 2013; Stanca et al., 2019) resulted in a rapidly varying tectono-stratigraphy along the Falkland Plateau and a conflicting assessment of the crustal architecture. The basins surrounding the islands have been under exploration for decades and Paleozoic deposits, similar to the ones cropping-out onshore the Falkland Islands, were penetrated by wells in the North Falkland Basin (well 14/9-1, Lohr and Underhill, 2015) and in the western basins (well Cruz x-1, Galeazzi, 1998). These local constraints, correlated with seismic reflection data, support the continental nature of the sedimentary basins north, south, and west of the Falkland Islands (Galeazzi, 1998; Bry et al., 2004; Tassone et al., 2008; Lohr and Underhill, 2015; Lovecchio et al., 2019), but the crust underlying the eastern basin remains uncertain.

The Falkland Plateau Basin is located between the Falkland Islands and the Maurice Ewing Bank. DSDP 330 cored metamorphic and igneous rocks on the western flank of Maurice Ewing Bank (Beckinsale et al., 1977) proving the continental nature of the block. The cored granites and gneisses are comparable with the ones cropping out in the western part of the FP, onshore the Falkland Islands at Cape Meredith (Beckinsale et al., 1977; Tarney, 1977), suggesting that the islands and the Maurice Ewing Bank originated from a continuous continental block that underwent extension and/or potential break-up during the fragmentation of Gondwana. This is supported by geochemical and isotopic analyses of their basement lithologies (Chemale et al., 2018).

The seismic refraction study across the FP and Scotia Sea by Ewing et al. (1971) is amongst the first attempts to describe the nature of the crust under the FPB. Based on the obtained velocities, Ewing et al. (1971) interpreted oceanic crust under the Falkland Trough, continental crust in the central part of the FPB (profile CD in Figure 1 of Ewing et al., 1971), whilst the northern escarpment bounding the basin showed velocities corresponding to continental basement. The latter interpretation remains uncertain due to the existence of steeply dipping structures and intense faulting (Ewing et al., 1971).

Further multichannel seismic reflections and sonobuoy reflection and refraction data were acquired during the cruises carried out by the Lamont-Doherty Geological Observatory. Analysis of these data suggested the presence of thick oceanic crust or highly attenuated continental crust underlying the FPB (Ludwig, 1983; Lorenzo and Mutter, 1988). Richards et al. (1996a), based on gravity modelling, interpreted a 16 km thick continental crust in the western part of the basin, and Barker (1999) placed the continent-ocean boundary along the NE-SW gravity high SE of the FI. Recent studies (Kimbell and Richards, 2008; Schimschal and Jokat, 2017, 2019b) brought new insights into the structure of the FPB. Based on gravity inversion and flexural modelling, Kimbell and Richards (2008) interpreted continental crust in the northern part of the FPB along the AFFZ, whereas the rest of the basin is interpreted as being underlain by thick oceanic crust or underplated thinned continental crust. Schimschal and Jokat (2017, 2019b) used wide-angle seismic data and potential field data modelling to confirm the presence of 35 km thick continental crust nearshore East Falkland, followed by a 90 km wide continent-ocean transition zone and a high velocity (up to 7.4 km/s) 11-20 km thick crust underlying the FPB, which was interpreted as thick oceanic crust. This led the same authors to postulate that the entire FPB is underlain by oceanic crust. Recent aeromagnetic data acquired along the Falkland Plateau Basin show the presence of magnetic reversal isochrons in the eastern part of the FPB (Eagles and Eisermann, 2020). Based on this, and the information from the refraction study of Schimschal and Jokat (2017), a FPB completely underlain by oceanic crust was interpreted by these authors as well. However, the seismic refraction survey of Schimschal and Jokat (2017, 2019b) consisted of a single profile which was extrapolated across the entire FPB, whereas the study of Eagles and Eisermann (2020) indicated the presence of oceanic crust with certainty only in the south-eastern corner of the FPB.

6.2.3 SW Gondwana reconstructions and the palaeoposition of the Falkland Plateau

The crustal architecture of the Falkland Plateau and the uncertainty around it are directly linked to its position and configuration prior to the break-up of Gondwana. The scarcity of data along the larger Falkland Plateau Basin hinders attempts to build a reliable crustal model and reconstruction of the area. The Falkland Islands Microplate (FIM) represents the contentious block of the plateau. Its position in a reconstructed Gondwana is controlled by the configuration of the larger plates of the supercontinent and has implications on the amount of extension that the Falkland Plateau Basin underwent and, in turn, on its crustal architecture. There are two main interpretations of the behaviour of the FIM during the fragmentation of Gondwana.

The first interpretation is based on stratigraphic correlations, fossil assemblages, ice flow directions, and structural similarities between the Falkland Islands and the South African margin, and palaeomagnetic and aeromagnetic data analysis, and invokes a clockwise rotation of the microplate of up to 120° during the early stages of fragmentation (Mitchell et al., 1986; Marshall, 1994; Mussett and Taylor 1994; Curtis and Hyam 1998; Trewin et al., 2002; Stone et al., 2009; Stanca et al., 2019; Chapters 4 and 5; Figure 6.2a). In this interpretation, the rotated Falkland Islands are located off the southeast coast of South Africa so that there is a correlation between the West Falkland Group and the Table Mountain, Bokkeveld, and Witteberg groups in South Africa (Adie, 1952b, cited by Marshall 1994), the Fitzroy Tillite Formation of the Falkland Islands and the Dwyka Group of South Africa (Curtis & Hyam 1998), the Upper Lafonian Group and the Ecca and Beaufort groups in South Africa (Trewin et al. 2002), and the Cape Meredith Complex and the Namaqua-Natal-Maud belt extending across South Africa and East Antarctica (Thomas et al., 1997; Jacobs et al., 2003; Jacobs and Thomas, 2004; Vorster et al., 2016). This model requires the FIM to be separate from the rest of the Falkland Plateau. Its boundaries correspond to the AFFZ or northern SNFB to the north (Marshall, 1994; Storey et al., 1999), the arcuate positive gravity anomaly (eastern margin of the Malvinas Basin; Marshall, 1994; Storey et al., 1999; Chapter 5) to the west, the NE-SW trending positive anomaly (western margin of the FPB; Richards et al., 1996b; Storey et al., 1999) or east of the Fitzroy and Volunteer sub-basins (Chapter 5) to the east, and the NSR to the south.

The second interpretation of the reconstruction of the Falkland Islands keeps the microplate in the same position relative to the southern part of South

American plate as today (Figure 6.2a). In this model the FPB would be the result of extension between South America and Africa or the plateau would represent the conjugate to the Weddell Sea, and the FPB opened in response to extension between Antarctica and West Gondwana (Lawrence et al., 1999; Eagles and Vaughan, 2009; Ramos et al., 2017; Chemale et al., 2018; Lovecchio et al., 2019; Eagles and Eisermann, 2020). Variations of the non-rotational model were favoured due to a lack of documented rotation-related deformation in the sedimentary basin-fills offshore the islands (Richards et al., 1996a) along with the absence of a mechanism for it. Stratigraphic and structural correlations between the West Falkland Group and northern Patagonia, the Fitzroy Tillite Formation and the Sauce Grande Tillite of the Ventania System, and the thrusts onshore the Falkland Islands and the ones in the north-eastern North Patagonian Massif are considered supporting arguments for this model (von Gosen, 2003; Ramos et al., 2017) along with correlations between magnetic reversal isochrons in the Falkland Plateau and Central Scotia and Weddell seas (Eagles and Eisermann, 2020).

The position of the plateau, and implicitly, the islands, in a Gondwana pre-break-up configuration is controlled by the space available at that time between Africa, South America, and East Antarctica. Considering a fixed position for South Africa, variations in the reconstructions of South America and Antarctica are impacting the extent and distribution of this space.

The fragmentation and fit of South America relative to Africa is of high importance as it can provide more constraints on the extension the plateau underwent, and the space that was available for a potential rotation of the FIM. A closer fit between the two major plates requires a pre-fragmentation of South America which has been achieved in various ways (König and Jokat, 2006; Torsvik et al., 2009; Müller et al., 2019). Its southern part (Patagonia) was reconstructed in a more eastern position by invoking the presence of a right-lateral fault north of the North Patagonian Massif (Ben-Avraham et al., 1993) or south of it, along the Gastre Fault System (Rapela and Pankhurst, 1992; König and Jokat, 2006; Torsvik et al., 2009). Field observations along the latter disproved its dextral kinematic (von Gosen and Loske, 2004; Franzese and Martino, 1998 in Ramos et al., 2017). Whereas this attempt to obtain a tighter fit between South America and Africa is based on movement along the boundaries of pre-defined sub-plates, Heine et al. (2013) and Müller et al. (2019) achieve a close fit by considering intra-plate deformation affecting South America during the break-up (i.e. by closing the sedimentary basins along the

eastern margin of South America; Figure 6.2). This scenario, however, positions Patagonia in a more south-western position than the one invoking dextral movement along the Gastre Fault System, requiring a correction of the position of the Falkland Islands in the same direction to avoid unrealistic gaps between the islands and the South American shelf (see Chapter 2, Section 2.3 for variations in the reconstruction of South America).

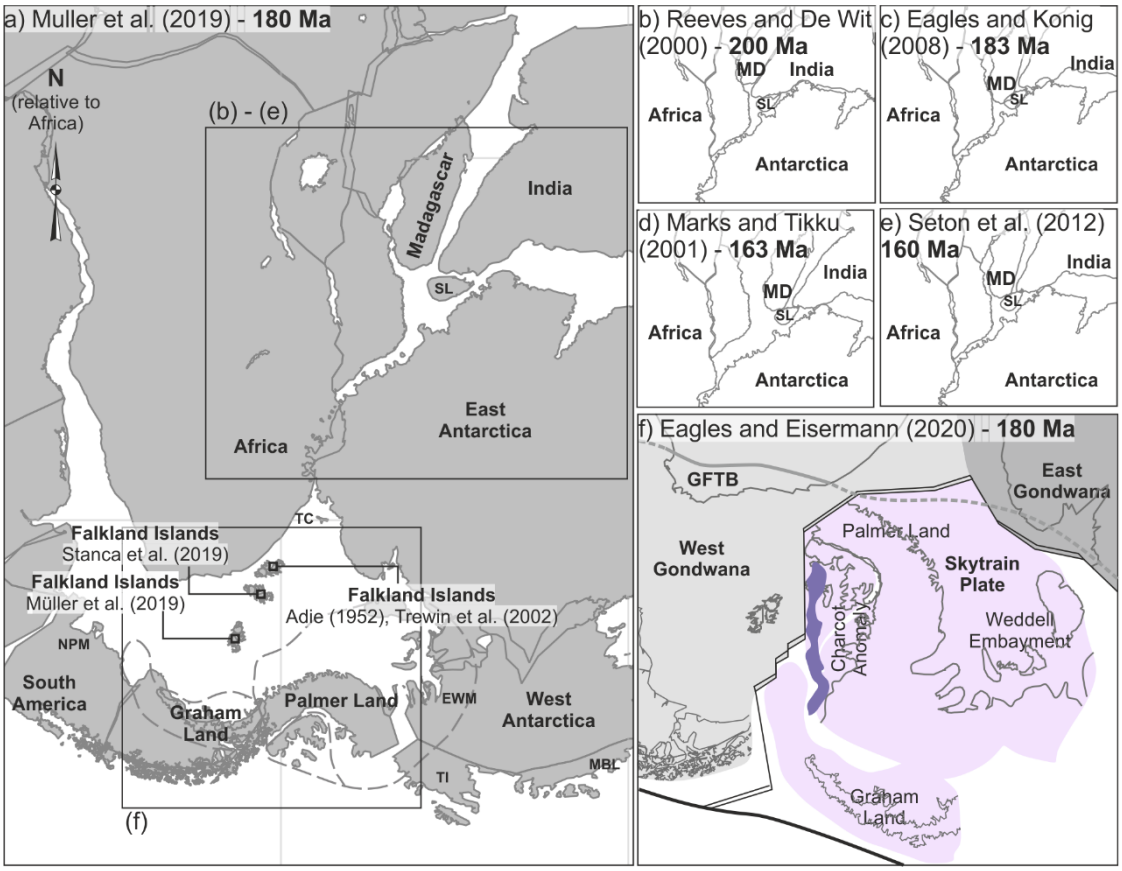

Figure 6.2 Differences in the palaeogeographic reconstruction of Gondwana; a) plate model after Müller et al. (2019) showing the fit between Africa, Antarctica, and South America and the different reconstructions of the Falkland Islands; stippled grey lines around the Antarctic Peninsula – boundaries of the Skytrain Plate in (f); b) to e) difference in the fit between Africa and East Antarctica from various authors for the Jurassic (redrawn after Nguyen et al., 2016); f) alternative reconstruction of the Antarctic Peninsula; EWM – Ellsworth Whitmore; MBL – Marie Byrd Land; MD – Madagascar; NPM – North Patagonia Massif; SL – Sri Lanka; TC – Tugela Cone; TI – Thurston Island

The reconstruction of East Antarctica, the smaller blocks of the West Antarctic region (Ellsworth Whitmore Terrane, Thurston Island, Marie Byrd Land), and the Antarctic Peninsula have implications on the position of the Falkland Plateau within Gondwana as well as on understanding its evolution. The now

eastern part of the Falkland Plateau (the Maurice Ewing Bank) is considered to have been connected to the southern part of the Tugela Cone (Figure 6.2) in the Natal Valley, offshore South Africa (Martin et al., 1982; Marshall, 1994) but there are reconstructions that position the MEB further north to achieve a tighter fit with East Antarctica (Storey et al., 1999; König and Jokat, 2006). This can increase the initial length of the Falkland Plateau and therefore decrease the amount of expected extension during the break-up of Gondwana (König and Jokat, 2006). Another importance of the reconstruction of the Antarctic blocks relates to the evolution of the now southern margin of the FP. This region would have been adjacent to West Antarctica (Figure 6.2) and was obscured during the formation of the North Scotia Ridge and opening of the Scotia Sea (Bry et al., 2004). Therefore, an understanding of the palaeoposition of East and West Antarctica could give us an indication of the architecture of this margin.

Although thoroughly studied, there are still variations in the reconstruction of East Antarctica in a Gondwana pre-break-up configuration. These are primarily due to different interpretations of the continent-ocean boundary, different times for the onset of rifting and drifting, and different interpretations of the pathways followed by the block in the early stages of the break-up (Reeves and De Wit, 2000; Marks and Tikku, 2001; König and Jokat, 2006; Eagles and König, 2008; Seton et al., 2012; Figure 6.2a-e). This has implications for the original length of the Falkland Plateau if using the reconstruction for the Maurice Ewing Bank after Storey et al. (1999). However, a more significant implication comes from the timing of the separation between East Antarctica and Africa as this marks the earliest time when both a driving force is present, and space generated for the Falkland Islands to rotate. Estimates of the timing of the East Antarctic drift onset varies from 165 Ma (Coffin and Rabinowitz, 1987; Marks and Tikku, 2001) through 167.2 Ma (König and Jokat, 2006), 170 Ma (Reeves and De Wit, 2000) to 183-177 Ma (Eagles and König, 2008). The rotation of the FIM is believed to have occurred relatively rapidly (Marshall, 1994; Stanca et al., 2019), after 178 Ma (Stone et al., 2008) and before the Early Cretaceous (Barker, 1999; Storey et al., 1999; Macdonald et al., 2003; Chapter 5). Therefore, a variation in the timing of drift onset of East Antarctica of 18 Ma has major implications on the timing and driving forces behind the rotation of the FIM.

One of the West Antarctic blocks crucial to understanding the evolution of the FP is the Ellsworth Whitmore (Mountains) Terrane (EWM in Figure 6.2), which

shares the same uncertainty in reconstruction as the FIM. The orientation and style of folding within the Ellsworth Whitmore Mountains have led to correlation of the deformation to the Gondwanide Orogen (Schopf, 1969 in Curtis and Storey, 1996), and its alignment with the Cape Fold Belt in Africa requires an anticlockwise rotation of ~90° (Curtis and Storey, 1996). This has been supported by subsequent palaeomagnetic data (Watts and Bramall, 1981; Grunow et al., 1987). The rotation is estimated to have occurred prior to 180-175 Ma (Curtis and Storey, 1996; Martin, 2007) either during the Gondwanide orogeny or later, during the early fragmentation of Gondwana (Curtis and Storey, 1996). Some interpretations consider that the rotation of the Ellsworth Whitmore Terrane and the FIM were coeval and/or due to the same external driving forces (Macdonald et al., 2003; Martin, 2007). However, the pre-break-up reconstruction of the Ellsworth Whitmore Mountains remains uncertain (Marshall, 1994; Curtis and Storey, 1996; Dalziel et al., 2000; Macdonald et al., 2003; Martin, 2007), thus hindering our understanding of the effect of its movement on the evolution of the Falkland Plateau.

The Antarctic Peninsula is another region from the Antarctic block that is closely related to the Falkland area. The peninsula is considered to represent a single block by most interpretations, being reconstructed south-west of Patagonia (König and Jokat, 2006; Seton et al., 2012; Müller et al., 2019; Figure 6.2a) prior to the break-up of Gondwana. Recent studies offer a different fragmentation of the West Antarctic region with the Graham Land as a separate plate in a more southern position than previously suggested for the Antarctic Peninsula (Eagles and Eisermann, 2020). The remainder of the Antarctic Peninsula (Palmer Land) is considered part of a larger new plate, Skytrain, along with the Weddell Embayment, and occupy a rotated position in the reconstruction, adjacent to the Falkland Islands (Eagles and Eisermann, 2020; Figure 6.2f). These two pre-break-up models of the peninsula suggest the Weddell Embayment and the Alexander Island and northern region of Palmer Land, respectively, as the conjugate to the southern part of the FP and have implications for the interpretation of the evolution of the plateau.

6.3 Data and methodology

6.3.1 Seismic reflection data and interpretation

The seismic reflection data used for this chapter comprise 2D and 3D data from seven vintages acquired between 1977 and 2014 by Falklands Oil and Gas Limited, WesternGeco, Noble Energy, Lamont-Doherty Earth Observatory, and

Geophysical Service Incorporated (Figure 6.1). All seismic reflection data have a vertical scale in two-way-time (TWT), and the maximum recorded length varies between 6 and 12 seconds TWT for the 2D data and is equal to 9 seconds TWT for the seismic cubes.

Five exploration wells (31/12-1, 41/07-1, 61/05-1, 61/17-1, and 61/25-1) and three DSDPs (327, 330, and 511) were tied to the seismic data for the horizon interpretation stage. Seismic and well data, except for the open-source Lamont-Doherty Earth Observatory 2D seismic reflection lines and the DSDP data, were provided courtesy of the Falkland Islands Government.

The seismic data were used to build a map of the depth to basement, interpret the near top Jurassic for the entire plateau (see full description of interpretation methodology in Chapters 4 and 5), and intra-Cretaceous and Cenozoic mega-sequences based on stratal terminations and seismic facies analysis (Mitchum et al., 1977; Hubbard et al., 1985a, b). 2D regional seismic reflection lines from the surveys acquired by Lamont-Doherty Earth Observatory, WesternGeco, and GSI were used for validating the crustal types distribution interpreted from gravity and magnetic data. This was carried out by evaluating changes in the seismic character across the Falkland Plateau and changes in amplitude considered a function of volcanism.

For the gravity modelling and inversion, a depth conversion of the modelled 2D seismic sections and horizon interpretations was carried out. A constant velocity of 1500 m/s was used for the water column. For the sediment infill, a v_0-k function ($v = v_0 + k(z-z_0)$, where v_0 – velocity at the top of the layer and ($z-z_0$) – the distance between the point of calculation and the top of the layer) was used, with v_0 = 1600 m/s, based on Schimschal and Jokat (2017), and k = 0.6 (averaged based on the P-wave velocities provided by the same study at different points in the basin). From the base of the sediments up until 15 s TWT depth, a constant velocity of 7000 m/s was used, the depth to Moho being input directly into the gravity modelling and inversion model from the calculations of Kimbell and Richards (2008) and Schimschal and Jokat (2019b), which were based on gravity modelling and isostatic analysis, and seismic refraction data, respectively.

6.3.2 Gravity and magnetic data and interpretation

The gravity data consist of the V24.1 1-minute satellite altimetry free-air gravity anomaly grid of (Sandwell et al., 2014) for the entire Falkland Plateau and for the southern part of South Africa. The magnetic anomaly data used for this

chapter are part of the AIRLAFONIA aerogeophysical survey (Eagles, 2019) acquired along the Falkland Plateau Basin by the Alfred Wegener Institute in 2017 - 2018. The computation of derivatives and testing of filters were carried in Geosoft's Oasis Montaj. Gravity and magnetic lineaments were mapped using the total horizontal (Cordell and Grauch, 1985) and the tilt derivatives (Miller and Singh, 1994; Verduzco et al., 2004; Oruç and Keskinsezer, 2008) of the free-air gravity anomaly and the reduced to pole total magnetic anomaly for the Falkland Plateau. A version of the free-air gravity data that underwent Butterworth bandpass filtering with cut-off wavelengths of 5-70 km (chosen by trial and error to resolve regional structures constrained by literature or seismic data) was used to enhance structural features and delineate areas with potentially different crustal types along the Falkland Plateau Basin. For South Africa a Butterworth bandpass filter with cut-off wavelengths of 10-85 km was chosen by trial to compare it against the one computed along the Falkland Plateau in order to facilitate the correlation of structural features.

6.3.3 2D gravity modelling

Geosoft Oasis Montaj GM-SYS Profile Modelling was used to generate 2D forward models (Talwani et al., 1959; Talwani and Heirtzler, 1964; Won and Bevis, 1987) along the 139 seismic reflection profile in Figure 6.1. This profile was considered suitable for the 2D gravity modelling stage because new seismic refraction data are available roughly along the same direction. The gravity data input was the free-air gravity anomaly grid of Sandwell et al. (2014). Two main models were considered based on the input for the depth to Moho. MKR-2D used the depths estimated by Kimbell and Richards (2008) from their isostatically compensated and forward gravity model, and MSJ-2D used the depths calculated based on seismic refraction data by Schimschal and Jokat (2019b), assuming that lines 139 and AWI-20130010 have a similar structure (Figure 6.1). The crust (from the base of the Mesozoic sediments to the Moho) was divided at its mid-point into an upper and lower crust. Lateral variations in density were accounted for by approximating the structure of the crust to a series of vertical prisms and/or by manipulating the boundary between the upper and lower crust in order to minimize the misfit between the observed and calculated gravity anomalies. A simplified model (with minimum lateral variations) was computed in the first stage to separate main crustal types. Iterative additions of details contributed to the understanding of the extent of areas with higher densities that might be indicative of intrusions.

The water density was set at 1.03 g/cc and the upper mantle at 3.33 g/cc (after Kimbell and Richards, 2008). The sedimentary cover was split into four layers with average densities (2.1 – 2.7 g/cc) based on Schimschal and Jokat (2017). The starting densities for the upper and lower crust were set at 2.75 g/cc and 2.95 g/cc, respectively, based on Kimbell and Richards (2008) and iteratively modified during the modelling process.

6.3.4 3D gravity inversion

Due to high crustal and structural lateral variations across the Falkland Plateau, the density distribution obtained from the 2D forward modelling was compared with results from 3D inversion. This stage was carried out using the VPmg software from Mira Geoscience which allows for 3D modelling and inversion using models consisting of vertical prisms (Fullagar et al., 2000, 2004, 2008; Fullagar and Pears, 2007).

The inputs were represented by the gravity-derived bathymetry of Smith and Sandwell (1997) which was considered a suitable approximation of the actual bathymetry for the scale of the study, and a depth-to-basement surface (Figure 6.3) obtained from the seismic reflection data across the plateau (interpretations from Chapter 4, 5, and this chapter). As for the forward modelling, two scenarios were considered with Moho from Kimbell and Richards (2008; MKR-3D) and Schimschal and Jokat (2019b; MSJ-3D).

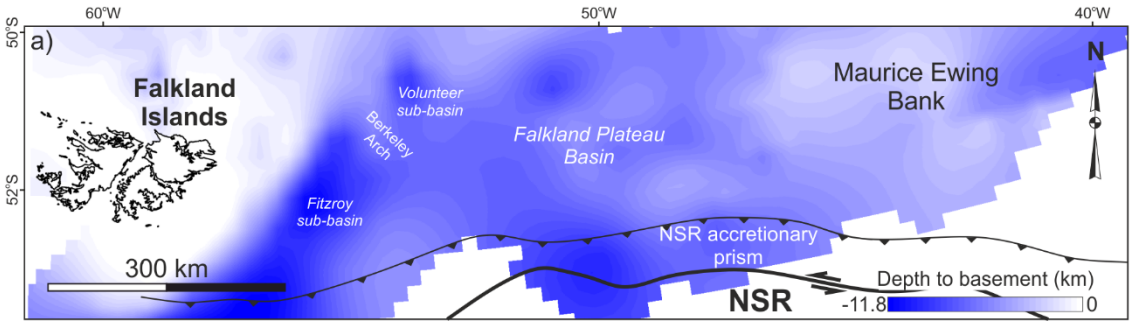

Figure 6.3 Depth to basement map for the Falkland Plateau Basin based on seismic reflection data interpretation (Chapter 4, 5, and this chapter)

A depth-to Moho surface based on an iteration of isostatically compensated modelling and forward gravity modelling of the area for the entire plateau is available from Kimbell and Richards (2008). In order to obtain a 3D surface of the Moho for the MSJ-3D scenario, two stages of geometrical inversion (using 50x50 km and 20x20 km prisms, respectively) were carried, using the Moho depths along the AWI-20130010 profile as pierce points (kept fixed during the inversion). The average densities used for this stage were 1.03 g/cc, 2.3 g/cc,

2.8 g/cc, and 3.33 g/cc for the water, sediments, crust, and upper mantle, respectively (averaged from Kimbell and Richards, 2008 and Schimschal and Jokat, 2019b). The maximum relative change in the depth of the Moho was set at 2% per iteration. The resulting Moho was re-gridded in Petrel in order to obtain a smoother surface and further used as input during the property inversion.

For this stage, a homogeneous inversion was used to obtain an estimation of the optimal starting density for the heterogeneous inversion for each layer. The widths of the model's prisms were 20x20 km, and the maximum change in density per iteration was set at 0.02 g/cc. The density ranges for the sedimentary cover and the crust (pre-Mesozoic sediments and basement) were set as 1.9-2.7 g/cc and 2.58-3.05 g/cc, respectively (based on Schimschal and Jokat, 2017) with the starting densities set at the average values of 2.3 g/cc for the sedimentary cover and 2.8 g/cc for the undifferentiated crust. The water density was set at 1.03 g/cc and the upper mantle at 3.33 g/cc. The homogeneous inversion yielded average densities of 2.4316 g/cc and 2.8328 g/cc, and 2.365 g/cc and 2.785 g/cc for the MKR-3D and MSJ-3D scenarios, respectively, for the sedimentary cover and crust, respectively. These are mentioned here as an aid for the following section.

For the heterogeneous inversion, the E-W and N-S widths of the model prisms were 20x20 km. The starting densities for the sediments and crust were 2.4 g/cc and 2.8 g/cc, respectively (as averaged for the 2 scenarios from the homogeneous inversion; see paragraph above) and the maximum absolute change in density per iteration was set at 0.05 g/cc. Prior to the heterogeneous inversion, a further vertical sub-celling of the sedimentary cover and crust was carried out, resulting in 5 km high cells within the vertical prisms. VPmg allows for three different types of weighting for the computed heterogeneous cells in order to prevent the concentration of densities near the surface of the model. Here a depth and a full distance weighting are used, and the results are compared. The depth weighting assumes that the gravitational effect decays with the inverse of the function squared (Li and Oldenburg, 1996, 1998), and the full distance weighting estimates the sensitivity of a cell to all data locations (Mira Geoscience, 2019; Figure A.9).

The maximum number of iterations was set at 25, 100, and 50 for the geometrical, homogeneous, and heterogeneous inversion, respectively, and the absolute data uncertainty (error) was set at 2 mGal. The upper and lower boundaries of the models were represented by the sea-level and a depth of -50

km, respectively. Laterally, the model extended ~1483 km E-W (from East Falkland past the Maurice Ewing Bank) and ~256 km N-S, covering the Falkland Plateau Basin. The depth-to Moho obtained from geometrical inversion along with the one available from Kimbell and Richards (2008) were used to calculate the crustal thickness along the Falkland Plateau along with thinning factors using the methodology of Hellinger and Sclater (1983).

6.3.5 Plate reconstruction

The plate reconstruction model for the Falkland Plateau region was carried out in GPlates and built on the global deformable plate model of Müller et al. (2019) with some modifications. The location of the pre-rift continent-ocean boundaries for South Africa and southern South America (although to a lesser extent) were edited (Figure A.12) so that they correspond to the high-low gravity anomaly break as shown by the satellite gravity data set of Sandwell et al. (2014) in order to obtain a close fit between the reconstructed plates (Macdonald et al., 2003). The initiation of westward movement of South America was set at ~167.2 Ma after König and Jokat (2006) to account for space generated due to rifting in the basins along the eastern margin of South America during the Early to Middle Jurassic (Lovecchio et al., 2018, 2019). The motion of the Antarctic Peninsula is also based on König and Jokat (2006). The model of Müller et al. (2019) incorporates the positions of East Antarctica after König and Jokat (2010) as far back as 148.8 Ma, followed by the tight fit position of Eagles and König (2008) at 177 Ma. The reconstructed positions for chron M24 (155 Ma) and the Jurassic Quiet Zone are adapted from König and Jokat (2006). The southward drift of Antarctica with respect to Africa is set at 167.2 Ma after König and Jokat (2006) to account for the emplacement of seaward-dipping reflectors and oceanization in the Mozambique Basin at 168.6-166.15 Ma and 164.1 Ma, respectively (Mueller and Jokat, 2017). The plate corresponding to the Falkland Plateau was split into two regions: Maurice Ewing Bank block (comprising the Maurice Ewing Bank and the south-eastern part of the Falkland Plateau Basin) and the FIM (comprising the Falkland Islands, North Falkland Basin, South Falkland Basin, area west of the islands up to the Malvinas Basin, and the western part of the FPB; Chapter 5). The starting position for the Maurice Ewing Bank was set to the southern part of the Tugela Cone (Durban Basin, Natal Valley; Marshall, 1994; König and Jokat, 2010). The onset of motion for the Maurice Ewing Bank was set at 140 Ma to account for Berriasian-Valanginian rifting and Late Valanginian oceanization in the Natal Valley (Baby et al., 2018) The boundary between the FIM and Patagonia was

set along the high gravity anomaly west of the Falkland Islands (Chapter 5) and northwards it was interpreted as separating the NE-SW trend of San Julian Basin from the North Falkland Basin (Figure 6.7). The model starts at 170 Ma, considering the rotation of the FIM did not occur prior to the Middle Jurassic as suggested by the analysis carried in Chapter 5. At this stage, the Ellsworth Whitmore Terrane was in its current-day position relative to West Antarctica (Curtis and Storey, 1996; Martin, 2007) and therefore its rotation is not accounted for in this model. The position of the FIM at 170 Ma is modified from Stanca et al. (2019) and Chapter 4 to eliminate the gaps between the islands and Patagonia while maintaining the fragmentation and deformation of South America from Müller et al. (2019). The rotation of the islands is modelled as ceasing at 145 Ma (based on Chapter 5). The rate of rotation is constrained by pre-set positions of the FIM at 155 Ma and 150 Ma so that the correlations between the local and regional σ_3 described in Chapter 5 are respected (coeval structural features along the FIM and south-western Gondwana have roughly the same orientation). The rigid plate reconstruction accounts for the opening of the Rocas Verdes Basin as described by Calderón et al. (2013). The model does not consider the Antarctic Peninsula fragmentation of Eagles and Eisermann (2020) as this does not account for the South American origin of South Georgia (Dalziel et al., 1975; Macdonald et al., 1987; Stone, 2015; Dalziel et al., 2021), nor for the sinistral wrenching interpreted along the western margin of the Falkland Plateau Basin based on seismic reflection data (Chapter 5; see Chapter 7 for the full discussion). The reconstructions are relative to Africa fixed in its present-day position. The plate codes and total reconstruction poles for south-western Gondwana are shown in Tables 6.1 and 6.2.

Table 6.1 Plate codes for the plate reconstruction model (see Figure 6.24 for plate extents and configuration)

Plate code	Plate name
SAM	South America Craton
PRB	Parana Basin Plate, South America
NPM	Colorado Subplate (North Patagonian Massif), South America
DMB	San Jorge Plate (Deseado Massif Block), South America
SSJ	Southernmost San Jorge Plate, South America
FIM	Falkland Islands Microplate

FP	Maurice Ewing Bank and the eastern Falkland Plateau Basin
SSP	Salado (Sub-) Micro-plate, South America
PMP	Pampean Terrane, South America
AFR	Africa
EANT	East Antarctica
ANTP	Antarctic Peninsula

Table 6.2 Finite rotations for the south-western Gondwana model

Age (Ma)	Moving plate	Fixed plate	Lat (deg)	Long (deg)	Angle (deg)	Source
0	PRB	SAM	0	0	0	present-day
180	PRB	SAM	0	0	0	Müller et al. (2019)
0	PMP	SSP	0	0	0	present-day
125	PMP	SSP	0	0	0	Heine et al. (2013)
150	PMP	SSP	0	0	0	Heine et al. (2013)
180	PMP	SSP	0	0	0	Müller et al. (2019)
0	SSP	SAM	0	0	0	present-day
124.1	SSP	SAM	0	0	0	Heine et al. (2013)
150	SSP	SAM	-33.02	-60.52	8.5	Heine et al. (2013)
180	SSP	SAM	-33.02	-60.52	8.5	Müller et al. (2019)
0	NPM	SSP	0	0	0	present-day
125	NPM	SSP	0	0	0	Heine et al. (2013)
167.2	NPM	SSP	-32.5	-59.58	4.9	after König and Jokat (2006)
180	NPM	SSP	-32.5	-59.58	4.9	after Müller et al. (2019)
0	DMB	NPM	0	0	0	present-day
125	DMB	NPM	0	0	0	Heine et al. (2013)
145	DMB	NPM	-41.11	-73.68	2.3	Heine et al. (2013)

180	DMB	NPM	-41.11	-73.68	2.3	Müller et al. (2019)
0	SSJ	DMB	0	0	0	present-day
80	SSJ	DMB	0	0	0	positions estimated based on Calderón et al. (2013, 2016)
100	SSJ	DMB	13.77	-144.21	-1.81	
120	SSJ	DMB	13.77	-144.21	-1.81	
140	SSJ	DMB	11.97	-148.23	-1.25	
154	SSJ	DMB	0	0	0	
180	SSJ	DMB	0	0	0	
0	FIM	DMB	0	0	0	present-day
140	FIM	DMB	0	0	0	this study
145	FIM	DMB	28.09	-58.23	-0.69	this study
150	FIM	DMB	-56.18	-58.0	14.56	this study
155	FIM	DMB	-53.64	-58.27	30.73	this study
167.2	FIM	DMB	-52.21	-57.09	77.76	this study
180	FIM	DMB	-52.21	-57.09	77.76	this study
0	FP	SAM	0	0	0	present-day
131	FP	SAM	0	0	0	this study
137	FP	SAM	49.81	127.73	3.42	this study
139	FP	SAM	50.11	129.22	6.68	this study
140	FP	SAM	49.57	131.20	7.54	this study
140	FP	AFR	48.01	-34.45	56.161	this study
180	FP	AFR	48.01	-34.45	56.161	this study
0	EANT	AFR	0	0	0	present-day
10.9	EANT	AFR	8.2	-49.4	1.53	Royer and Chang (1991)
20.1	EANT	AFR	10.7	-47.9	2.78	Royer and Chang (1991)
33.1	EANT	AFR	12	-48.4	5.46	Royer and Chang (1991)

47.9	EANT	AFR	9.73	-40.67	8.82	Cande et al. (2010)
55.9	EANT	AFR	9.86	-45.24	10.49	Cande et al. (2010)
67.7	EANT	AFR	0.1	-45.56	11.7	after Cande et al. (2010) and Bernard et al. (2005)
76.3	EANT	AFR	-4.6	-40.6	14.39	Bernard et al. (2005)
83.0	EANT	AFR	-0.45	-40.01	17.77	Nankivell (1998)
100.0	EANT	AFR	-3.06	-33.49	26.15	modified from Marks and Tikku (2001)
120.6	EANT	AFR	10.36	153.67	-41.56	Müller et al. (2008)
124.1	EANT	AFR	9.45	152.5	-42.91	Müller et al. (2008)
125.7	EANT	AFR	9.3	152.0	-43.71	Müller et al. (2008)
127.8	EANT	AFR	-8.63	-28.97	44.47	König and Jokat (2010)
128.9	EANT	AFR	-8.5	-29.16	45.07	König and Jokat (2010)
130.8	EANT	AFR	-8.27	-29.42	45.9	König and Jokat (2010)
132.6	EANT	AFR	-7.97	-29.76	47.04	König and Jokat (2010)
136.6	EANT	AFR	-7.75	-30.02	47.91	König and Jokat (2010)
138.9	EANT	AFR	-7.81	-30.27	48.74	König and Jokat (2010)
143.4	EANT	AFR	-7.29	-31.13	49.8	König and Jokat (2010)
147.1	EANT	AFR	-6.16	-31.54	50.72	König and Jokat (2010)
148.8	EANT	AFR	-6.79	-31.78	51.26	König and Jokat (2010)
155.0	EANT	AFR	-6.62	-32.00	51.93	König and Jokat

						(2006)
167.2	EANT	AFR	-5.20	-33.66	56.32	König and Jokat (2006)
177.0	EANT	AFR	7.8	146.00	-56.15	Eagles and König (2008)
180	EANT	AFR	7.8	146.00	-56.15	after Eagles and König (2008)
0	ANTP	EANT	0	0	0	present-day
111.1	ANTP	EANT	0	0	0	König and Jokat (2006)
147	ANTP	EANT	0	0	0	König and Jokat (2006)
167.2	ANTP	EANT	-73.74	-49.49	23.13	König and Jokat (2006)
180	ANTP	EANT	-73.74	-49.49	23.13	König and Jokat (2006)

The reliability of the rigid reconstruction was tested using the GPlates deformable modelling methodology (Gurnis et al., 2018; Müller et al., 2019). The deformable area (resolved topological network) was chosen by trial and error aiming to avoid edge effects when calculating strain rates and stretching/thinning factors and minimizing the front of unrealistic deformation. The south-western boundary was fixed along the western extents of the Pampean Terrane and Colorado, and San Jorge plates (Figure 6.5). Northward, the model was delimited by the present-day shoreline of Africa, which allowed only for the Outeniqua Basin to deform (Figure 6.5). A scenario where onshore South Africa south of the Kalahari Craton was included in the network was tested. However, using the coastline as the northern boundary minimized the front of unrealistic compression along the rest of South America during rotation while not yielding any significant differences in the thickness estimations along the Falkland Plateau compared to when the southern part of the Kalahari Craton was used. To the east, the deformable network extended up to the continent-ocean boundary defined for East Antarctica and the Antarctic Peninsula (Figure 6.5). This segment of the boundary was fixed to East Antarctica during movement. From 167.2 Ma onwards, the boundary starts switching to the transform fault along which East Antarctica drifted away

from Africa (Middle to Upper Jurassic in Figures 6.5, 6.6). After the onset of oceanic crust in the Weddell Sea at 147 Ma (König and Jokat, 2006), the eastern boundary completely switches to the southern extent of the Falkland Plateau as defined by Müller et al. (2019) (Lower Cretaceous in Figure 6.6). A rigid nucleus corresponding to the Falkland Islands was defined (Figures 6.5 and 6.6) in order to minimize the Mesozoic extension of the region; its limits were based on the free-air gravity anomaly and simplified in order for it not to impact the deformation occurring around the islands. A set of points were generated along the western and northern (present-day orientation) boundaries of the FIM, each with specific total reconstruction poles (Table 6.3). These would act as a boundary between the FIM and the South American plate during rotation and would facilitate the extension of the FIM. Their pre-deformation position was set by approximating an initial extent of the FIM based on the thickness map of Kimbell and Richards (2008). An original crustal thickness of 35 km was used based on the undeformed area from Kimbell and Richards (2008). Stretching factors estimated for the thickness corresponding to each of the points were used to approximate their Jurassic position, assuming mass conservation during deformation (see Figure 6.4 for an example of the calculations, and Figure 6.7a for an approximation of the Jurassic FIM western and northern extents). No points were generated for the eastern margin of the FIM in order to allow the area corresponding to the Falkland Plateau to extend freely (Figure 6.5). Crustal thickness points were generated for the entire deformable network for both the rotational (ROT) and non-rotational (NROT) scenarios (FIM fixed to the San Jorge Plate – finite rotation from Müller et al., 2019) from 170 Ma to 130 Ma. The latest stage was compared to the thickness map from Kimbell and Richards (2008) and the geometrical gravity inversion results from this study (model MSJ-3D) taking into consideration that the model does not account for the formation of the oroclinal bend of Patagonia nor for the Andean orogenesis and the formation of the North Scotia Ridge (e.g. Dalziel et al., 2013). An initial crustal thickness of 35 km was assumed at 170 Ma (based on the thickness of the undeformed areas in Kimbell and Richards, 2008). The spacing of the crustal thickness points was set at 0.15625° (density level of 8 in GPlates) with 0% random offset. The points falling outside the network as the deformation progressed were deactivated. A natural neighbour interpolation was used for the deformed network and strain accumulations were calculated for each time step. For both models, a scenario with break-up and oceanic crust generation (ROT-OC and NROT-OC) at ~164-163 Ma was modelled as

well (Figure 6.4). The rationale behind the timing of break-up and the extent of oceanic crust will be explained throughout this chapter.

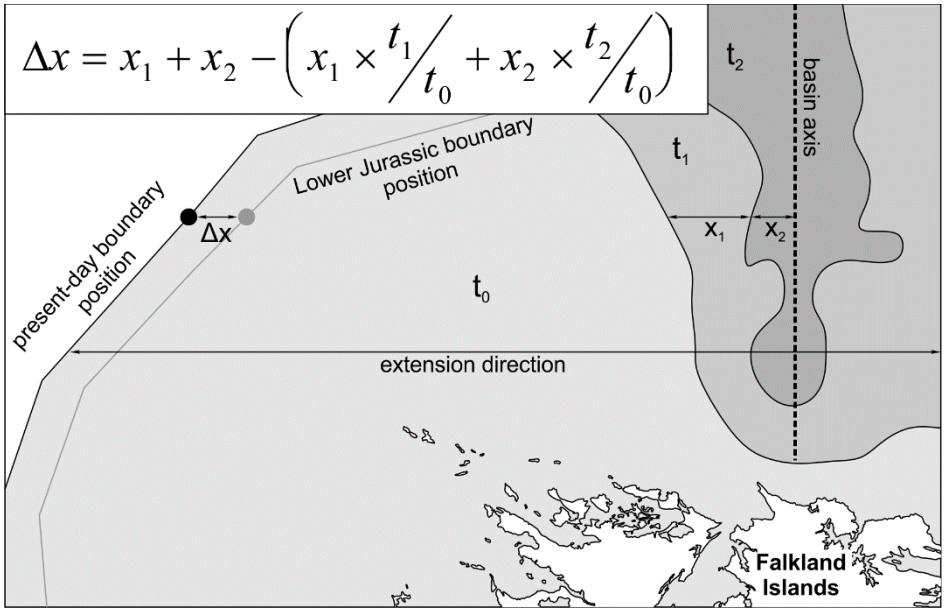

Figure 6.4 Example of the approximation of the Early Jurassic position of the points along the northern and western FIM boundaries; t_0 – unstretched crustal thickness; t_1 and t_2 – average extended crustal thicknesses within given isochores; x_1 and x_2 – lateral extent of thinned crust (parallel to the extension direction); Δx – difference in present-day and Early Jurassic position of a given point measured along the extension direction

Table 6.3 Finite rotations for points along the northern and western FIM boundary (Figure 6.5 - ROT) relative to the rigid FIM

Age (Ma)	Moving point	Reference plate	Lat (deg)	Long (deg)	Angle (deg)
0.0	1	FIM	0.880	-145.91	0.75
140.0	1	FIM	0.880	-145.91	0.75
162.0	1	FIM	-13.29	-163.72	0.01
170.0	1	FIM	0	0	0
0.0	2	FIM	4.65	-143.99	0.737
140.0	2	FIM	6.133	-141.66	0.93
162.0	2	FIM	-1.29	-151.62	-0.018
170.0	2	FIM	0	0	0
0	3	FIM	31.8098	-19.4383	-0.193

130	3	FIM	31.8098	-19.4383	-0.193
152	3	FIM	25.6782	-116.15528	-0.0279
170	3	FIM	0	0	0
0	4	FIM	38.7355	-53.1861	-0.1719
130	4	FIM	38.7355	-53.1861	-0.1719
152	4	FIM	24.9376	-118.8701	-0.0045
170	4	FIM	90	0	0
0	5	FIM	35.7662	-37.7633	-0.1647
130	5	FIM	35.7662	-37.7633	-0.1647
152	5	FIM	6.5395	18.2674	0.0151
170	5	FIM	90	0	0
0	6	FIM	37.9529	-60.9896	-0.1924
130	6	FIM	37.9529	-60.9896	-0.1924
152	6	FIM	35.7168	-86.3676	0.0387
170	6	FIM	90	0	0
0	7	FIM	29.4649	-104.5248	-0.2032
130	7	FIM	29.4649	-104.5248	-0.2032
152	7	FIM	29.2026	-107.075	0.0081
170	7	FIM	90	0	0
0	8	FIM	27.0918	-107.2588	-0.0845
130	8	FIM	27.0918	-107.2588	-0.0845
152	8	FIM	29.9014	-23.3153	0.0226
170	8	FIM	90	0	0

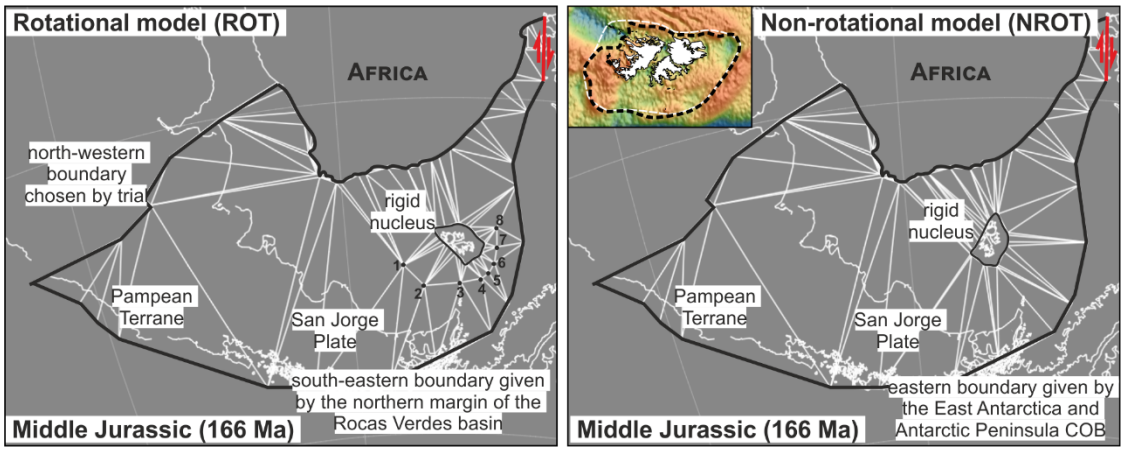

Figure 6.5 Deformable (resolved topological) networks for the rotational (ROT) and non-rotational (NROT) models; inset shows extent of rigid nucleus (black dashed line) overlain on the free-air gravity anomaly and the smoothed version incorporated in the deformable network (white dashed line); COB – continent-ocean boundary

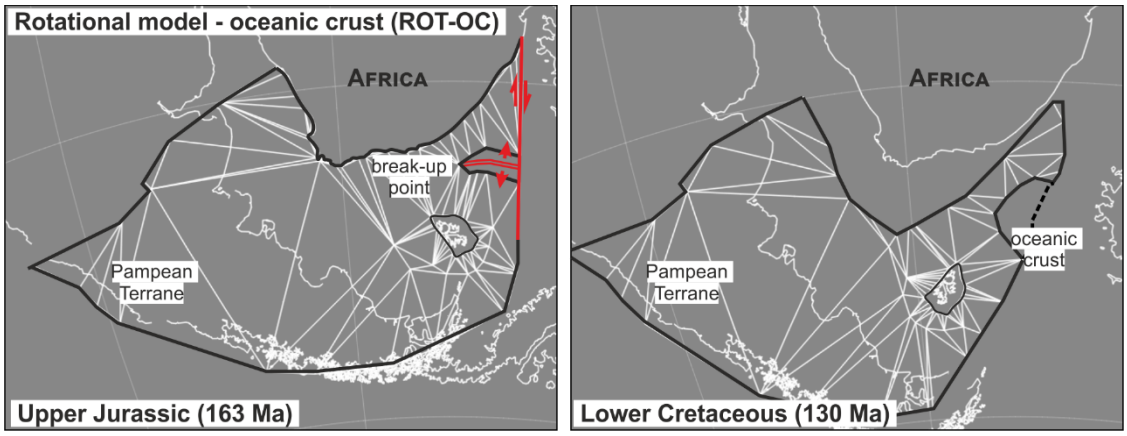

Figure 6.6 Evolution of the deformable (resolved topological) network for the rotational model with generation of oceanic crust (ROT-OC) at ~164 Ma

As the latitudinal position of the FIM for the rotation scenario was constrained by the space left available between the deformed South America, Africa, and Antarctica (i.e. in a more southern position than in previous reconstruction models incorporating a rotation of the FIM; Adie, 1952a; Mitchell et al., 1986; Trewin et al., 2002; Chapter 4), a plate model incorporating a more northern position was built as well (ROT-2) along with crustal thickness estimations. The constraints for the position were based on correlations between structures along the FIM and the rest of Gondwana, similar to ROT model above. The space between the FIM and Africa was based on the thinning factors derived from gravity inversion, as will be detailed later in the chapter, assuming mass conservation (changes in the thickness of the crust directly related to changes in lateral extent of the crust, similar to the methodology depicted in Figure 6.4).

The reconstruction of the San Jorge Plate was modified as well to minimize the gap between it and the FIM. Implications for these changes will be discussed in Chapter 7. The finite rotations differing from the main rotational model (ROT) are shown in Table 6.4.

Table 6.4 Finite rotations for the FIM and the San Jorge Plate for an alternative northern position of the FIM

Age (Ma)	Moving plate	Fixed plate	Lat (deg)	Long (deg)	Angle (deg)	Source
167.2	DMB	NPM	-41.76	-65.75	10.79	this study
180	DMB	NPM	-41.76	-65.75	10.79	this study
155	FIM	DMB	-55.37	-58.07	26.169	this study
167.2	FIM	DMB	-52.08	-56.152	69.43	this study
180	FIM	DMB	-52.08	-56.152	69.43	this study

6.4 Results

6.4.1 Crustal type distribution in the Falkland Plateau Basin

6.4.1.1 Variations in gravity and magnetic response, and seismic reflectivity

6.4.1.1.1 Gravity data interpretation

The bandpass filtered free-air gravity anomaly shows a mosaic of regions with different gravimetric signatures. West of the Falkland Islands a roughly N-S trending lineament describing an arc is interpreted as marking the western extent of the FIM (Chapter 5; Figure 6.7a). NE-SW striking anomalies are seen under the San Julian Basin, which here are correlated with its structural grain. These transition abruptly to the North Falkland Basin (NFB) region, which is characterised by N-S oriented lineaments that follow the main structural trend of the basin (Figure 6.7a).

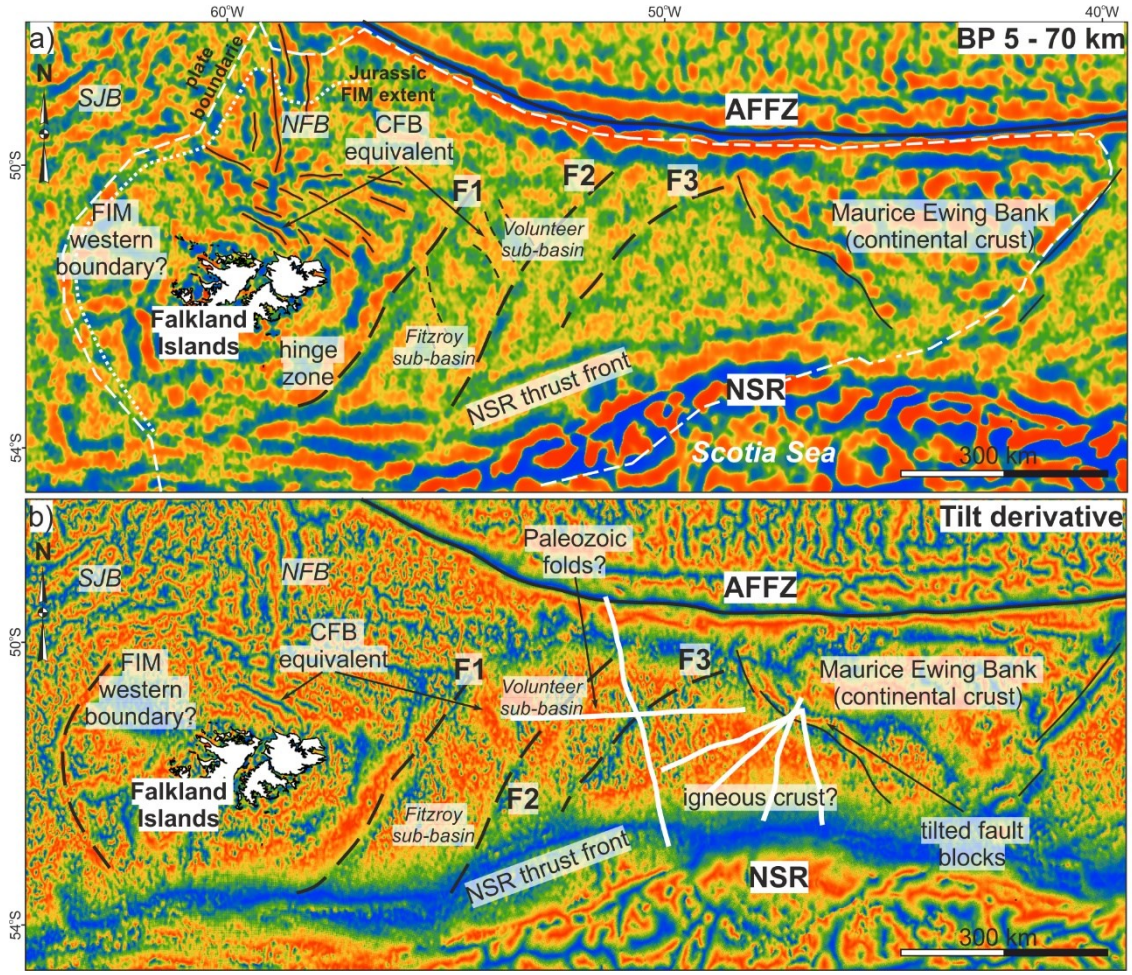

Figure 6.7 a) Bandpass filtered free-air gravity anomaly showing the trend of the Cape Fold Belt equivalent (Southern North Falkland Basin, Chapter 4) and the NE-SW potential shear zones; white dashed lines – Falkland Plateau boundary; white dotted line – FIM northern and western Jurassic extent; b) changes in the gravity signature as shown by the tilt derivative; black stippled lines mark potential fracture zones/crustal blocks boundaries; white lines – seismic sections in Figures 6.9 – 6.11; CFB – Cape Fold Belt; SJB – San Julian Basin

South of the NFB, an alternation of linear highs and lows follow a WNW-ESE strike underneath the Southern North Falkland Basin (SNFB). This is consistent with the trend of the half-grabens within this basin (the reactivated Cape Fold Belt (CFB) equivalent; Chapter 4; Figure 6.7a). This trend is mapped in the Volunteer sub-basin, ~300 km off the coast of East Falkland. The wavelength of the anomalies is relatively higher in this region which could be the result of an increase in the burial depth of the fold and thrust belt or related to larger scale variations in the basement topography and/or composition (Figure 6.7a). Underneath the Fitzroy sub-basin this trend is not as readily identified. This change in the gravimetric signature can be related to the sediment thickness, a

change in the nature of the crust or a change in the pre-Mesozoic distribution of the deformation. NE-SW oriented anomalies, cross-cutting the entire width of the FPB, are seen along the shelf break (F1) but also truncating the NW-SE trend of the Volunteer sub-basin to the east (F2; Figure 6.7a). These features have been interpreted as shear zones (Chapter 5). The rest of the Falkland Plateau Basin displays a chaotic distribution of gravimetric anomalies which transition to the east in the NW-SE and NE-SW lineaments-bounded domain of the Maurice Ewing Bank (Figure 6.7a).

The tilt derivative displays a similar distribution to the band-pass filtered free-air gravity anomaly, but with a few additions. A third basin-wide break in the gravity response following the same NE-SW trend as F1 and F2 in Figure 6.7a is identified on this derivative (F3; Figure 6.7b). This results in a separation of the Falkland Plateau Basin in two narrow slivers to the west and a triangular domain to the east (Figure 6.7). Another characteristic readily visible on the tilt derivative is the negative, E-W trending anomaly in the northern part of the FPB (Figure 6.7), the nature of which will be addressed in the next sections.

6.4.1.1.2 Magnetic data interpretation

The available magnetic data are restricted to the Falkland Plateau Basin and show a high amount of variability in the magnetic response from west to east (Figure 6.8). The region from the eastern coast of the Falkland Islands to the hinge line (F1 in Figure 6.7a and b) shows N-S trending anomalies (Figure 6.8a). These are interpreted as corresponding to the dyke swarm from Barker (1999). The hinge line itself displays isolated NE-SW striking linear magnetic anomalies (Figure 6.8) following the trend of the F1 gravity lineament in Figure 6.7. The positive magnetic anomalies associated with F1 could suggest a potential magmatic enrichment along this deformed margin of the basin (Figure 6.8a and b) as evidence of significant magmatism has been interpreted basinward (Chapter 5).

East of F1, isolated negative anomalies are separated by a WNW-ESE striking positive magnetic anomaly (Figure 6.8a and b). These are interpreted as corresponding to the Volunteer and Fitzroy sub-basins and the Berkeley Arch, respectively. The areas east and south of the Fitzroy sub-basin show a high positive magnetic response (Figure 6.8). These correspond to the sill complex interpreted in Chapter 5 and to the magmatic and volcanic province defined by Richards et al. (2013; Figure 6.8). The magnetic anomaly corresponding to the Berkeley Arch is truncated eastwards by a magnetic lineament readily seen on

the tilt derivative (Figure 6.8b). Its location corresponds to the F2 in Figure 6.7a and b.

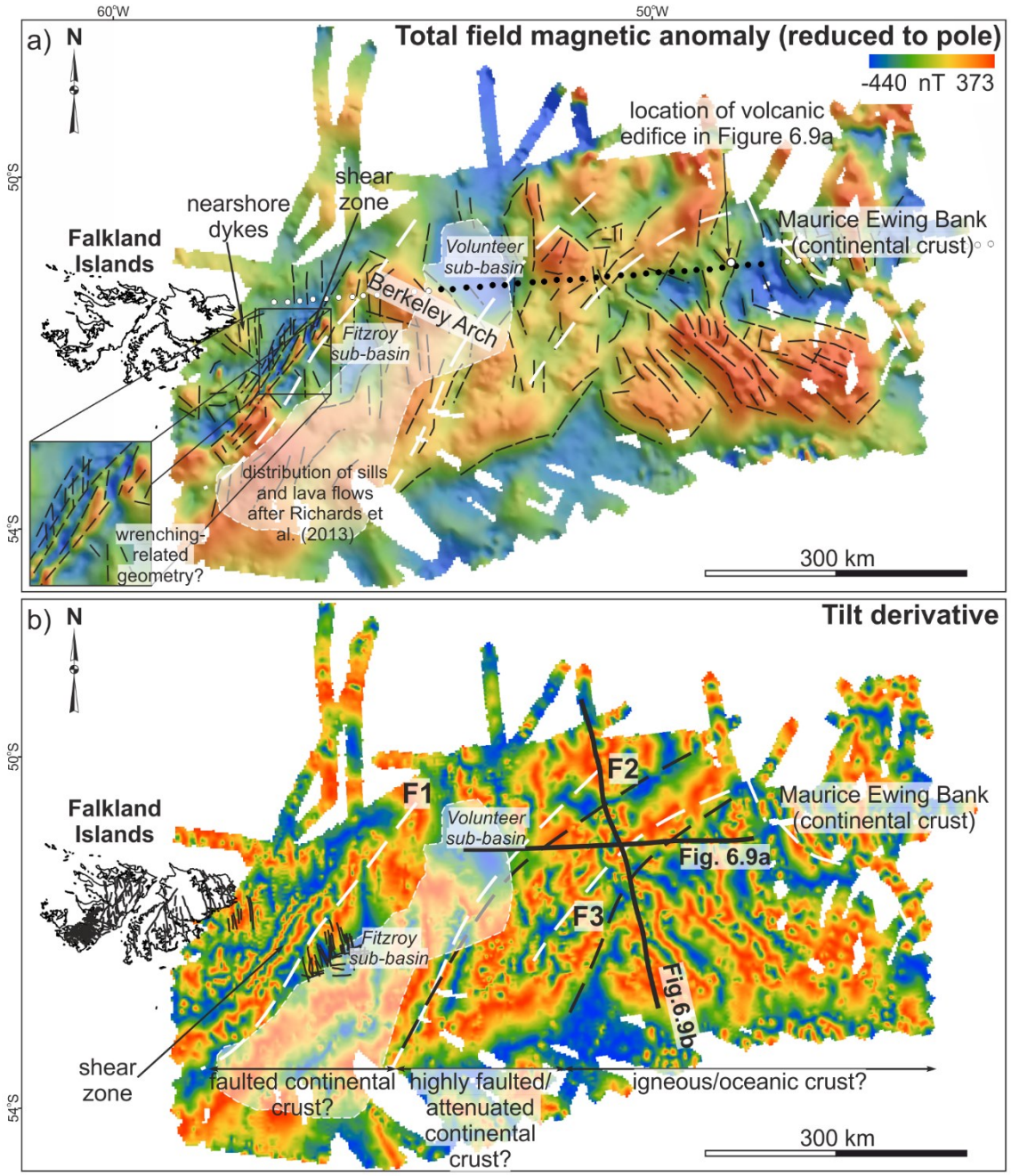

Figure 6.8 a) Reduced to pole total magnetic anomaly overlain by magnetic lineaments; dots mark ocean bottom seismometers locations from Schimschal and Jokat (2019b) with the black ones marking locations where oceanic crust was interpreted by the same study; b) tilt derivative along with the on- and nearshore dykes after Barker (1999) and Stone et al. (2009) and offshore dykes from Chapter 5 and the distribution of volcanics and magmatics after Richards et al. (2013); white stippled lines mark the fracture zones based on gravity data; black stippled lines mark the crustal boundaries as interpreted from the magnetic data

The remainder of the basin shows two distinct domains separated by F3 in Figure 6.7. The first one, west of F3, shows medium to high positive magnetic anomalies and a chaotic distribution of magnetic lineaments, with trends ranging from NE-SW and N-S to NW-SE (Figure 6.8). The domain east of F3 corresponds to the triangular zone delineated on gravity data west of the Maurice Ewing Bank (Figure 6.7). This region shows NW-SE to WNW-ESE magnetic stripes in the central and southern part of the domain (Figure 6.8) which are truncated to the west by F3. The northern part shows predominantly negative anomalies with weak NW-SE lineaments (Figure 6.8a). The magnetic lineations in the south-central part of this region are interpreted as magnetic reversal isochrons, consistent with the interpretation of Eagles and Eisermann (2020), characteristic of oceanic crust which transition to the north to potentially sheared (igneous?) crust or transitional crust (Figure 6.8a).

6.4.1.1.3 Seismic reflection data interpretation

Regional 2D seismic reflection data have been used to constrain the different crustal domains based on gravity and magnetic data. A seismic characterization of the F1 shear zone is reported in Chapter 5. Two near orthogonal seismic profiles crossing the F2-3 shear zones are shown in Figure 6.9, with each one intersecting the triangular domain between F3 and the Maurice Ewing Bank in different points. The seismic lines show a change in the seismic character of the Falkland Plateau Basin crust between each pair of shear zones.

Deformed sedimentary deposits of either Jurassic or Palaeozoic age are interpreted to extend up to 300 km offshore in the Volunteer sub-basin (Figure 6.9a). Along the F2 and between it and F3 the seismic response is characterized by a high degree of normal faulting, which could represent highly faulted and potentially attenuated continental crust (Figure 6.9a). The remainder of the crust up to the Maurice Ewing Bank is strongly reflective and in an elevated position compared to the rest of the basin on the E-W striking seismic line (Figure 6.9a). The high amplitudes are interpreted to be the result of volcanic and magmatic additions, whereas the elevation could suggest underplating or a transition to thick igneous crust (Figure 6.9a). This segment corresponds to the northern part of the triangular domain in Figures 6.7 and 6.8 which is associated with a negative magnetic response.

The ~N-S trending seismic line crosses the F2-3 shear zones and terminates in the crustal domain characterized my magnetic stripes (Figure 6.9b). The architecture of the basin and the seismic character varies abruptly southwards

from a highly elevated, transparent crustal block juxtaposed against the AFFZ and interpreted as continental in nature, to a ~8s TWT deep sedimentary basin just south of it, and further to a crustal domain characterised by high amplitudes and covered by pre-Upper Jurassic (?) deposits bounded to the top by an erosional unconformity (Figure 6.9b). Similar to the E-W profile, the high reflectivity is interpreted to be related to volcanic and magmatic additions. This, collated with the information from the magnetic data, would suggest that this segment of the profile is transitioning to oceanic crust southwards. However, the continent-ocean boundary is unclear. Dipping reflectors identified in this domain (Figure 6.9b) have been interpreted as subaerial volcanic flows by Lorenzo and Mutter (1988). However, evidence of faulting is seen above these reflectors, suggesting a sedimentary growth package for the shallowest of them. To the south, the high amplitudes of the oceanic domain can be readily seen continuing under the accretionary prism of the NSR (Figure 6.9a).

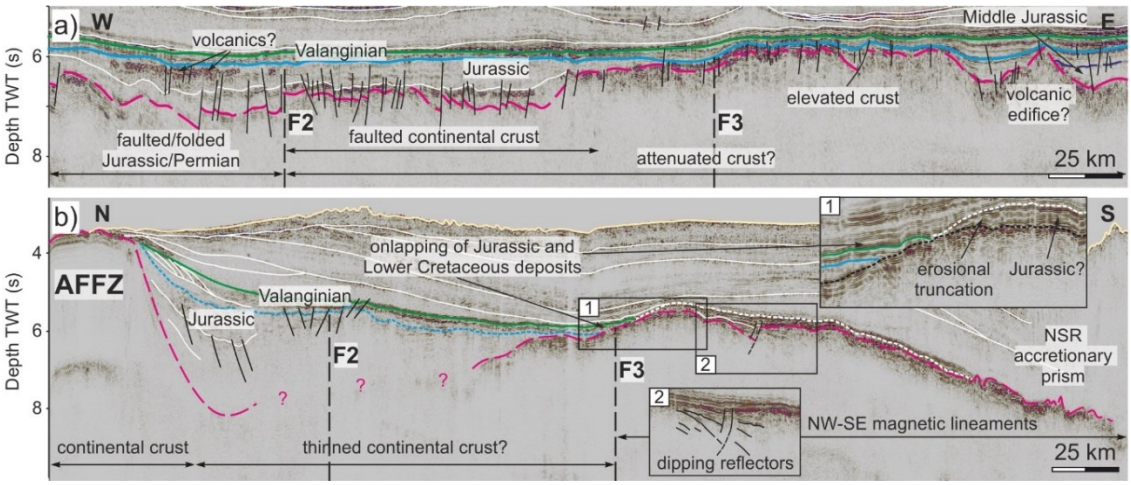

Figure 6.9 a) Seismic section showing the transition from Jurassic/Palaeozoic deposits to highly faulted crust and to an elevated, highly reflective domain; b) seismic section showing the N-S variation in crustal architecture in the FPB with uplifted continental crust to the north, deep Jurassic depocentre, and oceanic crust to the south; lines location in Figure 6.8b; NSR – North Scotia Ridge

Besides looking at the seismic characteristics of each of the three domains within the FPB, the area lying between F3 and the MEB shows some variation on the magnetic data and requires further analysis based on seismic data. Four additional regional lines crossing the magnetic lineaments interpreted as magnetic reversal isochrons were used for this analysis. These show a varied sediment architecture with no obvious continent-ocean transition (Figure 6.10, 6.11).

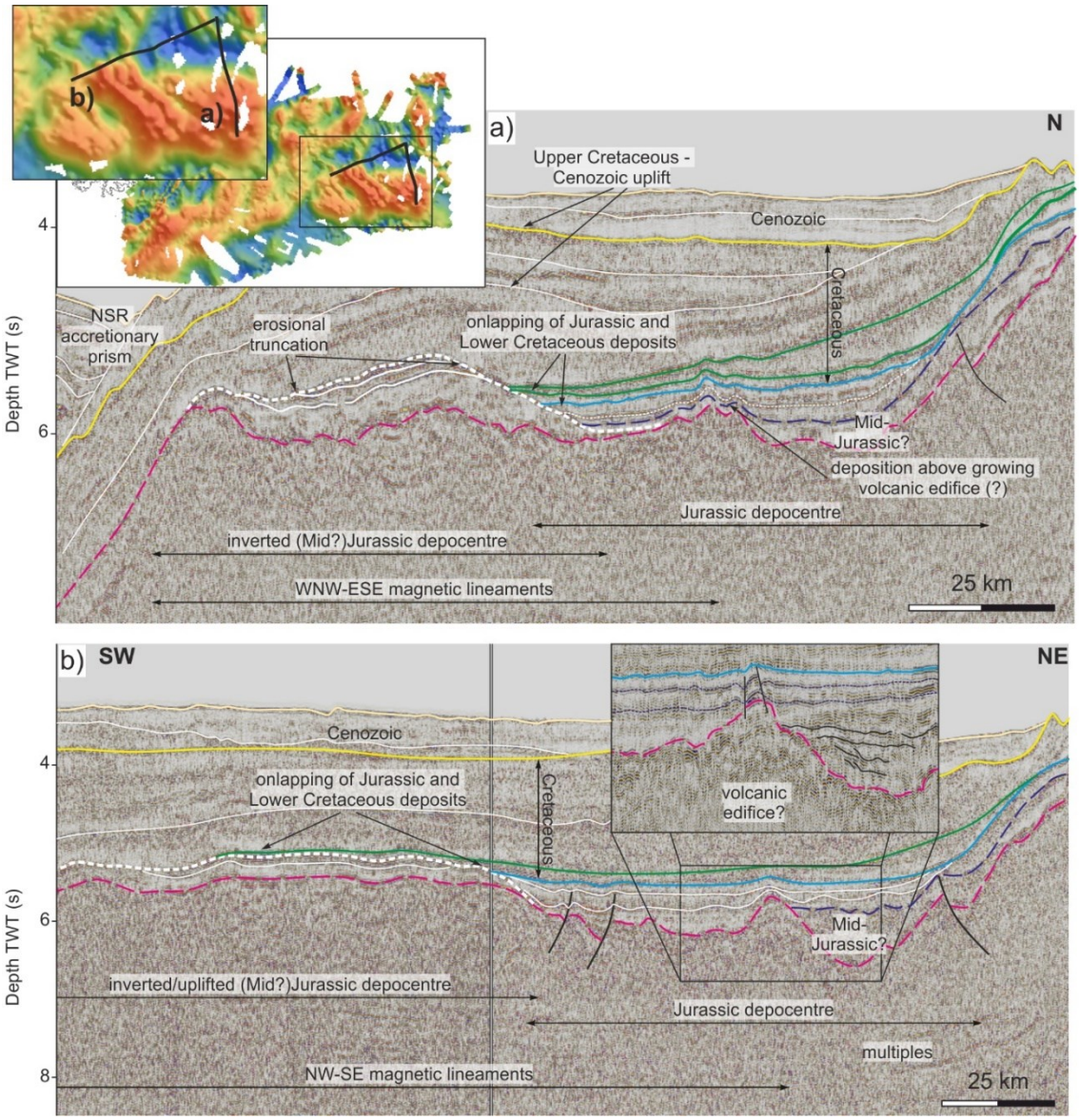

Figure 6.10 Seismic sections across the northern and western regions of the magnetic lineaments showing older uplifted Jurassic deposits onlapped by younger sediments and potential volcanic edifices bounding the northern extent of the magnetic lineaments

A Jurassic depocentre of ~0.8-0.9 s TWT thickness lies in the northern part of the triangular zone where negative magnetic anomalies were identified (Figures 6.10, 6.11). The northernmost and easternmost regional seismic profiles show Jurassic and Lower Cretaceous strata onlapping on an older sediment section bound to the top by an erosional unconformity (Figure 6.10). This is relatively thick and narrow on the easternmost section (Figure 6.10a) where it resembles an inverted/uplifted depocentre with strata potentially older than Middle Jurassic and thins and extends across a wider region on the northern profile (Figure 6.10b). These deposits are the same for sections in Figures 6.9b and 6.10b but it is unclear if they are related and coeval to the ones in Figure 6.10a.

No separation of these Jurassic deposits is seen on the two other seismic lines crossing the magnetic lineaments (Figure 6.11). However, the same onlap geometry of Lower Cretaceous strata onto the Jurassic section is identified in the S-SW of each section (Figure 6.11a and b), with an erosional truncation of the Jurassic sequence interpreted in the southern part of the profile in Figure 6.11a.

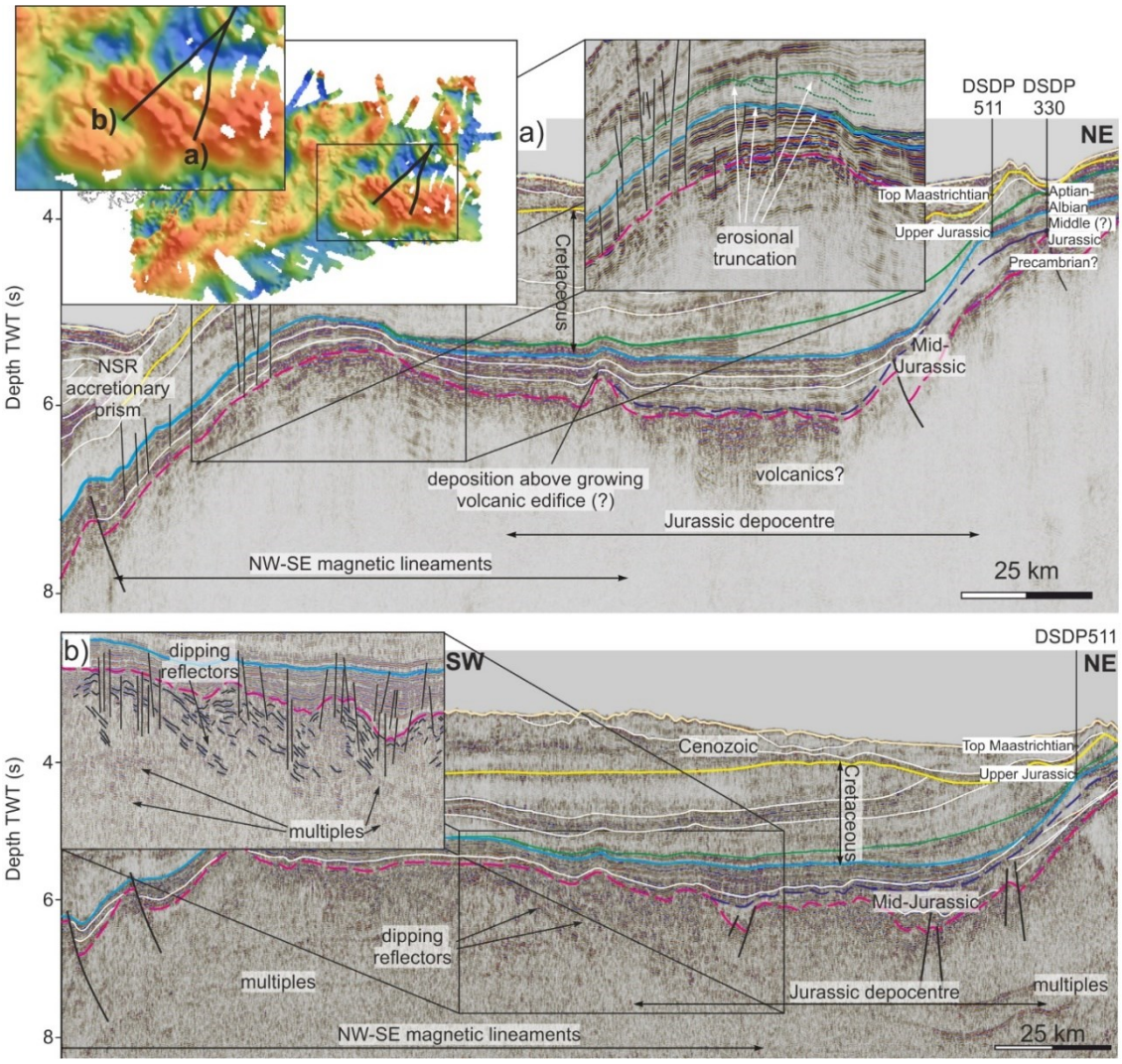

Figure 6.11 Seismic sections across the central part of the magnetic lineaments showing continuous deposition during the Jurassic and areas of high amplitudes (a) and dipping reflectors (b) within the acoustic basement

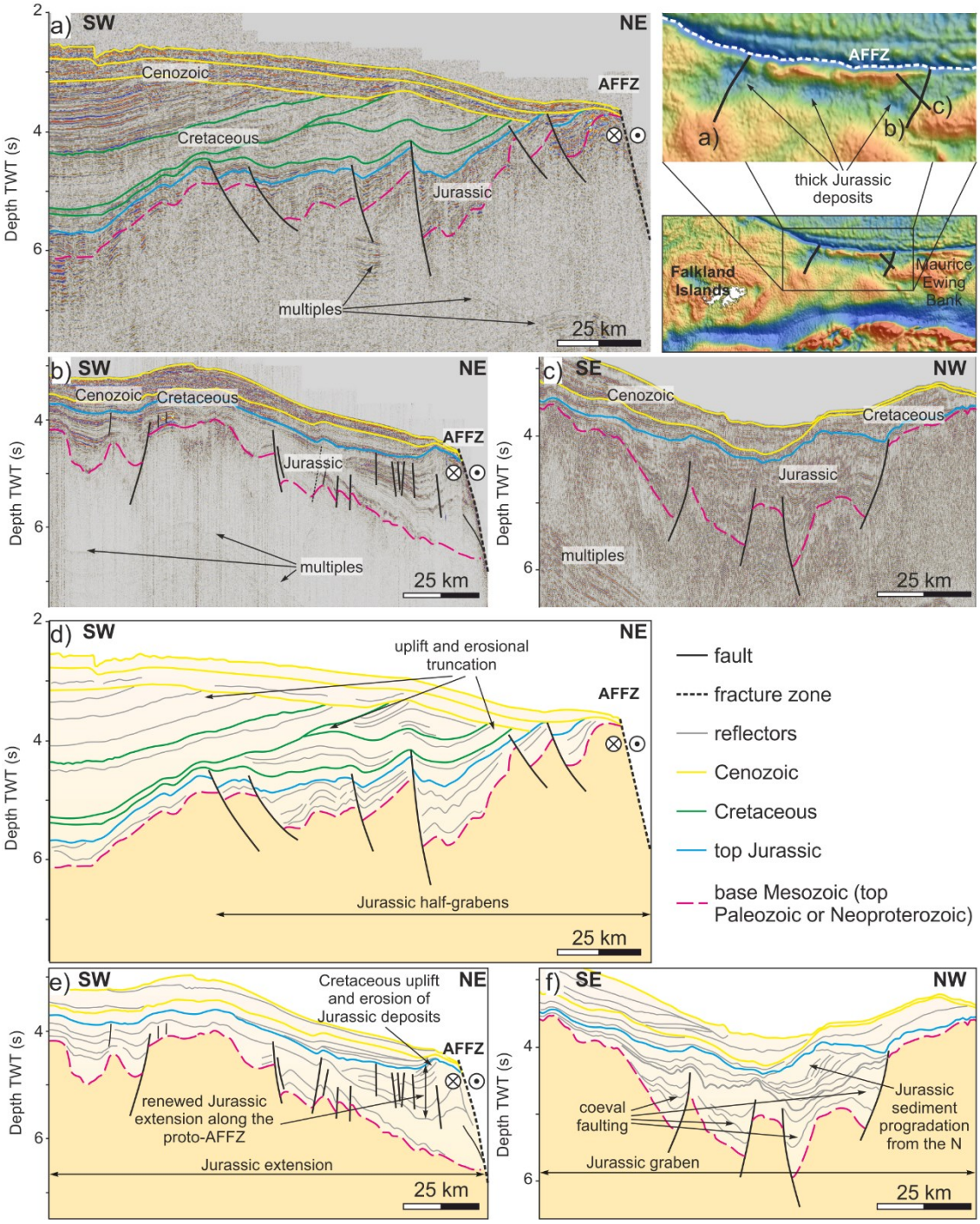

Figure 6.12 Seismic sections across the E-W trending negative gravity anomaly in the northern FPB showing Jurassic grabens and half-grabens and a high degree of lateral structural variability along the AFFZ; evidence of several unconformities (a, b, d, e) and sediment deformation can be readily seen and have been related to movement along the AFFZ and proto-AFFZ (extension and wrenching between the FIM and South Africa); line drawings of sections in a-c are shown in d-f in order to highlight sediment architecture; AFFZ – Agulhas-Falkland Fracture Zone

Gentle folding of the Cretaceous and Lower Cenozoic sections was identified locally (Figure 6.10a) suggesting further uplift from the south. On three of the four sections, the northern limit of the positive and striped magnetic domain corresponds to elevated features on the top basement of potential volcanic nature (Figures 6.10a, b and 6.11a). These are between 10 and 15 km wide and do not correspond to any isolated anomalies on the magnetic map. Jurassic strata thin above these features (Figures 6.10a and 6.11a) suggesting a coeval formation, although further folding and faulting of the Lower Cretaceous section is evidence of further growth (Figures 6.10a, b and 6.11a). Features resembling volcanic edifices are seen on the seismic reflection data in the negative magnetic anomaly domain as well (Figure 6.9a) where they relate to ridge-like structures on the magnetic map (Figure 6.8a).

A narrow negative gravity anomaly running parallel to the AFFZ in the northern part of the FPB has been identified in sub-section 6.4.1.1.1. On seismic reflection data this area corresponds to a series of Jurassic grabens and half-grabens overlying highly faulted crust interpreted here as continental (Figure 6.12). Evidence of differential Cretaceous and Cenozoic uplift is seen in the form of erosional truncations of Jurassic to Cenozoic deposits (Figure 6.12a, b, d, e) most likely related to processes along the AFFZ.

A summary interpretation of the crustal distribution as constrained by gravity, magnetic, and seismic data is shown in Figure 6.13. The seismic reflection data were not diagnostic for the nature of the crust in the distal part of the FPB or for the location of crustal type boundaries. Therefore, the crust underlying the Falkland Plateau Basin is subdivided into the following domains:

- a continental crust domain comprising the FIM, the region between F1 and F2, the crust adjacent to the AFFZ, and the MEB (1 in Figure 6.13);
- a domain of faulted and potentially attenuated and underplated continental (?) crust or sheared oceanic (based on Schimschal and Jokat, 2017) crust between F2 and F3 (2 in Figure 6.13);
- an uncertain domain comprising:
    - the northern region of the triangular zone (between F3 and the MEB; 3 in Figure 6.13) where the seismic reflection data suggests the presence of thicker (elevated) magma-enriched crust with a magnetic signature different than the interpreted oceanic crust to the south;
    - the central and eastern regions of the triangular zone (4 in Figure 6.13) where magnetic lineaments were mapped indicative of

magnetic reversal isochrons and oceanic crust, but pre-Middle Jurassic inverted basins were mapped on the seismic data across these lineaments;

- an oceanic domain corresponding to the southern magnetic reversal isochrons (5 in Figure 6.13).

The nature and implications of the region marked as uncertain in Figure 6.13 are discussed in Section 6.5.

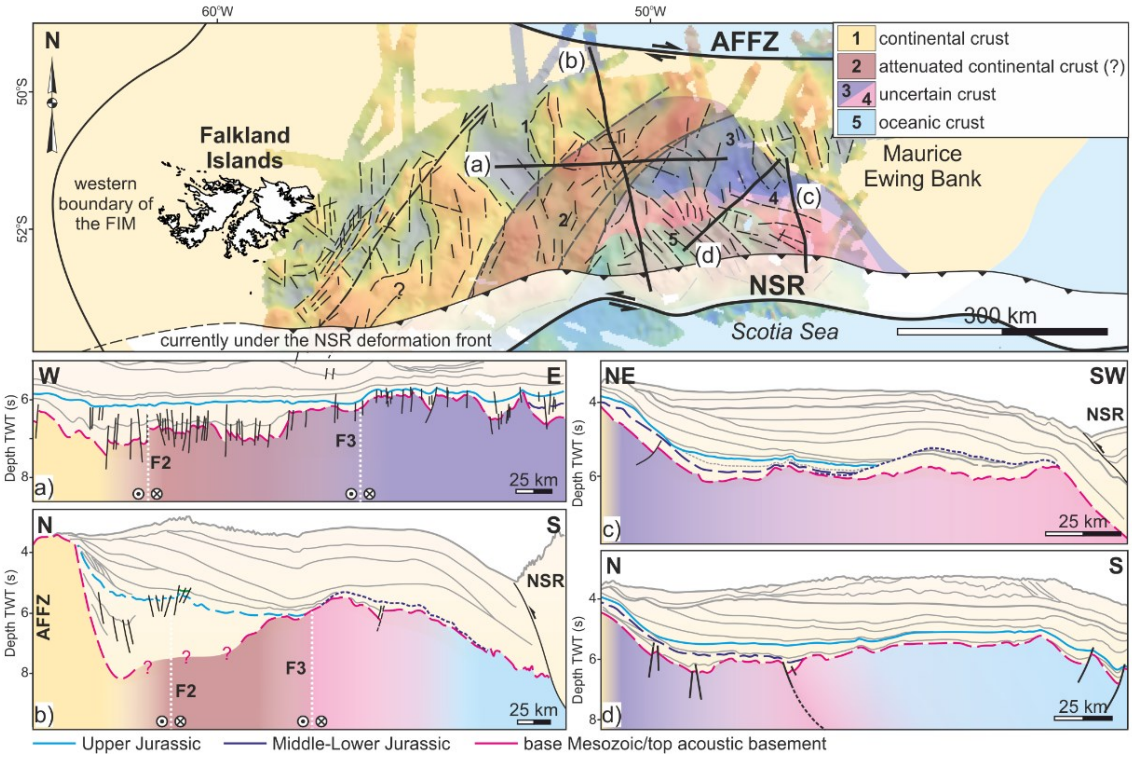

Figure 6.13 A model of the crustal type distribution and structure along the Falkland Plateau based on gravity, seismic reflection, and magnetic data overlain on the magnetic data, and type sections (a, b, c, and d, are line drawings of seismic sections in Figures 6.9, 6.10a and 6.11b; continental crust is considered to comprise the Maurice Ewing Bank, Falkland Islands with the Malvinas Basin, NFB, SFB, Volunteer and Fitzroy sub-basins, and the northern area along the AFFZ, with an uncertainty in the southern part of the Fitzroy sub-basin where the seismic response at depth is obscured by the extensive sill complex (Chapter 5); the eastern sliver of the FIM and the northern part of the triangular central region are both grouped under sheared and attenuated crust due to their high degree of faulting and/or high amplitudes on the seismic data and more chaotic character on the magnetic data; the area with magnetic lineaments is split in an oceanic domain to the south and an uncertain region to the north and east

6.4.1.2 Crustal density distribution based on gravity modelling and inversion

Subsequent to the interpretation of potential field and seismic reflection data, a lot of uncertainty remains in the nature and distribution of the crust under the FPB. Although seismic reflection data show folded Paleozoic deposits extending in the region between F1 and F2 (Figure 6.9a; Chapter 5), there is little seismic coverage further east in the basin with vintages of poor quality that makes a definitive characterization of crustal types difficult. Domains 2, 3, and 4 in Figure 6.13 remain of particular interest, and gravity modelling and inversion is employed to constrain the density distribution in this area of the plateau.

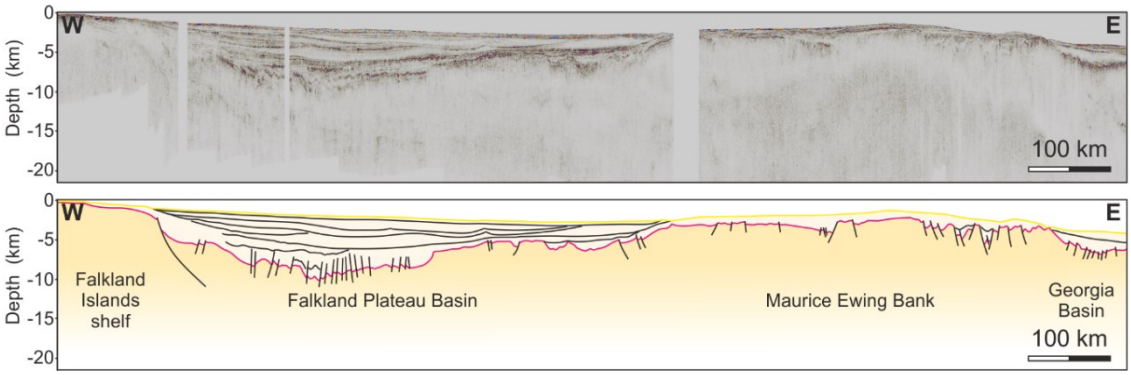

Figure 6.14 Uninterpreted and interpreted depth converted seismic profile 139 along which forward gravity modelling was carried out; light yellow – sediment infill; dark yellow – undifferentiated crust; line position shown in Figure 6.1; detailed interpretation of the central section corresponding to the Falkland Plateau Basin shown in Figure 6.9a

6.4.1.2.1 2D forward modelling results

The forward modelling results carried out along profile 139 in Figure 6.1 show different crustal architectures along the FPB based on the Moho model used as an input. For the MKR-2D model (depth to Moho from Kimbell and Richards, 2008), the modelled Falkland Islands eastern shelf and the Maurice Ewing Bank show a similar layering, with densities between 2.74 g/cc and 2.9 g/cc for the upper and lower crust, respectively, with lower densities being modelled for the easternmost section of the Maurice Ewing Bank (Figure 6.15a and b). Underneath the FPB an increase in density is modelled for the upper crust towards the Falklands shelf where densities of up to 2.83 g/cc are reached, whereas the lower crust is modelled as a homogeneous layer of 2.92-2.93 g/cc density (Figure 6.15a and b).

The MSJ-2D model (depth to Moho derived from Schimschal and Jokat, 2019b) shows a more complex density distribution. The Falklands shelf and Maurice Ewing Bank share some similarities with the first scenario (Figure 6.16a), but lower densities are modelled in the upper crust along the Falklands shelf and throughout a larger area in the eastern section of the Maurice Ewing Bank (Figure 6.16a and b). A high-density lower crust body is modelled for the Maurice Ewing Bank where the input Moho suggests a thicker crust than the first scenario. Along the FPB, crustal thickness and densities are relatively higher than for the first scenario, with the upper and lower crusts reaching densities of 2.88-2.9 g/cc and 3.05 g/cc, respectively (Figure 6.16).

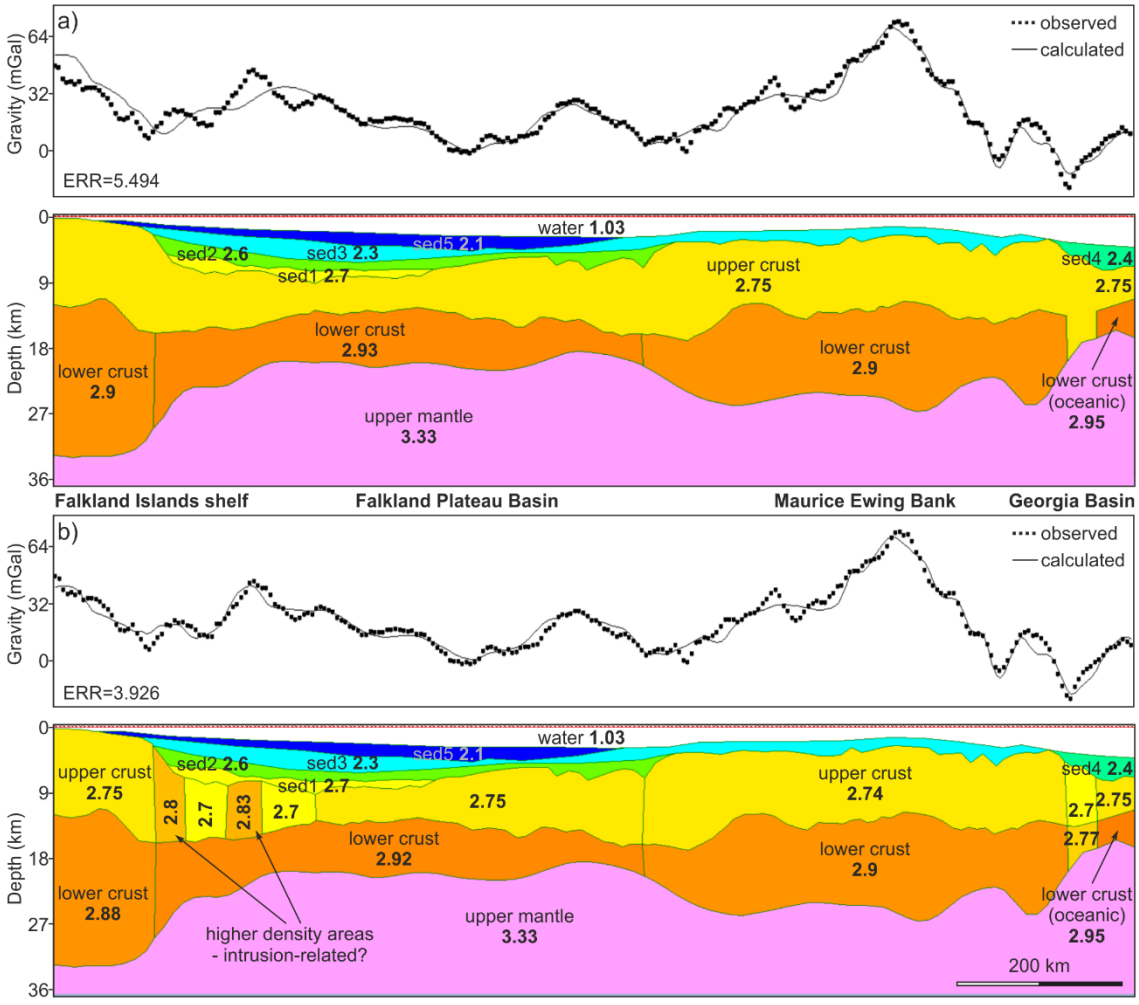

Figure 6.15 MKR-2D model; a) Simplified gravity forward model along line 139 showing little lateral variations in density between the Falkland Islands, Falkland Plateau Basin, and Maurice Ewing Bank; b) detailed gravity model showing isolated areas of higher densities along the shelf of the Falkland Islands; Moho based on Kimbell and Richards (2008); profile interpretation input for modelling shown in Figure 6.14; line position shown in Figure 6.1

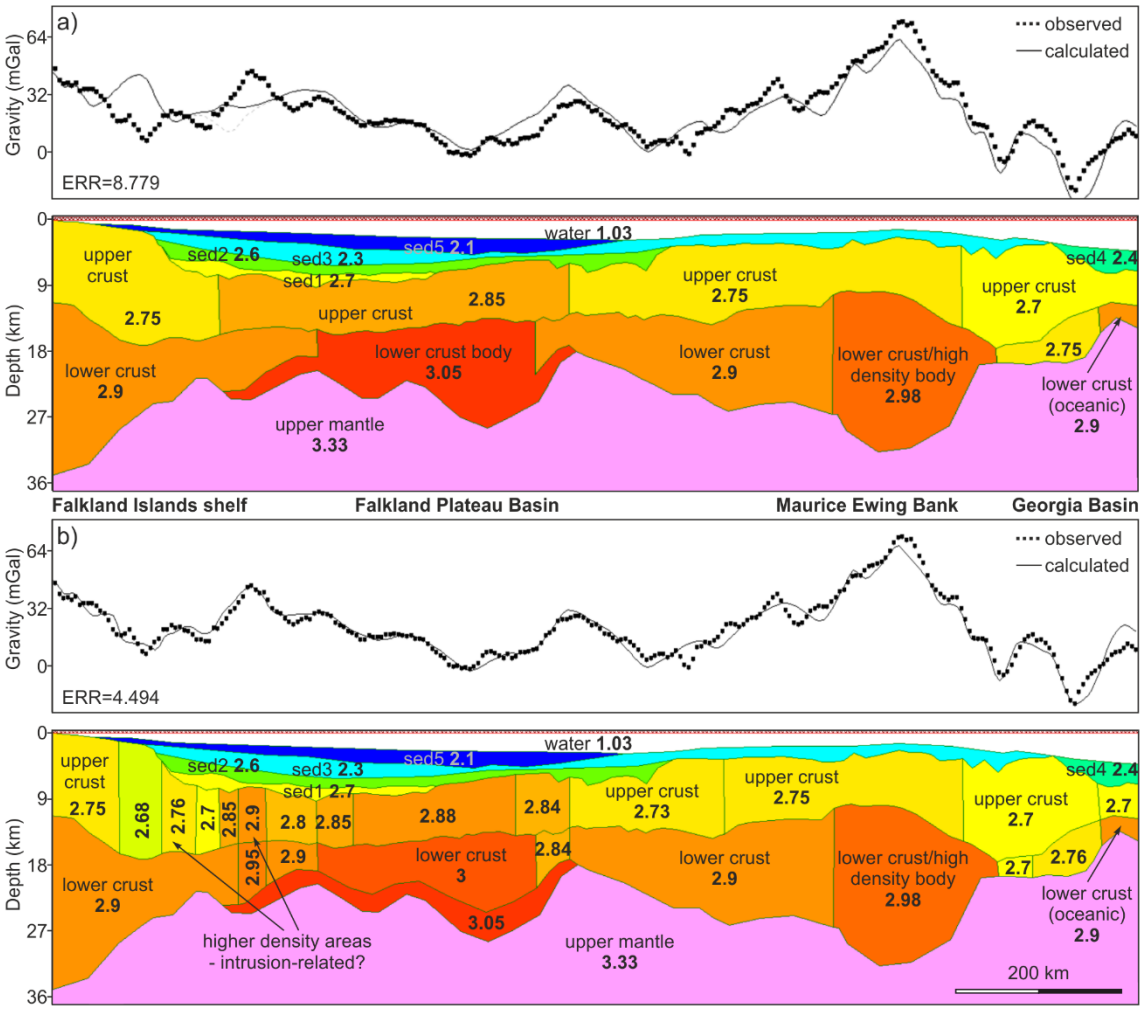

Figure 6.16 MSJ-2D model; a) Simplified gravity forward model along line 139 showing and increase in densities for the upper and lower crust underlying the Falkland Plateau Basin compared to the Falkland Islands platform and Maurice Ewing Bank; b) detailed gravity model showing narrow areas of relatively lower and higher densities than the surrounding crust nearshore the Falkland Islands; Moho based on Schimschal and Jokat (2019b); profile interpretation input for modelling shown in Figure 6.14; line position shown in Figure 6.1

6.4.1.2.2 3D inversion results

Due to the abrupt N-S changes in crustal architecture interpreted based on gravity, magnetic, and seismic reflection data (Figures 6.7, 6.8 and 6.13), 3D gravity inversion was further carried out across the entirety of the FPB and sections across profile 139 were compared against the 2D forward gravity modelling results.

A separation in the 3D density distribution across the FPB is observable between the two considered scenarios (MKR-3D and MSJ-3; Figure 6.17), which was due to the difference in crustal thicknesses. Although there are

many similarities between the proposed Moho morphologies from Kimbell and Richards (2008) and the one modelled after Schimschal and Jokat (2019b) (Figure 6.17a), there are differences in the depth to Moho, and consequently crustal thickness, underneath the FPB (Figures 6.18 and 6.19). The crust from Kimbell and Richards (2008) is thicker under the Fitzroy sub-basin, but thinner under the rest of the FPB compared to the inversion results for the MSJ-3D model (Figure 6.18, 6.19, 6.20). Largest differences occur in regions 3-5 where magmatic additions were inferred along with the presence of oceanic crust to the south (Figure 6.13), and under the Fitzroy sub-basin. The thickness of the 3-5 domain is relatively high compared to average oceanic crust thicknesses (typically less than 10 km); the mean crustal thickness estimated from the two models is ~15-16 km. The maximum thicknesses resulting from the two models were ~18 km for the MKR-3D scenario, and ~20 km for the MSJ-3D (Figure 6.18). This difference in thicknesses resulted in higher crustal densities being modelled during the heterogeneous inversion along the 3-4 regions for the MSJ-3D scenario (Figure 6.21b) when compared to the MKR-3D case (Figure 6.21a), which correlates with the interpreted igneous nature/addition of this crustal region. For both models, the densities predicted in region 5 were relatively high, indicative of volcanic material accretion, but not reaching typical oceanic crust densities (~3 g/cc; Figure 6.21). Regarding the Fitzroy sub-basin region, high densities were obtained for the MKR-3D scenario compared to the MSJ-3D model. However, the crust underlying the basin consists of folded Paleozoic units (Chapter 5). Extensive dyke and sill complexes would account for the high densities (Figures 6.15b, 6.16b, 6.21) and positive magnetic anomalies (Figure 6.8) interpreted along the hinge zone. Within the sedimentary infill of the FPB, the inversion yielded lower densities in regions 3-5 for MKR-3D when compared to the results from MSJ-3D (Figure 6.17).

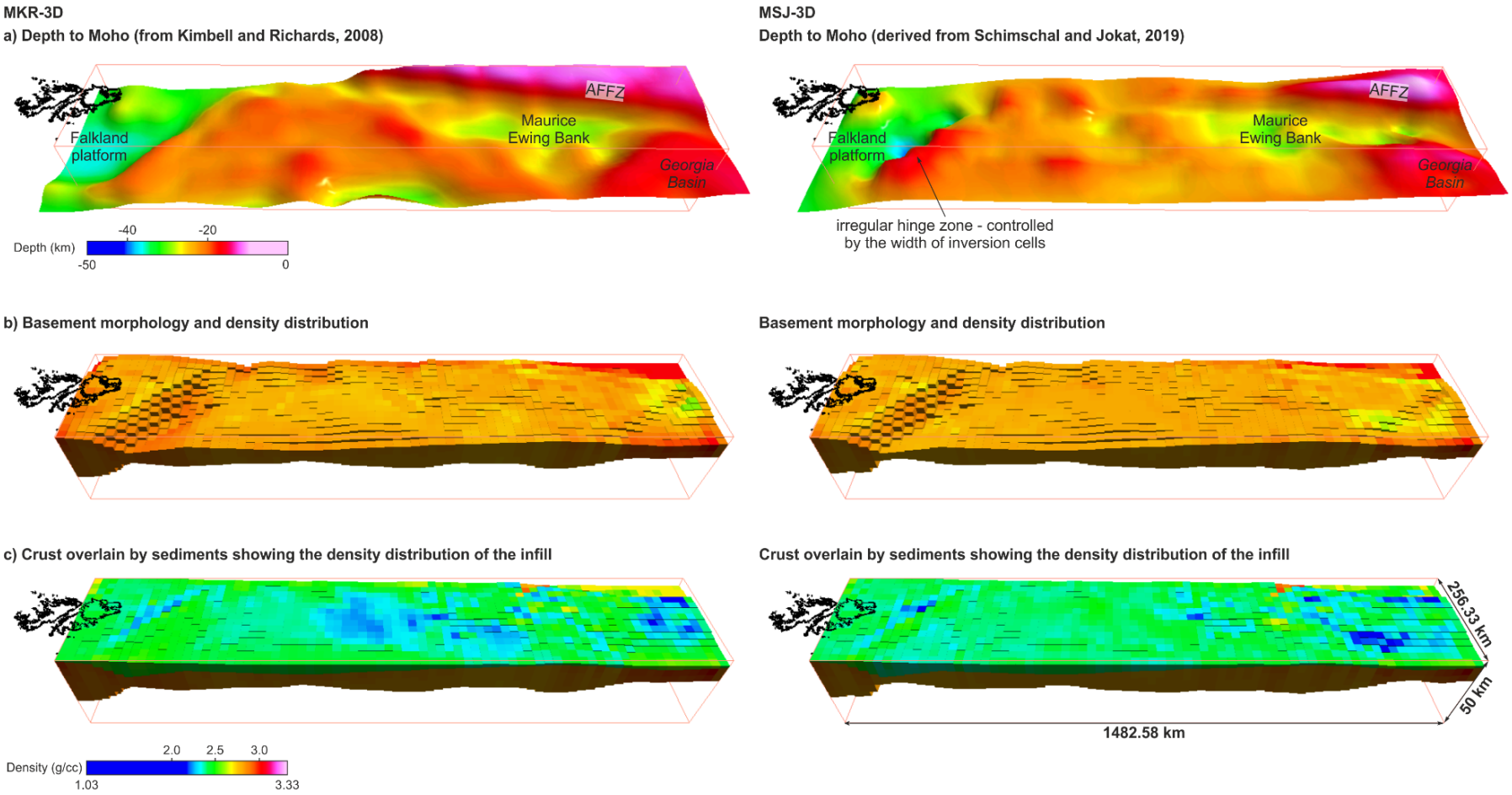

Figure 6.17 a) Morphology of the Moho from Kimbell and Richards (2008; MKR-3D) (left) and derived from Schimschal and Jokat (2019b; MSJ-3D) (right), and density distribution along the b) basement and c) sedimentary cover resulting from the 3D inversion

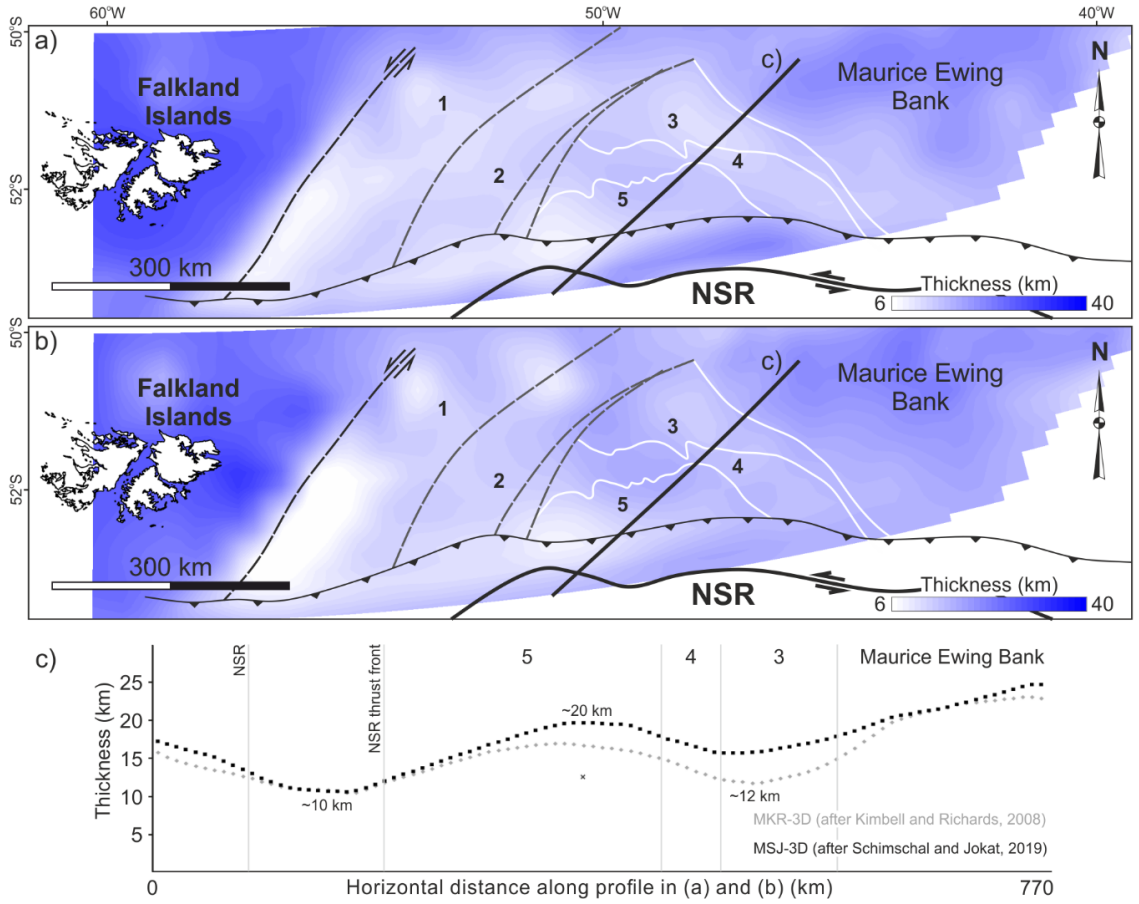

Figure 6.18 a) Crustal thickness calculated using the depth to Moho from Kimbell and Richards (2008) and top basement picked during this project (MKR-3D model); b) crust thickness based on the depth to Moho from Schimschal and Jokat (2019b) and 3D geometrical inversion (MSJ-3D model); c) comparison of crustal thicknesses across the 3-5 regions; profile position shown in (a) and (b)

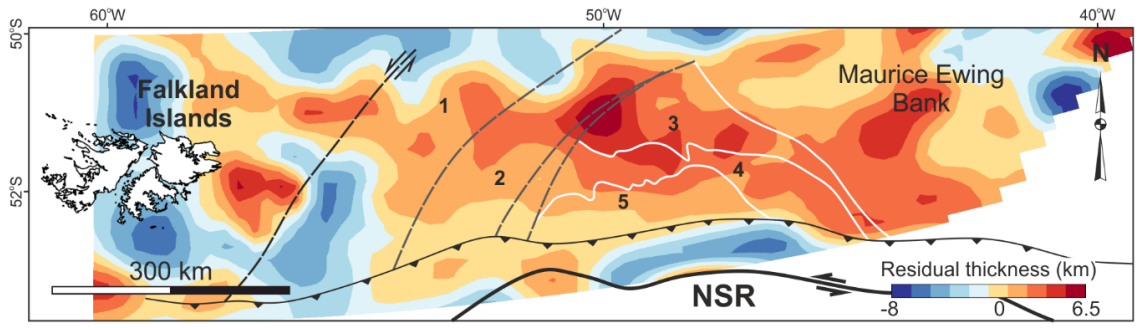

Figure 6.19 Residual thickness map obtained by subtracting the thickness of MKR-3D from MSJ-3D

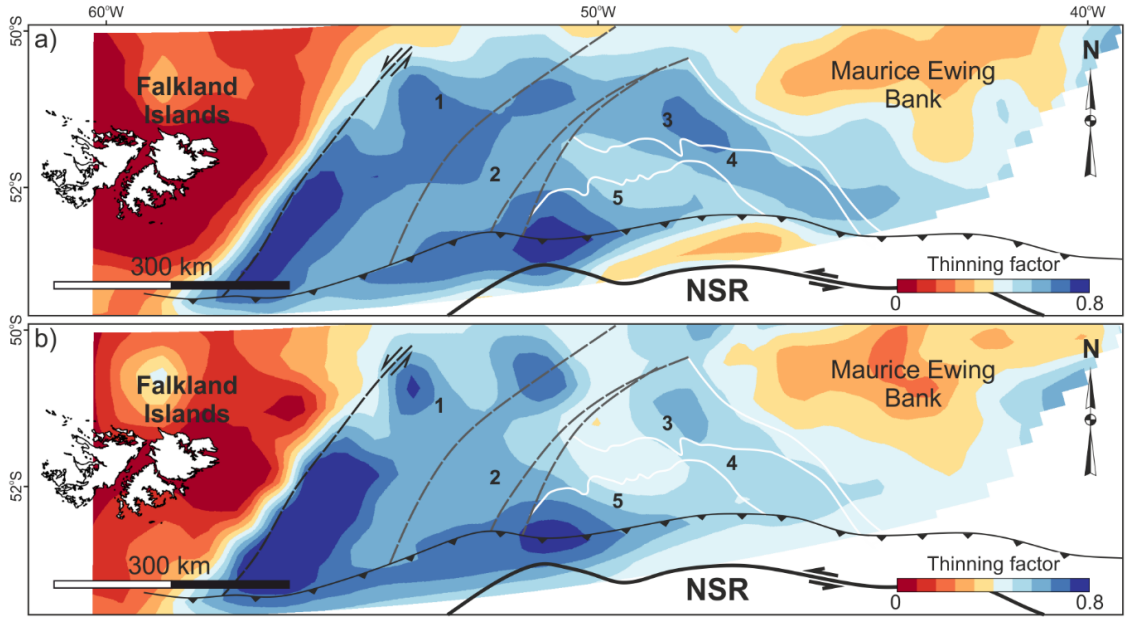

Figure 6.20 Thinning factors calculated from the crustal thickness estimated for a) the MKR-3D model (using the Moho model of Kimbell and Richards, 2008) and b) MSJ-3D model (using the Moho model derived from gravity inversion carried out in this chapter); thinning factor calculated as $1-t_f/t_i$ (where t_f is the current thickness of the crust and t_i is the original thickness assumed to be 35 km)

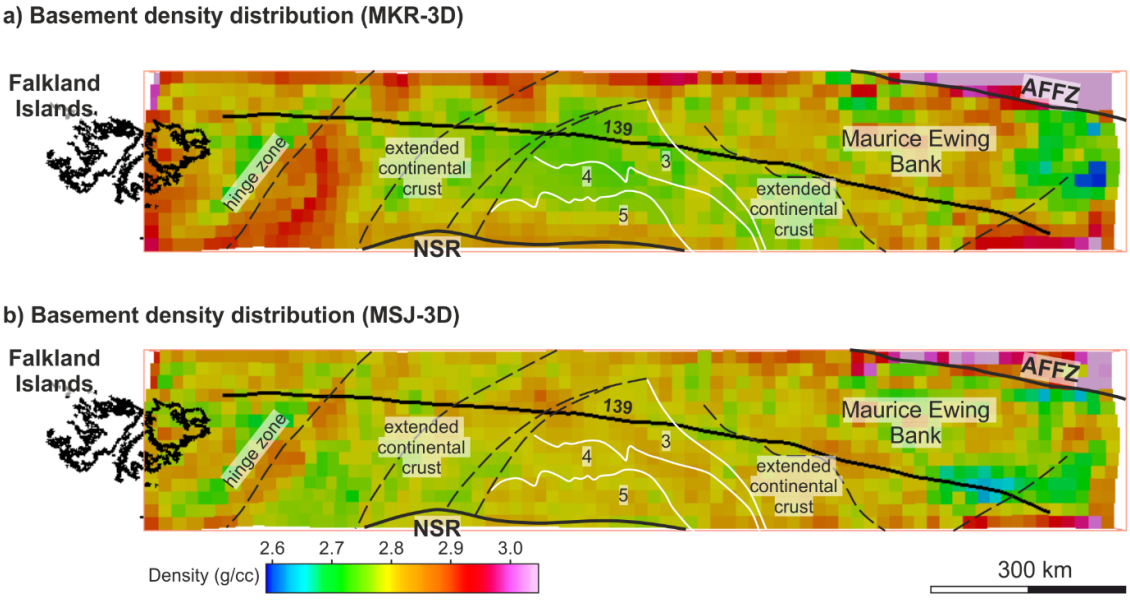

Figure 6.21 The 3D basement density distribution along the Falkland Plateau Basin and Maurice Ewing Bank for the two modelled scenarios using the full distance weighting showing high densities along the Falkland Islands shelf and Maurice Ewing Bank and a) relatively lower densities for the central and eastern Falkland Plateau Basin reaching the highest values under the Fitzroy sub-basin; b) high densities in the east-central part of the Falkland Plateau Basin and decreasing westwards (under the Fitzroy sub-basin)

East-west slices through the 3D models were taken along profile 139 for a direct comparison with the results from the 2D forward modelling. The inversion resulted in some variability in the density distribution based on the type of weighting used, with the full distance weighting yielding more geologically plausible results (no concentration of lower densities in the lower crust as seen in Figure 6.22a and eastern part of 6.23a). For the MKR-3D scenario, the crust underlying the FPB yielded relatively lower densities than the adjacent Falkland Islands platform and Maurice Ewing Bank (Figure 6.22) which contrasts with the results from 2D modelling (MKR-2D; Figure 6.15). The MSJ-3D model resulted in higher densities along the FPB than MKR-3D. The central part of the basin reached values of up to 2.86 g/cc, comparable to the Falklands shelf and the central part of the Maurice Ewing Bank, but lower than the densities estimated from 2D modelling (MSJ-2D; Figure 6.16). Lower densities along the eastern section of the MEB were obtained during inversion as well (Figure 6.23) compared to the 2D modelling (Figure 6.16).

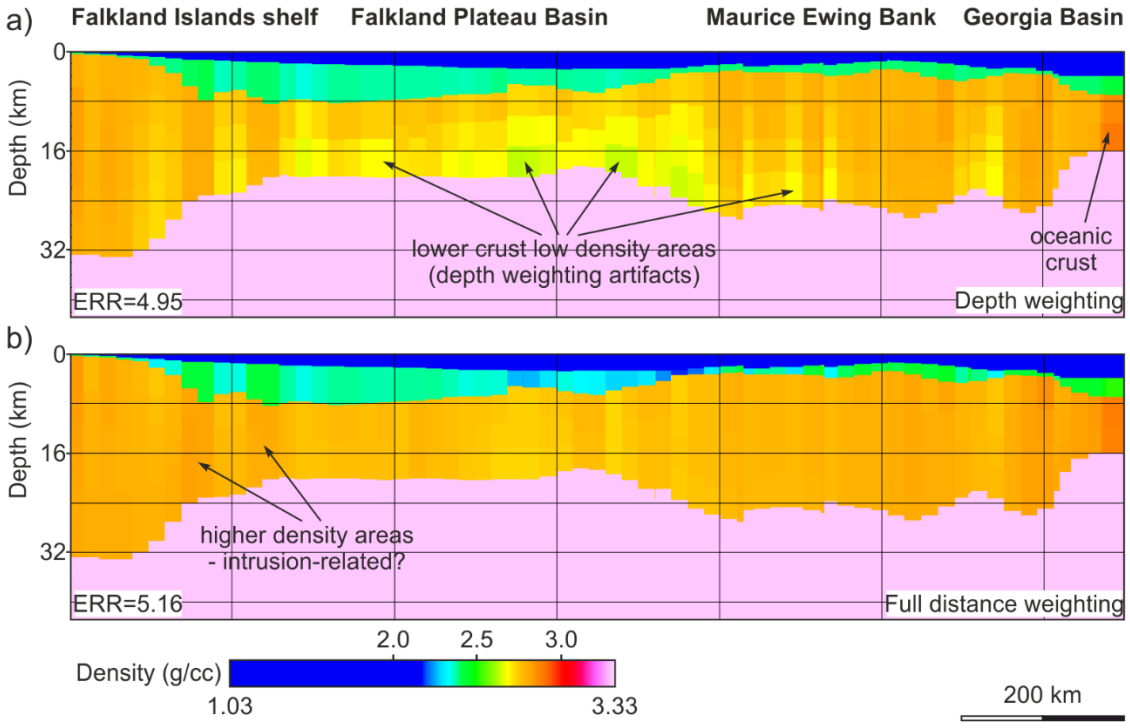

Figure 6.22 The results of the 3D gravity inversion (model MKR-3D) along line 139 using a) depth weighting and b) full distance weighting; Moho from Kimbell and Richards (2008); minimum-maximum estimated densities for sediments and crust across the Falkland Plateau Basin: (a) 2.226 – 2.569 g/cc and 2.58 – 3.05 g.cc, respectively; (b) 2.036 – 2.595 g/cc and 2.596 – 3.05 g/cc, respectively; line position shown in Figure 6.1

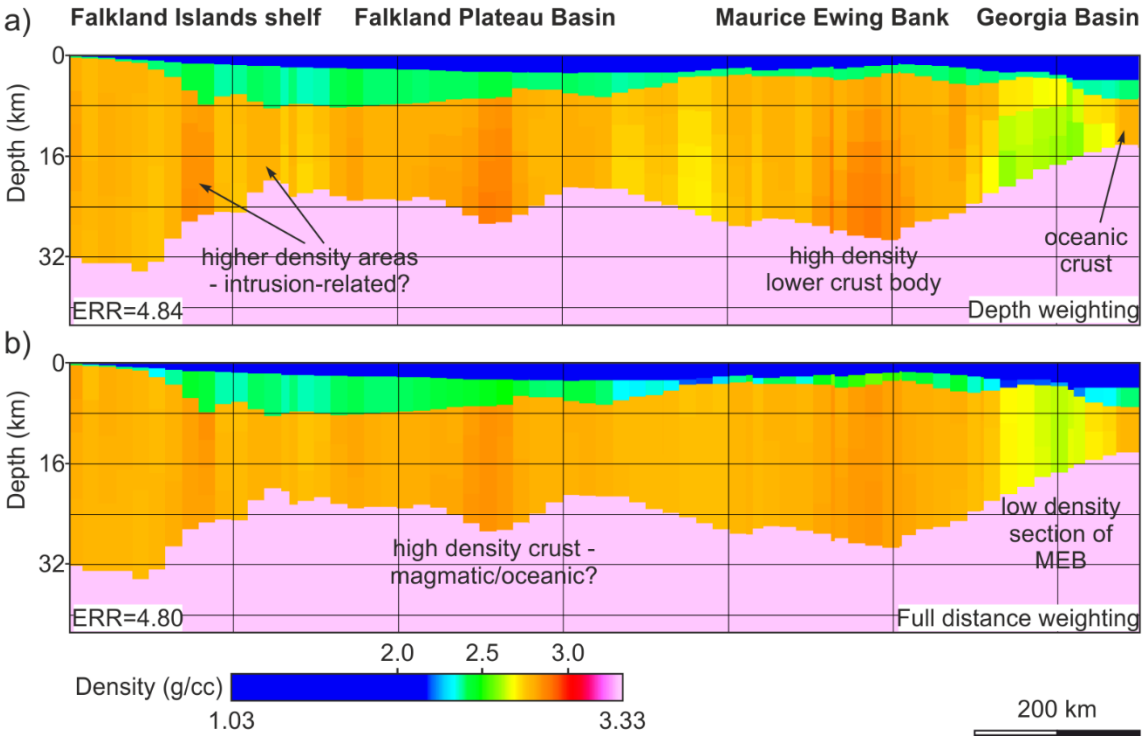

Figure 6.23 The results of the 3D gravity inversion (model MSJ-3D) along line 139 using a) depth weighting and b) full distance weighting; Moho from geometrical inversion constrained along AWI-20130010 from Schimschal and Jokat (2019b); minimum-maximum estimated densities for sediments and crust across the Falkland Plateau Basin: (a) 2.234 – 2.545 g/cc and 2.58 – 3.05 g.cc, respectively; (b) 2.077 – 2.613 g/cc and 2.63 – 3.05 g/cc, respectively; line position shown in Figure 6.1

6.4.2 Plate model

The crustal architecture across the FPB directly influences the plate reconstruction of the plateau and vice versa. Different plate configurations and evolutions of the plateau are considered in the following sections and compared and discussed against the observations from the gravity, magnetic, and seismic reflection data. The base of the plate reconstruction is shown in the rigid plate model, and four deforming plates scenarios are further considered (rotation of FIM with and without generation of oceanic crust and no rotation of the FIM with and without generation of oceanic crust) as a way to further validate the interpreted tectonic evolution of the plateau.

6.4.2.1 Rigid model

The rigid plate model shows the south-western Gondwana configuration at 170 Ma, 167.2 Ma, 160 Ma, 150 Ma, 140 Ma, and 130 Ma. The FIM is defined as follows: the northern boundary corresponds to the AFFZ, the eastern boundary

is F3 in Figure 6.7, the southern boundary is the North Scotia Ridge, and the western boundary is defined along the positive gravity anomaly (Figure 6.7b; Chapter 5).

The model starts at 170 Ma (after the rotation of the Ellsworth Whitmore Terrane - 180-175 Ma; Curtis and Storey, 1996; Martin, 2007) with the FIM rotated approximately 80° relative to southern South America, the Maurice Ewing Bank occupying the present-day position of the Tugela Cone, and Patagonia in a close fit to the Falkland Islands. The FIM starts in a more southern position than previous reconstruction models which is constrained by the fragmentation and deformation of the South American plate. This model uses the fragmentation and reconstruction suggested by Müller et al. (2019). This results in a more sinuous trend of the Gondwanide Fold and Thrust Belt (Figure 6.24 – Lower Jurassic stage) which, for the South Africa – Falklands region, was approximated using the reconstructed gravity trends along the FIM and South Africa (Figure 6.24 – top two maps).

The onset of clockwise rotation of the FIM was modelled as occurring at 167.2 Ma and here was related to the southward drift of East Antarctica (Chapter 5 and further discussed in Chapter 7). The dextral wrenching between West and East Gondwana might have generated a network of synthetic and antithetic shear zones (the present-day NE-SW trending F1-F3 in the FPB and the western and northern FIM boundaries; Figures 6.7, 6.8) that resulted in the isolation of the FIM (Figure 6.24 – Middle Jurassic; see Chapter 7 for the full discussion). The eastward movement of Patagonia generated at this stage extension in the basins along the eastern margin of South America and space to accommodate the rotation (Figure 6.24 – Middle Jurassic to Upper Jurassic 160 Ma). Correlations between the local and regional stress states suggest an intermediate rotated position for the FIM during the Late Jurassic (Chapter 5) when extension initiated between South America and Africa, in the Rocas Verdes Basin, and in the Weddell Sea (Figure 6.24 – Upper Jurassic 150 Ma; see Table 6.2 for the sources of each time-step). Generation of oceanic crust occurred in the Weddell Sea at 147 Ma (König and Jokat, 2006). The FIM was modelled to reach its present-day position relative to Patagonia at 145 Ma (Chapter 5). The Falkland Plateau reached its current extent at 130 Ma after the initiation of transform movement along the AFFZ (Baby et al., 2018; Figure 6.24 – Lower Cretaceous), as constrained by the movement of the MEB and South America.

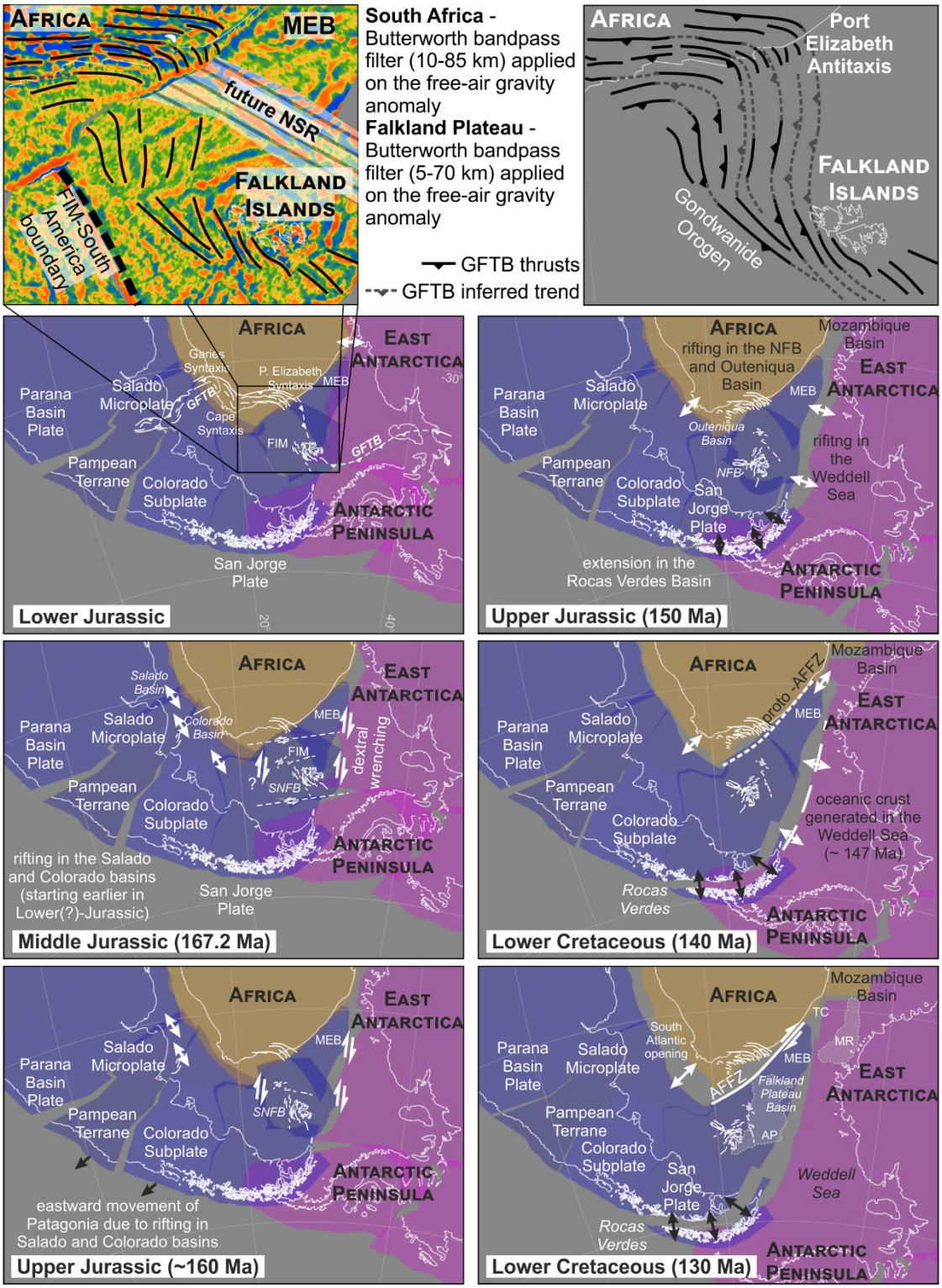

Figure 6.24 Butterworth bandpass filtered free-air gravity anomaly (Chapter 3) for the Falkland Plateau and South Africa and on- and offshore lineaments (top left); reconstructed trend of the Gondwana Fold and Thrust Belt (GFTB; top right); rigid plate reconstruction for south-western Gondwana (bottom six insets); AFFZ – Agulhas-Falkland Fracture Zone; AP – future Agulhas Plateau; FIM – Falkland Islands Microplate; MEB – Maurice Ewing Bank; MR – Mozambique Ridge; (S)NFB – (Southern) North Falkland Basin; TC – Tugela Cone

The closure of the Rocas Verdes Basin started at 100 Ma (Calderón et al., 2013, 2016), but is outside the time limits of this model. The overlapping area between the FIM and the eastern FPB and South Africa can be explained either through extension (pre-break-up, both the FIM and the plateau having smaller areal extents) or through the generation of oceanic crust.

The plate model is introduced in this chapter as it represents the base for the deforming plate models presented in next section, but the evolution of the Falkland Plateau in the context of south-western Gondwana will be fully discussed in Chapter 7.

6.4.2.2 Deforming plates model

The deforming plates model is used to test the reliability of the reconstruction by looking at the predicted crustal thicknesses and thinning factors and comparing these results to a non-rotational model and to present-day observations of the structure and architecture of the plateau.

The rotational model with no generation of oceanic crust (ROT) shows extension occurring in the Algoa and Gamtoos basins and the FPB during the Late Jurassic while the northern part (present-day orientation) of the FIM, the San Jorge Basin region, and the present-day Bredasdorp Basin were affected by compression due to the rotation of the FIM (Figure 6.25a). This compressional front migrated westward across the South American plate and eastwards in the Outeniqua Basin throughout the Late Jurassic and its extent and likely cause are discussed in Section 6.5.2. ENE-WSW extension (present-day reference system) occurred in the FPB (Figure 6.26b). West of the islands, in the Malvinas Trough (Malvinas Basin), the initial NNE-SSW and N-S strain orientation was subdued by a NNW-SSE extension throughout the Jurassic (Figure 6.27b). At the end of Jurassic and during the Early Cretaceous, southern Patagonia was affected by extension. At this stage, the FIM was fully rotated and the extension in the FPB was complete. Post-rotation and formation of the FPB, across the FIM, crust thins southwards and south-eastwards whereas on the Maurice Ewing side thinning occurs towards the south (Figure 6.25a – 130 Ma). Maximum thinning is seen under the South Falkland Basin, southern Fitzroy sub-basin, south-eastern FPB, and in the Malvinas Basin (Figures 6.25a – 130 Ma, 6.29b).

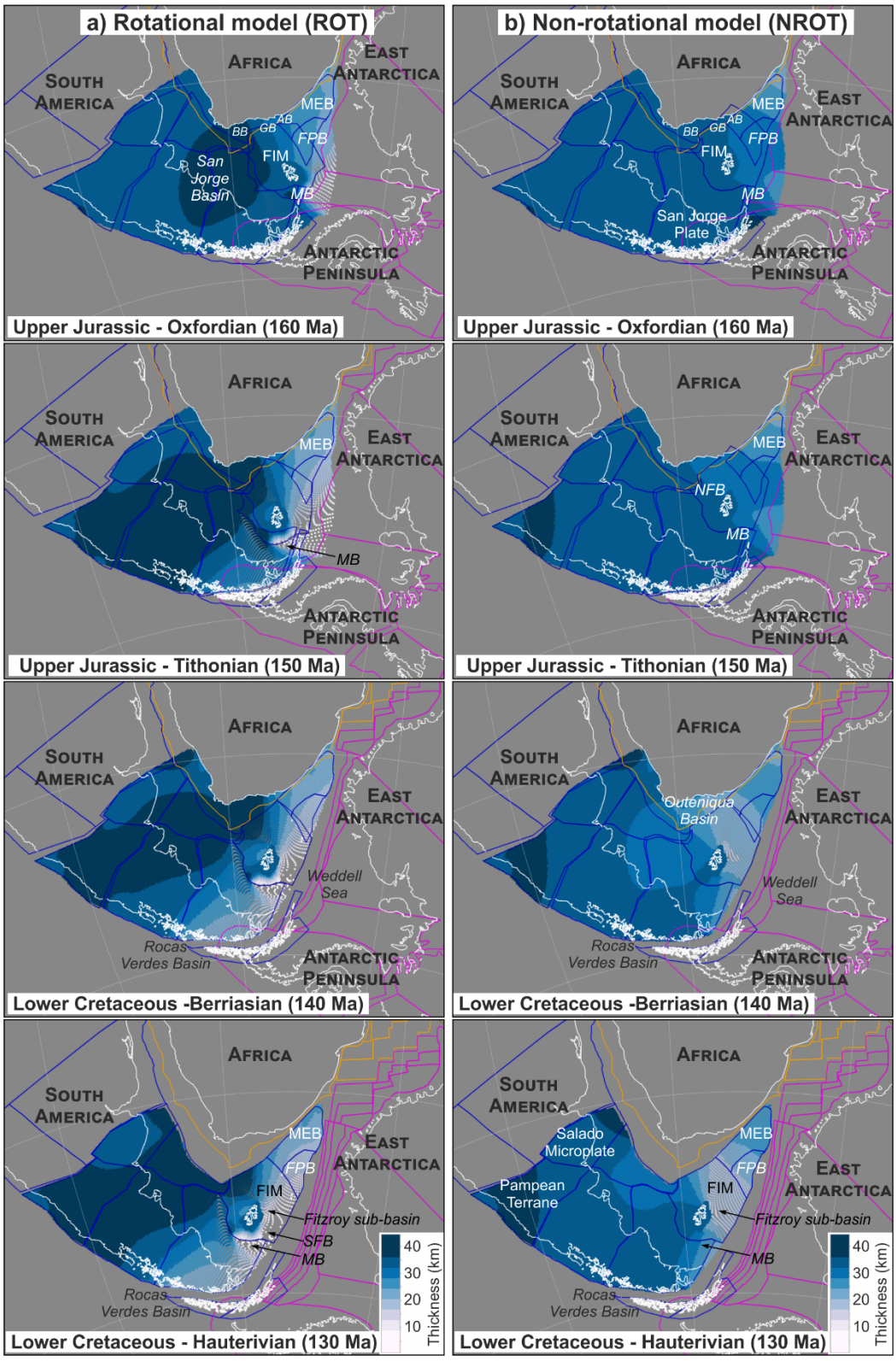

Figure 6.25 Deformable plate model for the Falkland Plateau showing the predicted crustal thickness for the rotational (ROT) and non-rotational (NROT) models when only extension with no oceanic crust generation occurs (160-130 Ma); AB – Algoa Basin; BB – Bredasdorp Basin; FIM – Falkland Islands Microplate; GB – Gamtoos Basin; MB – Malvinas Basin; SFB – South Falkland Basin

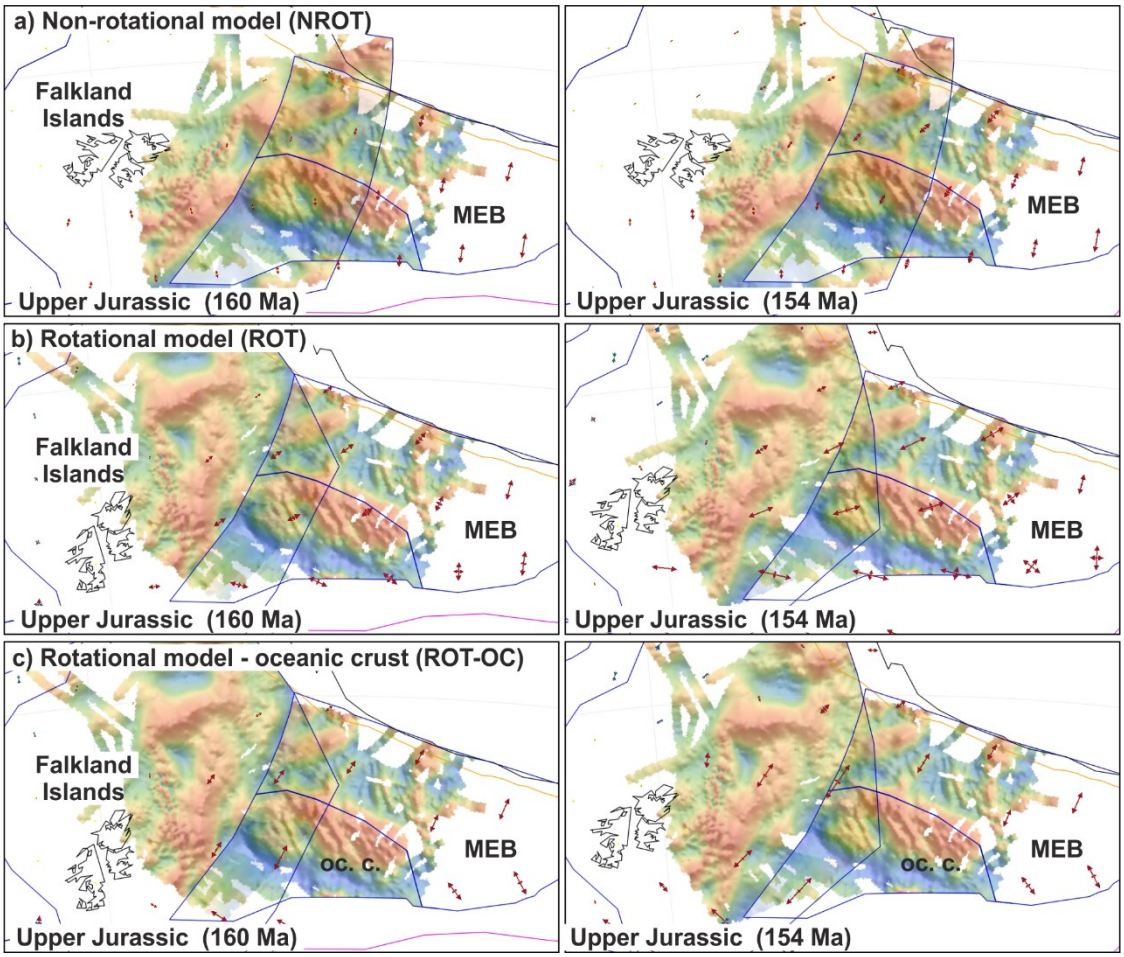

Figure 6.26 Azimuth of the principal component of the total strain across the magnetic stripes in the Falkland Plateau Basin showing a) a switch from N-S (oblique) extension to NE-SW (perpendicular) extension for the NROT model occurring at ~154 Ma; b) and c) a consistent extension direction perpendicular on the magnetic lineaments throughout the Late Jurassic for the rotational ROT and ROT-OC models; main difference seen along the south-eastern margin of the Maurice Ewing Bank (MEB) where the extension direction changes from NNE-SSW to NW-SE between the ROT and ROT-OC; lengths of total strain arrows are proportional to its relative magnitude; present-day orientation of South America; oc. c. – oceanic crust

For the second scenario (NROT), in which the FIM is part of the San Jorge Plate, the extension is initially concentrated south-east of the islands and along the MEB, migrating in the Outeniqua Basin and FPB throughout Late Jurassic and affecting the entire FPB and the NFB by the end of the Jurassic. Extension direction in the FPB changes from N-S to NE-SW throughout the Late Jurassic (Figure 6.26a). In the Malvinas Basin, a similar change in extension direction is seen as for the previous scenario (Figure 6.27a), but the relative strain magnitude is significantly lower. Compression affects the Pampean Terrane

and the Salado Microplate (Figure 6.25b – 150-130 Ma) and the likely cause is discussed in Section 6.5.2. The Early Cretaceous sees the end of FPB extension with most thinning occurring in the Fitzroy sub-basin. The crust thins towards the centre of the FPB across both the FIM and the Maurice Ewing Bank (Figures 6.25b – 130 Ma, 6.29a).

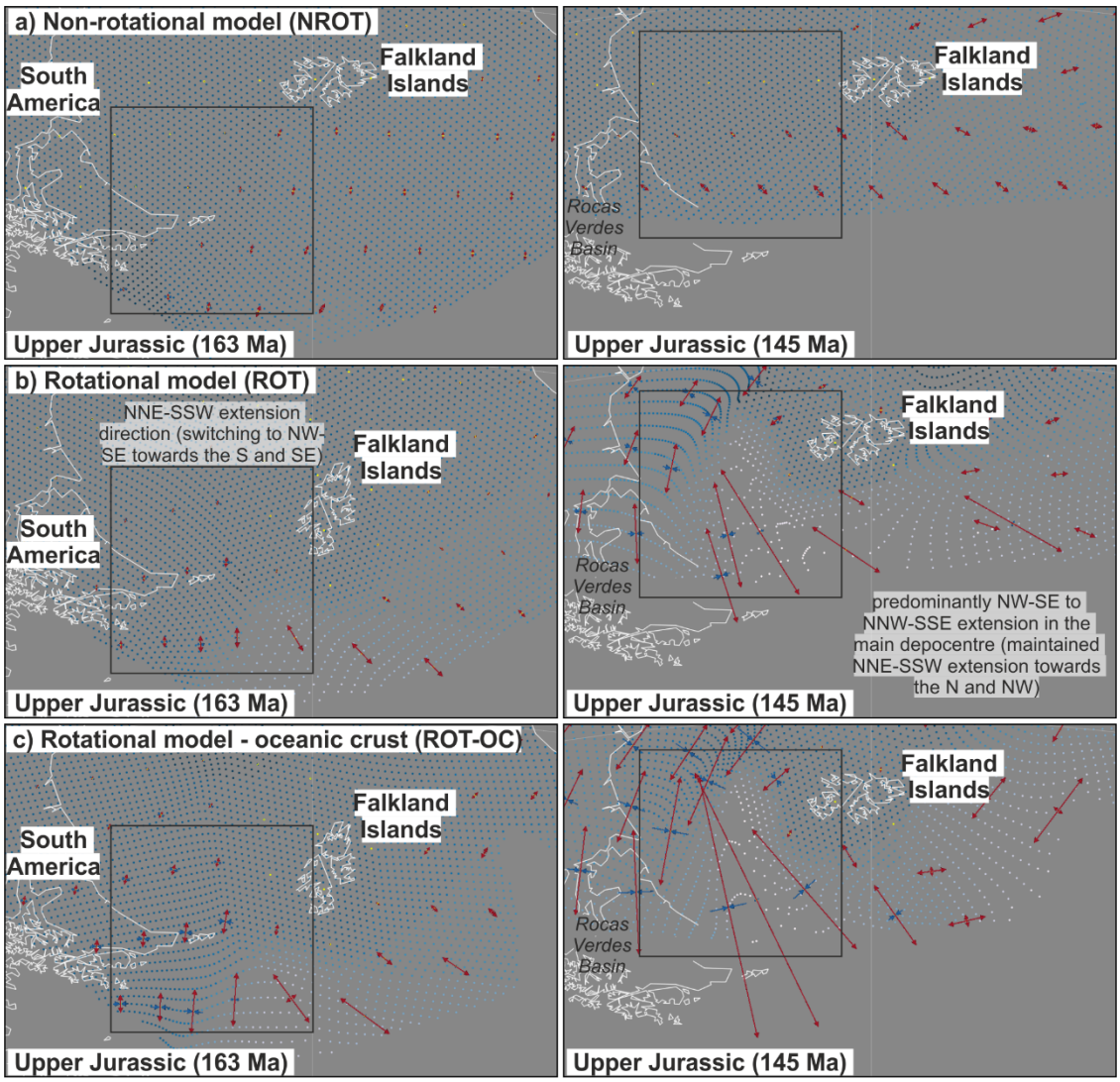

Figure 6.27 Azimuth of the principal component of the total strain in the Malvinas Basin (black rectangle) for the three models showing predominantly NNE-SSW extension which is further superimposed by NNW-SSE extension; strain magnitude increases from (a) to (c); present-day orientation of South America

The rotational model with generation of oceanic crust (ROT-OC) considers a maximum extent of the oceanic domain comprising regions 4-5 in Figure 6.13. The results show a regional thickness distribution similar to its continental crust counterpart. Differences are seen in the central part of the Falkland Plateau Basin where most thinning occurs for the oceanic crust generation scenario,

and across the Maurice Ewing Bank where, less extension is being modelled due to the Jurassic continental break-up (Figure 6.28, 6.29c). A non-rotational model with generation of oceanic crust (NROT-OC) was modelled as well (Figure A.13). This displays similarities with the NROT model (Figure 6.25b), but the results show a concentration of extension in the Volunteer sub-basin and along the AFFZ-adjacent portion of the FPB, with less extension modelled in the Malvinas Basin, Fitzroy sub-basin, and Maurice Ewing Bank. A summary of the results of the deforming plate models can be found in Table 6.5.

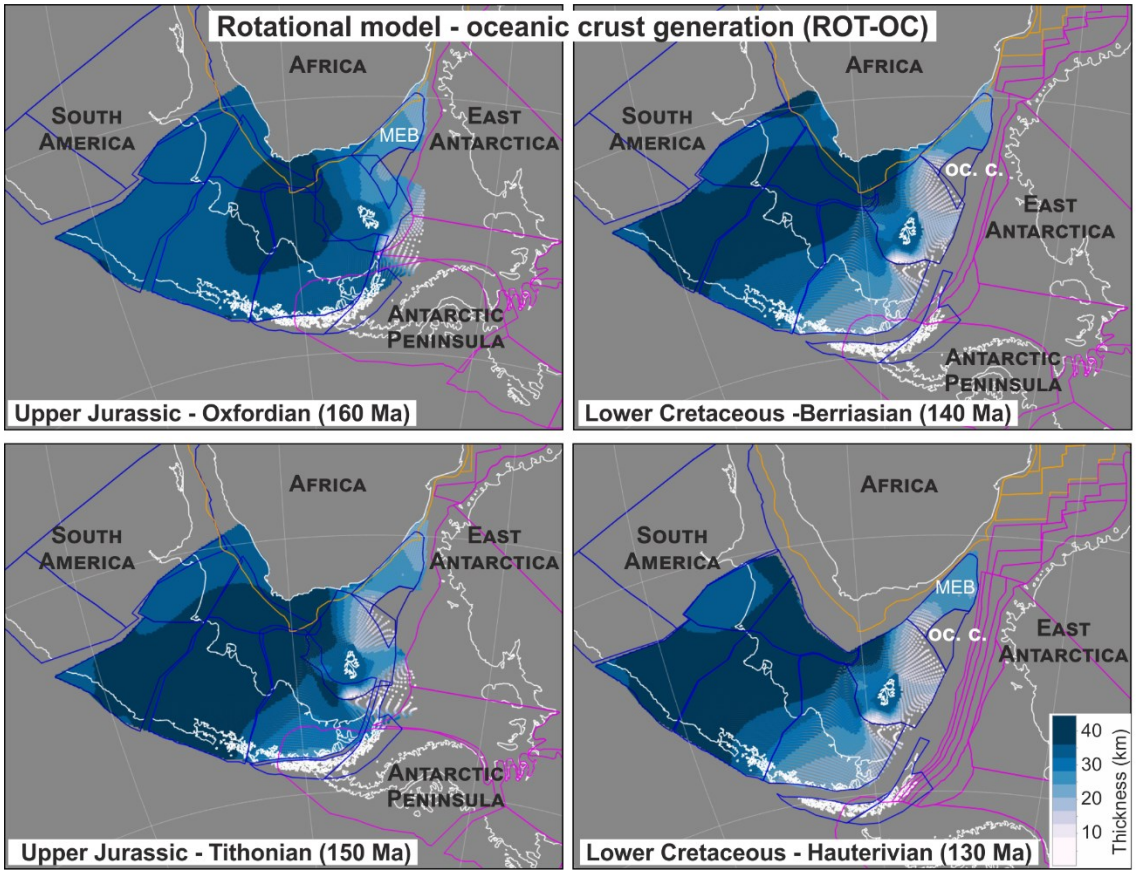

Figure 6.28 Deformable plate model for the Falkland Plateau for the rotational case with generation of oceanic crust (ROT-OC); oc. c. – oceanic crust; MEB – Maurice Ewing Bank

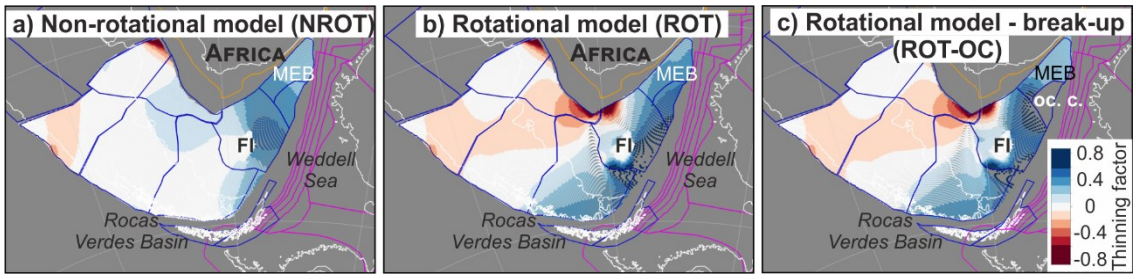

Figure 6.29 Thinning factors estimated for the deformable plate model for all three scenarios; FI – Falkland Islands; MEB – Maurice Ewing Bank; oc. c. – oceanic crust

Table 6.5 Summary of deformable plate reconstructions outcomes

SCENARIO	POSITIVE OUTCOMES	NEGATIVE OUTCOMES
No rotation (NROT and NROT-OC)	✓ thinning in the Fitzroy sub-basin for the NROT comparable to gravity inversion results ✓ extension occurring in the larger Outeniqua Basin from Late Jurassic ✓ changes in extension direction in the Malvinas Basin consistent with seismic data	✗ little extension in the Malvinas Basin ✗ little extension in the Falkland Plateau Basin during the Jurassic when potentially break-up occurs (for NROT) ✗ extension of the SW margin of the Maurice Ewing Bank not consistent with observations (present-day NW-SE trending faults)
Rotation (ROT and ROT-OC)	✓ extension along the western margin of the Maurice Ewing Bank consistent with faulting and lineations seen on seismic, gravity and magnetic data (ROT) ✓ significant thinning occurring in the Falkland Plateau Basin during the Jurassic, allowing for potential break-up (ROT) ✓ crustal thinning and shape of trough in the Malvinas Basin consistent with seismic data ✓ changes in extension direction in the Malvinas Basin consistent with seismic data ✓ extension of SE margin of the Maurice Ewing Bank consistent with observations (for ROT-OC)	✗ compression generated in the northern part of the FIM, Outeniqua Basin, and across the South American plate ✗ most extension modelled in the southern part of the Fitzroy sub-basin and in the South Falkland Basin and not around the potential oceanic domain (ROT) ✗ extension of the SW margin of the Maurice Ewing Bank not consistent with observations (present-day NW-SE trending faults; for ROT-OC)

A rigid plate model, crustal thickness distribution, and thinning factors for a more northern position of the FIM (model ROT-2) were further built and generated (Figures 6.30, A.14). The position was based on the reconstruction in Chapter 4 and the thinning factors estimated between F1 and F3 from the

gravity inversion (Figure 6.20). Thinning factors of ~0.6-0.65 would translate in a change in length between the F1 and F3 from the current ~300 km to ~105-120 km (Figure 6.30a, inset) which would fit between the Falkland Islands shelf (F1; what was believed to be the eastern extent of the FIM) and Africa. However, this position of the FIM results in a gap between the microplate and the South American plate as reconstructed by Müller et al. (2019) which requires adjustments in the reconstruction of the South American sub-plates (Figure 6.30a). The implications of changes in the latitudinal position of the FIM on the deformation of South America will be discussed in Chapter 7. The purpose of this secondary reconstruction is to show that the distribution of depocentres and overall morphology (thinning directions) of the Falkland Plateau obtained during rotation (Figures 6.25a - 130 Ma, 6.29b) are comparable for a tighter fit between the FIM and Africa and it will not impact the discussion in the following section. The main difference between ROT and ROT-2 arises from an overall thinner crust being estimated for the FPB (Figures 6.25a – 130 Ma, 6.30b).

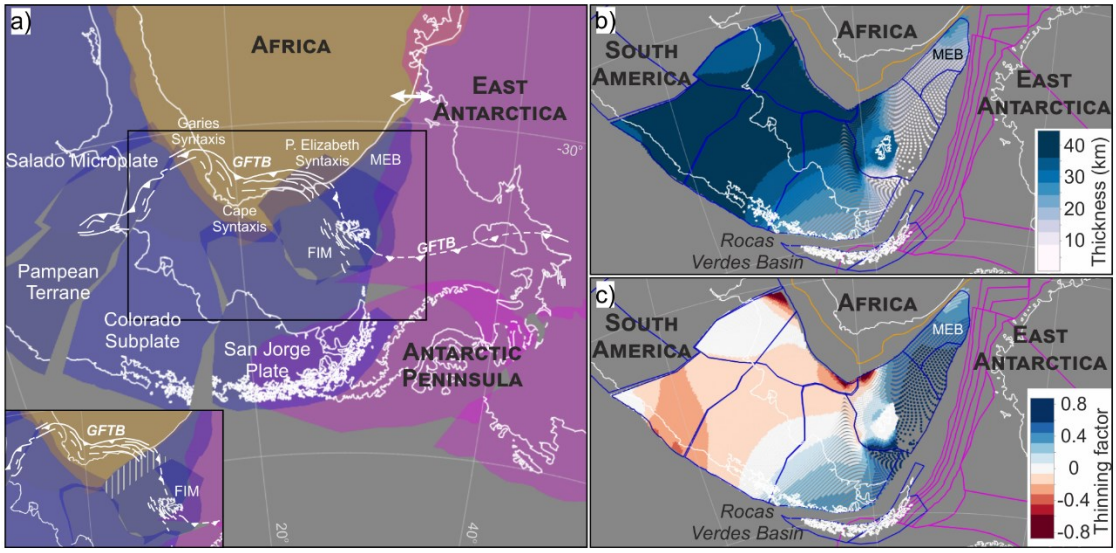

Figure 6.30 a) Alternative position for the FIM (model ROT-2) in a tighter fit to Africa and the changes needed along South America to accommodate this more northern position; rectangle shows extent of inset map; inset shows configuration from Figure 6.24 and the hatched area marks the eastern region of the FIM gained through extension; b) crustal thickness estimated for this more northern position; c) thinning factor across the deforming network; FIM – Falkland Islands Microplate; MEB – Maurice Ewing Bank

6.5 Discussion

The integration of seismic, gravity, and magnetic data, and deformable plate modelling have brought a lot of insights into the crustal architecture of the plateau. However, several areas of uncertainty and unanswered questions remain, which are addressed in this section. These are as follows:

1. the nature of the crust in the east-central part of the FPB (the region between F3 and MEB or areas 3-4 in Figure 6.13), and if not conclusive, the implications of each of the possibilities (Section 6.5.1.1);
2. the tectonic processes that led to the present-day architecture of the Falkland Plateau (i. e. Would a rotational or non-rotational model better account for the crustal and structural complexities seen along the plateau?) (Section 6.5.1.2).

6.5.1 Crustal architecture

6.5.1.1 Distribution of crustal types in the east-central part of the FPB

The nature of the crust under the Falkland Plateau Basin represents one of the obstacles in building a reliable reconstruction model of the South Atlantic that integrates the position of the Falkland Plateau. The lack of seismic reflection data that image the Mohorovičić discontinuity limited the use of gravity modelling and inversion but nonetheless insights can be gleaned from these methodologies when integrated with seismic facies and magnetic data analysis. The 2D forward gravity modelling and 3D gravity inversion for the two depth-to-Moho scenarios yielded densities that span the continental and oceanic range. The implications of both in the context of the interpreted seismic reflection and magnetic data are discussed in this section.

The models constrained with seismic refraction information from Schimschal and Jokat (2019b; MSJ-2D and MSJ-3D) yielded densities of up to 3.05 g/cc in the lower crust underneath regions 2 and 3 (Figure 6.13) of the FPB and a crustal thickness of up to 20 km which could be explained in two ways.

The first interpretation of the high densities is the presence of oceanic crust as suggested by Schimschal and Jokat (2017, 2019b) based on P-wave velocity analysis. This study and the one of Eagles and Eisermann (2020) support the presence of oceanic crust under regions 1 to 5 in Figure 6.13 (between F1, or east of it, and the MEB; black dots in Figure 6.8a). However, an interpretation more consistent with the presence of continental crust under region 1 is suggested in this study (Chapter 5; Figure 6.9). Oceanic crust was mapped

with higher certainty on magnetic data only within region 5 (Figure 6.13) but the high densities would suggest an oceanic domain spanning regions 2 to 5. The gravity modelling and inversion yielded crustal thicknesses of up to 20 km for central and eastern part of the FPB (Figures 6.16, 6.18, A.10), which would raise the question of the potential existence of an oceanic plateau. These are areas of thick oceanic crust (~30 km) that form relatively fast due to decompression melting above mantle plumes (the Mantle Plume hypothesis) or due to plate tectonics (the Plate Boundary hypothesis) (Zhang et al., 2020) and generate elevated topographies (~2-3 km higher) relative to typical oceanic crust domains (Courtillot and Renne, 2003; Kerr, 2014). Two such regions have been documented just offshore South Africa: the Agulhas Plateau and the Mozambique Ridge (Figure 6.24 – 130 Ma). These both have thicknesses between 20 and 24 km with P-wave velocities between 3.5 and 7.6 km/s and were formed between 100 and 95 Ma and 140 and 120 Ma, respectively (Parsiegla et al., 2008; König and Jokat, 2010; Gohl, 2011; Fischer et al., 2017). The two have been interpreted to be related to the migration of the Bouvet hotspot (Marks and Tikku, 2001; Parsiegla et al., 2008). However, the emplacement of the Agulhas Plateau has been estimated to have occurred after the Falkland Plateau cleared the coast of South Africa (Gohl and Uenzelmann-Neben, 2001). On the other hand, the model of emplacement for the Mozambique Ridge by Fischer et al. (2017) shows a migration of the eruption centres southwards where the ridge reaches its current southern extent by 130 Ma. Until this point, the ridge is located just east of the Maurice Ewing Bank (in a reconstructed model; Figure 6.24 – 130 Ma) and one can speculate that this magmatic province continued into the FPB. However, with the exception of an elevated region onto which Jurassic deposits onlap into the central part of the Falkland Plateau Basin (Figure 6.9b), the crust in the FPB seems to have formed before the end of the Jurassic (before ~145 Ma) section deposition (Figures 6.9a, 6.11). Prior to this, the large amount of magmatism and volcanism needed for the generation of an oceanic plateau occurred during the emplacement of the Karoo-Ferrar large igneous province (LIP) (174-184 Ma) (Jourdan et al., 2007). The reconstruction model from this study (Figure 6.24) suggests that not much extension occurred in the FPB prior to 170 Ma. However, back-arc extension associated with a high degree of underplating, magmatism, and volcanism occurred in the southern Weddell Sea at ~ 175 Ma (Jordan et al., 2017; Leat et al., 2018; Riley et al., 2020; see Chapter 5, Figure 5.21 for Weddell Sea rift configuration) which could have accounted for some degree of extension to propagate into the southern part of the FPB (Marshall,

1994). Nonetheless, not enough space existed at this time between the FI and the MEB in order to generate an oceanic domain comprising regions 2 to 5. Furthermore, the crust underneath the Weddell Sea Rift System is considered to be extended continental crust (Jordan et al., 2017) so it is unlikely that the FPB underwent enough extension for oceanic crust to be generated during this period. If this stage of crustal thinning, which overlaps the emplacement of the Karoo-Ferrar LIP, resulted in extensive volcanism and intrusion of the continental crust in the FPB, the crust underlying the regions 2-5 (Figure 6.13) is maybe similar to what has been interpreted in the Weddell Sea Rift System, but further extended and sheared (region 2) during the main stage of rifting in the FPB. However, with the exception of region 2 that displays significant deformation, little evidence of faulting and extension of this igneous crust is seen on the seismic (Figures 6.9b, 6.10, 6.11). Furthermore, DSDP 330 cored Oxfordian-Middle Jurassic sediments (Barker et al., 1977). Although difficult to map and extrapolate across the sparse seismic data, there are areas where these deposits were not interpreted (Figure 6.11) which would suggest oceanic crust generation occurring after their deposition but before the end of the Jurassic (Figure 6.9a). If no mantle plume is invoked for the formation of thick oceanic crust in the FPB, a simpler explanation would be its proximity to plate boundaries. The main extension stage in the plateau is interpreted as starting at 167.2 Ma when East Antarctica drifts away from Western Gondwana (König and Jokat, 2006) and continued all the way up to the Early Cretaceous (~140 Ma). If oceanic crust is generated in regions 2-5 during the end of Mid-Jurassic – beginning of Late Jurassic, the proximity of the plateau to the Weddell Sea spreading ridge, initiated at 147 Ma (König and Jokat, 2006), could account for additional volcanic material to be accreted to this crust. Intra-crust dipping reflectors and top crust topographical highs seen in the south-eastern part of the FPB (Figure 6.11) could be suggestive of lava flows and potential extrusion centres which are commonly associated with oceanic plateaus (Gohl and Uenzelmann-Neben, 2001).

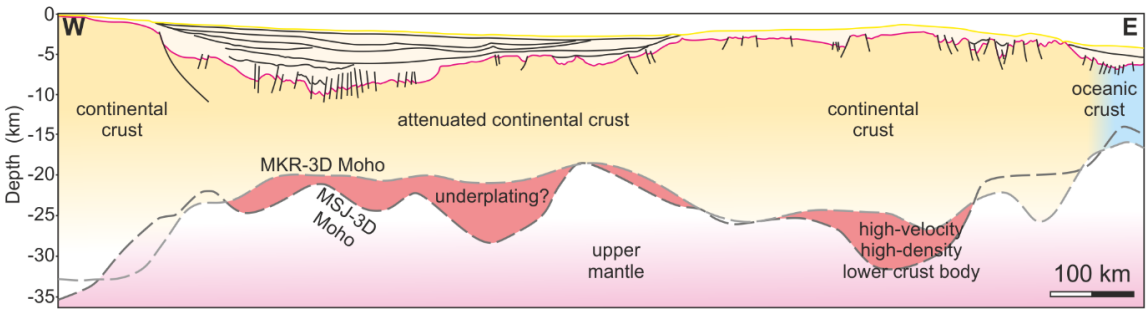

Figure 6.31 Potential interpretation of profile 139 showing attenuated and underplated continental crust underlying the Falkland Plateau Basin; line position shown in Figure 6.1

A second interpretation for the high densities from forward gravity modelling could be the presence of underplated continental crust (Figure 6.31). The P-wave velocities of the 3.05 g/cc dense lower crust are 7.2 – 7.4 km/s (Schimschal and Jokat, 2019b) which are not dissimilar to velocities and densities seen at the crust-mantle boundary in several transform systems (Lorenzo et al., 1991; Berndt et al., 2001; Klingelhöfer et al., 2005; Planert et al., 2017) where these velocities are associated with magmatic underplating or serpentinization of the upper mantle. Densities more typical of continental crust were obtained for MKR-2D and MKR-3D (Figures 6.15, 6.21, and 6.22), but invoking underplating or pockets of lower density (serpentinized?) upper mantle would be necessary in these scenarios as well to explain the low P-wave velocities at the crust/mantle boundary documented by Schimschal and Jokat (2017, 2019b). The presence of bodies with densities lower than the upper mantle would also result in an increase in the estimated densities for the crust underlying the FPB (Figure A.11). For the MKR-3D model in particular densities lower than the adjacent crustal blocks were modelled (Figure 6.22) for the FPB which contrast with both interpretations of the basin being underlain by oceanic crust or extended continental crust similar in composition to the Falkland shelf and MEB. For the scenario in which the lower crust densities in the FPB are correlated with underplating, regions 2 and 3 (Figure 6.13) would be underlain by extended, intruded, and underplated continental crust transitioning to the south and south-east to thick oceanic crust. Two possibilities for the location of the continent-ocean boundary (COB) can be considered. If the COB lies between regions 3 and 4, then the area comprising regions 4 and 5 would be underlain by oceanic crust thickened due to its closeness to the Weddell Sea spreading ridge (see paragraph above for full explanation). If the COB is located further south, between regions 4 and 5, then the crust in region 4 would be continental as well.

This interpretation of a non-oceanic nature of region 4 is supported by the sediment distribution mapped across the area. Although magnetic lineations were identified in this region (Figures 6.8 and 6.13), which might point to magnetic reversal isochrons typical of oceanic crust as seen in region 5 and as interpreted by Eagles and Eisermann (2020), thick successions of pre-Middle Jurassic sediments were deposited on top of this crust and then deformed, uplifted, and eroded (Figure 6.10). This suggests a different evolution between regions 4 and 5, with 4 needing to be a fully formed domain significantly earlier than region 5. A more plausible interpretation of region 4 is that it consists of continental crust and the magnetic lineations readily seen along it (Figure 6.8) represent a continuation of the Early Jurassic linear magnetic pattern of the Weddell Sea Rift System (Southern Weddell Magnetic Province in Jordan et al., 2017 and Chapter 5). In this case, the depocentres identified in Figure 6.10 would be coeval with the Weddell Sea Rift. It remains unclear if similar crust extends in regions 2 and 3. Region 3 exhibits a different magnetic signature than its southern adjacent domain. However, magnetic lineaments were mapped in this part of the FPB as well (Figure 6.8) but were locally associated with volcanic edifices on seismic data (Figure 6.9). The lineaments are sub-parallel to the magnetic reversal isochrons in region 5 (i.e. sub-perpendicular to the rifting direction) which might suggest that they were generated during extension in the FPB and acted as conduits for magmatic material. The lineaments change their strike from NW-SE to WNW-ESE towards the west (Figure 6.8) potentially due to shearing along the F3. Region 2 shows evidence of significant deformation potentially due to shearing between F2 and F3 (Figures 6.9a, 6.13) and P-wave velocities from Schimschal and Jokat (2017) point more towards the existence of oceanic crust although this is not clear on the seismic reflection data (Figure 6.9). The sliver between F2 and F3 could represent a mosaic of oceanic and highly deformed continental crust, sheared between the two fracture zones, with the oceanic component more predominant towards the south where region 2 is adjacent to 5 (Figure 6.13). The northern part of region 2 is overlain by relatively thick Jurassic deposits (Figure 6.9) which seem more suggestive of deposition above a thinned continental crust.

6.5.1.2 Implications of end-member reconstructions for the crustal architecture of the Falkland Plateau

The crustal thicknesses estimated from the deformable plate models show a high variability depending on the starting position of the FIM and its Mesozoic evolution (Figures 6. 25, 6.28, and 6.32).

Although oceanic crust was interpreted in the south-eastern part of the FPB (Figure 6.13), the most thinning estimated from the deforming plates reconstructions does not occur consistently in the vicinity of the oceanic domain (Figures 6.29 and 6.32). The presence of crustal heterogeneities or pre-existing structures would control the locus of deformation, but this is not accounted for by the model and could explain the discrepancies between the deformable plates modelling results and the interpretation of seismic, gravity, and magnetic data. More details on the limitations of this method are provided in the following section.

Model NROT-OC will not be considered separately as it shares significant similarities with the NROT and ROT-OC (for central FPB and MEB) models which the discussion will cover in detail. The NROT model suggests that thinning occurred roughly on a E-W direction (present-day orientation), with the most of it recorded in the Fitzroy sub-basin followed by the remainder of the FPB (Figures 6.29a and 6.32b). In contrast, the ROT model yields most thinning in the Malvinas Trough, the Southern Falkland Basin, and the southern part of the Fitzroy sub-basin (Figures 6.28a, 6.29b, and 6.32c). The rest of the plateau thins south-eastwards from the eastern shelf of the islands, and south-westwards from the MEB (Figure 6.32c). This results in a triangular zone of extension in the central part of the FPB. The ROT-OC model shows most thinning occurring in the Malvinas Trough and east and north-east of the oceanic domain in the FPB (region 2 in Figure 6.13; Figure 6.29c and 6.32d). Although extension was expected to occur on a similar orientation as for the ROT scenario, with the crust along the MEB thinning south-westwards (Figure 6.32c), this trend is not similar for the ROT-OC case (Figure 6.32d). The direction of thinning, sub-perpendicular to the breakup axis, is believed to be an artefact of the modelling and will be discussed in the limitations section.

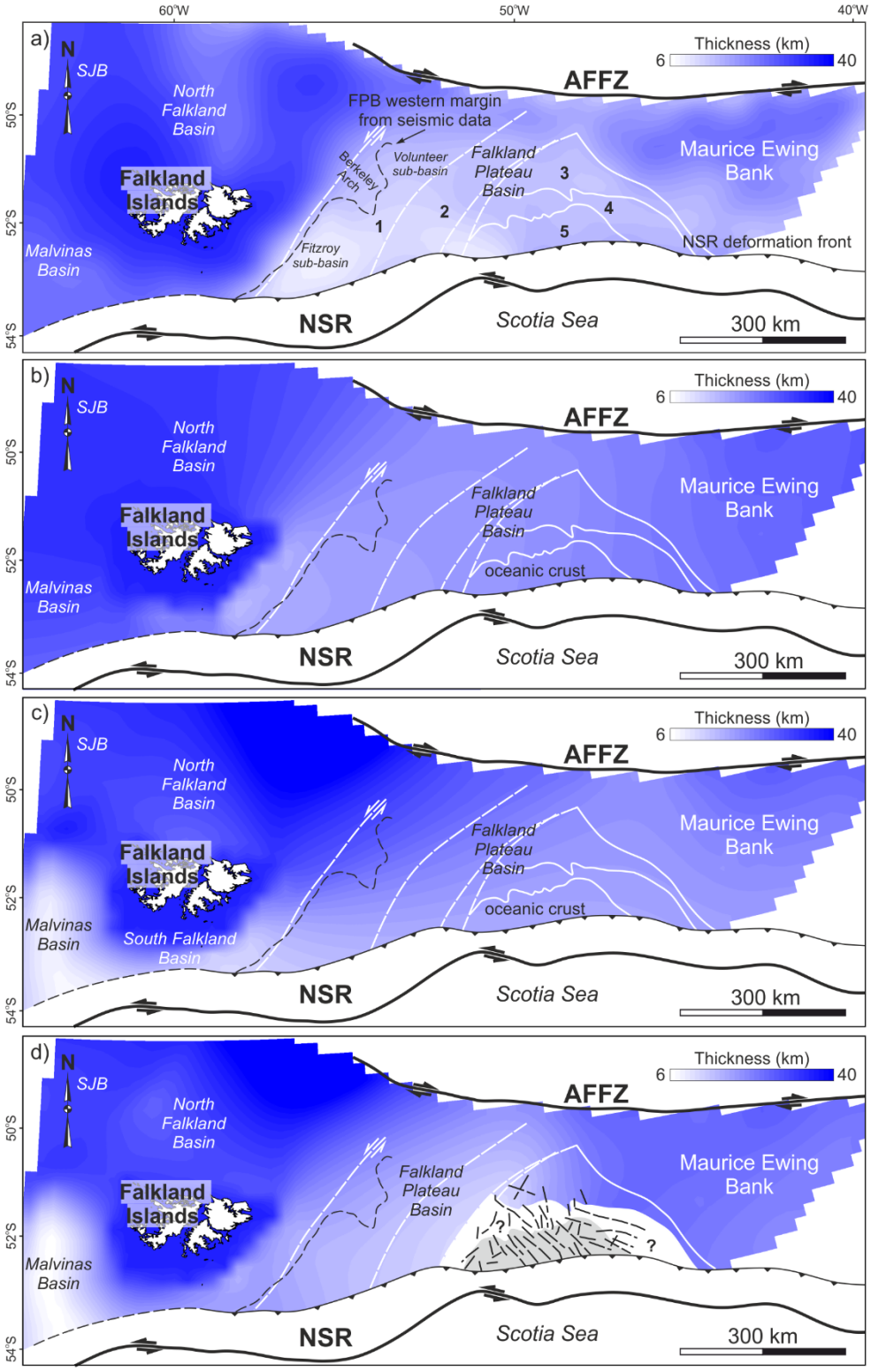

Figure 6.32 Crustal thickness across the Falkland Plateau from: a) Kimbell and Richards (2008); b) NROT model; c) ROT model; d) ROT-OC model overlain by the magnetic lineaments in regions 3-4; black stippled line - western extent of Falkland Plateau Basin depocentres; white dashed lines – F1 to F3; white lines – boundaries of regions 3-5; grey area in (d) – oceanic crust; AFFZ – Agulhas – Falkland Fracture Zone; NSR – North Scotia Ridge; SJB – San Julian Basin

All models predict that the thinning extends up to the predefined rigid block of the Falkland Islands (Figure 6.29 and 6.32). However, based on seismic reflection data (Chapter 5), significant crustal stretching does not occur west of the hinge zone (dashed black line in Figure 6.32). The deformation associated with the opening of the FPB consistently decreases towards the islands (Chapter 5). Defining the non-stretched area of the Falkland Islands as a rigid block during modelling concentrates the deformation along the boundaries of this block, which results in an underestimation of the crust thickness on the eastern shelf of the islands (Figure 6.32). This can be seen on the residual maps computed between the crustal thickness from MKR-3D and MSJ-3D, and crustal thickness from deforming plates modelling (Figures 6.34 and 6.35) as positive anomalies along the eastern shelf of the Falkland Islands.

There are several discrepancies between the crustal thicknesses estimated from gravity inversion and the ones from deforming plates modelling depending on which evolutionary model is invoked. The next sections cover these differences as seen across the main sedimentary basins of the plateau in order to understand if the variations are due to the used methodologies or the result of erroneous assumptions (rotation vs. no rotation of the FIM). These comparisons are collated with principal strain direction information (Figures 6.26, 6.27) from deforming plate modelling to constrain the validity of each model. The Southern Falkland Basin will not be included in the discussion as its present-day configuration was shaped by movement along the NSR which occurred outside the time limits of the deforming plates models. The crustal thicknesses estimated from the depth to Moho used in models MKR-3D and MSJ-3D will be referred to as the “gravity-derived thickness” for simplicity, although the depth to Moho in MKR-3D has been obtained through an iteration of isostatically compensated and forward gravity modelling (Kimbell and Richards, 2008).

6.5.1.2.1 Malvinas Basin

Little stretching occurs under the Malvinas Basin when the islands are kept fixed to Patagonia (NROT), comparable to the modelling results from MKR-3D (Figure 6.34a). However, when rotated, the FIM generates a thinned area similar in shape, albeit more northerly oriented, with the current basement trough in the Malvinas Basin (Figures 6.32c, d, 6.33 and 6.34b, c) where the greatest depths are estimated at ~11 km (Baristeas et al., 2013). When looking at the principal direction of the total accumulated strain along this trough, there is a change from NW-SE to NE-SW. The front of this change in the direction of

the total strain migrates northwards as the FIM rotates (Figure 6.27). This bi-directional orientation has been documented by several authors (Galeazzi, 1998; Ghiglione et al., 2010; Baristeas et al., 2013) and related to back-arc extension and the opening of the Weddell Sea and in this scenario the rotation of the FIM would be a contributor as well. NE-SW trending normal faults have been predominantly documented in the southern part of the basin (Baristeas et al., 2013) where the NW-SE extension is the most pronounced in the deforming plates model (Figure 6.27).

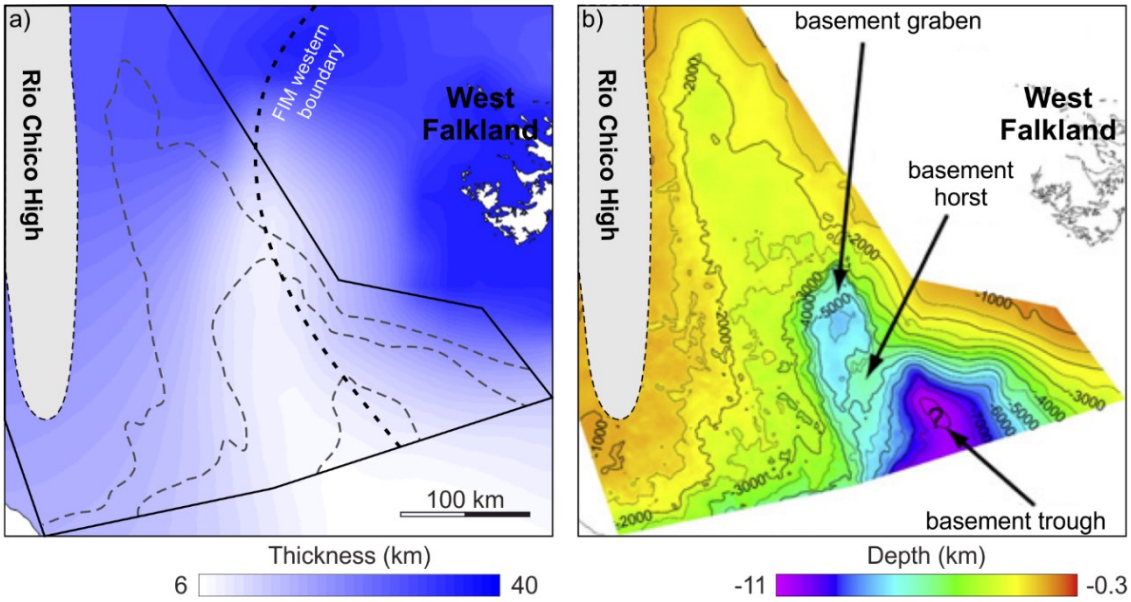

Figure 6.33 a) Shape of the Malvinas Basin as resulted from deforming plate modelling for ROT model (solely due to FIM rotation although other far-field stresses have been invoked for its formation (Baristeas et al., 2013)); grey dashed lines - depth contours from Baristeas et al. (2013) for comparison of overall shape; FIM western boundary shown and position of Rio Chico High; b) depth of Middle Jurassic interface in Malvinas Basin (modified after Baristeas et al., 2013); FIM – Falkland Islands Microplate

6.5.1.2.2 North Falkland Basin

The deforming plates models yield higher crustal thicknesses than the gravity-derived ones for the NFB (Figure 6.34 and 6.35). The exception is represented by the westernmost and easternmost parts of the SNFB region along which thicknesses are underestimated by the deforming plates models compared to the gravity-based ones (Figure 6.34 and 6.35). For the deforming plates modelling stage, a constant thickness was assumed for the whole Falkland Plateau. The differences seen along the SNFB could be accounted for by assuming a higher initial thickness for the SNFB region. The basin is

interpreted as a segment of the Cape Fold Belt reactivated in an extensional regime (Chapter 4; Richards and Fannin, 1997). Therefore, a thickened initial crust underlying the SNFB would be a reasonable assumption. Thicker crust was estimated north of the NFB (Figures 6.34b, c and 6.35b, c) by ROT and ROT-OC models compared to the thicknesses calculated from MKR-3D and MSJ-3D. This relates to the way deforming plates modelling accounts for the rotation of the FIM and is further detailed in the section on the limitations of the method. As detailed in Section 5.5.4 in Chapter 5, the rotation of the FIM was accommodated by intra-plate shearing as seen in California and the Bismarck Sea (Martinez and Taylor, 1996; Platt and Becker, 2013; Ingersoll and Coffey, 2017). The latter example shows less compression compared to what was expected for the rotation the microplate underwent, which was associated with material transport along the intra-plate shear zones from the compressed areas in the zones undergoing extension (Martinez and Taylor, 1996). This topic will be further discussed in Chapter 7.

Higher thicknesses resulted from the MKR-3D and MSJ-3D models compared to NROT for the area of the Falkland platform located east of the NFB (Figures 6.34a and 6.35a). This is due to the fact that the NROT model predicts early extension occurring in the now eastern part of the FIM (Figure 6.25b – Tithonian stage) with the end model showing a decrease in thinning towards the axis of the NFB (Figure 6.32b). This outcome is unsupported by seismic reflection data where maximum thinning corresponds to the NFB with little deformation affecting the eastern Falkland platform (area east of the NFB; Richards et al., 1996a; Lohr and Underhill, 2015).

6.5.1.2.3 Falkland Plateau Basin

There are many similarities between the thickness of the MEB blocks for the two methodologies used, with local underestimates by the deforming plates models (Figure 6.34 and 6.35). The crust under the FPB was predominantly overestimated by the deforming plates models when compared to the gravity derived ones (Figures 6.34 and 6.35) with few exceptions west and north-west of the oceanic domain (zones 2 and 3; Figures 6.34c and 6.35c). Underplating was interpreted in zones 2 and 3 which would not be accounted for by the deforming plates models where the final thicknesses are the result of tectonic thinning alone (i.e. later magmatic additions at the base of the crust are not modelled). This would account for the differences seen north and west of the oceanic domain in Figures 6.34c and 6.35c. More thinning is suggested to have occurred in the Fitzroy sub-basin by the gravity inversion results (Figures 6.34

and 6.35), particularly when looking at the MSJ-3D model (Figure 6.35). This is because a high volume of volcanism and magmatism is present within the Fitzroy sub-basin (Chapter 5) which would account for an increase in the global density of the crust and basin infill. Typical continental values were used for the geometrical gravity inversion, which resulted in over-thinned crust predicted under the sub-basin.

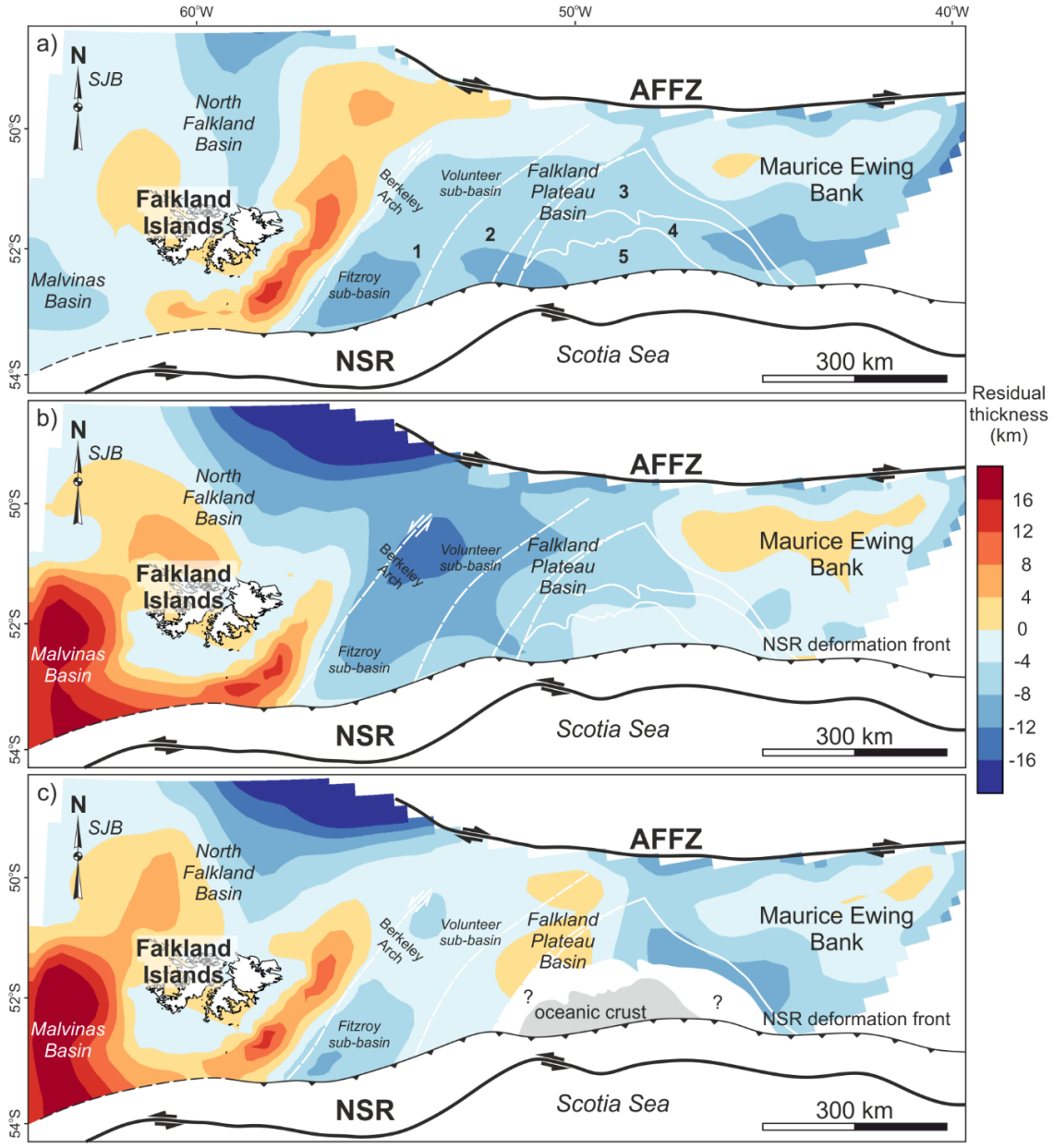

Figure 6.34 Residual thickness maps computed between the crustal thickness from MKR-3D across the Falkland Plateau and the deforming plates model – derived crustal thicknesses for: a) non-rotational (NROT); b) rotation without breakup (ROT); and c) rotation with breakup scenarios (ROT-OC); AFFZ – Agulhas – Falkland Fracture Zone; NSR – North Scotia Ridge

Along the Berkeley Arch and Volunteer sub-basin, the deforming plates models yielded higher thicknesses than the gravity-derived ones, particularly for the ROT model (Figure 6.34b and 6.35b). The Berkeley Arch is associated with a positive magnetic anomaly (Figure 6.8) which could suggest magmatic additions and higher densities than typical continental crust. This would result in more thinning to be estimated from gravity inversion. Furthermore, thickening associated with the rotation of the FIM is modelled during the plate reconstructions across this region, which would account for the difference as well (see limitations section for details). For the remainder of the FPB (region south-west of the MEB), the ROT model yielded smaller differences than NROT when compared to the thicknesses obtained from MKR-3D and MSJ-3D (Figures 6.34a, b and 6.35a, b). The ROT-OC model predicted thicknesses comparable to the NROT model between the MEB and region 5 (Figure 6.32b, d, 6.34a, c, and 6.35a, c). However, a thickness distribution and thinning orientation for the south-western margin of the MEB more similar to the ROT scenario (Figures 6.34b, 6.35b) is expected for this area when break-up occurs rather than the ROT-OC predictions (i.e. thinning perpendicular to the breakup axis).

The break-up of Gondwana was a major contributor to the development of the Falkland Plateau, from the Early Jurassic onwards. However, other events contributed to its current morphology which are not accounted for by the deforming plate modelling. The movement on the AFFZ could have resulted in further uplift and faulting of the northern area of the FPB. Furthermore, the formation of the North Scotia Ridge might have resulted in the southward tilting and faulting of the Falkland Plateau with a lot of the predicted oceanic crust covered by the folds and thrusts formed at the boundary with the Scotia Sea (white regions between the NSR and the NSR deformation front in Figures 6.34, 6.35).

Taking this into account, the crustal thickness distribution along with the total strain direction information shows that a rotation of the FIM (models ROT and ROT-OC) can more readily explain the crustal and structural complexities seen across the Falkland Plateau than when no rotation (NROT) is invoked. Rotation of the FIM leads to a similar extension history and depocentre morphology in the Malvinas Trough as supported by seismic data (Figure 6.33; Galeazzi, 1998; Baristeas et al., 2013), whereas very little extension occurs when the islands are fixed relative to Patagonia (Figures 6.25b, A.13). Little extension is suggested by the model of Kimbell and Richards (2008), but not supported by

seismic data (Baristeas et al., 2013; Chapter 5). Although back-arc extension and the opening of the Weddell Sea are considered the causes of the bi-directional fault network in the Malvinas Basin (Baristeas et al., 2013), the trough morphology and strain direction evolution yielded by the rotation deforming plate model shows significant similarities for it to be considered coincidental. Although all deforming plates models show extension perpendicular to the magnetic reversal isochrons in the FPB at some point during the Late Jurassic (Figure 6.26), there is significantly less thinning occurring for the NROT scenario compared to the ROT and ROT-OC (Figure 6.25 – Upper Jurassic). Furthermore, when the FIM is kept fixed to Patagonia, extension is only rotated perpendicular to the rift axis during the uppermost Jurassic (Figure 6.26a – 154Ma), and little extension and oriented obliquely occurs when oceanic crust is believed to be generated in the FPB (Figure 6.26a – 160 Ma), which makes the break-up modelled in NROT-OC less likely. In addition, the amount of thinning decreases southwards (present-day orientation) when no rotation is modelled (Figure 6.25b – Tithonian) which makes the breakup and generation of oceanic crust in the southern part of the FPB less likely. WNW-ESE trending fault blocks (Figures 6.7 and 6.8) were identified on the western side of the MEB which support the thinning direction seen in the ROT model (Figure 6.32c).

Model ROT-2 is considered separately as it includes modification of the South American sub-plate configuration not based on data analysed throughout this thesis but constrained by the expected northerly position of the FIM. A more comprehensive discussion on latitudinal changes of the FIM reconstruction can be found in Chapter 7. Here of importance is the similar thinning distribution between ROT-2 on one side and ROT and ROT-OC on the other when compared with MKR-3D and MSJ-3D in the Malvinas Basin, north of the Falkland Islands, and in the Volunteer sub-basin and along the Berkeley Arch (Figure 6.36). More thinning is estimated in the northern part of the FPB, along the AFFZ, and in the southern part of the Fitzroy sub-basin (Figure 6.36b). However, little faulting has been identified in the Fitzroy sub-basin (Chapter 5). Thinner crust is estimated west and north of the oceanic domain, similar to ROT-OC where the differences from the gravity-derived thicknesses were related to the presence of underplating. Along the MEB, the ROT-2 yielded more thinning than the gravity-derived models which is not supported by seismic data (Figure 6.31) and literature (Schimschal and Jokat, 2019a).

ROT-2 shows a fit to the present-day architecture of the western part of the plateau similar to ROT and ROT-OC. However, it overestimates the amount of thinning expected along the MEB. These inconsistencies will be addressed in Chapter 7.

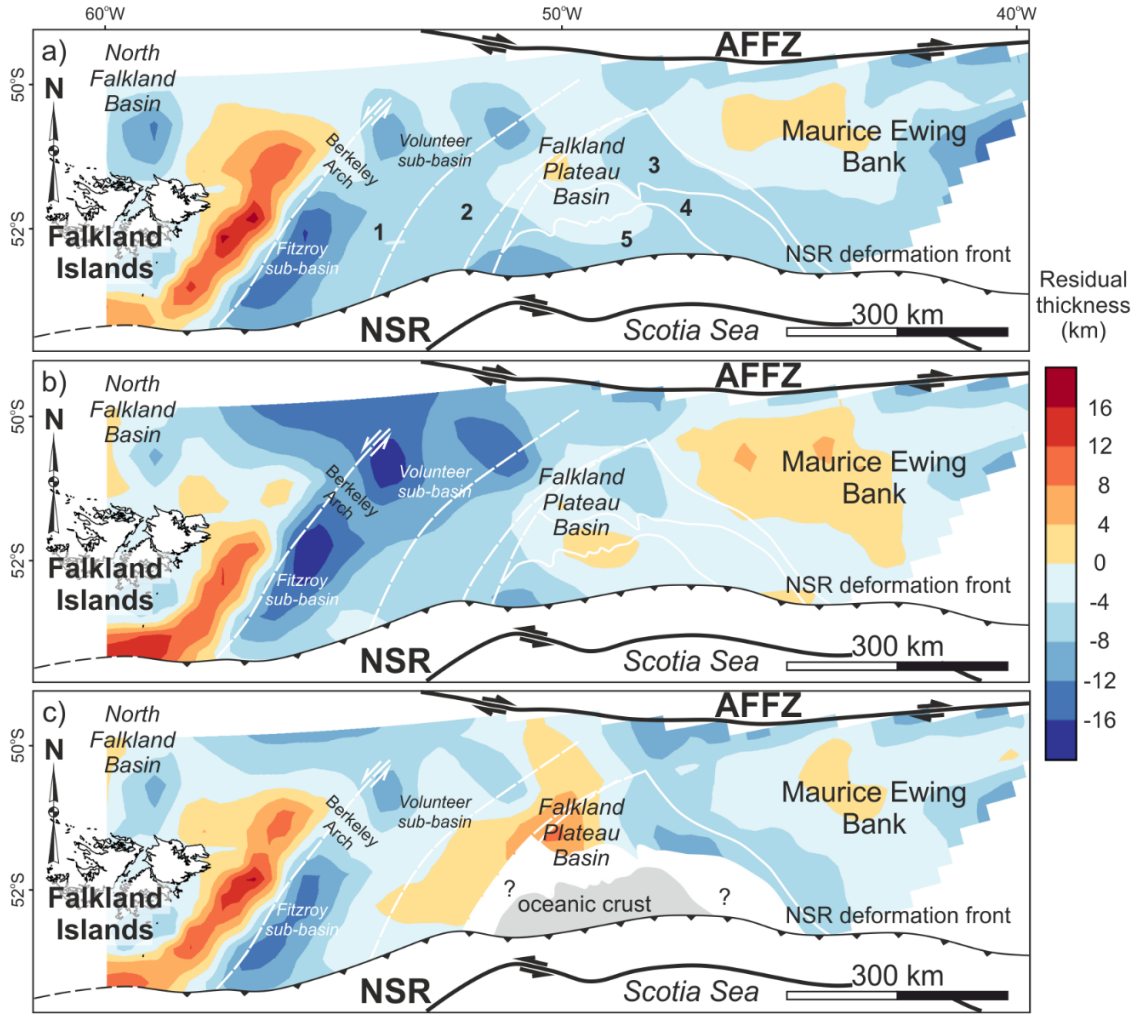

Figure 6.35 Residual thickness maps computed between the crustal thickness from geometrical gravity inversion (MSJ-3D) across the Falkland Plateau Basin and the deformable plate model – derived crustal thicknesses for: a) non-rotational (NROT); b) rotation without breakup (ROT); and c) rotation with breakup (ROT-OC) scenarios; AFFZ – Agulhas – Falkland Fracture Zone; NSR – North Scotia Ridge

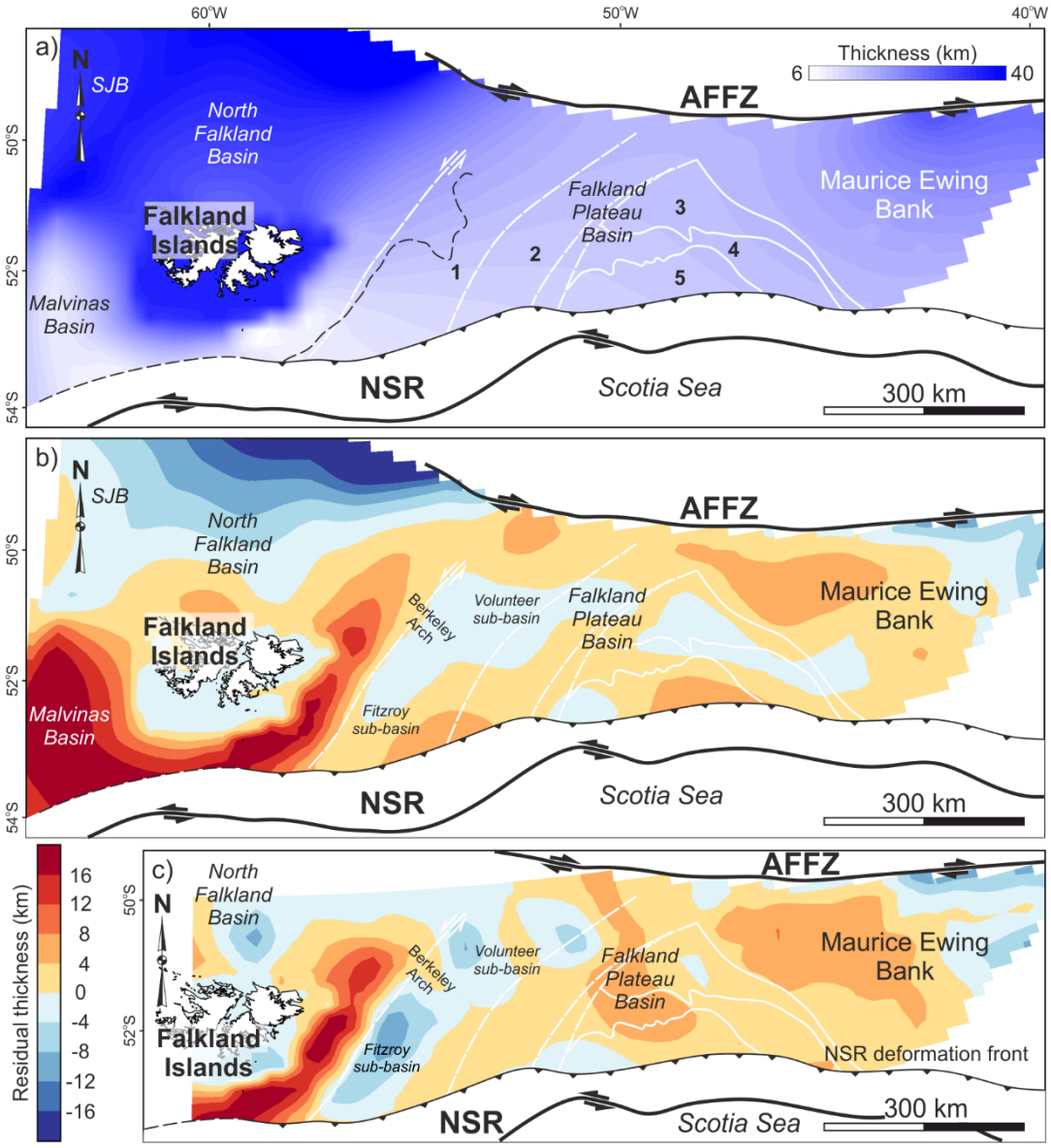

Figure 6.36 a) Crust thickness yielded by deforming plate model ROT-2; residual thickness maps computed between the crustal thickness from b) MKR-3D and c) geometrical gravity inversion (MSJ-3D) and the deformable plate model – derived crustal thicknesses across the Falkland Plateau

6.5.2 Limitations of the used methods

6.5.2.1 Gravity modelling and inversion

The density distribution along the Falkland Plateau Basin obtained from gravity modelling and inversion was used to constrain the nature of the crust underneath the basin. However, no control points were available from seismic reflection data for the Moho, the depth used in modelling and inversion being the result of gravity modelling and isostatic analysis (Kimbell and Richards, 2008) and/or seismic refraction data (Schimschal and Jokat, 2019b). The

difference between the two used Moho surfaces resulted in a wide range of densities for the Falkland Plateau Basin (2.6 - 3.05 g/cc) which spans the density ranges of both continental and oceanic crust, particularly when looking at the 2D forward modelling results. The inversion shows a more restricted range of densities, from 2.6 g/cc up to 2.8 g/cc. This difference in estimated densities raises the question of differences in the algorithms used and their reliability, and/or the importance of the method used based on the complexity of the area of study.

The structure of the Falkland Plateau is approximated with a simple three-layer model (Figure 6.37). The observed gravity is shown as well, but the purpose of this example is to compare the results of 2D and 3D modelling for an area with significant lateral crustal variations. During the 2D modelling, the geometry of this model is extruded laterally, and its gravimetric effect is calculated. The 2D gravity response of this in both GM-SYS and VPmg shows little difference (Figure 6.37). However, as soon as a lateral variation is introduced in the geometry of the interfaces (seabed, basement, Moho), the gravity response above the FPB is significantly different. As the density remains constant in each layer, this difference is most likely due to a laterally varying depth to basement and Moho which would have an effect on the response seen along profile 139. This off-section variation could result in an overestimation of the densities along profile 139 during 2D modelling. Whereas a difference is expected between the results of 2D and 3D gravity modelling, this example shows how drastic the differences can be and that a more critical approach should be adopted when choosing 2D gravity modelling over 3D.

The 3D property inversion in sub-section 6.4.1.2.2 takes into account the effect of off-section density heterogeneities which results in a global decrease in the estimated densities along profile 139 compared to the 2D forward modelling. The seismic data shows a change in the seismic character of the crust from north to south, as a function of the present volcanism, whilst the magnetic data support the presence of oceanic crust in the south-eastern part of the FPB. Although higher densities were modelled for regions 3-5 for the Moho based on Schimschal and Jokat (2019b; Figure 6.21b), the densities within the oceanic domain are underestimated when compared to typical oceanic crust densities. Significant lateral crustal changes occur north (oceanic crust of the Argentine Basin) and south (the NSR accretionary prism and the oceanic crust of the Scotia Sea) of the FP, which were not included in the inversion and can account for these inconsistencies.

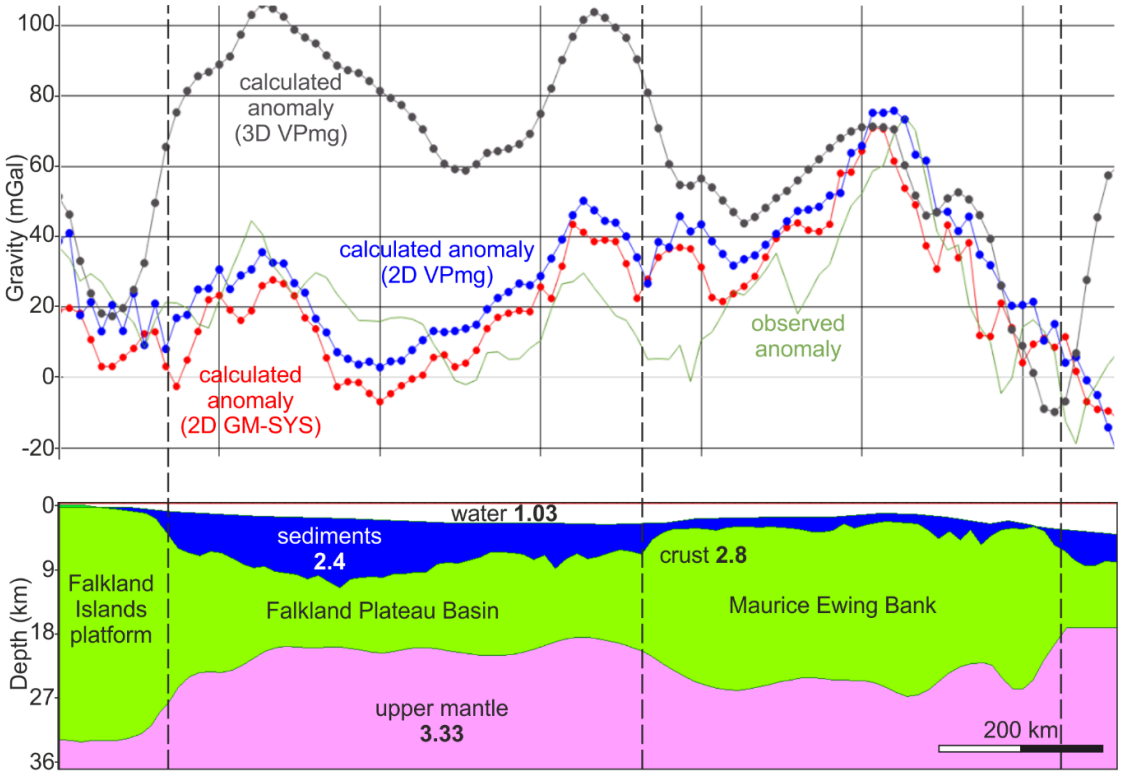

Figure 6.37 Gravity response of a three-layer model approximation of the Falkland Plateau; the 2D responses are similar for both used software; the 3D response shows an overlap above the Falkland Islands platform (where the crust does not show significant thickness variations laterally) and above the Maurice Ewing Bank; the 3D response diverges from the 2D ones on the western margin of the Maurice Ewing bank where the profile is between continental crust in the north and potentially oceanic crust in the south (Figure 6.13), the biggest difference occurring along the Falkland Plateau Basin; a separation is observed east of the Maurice Ewing Bank and it is most likely associated with edge effects, the 3D model not extending laterally as much as the 2D ones

The result of the geometrical gravity inversion showed some differences to observations from seismic reflection data. This was due to the heterogeneous density distribution within the continental crust of the FPB. Areas like the Fitzroy sub-basin and the Berkeley Arch, where significant volcanic additions were interpreted from seismic and magnetic data, were modelled as being underlain by overly thinned crust. However, this is not consistent with the seismic interpretation of the two areas (Chapter 5).

6.5.2.2 Deforming plates

The crustal thickness distribution along the plateau was predicted using the GPlates deformable modelling methodology. The setup of the model assumes

that the Falkland Plateau consisted of homogenous crust of constant thickness at 170 Ma, and that all deformation was not depth dependent.

South-western Gondwana was affected by multiple stages of extensional and compressional episodes prior to the start time of this model (Halbich, 1993; Thomas et al., 1993; Trouw and De Wit, 1999; Dalziel et al., 2000; Paton and Underhill, 2004; Tankard et al., 2009), with the Permo-Triassic orogeny and Triassic and Early Jurassic rifting being the youngest. This would have resulted in crustal thickness variation and the presence of heterogeneities which would affect the way the Jurassic and Cretaceous deformation was accommodated in the plateau and which cannot be accounted for in the model.

Another limitation of this methodology, as mentioned by Peace et al. (2019), is the presence of rigid boundaries both for the main deformable network but also for the pre-defined rigid blocks (i. e. the Falkland Islands block). These do not allow for the diffusion of the deformation in the surroundings of the network which results in increased or unrealistic compression/thickening against the boundaries of the model and in a concentration of the strain around the rigid blocks inside the deformable domain (Figures 6.25, 6.28). Similarly, for the models with generation of oceanic crust (ROT-OC and NROT-OC), the post-break-up extension leads to the thinning front to impinge onto the MEB side (around the defined rigid continent-ocean boundary), resulting in a crustal thinning direction parallel to the break-up axis (Figure 6.32d). On the other hand, for the rotation without generation of oceanic crust (ROT and ROT-2), the thinning direction stays perpendicular to the rift axis (parallel to the extension direction) (Figures 6.32c and 6.36a). The plate movement and deformation stages are the same for the ROT/ROT-2 and ROT-OC models, but the continent-ocean boundary added in the model acts as a barrier to the deformation resulting in a geologically unplausible architecture for the break-up scenario.

Furthermore, no constraints on the elastic thickness of the crust can be added. As a result, the deformation propagates unrealistically far from the source/the amplitude of the deformation is not geologically accurate (Figures 6.25, 6.28, 6.30b). If an intra-plate accommodation of the rotation via shear zones is inferred (Chapter 5) this cannot be accounted for during the deforming plate modelling which, collated with the previous issues, results in overestimation of the crustal thickness in the northern and north-eastern parts of the FIM when rotation is invoked (Figures 6.34 b, c and 6.35b, c). The modelling also shows some limitations when multiples stages of deformation on different directions

are invoked. Although extension on a NE-SW direction is suggested when looking at the azimuth of the principal component of the total strain for the non-rotational case (Figure 6.26a), the resulting crustal thickness reflects only the last E-W extension episode (Figure 6.32b).

The results of the modelling are highly dependent on the geometry of the defined plates and microplates and their finite rotations so there is a degree of uncertainty related to the reliability of the input data as well. As observed by Peace et al. (2019), this methodology is not suitable for transpressional and transtensional areas like the region modelled here, but nonetheless offers some insight into how a rotating microplate might affect the crust around it.

6.6 Conclusions

The crustal architecture underlying the Falkland Plateau Basin shows a higher degree of complexity than previously envisaged. Its east-central region comprises a mosaic of crustal types that resulted from the fragmentation of Gondwana. Typical continental crust, with varying degrees of extension, underlie the whole Falkland Platform, from the Malvinas Basin to F2 shear zone within the FPB, the Maurice Ewing Bank, and the region just south of the AFFZ. A sliver of highly faulted and potentially attenuated and underplated continental crust is located between F2 and F3. The remainder of the FPB comprises the area most affected by its breakup. Magma-enriched and underplated continental crust underlies the north-central part of this region, transitioning to the south to a thick oceanic domain.

A comparison between the present-day crustal thickness and architecture as constrained by gravity models, magnetic and seismic data, and the crustal thickness and architecture post-rotation, derived from deforming plate models, supports more similarities between the two when a rotation of the Falkland Islands Microplate is invoked. This process is associated with significant thinning in the Malvinas Trough and variations in the stress configuration affecting the basin, as the Falkland Islands Microplate reaches its current position relative to South America, and thinning along the Falkland Plateau Basin consistent with observation from seismic, gravity, and magnetic data.

Chapter 7 Discussion and conclusions

7.1 Introduction

In Chapters 4 to 6 several arguments were presented that support rotation of the Falkland Islands Microplate (FIM). A correlation between the fault geometries in the Algoa and Gamtoos basins and the Southern North Falkland Basin (SNFB) showed that these regions represent segments of the Gondwanide Fold and Thrust Belt reactivated in an extensional regime (Chapter 4). The presence and depth of a trans-crustal mega-décollement controlling the deformation in the SNFB supported this correlation (Chapter 4) as a similar interface was identified in South Africa, and further west, in the Colorado Basin. This was related to a long-lived structure that accommodated the formation of the Gondwanide Orogen (Hälbich, 1993; Paton et al., 2006; Lindeque et al., 2011; Pángaro and Ramos, 2012). Non-rotational reconstructions of the FIM would imply the presence of a separate structure of this size unrelated to the Gondwanide Fold and Thrust Belt, at a high angle to it, and not present in the basins west of the islands, which is considered unlikely. Correlations between structures on- and offshore the Falkland Islands and on- and offshore South America, Africa, and Antarctica support a rotated palaeoposition of the FIM until the Middle Jurassic, and that rotation occurred from this point up until ~Late Jurassic (Chapter 5). Evidence of wrenching along the western margin of the Falkland Plateau Basin (FPB) is also consistent with intra-plate deformation during clockwise rotation (Chapter 5). The complex structural and crustal architectures of the FPB, in conjunction with the orientation of the magnetic reversal isochrons identified in the south-eastern part of the basin, support a more complex evolution of the plateau than suggested by non-rotational models. Comparison between the estimated crustal thinning and strain orientation for both rotational and non-rotational models with present-day observations confirm a need for a rotation of the FIM to achieve a crustal architecture similar to that observed today along the plateau (Chapter 6).

However, there are uncertainties in the Jurassic horizon picked across the Volunteer sub-basin and Berkeley Arch (Chapter 5) which might impact the relative ages estimated for the wrenching identified in this region. Shearing along similar directions as identified in Chapter 5 occur during movement along

the Agulhas-Falkland Fracture Zone (AFFZ). This could be argued as the only mechanism for the shearing, rather than rotation of the FIM. However, the rest of the evidence presented in this thesis supports rotation. Furthermore, when considered with previously published studies on palaeomagnetic data, structural, stratigraphic, palaeocurrent, and ice flow directions correlations (Adie, 1952a, b; Mitchell et al., 1986; Mussett and Taylor, 1994; Thomas et al., 1997; Curtis and Hyam, 1998; Trewin et al., 2002; Stone et al., 2009), a rotated reconstruction of the FIM is the most compelling interpretation.

In this chapter, the reconstruction and rotation of the microplate will be discussed in the context of south-western Gondwana evolution. Due to its significant extent and high amount of rotation compared to analogue areas (Luyendyk et al., 1985; Martinez and Taylor, 1996; Neves et al., 2003; Ingersoll and Coffey, 2017; Horst et al., 2018), the causes and mechanisms for the separation and rotation of the FIM will be covered in Section 7.3. Besides the rotation of the microplate, the Falkland Plateau features a lot of characteristics typically documented along transform margins and marginal plateaus, which will be further discussed. Finally, the benefits and impact of an increased understanding of the behaviour, architecture, and evolution of the FIM on refining plate models will be covered in the last section.

7.2 The Mesozoic fragmentation of SW Gondwana; implications from the reconstruction of the FIM

The structural information presented in Chapters 4 and 5, in addition to the insights gained from gravity and plate modelling in Chapter 6, facilitated the development of a model of evolution for the Falkland Plateau. The model includes the driving force for rotation initiation and an estimate of the age of the rotation of the Falkland Islands Microplate (Figure 7.1), which will be further discussed in the context of the SW Gondwana evolution.

At the end of the Permo-Triassic, the Gondwanide Orogeny resulted in a trans-continental fold and thrust belt extending from Sierra de la Ventana, through the Colorado and Orange basins, Cape Fold Belt, Algoa and Gamtoos Basins, onshore the Falkland Islands (D1) and in the Southern North Falkland Basin, and through the Ellsworth and Pensacola Mountains (Chapter 4; Figure 7.2; Hälbich, 1993; Curtis, 2001; Bry et al., 2004; Paton et al., 2016; Stanca et al., 2019). The orogen was controlled by a trans-crustal mega-décollement interpreted to be a long-lived structure active throughout the tectonic history of Gondwana (Hälbich, 1993; Paton et al., 2006). Evidence of this décollement, or

a similar feature, has been reported under the Colorado, Karoo, Outeniqua, and SNFB basins (Chapter 3; Paton et al., 2006; Lindeque et al., 2011; Pángaro and Ramos, 2012; Stanca et al., 2019).

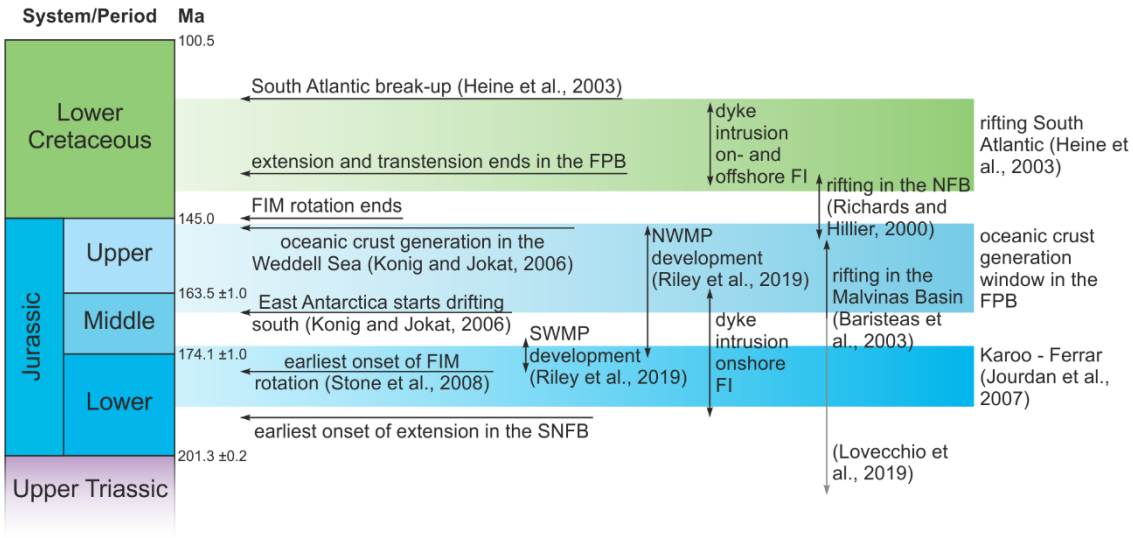

Figure 7.1 Timeline of the main events affecting SW Gondwana from Late Triassic to Early Cretaceous; NWMP - Northern Weddell Magnetic Province; SWMP - Southern Weddell Magnetic Province; timing of dyke emplacement onshore the Falkland Islands after Mussett and Taylor (1994), Thistlewood et al. (1997), Stone et al. (2008), and Stone et al. (2009)

Early signs that the supercontinent underwent break-up date from the Permian Karoo rifts and Triassic extension reported along South America (Uliana et al., 1989; Macdonald et al., 2003; Lovecchio et al., 2018; Macgregor et al., 2018; Lovecchio et al., 2020). Extensive volcanism and magmatism occurred throughout the Early Jurassic across Patagonia, Antarctica, and Africa, leading to the emplacement of the Chon Aike and Karoo-Ferrar magmatic provinces (Figure 7.2; Encarnación et al., 1996; Pankhurst et al., 1998; Macdonald et al., 2003; Riley et al., 2005; Jourdan et al., 2007). The Middle Jurassic southward motion of Antarctica from western Gondwana was preceded by alternating episodes of E-W and NNW-SSE extension (Chapter 5; Reeves, 2000; Le Gall et al., 2002; Paton and Underhill, 2004; Jourdan et al., 2007) that generated a complex network of structures in the Falkland – Weddell region and potentially a high degree of crustal fragmentation (Figure 7.2).

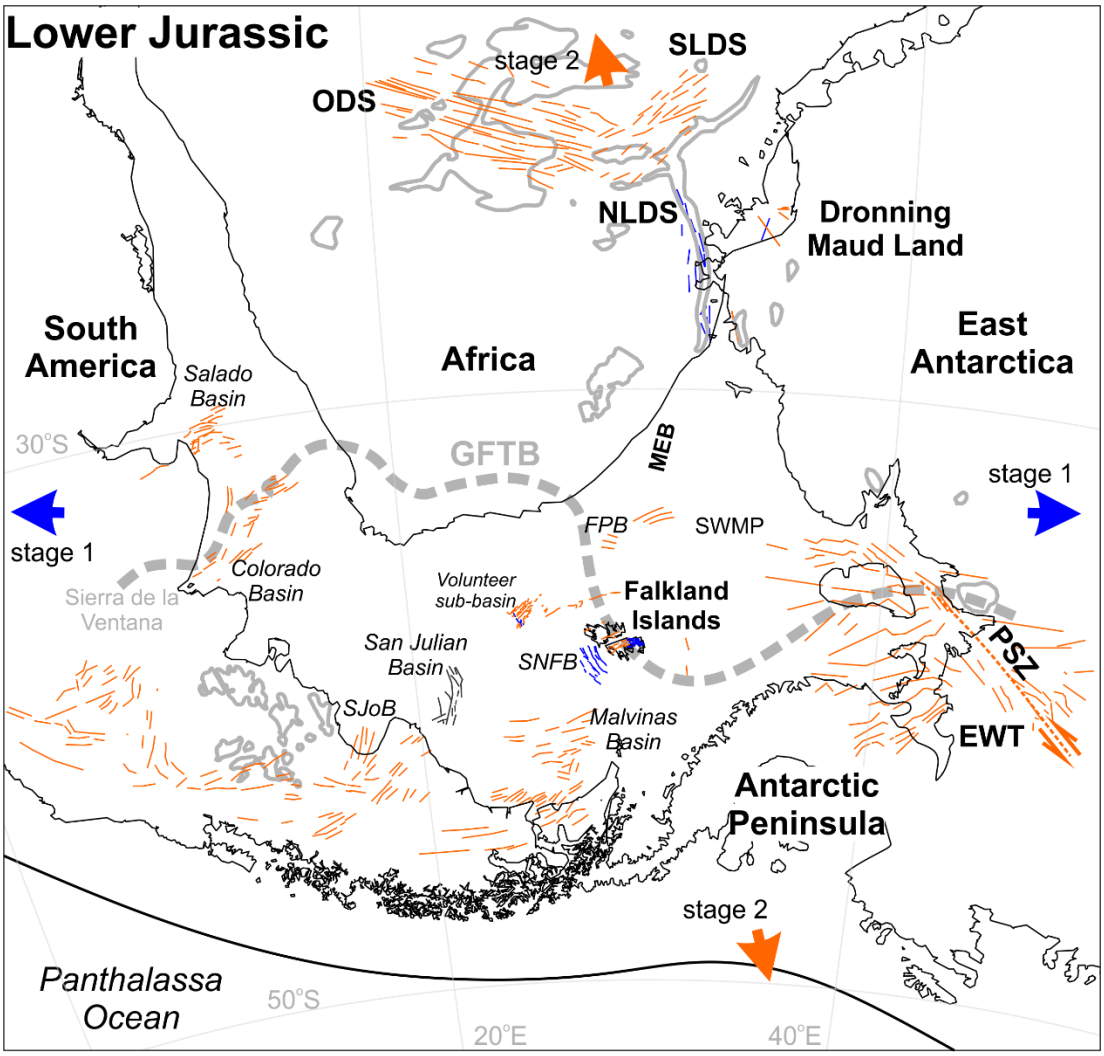

Figure 7.2 Early Jurassic configuration of south-western Gondwana along with active faults and synchronous dyke emplacement; blue and orange arrows show extension direction; fault colour matches the arrow colour of the phase they were coeval with; black faults – inactive faults; thick grey lines mark extent of Chon Aike and Karoo - DML (Dronning Maud Land) - Ferrar volcanics; EWT – Ellsworth-Whitmore Terrane; FPB – Falkland Plateau Basin; GFTB – Gondwana Fold and Thrust Belt; MEB – Maurice Ewing Bank; NLDS – Northern Lebombo dyke swarm; ODS – Okavango dyke swarm; PSZ – Pagano Shear Zone; SJoB – San Jorge Basin; SLDS – Save Limpopo dyke swarm; SNFB – Southern North Falkland Basin; SWMP - Southern Weddell Magnetic Province; SWMP framework from Jordan et al. (2017); South Africa simplified dyke network drawn after Gomez (2001); East Antarctica dykes drawn after Curtis et al. (2008); Falkland Islands dykes drawn after Stone et al. (2009); SNFB faults after Lohr and Underhill (2015) and Stanca et al. (2019); South America faults drawn after Lovecchio et al. (2019); Karoo lavas after Jourdan et al. (2007); Chon Aike lavas after Bouhier et al. (2017); DML-Ferrar lavas extent after Elliot (1992) and Elliot et al. (1999); plate configuration from Chapter 6

The first episode of E-W directed extension resulted in the emplacement of N-S trending dykes in Africa, East Antarctica, and the southern part of West Falkland (Chapter 5; Mussett and Taylor, 1994; Riley et al., 2005; Jourdan et al., 2007; Klausen, 2009). The offshore equivalent of the D1 belt onshore the Falkland Islands started undergoing reactivation in an extensional regime which resulted in the first stage of rifting in the SNFB with formation of half-grabens bounded by shallow-dipping listric faults (Chapters 4 and 5; Figure 7.2).

Before, or during, the rotation of the regional extension direction to an NNE-SSW orientation, the region between East and West Antarctica was affected by complex deformation as the Ellsworth Whitmore Terrane underwent ~90° of counter-clockwise rotation, although an older timing for this event has been postulated, coeval with the Gondwanide Orogeny (Curtis and Storey, 1996; Martin, 2007). As NNE-SSW extension occurred between East and West Gondwana, more dykes were intruded onshore Africa and the Falkland Islands, and normal faults affected the present-day western FPB (Volunteer and Fitzroy sub-basins), South America, and its offshore basins along a trend sub-parallel to the south-western margin of Gondwana or reactivating the older Gondwanide structures (Chapter 5; Figure 7.2; Mussett and Taylor, 1994; Le Gall et al., 2002; Jourdan et al., 2007; Lovecchio et al., 2018; Lovecchio et al., 2020). Sinistral shearing along the Pagano Shear Zone and early rifting in the southern Weddell Sea (Jordan et al., 2017; Riley et al., 2020) occurred at this stage, potentially extending into the proto-FPB (between the FIM and the Maurice Ewing Bank; Chapter 6; Figure 7.2).

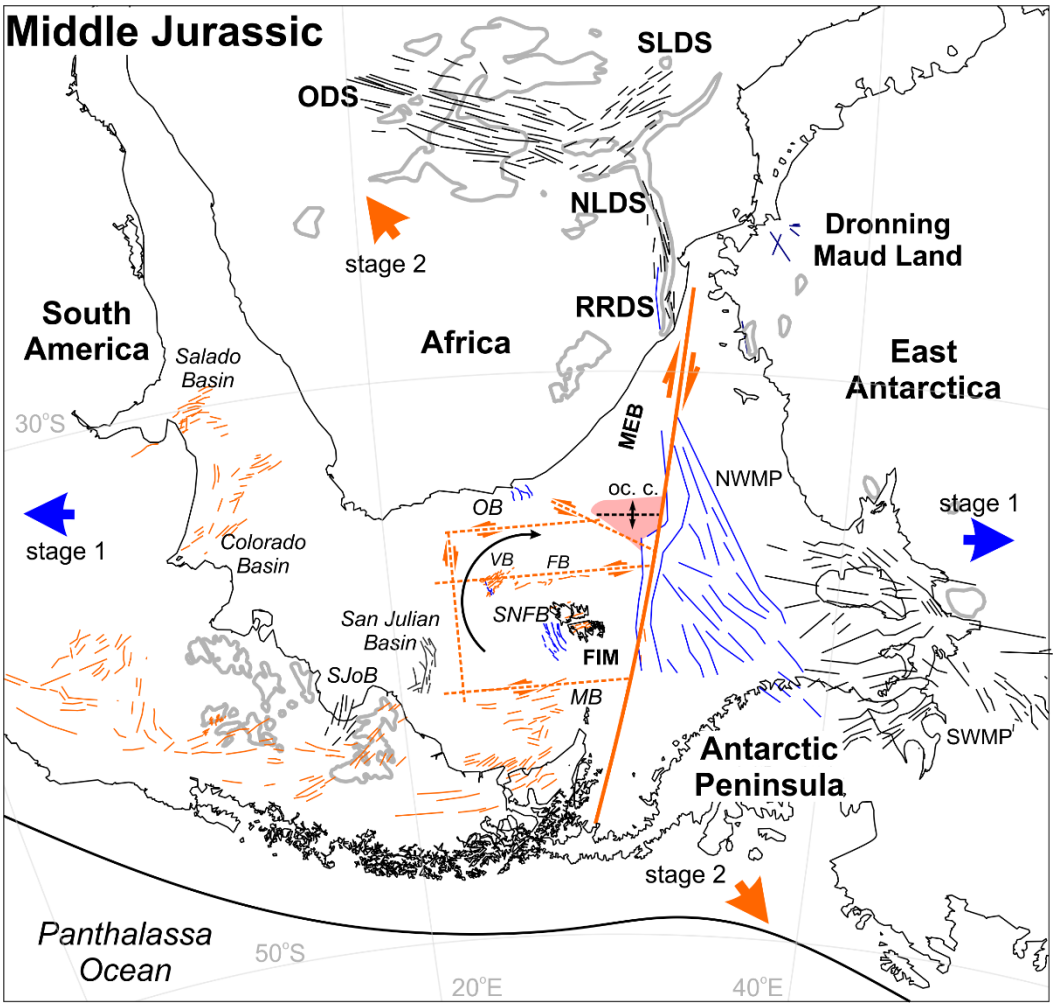

Figure 7.3 Middle Jurassic configuration of south-western Gondwana along with active faults and synchronous dyke emplacement; blue and orange arrows - extension direction; fault colour matches the arrow colour of the phase they were coeval with (n.b. some faults in South America might have been active during both phases; here are shown as a unit for simplicity); black faults/dykes – inactive; thick grey lines - extent of Chon Aike and Karoo - DML (Dronning Maud Land) - Ferrar volcanics; FB – Fitzroy sub-basin; MB - Malvinas Basin; MEB – Maurice Ewing Bank; NLDS – Northern Lebombo dyke swarm; NWMP – Northern Weddell Magnetic Province; OB – Outeniqua Basin; oc. c. – oceanic crust; ODS – Okavango dyke swarm; RRDS – Rooi Rand dyke swarm; SJoB – San Jorge Basin; SLDS – Save Limpopo dyke swarm; SNFB – Southern North Falkland Basin; SWMP - Southern Weddell Magnetic Province; VB – Volunteer sub-basin; SWMP from Jordan et al. (2017); South Africa dykes drawn after Gomez (2001); East Antarctica dykes drawn after Curtis et al. (2008); Falkland Islands dykes drawn after Stone et al. (2009); SNFB faults after Lohr and Underhill (2015) and Stanca et al. (2019); South America faults after Lovecchio et al. (2019); Karoo lavas after Jourdan et al. (2007); Chon Aike lavas after Bouhier et al. (2017); DML-Ferrar lavas after Elliot (1992) and Elliot et al. (1999); Outeniqua Basin faults after Paton et al. (2006) and Parsiegla et al. (2009)

A third stage of dyke intrusion along eastern Africa occurred at the beginning of the Middle Jurassic as extension between East and West Gondwana switched back to an E-W orientation (Figure 7.3; Chapter 5; Jourdan et al., 2007). The second rifting stage identified in the SNFB (Chapter 4; Lohr and Underhill, 2015) is interpreted to have occurred during this extensional episode, potentially in conjunction with early extension on the N-S trending fault segments in the Algoa and Gamtoos basins (NE Outeniqua Basin; Chapter 5; Figure 7.3). Extension was documented in the northern part of Weddell Sea Rift, cross-cutting the earlier rift-related structures (Figure 7.3; Jordan et al., 2017; Riley et al., 2020). This second rift system is interpreted to have been active until ~155 Ma (Figure 7.4; Grunow, 1993; Jordan et al., 2017; Riley et al., 2020).

At 167.2 Ma East Antarctica started drifting southward from western Gondwana (König and Jokat, 2006), leading to dextral wrenching between the Antarctic plate and the Falkland Plateau (Figure 7.3; König and Jokat, 2006). Sinistral strike-slip faults, antithetic to this dextral intra-continental fault zone and following the present-day orientation of the gravity lineaments/fracture zones (F1-F3) in the FPB (Chapter 6), contributed to the fragmentation of the Falkland Plateau (Figure 7.3). Motion along these fracture zones facilitated the delimitation and separation of the FIM from the surrounding plates and drag exerted by the southward movement of East Antarctica possibly initiated FIM rotation (Figures 7.3, 7.4).

The undocking of the islands from South Africa during the Middle Jurassic, which accompanied this rotation, resulted in more extension occurring in the FPB (Chapter 5) and along the South American plate as it started drifting westward (König and Jokat, 2006; Lovecchio et al., 2020). The westward drift of South America led to reorientation of the extension direction in the southern South Atlantic region along a roughly WSW-ENE direction (Figure 7.4; Paton and Underhill, 2004). This is recorded in the syn-rift sections in the north-eastern Outeniqua basin (Paton and Underhill, 2004) and the SNFB (Chapter 4; Lohr and Underhill, 2015; Stanca et al., 2019). Faults that trend oblique to the SNFB (trending E-W in the present-day orientation of the FIM) were identified in the northern part of the FIM (Chapter 4) and are related to the regional ~E-W directed extension between East and West Gondwana (Chapter 5). The ongoing rotation of the FIM away from the Maurice Ewing Bank was accommodated by extension along the proto-AFFZ and in the larger FPB, with break-up and generation of oceanic crust starting around Callovian to

Oxfordian times (Figures 7.1, 7.3), and sinistral shearing along the now NE-SW trending F1-F3 shear zones (Chapters 5 and 6; Figure 7.3). Evidence of magmatic enrichment has been interpreted along F1 based on magnetic data and gravity modelling (Chapter 6). The timing for it remains uncertain and it can be coeval with motion along the F1 or the Early Cretaceous volcanism interpreted in the Fitzroy sub-basin (Chapter 5). The dextral wrenching between East and West Gondwana (Figure 7.3) switched to rifting sub-perpendicular to the former wrenching direction during the Late Jurassic (Figure 7.4; Ghidella et al., 2002; König and Jokat, 2006). This led to the opening of the Weddell Sea (König and Jokat, 2006) and Rocas Verdes Basin (Calderón et al., 2013) and allowed for continued extension in the SNFB (Chapter 4; Ramos et al., 2017; Stanca et al., 2019) as the FIM completed its ~80° of clockwise rotation (Chapters 5 and 6; Figure 7.4). Continued rifting between South America and Africa resulted in the opening of the North Falkland Basin and the rest of the Outeniqua Basin (Figure 7.4; Chapter 5; Paton and Underhill, 2004), dyke emplacement onshore and offshore the Falkland Islands (Chapter 5; Figure 7.5), and continued extension in the FPB (Chapter 5; Figure 7.5).

This deformation in a rapidly changing stress configuration, along with the rotation of the FIM, could explain the complex crustal architecture across the FPB where sheared, attenuated, and underplated continental crust transitions to oceanic crust towards the south-eastern part of the FPB (Chapter 6; Figure 7.5). Break-up and oceanic crust formation occurred south-east of the FPB, in the Weddell Sea at 147 Ma (Figure 7.4; König and Jokat, 2006), which potentially led to a high volume of volcanic material to be accreted to the newly formed oceanic crust of the FPB. This resulted in thicker-than-normal crust underlying the oceanic domain in the south-eastern FPB (Figure 7.5). Growth of volcanic edifices is seen throughout the Late Jurassic (locally up to Early Cretaceous) indicative of this volcanic enrichment (Figures 6.9a, 6.10, and 6.11a in Chapter 6). The formation of the oceanic domain in the south-eastern part of the FPB was finalised before the end of the Late Jurassic, as evidenced by deposits of this age interpreted across the FPB (Figure 6.11 in Chapter 6). Soon after, the rotation of the FIM ceased at the end of the Jurassic and the microplate docked against the Patagonian plate.

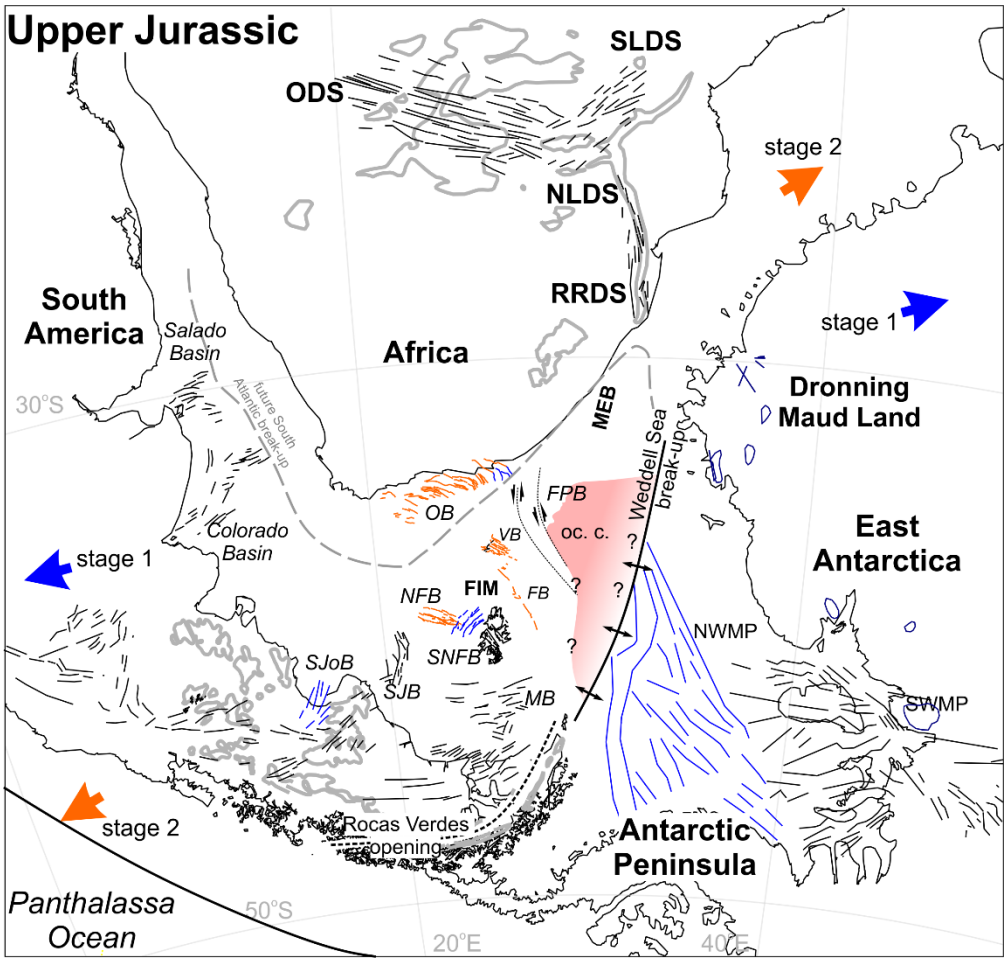

Figure 7.4 Late Jurassic configuration of south-western Gondwana along with active faults and synchronous dyke emplacement; blue and orange arrows - extension direction; fault colour matches the arrow colour of the phase they were coeval with; black faults/dykes – inactive; thick grey lines - extent of Chon Aike and Karoo - DML (Dronning Maud Land) - Ferrar volcanics; FB – Fitzroy sub-basin; FPB – Falkland Plateau Basin; MB - Malvinas Basin; MEB – Maurice Ewing Bank; NFB – North Falkland Basin; NLDS – Northern Lebombo dyke swarm; NWMP – Northern Weddell Magnetic Province; OB – Outeniqua Basin; oc. c. – oceanic crust; ODS – Okavango dyke swarm; RRDS – Rooi Rand dyke swarm; SJB – San Julian Basin; SJoB – San Jorge Basin; SLDS – Save Limpopo dyke swarm; SNFB – Southern North Falkland Basin; SWMP - Southern Weddell Magnetic Province; VB – Volunteer sub-basin; SWMP and NWMP from Jordan et al. (2017); South Africa dykes drawn after Gomez (2001); East Antarctica dykes drawn after Curtis et al. (2008); Falkland Islands dykes drawn after Stone et al. (2009); SNFB and NFB faults after Lohr and Underhill (2015) and Stanca et al. (2019); South America faults after Lovecchio et al. (2019); Karoo lavas after Jourdan et al. (2007); Chon Aike lavas after Bouhier et al. (2017); DML-Ferrar lavas after Elliot (1992) and Elliot et al. (1999); Outeniqua Basin faults after Paton et al. (2006) and Parsiegla et al. (2009); question marks in the Falkland Plateau Basin oceanic domain - uncertain southern extent

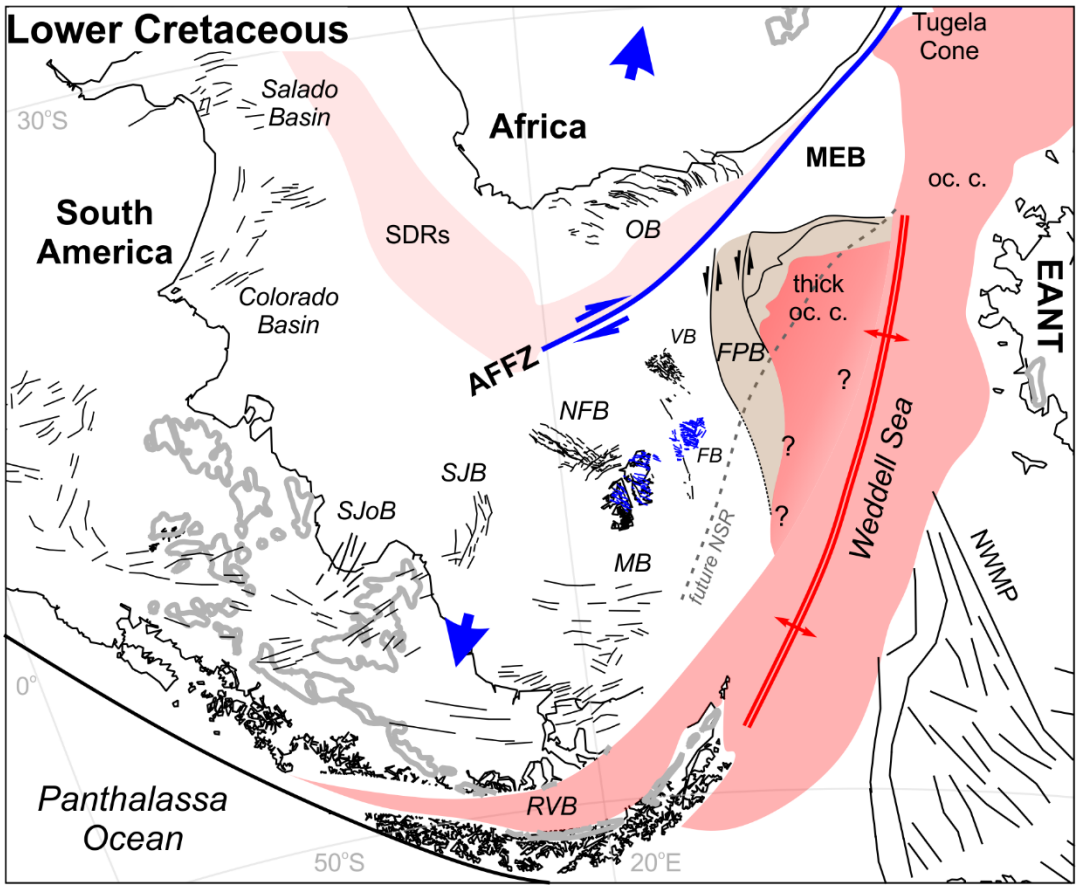

Figure 7.5 Early Cretaceous configuration of south-western Gondwana along with active faults and synchronous dyke emplacement in the Falkland Plateau; blue arrows show extension direction; black faults – fault configuration at this time in south-western Gondwana; thick grey lines mark extent of Chon Aike and Karoo - DML (Dronning Maud Land) - Ferrar volcanics; EANT – East Antarctica; FB – Fitzroy sub-basin; FPB – Falkland Plateau Basin; MB - Malvinas Basin; MEB – Maurice Ewing Bank; NFB – North Falkland Basin; NSR – North Scotia Ridge; NWMP – Northern Weddell Magnetic Province; OB – Outeniqua Basin; oc. c. – oceanic crust; RVB – Rocas Verdes Basin; SDR – seaward dipping reflectors; SJB – San Julian Basin; SJoB – San Jorge Basin; VB – Volunteer sub-basin; NWMP framework from Jordan et al. (2017); East Antarctica dykes drawn after Curtis et al. (2008); Falkland Islands onshore dykes drawn after Stone et al. (2009); SNFB and NFB faults after Lohr and Underhill (2015) and Stanca et al. (2019); South America fault network after Lovecchio et al. (2019); Karoo lavas extent after Jourdan et al. (2007); Chon Aike lavas extent after Bouhier et al. (2017); DML-Ferrar lavas extent after Elliot (1992) and Elliot et al. (1999); Outeniqua Basin fault network after Paton et al. (2006) and Parsiegla et al. (2009); extension direction after Paton and Underhill (2004); question marks in the Falkland Plateau Basin oceanic domain mark its uncertain southern extent and relation to the Weddell Sea oceanic crust; brown shades mark the interpreted intruded and underplated continental crust in the Falkland Plateau Basin

The rift and drift of South America away from Africa led to the development of the dextral AFFZ (Figure 7.5), which facilitated the separation of the Falkland Plateau from Africa during the Early Cretaceous (Baby et al., 2018). The now NE-SW trending lineaments (F1-F3) from the FPB were likely to have been reactivated to some extent as antithetic sinistral faults during the active stage of the AFFZ when minor plate readjustments were interpreted (Chapter 5). The plateau reached its current day extent at 130 Ma (Chapter 6; Figure 7.5) and continued moving as part of the South American plate during the opening of the southern South Atlantic. Its present-day configuration has been further shaped by Late Cretaceous – Cenozoic oblique compression from the south during the opening of the Scotia Sea and the formation of the North Scotia Ridge (see Figure 7.5 for future position of the North Scotia Ridge; the region of the FPB east of this ridge in Figure 7.5 was obscured during the opening of the Scotia Sea). However, the post-Early Cretaceous evolution of the Falkland Plateau is outside the scope of this thesis.

7.3 How do blocks/microplates form, rotate and deform in wrenching settings?

The fragmentation of Gondwana and the evolution of the Falkland Plateau were highly influenced by wrenching between East and West Gondwana, and Africa and South America (Chapters 4-6). This resulted in rapid variation in the stress state (Chapter 5) and rotations of microplates caught between these major tectonic plates (Chapters 4 and 5; Adie, 1952a; Mitchell et al., 1986; Marshall, 1994; Curtis and Storey, 1996; Trewin et al., 2002), which require a mechanistic explanation.

The current models for the vertical-axis rotation of blocks in strike-slip systems typically invoke a fragmentation and deformation predominantly controlled by Riedel geometries (Ron et al., 1984; Garfunkel and Ron, 1985; McKenzie and Jackson, 1986; Peacock et al., 1998). However, for continental blocks and microplates the location of their boundaries can be highly affected by inherited structures as in the case of the Victoria microplate, Romanche transform blocks, the Seychelles, the Sergipe and Sinai microplates (Szatmari and Milani, 1999; Salamon et al., 2003; Nemčok et al., 2016; Glerum et al., 2020).

For the case of the FIM, it is unclear why the fragmentation occurred along its present-day boundaries and on such a large scale. The inferred boundaries align with syn- and antithetic faults associated with the wrenching between East and West Gondwana (Section 7.2). However, the pre-break-up extensional

episodes that led to the drift of East Antarctica and the faulting in the SNFB and western side of the FPB (Figures 7.2, 7.3) could have generated areas of crustal weakness that controlled the locus of nucleation of microplate boundaries in the Jurassic. The present-day western boundary of the FIM remains of particular interest (Chapter 5). The uncertainties behind its existence and exact location have been one of the main arguments used against the rotation of the FIM, and the reasoning behind its location could offer some insights into why this microplate is so extensive. Based on the Siluro-Devonian faunal distribution across Brazil, Uruguay, Sierra Grande, South Africa, and the Falkland Islands (Clarke, 1913 and Baker, 1924 in Stone, 2016; Adie, 1952a; Pankhurst et al., 2006; Ramos et al., 2017), these terranes were part of Gondwana at this time. However, Patagonia is believed to have been accreted to the supercontinent during the late Paleozoic (Pankhurst et al., 2006; Ramos, 2008), although there is still some uncertainty regarding the accretion of the southernmost Patagonia (Deseado Massif) and the North Patagonian Massif (Ramos, 2008). If the Falkland Islands were already part of Gondwana during the collision of southern Patagonia, then one would expect a late Paleozoic suture to exist between the islands and the South American coast. The presence of this suture could explain the arcuate positive gravity anomaly along the eastern margin of the Malvinas Basin (Chapter 5). Furthermore, this area could have acted as a zone of weakness as suggested by significant thinning estimated in the Malvinas Trough compared to the rest of the Falkland platform (Baristeas et al., 2013; Chapter 5) and could have facilitated a separation of the FIM from the South American plate during the Jurassic.

In terms of the mechanism for rotation, several studies show that the coupling with the surrounding major plates can act as the main driving force for the rotation of a microplate (Schouten et al., 1993 and references therein; Searle et al., 1993; Glerum et al., 2020). However, there have been documented instances where mantle drag at the base of the microplate can be a contributor to its motion (Neves et al., 2003; Calais et al., 2006). The FIM represents a particular case due to its size and amount of rotation. It has formed and developed adjacent to the West Antarctic region in which major block readjustments have been documented throughout the Mesozoic (Watts and Bramall, 1981; Grunow et al., 1987; Curtis and Storey, 1996; Martin, 2007). The opposite sense of rotation, but of a comparable amount, of the Ellsworth Whitmore Terrane has led previous studies to correlate their rotations and assign them to the same event/process (Macdonald et al., 2003; Martin, 2007).

The initiation of FIM extension and rotation is difficult to pinpoint due to the lack of age constraints for the oldest syn-rift deposits. However, there is evidence that it was still ongoing during the Middle and Late Jurassic (Chapter 5 and 6), after the completion of rotation of the Ellsworth Whitmore Terrane at 175-180 Ma (Grunow et al., 1987). However, the comparable extent and amount of rotation of the two microplates could suggest that the area in which they developed was characterised by geodynamic conditions favourable for such complex motions to occur. This idea was at the base of the double-saloon-door model of Martin (2007) for block rotations in Gondwana. Similar to the interpretation proposed by Martin (2006) for the Mediterranean, this model related the mirrored rotations of the FIM and Ellsworth Whitmore Terrane to slab rollback along the Panthalassa Ocean – SW Gondwana subduction zone (Figure 7.6). This mechanism is not dissimilar to the trench suction forces postulated by Ben-Avraham et al. (1993) as being responsible for the vertical-axis block rotations documented in south-western Gondwana.

Evidence of Late Triassic to Late Jurassic rollback and steepening of the subducted slab came from studies on the migration of the locus of magmatism along Patagonia (Echaurren et al., 2017) and the Antarctic Peninsula (Storey et al., 1992), and changes in the extension direction along the South American plate (Lovecchio et al., 2019, 2020). The perpendicular orientation of the Weddell Sea opening in the Late Jurassic compared to the subduction zone along the western margin of Gondwana (Figure 7.4) was explained through a slab tear of the subducted plate occurring along the wrenching zone between East and West Gondwana (Figure 7.3; Lovecchio et al., 2019). The tear would have accentuated a mirrored slab rollback decreasing westward along East Gondwana (Figure 7.6) and eastward across West Gondwana, and would have generated a thermal anomaly responsible for the break-up in the Weddell Sea during the Late Jurassic (Lovecchio et al., 2019). Numerical modelling of mantle flow under retreating trenches show an increase in the trench-directed flow above a slab undergoing rollback (Sternai et al., 2014). This can result in rotations in the overriding plate due to differential mantle drag at its base (Sternai et al., 2014; Figure 7.6).

If this was the case in south-western Gondwana, then the interpretation of the counter-clockwise rotation of the Ellsworth Whitmore Terrane would have been driven by this differential rollback (increasing westward) of the Panthalassan plate as suggested by Martin (2007). However, the rotation of the FIM potentially occurred and continued after the rotation of the Ellsworth Whitmore

Terrane ceased. This was probably related to later tectonic delimitation of the microplate, during the successive extensional episodes that preceded the drift of East Antarctica (Chapter 5; Figures 7.2, 7.3). As the dextral wrenching between East and West Gondwana started (König and Jokat, 2006), the delimitation of the FIM reached its completion (Figure 7.3). The southward movement of East Antarctica was most likely responsible for drag along the margin of the FIM and initiated the rotation of the microplate, as originally speculated by Taylor and Shaw (1989). However, the dextral wrenching between East Antarctica and West Gondwana switched to rifting in the Late Jurassic with the opening of the Weddell Sea (Ghidella et al., 2002; König and Jokat, 2006; Figure 7.4). At this point any coupling between the FIM and East Antarctica would have ceased. The remainder of the FIM rotation would have been driven by mantle flow which, due to the differential rollback, would have increased eastward and maintained the clockwise rotation of the FIM (Figure 7.6). It is unclear if ridge push from the Weddell Sea and the oceanic domain opening in the FPB (Figures 7.3, 7.4) contributed to the rotation as well.

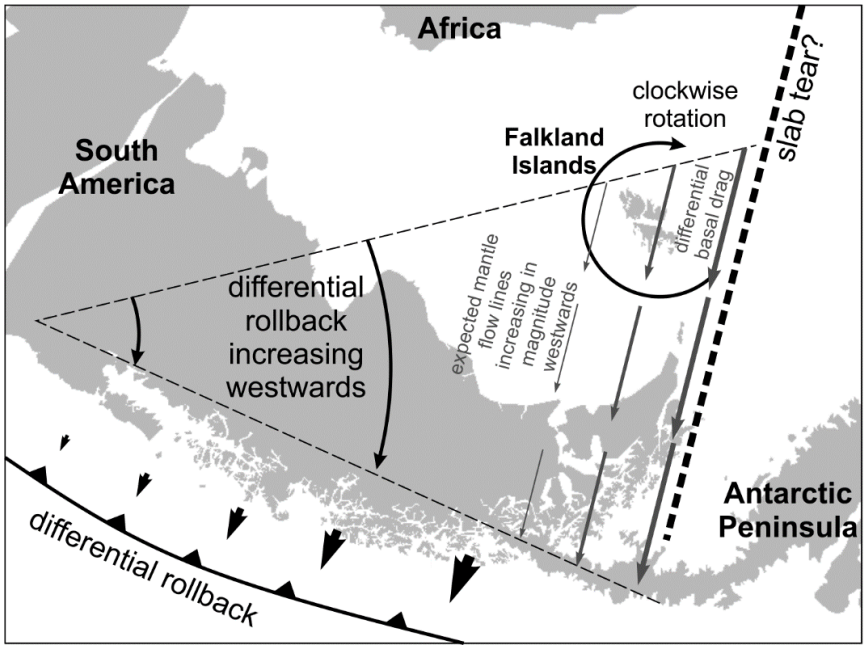

Figure 7.6 Jurassic configuration of SW Gondwana showing differential rollback and slab tear along the Panthalassan margin and a schematic depiction of differential mantle flow, increasing eastward and resulting in differential drag at the base of the Falkland Islands Microplate, which maintained the clockwise rotation; rough position of the inferred slab tear and hinge point for the slab rollback drawn after Lovecchio et al. (2019); the Ellsworth Whitmore Terrane is located in the region east of the Falkland Islands and the mantle flow under this region would be a mirrored version of the one shown below the Falkland Islands (increasing westward)

Another insight into the forces that drove microplate rotation comes from the behaviour of the FIM during the drift of South America away from Africa. The FIM rotation occurred during the wrenching and rifting phases between East and West Gondwana in the Middle to Late Jurassic, but it is affected by wrenching along the AFFZ only in the Early Cretaceous (Baby et al., 2018). Although evidence of shear is seen along the western margin of the FPB, similar to the deformation related to rotation, local and regional stress field correlations (Chapter 5; Stone et al., 2008), aeromagnetic modelling (Stone et al., 2009), and palaeomagnetic data (Stone et al., 2008) suggest that the rotation of the FIM had already ceased at this time. Therefore, the drag along the edge of the African plate was not sufficient to re-initiate rotation in the lack of a mantle flow component or there was little coupling between the FIM and Africa post-rotation for the latter to exert any significant drag during wrenching.

Although some of the models for vertical-axis rotation support a rigid behaviour of the blocks (Ron et al., 1984; Garfunkel and Ron, 1985; McKenzie and Jackson, 1986), some degree of deformation is postulated by others (Dibblee, 1977 in Peacock et al., 1998; Peacock et al., 1998). Complex fault networks have been interpreted and associated with intra-plate deformation during rotation in Northern Iceland and along the Easter and Sinai microplates (Neves et al., 2003; Salamon et al., 2003; Horst et al., 2018). Areas like California and Manus microplate show deformation more consistent with bookshelf tectonism (Luyendyk et al., 1985; Jackson and Molnar, 1990; Martinez and Taylor, 1996; Ingersoll and Coffey, 2017) where the rotating blocks are expected to behave rigidly during rotation (Ron et al., 1984; Garfunkel and Ron, 1985; McKenzie and Jackson, 1986). However, space issues have been raised for these types of models in the corners of the blocks where compression or extension would be expected (Dibblee, 1977; Peacock et al., 1998). In the example of the Manus microplate less compression than expected was identified in the corners of the blocks suggesting a transport from the compressed corners to the corners undergoing extension (Martinez and Taylor, 1996). In addition, along the San Andreas Fault observations along intra-block faults showed they die out towards the zone-bounding faults and the blocks underwent internal deformation (Dibblee, 1977 in Peacock et al., 1998). This would be more consistent with the interpretation of Peacock et al. (1998) with intra-plate strike-slip zones and normal and thrust faults accommodating deformation (Figure 7.7b). In the case of the FIM, significant deformation is seen at several scales on both seismic and gravity data. Although complex and suggestive of multiple superimposed deformation stages, the fault networks along the microplate

follow three distinct trends: NE-SW, WNW-ESE, and N-S (Chapter 5). The regional NE-SW fracture zones point toward an incipient fragmentation of the FIM during rotation which would result in a more classical bookshelf geometry (Figure 7.7). However, there is no indication from the available data that these fracture zones are trans-crustal and that much lateral movement occurred between the sub-blocks themselves. Normal faults on two almost orthogonal directions developed along the FIM during its Jurassic rotation. Although related to distinct regional extensional episodes (Chapter 5), the now NE-SW trending normal faults along the Berkeley Arch follow the same trend suggested by Peacock et al. (1998) for the extensional corners of their quasi-continuous model (Figure 7.7). Furthermore, shearing along conjugate directions (WNW-ESE and NNE-SSW along the western margin of the FPB; Figure 7.7) has been interpreted along the FIM. This is consistent with the type of intra-block deformation suggested by Peacock et al. (1998). Moreover, wrenching identified at different scales was interpreted along the western margin of the FPB on the gravity and seismic data (Figure 7.8), which supports the fractal model for rotations of Peacock et al. (1998).

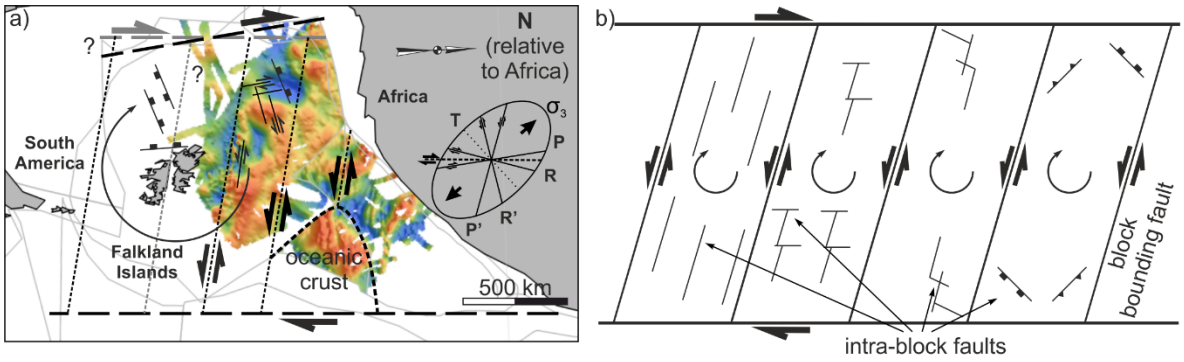

Figure 7.7 a) Fault configuration along the FIM during the break-up of Gondwana; b) expected fault networks within rotating blocks (drawn after Peacock et al., 1998); note similarities in the types and trend of faults identified along the FIM and the model of Peacock et al. (1998); it remains unclear if the NE-SW trending faults fragment the FIM and act as the block-bounding faults in Peacock et al. (1998)'s model or merely as intra-block faults

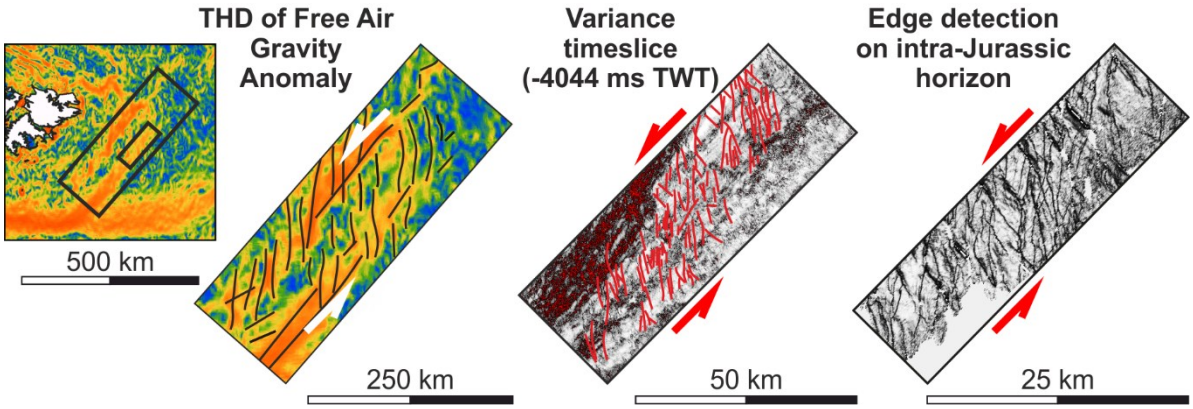

Figure 7.8 Evidence of wrenching occurring at different scales along the western margin of the Falkland Plateau Basin

7.4 Crustal, structural, and stratigraphic architectures along transform margins

The Falkland Plateau is an example of a transform margin, currently bound by one of the longest-lived and highest offset transform faults on Earth, the Agulhas-Falkland Fracture Zone (Ben-Avraham et al., 1997; Mercier de Lépinay et al., 2016). The plateau represents a classic example of a transform marginal plateau (*sensu* Loncke et al., 2020) which has undergone a multi-stage evolution during the fragmentation of Gondwana, and its study provides an excellent opportunity for gaining more detailed insights into the architecture of these tectonic settings.

Transform motion along the AFFZ is believed to have initiated during the Early Cretaceous (Valanginian) although extension along a proto-AFFZ would have started in the Middle Jurassic (Baby et al., 2018). The findings presented throughout Chapters 4 to 6 support a rotation of a sub-plate of the plateau (the FIM) from Middle to Late Jurassic, which would require a proto-AFFZ along the now northern boundary of the FIM to have facilitated this rotation. The separation of the FIM and initiation of rotation was associated with early rifting and dextral wrenching between East and West Gondwana (Chapters 5 and 6; Section 7.2; Taylor and Shaw, 1989) and was responsible for the formation of the main crustal domains along the plateau and varied structural styles. Although the present-day configuration of the Falkland Plateau is not fully the result of movement along the AFFZ, its formation was highly impacted by intra-continental wrenching (as documented in the early stages of transform formation), between East and West Gondwana, and South America and Africa. Therefore, its current architecture can be discussed in the context of current

understanding of transform margin development and transform marginal plateaus.

7.4.1 Structural network

Fault networks that formed along transform margins can be highly complex, particularly due to the early stages of intra-continental wrenching (Scrutton, 1979; Mascle and Blarez, 1987; Benkhelil et al., 1995; Antobreh et al., 2009; Nemcok et al., 2016). The complexity increases when the transform margin is associated with a marginal plateau as the latter would have undergone at least one other stage of deformation prior to transform motion (Mercier de Lépinay et al., 2016).

The pre-AFFZ deformation stage along the Falkland Plateau is related to intra-continental wrenching, but between East and West Gondwana, and a rotation of the FIM (Chapters 5 and 6). Therefore, the present-day structural configuration shows the superimposition of two wrenching events combined with vertical-axis block rotation and followed by extension related to the separation from Africa along the AFFZ and the opening of the South Atlantic. This resulted in several fault networks with the following trends: NE-SW, WNW-ESE, and N-S (Chapters 4 and 5).

The formation of WNW-ESE trending normal faults predominantly reactivated Paleozoic compressional features north and north-east of the Falkland Islands during early stages of extension in SW Gondwana (Chapters 4 and 5). A control of inherited structures on the morphology and deformation along transform marginal plateaus has been documented along several plateaus, including Vøring, Exmouth, and Guinea (Benkhelil et al., 1995; Pryer et al., 2002; l'Anson et al., 2019; Loncke et al., 2020). The present-day shape of the Vøring Plateau has been influenced by pre-existing Proterozoic structures (Loncke et al., 2020), and the Paleozoic and Mesozoic en-échelon normal faults across the Exmouth Plateau show a strong control of the Precambrian and Paleozoic fabrics, respectively (Pryer et al., 2002; l'Anson et al., 2019). Furthermore, a change from margin-parallel normal faults along the Guinea margin to a sub-perpendicular orientation has been related to pre-existing structures (Benkhelil et al., 1995). More evidence of structural inheritance can be seen in the predominant type of shears formed along the FIM during wrenching (P, R', and P' shears; Figures 6.24, 7.7), which form instead of typical R shears, similar to observations made in Equatorial Atlantic (Nemčok et al., 2016).

NE-SW trending normal faults and wrenching on the same direction were interpreted along the FPB and related to wrenching between East and West Gondwana and a rotation of the FIM (Chapters 5 and 6). N-S trending en-échelon faults accommodated intra-plate shearing during rotation and during incipient motion along the AFFZ east of the Falkland Islands (Chapter 5; Figure 7.9d-f). The presence of strike-slip faults and strike-slip related geometries (e.g. en-échelon and pull-apart geometries) are commonly identified along transform margins (Figure 7.9). Margin-parallel negative flower structures and normal faults related to oblique extension have been documented in the eastern part of the Côte d'Ivoire – Ghana margin (Antobreh et al., 2009). These transition to the south-west to a sheared domain of en-échelon strike-slip faults, adjacent to the transform fault bounding the margin, and switch to the north-west to a domain of sub-perpendicular normal faults formed in a pull-apart setting (Basile et al., 1993; Antobreh et al., 2009). Along the Exmouth Plateau Paleozoic en-échelon normal faults are restricted near-shore, whereas the plateau itself shows a strong deformation related to the Mesozoic rifting with normal faults distributed in an en-échelon geometry (Figure 7.9a-c; Pryer et al., 2002; McHarg et al., 2018; l'Anson et al., 2019).

Localised compression and inversion of the WNW-ESE trending faults was documented during the rotation of the FIM (Chapter 5). Where compressional features were identified along other transform marginal plateaus, they were more extensive and related to transpression along the transform-bounding fault. En-échelon compressional structures and inversion of pre-existent normal and strike-slip faults were documented along the Côte d'Ivoire - Ghana margin (Attoh et al., 2004). The conjugate Guinea and Demerara plateaus show a superimposition of extensional and compressional structural styles (Benkhelil et al., 1995; Basile et al., 2013). Margin parallel folds and inverted normal faults were reported along the Guinea margin due to a change from transtension to transpression along the transform-bounded margin (Benkhelil et al., 1995). On the Demerara side the compressional and extensional features are considered coeval and related to transform motion (Basile et al., 2013). However, on the Falkland Plateau side it is unclear if the compression is due to wrenching or the rotation of the FIM (Chapter 5). Furthermore, thrusting and folding are highly localised compared to the aforementioned examples. The scarcity of compressional features along the FIM was associated with generation of accommodation space between South America, Africa, and Antarctica at a faster rate than the rate of rotation and/or wrenching (Chapter 5).

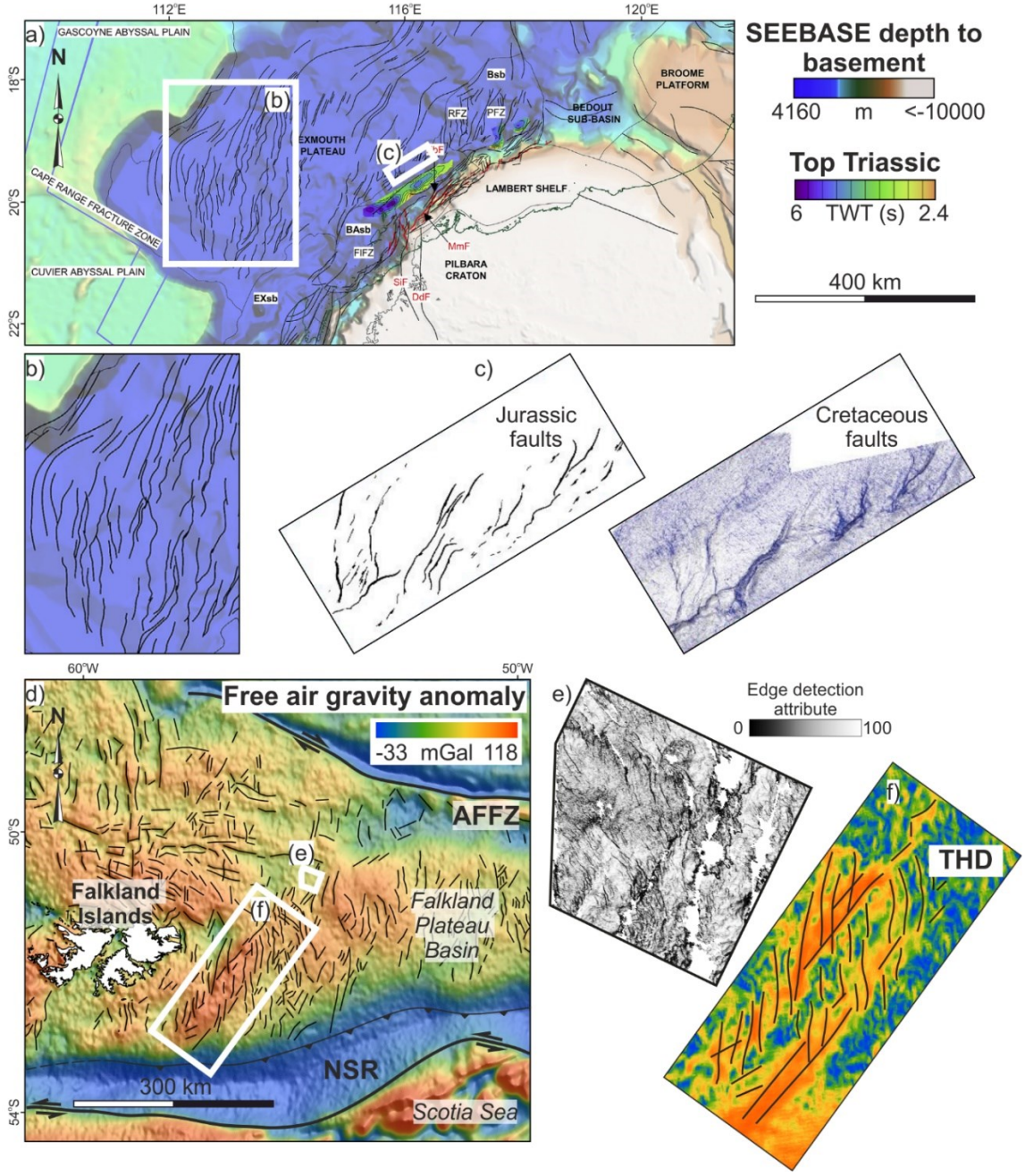

Figure 7.9 Examples of fault networks along transform marginal plateaus; a) example from the Exmouth Plateau (compiled after McHarg et al., 2018 and l'Anson et al., 2019) showing en-échelon fault distribution (b and c) similar to deformation identified in the Falkland Plateau Basin (d, e, and f)

N-S trending normal faults along the FIM were also related to the opening of the South Atlantic. These overprinted the reactivated WNW-ESE Paleozoic structures north of the Falkland Islands, where they generated extensive grabens (Richards et al., 1996a; Lohr and Underhill, 2015) and contributed to the present-day complex structural architecture of the plateau.

7.4.2 Crustal architecture

Juxtaposition of highly varied crustal types has been documented along several transform marginal plateaus including the conjugate Sao Paolo and Walvis plateaus and the South Tasman Rise (Royer and Rollet, 1997; Evain et al., 2015; Fromm et al., 2017; Planert et al., 2017; Loncke et al., 2020). Similarly, the Falkland Plateau has been interpreted as a mosaic of continental and oceanic crust (Chapters 4-6), namely underlying the FPB (Chapter 6). Thinned continental crust was interpreted along the western and northern margins of the FPB, whereas thick oceanic crust underlies the south-eastern corner of the basin. The two domains are separated by sheared, intruded, and underplated continental crust (Chapter 6). Underplating of thinned continental crust with high volcanic and magmatic additions and/or serpentinization of the upper mantle (P-wave velocities higher than 7 km/s; densities of ~3-3.1 g/cc) have been documented under a number of transform marginal plateaus like Vøring, Rockall, Exmouth, and Walvis (Lorenzo, et al., 1991; Berndt et al., 2001; Klingelhöfer et al., 2005; Planert et al., 2017; Loncke et al., 2020). Similar velocities and densities have been reported at the crust/mantle boundary in the FPB (Schimschal and Jokat, 2017, 2019b). The oceanic domain interpreted in the FPB consists of thicker than normal oceanic crust (up to 20 km) and has been associated with magmatic and volcanic accretion due to closeness to the Weddell Sea rift axis (Chapter 6, Section 7.2) or to the presence of a localised mantle thermal anomaly (Schimschal and Jokat, 2019b). Although not as common, where documented (e.g. western part of the Walvis plateau), thick oceanic crust was related to the presence of a hotspot (Tristan Da Cunha hotspot; Fromm et al., 2017).

7.4.3 Volcanism

Widespread volcanism has been documented along transform margins and their associated marginal plateaus, either during transform margin development or during the deformation phases that preceded transform motion (Loncke et al., 2020). Along the Falkland Plateau several episodes of volcanism and magmatism have been identified. The first episodes (188 ± 2 to 190 ± 4 Ma and 162 ± 6 to 178.6 ± 4.9 Ma; Mussett and Taylor, 1994; Stone et al., 2008, 2009) consisted of dyke intrusion and have been related to the emplacement of the Karoo-Ferrar large igneous province (Mussett and Taylor, 1994; Mitchell et al., 1999). These were coeval to early extension documented along the FIM and potentially early stages of rotation of the FIM and wrenching between East and West Gondwana (Chapters 5 and 6; Section 7.2). Another episode (121 ± 1.2

Ma to 138 ± 4 Ma; Stone et al., 2008; Richards et al., 2013; Chapter 5) of dykes, sills, and lava emplacement was synchronous to the opening of the South Atlantic (Stone et al., 2009; Stone, 2016; Chapter 5) and the wrenching and active transform phase of the AFFZ, as constrained by Baby et al. (2018). Commonly, the timing of volcanism and magmatism along marginal plateaus can vary and be coeval to any of the deformational episodes that preceded the initiation of transform movement (Loncke et al., 2020). Similar to the Karoo-Ferrar-related episodes of dyke emplacement onshore the Falkland Islands, the main volcanic activity of several transform marginal plateaus has occurred prior to transform motion (Loncke et al., 2020). This was due to early deformation coeval with, and adjacent to, the main volcanic events that affected Gondwana prior to and during its fragmentation (e.g. Karoo-Ferrar, Central Atlantic Magmatic Province, Paraná-Etendeka flood-basalt province; Encarnación et al., 1996; Marzoli et al., 1999; Trumbull et al., 2007; Hastie et al., 2014; Foulger, 2018; Loncke et al., 2020). Examples include the Sao Paulo – Walvis conjugate pair and the Tasman region (Storey, 1995; Elliott et al., 2009; Fromm et al., 2017; Loncke et al., 2020). Regarding transform margin formation in general, their active stage of development has been related to volcanism (Benkhelil et al., 1995; Lorenzo, 1997; Lorenzo and Wessel, 1997). This is consistent with the timing of the last episode documented along the Falkland Plateau, which was synchronous to the opening of the South Atlantic and movement along the AFFZ (Stone et al., 2008; Richards et al., 2013; Chapter 5).

7.4.4 Vertical movements

Transform margins are frequently associated with marginal ridges/highs, the formation of which remains uncertain (Basile, 2015; Mercier de Lépinay et al., 2016; Nemčok et al., 2016). Tectonic, flexural, and thermal processes have been invoked to explain their development. Each of these processes impacts the timing of the ridge formation in the transform margin development (during intra-continental and active transform stages for first two mechanisms and post-transform for the latter; Le Pichon and Fox, 1971; Scrutton, 1979; Mascle and Blarez, 1987; Lorenzo et al., 1991; Basile et al., 1998; Basile and Allemand, 2002; Attoh et al., 2004; Nemčok et al., 2013; Basile, 2015). It remains unclear which process is dominant in different regions and why. Unfortunately, the Falkland segment of the AFFZ is intersected by few seismic reflection lines with only six crossing the marginal ridge (as constrained by bathymetric and gravity data). Two of these sections do not have age constraints on the overlying

sediment cover and were not included here. However, some insight can be gained from the architecture of the other four (Figure 7.10).

The northern part of the FPB consists of an E-W elongated Jurassic depocentre infilling tilted fault blocks (Chapter 6; Figure 7.10). Extensive erosional unconformities, stratal geometries, and changes in the bathymetry provide evidence for uplift occurring further north, along the AFFZ, with generation of basement highs (the Falkland Escarpment; Figure 7.10). This is similar to architectures documented along the Côte d'Ivoire – Ghana margin where the basement is uplifted and tilted away from the transform and underwent erosion and flexural uplift (Basile et al., 1998; Nemčok et al., 2013). However, similar tilting is observed only on the westernmost section (Figure 7.10a) with two of the sections showing structures similar to horsts bounding the Jurassic grabens to the south (Figure 7.10b, c). Further east, north of the MEB, thick sections of sedimentary deposits were uplifted along the transform fault (Figure 7.10d), similar to regions along the Exmouth Plateau (Mercier de Lépinay et al., 2016) where they were related to thicker crust due to the addition of underplates at its base (Lorenzo et al., 1991). The basement underlying the uplifted Jurassic depocentre shows tilting towards the AFFZ (Figure 7.10d). However, the composition of the ridge alone along with the tilting direction are not enough to infer a mechanism for the uplift. Time constraints provided by the geometry of the overlying sediments are required from stratigraphic analysis (Mercier de Lépinay et al., 2016).

However, along the Falkland segment of the AFFZ the timing of the uplift remains contentious. The westernmost two sections show Lower Cretaceous deposits either prograding down the slope created by the rising ridge or thinning towards the AFFZ before they are truncated (Figure 7.10a, b) suggesting a coeval initial uplift. Same timing for uplift from the north is interpreted in Chapter 5 (Figure 5.7h, i; Section 5.4.1) and would be related to wrenching or active transform motion along the AFFZ (Baby et al., 2018). This timing is more commonly related to tectonic or flexural (unloading related to erosion) processes (Mercier de Lépinay et al., 2016).

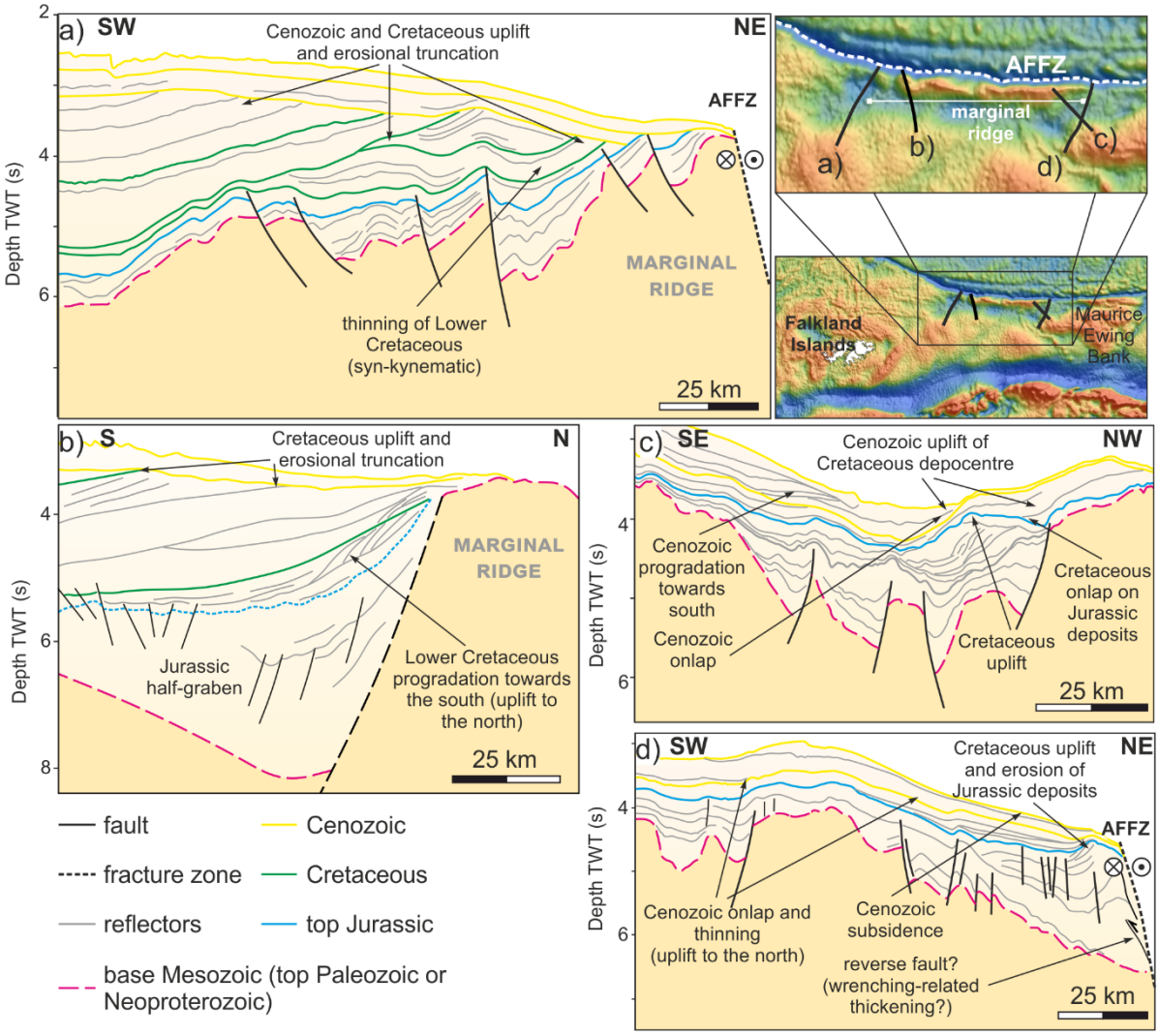

Figure 7.10 Interpreted sections across the Falkland Escarpment showing erosional truncations of Jurassic-Cenozoic strata and stratal geometries indicative of vertical movements along the marginal ridge

Significant erosion can be inferred from the truncated reflectors in Figure 7.10a, which, when linked to the absence of evidence for compression along the AFFZ (Figure 7.10), might point to a flexural process. More data are required to constrain this. Towards the east, limited chronological constraints exist within the Cretaceous section (Figure 7.10c, d). Some degree of deformation occurs during this period, as suggested by onlapping geometries and erosional truncations (Figure 7.10c, d), but it is unclear during which stage of transform fault development it occurred. Furthermore, the Cretaceous section is significantly thinner than in the west, which might suggest a more elevated position during deposition or extensive erosion (Figure 7.10c, d). Some evidence of faulting under the folded Jurassic section in Figure 7.10d could point to tectonic thickening. This is very localised, and it is unclear if it

contributed significantly to the overall uplift. Underplating was interpreted further south in the basin (Chapter 6), but there is no evidence for its northern extent to argue for a similar cause of uplift as for the Exmouth Plateau (Lorenzo et al., 1991). Onlapping geometries can be observed in the Cenozoic section of the sedimentary infill (Figure 7.10c, d), which might point to a post-transform vertical movement, typically associated with thermal processes (Mercier de Lépinay et al., 2016). Section in Figure 7.10d also shows a downward warping of the margin with the Cenozoic deposits, thinning towards the AFFZ during their deposition, in a more subsided position, which would support thermal uplift occurring prior to this, followed by cooling and subsidence.

7.5 Microplate control on regional reconstructions

Unravelling the crustal and structural architecture of areas such as the Falkland Plateau, along with understanding their behaviour during supercontinent fragmentation, can provide significant insights into plate reconstructions. In this example, the evolution of the plateau offers constraints on the pre-break-up position of the FIM, which in turn can shed more light on the pre-break-up position of the major plates of south-western Gondwana.

The plate model presented in Chapter 6 (and discussed in Section 7.2) is based on the fragmentation and reconstruction of South America, East Antarctica, and the Antarctic peninsula after König and Jokat (2006), Eagles and König (2008), König and Jokat (2010), and Muller et al. (2019). However, there have been different models for the fragmentation of the South American plate and the West Antarctic region, which explain the deformation associated with the break-up of Gondwana in various ways (Lawver et al., 1999; Macdonald et al., 2003; König and Jokat, 2006; Torsvik et al., 2009; Heine et al., 2013; Eagles and Eisermann, 2020). These strongly impact the space available for the reconstruction of the Falkland Plateau and its tectonic evolution in the context of Gondwana breakup. The pre-break-up position of the FIM postulated in this thesis along with the correlations carried between the FIM and the surrounding plates both in this thesis and in previous studies, can offer more constraints on the evolution of the southern South Atlantic and Weddell Sea regions.

7.5.1 Deformation along the South American plate

Several ways of representing deformation across South America and achieving a tighter fit between it and Africa have been proposed (e.g. Lawver et al., 1999;

Macdonald et al., 2003; König and Jokat, 2006; Torsvik et al., 2009; Heine et al., 2013; Chapter 2). Some of these models argue for the existence of trans-continental shear zones splitting the South American plate into rigid sub-plates (Lawver et al., 1999; Macdonald et al., 2003; König and Jokat, 2006; Torsvik et al., 2009). Lateral movement of up to 500 km was invoked along the shear zone bounding Patagonia to the north in order to obtain a close fit between the sub-plate and Africa (Torsvik et al., 2009). However, no supporting evidence for this motion has been found onshore (von Gosen and Loske, 2004). More recent studies argue for a different fragmentation of the South American plate where intra-plate deformation is undertaken by small rotations of sub-plates occurring as the main basins across and offshore South America are opening, as demonstrated by Heine et al. (2013) and incorporated in a global plate model by Muller et al. (2019). These different interpretations of the deformation across South America result in different scenarios for the space available during the evolution of the Falkland Plateau, and the amount of lateral movement that occurred along the AFFZ in the early stages of its development. Without further constraints on these two elements, speculations will remain.

Besides the space issues identified between South America and Africa for a rigid reconstruction of the former (Bullard et al., 1965), the need for a tighter fit between Patagonia and Africa arose from the rotational model of the Falkland Islands, which positioned the islands near Port Elizabeth in South Africa (Figure 7.11a; Adie, 1952a; Mitchell et al., 1986; Marshall, 1994; Trewin et al., 2002). As pointed out by Marshall (1994), this reconstruction of the islands generated space between them and Patagonia, which could only be solved by deforming the South American plate during reconstruction. More recent studies arguing for a FPB fully underlain by oceanic crust have pointed out a similar space issue when closing the FPB (Schimschal and Jokat, 2019b). The interpretation shown in this thesis argues for a less extensive oceanic domain but nonetheless formed during a rotation of the islands (Chapter 6).

Here, three positions for the rotated FIM are discussed, along with their implications on the deformation of South America. The first model (Figure 7.11a) is derived from literature and based on the original reconstruction of Adie (1952a) in which the islands are located between 42±6°S and 47±5°S (Mitchell et al., 1986), adjacent to south-eastern South Africa, and rotated by ~120° relative to their Cretaceous position (Adie, 1952a; Mitchell et al., 1986; Taylor and Shaw, 1989; Trewin et al., 2002). This position requires ~500 km dextral displacement to have occurred between Patagonia and the rest of

South America (Marshall, 1994; Torsvik et al., 2009). The second model is the one presented in this thesis (Chapter 6; Section 7.2) and shown in Figure 7.11b. In this model the FIM fits in the space available between a deformed South America (after Muller et al., 2019) and Africa and is rotated by ~80° compared to its Cretaceous position. This reconstruction of the FIM does not require more deformation of the South American plate than already documented by Heine et al. (2013) and included in the plate model of Müller et al. (2019). The third model (the alternative reconstruction presented in Chapter 6; Figure 7.11c) positions the FIM between the first two models, and requires further deformation of the South American plate, here accounted for by rotation of the San Jorge Plate.

Model 1

Stratigraphic correlations between the Permian sedimentary sequence cropping out onshore the Falkland Islands and South Africa suggested an adjacent palaeoposition (~200 km apart; Figure 7.11a) of the two during deposition (Trewin et al., 2002), with sediments sourced from the fold and thrust belt forming to the south and south-west, as supported by palaeocurrent data (Veevers et al., 1994; Macdonald et al., 2003). This is supported by the preliminary range of palaeolatitudes derived from palaeomagnetic data (Mitchell et al., 1986).

As pointed out by Marshall (1994), this position of the FIM requires Patagonia to have been in a more northern position compared to the rest of South America prior to the fragmentation of Gondwana. This relative movement has been achieved by invoking ~500 km of dextral movement along the Gastre Fault System of Rapela and Pankhurst (1992) during the Jurassic (Figure 7.11 a; Marshall, 1994; Macdonald et al., 2003; Torsvik et al., 2009). However, more recent studies carried in the North Patagonian Massif do not support the presence of a Mesozoic dextral Gastre (Franzese and Martino,1998 in Ramos et al., 2017; von Gosen and Loske, 2004). An alternative fragmentation and deformation of the South American plate (Figure 7.11b) provides a closer fit between Patagonia and Africa (Heine et al., 2013; Müller et al., 2019) than when no deformation is invoked, but still leaves a gap of ~400 km between the FIM and Patagonia. Furthermore, almost the entirety of the FPB is overlapping either South Africa or the FIM in this scenario whereas a big part of the MEB underlies the FIM as well (Figure 7.11a), suggesting much more extension then estimated in this thesis (Chapter 6) and/or previously published for both the MEB and the FPB.

Model 2

Following the South American plate fragmentation of Muller et al. (2019), the closest fit that can be obtained between the FIM and South Africa without generating space between the Falkland Islands and Patagonia is shown in Figure 7.11b. The D1 fold and thrust belt onshore the Falkland Islands is considered a continuation of the Cape Fold Belt in South Africa (Du Toit, 1927; Adie, 1952a; Curtis and Hyam, 1998), and the offshore SNFB was originally part of this fold and thrust belt as well (Chapter 4; Richards and Fannin, 1997). The comparison carried between the SNFB and the Algoa and Gamtoos basins in Chapter 4 suggests that these are along-strike equivalents, and that their orientation supports an oroclinal bend in the Gondwanide Orogen at Port Elizabeth. This bend was first suggested by Johnston (2000) and the ~90° change in strike of the Cape Fold Belt was confirmed by later studies on the origin of the change in structural trend in the Gamtoos Basin (Paton and Underhill, 2004). Several oroclinal bends (Colorado, Garies, Cape; Figure 7.11b) have been identified along the entirety of the Gondwanide Fold and Thrust Belt (De Beer, 1992; Paton et al., 2016). These are believed to have been controlled by the extent of the Kalahari Craton in Africa and the Rio de la Plata Craton in South America (De Beer, 1995; Pángaro and Ramos, 2012). Alternatively, an oblique component to the collisional event leading to the Gondwanide orogeny has been invoked as a control for the Cape and Port Elizabeth antitaxial bends (Johnston, 2000; Tankard et al., 2009). Regardless of their origin, the existence of the Port Elizabeth antitaxis, while supporting less rotation of the FIM (Chapter 4; Stanca et al., 2019), also implies a second bend of the Gonwanide orogen east of the reconstructed FIM (Figure 7.11b) so that the trend joins the Ellsworth and Pensacola Mountains in Antarctica. Although this is a reasonable assumption considering the variation in structural and rheological inheritance across south-western Gondwana (De Beer, 1995; Tankard et al., 2009; Pángaro and Ramos, 2012), the FIM reconstruction presented in this thesis, as constrained by the South American intra-plate deformation after Muller at al. (2019), introduces a dramatic bend in the orogen (Figure 7.11b) that might require further considerations.

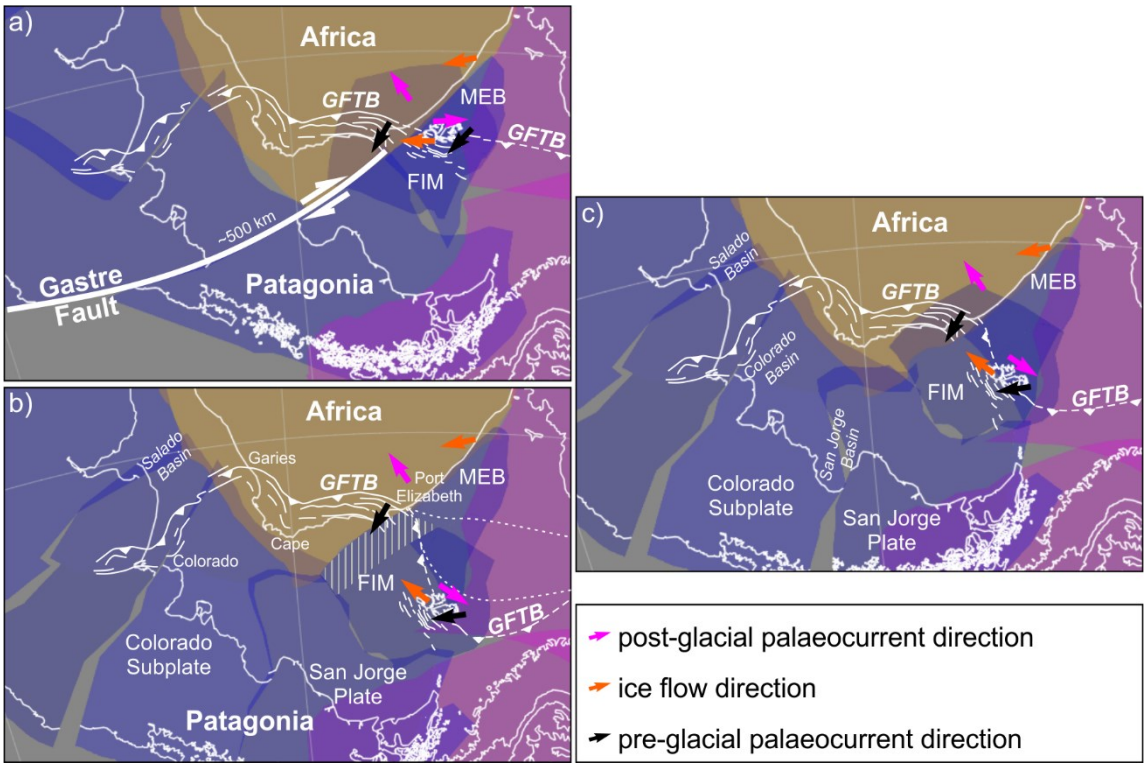

Figure 7.11 a) Model 1; reconstruction of the Falkland Islands after Trewin et al. (2002); fragmentation of northern Patagonia after Seton et al. (2012); Gastre Fault position after König and Jokat (2006) and displacement after Torsvik et al. (2009); b) Model 2; reconstruction of the FIM from Chapter 6 showing the position of the oroclinal bends along the GFTB; hatched area – area estimated to be added through extension; stippled lines – trend of the GFTB from reconstructions in (a) and (c); c) Model 3; tight fit reconstruction of the FIM and the position needed for southern Patagonia (San Jorge Plate) to minimize gaps between it and the islands; FIM – Falkland Islands Microplate; GFTB – Gondwana Fold and Thrust Belt; MEB – Maurice Ewing Bank

Besides the extensive oroclinal bend, the space between the Falkland Islands and the South African coastline varies significantly between models 1 and 2 (Figure 7.11a, b). Crustal thickness estimates from gravity inversion, along with the range of calculated thinning factors (Chapter 6) suggest that the eastern un-stretched extent of the FIM was bigger than previously thought (see un-hatched area between the Falkland Islands and South Africa in Figure 7.11b compared to Figure 7.11a; Richards et al., 1996b; Storey et al., 1999). This, combined with the correlation between SNFB and Gamtoos and Algoa basins point to a larger initial distance between the Falkland Islands and the South African coast than previously thought (Model 1; Figure 7.11a), but smaller than the one used in the plate model based on Muller et al. (2019; Model 2; Figure 7.11b). This would generate a gap between the un-stretched FIM and the

South African coastline (the size of the hatched area in Figure 7.11b) or would require an explanation for the loss of that crustal segment (i.e. shearing and fragmentation during rotation and movement along the AFFZ, and accretion of the crustal blocks to the Falkland Escarpment or the Diaz Marginal Ridge, south of the Outeniqua Basin).

The overestimated distance between the Falkland Islands and the South African coastline in Model 2 also translates into the sections compared and correlated by Trewin et al. (2002) onshore South Africa and the Falklands to be situated further apart. However, this reconstruction does not hinder a correlation between the Karoo Basin infill and the Lafonia Supergroup, which would still be part of the same sedimentary basin fed from the rising Gondwanide Fold and Thrust Belt. Palaeocurrent directions from Trewin et al. (2002) would still support a sediment sourced from the south and south-west but diverging away from the rising Port Elizabeth oroclinal bend (Figure 7.11b).

Model 3

The tightest fit between FIM and Africa that accounts for the estimated space between the FIM and the South African coast (Chapter 6), and the along-strike continuation of the SNFB and Algoa-Gamtoos (Chapter 4) was also built in Chapter 6 and shown in Figure 7.11c. Similar to Model 2, the southern part of East Falkland would still have been a segment of the Karoo Basin with sedimentation direction controlled by the sinuous trend of the Gondwanide Fold and Thrust Belt (Figure 7.11c). This position would be more consistent with ice flow from East Antarctica (orange arrows in Figure 7.11; Stone and Thompson, 2005) than for Model 2 where a more complicated trend whould be invoked. The range of palaeolatitudes for the FIM estimated from the onshore dykes and approximated from South Africa dolerites based on a reconstructed FIM is relatively wide (42±6°S-47±5°S; Mitchell et al., 1986). All three models are located within the error, although the values obtained directly from the dykes onshore the Falkland Islands argue for a position of the FIM as given by Model 1. However, as mentioned by Mitchell et al. (1986), their analysis was carried out on a small number of samples and further palaeomagnetic data would be required to constrain the range of palaeolatitudes for the FIM.

Similar to Model 1, the fit in Model 3 requires a more extensive deformation of the South American plate. This was achieved by rotating the San Jorge Plate counter-clockwise until the gap been it and FIM was minimized (Figure 7.11c). In Model 2, the rotation of Patagonia as South America rifts away from Africa has been accomodated by deformation in the Colorado and Salado basins

while little movement occurred between the San Jorge and Colorado sub-plates (Figure 7.11b; Heine et al., 2013; Muller et al., 2019). Palaeomagnetic data from the Deseado (on San Jorge Plate) and North Patagonian (on Colorado Sub-plate) massifs showed that sample localities from the former yielded Jurassic - Early Cretaceous clockwise rotations of up to 20° more than the latter (Geuna et al., 2000; Somoza et al., 2008), which could support a more northern position of the San Jorge Plate. The San Jorge Basin, situated between the two massifs (Figure 7.11c), shows evidence of Triassic - Early Jurassic and Late Jurassic - Early Cretaceous extension, which resulted in ~3 km thick deposits (Fitzgerald et al., 1990; Homovc and Constantini, 2001), which could have accommodated this rotation of the San Jorge Plate. Compression on a ~N-S (present-day) direction has been documented in Central Patagonia throughout the Jurassic (Navarrete et al., 2016) and correlated to similar evidence in Northern and Southern Patagonia (Naipauer et al., 2012; Navarrete et al., 2019). This has been interpeted as related to far-field stresses, such as the early opening of the Weddell Sea and the North Atlantic (Navarrete et al., 2016, 2019), but would align with the expected contraction for clockwise rotations of the Patagonian sub-plates, including the San Jorge Plate. However, more detailed analysis on the amount of extension in the on- and offshore sedimentary basins collated with amount of compression is needed to confirm the validity of this hypothesis.

Furthermore, Section 6.5.1.2 argues that the deforming plate model for this reconstruction of the FIM underestimated the crustal thickness under the MEB (Figure 6.36). However, it is unclear if the present-day morphology of the MEB has been controlled by structural inheritance and thus would not undergo significant extension for a more northern positon of the FIM under normal geological conditions.

In summary, all three models for the reconstruction of the FIM presented here have drawbacks, which require further analysis in order to constrain the configuration of the South American sub-plates prior to the break-up of Gondwana. Model 1 requires a significant deformation of the South American plate that needs to be explained by not invoking movement along the disproved Gastre Fault. Furthermore, this reconstruction requires far more extension along the Falkland Plateau than documented and does not account for the correlation between the SNFB and Algoa-Gamtoos region and the segment of the FPB interpreted to have lain between the FIM and South Africa (Chapter 6). A fit of the FIM in current plate models for the South Atlantic (Model 2; Figure

7.11b), although complying to the already interpreted deformation of the major plates in south-western Gondwana, requires further clarification of the sinuous trend of the Gondwanide Fold and Thrust Belt between Africa and Antarctica and of the region between the un-stretched FIM and South Africa. A more northern position of the FIM (Model 3; Figure 7.11c) would fit the observations previously published for the Falkland Plateau along with the ones presented throughout this thesis (Chapters 4-6). However, the deformation of the South American plate required to achieve this fit (Figure 7.11c) remains to be validated.

7.5.2 Pre-break-up configuration of the West Antarctic

Beside the space between South America and Africa controlling the reconstruction of the Falkland Plateau, of significant importance is the configuration of the West Antarctic blocks (Weddell Sea region). Due to the formation of the North Scotia Ridge and opening of the Scotia Sea starting in the Late Cretaceous (Barker and Griffiths, 1972; Dalziel et al., 2013), the southern margin of the Falkland Plateau was obscured. There are, therefore, different models for the way in which the fragmentation of West and East Gondwana was recorded along the Falkland Plateau. Several models argue for only the southern margin of the plateau being affected by wrenching related to movement between East and West Gondwana, which switched to extension and break-up during the Jurassic (König and Jokat, 2006; Lovecchio et al., 2020). Other studies support an evolution of the FPB more shaped by the extension between East and West Gondwana (Eagles and Vaughan, 2009; Reeves et al., 2016; Eagles and Eisermann, 2020), with break-up occurring between the northern Falkland Plateau – Maurice Ewing Bank and the West Antarctic region (Eagles and Eisermann, 2020; Figure 6.2f in Chapter 6).

In the reconstruction presented in Chapter 6 (Figures 6.24) and Section 7.2, the wrenching between East and West Gondwana is responsible for the initiation of FIM rotation, and the overall crustal architecture of the FPB. This interpretation, and that of Eagles and Eisermann (2020), both support a significant contribution of the relative motion between East and West Gondwana on the formation of the FPB. However, there are disparities between the reconstructions presented in this thesis and the model for the Weddell Sea proposed by Eagles and Eisermann (2020).

The crustal and structural architectures presented in Chapters 4-6 indicate that the plateau underwent a more complex evolution than pure extension related to the opening of the South Atlantic. Dextral and sinistral shearing interpreted

along the FPB (Chapter 5), rapid changes in the stress state (Chapter 4 and 5), and the presence of sheared, high velocity crust truncating a thick oceanic domain (Chapter 6) suggest a strong control by wrench tectonics on the formation of the plateau. Compared to more simplistic models for the evolution of the plateau incorporated in reconstructions of the South Atlantic (König and Jokat, 2006; Schimschal and Jokat, 2019b; Lovecchio et al., 2020), the interpretation of Eagles and Eisermann (2020) does account for a higher degree of shearing along the FPB. However, the same study of Eagles and Eisermann (2020) argues for no rotation of the FIM. The plate configuration proposed by Eagles and Eisermann (2020) cannot be incorporated into a rotational model either as Palmer Land and Alexander Island occupy the position of a rotated FIM (Figure 6.2). Furthermore, this model, similar to the interpretation of Schimschal and Jokat (2017, 2019b), argues for oceanic crust underlying the entirety of the FPB. Seismic reflection data (Chapters 5 and 6) show that the western margin of the FPB is still underlain by continental crust. Thick Jurassic depocentres are seen further east in the basin (Figures 6.9, 6.10), which are more supportive of deposition above a faulted continental crust with the high P-wave velocities of Schimschal and Jokat (2017, 2019b) pointing towards magmatic enrichment and/or underplating and oceanic crust restricted to the south-eastern corner of the FPB. Moreover, the break-up between the Skytrain of Eagles and Eisermann (2020) and the Falkland Plateau requires a right-lateral transform fault along the western margin of the FPB. Although, as mentioned by the authors, evidence of dextral strike-slip has been documented onshore the islands and was related to movement along the Falkland Sound Fault (parallel to the western margin of the FPB). However, seismic reflection, gravity, and magnetic data interpretation show evidence of sinistral wrenching occurring along the NE-SW trending western margin of the FPB. Inconsistencies of the model of Eagles and Eisermann (2020) with current interpretations of the evolution of the southern margin of the Falkland Plateau (i. e. South Georgia origin and evolution) were also pointed out by a recent review of Dalziel et al. (2021).

Similar to the reconstruction of the South American plate discussed in the previous sub-section, it is of high importance that microplate and microcontinents are considered when building a plate model as they can provide valuable information on the validity of existing reconstructions. Information on the evolution of the continental blocks sheared along the northern margin of the Scotia Sea (e.g. South Georgia; Dalziel et al., 1975, 2013, 2021; Macdonald et al., 1987), and of the Falkland Plateau can provide

more constraints on the reconstruction of West Antarctic region in a Gondwana pre-break-up configuration.

7.6 Suggested future research

7.6.1 Falkland Plateau – Outeniqua basins comparative study

A strong argument for the rotation of the Falkland Islands stems from the extensive correlative work carried out between the structures and stratigraphy onshore the islands and South Africa (Adie, 1952a; Thomas et al., 1997; Curtis and Hyam, 1998; Jacobs et al., 1999; Trewin et al., 2002; Vorster et al., 2016). Similarly, a comparison and correlation between the Southern North Falkland Basin and published sections from the Algoa and Gamtoos basins was carried out in Chapter 4 (Stanca et al., 2019). However, a more thorough analysis of seismic reflection data from both sides of the AFFZ could provide additional constraints for the pre-break-up position of the Falkland Islands. The two seismic cubes analysed in Chapter 5 show complex fault networks developed during Jurassic - Early Cretaceous as fragmentation occurred across south-western Gondwana (Chapter 5). The FINA cube covering the Berkeley Arch and part of the Volunteer sub-basin, in particular, shows upper crust reflectivity and several superimposed fault networks (Figure 7.12) which would require more detailed mapping. Furthermore, a comparison with the Outeniqua sub-basins could provide more constraints on the evolution of the FIM relative to Africa.

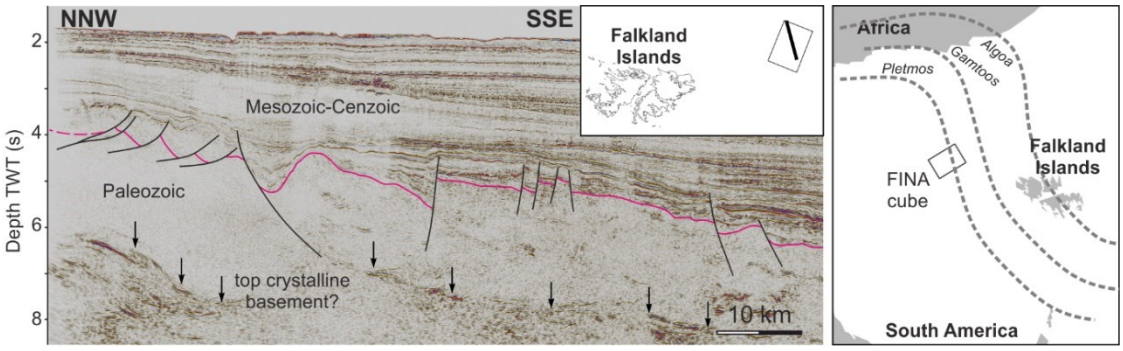

Figure 7.12 Section through the FINA cube showing faulting style and crust reflectivity (left); reconstructed position of the cube relative to the Outeniqua sub-basins offshore South Africa (right); dashed grey lines – rough trend of the Gondwanide orogen

The FISA cube in the Fitzroy sub-basin shows channel incisions and canyon formation occurring during the Early Cretaceous (Chapter 5). Uplift and extensive canyon formation has been documented in the Algoa and Gamtoos basins during this time (McMillan, 2003; Baby et al., 2018) and related to

movement along the AFFZ (Baby et al., 2018). A correlative study between the Lower Cretaceous sections of the two areas can provide more insights into the post-rotation syn-transform evolution of the two margins.

7.6.2 Berkeley Arch – Volunteer sub-basin structural analysis

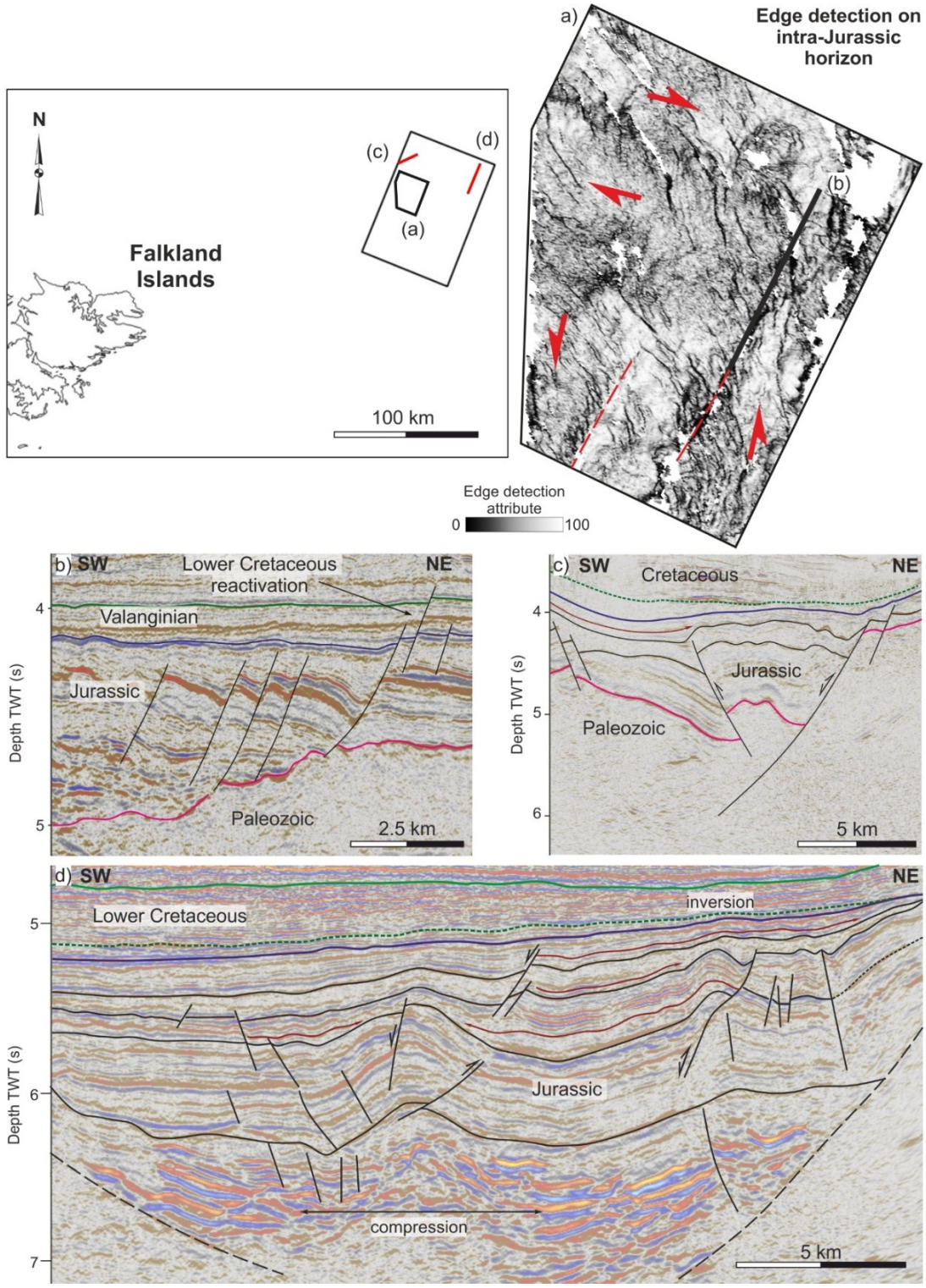

Figure 7.13 Variety of structural styles interpreted in the FINA cube, along the Berkeley Arch and Volunteer sub-basin

As mentioned above, the seismic cube along the Berkeley Arch and the Volunteer sub-basin displays a complex interplay of several fault trends with evidence of localized inversion and dextral and sinistral wrenching superimposed on the interpreted normal faults (Figures 7.12 and 7.13). A more detailed interpretation of the fault network in this area would facilitate a thorough palaeostress analysis of this region of the Falkland Plateau Basin. This would provide more information and fine-scale adjustments on the local stress variation discussed in Chapter 5.

7.6.3 Source-to-sink analysis

The source of the sediment infill of the sedimentary basins along the Falkland Plateau in correlation with sediment transport routes are crucial factors to know in order to understand the palaeogeography of an area and, for instance, the distribution and quality of petroleum system elements. Richardson et al. (2017) analysis of eroded versus deposited material for southern South Africa supports the deposition of significant sediments derived from onshore South Africa in the Falkland Plateau basins in the Late Jurassic and Early Cretaceous (Figure 7.14b). However, due to uncertainties in the reconstruction of the Falkland Plateau, it remains unclear which areas acted like sediment sources prior to this and along which pathways the sediment transport occurred. Thomson et al. (2002) documented a phase of cooling onshore the Falkland Islands during the Early to Middle Jurassic based on apatite fission track and vitrinite reflectance data. The same study correlated this cooling episode with uplift preceding the break-up of Gondwana which would result in the Falkland Islands being high ground during this time (i.e. source for sedimentation in the opening Falkland Plateau Basin; Figure 7.14a). Evidence of prograding Jurassic sediments in the north-eastern part of the Falkland Plateau Basin (Figure 7.10c) supports sediment input from the north as suggested by Richardson et al. (2017). However, more geochronological constraints and provenance studies would be required to understand the source and transport routes for the sedimentary infill of the Falkland Plateau basins in the context of the revised reconstruction presented in this thesis.

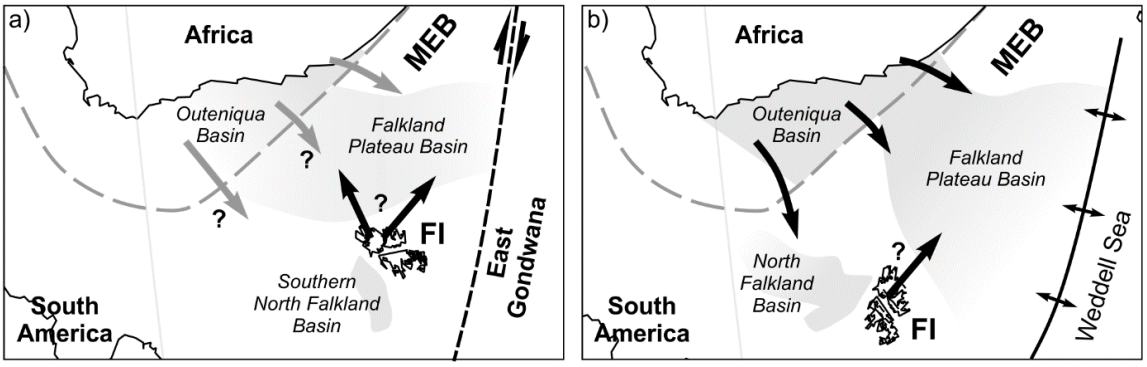

Figure 7.14 a) Middle Jurassic and b) Late Jurassic reconstruction of the Falkland Plateau showing potential sediment sources for the opening Falkland Plateau basins; black arrows in (b) from South Africa to the Falkland Plateau basins from Richardson et al. (2017); FI – Falkland Islands; MEB – Maurice Ewing Bank

7.6.4 Falkland Escarpment – Diaz Marginal Ridge study

The Falkland Escarpment has been only briefly discussed in this thesis, due to limited data along it, particularly chronological constraints. However, the development of transform marginal highs or ridges remains uncertain (Basile and Allemand, 2002; Basile, 2015 and references therein). The Falkland Escarpment and its counterpart on the conjugate Agulhas margin, the Diaz Marginal Ridge, formed at the Early Cretaceous gateway into the South Atlantic (Pérez-Díaz and Eagles, 2017). Therefore, understanding their development can offer us significant insight into how the deep oceanic connectivity was established and evolved as Gondwana dispersed. Furthermore, the sedimentary cover of the two ridges shows a strong control of the oceanic currents present in these two areas: the Agulhas Current and secondary branches of the Antarctic Circumpolar Current (Figure 7.15; Schlüter and Uenzelmann-Neben, 2007; Nicholson and Stow, 2019). A study of stratigraphic geometries above the Falkland Escarpment and the Diaz Marginal Ridge would give an indication of how these two important oceanic currents have established and evolved. The findings would build on the work of Schlüter and Uenzelmann-Neben (2007), Hall et al. (2017), Nicholson and Stow (2019), and Nicholson et al. (2020) carried out in the Agulhas Plateau, Transkei Basin, western Falkland Plateau Basin, South Falkland Basin, and Burdwood Bank. A comparative approach for the study of the two marginal ridges would be favoured in order to understand the impact the movement along the AFFZ had on palaeobathymetry. This, in turn, would provide more insight into the evolution of oceanic connectivity and the palaeoclimate, and would feed into current climate models and climate monitoring endeavours. However, as

detailed in Section 7.4.4, more chronological constraints would be needed, primarily on the Falkland side, to constrain the sedimentary section covering the Falkland Escarpment.

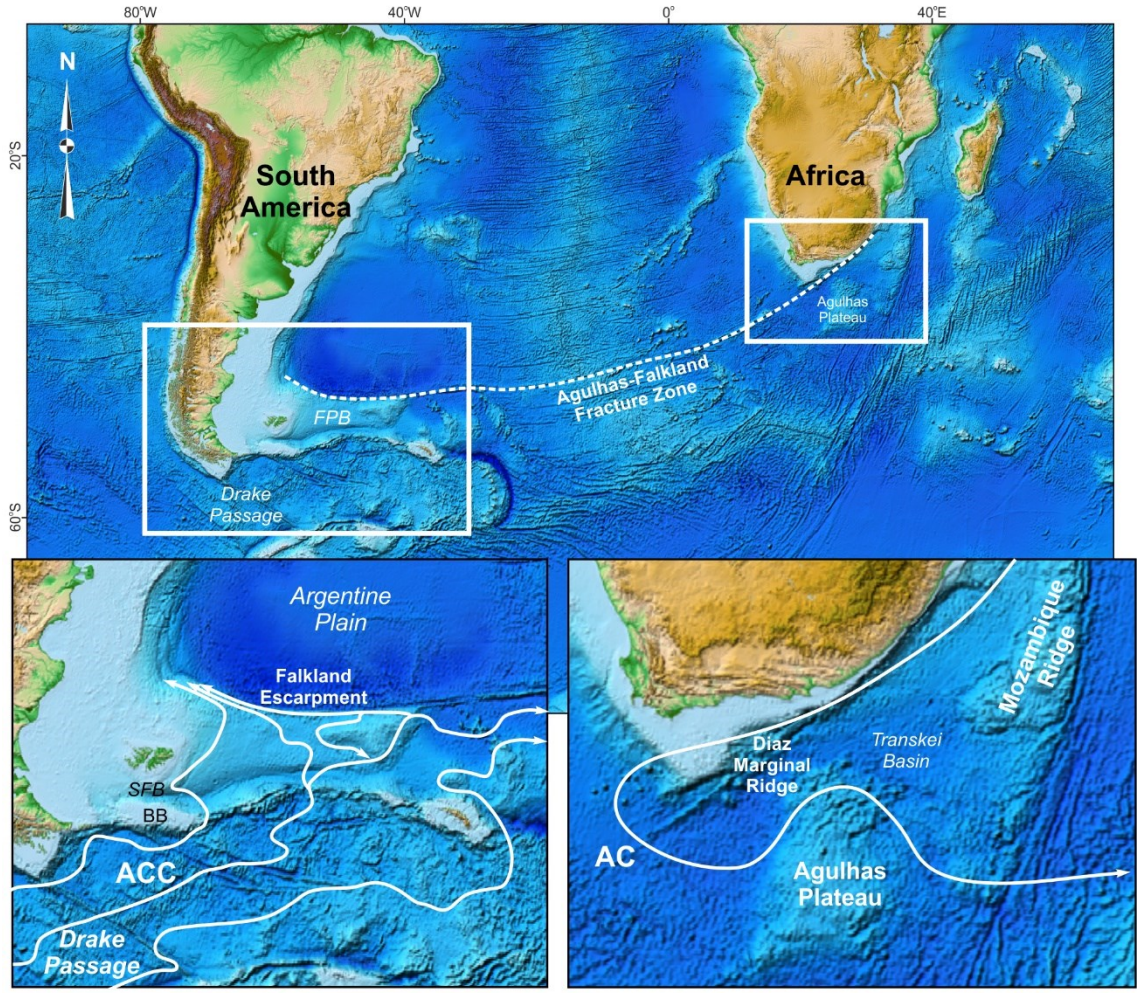

Figure 7.15 Position of the Falkland Escarpment and Diaz Marginal Ridge and the paths of the Antarctic Circumpolar Current (ACC) and Agulhas Current (AC); oceanic currents from Arhan et al. (2002), Hall et al. (2017), and Dalziel et al. (2021); BB – Burdwood Bank; FPB – Falkland Plateau Basin; SFB – South Falkland Basin

7.7 Conclusions

7.7.1 What are the implications of the reconstruction of the FIM on the fragmentation of SW Gondwana and how do microplates control regional reconstructions?

Correlations between structures on- and offshore the Falkland Islands, and on- and offshore Africa, South America, and Antarctica along with evidence for wrenching in the Falkland Plateau Basin and the deforming plates modelling

results, point towards an ~80° clockwise rotation of the Falkland Islands Microplate during the break-up of Gondwana. This, in combination with estimates on the extent of the Falkland Islands Microplate prior to break-up, suggest a more southerly reconstructed position of the islands than previously suggested, but more northward than the position allowed by current plate reconstructions of the South Atlantic (Figure 7.11). This results in more deformation of the South American plate than most recent studies argue for, which remains to be validated. Furthermore, the rotated reconstruction along with the sense of shear identified along the western margin of the Falkland Plateau Basin argues against the Skytrain evolution recently postulated for the West Antarctic region. This study highlights the importance of smaller tectonic plates in constraining the pre-break-up configuration of major plates like South America and Antarctica.

Regarding the processes related to the break-up of Gondwana, the analysis of the Falkland Plateau revealed that the fragmentation of East and West Gondwana was preceded by rapid changes in the stress configuration with alternating episodes of extension on roughly orthogonal directions resulting in complex fault and dyke networks. These extensional stages were coeval with rifting in the southern Weddell Sea, which continued in the Falkland Plateau Basin. The southern Weddell Sea rifting culminated with dextral wrenching between East and West Gondwana that initiated a clockwise rotation of the Falkland Islands Microplate. The vertical-axis rotation resulted in continental break-up and oceanic crust generation in the south-eastern corner of the Falkland Plateau Basin that underwent significant magmatic additions due to its closeness to the Weddell Sea rift axis. The Falkland Islands Microplate docked against the South American plate at the end of the Jurassic when its rotation ceased.

7.7.2 How do blocks/microplates form, rotate and deform in wrenching settings?

The delimitation of the Falkland Islands Microplate might have been controlled by inherited structures to some degree. The now western boundary could have been generated along a Paleozoic suture between the Falkland Islands and Gondwana on one side and Patagonia on the other side. The position of the remainder of the boundaries could have been facilitated by the alternating stages of extension that preceded the rotation of the islands. These generated areas of thinned crust along which strike-slip faults antithetic to the main dextral zone between East and West Gondwana nucleated.

The early stages of rotation of the Falkland Islands Microplate were controlled by the drag exerted by the southward drift of East Antarctica (edge-driven mechanism). However, as the wrenching between East and West Gondwana switched to rifting in the Jurassic, a secondary driving force is proposed to have maintained the rotation of the islands (i.e. basal mantle drag). This, in correlation with the opposite-sense of rotation but of comparable amount of the Ellsworth Whitmore Terrane in West Antarctica, points towards differential mantle flow related to differential rollback along the Panthalassan margin as the driving force maintaining the rotation of the Falkland Islands Microplate.

During the rotation, the Falkland Islands Microplate underwent intra-plate deformation at multiple scales similar to previously published models for rotating blocks. Sinistral and dextral wrenching along roughly orthogonal directions was identified across the microplate along with evidence of extension and localized compression consistent with a clockwise rotation.

7.7.3 What crustal, structural, and stratigraphical architectures can be seen along transform margins?

The architecture of the Falkland Plateau shows some similarities with other examples of transform margins documented around the globe, but its tectonic history prior to motion along the AFFZ has highly impacted its structure. Fault networks with elements indicative of wrenching (i.e. en-échelon geometries) commonly found along transform margins have been identified along the Falkland Plateau as well. However, these were initiated during the rotation of the Falkland Islands Microplate during the wrenching between East and West Gondwana and potentially later reactivated during the wrenching stage of the AFFZ. The crustal architecture of transform margins and marginal plateaus is highly varied as well and the Falkland Plateau is a clear example of this as it displays a mosaic of continental and thick oceanic crust. Volcanic additions, emplaced both before and during the wrenching and active transform phases of the AFFZ, were identified, which is a common occurrence along transform marginal plateaus. Another typical feature of transform margins is the presence of marginal ridges like the Falkland Escarpment. Uplift along these ridges can occur through different processes and in different stages of transform margin development. The stratal geometries and style of faulting point more towards flexural and thermal processes. However, few seismic lines and limited age constraints were available above the Falkland Plateau ridge to understand the nature of the vertical movements along the AFFZ with more certainty.

7.7.4 Concluding statement

The study of the Falkland Plateau has provided more evidence into its tectonic evolution and the motion of the Falkland Islands Microplate during the early fragmentation of Gondwana. Correlations between the interpreted and published structural networks offshore and onshore the Falkland Islands with the ones from South America, Africa, and Antarctica support a ~80° clockwise rotation of the islands occurring during the Middle-Late Jurassic. The rotation was facilitated by wrenching between the south-western Gondwanian tectonic plates, which led to a complex mosaic of intruded and underplated continental and thick oceanic crust underlying the Falkland Plateau Basin. The overall architecture of the Falkland Plateau shares similarities with other transform margins around the globe and supports the variability documented along marginal plateaus. The analysis of the structural network along the Falkland Islands Microplate also sheds more light onto the rapid changes in the stress state that preceded the break-up of Gondwana. The resulting fault networks correlated with the syn-rotation deformation demonstrates an applicability of current mechanisms for rotation to the case of the Falkland Islands Microplate. In addition, the processes documented along the southern margin of south-western Gondwana (e.g. subduction along the Panthalassan margin, rollback of the subducting plate, counter-clockwise rotation of the Ellsworth Whitmore Terrane) supports a geodynamic control for the Falkland Islands Microplate rotation. Lastly, discussion of how variations in the pre-break-up position of the Falkland Islands impacts the fragmentation and configuration of South America and West Antarctica highlighted the importance of understanding the evolution of microplates for building reliable regional plate models. The outcomes of this thesis build upon current knowledge on transform margins and the complex processes associated with continental break-up and pave the way for future (palaeo)climatology-related research.

References

Adie, R. J. 1952a. The Position of the Falkland Islands in a Reconstruction of Gondwanaland. Geological Magazine, 89(6), pp. 401-410. https://doi.org/10.1017/S0016756800068102

Adie, R. J. 1952b. Representatives of the Gondwana system in the Falkland Islands. In: Teichert, C. (ed.) Symposium sur le Seriés de Gondwana. 19th International Geological Congress, Algiers, pp. 385-392.

Aldiss, D. T. and Edwards, E. J. 1999. The geology of the Falkland Islands. British Geological Survey Technical Report WC/99/10. Retrieved from http://nora.nerc.ac.uk/507542/

Allmendinger, R. W. 2020. Rick Allmendinger's Stuff. Available at: http://www.geo.cornell.edu/geology/faculty/RWA/programs/stereonet.html

Amante, C. and Eakins, B.W. 2009. ETOPO1 1 Arc-Minute Global Relief Model: Procedures, Data Sources and Analysis. NOAA Technical Memorandum NESDIS NGDC-24. National Geophysical Data Center, NOAA. doi:10.7289/V5C8276M [21 August 2021].

Antobreh, A. A., Faleide, J. I., Tsikalas, F., and Planke, S. 2009. Rift-shear architecture and tectonic development of the Ghana margin deduced from multichannel seismic reflection and potential field data. Marine and Petroleum Geology, 26(3), pp. 345–368. doi: 10.1016/j.marpetgeo.2008.04.005.

Arhan, M., Naveira Garabato, A. C., Heywood, K. J., and Stevens, D. P. 2002. The Antarctic Circumpolar Current between the Falkland Island and South Georgia. Journal of Physical Oceanography, 32(6), pp. 1914–1931. doi: 10.1175/1520-0485(2002)032<1914:TACCBT>2.0.CO;2.

Armstrong, R.A., Bristow, J.W., and Cox, K.G. 1984. The Rooi Rand dyke swarm, southern Lebombo. In: Erlank, A.J. (ed.) Petrogenesis of the volcanic rocks of the Karoo province. Geological Society of South Africa, Special Publications, 13, pp. 77–86.

Attoh, K. Brown, L., Guo, J., and Heanlein, J. 2004 Seismic stratigraphic record of transpression and uplift on the Romanche transform margin, offshore Ghana. Tectonophysics, 378(1–2), pp. 1–16. doi: 10.1016/j.tecto.2003.09.026.

Baby, G., Guillocheau, F., Boulogne, C., Robin, C., and Dall'Asta, M. 2018. Uplift history of a transform continental margin revealed by the stratigraphic record : The case of the Agulhas transform margin along the Southern African Plateau DOME. Tectonophysics, 731–732, pp. 104–130. doi: 10.1016/j.tecto.2018.03.014.

Baker, H. A. 1924. Final Report on Geological Investigations in the Falkland Islands, 1920-1922. Stanley: Falkland Islands Government Printer, p. 38

Baranov, V. and Naudy, H. 1964. Numerical calculation of the formula of reduction to the magnetic pole. Geophysics, 29(1), pp. 67–79. doi: https://doi.org/10.1190/1.1439334

Baristeas, N., Anka, Z., di Primio, R., Rodriguez, J. F., Marchal, D., and Dominguez, F. 2013. New insights into the tectono-stratigraphic evolution of the Malvinas Basin, offshore of the southernmost Argentinean continental margin. Tectonophysics, 604, pp. 280–295. https://doi.org/10.1016/j.tecto.2013.06.009

Barker, P. F. and Griffiths, D. H. 1972. The Evolution of the Scotia Ridge and Scotia Sea. Philosophical Transactions of the Royal Society of London. Series A, Mathematical and Physical Sciences, 271(1213), pp. 151–183.

Barker, P. F. 1977. Correlations between Sites on the Eastern Falkland Plateau by Means of Seismic Reflection Profiles, Leg 36, DSDP. Initial Reports of the Deep Sea Drilling Project, 36. doi: 10.2973/dsdp.proc.36.128.1977.

Barker, P. F., Dalziel, I. W. D., Dinkelman, M. G., Elliot, D. H., Gombos, A. M., Jr., Lonardi, A., Plafker, G., Tarney, J., Thompson, R. W., Tjalsma, R. C., von der Borch, C. C., Wise, S. W., Jr., Harris, W. K., and Sliter, W. V. 1977. Site 330. Texas A and M University, Ocean Drilling Program, College Station, TX, United States. doi:10.2973/dsdp.proc.36.106.1977

Barker, P. F. 1999. Evidence for a volcanic rifted margin and oceanic crustal structure for the Falkland Plateau Basin. Journal of the Geological Society, 156, pp. 889–900. doi: 10.1144/gsjgs.156.5.0889.

Barker, P. F. and Thomas, E. 2004. Origin, signature and palaeoclimatic influence of the Antarctic Circumpolar Current. Earth-Science Reviews, 66(1–2), pp. 143–162. doi: 10.1016/j.earscirev.2003.10.003.

Basile, C., Mascle, J., Popoff, M., Bouillin, J. P., and Mascle, G. 1993. The Ivory Coast-Ghana transform margin: a marginal ridge structure deduced from seismic data. Tectonophysics, 222, pp. 1–19.

Basile, C., Mascle, J., Benkhelil, J., and Bouillin, J.-P. 1998 Geodynamic evolution of the Cote d'Ivoire-Ghana transform margin: an overview of Leg 159 results. Proceedings of the Ocean Drilling Program, Scientific Results, 159, pp. 101–110.

Basile, C. and Allemand, P. 2002. Erosion and flexural uplift along transform faults. Geophysical Journal International, 151(2), 646–653. https://doi.org/10.1046/j.1365-246X.2002.01805.x

Basile, C., Mascle, J., and Guiraud, R. 2005. Phanerozoic geological evolution of the Equatorial Atlantic domain. Journal of African Earth Sciences, 43(1–3), pp. 275–282. doi: 10.1016/j.jafrearsci.2005.07.011.

Basile, C., Maillard, A., Patriat, M., Gaullier, V., Loncke, L., Roest, W., Mercier de Lépinay, M., and Pattier, F. 2013. Structure and evolution of the Demerara Plateau, offshore French Guiana: Rifting, tectonic inversion and post-rift tilting at transform-divergent margins intersection. Tectonophysics, 591, pp. 16–29. doi: 10.1016/j.tecto.2012.01.010.

Basile, C. 2015. Transform continental margins - part 1: Concepts and models. Tectonophysics, 661, pp. 1–10. doi: 10.1016/j.tecto.2015.08.034.

Beck, M. E. 1976. Discordant paleomagnetic pole positions as evidence of regional shear in the western Cordillera of North America. American Journal of Science, pp. 694–712. doi: 10.2475/ajs.276.6.694.

Beckinsale, R.D., Tarney, J., Darbyshire, D.P.F., and Humm, M. J. 1977. Re-Sr and K-Ar age determinations on samples of the Falkland Plateau basement at site 330, DSDP. Initial Reports of the Deep Sea Drilling Project, 71, 36, pp. 923–927.

Bellahsen, N., Leroy, S., Autin, J., Razin, P., D'Acremont, E., Sloan, H., Pik, R., Ahmed, A., and Khanbari, K. 2013. Pre-existing oblique transfer zones

and transfer/transform relationships in continental margins: New insights from the southeastern Gulf of Aden, Socotra Island, Yemen. Tectonophysics, 607, pp. 32–50. doi: 10.1016/j.tecto.2013.07.036.

Ben-Avraham, Z., Hartnady, C. J. H., and Malan, J. A. 1993. Early tectonic extension between the Agulhas Bank and the Falkland Plateau due to the rotation of the Lafonia microplate. Earth and Planetary Science Letters, 117(1–2), pp. 43–58. https://doi.org/10.1016/0012-821X(93)90116-Q

Ben-Avraham, Z., Hartnady, C. J. H., and Kitchin, K. A. 1997. Structure and tectonics of the Agulhas-Falkland fracture zone. Tectonophysics, 282, pp. 83-98.

Benkhelil, J., Mascle, J., and Tricart, P. 1995. The Guinea continental margin: an example of a structurally complex transform margin. Tectonophysics, 248(1–2), pp. 117–137. doi: 10.1016/0040-1951(94)00246-6.

Bernard, A., Munschy, M., Rotstein, Y., and Sauter, D. 2005. Refined spreading history at the Southwest Indian Ridge for the last 96 Ma, with the aid of satellite gravity data. Geophysical Journal International, 162(3), pp. 765–778. doi: 10.1111/j.1365-246X.2005.02672.x.

Berndt, C., Mjelde, R., Planke, S., Shimamura, H., and Faleide, J. I. 2001. Controls on the tectono-magmatic evolution of a volcanic transform margin: The Vøring transform margin, NE Atlantic. Marine Geophysical Researches, 22(3), pp. 133–152. doi: 10.1023/A:1012089532282.

BHP Billiton Petroleum. 2010. Well completion report, Toroa-1, FI 61/05-1. Unpublished

Biari, Y., Klingelhoefer, F., Franke, D., Funck, T., Loncke, L., Sibuet, J. C., Basile, C., Austin, J. A., Rigoti, C. A., Sahabi, M., Benabdellouahed, M., and Roest, W. R. 2021. Structure and evolution of the Atlantic passive margins: A review of existing rifting models from wide-angle seismic data and kinematic reconstruction. Marine and Petroleum Geology, 126, p. 104898. doi: 10.1016/j.marpetgeo.2021.104898.

Bird, D. 2001. Shear margins: Continent-ocean transform and fracture zone boundaries. The Leading Edge, 20(2), p. 150. doi: 10.1190/1.1438894.

Bouhier, V. E., Franchini, M. B., Caffe, P. J., Maydagán, L., Rapela, C. W., and Paolini, M. 2017. Petrogenesis of volcanic rocks that host the world-class Ag–Pb Navidad District, North Patagonian Massif: Comparison with the Jurassic Chon Aike Volcanic Province of Patagonia, Argentina. Journal of Volcanology and Geothermal Research, 338, pp. 101–120. doi: 10.1016/j.jvolgeores.2017.03.016.

Bransden, P. J. E., Burges, P., Durham, M. J., and Hall, J. G. 1999. Evidence for multi-phase rifting in the North Falklands Basin. Geological Society, London, Special Publications, 153(1), pp. 425–443. https://doi.org/10.1144/gsl.sp.1999.153.01.26

Broad, D.S., Jungslager, E.H.A., McLachlan, I.R., and Roux, J. 2006. Offshore Mesozoic basins. In: Johnson, M.R., Anhaeusser, C.R., Thomas, R.J. (eds.) The Geology of South Africa. Geological Society of South Africa and Council for Geoscience, Johannesburg, pp. 553–571.

Bry, M., White, N., Singh, S., England, R., and Trowell, C. 2004. Anatomy and formation of oblique continental collision: South Falkland basin. Tectonics, 23(4), pp. 1–20. doi: 10.1029/2002TC001482.

Bullard, E., Everett, J. E., and Smith, A. G. 1965. The fit of the continents around the Atlantic. Philosophical Transactions of the Royal Society of London. Series A, Mathematical and Physical Sciences, 258(1088), pp. 41–51. doi: 10.1098/rsta.1965.0020.

Calais, E., Ebinger, C. J., Hartnady, C., and Nocquet, J. M. 2006. Kinematics of the East African Rift from GPS and earthquake slip vector data. Geological Society Special Publication, 259, pp. 9–22. doi: 10.1144/GSL.SP.2006.259.01.03.

Calderón, M., Prades, C. F., Hervé, F., Avendaño, V., Fanning, C. M., Massonne, H. J., Theye, T., and Simonetti, A. 2013. Petrological vestiges of the Late Jurassic-Early Cretaceous transition from rift to back-arc basin in southernmost Chile: New age and geochemical data from the Capitán Aracena, Carlos III, and Tortuga ophiolitic complexes. Geochemical Journal, 47(2), pp. 201–217. doi: 10.2343/geochemj.2.0235.

Calderón, M., Herve, F., Fuentes, F., Fosdick, J. C., Sepulveda, F., and Galaz, G. 2016. Tectonic Evolution of Paleozoic and Mesozoic Andean

Metamorphic Complexes and the Rocas Verdes Ophiolites in Southern Patagonia. In Ghiglione, M. C. (ed.) Geodynamic Evolution of the Southernmost Andes. Switzerland: Springer International Publishing, pp. 6–37. doi: 10.1007/978-3-319-39727-6.

Cande, S. C., Patriat, P., and Dyment, J. 2010. Motion between the Indian, Antarctic and African plates in the early Cenozoic. Geophysical Journal International, 183(1), pp. 127–149. doi: 10.1111/j.1365-246X.2010.04737.x.

Channell, J. E. T., Erba, E., Nakanishi, M., and Tamaki, K. 1995. Late Jurassic-early Cretaceous time scales and oceanic magnetic anomaly block models. In: Berggren, W. A. et al. (eds) Geochronology, time scales and global stratigraphic correlation. SEPM Special Publications, pp. 51–64. doi: 10.2110/pec.95.04.0051.

Chemale, F., Ramos, V. A., Naipauer, M., Girelli, T. J., and Vargas, M. 2018. Age of basement rocks from the Maurice Ewing Bank and the Falkland/Malvinas Plateau. Precambrian Research, 314, pp. 28–40. doi: 10.1016/j.precamres.2018.05.026.

Cingolani, C.A. and Varela, R. 1976. Investigaciones geolgicas y geocronologicas en el extremo sur de la Isla Gran Malvina, sector de Cabo Belgrano (Cabo Meredith), Isla Malvinas. In: Actas 6 Congreso Geologico Argentino, 1. La Asociacion Geologica Argentina, Bahia Blanca, Buenos Aires, pp. 457–480.

Clarke, J. M. 1913. Fósseis Devonianos do Paraná. Monographia do Serviço Geológico y Mineralógico do Brasil, 1, p. 353

Coffin, M. F. and Rabinowitz, P. D. 1987. Reconstruction of Madagascar and Africa: Evidence from the Davie Fracture Zone and Western Somali Basin. Journal of Geophysical Research, 92(B9), p. 9385. doi: 10.1029/jb092ib09p09385.

Collier, J. S., McDermott, C., Warner, G., Gyori, N., Schnabel, M., McDermott, K., and Horn, B. W. 2017. New constraints on the age and style of continental breakup in the South Atlantic from magnetic anomaly data. Earth and Planetary Science Letters, 477, pp. 27–40. doi: 10.1016/j.epsl.2017.08.007.

Collinson, J. W., Hammer, W. R., Askin, R. A., and Elliot, D. H. 2006. Permian-Triassic boundary in the central Transantarctic Mountains, Antarctica. Bulletin of the Geological Society of America, 118(5–6), pp. 747–763. doi: 10.1130/B25739.1.

Cordell, L. and Grauch, V.J.S. 1985. Mapping Basement Magnetization Zones from Aeromagnetic Data in the San Juan Basin, New Mexico. In: Hinze, W.J. (ed.) The Utility of Regional Gravity and Magnetic Anomaly Maps. Society of Exploration Geophysicists, Tulsa, pp. 181-197.

Courtillot, V. E. and Renne, P. R. 2003. On the ages of flood basalt events. C. R. Geoscience, 335, pp. 113–140. doi: 10.1016/S1631-0713(03)00006-3.

Covault, J. A. 2011. Submarine fans and canyon-channel systems: A review of processes, products, and models. Nature Education Knowledge, 3(10).

Crowell, J. C. and Frakes, L. A. 1972. Late Paleozoic Glaciation: Part V, Karoo Basin, South Africa. Geological Society of America Bulletin, 83, pp. 2887–2912.

Cunningham, A. P., Barker, P. F., and Tomlinson, J. S. 1998. Tectonics and sedimentary environment of the North Scotia Ridge region revealed by side-scan sonar. Journal of the Geological Society, London, 155, pp. 941–956.

Curtis, M. L., Riley, T. R., Owens, W. H., Leat, P. T., and Duncan, R. A. 2008. The form, distribution and anisotropy of magnetic susceptibility of Jurassic dykes in H.U. Sverdrupfjella, Dronning Maud Land, Antarctica. Implications for dyke swarm emplacement. Journal of Structural Geology, 30(11), pp. 1429–1447. doi: 10.1016/j.jsg.2008.08.004.

Curtis, M. L. 2001. Tectonic history of the Ellsworth Mountains, West Antarctica: Reconciling a Gondwana enigma. Bulletin of the Geological Society of America, 113(7), pp. 939–958. doi: 10.1130/0016-7606(2001)113<0939:THOTEM>2.0.CO;2.

Curtis, M. L. and Hyam, D. M. 1998. Late Palaeozoic to Mesozoic structural evolution of the Falkland Islands: a displaced segment of the Cape Fold Belt. Journal of the Geological Society, 155(1), pp. 115–129. https://doi.org/10.1144/gsjgs.155.1.0115

Curtis, M. L. and Storey, B. C. 1996. A review of geological constraints on the pre-break-up position of the Ellsworth Mountains within Gondwana: implications for Weddell Sea evolution. Geological Society, London, Special Publications, 108(1), pp. 11–30. doi: 10.1144/GSL.SP.1996.108.01.02.

Dalziel, I. W. D., Dott, R. H., Winn, R. D., and Bruhn, R. L. 1975. Tectonic relations of south Georgia island to the southernmost Andes. Bulletin of the Geological Society of America, 86(7), pp. 1034–1040. doi: 10.1130/0016-7606(1975)86<1034:TROSGI>2.0.CO;2

Dalziel, I. W. D., Lawver, L. A., and Murphy, J. B. 2000. Plumes, orogenesis, and supercontinental fragmentation. Earth and Planetary Science Letters, 178(1–2), 1–11. https://doi.org/10.1016/S0012-821X(00)00061-3

Dalziel, I. W. D. and Lawver, L. A. 2001. The lithospheric setting of the West Antarctic Ice Sheet. The West Antarctic ice sheet: behaviour and environment; Antarctic Research Series, 77, pp. 29–44.

Dalziel, I. W. D., Lawver, L. A., Norton, I. O., and Gahagan, L. M. 2013. The Scotia Arc: Genesis, Evolution, Global Significance. Annual Review of Earth and Planetary Sciences, 41(1), pp. 767–793. doi: 10.1146/annurev-earth-050212-124155.

Dalziel, I. W. D., Macdonald, D. I.M., Stone, P., and Storey, B. C. 2021. South Georgia microcontinent: Displaced fragment of the southernmost Andes. Earth-Science Reviews, 220(May), p. 103671. doi: 10.1016/j.earscirev.2021.103671.

De Beer, C.H. 1992. Structural evolution of the Cape Fold Belt syntaxis and its influence on syntectonic sedimentation in the SW Daroo Basin. In: de Wit, M.J. and Ransome, I.G.D. (eds.) Inversion Tectonics of the Cape Fold Belt, Karoo and Cretaceous Basins of Southern Africa. Balkema Publishers, Rotterdam, pp. 197–206.

De Beer, C. H. 1995. Fold interference from simultaneous shortening in different directions: the Cape Fold Belt syntaxis. Journal of African Earth Sciences, 21(1), pp. 157–169. doi: 10.1016/0899-5362(95)00084-7.

Del Ben, A. and Mallardi, A. 2004. Interpretation and choronostratigraphic mapping of multichannel seismic reflection profile I95167, Eastern Falkland Plateau (South Atlantic). Marine Geology, 209, pp. 347-361.

Dibblee, T.W. 1977. Strike-slip tectonics of the San Andreas Fault and its role in Cenozoic basin evolution. In: Sylvester, A.G. (Ed.), Wrench Fault Tectonics. American Association of Petroleum Geologists, Reprint 29, pp. 159–172.

Dodd, T. J. H. and McCarthy, D. J. 2016. The Berkley Arch: Seaward Dipping Reflectors or a missing slice of the Cape Fold Thrust Belt? In: The Roberts Conference Passive Margins. doi: 10.13140/RG.2.2.13836.97928.

Donnadieu, Y., Pucéat, E., Moiroud, M., Guillocheau, F., and Deconinck, J. F. 2016. A better-ventilated ocean triggered by Late Cretaceous changes in continental configuration. Nature Communications, 7. doi: 10.1038/ncomms10316.

Du Toit, A.L. 1927. A Geological Comparison of South America and South Africa. Carnegie Institution of Washington, Washington.

Du Toit, A.L. 1937. Our Wandering Continents. Oliver and Boyd, London.

Durrheim, R. J. 1987. Seismic reflection and refraction studies of the deep structure of the Agulhas Bank. Geophysical Journal of the Royal Astronomical Society, 89(1), pp. 395–398. https://doi.org/10.1111/j.1365-246X.1987.tb04437.x

Eagles, G. 2000. Modelling plate kinematics in the Scotia Sea. Ph.D. Thesis, University of Leeds.

Eagles, G. and König, M. 2008. A model of plate kinematics in Gondwana breakup. Geophysical Journal International, 173(2), pp. 703–717. doi: 10.1111/j.1365-246X.2008.03753.x.

Eagles, G. and Vaughan, A. P. M. 2009. Gondwana breakup and plate kinematics: Business as usual. Geophysical Research Letters, 36(10), pp. 2–5. doi: 10.1029/2009GL037552.

Eagles, G. 2019. Links to master tracks in different resolutions from POLAR 6 flight FALKLANDS_2018_1811080301. PANGAEA, https://doi.org/10.1594/PANGAEA.897432,

Eagles, G. 2019. Master tracks in different resolutions during POLAR 6 campaign FALKLANDS_2018 (AIRLAFONIA). Alfred Wegener Institute, Helmholtz Centre for Polar and Marine Research, Bremerhaven, PANGAEA, https://doi.org/10.1594/PANGAEA.897441

Eagles, G. and Eisermann, H. 2020. The Skytrain plate and tectonic evolution of southwest Gondwana since Jurassic times. Sci. Rep. Nature Publishing Group UK, 10(1), pp. 1–17. doi: 10.1038/s41598-020-77070-6.

Echaurren, A. Oliveros, V., Folguera, A., Ibarra, F., Creixell, C., and Lucassen, F. 2017. Early andean tectonomagmatic stages in North Patagonia: Insights from field and geochemical data. Journal of the Geological Society, 174(3), pp. 405–421. doi: 10.1144/jgs2016-087.

Echavarría, L. E., Schalamuk, I. B., and Etcheverry, R. O. 2005. Geologic and tectonic setting of Deseado Massif epithermal deposits, Argentina, based on El Dorado-Monserrat. Journal of South American Earth Sciences, 19(4), pp. 415–432. https://doi.org/10.1016/j.jsames.2005.06.005

Elliot, D. H. 1992. Jurassic magmatism and tectonism associated with Gondwanaland break-up: An Antarctic perspective. Geological Society, London, Special Publications, 68(68), pp. 165–184. doi: 10.1144/GSL.SP.1992.068.01.11.

Elliot, D. H., Fleming, T. H., Kyle, P. R., and Foland, K. A. 1999. Long-distance transport of magmas in the Jurassic Ferrar Large Igneous Province, Antarctica. Earth and Planetary Science Letters, 167(1–2), pp. 89–104. doi: 10.1016/S0012-821X(99)00023-0.

Elliott, G. M., Berndt, C., and Parson, L. M. 2009. The SW African volcanic rifted margin and the initiation of the Walvis Ridge, South Atlantic. Marine Geophysical Research, 30(3), pp. 207–214. doi: 10.1007/s11001-009-9077-x.

Encarnación, J., Fleming, T. H., Elliot, D. H., and Eales, H. V. 1996. Synchronous emplacement of Ferrar and Karoo dolerites and the early

breakup of Gondwana. Geology, 24(6), pp. 535–538. doi: 10.1130/0091-7613(1996)024<0535:SEOFAK>2.3.CO;2.

England, P., Houseman, G., and Sonder, L. 1985. Length Scales for Continental Deformation in Convergent, Divergent, and Strike-Slip Environments: Analytical and Approximate Solutions for a Thin Viscous Sheet Model. Journal of Geophysical Research, 90(B5), pp. 3551–3557.

Evain, M., Afilhado, A., Rigoti, C., Loureiro, A., Alves, D., Klinelhoefer, F., Schnurle, P., Feld, A., Fuck, R., Soares, J., Vinicius de Lima, M., Corela, C., Matias, L., Benabdellouahed, M., Baltzer, A., Rabineau, M., Viana, A., Moulin, M., and Aslanian, D. 2015. Deep structure of the Santos Basin-São Paulo Plateau System, SE Brazil. Journal of Geophysical Research: Solid Earth, 120, pp. 5401–5431. doi: 10.1002/2015JB012608.Received.

Evjen, H. M. 1936. The place of the vertical gradient in gravitational interpretations. Geophysics, 1(1), pp. 127-136.

Ewing, J. I., Ludwig, W. J., Ewing, M., and Eittreim, S. L. 1971. Structure of the Scotia Sea and Falkland Plateau. Journal of Geophysical Research, 76(29), pp. 7118-7137.

Falkland Oil and Gas Limited. 2013. Geological well completion report, Scotia East D, FI 31/12-1. Unpublished

Figari, E. G., Scasso, R. A., Cúneo, R. N., and Escapa, I. 2015. Estratigrafía y evolución geológica de la Cuenca de Cañadón Asfalto, Provincia del Chubut, Argentina. Latin American Journal of Sedimentology and Basin Analysis, 22(2), pp. 135–169.

Fischer, M. D., Uenzelmann-Neben, G., Jacques, G., and Werner, R. 2017. The Mozambique Ridge: a document of massive multistage magmatism. Geophysical Journal International, 208, pp. 449–467. doi: 10.1093/gji/ggw403.

Fitzgerald, M. G., Mitchum, R. M., Uliana, M. A., and Biddle, K. T. 1990. Evolution of the San Jorge Basin, Argentina. American Association of Petroleum Geologists Bulletin, 74(6), pp. 879-920.

Foulger, G. R. 2018. Origin of the South Atlantic igneous province. Journal of Volcanology and Geothermal Research, 355, pp. 2–20. doi: 10.1016/j.jvolgeores.2017.09.004.

Frakes, L. A. and Crowell, J. C. 1967. Facies and Paleogeography of Late Paleozoic Diamictite, Falkland Islands. Geological Society of America Bulletin, 78, pp. 37–58.

Frakes, L. A. and Crowell, J. C. 1968. Late Palaeozoic glacial facies and the origin of the South Atlantic Basin. Nature, 217(5131), pp. 837–838. doi: 10.1038/217837a0.

Frakes, L. A. and Crowell, J. C. 1969. Late Paleozoic Glaciation:I, South America. Geological Society of America Bulletin, 80, pp. 1007–1042.

Franzese, J., Martino, R. 1998. Aspectos cinemáticos y tectónicos de la zona de cizalla de Gastre en la sierra de Calcatapul, provincia de Chubut, Argentina. X Congreso Latinoamericano de Geología y VI Congreso Nacional de Geología Economica, Actas II, 3.

Fromm, T., Jokat, W., and Behrmann, J. H. 2017. Interaction between a hotspot and a fracture zone: The crustal structure of Walvis Ridge at 6° E. Tectonophysics, 716, pp. 108–120. doi: 10.1016/j.tecto.2017.03.001

Fullagar, P.K., Hughes, N., and Paine, J. 2000, Drilling-constrained 3D gravity interpretation. Exploration Geophysics, 31, pp. 17-23.

Fullagar, P.K., Pears, G.A., Hutton, D., and Thompson, A. 2004, 3D gravity & aeromagnetic inversion, Pillara region, W.A. Exploration Geophysics, 35, pp. 142-146.

Fullagar, P.K. and Pears, G.A. 2007, Towards Geologically Realistic Inversion. In: Proceeding of Exploration 07: Fifth Decennial International Conference on Mineral Exploration, Toronto.

Fullagar, P.K., Pears, G.A., and McMonnies, B. 2008. Constrained inversion of geological surfaces - pushing the boundaries. The Leading Edge, 27(1), pp. 98-105.

Galeazzi, J. S. 1998. Structural and Stratigraphic Evolution of the Western Malvinas Basin, Argentina. AAPG Bulletin, 82(4), pp. 596–636.

Garcia, E. S., Sandwell, D. T., and Smith, W. H. F. 2014. Retracking cryosat-2, envisat and jason-1 radar altimetry waveforms for improved gravity field recovery. Geophysical Journal International, 196(3), pp. 1402–1422. doi: 10.1093/gji/ggt469.

Garfunkel, Z. and Ron, H. 1985. Block rotation and deformation by strike-slip faults. The properties of a type of macroscopic discontinuous deformation. Journal of Geophysical Research, 90(B10), pp. 8589–8602. doi: 10.1029/JB090iB10p08589

GEBCO Compilation Group. 2020. GEBCO 2020 Grid (doi:10.5285/a29c5465-b138-234d-e053-6c86abc040b9)

Geosoft Inc. 2020. Seequent Support. Oasis Montaj [Online]. [Accessed 8 August 2021]. Available from: https://help.seequent.com/Oasis-montaj/9.9/en/Content/gxhelp/fft2con/fft2con_btwrb.htm

Geuna, S. E., Somoza, R., Vizán, H., Figari, E. G., and Rinaldi, C. A. 2000. Paleomagnetism of Jurassic and Cretaceous rocks in central Patagonia: A key to constrain the timing of rotations during the breakup of southwestern Gondwana? Earth and Planetary Science Letters, 181(1–2), pp. 145–160. doi: 10.1016/S0012-821X(00)00198-9.

Ghidella, M. E., Yáñez, G., and LaBrecque, J. L. 2002. Revised tectonic implications for the magnetic anomalies of the western Weddell Sea. Tectonophysics, 347(1–3), pp. 65–86. doi: 10.1016/S0040-1951(01)00238-4.

Ghiglione, M. C., Quinteros, J., Yagupsky, D., Bonillo-Martínez, P., Hlebszevtich, J., Ramos, V. A., Vergani, G., Figueroa, D., Quesada, S., and Zapata, y. T. 2010. Structure and tectonic history of the foreland basins of southernmost South America. Journal of South American Earth Sciences, 29(2), pp. 262–277. doi: 10.1016/j.jsames.2009.07.006.

Giorgis, S., Markley, M., and Tikoff, B. 2004. Vertical-axis rotation of rigid crustal blocks driven by mantle flow. Geological Society, London, Special Publications, 227(1), pp. 83–100. doi: 10.1144/GSL.SP.2004.227.01.05.

Glerum, A., Brune, S., Stamps, D. S., and Strecker, M. R. 2020. Victoria continental microplate dynamics controlled by the lithospheric strength

distribution of the East African Rift. Nature Communications, 11(1), pp. 1–15. doi: 10.1038/s41467-020-16176-x.

Gohl, K. and Uenzelmann-Neben, G. 2001. The crustal role of the Agulhas Plateau, southwest Indian Ocean: Evidence from seismic profiling. Geophysical Journal International, 144(3), pp. 632–646. doi: 10.1046/j.1365-246X.2001.01368.x.

Gohl, K. 2011. Growth and dispersal of a Southeast African large igneous province. South African Journal of Geology, 114. doi: 10.2113/gssajg.114.3-4.379.

Gomez, S. C. 2001. A catalogue of dykes from aeromagnetic surveys in eastern and southern Africa. Enschede: The International Institute for Aerospace Survey and Earth Sciences (ITC).

González, P. D., Tortello, M. F., Damborenea, S. E., Naipauer, M., Sato, A. M., and Varela, R. 2013. Archaeocyaths from South America: Review and a new record. Geological Journal, 48(2–3), pp. 114–125. doi: 10.1002/gj.2415.

Grunow, A. M., Kent, D. V., and Dalziel, I. W. D. 1987. Mesozoic evolution of West Antarctica and the Weddell Sea Basin: new paleomagnetic constraints. Earth and Planetary Science Letters, 86(1), pp. 16–26. doi: 10.1016/0012-821X(87)90184-1.

Grunow, A. M. 1993. New paleomagnetic data from the Antarctic Peninsula and their tectonic implications. Journal of Geophysical Research, 98(B8). doi: 10.1029/93jb01089.

Gurnis, M., Yang, T., Cannon, J., Turner, M., Williams, S., Flament, N., and Müller, R. D. 2018. Computers and Geosciences Global tectonic reconstructions with continuously deforming and evolving rigid plates. Computers and Geosciences, 116, pp. 32–41. doi: 10.1016/j.cageo.2018.04.007.

Hälbich, I. W. 1993. The Cape Fold Belt—Agulhas Bank Transect across the Gondwana Suture in southern Africa. American Geophysical Union Special Publication, 202, AGU Press, Washington.

Hall, I. R., Hemming, S.R., LeVay, L.J., Barker, S., Berke, M.A., Brentegani, L., Caley, T., Cartagena-Sierra, A., Charles, C.D., Coenen, J.J., Crespin, J.G., Franzese, A.M., Gruetzner, J., Han, X., Hines, S.K.V., Jimenez Espejo, F.J., Just, J., Koutsodendris, A., Kubota, K., Lathika, N., Norris, R.D., Periera dos Santos, T., Robinson, R., Rolinson, J.M., Simon, M.H., Tangunan, D., van der Lubbe, J.J.L., Yamane, M., and Zhang, H. 2017. Site U1475. Proceedings of the International Ocean Discovery Program 361. doi: 10.14379/iodp.proc.361.104.2017.

Harley, S. and Kelly, N. 2007. Chapter 3.2 Ancient Antarctica: The Archaean of the East Antarctic Shield. Developments in Precambrian Geology, 15, pp. 149-186.

Hastie, W. W., Watkeys, M. K., and Aubourg, C. 2014. Magma flow in dyke swarms of the Karoo LIP: Implications for the mantle plume hypothesis. Gondwana Research, 25(2), pp. 736–755. doi: 10.1016/j.gr.2013.08.010.

Heine, C., Zoethout, J., and Müller, R. D. 2013. Kinematics of the South Atlantic rift. Solid Earth, 4(2), pp. 215–253. doi: 10.5194/se-4-215-2013.

Heiskanen, W. and Moritz, H. 1967. Physical Geodesy. W.H Freeman and Co., San Fransisco and London. Geological Magazine, 104(3), pp. 302-302. doi:10.1017/S0016756800048834

Hellinger, S. J. and Sclater, J. G. 1983. Some comments on two-layer extensional models for the evolution of sedimentary basins. Journal of Geophysical Research, 88(B10), pp. 8251–8269. doi: 10.1029/JB088iB10p08251.

Henza, A. A., Withjack, M. O., and Schlische, R. W. 2010. Normal-fault development during two phases of non-coaxial extension : An experimental study. Journal of Structural Geology, 32(11), pp. 1656–1667. doi: 10.1016/j.jsg.2009.07.007.

Hodgkinson, R. 2002. Structural studies in the Falkland Islands, South Atlantic. Unpublished PhD Thesis, University of Birmingham, UK.

Hole, M. J., Ellam, R. M., Macdonald, D. I. M., and Kelley, S. P. 2016. Gondwana break-up related magmatism in the Falkland Islands. Journal of the Geological Society, 173(1), pp. 108–126. doi: 10.1144/jgs2015-027.

Homovc, J. F. and Constantini, L. 2001. Hydrocarbon exploration potential within intraplate shear-related depocenters: Deseado and San Julian basins, southern Argentina. AAPG Bulletin, 85(10), pp. 1795–1816.

Horst, A. J., Karson, J. A., and Varga, R. J. 2018. Large Rotations of Crustal Blocks in the Tjörnes Fracture Zone of Northern Iceland. Tectonics, 37(6), pp. 1607–1625. doi: 10.1002/2016TC004371.

Hubbard, R.J., Pape, J., and Roberts, D.G. 1985a. Depositional sequence mapping as a technique to establish tectonic and stratigraphic framework and evaluate hydrocarbon potential on a passive continental margin. In: Berg, O.R. and Woolverton, D. (eds) Seismic Stratigraphy II: An Integrated Approach to Hydrocarbon Exploration. American Association of Petroleum Geologists, Memoir, 39, pp. 79-91.

Hubbard, R.J., Pape, J., and Roberts, D.G. 1985b. Depositional sequence mapping to illustrate the evolution of a passive continental margin. In: Berg, O.R. and Woolverton, D. (eds) Seismic Stratigraphy II: An Integrated Approach to Hydrocarbon Exploration. American Association of Petroleum Geologists, Memoir, 39, pp. 93-115.

I'Anson, A., Elders, C., and McHarg, S. 2019. Marginal fault systems of the Northern Carnarvon Basin: Evidence for multiple Palaeozoic extension events, North-West Shelf, Australia. Marine and Petroleum Geology, 101, pp. 211–229. doi: 10.1016/j.marpetgeo.2018.11.040.

Ingersoll, R. V. and Coffey, K. T. 2017. Transrotation Induced by Crustal Blocks Moving through Restraining Double Bends, with Southern California Examples. The Journal of Geology, 125, pp. 551–559. https://doi.org/10.1086/692654

Jackson, J. and Molnar, P. 1990. Active faulting and block rotations in the western Transverse Ranges, California. Journal of Geophysical Research, 95(B13). doi: 10.1029/jb095ib13p22073.

Jacobs, J., Thomas, R. J., Armstrong, R. A., and Henjes-Kunst, F. 1999. Age and thermal evolution of the Mesoproterozoic Cape Meredith Complex, West Falkland. Journal of the Geological Society, 156(5), pp. 917–928. doi: 10.1144/gsjgs.156.5.0917.

Jacobs, J., Bauer, W., and Fanning, C. M. 2003. Late Neoproterozoic/Early Palaeozoic events in central Dronning Maud Land and significance for the southern extension of the East African Orogen into East Antarctica. Precambrian Research, 126(1–2), pp. 27–53. doi: 10.1016/S0301-9268(03)00125-6.

Jacobs, J. and Thomas, R. J. 2004. Himalayan-type indenter-escape tectonics model for the southern part of the late Neoproterozoic-early Paleozoic East African-Antarctic orogen. Geology, 32(8), pp. 721–724. doi: 10.1130/G20516.1.

Johnson, M. R. 1991. Sandstone petrography, provenance and plate tectonic setting in Gondwana context of the southeastern Cape-Karoo Basin. South African Journal of Geology, 94(2–3), pp. 137–154.

Johnston, S. T. 2000. The Cape Fold Belt and Syntaxis and the rotated Falkland Islands: dextral transpressional tectonics along the southwest margin of Gondwana. Journal of African Earth Sciences, 31(1), pp. 51-63.

Jokat, W., Boebel, T., König, M., and Meyer, U. 2003. Timing and geometry of early Gondwana breakup. Journal of Geophysical Research: Solid Earth, 108(B9). doi: 10.1029/2002jb001802.

Jordan, T. A., Ferraccioli, F., and Leat, P. T. 2017. New geophysical compilations link crustal block motion to Jurassic extension and strike-slip faulting in the Weddell Sea Rift System of West Antarctica. Gondwana Research, 42, pp. 29–48. doi: 10.1016/j.gr.2016.09.009.

Jourdan, F., Féraud, G., Bertrand, H., and Watkeys, M. K. 2007. From flood basalts to the inception of oceanization: Example from the 40Ar/ 39Ar high-resolution picture of the Karoo large igneous province. Geochemistry, Geophysics, Geosystems, 8(2). doi: 10.1029/2006GC001392.

Kerr, A. C. 2014. Oceanic Plateaus. In: Holland, H. C. and Turekian, K. (eds) Treatise on Geochemistry, Volume 3: Geochemistry of the Earth's Crust. 2nd edition. Elsevier, pp. 631–667. doi: 10.1007/978-94-007-6644-0.

Kimbell, G. S. and Richards, P. C. 2008. The three-dimensional lithospheric structure of the Falkland Plateau region based on gravity modelling.

Journal of the Geological Society, 165(4), pp. 795–806. https://doi.org/10.1144/0016-76492007-114

Kimura, H., Itoh, Y., and Tsutsumi, H. 2004. Quaternary strike-slip crustal deformation around an active fault based on paleomagnetic analysis: A case study of the Enako fault in central Japan. Earth and Planetary Science Letters, 226(3–4), pp. 321–334. doi: 10.1016/j.epsl.2004.08.003.

Kimura, H., Ishikawa, N., and Sato, H. 2011. Estimation of total lateral displacement including strike-slip offset and broader drag deformation on an active fault: Tectonic geomorphic and paleomagnetic evidence on the Tanna fault zone in central Japan. Tectonophysics, 501(1–4), pp. 87–97. doi: 10.1016/j.tecto.2011.01.016.

Klausen, M. B. 2009. The Lebombo monocline and associated feeder dyke swarm: Diagnostic of a successful and highly volcanic rifted margin? Tectonophysics, 468(1–4), pp. 42–62. doi: 10.1016/j.tecto.2008.10.012.

Klingelhöfer, F., Edwards, R. A., Hobbs, R. W., and England, R. W. 2005. Crustal structure of the NE Rockall Trough from wide-angle seismic data modelling. Journal of Geophysical Research: Solid Earth, 110(11), pp. 1–25. doi: 10.1029/2005JB003763.

König, M. and Jokat, W. 2006. The Mesozoic breakup of the Weddell Sea. Journal of Geophysical Research Solid Earth, 111(12), pp. 1–28. doi: 10.1029/2006JB004035.

Konig, M. and Jokat, W. 2010. Advanced insights into magmatism and volcanism of the potential field data. Geophysical Journal International, 180, pp. 158–180. doi: 10.1111/j.1365-246X.2009.04433.x.

Lamb, S. H. 1987. A model for tectonic rotations about a vertical axis. Earth and Planetary Science Letters, 84(1), pp. 75–86. doi: 10.1016/0012-821X(87)90178-6.

Lawrence, S. R., Johnson, M., Tubb, S. R., and Marshallsea, S. J. 1999. Tectono-stratigraphic evolution of the North Falkland region. Geological Society, London, Special Publications, 153(1), pp. 409–424. https://doi.org/10.1144/GSL.SP.1999.153.01.25

Lawver, L. A., Gahagan, L. M., and Dalziel, I. W. D. 1999. A tight fit - Early Mesozoic Gondwana, a plate reconstruction perspective. Memoirs of National Institute of Polar Research, Special Issue, 53, pp. 214–229.

Le Gall, B., Tshoso, G., Jourdan, F., Féraud, G., Bertrand, H., Tiercelin, J. J., Kampunzu, A. B., Modisi, M. P., Dyment, J., and Maia, M. 2002. 40Ar/39Ar geochronology and structural data from the giant Okavango and related mafic dyke swarms, Karoo Igneous province, Northern Botswana. Earth and Planetary Science Letters, 202(3–4), pp. 595–606. doi: 10.1016/S0012-821X(02)00763-X.

Le Gall, B., Tshoso, G., Dyment, J., Kampunzu, A. B., Jourdan, F., Féraud, G., Bertrand, H., Aubourg, C., and Vétel, W. 2005. The Okavango giant mafic dyke swarm (NE Botswana): Its structural significance within the Karoo Large Igneous Province. Journal of Structural Geology, 27(12), pp. 2234–2255. doi: 10.1016/j.jsg.2005.07.004.

Leat, P. T., Jordan, T. A., Flowerdew, M. J., Riley, T. R, Ferraccioli, F., and Whitehouse, M. J. 2018. Jurassic high heat production granites associated with the Weddell Sea rift system , Antarctica. Tectonophysics, 722, pp. 249–264. doi: 10.1016/j.tecto.2017.11.011.

Li, Y. and Oldenburg, D.W. 1996. 3D inversion of magnetic data. Geophysics, 61, pp. 394-408.

Li, Y. and Oldenburg, D.W. 1998. 3-D inversion of gravity data. Geophysics, 63, pp. 109-119.

Lindeque, A., De Wit, M. J., Ryberg, T., Weber, M., and Chevallier, L. 2011. Deep crustal profile across the Southern Karoo basin and Beattie magnetic anomaly, South Africa: An integrated interpretation with tectonic implications. South African Journal of Geology, 114(3-4), pp. 265-292. https://doi.org/10.2113/gssajg.114.3-4.265

Little, T. A. and Roberts, A. P. 1997. Distribution and magnitude of Neogene to present-day vertical-axis rotations, Pacific-Australia plate boundary zone, South Island, New Zealand. Journal of Geophysical Research, 102, pp. 20447-20468.

Lohr, T. and Underhill, J. R. 2015. Role of rift transection and punctuated subsidence in the development of the North Falkland Basin. Petroleum

Geoscience, 21(2–3), pp. 85–110. https://doi.org/10.1144/petgeo2014-050

Loncke, L., Roest, W. R., Klingelhoefer, F., Basile, C., Graindorge, D., Heuret, A., Marcaillou, B., Museur, T., Fanget, A. S., and Mercier de Lépinay, M. 2020. Transform Marginal Plateaus. Earth-Science Reviews, 203, p. 102940. doi: 10.1016/j.earscirev.2019.102940.

López De Luchi, M. G. and Rapalini, A. E. 2002. Middle Jurassic dyke swarms in the North Patagonian Massif: The Lonco trapial formation in the Sierra de Mamil Choique, Río Negro province, Argentina. Journal of South American Earth Sciences, 15(6), pp. 625–641. doi: 10.1016/S0895-9811(02)00083-4.

Lorenzo, J. M. and Mutter, J. C. 1988. Seismic stratigraphy and tectonic evolution of the Falkland/Malvinas Plateau. Revista Brasileira de Geociências, 18(2), pp. 191-200.

Lorenzo, J. M., Mutter, J. C., Larson, R. L., Buhl, P., Diebold, J. B., Alsop, J., Hopper, J., Falvey, D., Williamson, P., and Brassil, F. 1991. Development of the continent-ocean transform boundary of the southern Exmouth Plateau. Geology, 19, pp. 843–846.

Lorenzo, J. M. 1997. Sheared continent – ocean margins : an overview. Geo-Marine Letters, 17, pp. 1-3

Lorenzo, J. M. and Wessel, P. 1997. Flexure across a continent-ocean fracture zone: the northern Falkland/Malvinas Plateau, South Atlantic. Geo-Marine Letters, 17, pp. 110–118. https://doi.org/10.1007/s003670050015

Lovecchio, J. P., Rohais, S., Joseph, P., Bolatti, N. D., Kress, P. R., Gerster, R., and Ramos, V. A. 2018. Multistage rifting evolution of the Colorado basin (offshore Argentina): Evidence for extensional settings prior to the South Atlantic opening. Terra Nova, 30(5), pp. 359–368. doi: 10.1111/ter.12351.

Lovecchio, J. P., Naipauer, M., Cayo, L. E., Rohais, S., Giunta, D., Flores, G., Gerster, R., Bolatti, N. D., Joseph, P., Valencia, V. A., and Ramos, V. 2019. Rifting evolution of the Malvinas basin, offshore Argentina: New constrains from zircon U–Pb geochronology and seismic characterization.

Journal of South American Earth Sciences, 95, p. 102253. doi: 10.1016/j.jsames.2019.102253.

Lovecchio, J. P. Rohais, S., Joseph, P., Bolatti, N. D., and Ramos, V. A. 2020. Mesozoic rifting evolution of SW Gondwana: A poly-phased, subduction-related, extensional history responsible for basin formation along the Argentinean Atlantic margin. Earth-Science Reviews, 203, p. 103138. doi: 10.1016/j.earscirev.2020.103138.

Ludwig, W. J., Ewing, J. I., and Ewing, M. 1968. Structure of the Argentine continental margin. The American Association of Petroleum Geologists Bulletin, 52(12), pp. 2337–2368.

Ludwig, W. J., Windisch, C. C., Houtz, R. E., and Ewing, J. I. 1978. Structure of Falkland Plateau and Offshore Tierra del Fuego, Argentina. In: Watkins, J. S., Montadert, L. and Dickerson, P. W. (eds.) Geological and Geophysical Investigations of Continental Margins, American Association of Petroleum Geologists, Memoir, 29, pp. 125–137.

Ludwig, W.J., Krasheninnikov, V. A., Basov, I. A., Bayer, U., Bloemendal, J., Bornhold, B., Ciesielski, P., Goldstein, E. H., Robert, C., Salloway, J. C., Usher, J. L., von der Dick, H., Weaver, F. M., and Wise, S. W. 1980. Site 512. Initial Reports of the Deep Sea Drilling Project, 71.

Ludwig, W. J. 1983. Geologic Framework of the Falkland Plateau. Initial Reports of the Deep Sea Drilling Project, 71, pp. 281–293. doi: 10.2973/dsdp.proc.71.107.1983.

Ludwig, W.J., Krasheninnikov, V. A., Basov, I. A., Bayer, U., Bloemendal, J., Bornhold, B., Ciesielski, P., Goldstein, E. H., Robert, C., Salloway, J. C., Usher, J. L., von der Dick, H., Weaver, F. M., and Wise, S. W. 1983. Site 511. Initial Reports of the Deep Sea Drilling Project, 71, pp. 21–109. doi: doi:10.2973/dsdp.proc.71.102.1983.

Luyendyk, B. P., Kamerling, M. J., Terres, R. R., and Hornafius, J. S. 1985. Simple shear of southern California during Neogene time suggested by paleomagnetic declinations. Journal of Geophysical Research, 90(B14), pp. 454–466. doi: 10.1029/jb090ib14p12454.

Macdonald, D. I. M., Storey, B. C., and Thomson, J. W. 1987. South Georgia. BAS GEOMAP Series. Cambridge. doi: 10.1038/099272a0.

Macdonald, D., Gomez-Perez, I., Franzese, J., Spalletti, L., Lawver, L., Gahagan, L., Dalziel, I., Thomas, C., Trewin, N., Hole, M., and Paton, D. 2003. Mesozoic break-up of SW Gondwana: implications for regional hydrocarbon potential of the southern South Atlantic. Marine and Petroleum Geology, 20, pp. 287-308.

Macgregor, D., Argent, J., and Sansom, P. 2018. Introduction to the thematic set: Tectonics and petroleum systems of East Africa – Part II. Petroleum Geoscience, 24(3), pp. 245–246. doi: 10.1144/petgeo2018-080.

Magee, C. and Jackson, C. A. 2019. [Pre-print] How do normal faults grow above dykes? doi: 10.31223/osf.io/ahxn5

Marks, K. M. and Tikku, A. A. 2001. Cretaceous reconstructions of East Antarctica , Africa and Madagascar. Earth and Planetary Science Letters, 186, pp. 479–495.

Marshall, J. E. A. 1994. The Falkland Islands: A key element in Gondwana paleogeography. Tectonics, 13(2), pp. 499–514.

Martin, A. K., Hartnady, C. J. H., and Goodlad, S. W. 1981. A revised fit of South America and South Central Africa. Earth and Planetary Science Letters, 54(2), pp. 293–305. doi: 10.1016/0012-821X(81)90012-1.

Martin, A. K. Goodlad, S. W., Hartnady, C. J. H., and du Pleiss, A. 1982. Cretaceous palaeopositions of the Falkland Plateau relative to southern Africa using Mesozoic seafloor spreading anomalies. Geophysical Journal of the Royal Astronomical Society, 71, pp. 567–579. doi: 10.1016/0198-0254(83)90163-2.

Martin, A. K. 2006. Oppositely directed pairs of propagating rifts in back-arc basins: Double saloon door seafloor spreading during subduction rollback. Tectonics, 25(3), pp. 1–21. doi: 10.1029/2005TC001885.

Martin, A. K. 2007. Gondwana breakup via double-saloon-door rifting and seafloor spreading in a backarc basin during subduction rollback. Tectonophysics, 445(3–4), pp. 245–272. doi: 10.1016/j.tecto.2007.08.011.

Martinez, F. and Taylor, B. 1996. Backarc spreading, rifting, and microplate rotation, between transform faults in the Manus Basin. Marine Geophysical Research, 18(2–4), pp. 203–224. doi: 10.1007/BF00286078.

Marzoli, A., Renne, P. R., Piccirillo, E. M., Ernesto, M., Bellieni, G., and De Min, A. 1999. Extensive 200-million-year-old continental flood basalts of the Central Atlantic Magmatic Province. Science, 284, pp. 616–618. doi: 10.1126/science.284.5414.616.

Mascle, J. and Blarez, E. 1987. Evidence for transform margin evolution from the Ivory Coast-Ghana continental margin. Nature, 326, pp. 378-381.

Mascle, J., Mougenot, D., Blarez, E., Marinho, M., and Virlogeux, P. 1987. African transform continental margins: Examples from Guinea, the Ivory Coast and Mozambique. Geological Journal, 22(2 S), pp. 537–561. doi: 10.1002/gj.3350220632.

Maslanyj, M. P., Light, M. P.R., Greenwood, R. J., and Banks, N. L. 1992. Extension tectonics offshore Namibia and evidence for passive rifting in the South Atlantic. Marine and Petroleum Geology, 9(6), pp. 590–601. doi: 10.1016/0264-8172(92)90032-A.

McCarthy, D., Aldiss, D., Arsenikos, S., Stone, P., and Richards, P. 2017. Comment on “Geophysical evidence for a large impact structure on the Falkland (Malvinas) Plateau”. Terra Nova, 29, pp. 411–415.

McHarg, S., l’Anson, A., and Elders, C. 2018. The Permian and Carboniferous extensional history of the Northern Carnarvon Basin and its influence on Mesozoic extension. In: ASEG Extended Abstracts, pp. 1–8. doi: 10.1071/aseg2018abm3_1b.

McKenzie, D. and Jackson, J. 1986. A block model of distributed deformation by faulting. Journal of the Geological Society, 143(2), pp. 349–353. doi: 10.1144/gsjgs.143.2.0349.

McMillan, I.K., Brink, G.J., Broad, D.S., and Maier, J.J. 1997. Late Mesozoic sedimentary basins off the south coast of South Africa. In: Selly, R.C. (ed.) Sedimentary Basins of the World, 3. Elsevier, Amsterdam, 319-376.

McMillan, I. K. 2003. Foraminiferally defined biostratigraphic episodes and sedimentation pattern of the Cretaceous drift succession (Early Barremian to Late Maastrichtian) in seven basins on the South African and southern Namibian continental margin. South African Journal of Science, 99(11-12), pp. 537–576.

Mercier de Lépinay, M., Loncke, L., Basile, C., Roest, W. R., Patriat, M., Maillard, A., and De Clarens, P. 2016. Transform continental margins – Part 2: A worldwide review. Tectonophysics, 693, pp. 96–115. https://doi.org/10.1016/j.tecto.2016.05.038

Miller, H. G. and V. Singh. 1994. Potential field tilt—A new concept for location of potential field sources. Journal of Applied Geophysics, 32, pp. 213–217.

Mira Geoscience. 2019. VPutility 1.1 - User guide

Mitchell, C., Taylor, G. K., Cox, K. G., and Shaw, J. 1986. Are the Falkland Islands a rotated microplate? Nature, 319 (6049), pp. 131–134. https://doi.org/10.1038/319131a0

Mitchell, C., Ellam, R. M., and Cox, K. G. 1999. Mesozoic dolerite dykes of the Falkland Islands: petrology, petrogenesis and implications for geochemical provinciality in Gondwanaland low-Ti basaltic rocks. Journal of the Geological Society, 156, pp. 901-916.

Mitchum, R.M. Jr., Vail, P.R., and Sangree, J.B. 1977. Seismic stratigraphy and global changes of sea level; part 6, stratigraphic interpretation of seismic reflection patterns in depositional sequences. In: Payton, C. E. (ed.) Seismic Stratigraphy; Applications to Hydrocarbon Exploration. American Association of Petroleum Geologists, Memoir, 26, pp. 117-134.

Mohammed, M., Paton, D., Collier, R. E. L., Hodgson, N., and Negonga, M. 2017. Interaction of crustal heterogeneity and lithospheric processes in determining passive margin architecture on the southern Namibian margin. Geological Society, London, Special Publications, 438(1), pp. 177–193. doi: 10.1144/SP438.9.

Molnar, P. and Gipson, J.M. 1994. Very long baseline interferometry and active rotations of crustal blocks in the Western Transverse Ranges, California. Geological Society America Bulletin, 106, pp. 594-606.

Moreira, P. and Fernández, R. R. 2015. La Josefina Au-Ag deposit (Patagonia, Argentina): A Jurassic epithermal deposit formed in a hot spring environment. Ore Geology Reviews, 67, pp. 297–313.

Mosquera, A. and Ramos, V. A. 2006. Intraplate deformation in the Neuquén Embayment. Geological Society of America Special Papers, 407(05), pp. 97–123. doi: 10.1130/2006.2407(05).

Mueller, C. O. and Jokat, W. 2017. Geophysical evidence for the crustal variation and distribution of magmatism along the central coast of Mozambique. Tectonophysics, 712–713, pp. 684–703. doi: 10.1016/j.tecto.2017.06.007.

Müller, R. D., Sdrolias, M., Gaina, C., and Roest, W. R. 2008. Age, spreading rates, and spreading asymmetry of the world's ocean crust. Geochemistry, Geophysics, Geosystems, 9(4), pp. 1–19. doi: 10.1029/2007GC001743.

Müller, R. D., Zahirovic, S., Williams, S. E., Cannon, J., Seton, M., Bower, D. J., Tetley, M., Heine, C., Le Breton, E., Liu, S., Russell, S. H. J., Yang, T., Leonard, J., and Gurnis, M. 2019. A global plate model including lithospheric deformation along major rifts and orogens since the Triassic. Tectonics, 38(6), pp. 1884–1907. doi: 10.1029/2018TC005462.

Muntingh, A. 1993. Geology, prospects in Orange Basin offshore western South Africa. Oil & Gas Journal, 91(4), pp. 106–109.

Mussett, A. E. and Taylor, G. K. 1994. 40Ar-39Ar ages for dykes from the Falkland Islands with implications for the break-up of southern Gondwanaland. Journal of the Geological Society, 151(1), pp. 79–81. https://doi.org/10.1144/gsjgs.151.1.0079

Mutter, J. C., Roger Buck, W., and Zehnder, C. M. 1988. Convective partial melting: A model for the formation of thick basaltic sequences during the initiation of spreading. Journal of Geophysical Research, 93(B2), pp. 1031–1048.

Mutter, J. C. and Larson, R. L. 1989. Extension of the Exmouth Plateau, offshore northwestern Australia: deep seismic reflection/refraction evidence for simple and pure shear mechanisms. Geology, 17(1), pp. 15–18. doi: 10.1130/0091-7613(1989)017<0015:EOTEPO>2.3.CO;2.

Naipauer, M., García Morabito, E., Marques, J. C., Tunik, M., Rojas Vera, E. A., Vujovich, G. I., Pimentel, M. P., and Ramos, V. A. 2012. Intraplate Late Jurassic deformation and exhumation in western central Argentina:

Constraints from surface data and U-Pb detrital zircon ages. Tectonophysics, 524–525, pp. 59–75. doi: 10.1016/j.tecto.2011.12.017.

Nankivell, A. P. 1998. Tectonic evolution of the Southern Ocean between Antarctica, South America and Africa over the past 84 Ma. PhD Thesis. University of Oxford.

Navarrete, C., Gianni, G., Echaurren, A., Kingler, F. L., and Folguera, A. 2016. Episodic Jurassic to Lower Cretaceous intraplate compression in Central Patagonia during Gondwana breakup. Journal of Geodynamics, 102, pp. 185–201. doi: 10.1016/j.jog.2016.10.001.

Navarrete, C., Gianni, G., Christiansen, R., Kamerbeek, Y., Periale, S., and Folguera, A. 2019. Jurassic intraplate contraction of southern Patagonia: The El Tranquilo Anticline area, Deseado Massif. Journal of South American Earth Sciences, 94, p. 102224. doi: 10.1016/j.jsames.2019.102224.

Nelson, M. R. and Jones, C. H. 1987. Paleomagnetism and crustal rotations along a shear zone, Las Vegas Range, southern Nevada. Tectonics, 6(1), pp. 13–33. doi: 10.1029/TC006i001p00013.

Nemčok, M., Henk, A., Allen, R., Sikora, P. J., and Stuart, C. 2013. Continental break-up along strike-slip fault zones; observations from the equatorial Atlantic. Geological Society Special Publication, 369(1), pp. 537–556. doi: 10.1144/SP369.8.

Nemčok, M., Sinha, S. T., Doré, A. G., Lundin, E. R., Mascle, J., and Rybár, S. 2016. Mechanisms of microcontinent release associated with wrenching-involved continental break-up; a review. Geological Society, London, Special Publications, 431, pp. 323–359. doi: 10.1144/SP431.14.

Nemčok, M., Rybár, S., Sinha, S. T., Hermeston, S. A., and Ledvényiová, L. 2016. Transform margins: development, controls and petroleum systems – an introduction Dynamic development. Geological Society, London, Special Publications, pp. 1–38. doi: 10.1144/SP431.15.

Neves, M. C., Searle, R. C., and Bott, M. H. P. 2003. Easter microplate dynamics. Journal of Geophysical Research: Solid Earth, 108(B4), pp. 1–12. doi: 10.1029/2001jb000908.

Nicholson, U., Libby, S., Tappin, D. R., and McCarthy, D. 2020. The Subantarctic Front as a sedimentary conveyor belt for tsunamigenic submarine landslides. Marine Geology, 424, p. 106161. doi: 10.1016/j.margeo.2020.106161.

Nicholson, U. and Stow, D. 2019. Erosion and deposition beneath the Subantarctic Front since the Early Oligocene. Scientific Reports, 9(1), pp. 1–9. doi: 10.1038/s41598-019-45815-7.

Nguuri, T. K., Gore, J., James, D. E., Webb, S. J., Wright, C., Zengeni, T. G., Gwavava, O., Snoke, J. A., and Kaapvall Seismic Group. 2001. Crustal structure beneath southern Africa and its implications for the formation and evolution of the Kaapvaal and Zimbabwe cratons. Geophysical Research Letters, 28(13), pp. 2501–2504. https://doi.org/10.1029/2000GL012587

Nguyen, L. C., Hall, S. A., Bird, D. E., and Ball, P. J. 2016. Reconstruction of the East Africa and Antarctica continental margins. Journal of Geophysical Research: Solid Earth, (2), pp. 3782–3803. doi: 10.1002/2015JB012608.Received.

NOAA National Geophysical Data Center. 2009. ETOPO1 1 Arc-Minute Global Relief Model. NOAA National Centers for Environmental Information. Accessed 2 August 2021.

Nürnberg, D. and Müller, R. D. 1991. The tectonic evolution of the South Atlantic from Late Jurassic to present. Tectonophysics, 191(1–2), pp. 27–53. doi: 10.1016/0040-1951(91)90231-G.

Oldenburg, D., Levy, S., and Whittall, K. 1981. Wavelet estimation and deconvolution. Geophysics, 46, pp. 1528– 1542.

Oruç, B. and Keskinsezer, A. 2008. Structural setting of the northeastern Biga Peninsula (Turkey) from tilt derivatives of gravity gradient tensors and magnitude of horizontal gravity components. Pure and Applied Geophysics, 165, pp. 1913–1927.

Pángaro, F. and Ramos, V. A. 2012. Paleozoic crustal blocks of onshore and offshore central Argentina: New pieces of the southwestern Gondwana collage and their role in the accretion of Patagonia and the evolution of

Mesozoic south Atlantic sedimentary basins. Marine and Petroleum Geology, 37, pp. 162-183.

Pankhurst, R. J. and Rapela, C. W. 1998. The proto-Andean margin of Gondwana. Geological Society, London, Special Publication, 142, pp. 1–9. doi: 10.1016/s1342-937x(05)70249-5.

Pankhurst, R. J., Leat, P. T., Sruoga, P., Rapela, C. W., Márquez, M., Storey, B. C., and Riley, T. R. 1998. The Chon Aike province of Patagonia and related rocks in West Antarctica: a silicic large igneous province. Journal of Volcanology and Geothermal Research, 81(1–2), pp. 113–136. doi: 10.1016/S0377-0273(97)00070-X.

Pankhurst, R. J., Riley, T. R., Fanning, C. M., and Kelley, S. P. 2000. Episodic silicic volcanism in Patagonia and the Antarctic Peninsula: Chronology of magmatism associated with the break-up of Gondwana. Journal of Petrology, 41(5), pp. 605–625. doi: 10.1093/petrology/41.5.605.

Pankhurst, R. J., Rapela, C. W., Fanning, C. M., and Márquez, M. 2006. Gondwanide continental collision and the origin of Patagonia. Earth-Science Reviews, 76(3–4), pp. 235–257. doi: 10.1016/j.earscirev.2006.02.001.

Papini, M. and Benvenuti, M. 2008. The Toarcian-Bathonian succession of the Antsiranana Basin (NW Madagascar): Facies analysis and tectono-sedimentary history in the development of the East Africa-Madagascar conjugate margins. Journal of African Earth Sciences, 51(1), pp. 21–38. doi: 10.1016/j.jafrearsci.2007.11.003.

Parsiegla, N., Gohl, K., and Uenzelmann-Neben, G. 2007. Deep crustal structure of the sheared South African continental margin: First results of the Agulhas-Karoo Geoscience Transect. South African Journal of Geology, 110(2–3), pp. 393–406. doi: 10.2113/gssajg.110.2-3.393.

Parsiegla, N., Gohl, K., and Uenzelmann-Neben, G. 2008. The Agulhas Plateau: structure and evolution of a Large Igneous Province. Geophysical Journal International, 174(1), pp. 336–350. doi: DOI 10.1111/j.1365-246X.2008.03808.x.

Parsiegla, N., Stankiewicz, J., Gohl, K., Ryberg, T., and Uenzelmann-Neben, G. 2009. Southern African continental margin: Dynamic processes of a

transform margin. Geochemistry, Geophysics, Geosystems, 10(3). https://doi.org/10.1029/2008GC002196

Paton, D. A. and Underhill, J. R. 2004. Role of crustal anisotropy in modifying the structural and sedimentological evolution of extensional basins: The Gamtoos Basin, South Africa. Basin Research, 16(3), pp. 339–359. https://doi.org/10.1111/j.1365-2117.2004.00237.x

Paton, D. A. and Underhill, J. R. 2004. Role of crustal anisotropy in modifying the structural and sedimentological evolution of extensional basins: The Gamtoos Basin, South Africa. Basin Research, 16(3), pp. 339–359. doi: 10.1111/j.1365-2117.2004.00237.x.

Paton, D. A. 2006. Influence of crustal heterogeneity on normal fault dimensions and evolution: southern South Africa extensional system. Journal of Structural Geology, 28(5), pp. 868-886.

Paton, D. A., Macdonald, D. I. M., and Underhill, J. R. 2006. Applicability of thin or thick skinned structural models in a region of multiple inversion episodes; southern South Africa. Journal of Structural Geology, 28(11), pp. 1933–1947. https://doi.org/10.1016/j.jsg.2006.07.002

Paton, D.A., Mortimer, E.J., and Hodgson, N. 2016. The missing piece of the South Atlantic jigsaw: when continental break-up ignores crustal heterogeneity. Special Publication of the Geological Society London, 438, pp. 195-210. doi: 10.1144/SP438.8

Peace, A. L., Welford, J. K., Ball, P. J., and Nirrengarten, M. 2019. Deformable plate tectonic models of the southern North Atlantic. Journal of Geodynamics, 128, pp. 11–37. doi: 10.1016/j.jog.2019.05.005.

Peace, A. L., Phethean, J.J.J., Franke, D., Foulger, G.R., Schiffer, C., Welford, J.K., McHone, G., Rocchi, S., Schnabel, M., and Doré, A.G. 2020. A review of Pangaea dispersal and Large Igneous Provinces – In search of a causative mechanism. Earth-Science Reviews, 206, p. 102902. doi: 10.1016/j.earscirev.2019.102902.

Peacock, D. C. P., Anderson, M. W., Morris, A., and Randall, D. E. 1998. Evidence for the importance of “small” faults on block rotation. Tectonophysics, 299, pp. 1–13.

Pérez-Díaz, L. and Eagles, G. 2017. South Atlantic paleobathymetry since early Cretaceous. Scientific Reports, 7(1), pp. 1–16. doi: 10.1038/s41598-017-11959-7.

Le Pichon, X. and Fox, P. J. 1971. Marginal offsets, fracture zones, and the early opening of the North Atlantic. Journal of Geophysical Research, 76(26), pp. 6294–6308. doi: 10.1029/jb076i026p06294.

Planert, L., Behrmann, J., Jokat, W., Fromm, T., Ryberg, T., Weber, M., and Haberland, C. 2017. The wide-angle seismic image of a complex rifted margin, offshore North Namibia: Implications for the tectonics of continental breakup. Tectonophysics, 716, pp. 130–148. doi: 10.1016/j.tecto.2016.06.024.

Platt, J. P. and Becker, T. W. 2013. Kinematics of rotating panels of E-W faults in the San Andreas system: What can we tell from geodesy? Geophysical Journal International, 194(3), pp. 1295–1301. doi: 10.1093/gji/ggt189.

Platt, N. H. and Philip, P. R. 1995. Structure of the southern Falkland Islands continental shelf: initial results from new seismic data. Marine and Petroleum Geology, 12(7), pp. 759-771.

Pryer, L. L., Romine, K.K., Loutit, T.S., and Barnes, R.G. 2002. Carnarvon Basin Architecture and Structure Defined By the Integration of Mineral and Petroleum Exploration Tools and Techniques. The APPEA Journal, 42(1), pp. 287–309. doi: 10.1071/aj01016.

Rabinowitz, P. D. and Labrecque, J. 1979. The Mesozoic South Atlantic Ocean and evolution of its continental margins. Journal of Geophysical Research, 84(B11), pp. 5973–6002. doi: 10.1029/JB084iB11p05973.

Ramos, V. A. 2008. Patagonia: A Paleozoic continent adrift? Journal of South American Earth Sciences, 26(3), pp. 235–251. https://doi.org/10.1016/j.jsames.2008.06.002

Ramos, V. A., Vujovich, G., Martino, R., and Otamendi, J. 2010. Pampia: A large cratonic block missing in the Rodinia supercontinent. Journal of Geodynamics, 50(3–4), pp. 243–255. doi: 10.1016/j.jog.2010.01.019.

Ramos, V. A., Cingolani, C., Junior, F. C., Naipauer, M., and Rapalini, A. 2017. The Malvinas (Falkland) Islands revisited: The tectonic evolution of

southern Gondwana based on U-Pb and Lu-Hf detrital zircon isotopes in the Paleozoic cover. Journal of South American Earth Sciences, 76. https://doi.org/10.1016/j.jsames.2016.12.013

Rapalini, A. E. and Lopez De Luchi, M. 2000. Paleomagnetism and magnetic fabric of Middle Jurassic dykes from Western Patagonia, Argentina. Physics of the Earth and Planetary Interiors, 120(1), pp. 11–27. doi: 10.1016/S0031-9201(00)00140-0.

Rapela, C. W. and Pankhurst, R. J. 1992. The granites of northern Patagonia and the Gastre Fault System in relation to the break-up of Gondwana. Geological Society, London, Special Publications, 68(1), pp. 209–220. https://doi.org/10.1144/GSL.SP.1992.068.01.13

Reeves, C. 2000. The geophysical mapping of Mesozoic dyke swarms in southern Africa and their origin in the disruption of Gondwana. Journal of African Earth Sciences, 30(3), pp. 499–513.

Reeves, C. and De Wit, M. 2000. Making ends meet in Gondwana: Retracing the transforms of the Indian Ocean and reconnecting continental shear zones. Terra Nova, 12(6), pp. 272–280. doi: 10.1046/j.1365-3121.2000.00309.x.

Reeves, C. V., Teasdale, J. P., and Mahanjane, E. S. 2016. Insight into the Eastern Margin of Africa from a new tectonic model of the Indian Ocean. Geological Society, London, Special Publications, 431(1), pp. 299–322. https://doi.org/10.1144/SP431.12

Rex, D.C. and Tanner, P.W.G. 1982. Precambrian age for gneisses at Cape Meredith in the Falkland Islands. In: Craddock, C. (ed.) Antarctic Geoscience Symposium on Antarctic Geology and Geophysics, Madison, Wisconsin, U.S.A. University of Wisconsin Press, Madison, pp. 107–110.

Richards, P. C., Gatliff, R. W., Quinn, M. F., Fannin, N. G. T., and Williamson, J. P. 1996a. The geological evolution of the Falkland Islands continental shelf. Geological Society, London, Special Publications, 108(1), pp. 105–128. https://doi.org/10.1144/GSL.SP.1996.108.01.08

Richards, P. C., Gatliff, R. W., Quinn, M. F., and Fannin, N. G. T. 1996b. Petroleum potential of the Falkland Islands offshore area. Journal of

Petroleum Geology, 19(2), pp. 161–182. doi: 10.1111/j.1747-5457.1996.tb00423.x.

Richards, P. C. and Fannin, N. G. T. 1997. Geology of the North Falkland Basin. Journal of Petroleum Geology, 20(2), pp. 165–183. https://doi.org/10.1111/j.1747-5457.1997.tb00771.x

Richards, P. C. and Hillier, B. V. 2000. Post-drilling analysis of the North Falkland Basin-Part 1: Tectono-stratigraphic framework. Journal of Petroleum Geology, 23(3), pp. 253–272. https://doi.org/10.1111/j.1747-5457.2000.tb01019.x

Richards, P. C., Duncan, I., Phipps, C., Pickering, G., Grzywacz, J., Hoult, R., and Merritt, J. 2006. Exploring for fan and delta sandstones in the offshore Falklands basins. Journal of Petroleum Geology, 29(3), pp. 199-214.

Richards, P. C., Stone, P., Kimbell, G. S., McIntosh, W. C., and Phillips, E. R. 2013. Mesozoic magmatism in the Falkland Islands (South Atlantic) and their offshore sedimentary basins. Journal of Petroleum Geology, 36(1), pp. 61–73.

Richardson, J. C., Hodgson, D. M., Paton, D., Craven, B., Rawcliffe, A., and Lang, A. 2017. Where is my sink? Reconstruction of landscape development in southwestern Africa since the Late Jurassic. Gondwana Research, 45, pp. 43-64. https://doi.org/10.1016/j.gr.2017.01.004

Riley, T. R., Leat, P. T., Curtis, M. L., Millar, I. L., Duncan, R. A., and Fazel, A. 2005. Early – Middle Jurassic dolerite dykes from Western Dronning Maud Land (Antarctica): Identifying mantle sources in the Karoo Large Igneous Province. Journal of Petroleum Geology, 46(7), pp. 1489–1524. doi: 10.1093/petrology/egi023.

Riley, T. R., Jordan, T. A. R. M., Leat, P. T., Curtis, M. L., and Millar, I. L. 2020. Magmatism of the Weddell Sea rift system in Antarctica: Implications for the age and mechanism of rifting and early stage Gondwana breakup. Gondwana Research, 79, pp. 185-196. doi: 10.1016/j.gr.2019.09.014.

Rockhopper Exploration Plc. 2012. [In-house presentation] The East Falklands Basin. Available at:

http://ww7.investorrelations.co.uk/fogl/uploads/companypresentations/TheEastFalklandsBasin-2012DrillingProgramme.pdf

Roest, W.R., Verhoef, J., and Pilkington, M. 1992. Magnetic interpretation using the 3-D analytic signal. Geophysics, 57, pp. 116–125.

Ron, H., Freund, R., and Garfunkel, Z. 1984. Block rotation by strike-slip faulting: structural and paleomagnetic evidence. Journal of Geophysical Research, 89(B7), pp. 6256–6270.

Royer, J.-Y. and Chang, T. 1991. Evidence for Relative Motions Between the Indian and Australian Plates During the Last 20 m.y. From Plate Tectonic Reconstructions: Implications for the Deformation of the Indo-Australian Plate. Journal of Geophysical Research, 96(B7), pp. 11779–11802.

Royer, J. Y. and Rollet, N. 1997. Plate-tectonic setting of the Tasmanian region. Australian Journal of Earth Sciences, 44(5), pp. 543–560. doi: 10.1080/08120099708728336.

Sage, F., Basile, C., Mascle, J., Pontoise, B., and Whitmarsh, R. B. 2000. Crustal structure of the continent- ocean transition off the Côte d'Ivoire - Ghana transform margin: implications for thermal exchanges across the palaeotransform boundary. Geophysical Journal International, 143, pp. 662–678.

Salamon, A., Hofstetter, A., Garfunkel, Z., and Ron, H. 2003. Seismotectonics of the Sinai subplate - The eastern Mediterranean region. Geophysical Journal International, 155(1), pp. 149–173. doi: 10.1046/j.1365-246X.2003.02017.x.

Sandwell, D. T., Müller, R. D, Smith, W. H. F., Garcia, E., and R. Francis. 2014. New global marine gravity model from CryoSat-2 and Jason-1 reveals buried tectonic structure. Science, 346(6205), pp. 65-67, doi: 10.1126/science.1258213

Santos, J. O. S., Chernicoff, C. J., Zappettini, E. O., McNaughton, N. J., and Hartmann, L. A. 2019. Large geographic and temporal extensions of the Río de la Plata Craton, South America, and its metacratonic eastern margin. International Geology Review, 61(1), pp. 56–85. doi: 10.1080/00206814.2017.1405747.

Scasso, R. A. and Mendia, J. E. 1985. Rasgos estratigraficos y paleoambientales del Paleozoico de las Islas Malvinas. Asociacion Geologica Argentina, Revista XL, pp. 26–50.

Schimschal, C. M. and Jokat, W. 2017. The crustal structure of the continental margin east of the Falkland Islands. Tectonophysics, 724-725, pp. 234-253. https://doi.org/10.1016/j.tecto.2017.11.034

Schimschal, C. M. and Jokat, W. 2019a. The crustal structure of the Maurice Ewing Bank. Tectonophysics, p. 228190. doi: 10.1016/j.tecto.2019.228190.

Schimschal, C. M. and Jokat, W. 2019b. The Falkland Plateau in the context of Gondwana breakup. Gondwana Research. International Association for Gondwana Research, 68, pp. 108–115. doi: 10.1016/j.gr.2018.11.011.

Schlüter, P. and Uenzelmann-Neben, G. 2007. Seismostratigraphic analysis of the Transkei Basin: A history of deep sea current controlled sedimentation. Marine Geology, 240(1–4), pp. 99–111. doi: 10.1016/j.margeo.2007.02.015.

Schopf, J. M. 1969. Ellsworth Mountains: position in West Antarctica due to sea-floor spreading. Science, 164, pp. 63-66.

Schouten, H., Klitgord, K., and Gallo, G. 1993. Edge-driven microplate kinematics. Journal of Geophysical Research, 98(B4), pp. 6689–6701.

Schreider, A. A., Mazo, E. L., Bulychev, A. A., Schreider, A. A., Gilod, D. A., and Kulikova, M. P. 2011. The structure of the Falkland Basin's lithosphere. Oceanology, 51(5), pp. 866–875. https://doi.org/10.1134/S0001437011050171

Scrutton, R. A. 1979. On sheared passive continental margins. Tectonophysics, 59, pp. 293–305.

Searle, R. C., Bird, R. T., Rusby, R. I., and Naar, D. F. 1993. The development of two oceanic microplates: Easter and Juan Fernandez microplates, East Pacific Rise. Journal of the Geological Society, 150(5), pp. 965–976. doi: 10.1144/gsjgs.150.5.0965.

Sengör, A. M. and Burke, K. 1978. Relative timing of rifting and volcanism on Earth and its tectonic implications. Geophysical Research Letters, 5(6), pp. 419–421.

Seton, M., Müller, R. D., Zahirovic, S., Gaina, C., Torsvik, T., Shephard, G., Talsma, A., Gurnis, M., Turner, M., Maus, S., and Chandler, M. 2012. Global continental and ocean basin reconstructions since 200 Ma. Earth Science Reviews, 113(3–4), pp. 212–270. doi: 10.1016/j.earscirev.2012.03.002.

Shone, R.W., Nolte, C.C., and Booth, P.W.K. 1990. Pre-Cape rocks of the Gamtoos area - a complex tectonostratigraphic package preserved as a horst block. South African Journal of Geology, 93, pp. 616-621.

Smith, W. H. F. and Sandwell, D. T. 1997. Global seafloor topography from satellite altimetry and ship depth soundings. Science, v. 277, pp. 1957-1962.

Soares F., J. R. S., Miranda, A. P., and de Figueiredo, A. M. F. 2000. Geological and geophysical interpretation of the San Julian basin-offshore Argentina. Geophysical Monograph Series, 115, pp. 193–209. https://doi.org/10.1029/GM115p0193

Somoza, R., Vizán, H., and Taylor, G. K. 2008. Tectonic rotations in the Deseado Massif, southern Patagonia, during the breakup of Western Gondwana. Tectonophysics, 460(1–4), pp. 178–185. doi: 10.1016/j.tecto.2008.08.004.

Sonder, L. J., Jones, C. H., Salyards, S. L., and Murphy, K. M. 1994. Vertical axis rotations in the Las Vegas Valley Shear Zone, southern Nevada: Paleomagnetic constraints on kinematics and dynamics of block rotations. Tectonics, 13(4), pp. 769–788. doi: 10.1029/94TC00352.

Stanca, R. M., Paton, D. A., Hodgson, D. M., McCarthy, D. J., and Mortimer, E. J. 2019. A revised position for the rotated Falkland Islands microplate. Journal of the Geological Society London, 176, pp. 417–429.

Stankiewicz, J. and De Wit, M. 2013. 3.5 billion years of reshaped Moho, southern Africa. Tectonophysics, 609, pp. 675–689. https://doi.org/10.1016/j.tecto.2013.08.033

Stankiewicz, J., Parsiegla, N., Ryberg, T., Gohl, K., Weckmann, U., Trumbull, R., and Weber, M. 2008. Crustal structure of the southern margin of the African continent: Results from geophysical experiments. Journal of Geophysical Research: Solid Earth, 113(10), pp. 1–15. https://doi.org/10.1029/2008JB005612

Sternai, P., Jolivet, L., Menant, A., Gerya, T. 2014. Driving the upper plate surface deformation by slab rollback and mantle flow. Earth and Planetary Science Letters, 405, pp. 110–118. doi: 10.1016/j.epsl.2014.08.023.

Stone, P. and Thomson, M. R. 2005. Archaeocyathan limestone blocks of likely Antarctic origin in Gondwanan tillite from the Falkland Islands. Geological Society, London, Special Publications, 246(1), pp. 347–357. https://doi.org/10.1144/GSL.SP.2005.246.01.14

Stone, P., Richards, P. C., Kimbell, G. S., Esser, R. P., and Reeves, D. 2008. Cretaceous dykes discovered in the Falkland Islands: implications for regional tectonics in the South Atlantic. Journal of the Geological Society, 165(1), pp. 1–4. https://doi.org/10.1144/0016-76492007-072

Stone, P., Kimbell, G. S., and Richards, P. C. 2009. Rotation of the Falklands microplate reassessed after recognition of discrete Jurassic and Cretaceous dyke swarms. Petroleum Geosciences, 15(3), pp. 279–287.

Stone, P., Thomson, M. R. A., and Rushton, A. W. A. 2012. An Early Cambrian archaeocyath–trilobite fauna in limestone erratics from the Upper Carboniferous Fitzroy Tillite Formation, Falkland Islands. Earth and Environmental Science Transactions of the Royal Society of Edinburgh, 102, pp. 201–225.

Stone, P. 2015. Geological exploration of South Atlantic islands and its contributions to the continental drift debate of the early 20th century. Proceedings of the Geologists' Association, 126(2), pp. 266–281. https://doi.org/10.1016/j.pgeola.2015.01.001

Stone, P. 2016. Geology reviewed for the Falkland Islands and their offshore sedimentary basins, South Atlantic Ocean. Earth and Environmental Science Transactions of the Royal Society of Edinburgh, 106(2), pp. 115–143. https://doi.org/10.1017/S1755691016000049

Storey, B. C., Alabaster, T., Hole, M. J., Pankhurst, R. J., and Wever, H. E. 1992. Role of subduction-plate boundary forces during the initial stages of Gondwana break-up: Evidence from the proto-Pacific margin of Antarctica. Geological Society Special Publication, 68(68), pp. 149–163. doi: 10.1144/GSL.SP.1992.068.01.10.

Storey, B. C. 1995. The role of mantle plumes in continental breakup: case histories from Gondwanaland. Nature, 377, pp. 301–308.

Storey, B. C., Curtis, M. L., Ferris, J. K., Hunter, M. A., and Livermore, R. A. 1999. Reconstruction and break-out model for the Falkland Islands within Gondwana. Journal of African Earth Sciences, 29(1), pp. 153–163.

Szatmari, P. and Milani, E. J. 1999. Microplate rotation in northeast Brazil during South Atlantic rifting: Analogies with the Sinai microplate. Geology, 27(12), pp. 1115–1118. doi: 10.1130/0091-7613(1999)027<1115:MRINBD>2.3.CO;2.

Talwani, M., Worzel, J. L., and Landisman, M. 1959. Rapid Gravity Computations for Two-Dimensional Bodies with Application to the Mendocino Submarine Fracture Zone. Journal of Geophysical Research, 64(1), pp. 49-59, doi:10.1029/JZ064i001p00049.

Talwani, M. and Heirtzler, J. R. 1964. Computation of magnetic anomalies caused by two dimensional structures of arbitrary shape. Computers in the mineral industries, part 1: Stanford University publications. Geol. Sciences, 1, pp. 464–480.

Tankard, A.J., Jackson, M.P.A., Eriksson, K.A., Hobday, D.K., Hunter, D.R., and Minter, W.E.L. 1982. Crustal Evolution of Southern Africa. Spring-Verlag, New York.

Tankard, A., Welsink, H., Aukes, P., Newton, R., and Stettler, E. 2009. Tectonic evolution of the Cape and Karoo basins of South Africa. Marine and Petroleum Geology, 26(8), pp. 1379–1412. https://doi.org/10.1016/j.marpetgeo.2009.01.022

Tarney, J. 1977. Petrology, mineralogy, and geochemistry of the Falkland Plateau basement rocks, site 330, Deep Sea Drilling Project. Initial Reports of the Deep Sea Drilling Project, 36, pp. 893–921.

Tassone, A., Lodolo, E., Menichetti, M., Yagupsky, D., Caffau, M., and Vilas, J. F. 2008. Seismostratigraphic and structural setting of the Malvinas Basin and its southern margin (Tierra del Fuego Atlantic offshore). Geologica Acta, 6(1), pp. 55–67.

Taylor, G. K. and Shaw, J. 1989. The Falkland Islands: New palaeomagnetic data and their origin as a displaced terrane from Southern Africa. Deep Structure and Past Kinematics of Accreted Terranes, 50, pp. 59-72.

Thistlewood, L., Leat, P. T., Millar, I. L., Storey, B. C., and Vaughan, A. P. M. 1997. Basement geology and Palaeozoic-Mesozoic mafic dykes from the Cape Meredith Complex, Falkland Islands: a record of repeated intracontinental extension. Geological Magazine, 134(3), pp. 355-367.

Thistlewood, L. and Randall, D. 1998. Palaeomagnetic studies of West Gondwanan microplates. Journal of African Earth Sciences, 27 (1A: Gondwana 10: Event Stratigraphies of Gondwana (abstracts)), p. 227.

Thomas, R.J., Von Veh, M.W., and McCourt, S. 1993. The tectonic evolution of southern Africa: an overview. Journal of African Earth Sciences, 16, pp. 5-24.

Thomas, R. J., Jacobs, J., and Weber, K. 1997. Geology of the Mesoproterozoic Cape Meredith Complex, West Falkland. The Antarctica Region, Geological Evolution and Processes, pp. 21–30.

Thomas, R. J., Jacobs, J., and Eglington, B. M. 2000. Geochemistry and isotopic evolution of the Mesoproterozoic Cape Meredith Complex, West Falkland. Geological Magazine, 137(5), pp. 537–553. doi: 10.1017/S0016756800004519.

Thompson, R. W. 1977. Mesozoic Sedimentation on the Eastern Falkland Plateau. Initial Reports of the Deep Sea Drilling Project, 36, 36, p. 877891. doi: 10.2973/dsdp.proc.36.122.1977.

Thomson, K. 1998. When did the Falklands rotate? Marine and Petroleum Geology, 15(8), pp. 723-736

Thomson, K. and Underhill, J.R. 1999. Frontier exploration in the South Atlantic: structural prospectivity in the North Falkland Basin. AAPG bulletin, 83(5), pp. 778-797.

Thomson, K., Hegarty, K. A., Marshallsea, S. J., and Green, P. F. 2002. Thermal and tectonic evolution of the Falkland Islands: Implications for hydrocarbon exploration in the adjacent offshore region. Marine and Petroleum Geology, 19(2), pp. 95–116. doi: 10.1016/S0264-8172(02)00005-3.

Tinker, J., de Wit, M., and Brown, R. 2008. Mesozoic exhumation of the southern Cape, South Africa, quantified using apatite fission track thermochronology. Tectonophysics, 455(1–4), pp. 77–93. https://doi.org/10.1016/j.tecto.2007.10.009

Torsvik, T. H., Rousse, S., Labails, C., and Smethurst, M. A. 2009. A new scheme for the opening of the South Atlantic Ocean and the dissection of an Aptian salt basin. Geophysical Journal International, 177(3), pp. 1315–1333. doi: 10.1111/j.1365-246X.2009.04137.x.

Trewin, N. H., Macdonald, D. I. M., and Thomas, C. G. C. 2002. Stratigraphy and sedimentology of the Permian of the Falkland Islands; lithostratigraphic and palaeoenvironmental links with South Africa. Journal of the Geological Society, 159(1), pp. 5–19. https://doi.org/10.1144/0016-764900-089

Trouw, R. A. J. and De Wit, M. J. 1999. Relation between the Gondwanide Orogen and contemporaneous intracratonic deformation. Journal of African Earth Sciences, 28(1), pp. 203–213. https://doi.org/10.1016/S0899-5362(99)00024-X

Trumbull, R. B., Reid, D. L., de Beer, C., van Acken, D., and Romer, R. L. 2007. Magmatism and continental breakup at the west margin of southern Africa: A geochemical comparison of dolerite dikes from northwestern Namibia and the Western Cape. South African Journal of Geology, 110(2–3), pp. 477–502. doi: 10.2113/gssajg.110.2-3.477.

Uchupi, E. 1989. The tectonic style of the atlantic mesozoic rift system. Journal of African Earth Sciences, 8(2–4), pp. 143–164. doi: 10.1016/S0899-5362(89)80021-1.

Uliana, M. A., Biddle, K., and Cerdán, J. 1989. Mesozoic extension and the formation of Argentina sedimentary basins. Extensional Tectonics and

Stratigraphy of the North Atlantic Margin. AAPG Memoir, 46(3), pp. 599–613.

Van Hinsbergen, D. J. J., Buiter, S. J. H., Torsvik, T. H., Gaina, C., and Webb, S. J. 2011. The formation and evolution of Africa from the Archaean to present: Introduction. Geological Society, London, Special Publication, 357(1), pp. 1–8. doi: 10.1144/SP357.1.

Vargas, M. R. de, Chemale, F., and Girelli, T. 2021. Remnant of upper granulite continental crust in the Maurice Ewing Bank Complex (DSDP site 330, east Falkland-Malvinas Plateau) and role in Grenville orogeny. Lithos, 386–387, p. 106041. doi: 10.1016/j.lithos.2021.106041.

Veevers, J. J., Cole, D. I., and Cowan, E. J. 1994. Southern Africa: Karoo Basin and Cape Fold Belt. Geological Society of America, Memoir, 184, pp. 223–279. https://doi.org/10.1130/MEM184-p223

Verduzco, B., Fairhead, J. D., Green, C. M., and MacKenzie, C. 2004. The meter reader—New insights into magnetic derivatives for structural mapping. The Leading Edge, 23, pp. 116–119.

Von Gosen, W. 2003. Thrust tectonics in the North Patagonian Massif (Argentina): Implications for a Patagonia plate. Tectonics, 22(1). https://doi.org/10.1029/2001TC901039

Von Gosen, W. and Loske, W. 2004. Tectonic history of the Calcatapul Formation, Chubut province, Argentina, and the “Gastre fault system.” Journal of South American Earth Sciences, 18(1), pp. 73–88. https://doi.org/10.1016/j.jsames.2004.08.007

Vorster, C., Kramers, J., Beukes, N., and van Niekerk, H. 2016. Detrital zircon U-Pb ages of the Palaeozoic Natal Group and Msikaba Formation, Kwazulu-Natal, South Africa: Provenance areas in context of Gondwana. Geological Magazine, 153(3), pp. 460–486. doi: 10.1017/S0016756815000370.

Watts, D. R. and Bramall, A. M. 1981. Palaeomagnetic evidence for a displaced terrain in Western Antarctica. Nature, 293(5834), pp. 638–640. doi: 10.1038/293638a0.

Weber, M., Abu-Ayyash, K., Abueladas, A., Agnon, A., Al-Amoush, H., Babeyko, A., Bartov, Y., Baumann, M., Ben-Avraham, Z., Bock, G., Bribach, J., El-Kelani, R., Förster, A., Förster, H. J., Frieslander, U., Garfunkel, Z., Grunewald, S., Götze, H. J., Haak, V., Haberland, C., Hassouneh, M., Helwig, S., Hofstetter, A., Jäckel, K. H., Kesten, D., Kind, R., Maercklin, N., Mechie, J., Mohsen, A., Neubauer, F. M., Oberhänsli, R., Qabbani, I., Ritter, O., Rümpker, G., Rybakov, M., Ryberg, T., Scherbaum, F., Schmidt, J., Schulze, A., Sobolev, S., Stiller, M., Thoss, H., Weckmann, U., and Wylegalla, K. 2004. The crustal structure of the Dead Sea transform. Geophysical Journal International, 156(3), pp. 655–681. doi: 10.1111/j.1365-246X.2004.02143.x.

Weber, M., Abu-Ayyash, K., Abueladas, A., Agnon, A., Alasonati-Tašárová, Z., Al-Zubi, H., Babeyko, A., Bartov, Y., Bauer, K., Becken, M., Bedrosian, P. A., Ben-Avraham, Z., Bock, G., Bohnhoff, M., Bribach, J., Dulski, P., Ebbing, J., El-Kelani, R., Förster, A., Förster, H. J., Frieslander, U., Garfunkel, Z., Goetze, H. J., Haak, V., Haberland, C., Hassouneh, M., Helwig, S., Hofstetter, A., Hoffmann-Rotrie, A., Jäckel, K. H., Janssen, C., Jaser, D., Kesten, D., Khatib, M., Kind, R., Koch, O., Koulakov, I., Laske, G., Maercklin, N., Masarweh, R., Masri, A., Matar, A., Mechie, J., Meqbel, N., Plessen, B., Möller, P., Mohsen, A., Oberhänsli, R., Oreshin, S., Petrunin, A., Qabbani, I., Rabba, I., Ritter, O., Romer, R. L., Rümpker, G., Rybakov, M., Ryberg, T., Saul, J., Scherbaum, F., Schmidt, S., Schulze, A., Sobolev, S. V., Stiller, M., Stromeyer, D., Tarawneh, K., Trela, C., Weckmann, U., Wetzel, U., and Wylegalla, K. 2009. Anatomy of the Dead Sea Transform from lithospheric to microscopic scale. Reviews of Geophysics, 47(2), pp. 1–44. doi: 10.1029/2008RG000264.

Withjack, M. and Jamison, W. R. 1986. Deformation produced by oblique rifting. Tectonophysics, 126, pp. 99–124.

Won, I. J. and Bevis, M. 1987. Computing the gravitational and magnetic anomalies due to a polygon: Algorithms and Fortran subroutines. Geophysics, 52(2), pp. 232–238. https://doi.org/10.1190/1.1442298

Wright, J. B. 1976. Fracture systems in Nigeria and initiation of fracture zones in the South Atlantic. Tectonophysics, 34, pp. 43–47.

Zhang, J., Luo, Y., and Chen, J. 2020. Oceanic Plateau Formation Implied by Ontong Java Plateau, Kerguelen Plateau and Shatsky Rise. Journal of

Ocean University of China, 19(2), pp. 351–360. doi: 10.1007/s11802-020-4246-2.

Appendix

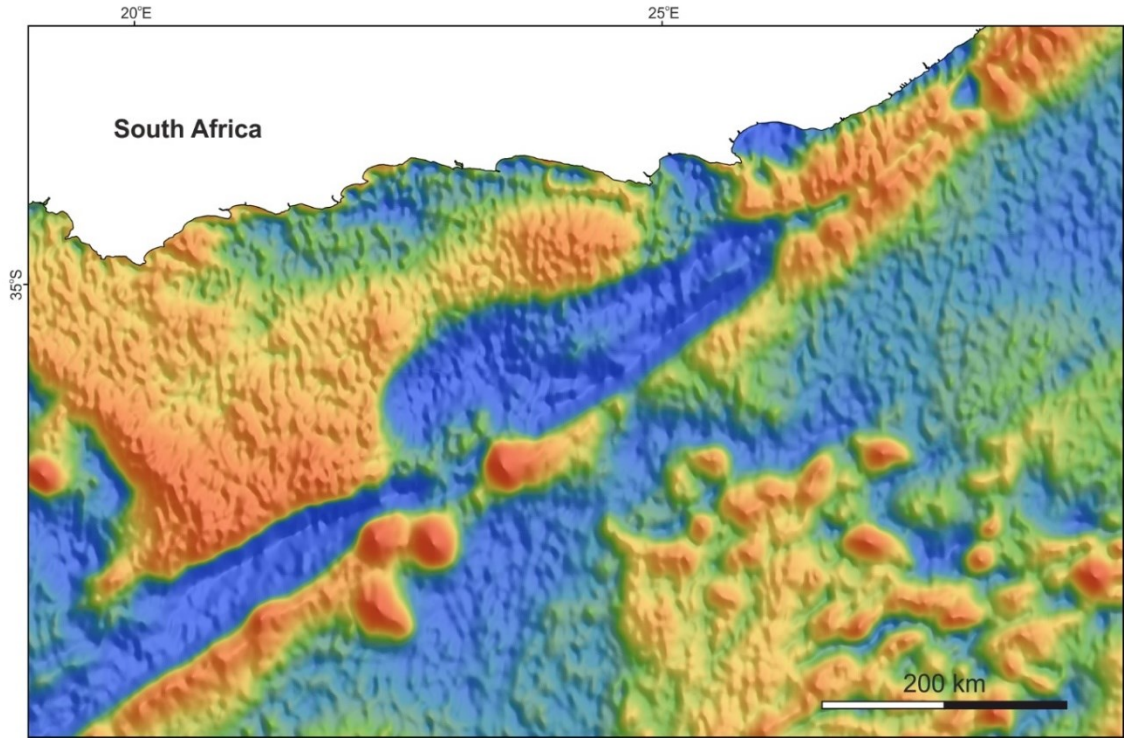

Figure A.1 Free-air gravity anomaly offshore South Africa (Sandwell et al., 2014)

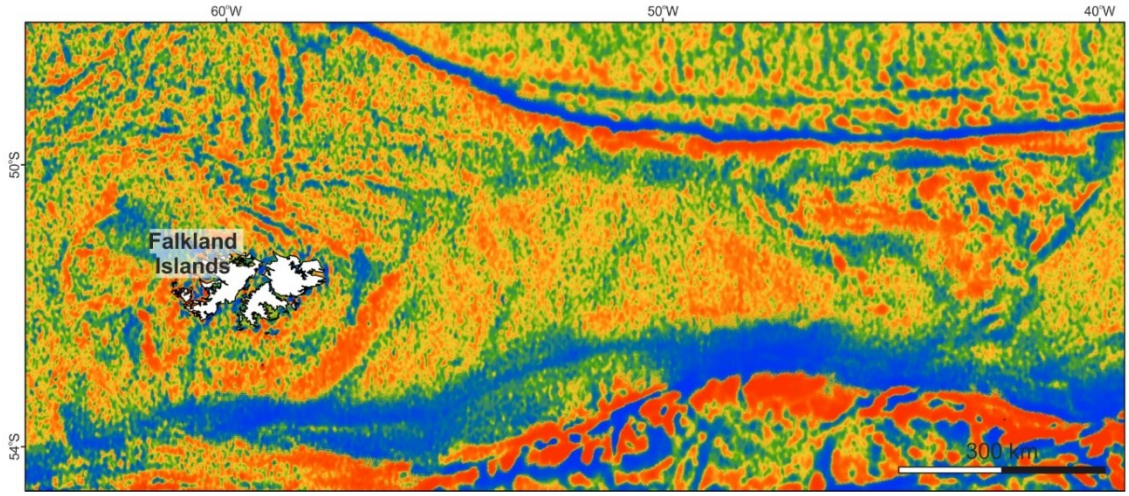

Figure A.2 First vertical derivative of the free-air gravity anomaly along the Falkland Plateau (Sandwell et al., 2014)

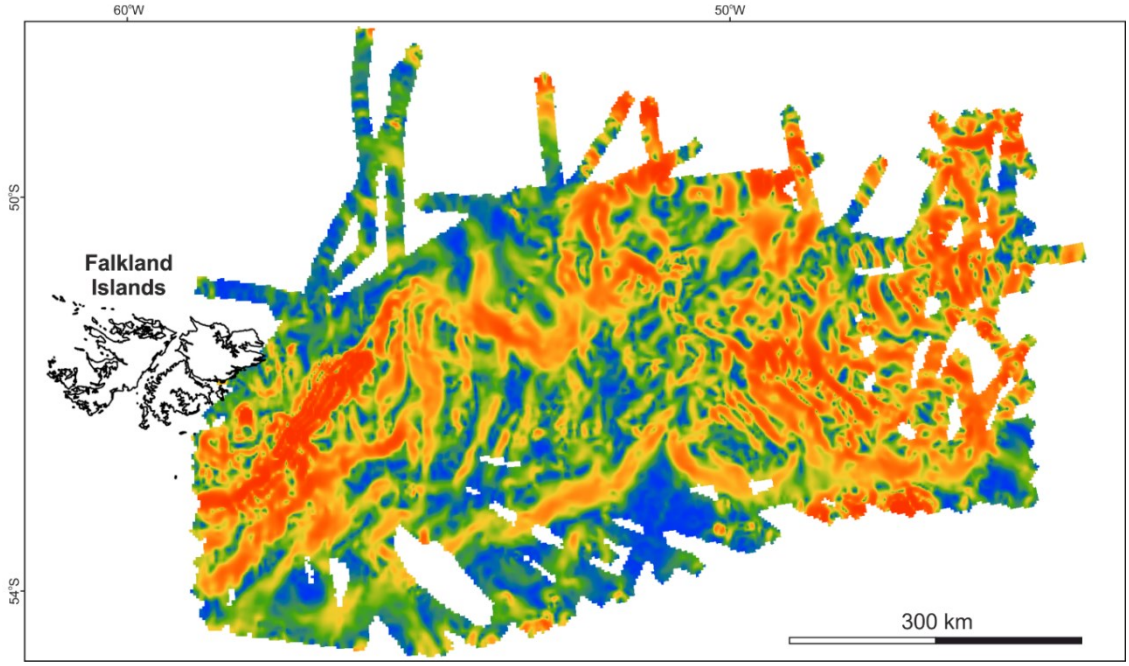

Figure A.3 Total horizontal derivative of the reduced to pole total field magnetic anomaly (Eagles, 2019)

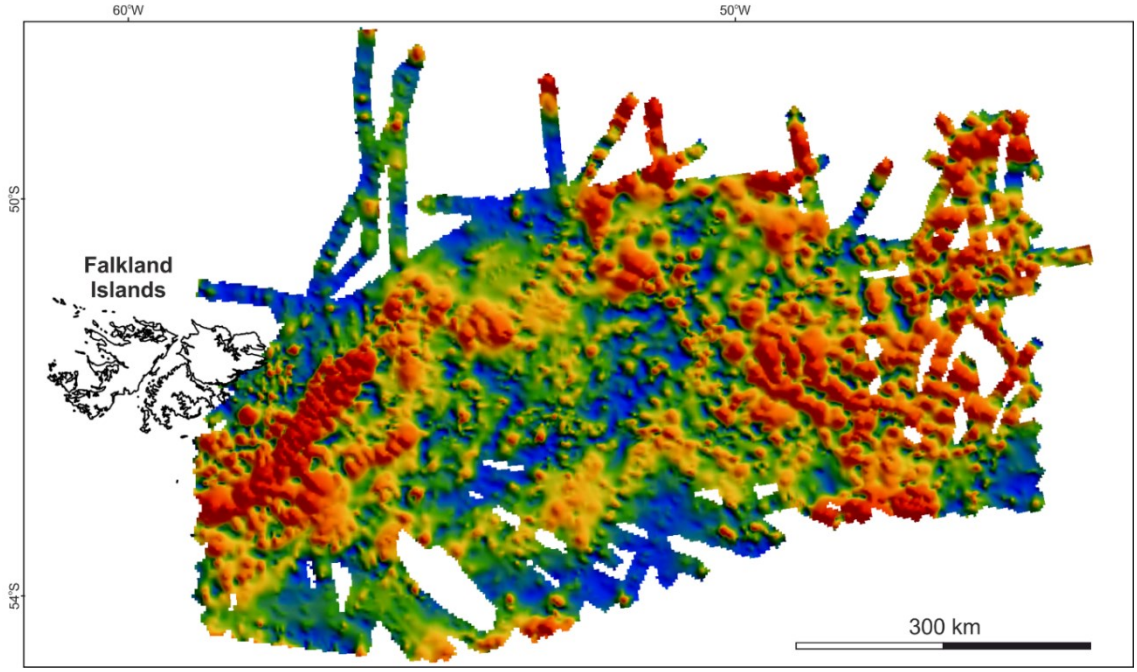

Figure A.4 Analytic signal of the total field magnetic anomaly (Eagles, 2019)

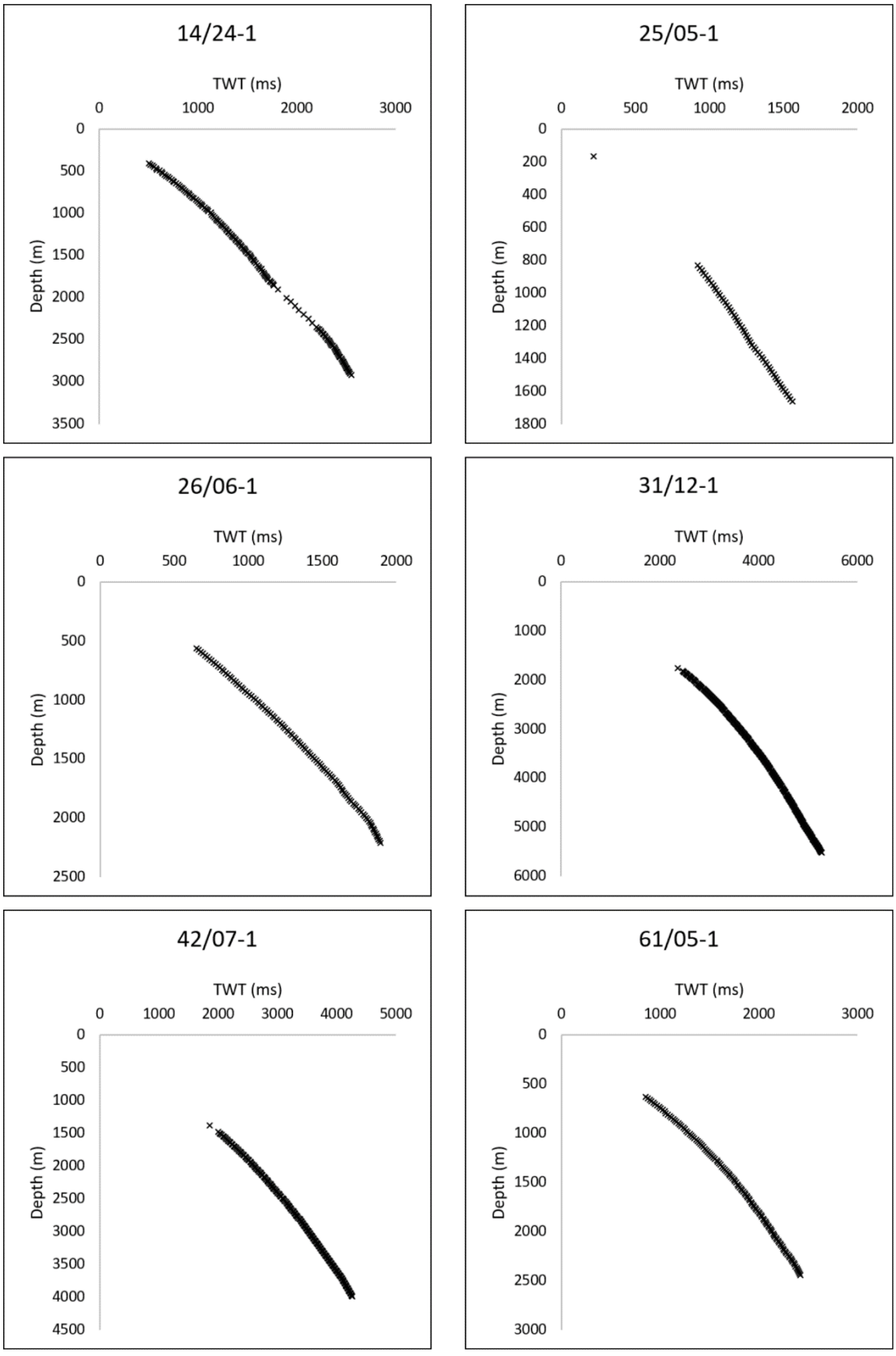

Figure A.5 Time-depth relationships available for the used wells

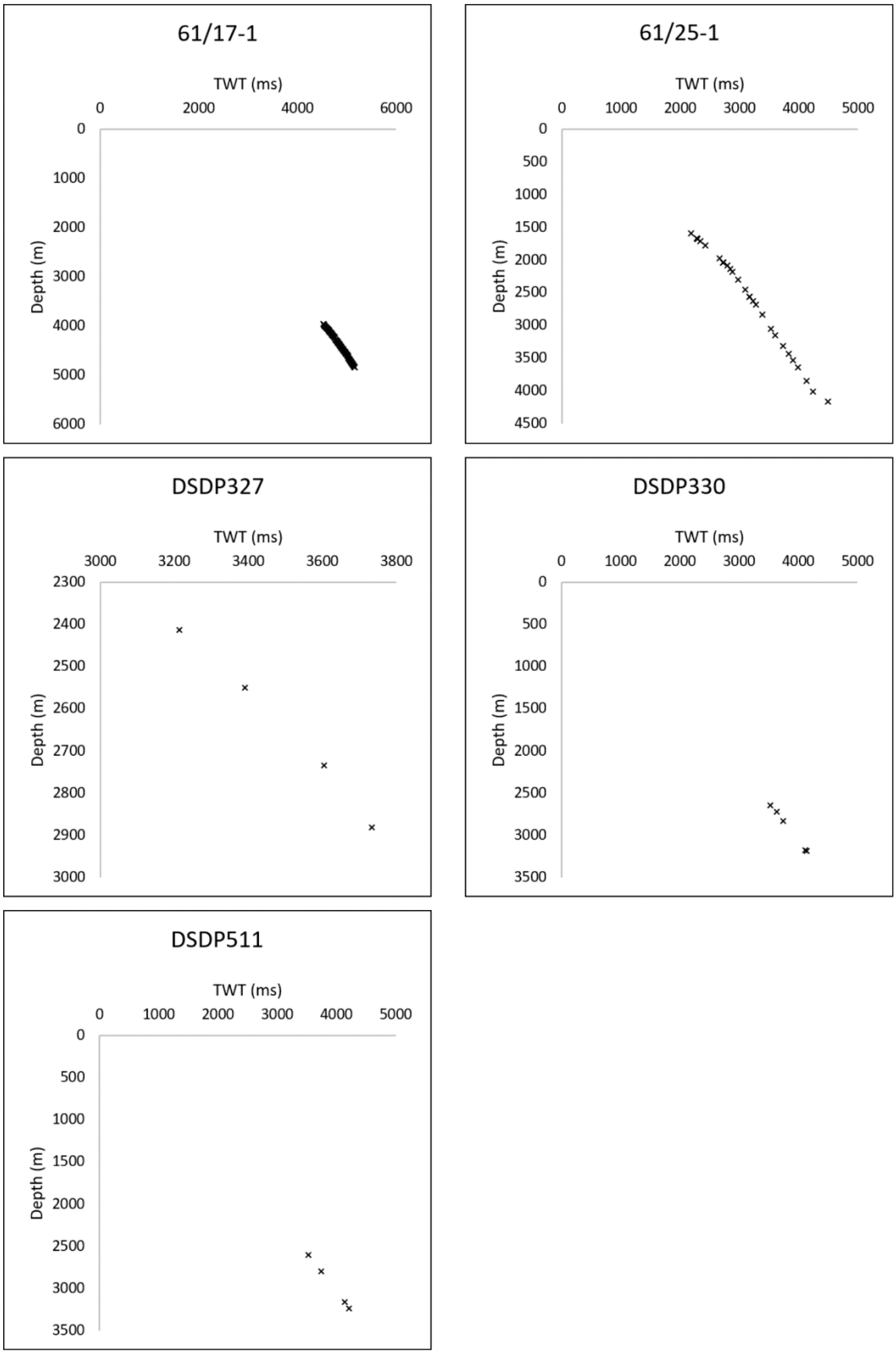

Figure A.5 (continuation) Time-depth relationships available for the used wells

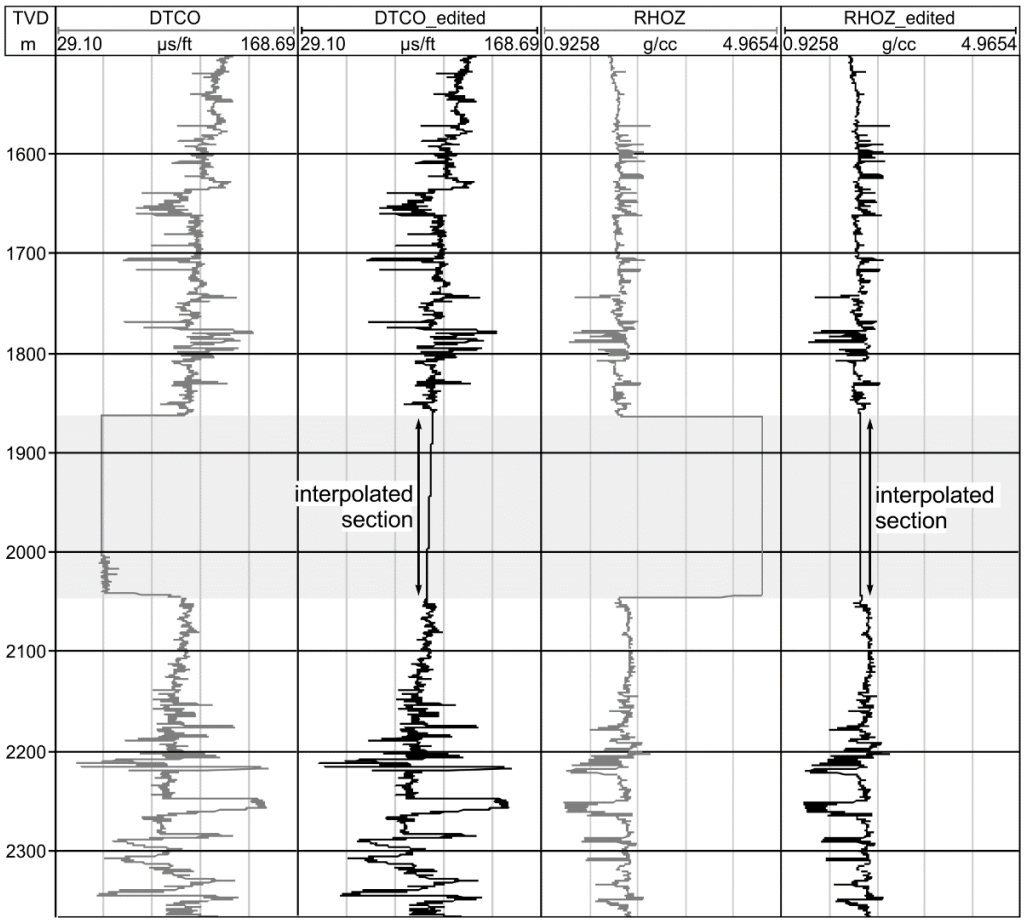

Figure A.6 Example of well logs where interpolation was required for specific intervals (shaded in grey) along which erroneous measurements were acquired; DTCO – original sonic log; DTCO_edited – sonic log after interpolation; RHOZ – density log; RHOZ_edited – density log after interpolation

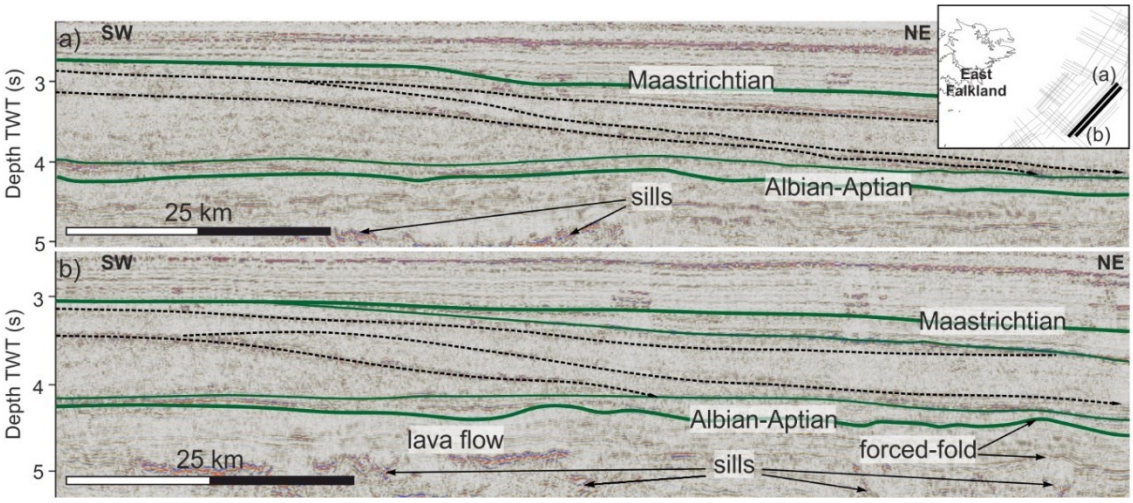

Figure A.7 Sections through the Fitzroy sub-basin showing progradation of Upper Cretaceous deposits (between the green horizons) from the SW, sills and lava flows distribution, and associated forced-folding of the Albian-Aptian marker

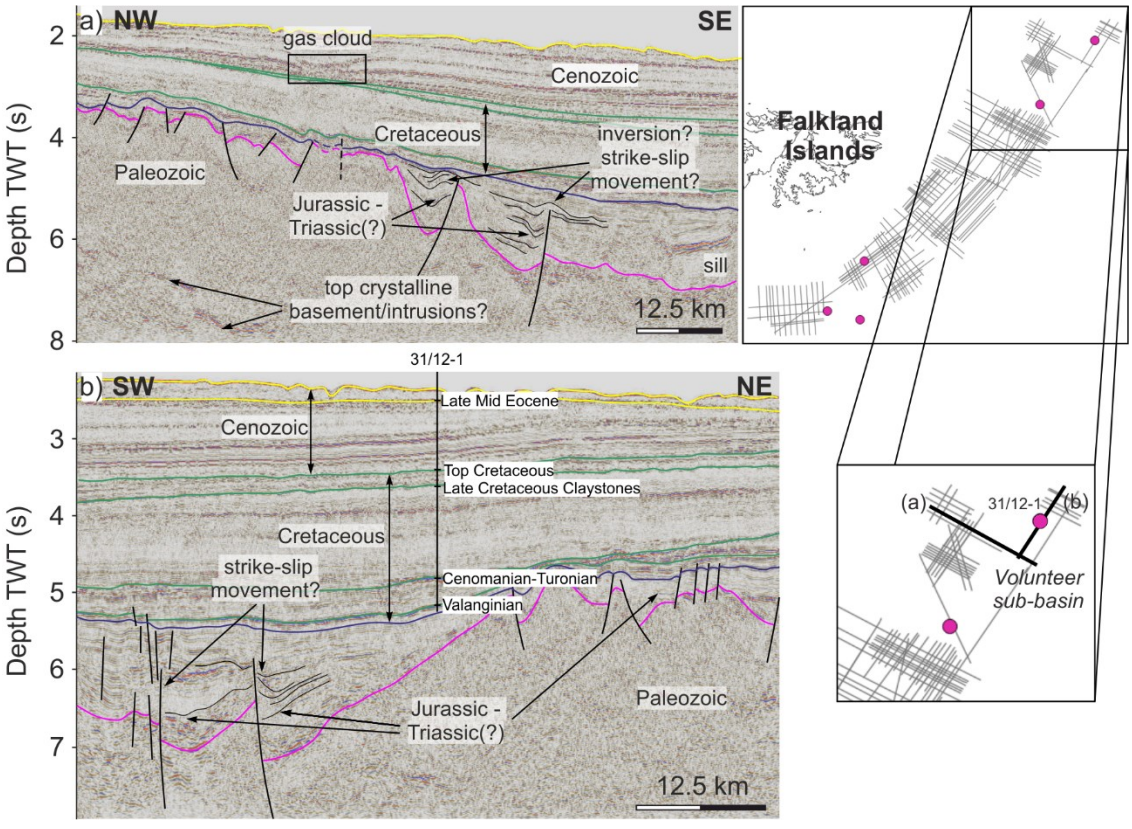

Figure A.8 Section through the north-western part of the Volunteer sub-basin showing Jurassic half-grabens and along-faults deformation potentially related to wrenching

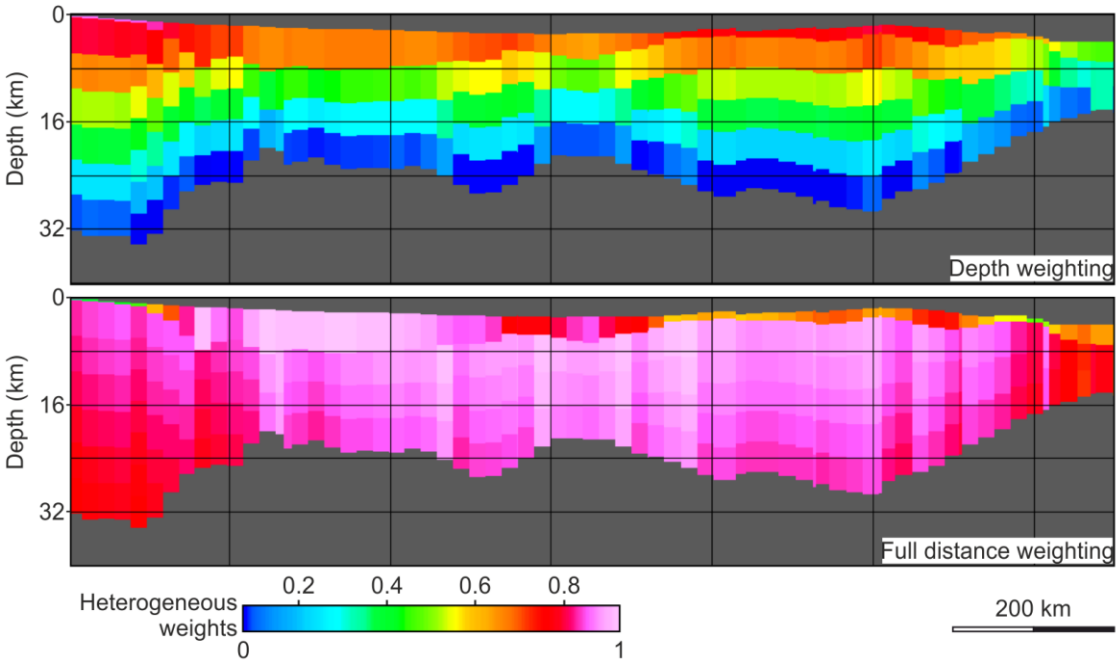

Figure A.9 Example of weight distribution based on the used weighting algorithm; larger values correspond to cells more likely to undergo changes in density in order to minimize the misfit between the observed and calculated gravity anomaly (i.e. depth weighting results in the shallower part of the model undergoing increases and decreases in density during the inversion process and can result in a concentration of big densities close to the surface)

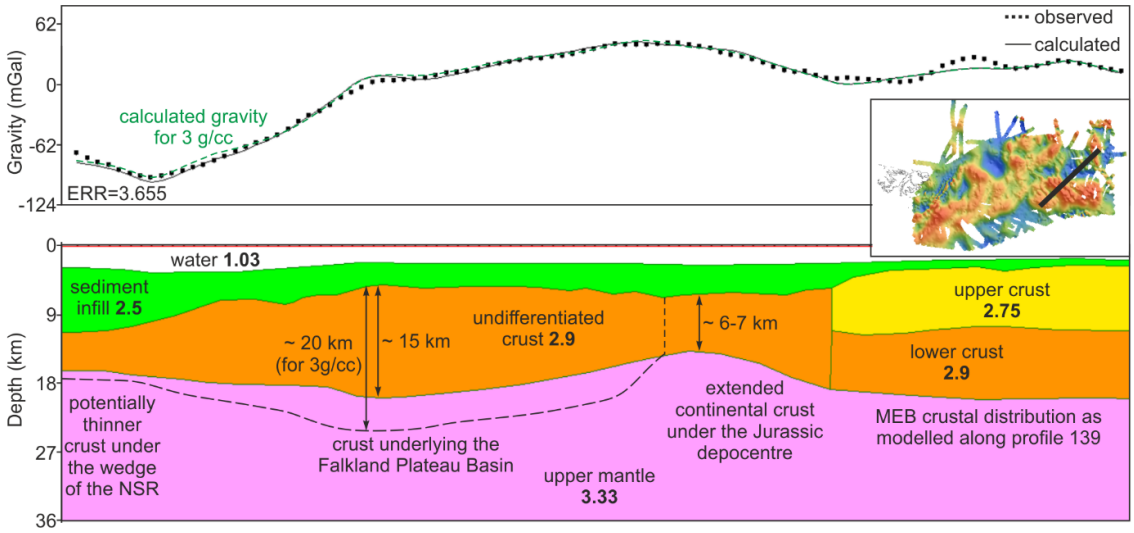

Figure A.10 2D forward gravity model along a profile cross-cutting the oceanic domain in the Falkland Plateau Basin; the sediment infill is considered to have an average density of 2.5 g/cc (the equivalent of the density distribution modelled for profiles 139); the crust under the FPB is also considered a homogenous block for simplicity; the calculated anomaly and error (misfit between the observed and calculated gravity anomaly) are for a crust of 2.9 g/cc; the fit for oceanic crust (3 g/cc) is shown in green, with the required thickness for the oceanic domain to minimize the misfit shown as the black dashed line in the section

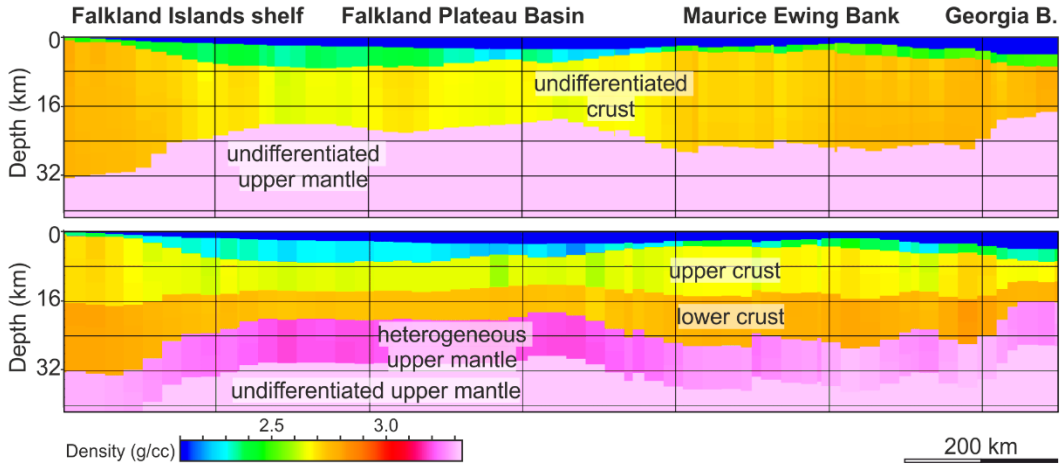

Figure A.11 Example of inversion results along profile 139 showing undifferentiated crust and mantle (top) and relatively lower densities for the Falkland Plateau Basin compared to the Maurice Ewing Bank and the Falkland Platform; layered crust (split at mid-point similar to the methodology described for the 2D forward modelling in Chapter 6) and heterogeneous upper mantle (bottom; first 10 km) showing that densities for the Falkland Plateau Basin more comparable to the Falkland platform and the Maurice Ewing Bank are obtained if lower densities are modelled for the upper mantle (underplating or serpentinization?); for the bottom model the range of densities for the upper crust was 2.58-2.96 g/cc, for the lower crust 2.7-3.05 g/cc, and for the upper mantle 2.9-3.33 g/cc

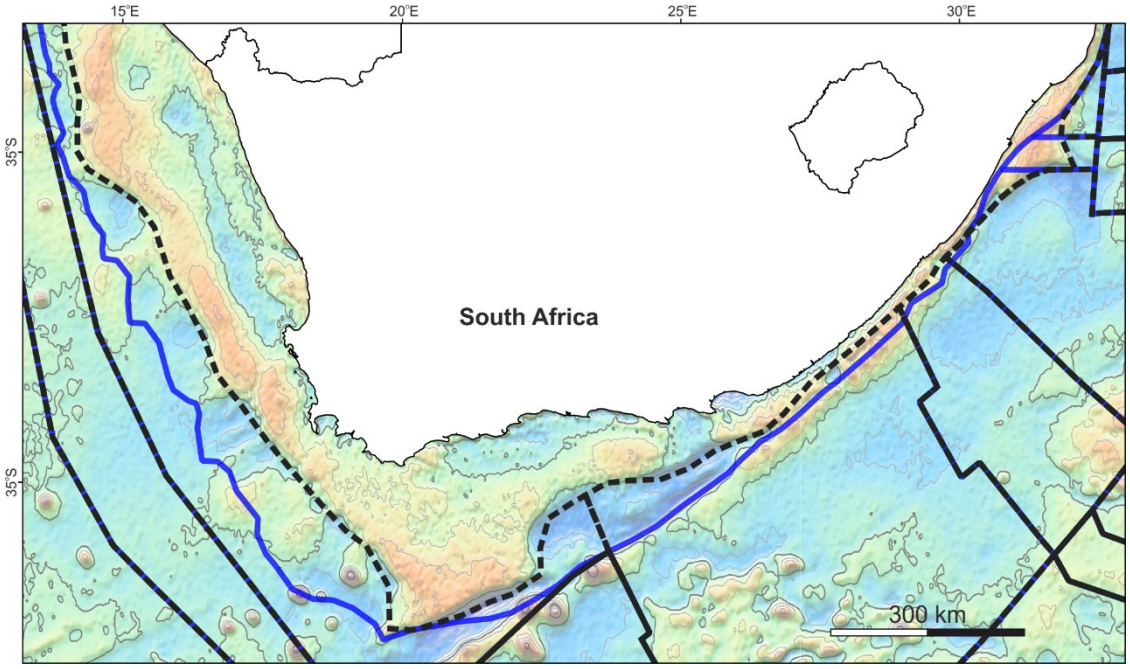

Figure A.12 Plate boundaries for South Africa and offshore basins from Müller et al. (2019) (blue); re-drawn plate boundaries (black dashed lines); gravity data from Sandwell et al. (2014)

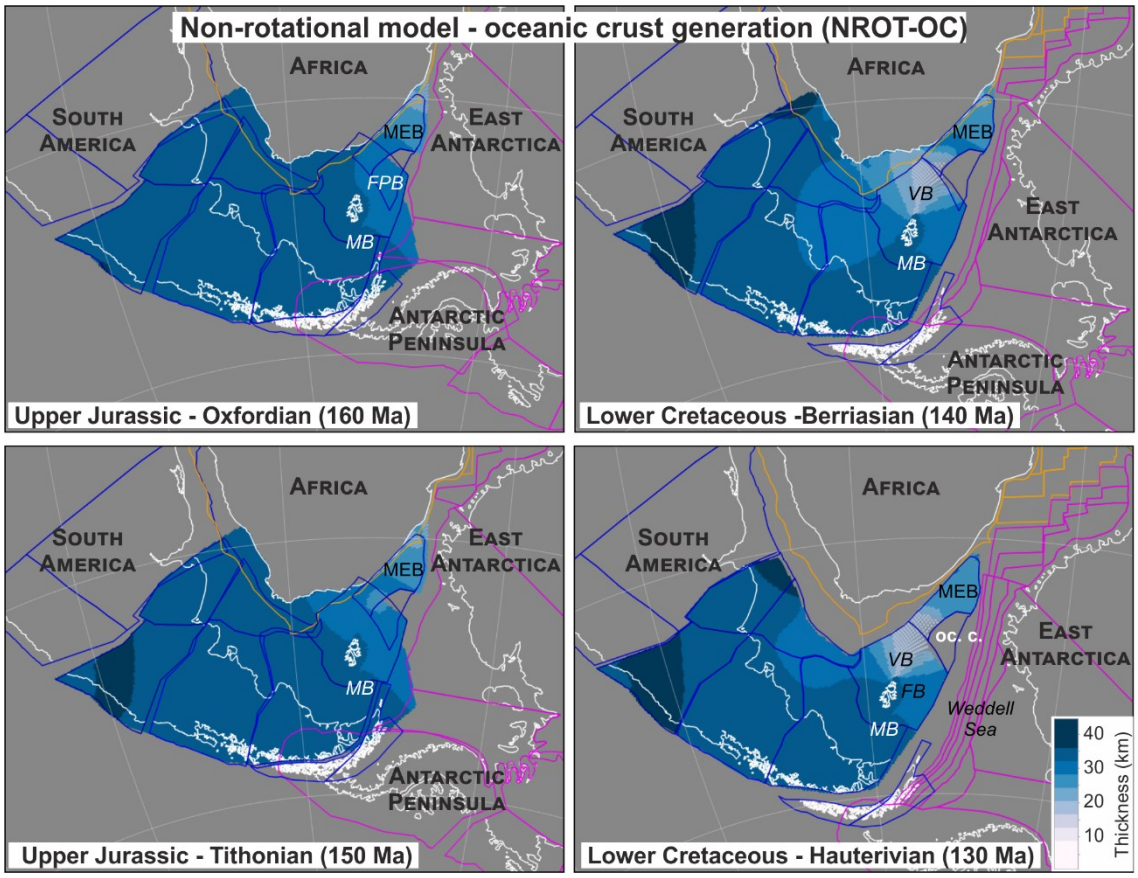

Figure A.13 Deforming plate model for a non-rotational scenario with break-up and generation of oceanic crust; FB – Fitzroy sub-basin; FPB – Falkland Plateau Basin; MB – Malvinas Basin; MEB – Maurice Ewing Bank; oc. c. – oceanic crust; VB – Volunteer sub-basin

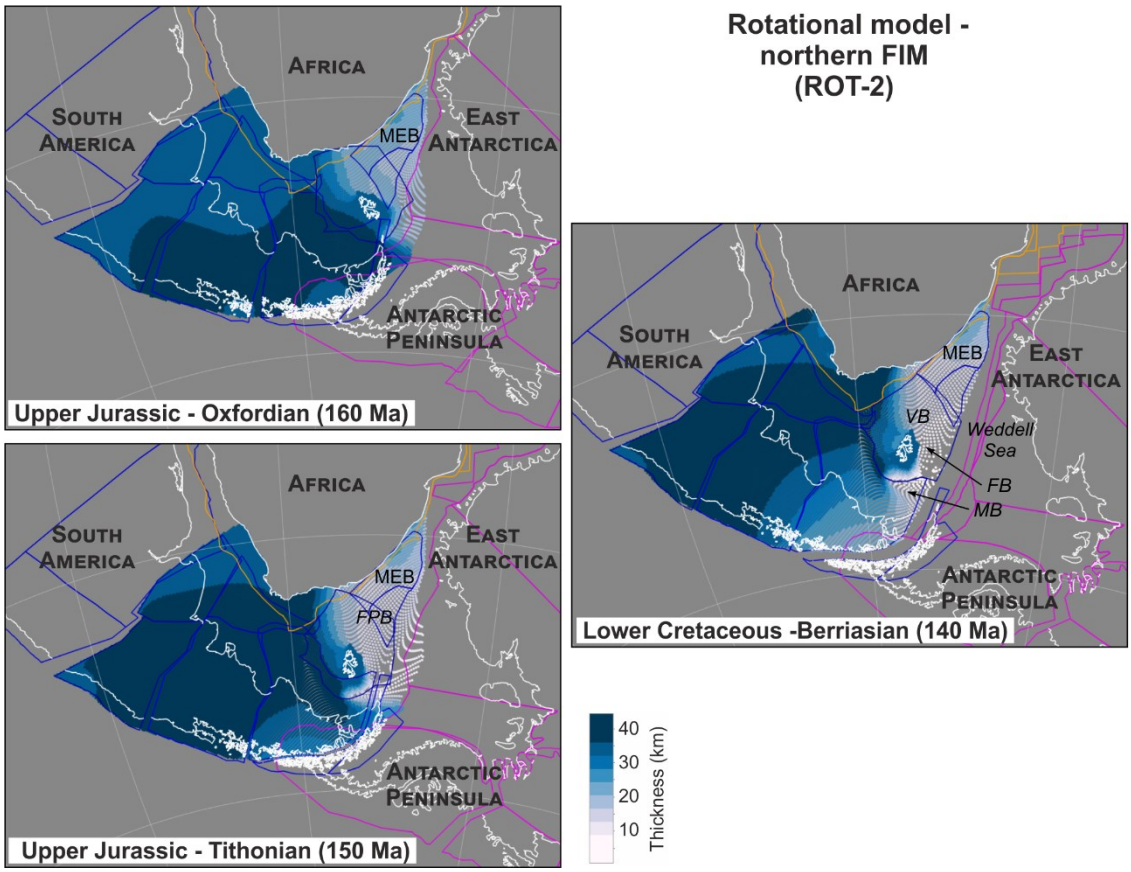

Figure A.14 Time steps of the deforming plate model built on rigid model ROT-2 (northern position of the FIM)